Geotechnical aspects of tunnelling in discontinuous rock, with particular reference to the lower chalk

Priest, S. D.

GEOTECHNICAL ASPECTS OF TUNNELLING IN DISCONTINUOUS ROCK, WITH PARTICULAR REFERENCE TO THE LOWER CHALK

by

S.D. Priest

being a thesis submitted in partial fulfilment of the requirements for the degree of Doctor of Philosophy in the University of Durham.

September 1975

GEOTECHNICAL ASPECTS OF TUNNELLING IN DISCONTINUOUS ROCK, WITH PARTICULAR REFERENCE TO THE LOWER CHALK

ABSTRACT

Discontinuities, defined as breaks or interruptions of the mechanical properties of a solid, are recognised in the literature as being of vital importance in controlling the behaviour of rock during tunnelling. This thesis presents a detailed study of an experimental tunnel excavated in discontinuous rock (Lower Chalk) at Chinnor in Oxfordshire. The work falls into three main areas of study.

Prior to tunnel excavation, detailed discontinuity surveys were carried out using an orthogonal scanline technique on exposed faces in the Chinnor quarry and in a 3m diameter shaft. This work, supported by subsequent surveys in the tunnel during its excavation, established - in numerical terms - the discontinuity characteristics of the Lower Chalk at Chinnor.

Ground behaviour during tunnel excavation was monitored in boreholes and in a trench excavated across the tunnel line. Ground movement results, when viewed in the light of data obtained from finite element analyses, have emphasised the non-elastic discontinuous response of the ground. The actual behaviour of the ground at Chinnor was found to be equivalent to that of a material having a deformation modulus that was approximately 1/20th of the Young's modulus of chalk determined from laboratory tests on intact samples. This modulus reduction was a direct result of the interaction between the tunnel excavation system and the discontinuous ground.

Having established the role of discontinuities in controlling the behaviour of the ground during tunnelling, and recognising the importance of discontinuity spacing as an index of discontinuity frequency, a detailed study of various statistical and geotechnical aspects of discontinuity spacings in rock is presented. The distribution of discontinuity spacing values obtained from measurements in three tunnels in the UK was found to closely follow a negative exponential distribution. The implications of this relation are that a single parameter expression can be adopted to describe the discontinuity spacing characteristics. By integrating this expression between the appropriate limits, a formula giving a precise value for the RQD (Rock Quality Designation) of the rock exposed can be obtained. In addition, important conclusions concerning optimum sample size and precision can be made once the discontinuity spacing distribution has been described in these simple mathematical terms.

Subsidiary to the three main areas of study outlined above, three additional peripheral subjects are considered. These include an evaluation of the hydrological characteristics of the chalk and an examination of chalk cutability. In addition, data concerning the shear strength characteristics of discontinuity surfaces in the chalk (obtained from laboratory tests) are incorporated in an analysis of stability near the tunnel at Chinnor, using a computer program on file at the University of Durham.

ACKNOWLEDGEMENTS

The work presented in this thesis forms a part of a research project run by the Transport and Road Research Laboratory (TRRL) conducted, in the main, at Chinnor in Oxfordshire. The author expresses his gratitude to all members of the research team at Chinnor for their assistance and co-operation on site. In particular the author would like to thank Mr G. H. Alderman (of TRRL) and Mr K. Kemp for their assistance in data collection, Mr J. Travers (of Sir Robert McAlpine and Sons Ltd.) for providing access to the tunnel and shaft, Mr P. Bilson (of the Rugby Portland Cement Co. Ltd.) for providing access to the quarry and Mr B. Wareham (of Soil Mechanics Ltd.) for providing site investigation data.

The author would also like to thank the following: Mr H. Eadie (of Babtie Shaw and Morton) and the Kielder Experimental Tunnel Steering Committee for providing access to the tunnel in Rogerley quarry, Mr I. Hill (of Mott Hay and Anderson) and Mr H. Smith (of Rio Tinto Zinc) for providing access to the Channel Tunnel, Dr. E.T. Brown (of Imperial College) for advice and assistance on site at the Channel Tunnel and Mr R. G. Hardy of the Department of Geological Sciences, University of Durham, for carrying out X-ray analyses on samples from Chinnor.

The author is also indebted to Mr J.B. Boden (TRRL) for advice and encouragement during the early stages of the work and Dr J.A. Hudson for many stimulating discussions and ideas. The author would also like to thank members of TRRL for their assistance and co-operation during the preparation of this thesis, in particular Mr H. J. Hignett for advice on rock cutting, Mr M. P. O'Reilly for providing access to the facilities of Tunnels Division, Mrs L.I. Foote of Technical Illustrations for

assistance with diagram preparation and the various members of the typing pool especially Mrs B. Wilson for typing the thesis.

Finally, the author would like to express his gratitude to his supervisors Dr P. B. Attewell and Dr I. W. Farmer of the Engineering Geology Laboratories, University of Durham for their valuable assistance and instruction during the past three years.

Financial support for this research project was provided at the outset by the Natural Environment Research Council in the form of a Studentship and latterly by the Transport and Road Research Laboratory, Department of the Environment in the form of a Research Contract to Drs. Attewell and Farmer.

TABLE OF CONTENTS

List of Figures

List of Tables

List of Plates

CHAPTER 1

TUNNELLING IN DISCONTINUOUS ROCK

1.1 Introduction

The use of tunnels in the urban environment is rapidly becoming a viable proposition as land costs rise and environmental awareness increases. The greatest single factor now restricting the use of tunnels is their cost. Where the cost differential between surface and subsurface construction is small, tunnelling becomes the most attractive proposition because surface land wastage is minimised.

O'Reilly and Munton (1972) considered the cost, merits and problems involved in putting urban roads in tunnels. They emphasised that a large percentage of tunnel costs are time dependent such that significant savings may result from faster tunnelling. Slow tunnelling is often a direct result of adverse ground conditions, consequently improved methods that allow faster tunnelling in bad conditions are likely to reduce costs. In weak cohesionless sands and gravels the bentonite tunnelling machine (Bartlett *et al*, 1973) offers the possibility of rapid tunnelling in unstable or waterlogged conditions. In very strong rock the factor limiting the rate of tunnelling is often the rate at which the rock can be excavated, in which case improvements in rock cutting technology will lead to reduced costs. However, for many near surface tunnels in rock the quality of the ground as a tunnelling medium is controlled not by the intact strength of the material but by the breaks or interruptions (discontinuities) in the mechanical properties.

In general engineering practice many authors have recognised the major role played by discontinuities in controlling the behaviour of a

rock mass (Trollope, 1968; Jaeger and Cook, 1969; Hoek and Bray, 1974).

The following dicontinuity characteristics were listed by Piteau (1970) as having particular engineering significance:

(a) Nature of their occurrence, that is, whether occurring singly or in sets;
(b) Orientation and position in space;
(c) Continuity;
(d) Intensity;
(e) Surface geometry;
(f) Genetic type;
(g) Nature and thickness of the joint fill.

There are many engineering situations in which a knowledge of the discontinuity characteristics of a rock mass is of importance and a variety of approaches can be adopted to analyse the stability and behaviour of a given rock mass utilizing discontinuity characteristics. A commonly-used technique is that applied to evaluation of slope stability, based on considerations of discontinuity orientation viewed in terms of factors of safety against failure along critical discontinuity surfaces (Attewell and Woodman 1971; Hoek *et al.* 1973).

Deere *et al.* (1969) suggested that rock should be considered discontinuous in terms of tunnelling when the ratio of fracture spacing to tunnel diameter is between the approximate limits of 1/5 and 1/100, concluding that for a range outside these limits the rock may be considered continuous, though possibly anisotropic. Following this definition Robertson (1974) stated that if the ratio of discontinuity spacing to tunnel diameter indicates that the tunnel will behave as if it were in a discontinuous

material the intact rock properties provide only upper bounds to the rock mass properties. The spacing, orientation, shear strength and deformational characteristics of the discontinuities govern the deformations and stress distributions that occur round the tunnel.

The problem of discontinuities in tunnel engineering was examined, largely qualitatively, by Terzaghi (1946). He assessed the influence of rock conditions on the load acting on the tunnel supports, in particular the relation between the amount of overbreak developing and the orientation of discontinuities with respect to the tunnel. In general he concluded that the maximum height of overbreak is approximately 0.5 B (where B is the tunnel width) and that this condition determined the maximum value which the load on the roof support could assume in fractured rock. Cording and Mahar (1974) extended the work of Terzaghi into more quantitative terms. They examined the effect of discontinuities on the behaviour of rock in tunnels and concluded that discontinuities having a strike direction within 25^{o} of the tunnel axis direction caused the greatest stability problems. They also found that instability was exacerbated by the presence of intersecting discontinuity planes.

Hobbs (1973, 1974), examining the settlement of structures on chalk, advocated the use of a rock mass factor j to quantify the effect of discontinuities on the expected performance of the intact rock. Defining j as "the ratio of the deformability of the rock mass within any readily identifiable lithological and structural component to that of the deformability of the intact rock comprising the component" he went on to consider the relation between j and fracture frequency. The work of Hobbs is considered further in Chapter 8 where the concept of the 'j-factor' is applied to the specific problem of tunnel engineering.

An alternative method of studying the behaviour of discontinuous rock is the use of mechanical or theoretical models. In the following paragraphs a brief outline of some of the more recent work is presented.

Zienkiewicz *et al.* (1968) and Einstein *et al.* (1970) adopted finite element analysis techniques to model the behaviour of discontinuous rock masses. Einstein *et al.* (1970), combining their theoretical analyses with model studies, concluded that the transition from brittle to ductile behaviour in the rock mass coincides with the transition from sliding along a pre-existing joint to fracture through the intact material. They also concluded that multiple joints have a systematic influence on strength and deformability depending on joint orientiation, joint spacing and the number of joint sets. Einstein and Hirschfeld (1973), developing these ideas further using model studies, concluded that deformability in the direction of an applied principal stress increases as the joint spacing decreases.

Sapegin and Karpov (1969) applied theoretical techniques to the analysis of the deformation characteristics of a discontinuous rock mass considered as a medium composed of blocks. They concluded that deformations resulting from load tests, calculated using the theory of discrete media, gave a better approximation to rock mass behaviour than those based on simple elastic theory. Heuzé *et al.* (1970) applied theoretitcal techniques to the analysis of deformability tests in jointed rock using joint perturbation and "no-tension" finite element solutions. They concluded that the good agreement between their theoretical results and field deformability tests indicated an appreciable deviation from linear elastic behaviour in the rock mass.

Singh (1973) used theoretical techniques to obtain general constitutive equations giving a continuum characterisation of jointed rock masses

using joint stress concentration factors. He found that stress concentration factors computed independently from finite element analyses agreed well with those obtained for the continuum characterisation. The complicated nature of this approach, however, limits its applicability to highly simplified situations of stress and discontinuity geometry.

The validity of the above theoretical models in describing the behaviour of a discontinuous rock mass, whilst confirmed for specific cases such as compressive loading, is debatable when applied to the complex stress situation found near a tunnel. These studies do, however, serve to indicate some of the main factors that could control the behaviour of discontinuous rock; in general suggesting that discontinuous rock cannot be regarded as a simple elastic medium, but rather as a complicated structure whose behaviour is critically modified by the discontinuity characteristics, in particular discontinuity spacing.

Another approach commonly adopted in analysing the problems of discontinuities in tunnels is to use practical, and largely empirical, methods. A variety of techniques for monitoring ground conditions in tunnels has been suggested. Proctor (1971) and Watkins (1971) advocate the use of standardised descriptive terminology for mapping conditions in tunnels. Piteau (1970, 1973) advocated the adoption of more rigorous quantitative techniques based on sampling of rock conditions along scanlines set up in the tunnel.

There is a wide range of existing rock mass classification systems, based on discontinuity characteristics, intact rock properties, geology and hydrological characteristics. Some of the more comprehensive systems are described in Coates (1964), Deere (1968) and Franklin (1970). In tunnel engineering it is common practice to use the index of rock properties obtained from examination of exposed faces or borehole cores

to give an indication of the suitability of the ground for tunnelling. Wickham and Tiedemann (1971) described a method of evaluating the quality of a rock mass to give a rock structure rating, ranging from 0-100. Lauffer (1960), Obert and Rich (1971), Bieniawski (1973) and Barton *et al.* (1974) have proposed a variety of detailed rock classification systems linked to support requirements in tunnels. In all these classification systems discontinuity characteristics play a major role in dictating the magnitude of the rock quality indices. In particular rock quality expressed as a Rock Quality Designation (RQD), initially proposed by Deere (1964), is widely accepted as a reliable index of discontinuity frequency. The adoption of discontinuity frequency (or discontinuity spacing) as an indication of the likely behaviour of a rock mass during tunnelling is a logical application of the results of the theoretical studies outlined above.

In their classification systems Bieniawski (1973) and Barton *et al.* (1974) take into account the relative importance of the various rock properties in controlling tunnel stability. In both systems discontinuity characteristics are heavily weighted as being important. Goodman and Duncan (1969) and Bieniawski (1971) emphasised that in addition to discontinuity characteristics the behaviour of a jointed rock mass is dependent on the nature of the intact material and the applied stress field. Therefore any analysis of the geotechnical aspects of tunnelling in discontinuous rock cannot be divorced from considerations of these factors.

Examination of the literature shows that there is no lack of theoretical studies of discontinuous rock masses, rock classification systems or tunnel case history studies when considered as separate items. There is, however, a distinct lack of literature describing integrated studies combining these approaches in the examination of one specific tunnelling

situation. Fairhurst (1969) writes: "Mere increase in the sophistication of mathematical formulation of a problem is of little value if the correspondingly required physical details are not available. Conversely, acquisition of experimental data without guidance from theoretical hypothesis is at best expensive and wasteful, and often misleading." It is the aim of this thesis to examine the geotechnical aspects of tunnelling in discontinuous rock by studying in detail one particular tunnel excavated in Lower Chalk. The examination will combine practical and theoretical approaches with particular emphasis on the collection, evaluation and interpretation of rock quality data in terms of the practical and theoretical results.

1.2 Discontinuity characteristics

The non-genetic term "discontinuity" defines a mechanical break or interruption of the properties of a solid (Fookes and Denness, 1969; John, 1971). The term "discontinuity" is therefore adopted in this thesis to describe all joints, fractures, faults, bedding planes and laminations formed as a result of either brittle fracture or sedimentation (Braybrooke, 1966). Discontinuities formed in the rock prior to exposure or disturbance are termed "inherited discontinuities", those formed as a result of weathering or excavation are termed "imposed discontinuities". In order to determine the influence of discontinuities on the behaviour of rock in a tunnelling situation, it is first necessary to assess the relevant discontinuity characteristics of the material.

Expanding on the conclusions of Piteau (1970), discontinuities can be described in terms of the following characteristics:

(a) Orientation of the discontinuity surface; expressed, for example, as a dip from the horizontal and azimuth of the dip direction.

(b) Discontinuity intensity; expressed as discontinuity frequency, average spacing, or total area of discontinuities per unit volume of rock.

(c) Discontinuity size; expressed as the trace length or area of the discontinuity.

(d) Surface geometry.

In addition, it may be necessary to consider the shear strength of the discontinuity surface; this strength is partly influenced by the characteristics described above and partly by other characteristics which may only be described qualitatively:

(a) Mineralogy of the fill material (if any) between the discontinuity surfaces.

(b) Mineralogy of the intact rock.

(c) Degree of weathering.

(d) Presence or absence of water.

Classification of discontinuities in terms of shear strength was discussed by Goodman (1970). He considered the results of shear tests on discontinuity surfaces and proposed a basically qualitative scheme for relating discontinuity surface-type and shear displacement to the peak and residual shear strengths. Fookes and Denness (1969) proposed a detailed system for classifying discontinuities in stiff clays in terms of type, size, surface geometry, surface markings, fabric (discontinuity orientation patterns), and intensity. These classification systems, though comprehensive, shed no further light on the influence of discontinuities on the engineering properties of the ground. The use of these systems is therefore regarded as inappropriate in the context of the present studies.

Ward *et al.* (1968) produced a classification system for chalk based on the degree of weathering and discontinuity characteristics of the material. In their system the chalk is given a grade, ranging from I - V, to indicate its quality as a foundation material (Table 1.1). The applicability of this system for classifying the Lower Chalk at Chinnor is discussed in Chapter 2.

Table 1.1

Classification of chalk
(After Ward *et al.* 1968)

Grade	Brief description
V	Structureless remoulded chalk, containing lumps of intact chalk.
IV	Partly weathered chalk, joint spacing 0.01m to 0.06m joint opening up to 0.02m, often infilled with remoulded chalk and fragments.
III	Rubbly to blocky unweathered chalk, joint spacing 0.06m to 0.20m, joint opening up to 3mm sometimes infilled with fragments.
II	Blocky medium hard chalk, joint spacing greater than 0.20m joints closed.
I	As for Grade II but harder and more brittle.

1.3 Assessment of discontinuity characteristics

When attempting to determine the influence of discontinuities on the behaviour of ground under a given engineering situation it is necessary to balance two requirements:

(a) Knowledge is required of those discontinuity characteristics most significantly dictating the behaviour of the ground.

(b) Knowledge can only be gained concerning those discontinuity characteristics amenable to evaluation using practicable survey techniques.

The discontinuity characteristics most likely to influence the behaviour of material both during and following tunnel excavation are orientation, intensity, and shear strength properties, (Bieniawski, 1971). There are four direct methods for assessing the orientation and intensity of discontinuities exposed at a face:

(a) Random measurement of discontinuity orientation.

This is often coupled with qualitative visual assessment of discontinuity frequency which may be summarised as a sketch diagram showing the discontinuity pattern.

(b) Block technique.

This involves the excavation and removal of a block of material followed by detailed measurement of discontinuity orientation, geometry, spacing and area during careful dissection of the block.

(c) Cavity technique

This involves the measurement of the characteristics outlined in (b), but by excavation and dissection of *in situ* material.

(d) Scanline technique.

This involves the measurement of discontinuity spacing, orientation and trace length at points where the discontinuities intersect scanlines (measuring tapes) set up on the exposure.

The method (a) is used widely by geologists and engineers for assessing discontinuity characteristics; this method is, however, highly subjective and unsuitable for rigorous numerical characterisation requirements.

Methods (b) and (c) were developed by Fookes and Denness (1969), for use in fissured Cretaceous sediments. The techniques, exhaustive and time consuming, provide detailed information about small volumes of highly fissured material, but become inappropriate in materials where discontinuity size or spacing are large compared with the sample volume.

The scanline method (d) was initially proposed by Jennings (1968) and extended by Piteau (1970). The technique is particularly suited to obtaining discontinuity data from large areas of rock face in a comparatively short time. Scanlines do, however, when taken singly, introduce a bias into the data since scanlines tend to intersect discontinuities inclined at a large angle to the scanline direction. This effect was noted by Terzaghi (1965) in connection with sampling by boreholes. The bias can be largely eliminated by taking three orthogonal scanlines of equal lengths at each survey location. In this way a largely unbiased 3-dimensional characterisation of the rock mass is produced.

When attempting to evaluate the problems of tunnelling in discontinuous rock, indexing using the scanline technique is considered to be the most desirable, for the following reasons:

(a) The scanline technique produces an index of discontinuity intensity in the form of an average spacing between discontinuities measured

along a line, the index of spacing is thus directly comparable with fracture spacing measurements taken from borehole cores. It is therefore possible to compare borehole site investigation data directly with data from scanline surveys taken both inside and outside the tunnel.

(b) Scanline surveys can be taken relatively quickly, so making it possible to measure discontinuities between shifts without disturbing excavation and construction work.

(c) The scale of the scanline survey can be made equal to that of the tunnel. Thus, discontinuity patterns sampled during the survey will reflect the average values and variability expected to occur in the zone of influence of tunnelling.

To determine the shear strength properties of discontinuity surfaces Hoek (1970) recommends the use of shear box tests. These tests, performed on actual discontinuity surfaces, reproduce as accurately as is possible, conditions obtaining in the rock mass (subject to the inherent limitations of the shear box). In this way, the behaviour of discontinuity surfaces under stress is determined directly. This method has obvious advantages over indirect methods involving the inference of shear strength properties from visual examination of the discontinuity surfaces.

1.4 The mechanised tunnelling trials at Chinnor

Much of the work described in this thesis was carried out in conjunction with the Transport and Road Research Laboratory (TRRL) during mechanised tunnelling trials in Lower Chalk at Chinnor in Oxfordshire. The opportunity for participation formed a logical extension of earlier analytical work, performed by research workers at Durham, into discontinuity

controls on stability. The possibility of studying the relation between discontinuities and ground behaviour during controlled tunnelling operations was a particularly attractive proposition. Accordingly, a research contract to finance the work was formulated by the Engineering Geology Laboratories and TRRL.

Tunnelling research at Chinnor was carried out under the general direction of Tunnels Division, TRRL. The Consulting Engineer for the project was Mott, Hay and Anderson. The main contract for the design of a full-face tunnelling machine and for tunnel construction at Chinnor was awarded to Sir Robert McAlpine and Sons Ltd. The machine, constructed by Peter Brotherhood Ltd in Peterborough, was delivered on site at Chinnor in October 1973. This machine, shown in Figure 1.1, consists of a 5m diameter full-face cutting head, housed in a shield, jacking against a two-section reaction ring (Plate 1.1). More detailed specifications of the tunnelling machine are given in Appendix A, after Hignett and Boden (1974). The excavated tunnel was supported using mining arches - spaced at 1m intervals - in conjunction with wire mesh (Plate 1.2). The general layout of the site, in the Rugby Portland Cement Company quarry at Chinnor, and the proposed tunnel line are shown in Figure 1.2. An aerial view of the site at Chinnor is shown in Plate 1.3.

The principal objective of the tunnelling trials, described in Hignett and Boden (1974), was to "obtain numerical data on the performance of tunnelling machines and examine how this is affected by various factors, e.g. arrangements of cutting tools." In particular the relation between the full-scale situation and the results of single-tool and multiple-tool cutting experiments in the laboratory and at pilot scale respectively were to be examined. The results of the laboratory and pilot scale experiments are described by Roxborough and Rispin (1972; 1973) and by Hignett (1974).

A part of the author's work at Chinnor was to index the discontinuity characteristics of the rock encountered during tunnelling. In this way, rock variability was monitored such that variation in machine performance resulting from modification of the cutting head design could be distinguished from that caused by variation in ground conditions.

A two-stage site investigation programme at Chinnor, involving the sinking of a total of eleven 131mm diameter diamond core drill holes, was carried out by Soil Mechanics Ltd. in order to (a) provide data for tunnel route selection, and (b) provide detailed information about the tunnel route once selected. In addition, a 3m diameter shaft was sunk near to the proposed tunnel line in order to allow detailed examination of the *in situ* chalk. A secondary objective of this site investigation programme was to assess critically the effectiveness of the site investigation techniques.

1.5 General geology of the Chalk

The Chalk, forming the upper calcareous series of the Upper Cretaceous, is divided into three groups of fossil zones: The Upper Chalk (Senonian), the Middle Chalk (Turonian) and the Lower Chalk (Cenomanian). The total thickness of the Chalk below the base of the Tertiary formations is commonly between 200m and 300m, which in south-east England is generally composed of equal thicknesses of Lower, Middle and Upper Chalk. The following typical features, described by Higginbottom (1966) are developed with great uniformity in the Upper Chalk:

1. A high calcium carbonate content (approximately 98%), resulting in a pure white colouration and a fine uniform texture of comparative softness.

2. An abundance of flint, occurring as irregular nodules, continuous bands or inclined veins.

In the Middle Chalk, whilst flints are usually scarce or absent, the high proportion of broken shells may impart a hard gritty texture to the rock. With increasing depth in the Middle Chalk the material becomes less uniform and shows a tendency towards alteration into hard cemented bands or nodules.

The lithology of the Lower Chalk is dominated by an absence of flints and a comparatively lower calcium carbonate content which decreases with depth in the sequence from approximately 90% near the junction with the Middle Chalk to values less than 45% near the base of the Chalk. The Lower Chalk formation can be divided into two main lithological units, the Grey Chalk and the lower Chalk Marl, separated by the mid-Cenomanian non-sequence. The Grey Chalk, developed above this non-sequence has a higher calcium carbonate content than the Chalk Marl and is consequently much harder and resistant to weathering. The Chalk Marl, having a lower calcium carbonate content, is dominated by the presence of soft marly zones of chalk which make the material exceptionally weak when wet.

A zonation of the Lower Chalk based on a microfossil zonal scheme formulated by D. J. Carter is presented in Bruckshaw *et al.* (1961). This scheme serves to separate the Lower Chalk into numbered zones delimited by the presence or absence of selected microfossils. By examining the microfossils present at Chinnor it was possible to put the Lower Chalk at Chinnor into the more general context of this zonation scheme. This work, described in Chapter 3, indicated that operations at Chinnor were largely confined to the Chalk Marl lithological unit of the Lower Chalk. The Chalk Marl is located below the mid-Cenomanian non-sequence, which at

Chinnor served to cut out a significant proportion of the Lower Chalk due to the influence of the mid-Berkshire swell. A description of the lithology and micropalaeontology of the Lower Chalk at Chinnor is presented in Chapter 3 and Appendix F.

Figure 1.3 shows a diagrammatic geological section across the Chinnor area summarising the main features of Chalk stratigraphy described above. This section is taken along a northwest-southeast line, parallel to the dip direction of the Chalk bedding which is inclined at an angle of approximately 3^{o} to the southeast. It is clear that Chinnor is situated at the base of the scarp slope of the Chilterns. These hills, running in a line from northeast to southwest are composed largely of Middle and Upper Chalk, the strike direction of which largely dictates the line of the hills.

1.6 Structure of the thesis

The work in this thesis falls into three main areas of study:

1. Collection and evaluation of rock quality data, in particular discontinuity characteristics. This work, performed on exposed faces in the Chinnor quarry, the 3m diameter shaft and the 5m diameter tunnel, together with a summary of the two-stage site investigation is presented in Chapters 2, 3 and 5.

2. Evaluation of the geotechnical aspects of tunnelling in the discontinuous chalk, drawing on data concerning:

    (a) Rock quality (Chapters 2, 3 and 5).
    (b) Ground movements caused by tunnelling at Chinnor (Chapter 7).

(c) Ground movements predicted using theoretical models, adopting finite element analytical techniques (Chapter 8).

3. Having established the role of discontinuities in controlling the behaviour of the ground during tunnelling, and recognising the importance of discontinuity spacing as an index of discontinuity frequency, a detailed study of various statistical and geotechnical aspects of discontinuity spacings in rock is presented. This work, described in Chapter 11, is presented in the context of:

   (a) Discontinuity spacing data from Chinnor.
   (b) Discontinuity spacing data from two other tunnels in the UK, plus relevant data from the literature.
   (c) A theoretical statistical analysis in terms of the negative exponential distribution.

Subsidiary to the three main areas of study outlined above, three additional peripheral subjects are considered:

1. Hydrological characteristics of the Chalk, including predictions of possible water make in the Chinnor tunnel (Chapter 4).

2. Cutability of the chalk (Chapter 6).

3. Evaluation of the shear strength characteristics of discontinuity surfaces in the Lower Chalk at Chinnor (Chapter 9). In Chapter 10 these data are incorporated in an anlysis of stability near the tunnel at Chinnor using a computer program on file at the University of Durham, the background logic of which is described in Attewell and Woodman (1971).

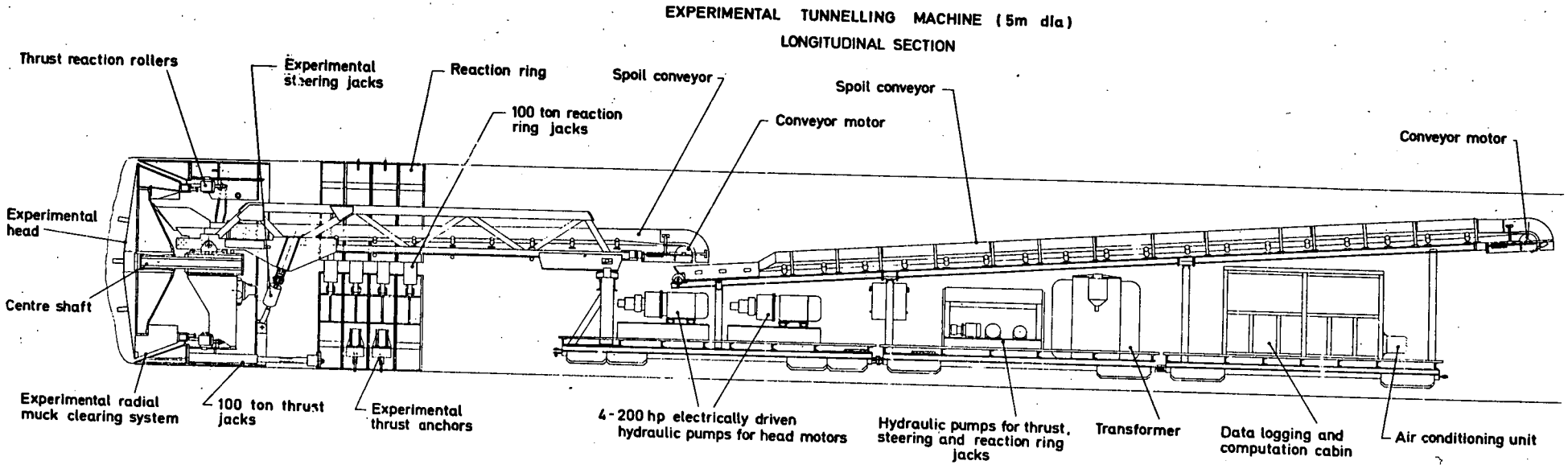

Fig. 1.1 THE McALPINE TUNNELLING MACHINE.

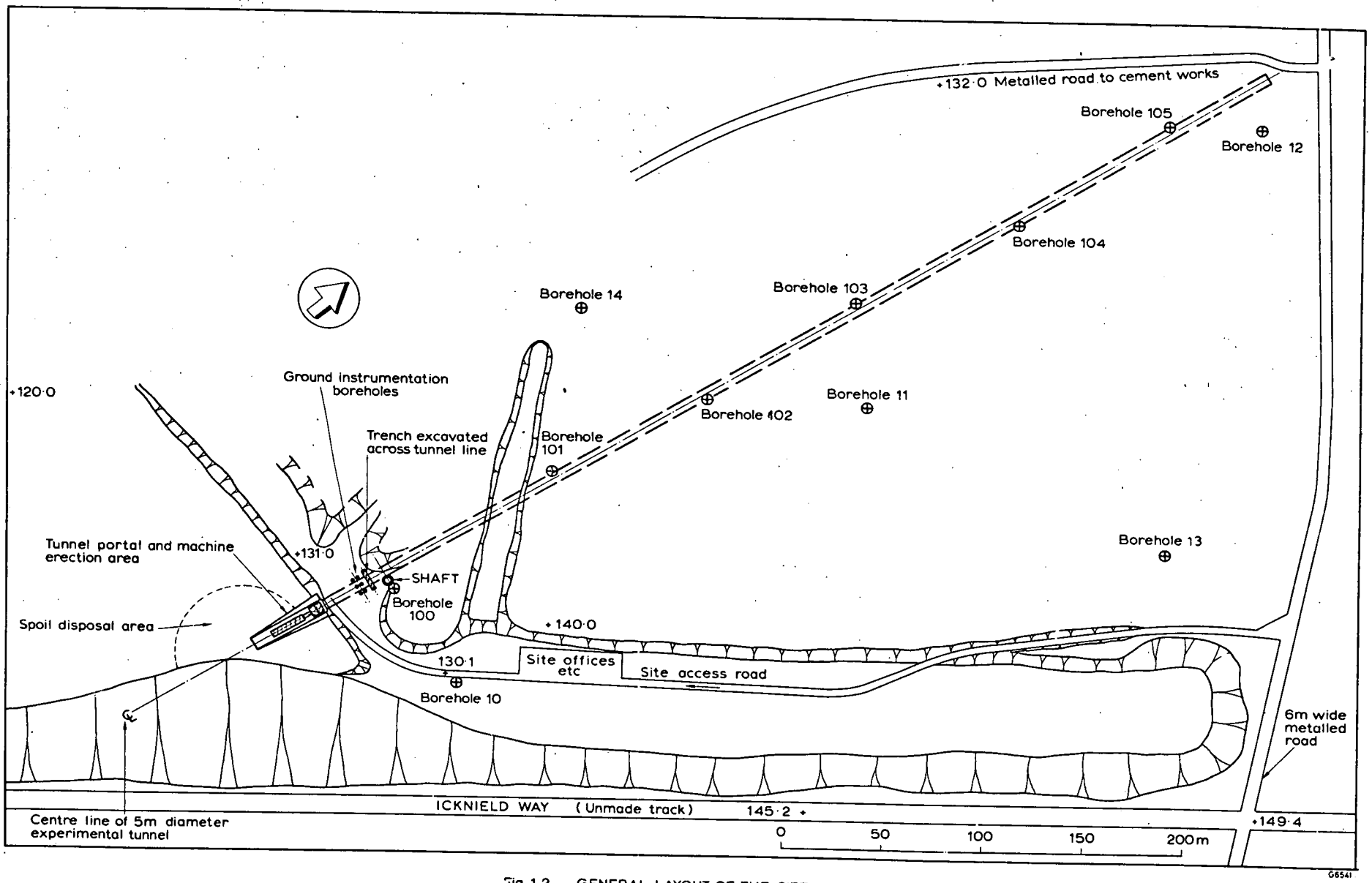

Fig. 1.2 GENERAL LAYOUT OF THE SITE AT CHINNOR

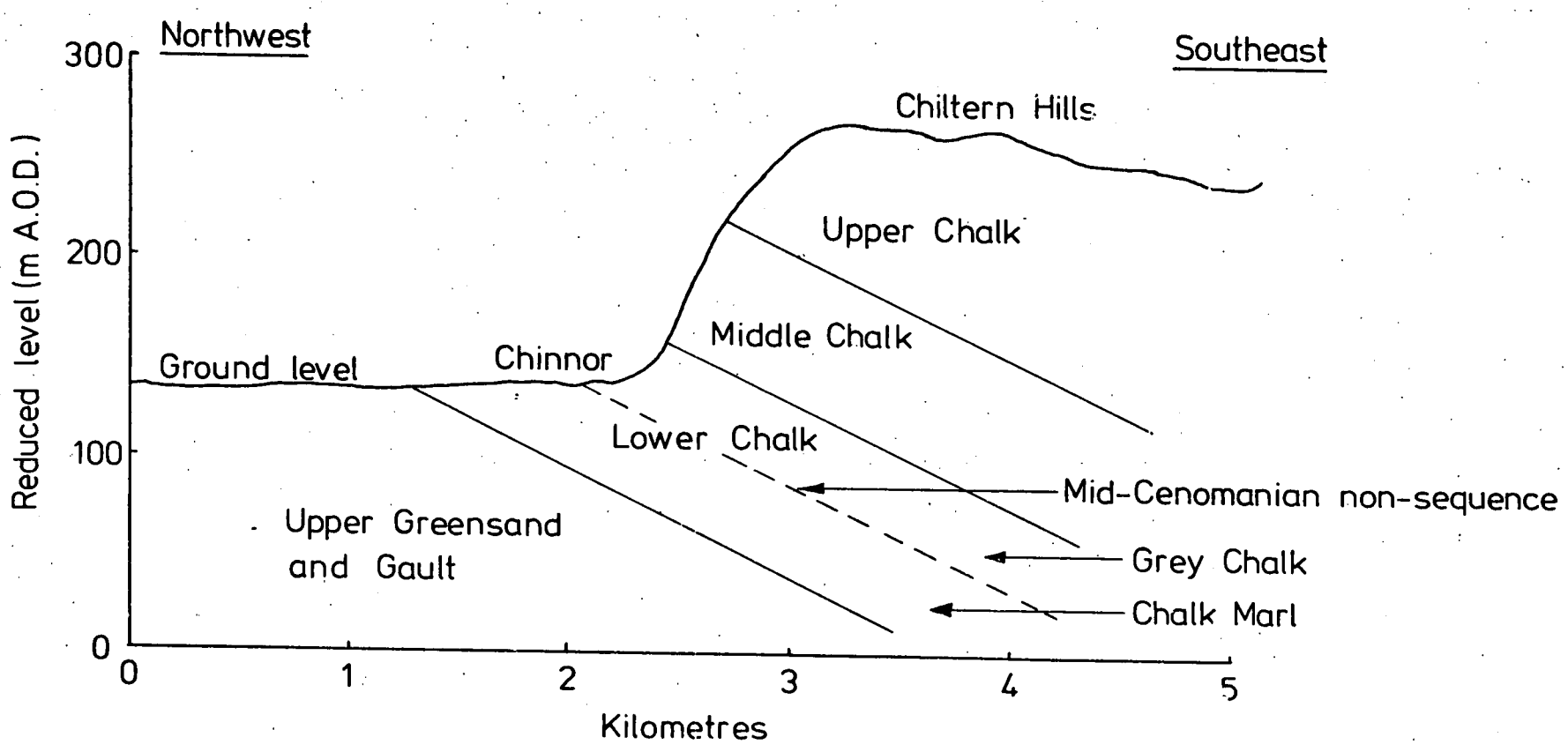

Fig. 1.3 DIAGRAMMATIC GEOLOGICAL SECTION ACROSS THE CHINNOR AREA.

Plate 1.1 THE McALPINE TUNNELLING MACHINE AT CHINNOR.

Photograph taken from chainage 5m (approx.) looking in the tunnel drive direction.

Plate 1.2 THE CHINNOR TUNNEL

(Looking north)

Plate 1.3 AERIAL VIEW OF THE SITE AT CHINNOR.

CHAPTER 2

ASSESSMENT OF DISCONTINUITY CHARACTERISTICS OF THE LOWER CHALK USING SCANLINES ON EXPOSED FACES IN THE CHINNOR QUARRY

2.1 Introduction

Before tunnelling at Chinnor began, a preliminary assessment of the discontinuity characteristics of chalk exposed at faces in the quarry was undertaken. These preliminary surveys were designed to: (a) give an indication of conditions that could be expected in the tunnel, and (b) allow comparison between the results of discontinuity surveys taken in the tunnel, in the shaft and at the exposed quarry faces, thus allowing an assessment of the effectiveness of the quarry face surveys in predicting conditions underground.

2.2 Survey technique

Discontinuity characteristics were measured along scanlines (measuring tapes) set up vertically and horizontally on exposed faces. Surveys were completed at ten locations in the quarry shown on the map in Figure 2.1. Where possible, three orthogonal scanlines were set up on a rock abutment, permitting a three-dimensional characterisation of the rock; this was possible at locations 1, 7, 8, and 10. At locations 2, 3, 4 and 5 a vertical face only was available, restricting the survey to one vertical and one horizontal scanline. At locations 6 and 9 a single horizontal scanline only was possible. Plate 2.1 shows the chalk face at survey location number 10, the tunnel portal face.

At the time of the surveys all faces except at location 6 were disused and had probably been exposed for several weeks. At the time of

the survey, the face at location 6 was being regularly worked.

The length of the scanlines set up was dictated by conditions at the face; in general scanline lengths ranged from 3m to 13m. At each location the rock was scanned along the measuring tape starting from the zero end. At points where discontinuities intersected the tape, the following characteristics were recorded:

(a) Distance of the intersection point along the scanline (D), taken to the nearest 0.01m.

(b) Orientation of the discontinuity, measured using a compass-clinometer, and recorded as the geographical azimuth (000^{o} to 360^{o}, counting in clockwise rotation) of the direction of maximum discontinuity dip and the amount (00^{o} to 90^{o}) of this maximum dip. Azimuth directions were taken relative to magnetic north, read to the nearest degree, then adjusted for magnetic declination. The dip was taken as the maximum angle (00^{o} to 90^{o}) between the discontinuity surface and the horizontal, again read to the nearest degree. Thus the reading 090/40 is the orientation of a discontinuity dipping at an angle of 40^{o} to the east.

(c) Trace length of the discontinuity, extending to the right (L_1) and left (L_2) sides of the tape (facing the zero end). The raw data (a), (b) and (c) for all scanlines are listed in Appendix B.

(d) Geometry and structure of the discontinuity, that is, whether planar or curved, open or closed and the nature of the fill, if any.

The discontinuities measured were those that visibly interrupted the mechanical properties of the solid and were thought likely to modify

significantly the mass behaviour of the rock. Microscopic hairline fractures were not measured. There was therefore this degree of personal selectivity.

Evaluation of discontinuity trace length proved to be a largely subjective process since the visible trace length of each discontinuity was, in many cases, more a function of the geometry of the face rather than the size of the discontinuity. Values of trace length, exhaustively collected to the best of the author's ability, are, however, presented in Appendix B for completeness. Processing of the trace length data has not been undertaken in this thesis for the reasons outlined above, but rather discontinuity intensity is considered in terms of mean discontinuity spacing.

2.3 Processing of results

Each scanline was given a reference number to indicate the location, and a reference letter to differentiate between scanlines at each location. For each scanline, consecutive intersection distances (D) were subtracted to give discontinuity spacing values, calculated to the nearest centimetre. Spacing values taken on the one, two or three scanlines at each location were then aggregated to enable the production of a discontinuity spacing histogram for each survey location. In this aggregation an integral correction factor was applied, to correct for scanline length. This correction was necessary because scanlines within each location could not always be set up having equal lengths. If the lengths of scanlines a, b and c at a given location are L_a, L_b and L_c; and $L_a \neq L_b \neq L_c$, then a correction for scanline length is required. If, say, $L_a > L_b > L_c$ then the integral correction factors A, B and C adopted for each scanline are:

$$A = \text{INT}\frac{(L_a)}{(L_a)} = 1$$

$$B = \text{INT}\frac{(L_a)}{(L_b)}$$

$$C = \text{INT}\frac{(L_a)}{(L_c)}$$

where "INT" indicates the nearest integer to the quotient in brackets.

For scanlines in two dimensions a correction factor equating vertical and horizontal scanline lengths was adopted, calculated in a similar way to that described above for three dimensions. The application of the scanline correction factor is summarised in Figure 2.2. The integral correction factors were applied to each discontinuity thus doubling, trebling or even multiplying further the volume of data for the particular scanline, according to the value of the correction factor. Although there is some statistical logic in adopting such a normalizing procedure, there is still an intuitive objection to the "manufacturing" of data.

It is partly for this latter reason that the normalizing techniques advocated by Terzaghi (1965) have not been adopted here. Terzaghi suggested that the number of discontinuities N_α intersecting a scanline at an angle α should be replaced by a value N_{90} respresenting the number of discontinuities with the same orientation that would have been observed had the scanline intersected the discontinuities at an angle of 90^o, where

$$N_{90} = \frac{N_\alpha}{\sin \alpha} .$$

At first sight this appears to be an attractive technique, however,

practical application involves complicated three-dimensional geometry and the eventual production of non-integral discontinuity occurrences, that is, the problematical occurrence of, say, 1.3 discontinuities having a given orientation. The avoidance of such occurrences may require a ten-fold multiplication of the volume of data for a given scanline, thus imposing an artificial discontinuity spacing distribution and false mean spacing value. It is recognised that for the purposes of plotting discontinuity orientation data from single scanlines the approach advocated by Terzaghi has distinct advantages. However, for largely qualitative interpretation of orientation data it is felt that the orthogonal scanline technique, used in conjunction with the simple correction procedures described above, is preferable.

By taking orthogonal scanlines of equal lengths, preferential selection of discontinuity spacing values along a single line was avoided, and a largely unbiased three-dimensional characterisation of the rock mass was obtained. Corrected discontinuity spacing histograms for each of the survey locations are shown in Figures 2.3 to 2.12. Additional data concerning each of the separate scanlines at each location are tabulated in these Figures. These tabulated data include scanline lengths, face and scanline orientations, together with values of mean discontinuity spacing and mean dip, plus the respective standard deviations for these mean values. These data are summarised for each location in Table 2.1. Figure 2.13 shows a summary discontinuity spacing histogram for the aggregated readings from locations 1 to 10.

Figures 2.3 to 2.12 also include a fitted negative exponential probability density distribution, calculated in each case for the appropriate parameter $\hat{\lambda}$ equal to the reciprocal of the mean discontinuity spacing at each survey location. These fitted curves and the negative

Table 2.1 Discontinuity data from scanlines in the quarry

Scanline location (Figure 2.1)	Corrected total scanline length (m)	Corrected number of discontinuities measured	Mean discontinuity spacing (m)	Spacing, standard deviation (m)	Mean discontinuity dip, (degrees)	Dip, standard deviation, (degrees)
1	16.16	256	0.063	0.038	57.06	26.03
2	20.09	325	0.062	0.050	64.71	21.59
3	18.10	273	0.066	0.062	62.24	21.79
4	20.17	275	0.073	0.063	63.29	19.58
5	27.81	424	0.066	0.061	57.25	26.39
6	13.00	98	0.133	0.105	64.20	19.61
7	36.64	561	0.065	0.063	51.88	24.18
8	34.50	457	0.075	0.068	62.07	20.81
9	10.60	191	0.056	0.049	54.94	21.55
10	19.00	302	0.063	0.058	51.49	25.64

exponential distribution are discussed fully in Chapter 11.

Discontinuity orientation data were processed using a computer program on file in the Engineering Geology Laboratories, University of Durham. The program rapidly processes large volumes of orientation data and displays the resulting discontinuity fabric, smoothed and contoured, on an upper or lower hemisphere projection or, if required, a whole sphere projection (Attewell and Woodman 1971). Further details concerning the construction and interpretation of the upper hemisphere projections that were used in this work are given in Appendix C.

Orientation data, corrected for scanline length and taken from each of the survey locations, were processed using the program described above (and in Appendix C). The resulting equal area projections are shown in Figures 2.14 to 2.23.

The use of orthogonal scanlines, corrected for scanline length largely obviated the possibility of preferential sampling of one particular discontinuity set. However, at locations 6 and 9, the use of a single horizontal scanline will have led to preferential sampling of sub-vertical discontinuities, and a consequent introduction of bias into the equal area projections. Data from locations 6 and 9 are therefore omitted from Figure 2.24, showing the discontinuity orientation fabric for aggregated data from the survey locations in the quarry.

2.4 Discussion of results

Examination of Figures 2.3 to 2.12 reveals that overall mean discontinuity spacing values for rock examined along orthogonal scanlines at locations 1, 2, 3, 4, 5, 7, 8, 9 and 10 range from 0.056m to 0.075m.

The higher mean spacing value of 0.133m for the freshly exposed rock at location 6 indicates that length of exposure of the chalk is a factor controlling discontinuity frequency. It is likely that weathering effects acting on the rock following exposure, emphasised the hitherto invisible hairline discontinuities, causing a reduction in mean discontinuity spacing with time. Fookes and Denness (1969) found that weathering effects, whilst having no apparent influence on the discontinuity orientation-fabric or size of discontinuities, did tend to increase significantly the intensity of fissuring. Fookes and Denness also found that the age of exposure influenced the discontinuity characteristics by increasing the proportion of non-planar discontinuities. This latter effect was not, however, found in the Lower Chalk at Chinnor. It is probable that the additional discontinuities, exposed by the processes described above, when present as incipient hairline fractures in the unexposed rock mass would not significantly modify the mechanical properties of the rock.

Application of the chalk classification system of Ward *et al.* (1968), described in Chapter 1, shows that the Lower Chalk in the quarry at Chinnor is, in general, all Grade III. This system therefore, whilst serving to place the quality of the chalk at Chinnor in the more general context of chalk quality, is not an effective tool for describing the variation of chalk properties within the site at Chinnor. In this thesis, therefore, chalk quality will be described using numerical parameters rather than descriptive terms or classification systems.

Table 2.1 indicates that the mean discontinuity dip values at locations 1 - 10 range from 51.49^{o} to 64.71^{o}. These values together with the equal area projections shown in Figures 2.14 to 2.23, show that there is no tendency for the discontinuities at Chinnor to be orientated in either a predominantly vertical or a predominantly horizontal attitude.

The close similarity between mean spacing values taken from vertical and horizontal scanlines set up in the quarry (Figures 2.3 to 2.12) tends to confirm this conclusion, since, for example, a lower mean spacing on a vertical scanline compared with a horizontal one at the same location indicates the possibility (but does not confirm the presence) of predominantly sub-horizontal discontinuities. This effect is discussed further in Chapter 3.

Examination of the mean dip values for the individual scanlines in Figures 2.3 to 2.12 indicates that preferential sampling of sub-horizontal discontinuities on vertical scanlines and sub-vertical discontinuities on horizontal scanlines leads to a lower mean discontinuity dip for the vertical scanlines than the horizontal scanlines. This emphasises the necessity of taking scanline surveys in orthogonal directions when attempting to assess the true 3-dimensional discontinuity characteristics of a rock mass.

The discontinuity spacing histograms shown in Figures 2.3 to 2.12 indicate a broadly similar distribution of discontinuity spacing values for all survey locations. It is apparent that the frequency of occurrence of a given discontinuity spacing value decreases exponentially as the magnitude of the spacing value increases, such that, in general, the smaller discontinuity spacings are more frequent. This effect is discussed further in Chapter 11.

Equal area projections shown in Figures 2.14 to 2.23 reveal broadly similar patterns of discontinuity orientation at the various locations in the Chinnor quarry. There are four basic components to the orientation fabrics, developed to a lesser or greater extent at each of the survey locations:

(1) A sub-horizontal set of discontinuities dipping at low angles (15^{o}) to the northwest. This set is well developed at all survey locations, except 6 and 9 where the use of a single horizontal scanline only, introduced a bias against sampling sub-horizontal discontinuities.

(2) A sub-vertical set dipping steeply ($\simeq 70^{o}$) to the northwest and southeast. The northwesterly dipping component of this set is well developed at all survey locations.

(3) A sub-vertical set dipping steeply ($\simeq 70^{o}$) to the northeast and southwest. The southwesterly dipping component of this set is often poorly developed, or in some cases swings round to dip to the south and merge with the southeasterly steeply dipping set.

(4) A randomly orientated component, showing no preferred orientation, but developed to varying degrees at each survey location.

The overall pattern of discontinuity orientation in the Chinnor quarry shown in Figure 2.24 summarises the general patterns described above. Because a large volume of data (2,899 readings) was used in Figure 2.24, the randomly orientated set of discontinuities (set 4) becomes self-cancelling and is smoothed out of the projection.

The bedding in the Chalk at Chinnor is of a very flat even nature, showing a low dip (approximately 3^{o}) to the southeast (Figure 2.25). This, together with the absence of any marked folding or faulting, suggests that the Chalk in this area has not suffered any severe tectonic activity. It is therefore likely that the spatial and orientation density distributions of discontinuities at Chinnor are a reflection of geomorphological rather than regional tectonic controls. This effect (not confined to the

Lower Chalk at Chinnor) is a characteristic of the Chalk in general that is widely acknowledged in the literature (Higginbottom, 1966; Foster, 1974).

It is probable that the clusters of discontinuity orientation in the Chalk at Chinnor, described in the previous paragraphs, reflect stress release effects resulting from erosion of the scarp slope of the Chilterns (Figure 2.25). Chinnor, situated at the base and to the northwest of this scarp slope, was at one time covered with approximately 200m of Middle and Upper Chalk, now eroded. Progressive erosion resulting in the migration of the northwesterly dipping scarp slope across the Chinnor area probably accounts for the well developed orientation concentration of discontinuities dipping to the northwest, parallel to the stress release surface of the scarp slope. Additional more randomly orientated discontinuities at Chinnor may partly be a result of stress effects induced by frost action and a fluctuating ground water level.

2.5 Summary and conclusions

(1) Discontinuity characteristics were measured along scanlines set up on exposed faces in the Chinnor quarry.

(2) By using orthogonal scanline techniques in conjunction with an integral correction factor (to allow for variable scanline length) a largely unbiased 3-dimensional characterisation of the rock mass was produced.

(3) Mean discontinuity spacing values on faces exposed for several months ranged from 0.056m to 0.075m. A freshly exposed face gave a mean spacing value of 0.133m. All chalk encountered was found to be Grade III in the classification system of Ward *et al.* (1968).

(4) It is thought likely that weathering effects acting on the rock emphasised hitherto invisible hairline discontinuities causing a reduction in mean discontinuity spacing on faces exposed for several weeks until degradation processes exposed a new face.

(5) Discontinuity spacing histograms revealed that, at all survey locations, the frequency of a given discontinuity spacing value decreased exponentially as the magnitude of the spacing value increased.

(6) Discontinuity orientation data were computer plotted on upper hemisphere equal-area projections. Discontinuity orientation fabrics for the survey locations in the quarry were found to consist of four basic discontinuity orientation sets, developed to a lesser or greater extent at each survey location. It is probable that spatial and orientation density distributions of discontinuities at Chinnor reflect geomorphological controls, such as stress release effects, resulting from erosion of the scarp slope of the Chilterns.

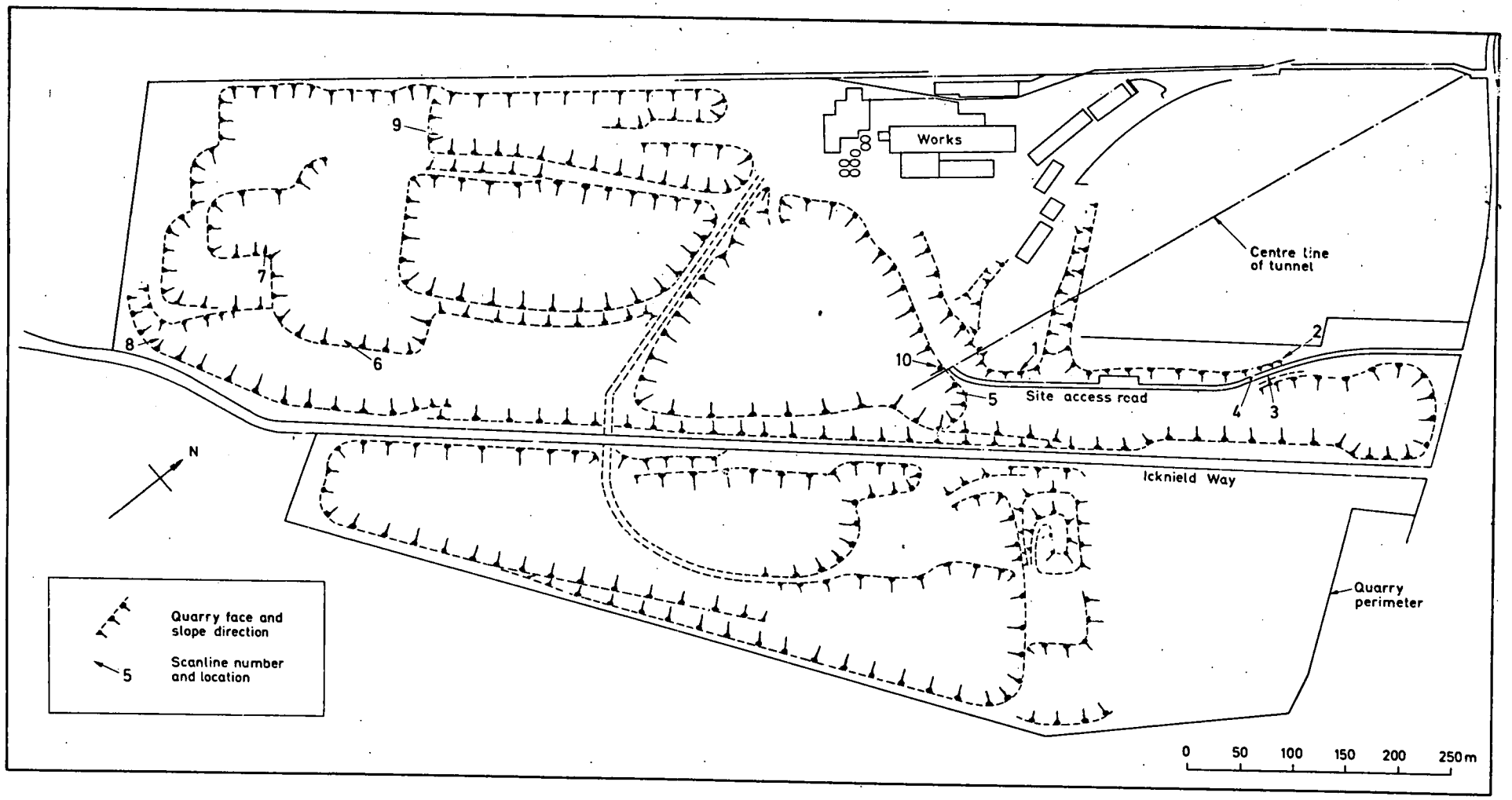

Fig. 2.1 DISCONTINUITY SURVEY LOCATIONS IN THE CHINNOR QUARRY

a. Actual scanline configuration

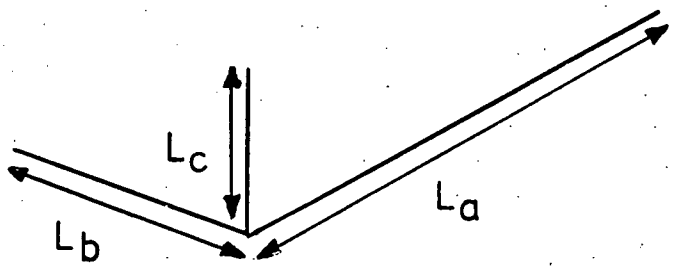

$A = 1$

$B = \frac{L_a}{L_b} \approx 2$

$C = \frac{L_a}{L_c} \approx 3$

b. Corrected scanline configuration

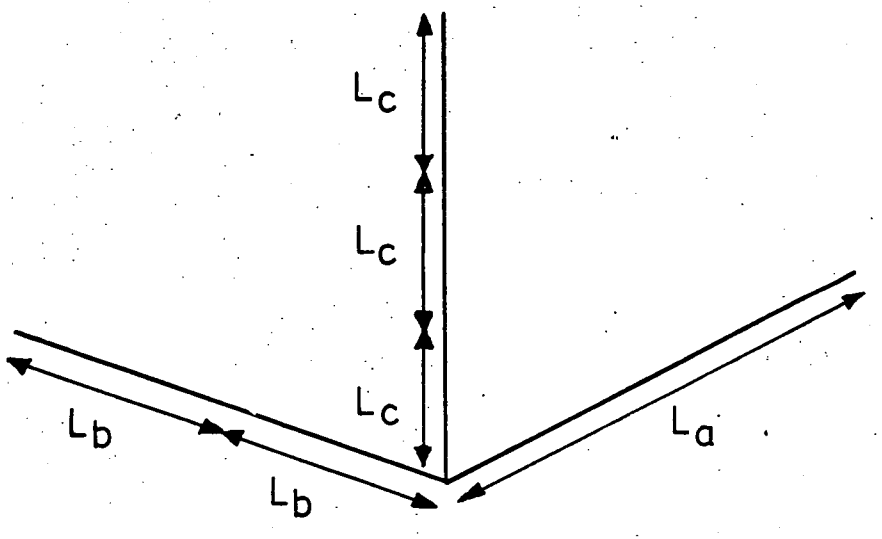

Data from scanline b are doubled

Data from scanline c are trebled

Fig. 2.2 APPLICATION OF THE SCANLINE CORRECTION FACTOR.

Scanline	Face orientation	Scanline orientation	Scanline length (m)	Integral correction factor	Mean discontinuity spacing (m)	Spacing, standard deviation (m)	Mean discontinuity dip, (degrees)	Dip, standard deviation, (degrees)
1A	130/80	037/00	4·49	1	0·077	0·053	68·63	13·38
1B	074/78	350/08	5·85	1	0·068	0·038	62·79	24·26
1C	165/70	165/70	2·91	2	0·052	0·024	46·60	28·60
1A + 1B +(2×1C)	—	—	16·16	—	0·063	0·038	57·06	26·03
Corrected total number of spacing values = 256								

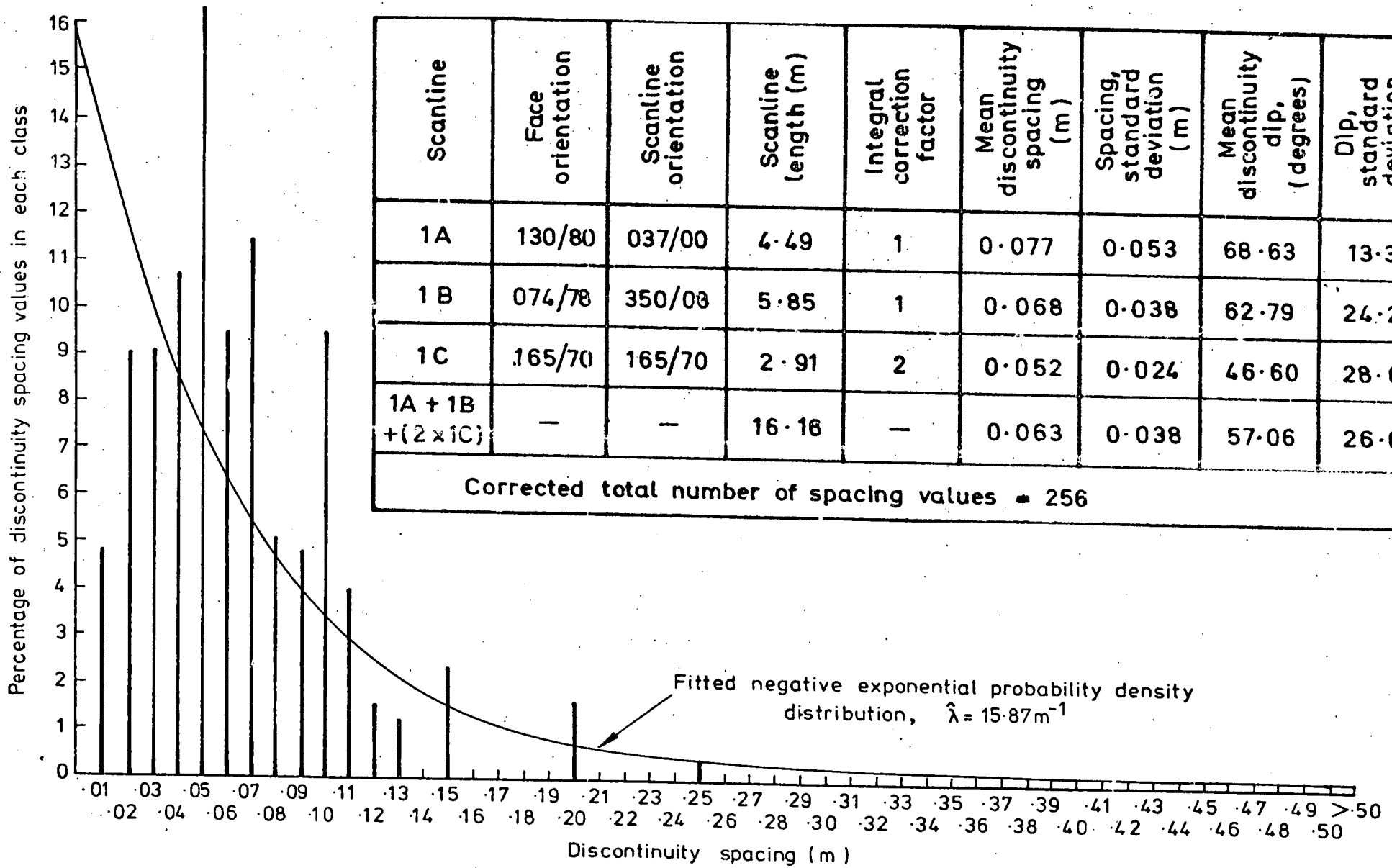

Fig. 2.3 DISCONTINUITY SPACING HISTOGRAM, CHINNOR QUARRY LOCATION 1

Scanline	Face orientation	Scanline orientation	Scanline length (m)	Integral correction factor	Mean discontinuity spacing (m)	Spacing, standard deviation (m)	Mean discontinuity dip, (degrees)	Dip, standard deviation, (degrees)
2 A	128/84	218/05	10·67	1	0·061	0·052	65·59	21·14
2 B	125/76	126/68	3·14	3	0·063	0·047	63·68	22·29
2A+(3x2B)	—	—	20·09	—	0·062	0·050	64·71	21·59
Corrected total number of spacing values = 325								

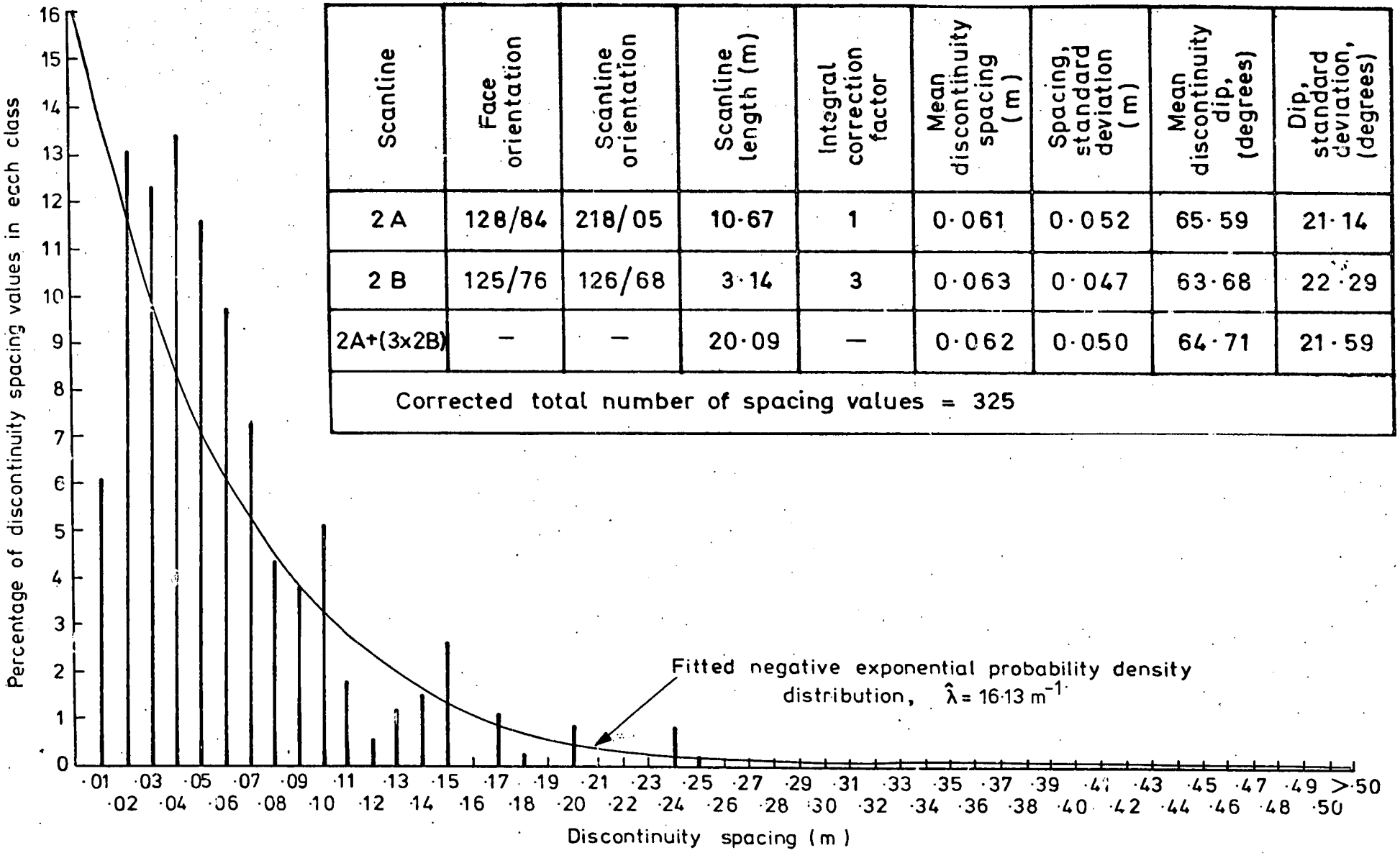

Fig. 2.4 DISCONTINUITY SPACING HISTOGRAM, CHINNOR QUARRY LOCATION 2

Scanline	Face orientation	Scanline orientation	Scanline length (m)	Integral correction factor	Mean discontinuity spacing (m)	Spacing, standard deviation (m)	Mean discontinuity dip, (degrees)	Dip, standard deviation, (degrees)
3A	307/80	224/04	9·20	1	0·056	0·046	67·39	21·69
3B	308/73	307/77	4·45	2	0·082	0·078	54·45	19·69
3A + (2x3B)	—	—	18·10	—	0·066	0·062	62·24	21·79
Corrected total number of spacing values = 273								

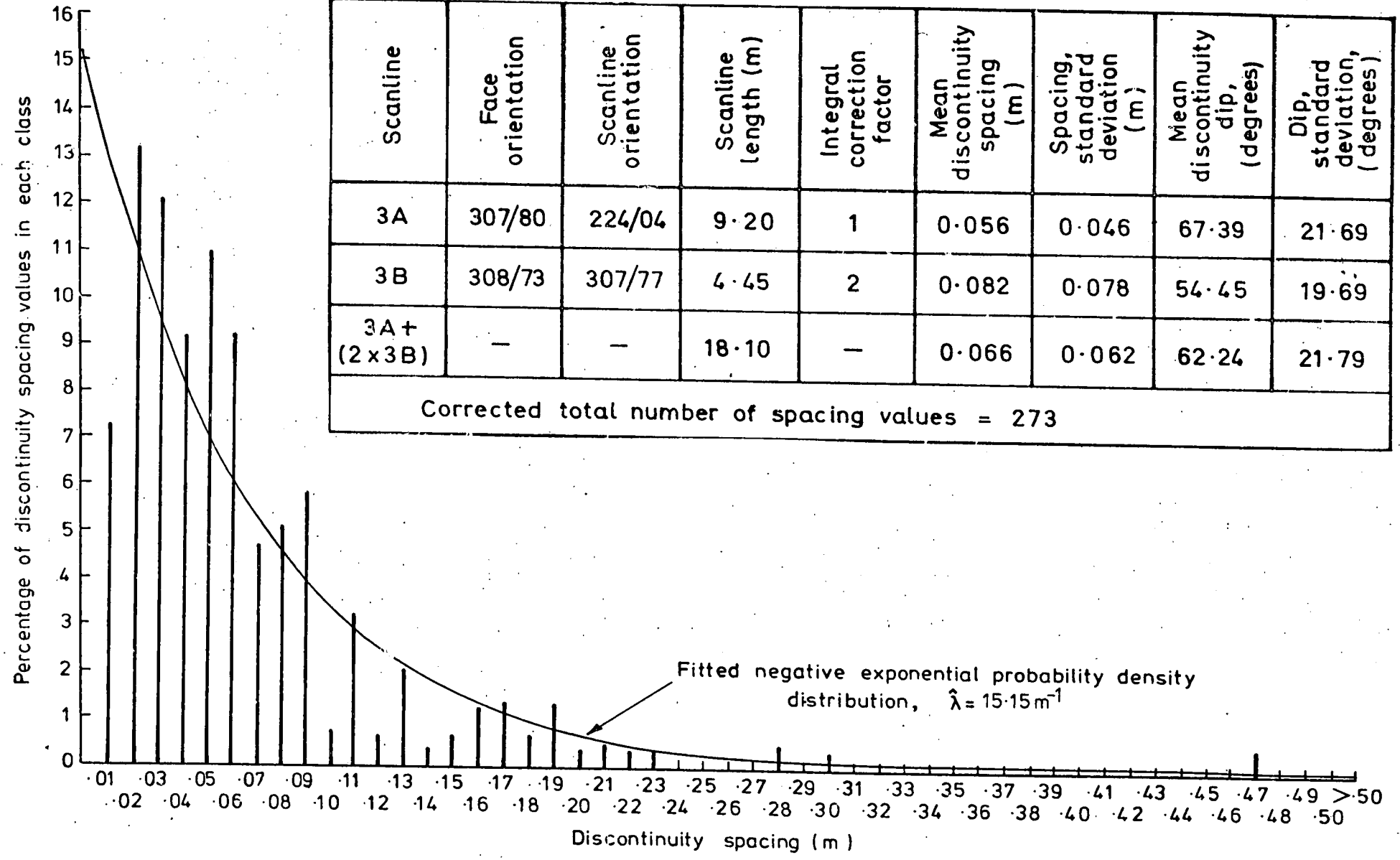

Fig. 2.5 DISCONTINUITY SPACING HISTOGRAM, CHINNOR QUARRY LOCATION 3

Scanline	Face orientation	Scanline orientation	Scanline length (m)	Integral correction factor	Mean discontinuity spacing (m)	Spacing, standard deviation (m)	Mean discontinuity dip, (degrees)	Dip, standard deviation, (degrees)
4A	107/79	211/05	10·57	1	0·070	0·065	65·18	19·07
4B	119/76	120/80	4·80	2	0·077	0·061	60·95	20·11
4A + (2×4B)	—	—	20·17	—	0·073	0·063	63·29	19·58
Corrected total number of spacing values = 275								

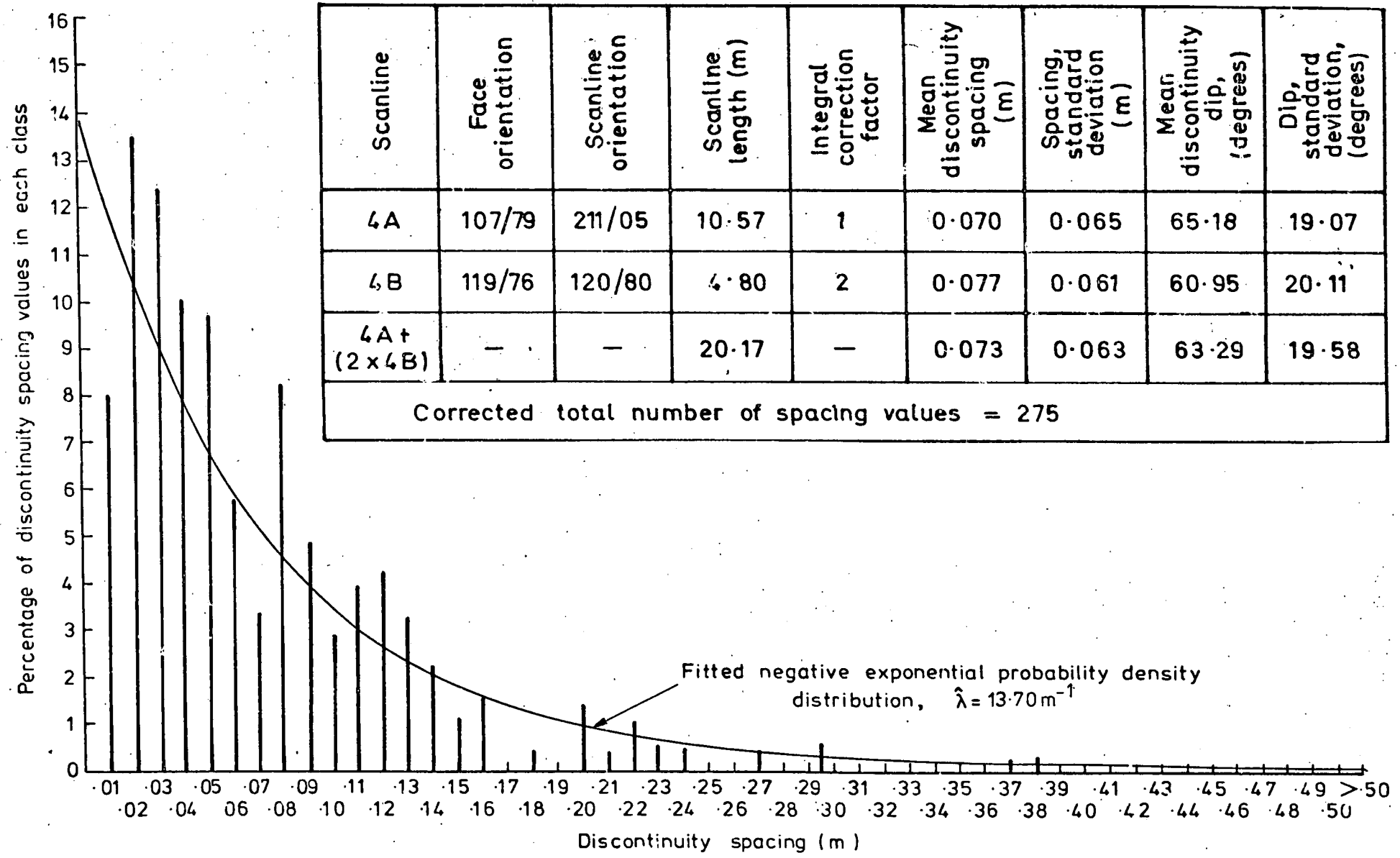

Fig. 2.6 DISCONTINUITY SPACING HISTOGRAM, CHINNOR QUARRY LOCATION 4

Scanline	Face orientation	Scanline orientation	Scanline length (m)	Integral correction factor	Mean discontinuity spacing (m)	Spacing, standard deviation (m)	Mean discontinuity dip, (degrees)	Dip, standard deviation, (degrees)
5A	000/82	263/07	13·21	1	0·087	0·083	59·55	23·52
5 B	200/70	172/70	3·65	4	0·054	0·040	55·97	27·97
5A + (4 x 5B)	—	—	27·81	—	0·066	0·061	57·25	26·39
Corrected total number of spacing values = 424								

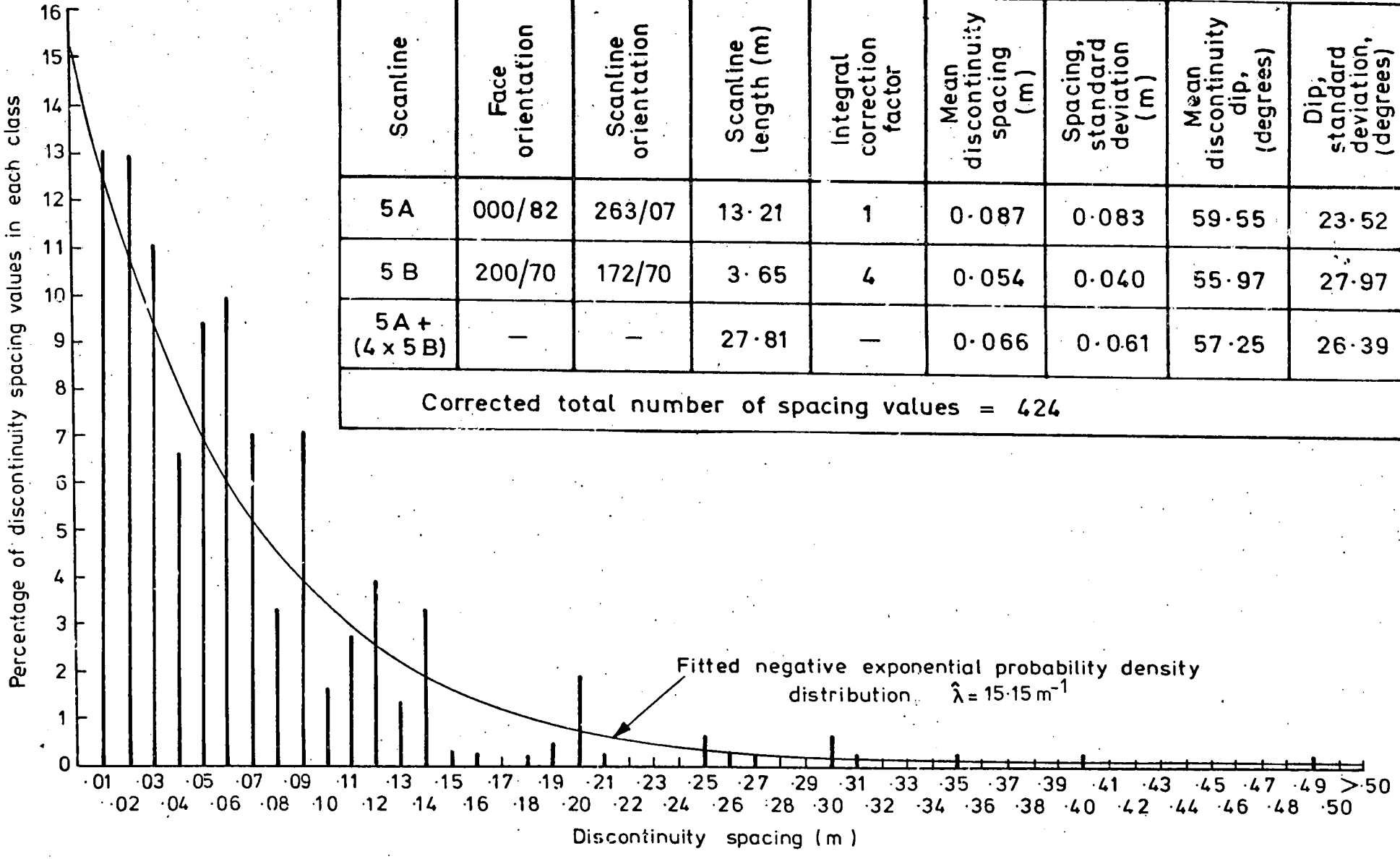

Fig. 2.7 DISCONTINUITY SPACING HISTOGRAM, CHINNOR QUARRY LOCATION 5

Scanline	Face orientation	Scanline orientation	Scanline length, (m)	Mean discontinuity spacing (m)	Spacing, standard deviation (m)	Mean discontinuity dip, (degrees)	Dip, standard deviation (degrees)
6A	300/75	210/02	13·00	0·133	0·105	64·20	19·61
Total number of spacing values = 98							

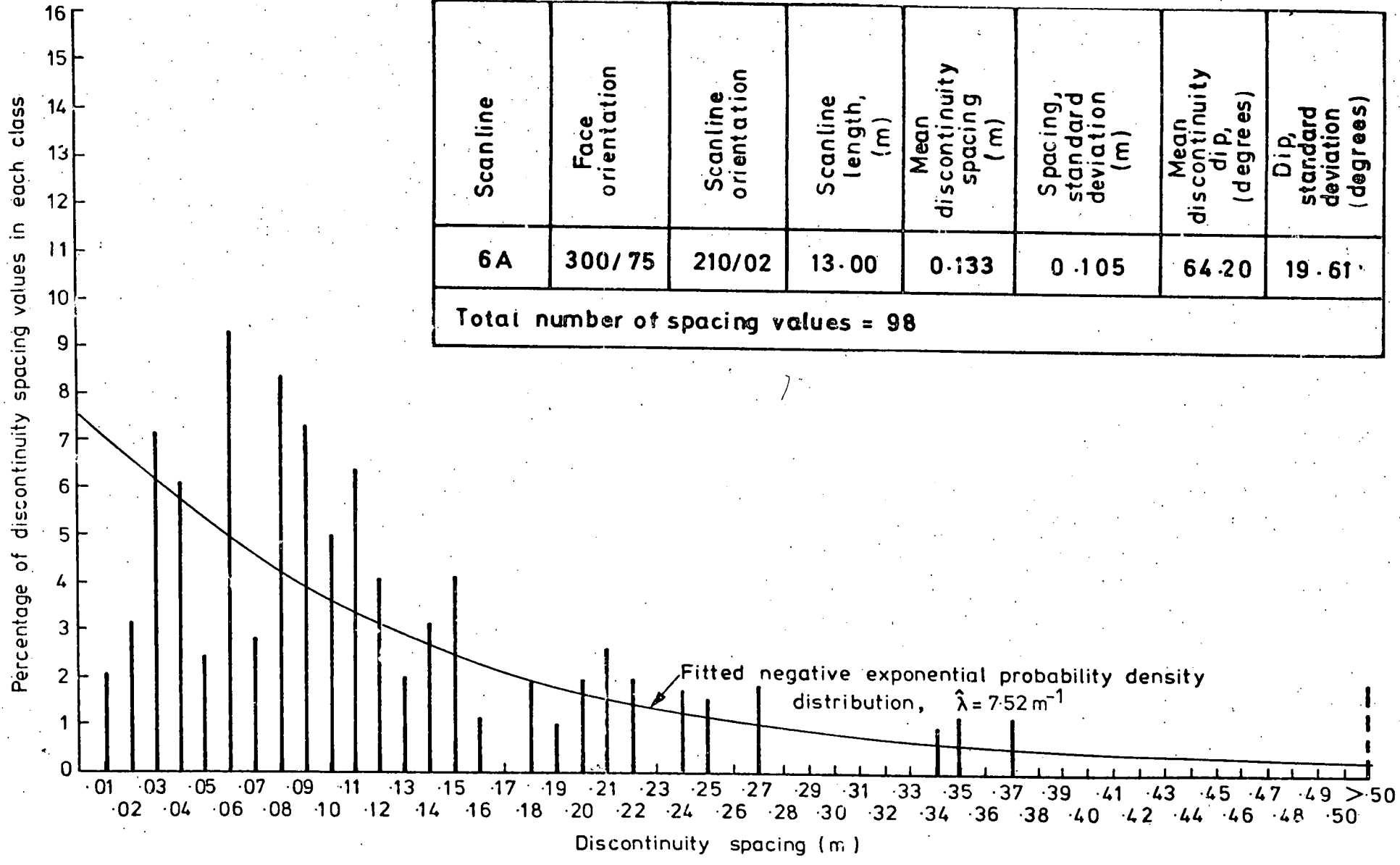

Fig. 2.8 DISCONTINUITY SPACING HISTOGRAM, CHINNOR QUARRY LOCATION 6

Scanline	Face orientation	Scanline orientation	Scanline length (m)	Integral correction factor	Mean discontinuity spacing (m)	Spacing, standard deviation (m)	Mean discontinuity dip, (degrees)	Dip, standard deviation, (degrees)
7A	045/80	140/02	10·01	1	0·060	0·044	56·74	21·36
7B	322/82	055/08	13·40	1	0·084	0·083	54·74	21·63
7C	343/76	348/79	4·41	3	0·057	0·056	46·41	26·75
7A + 7B + (3x7C)	—	—	36·64	—	0·065	0·063	51·88	24·18
Corrected total number of spacing values = 561								

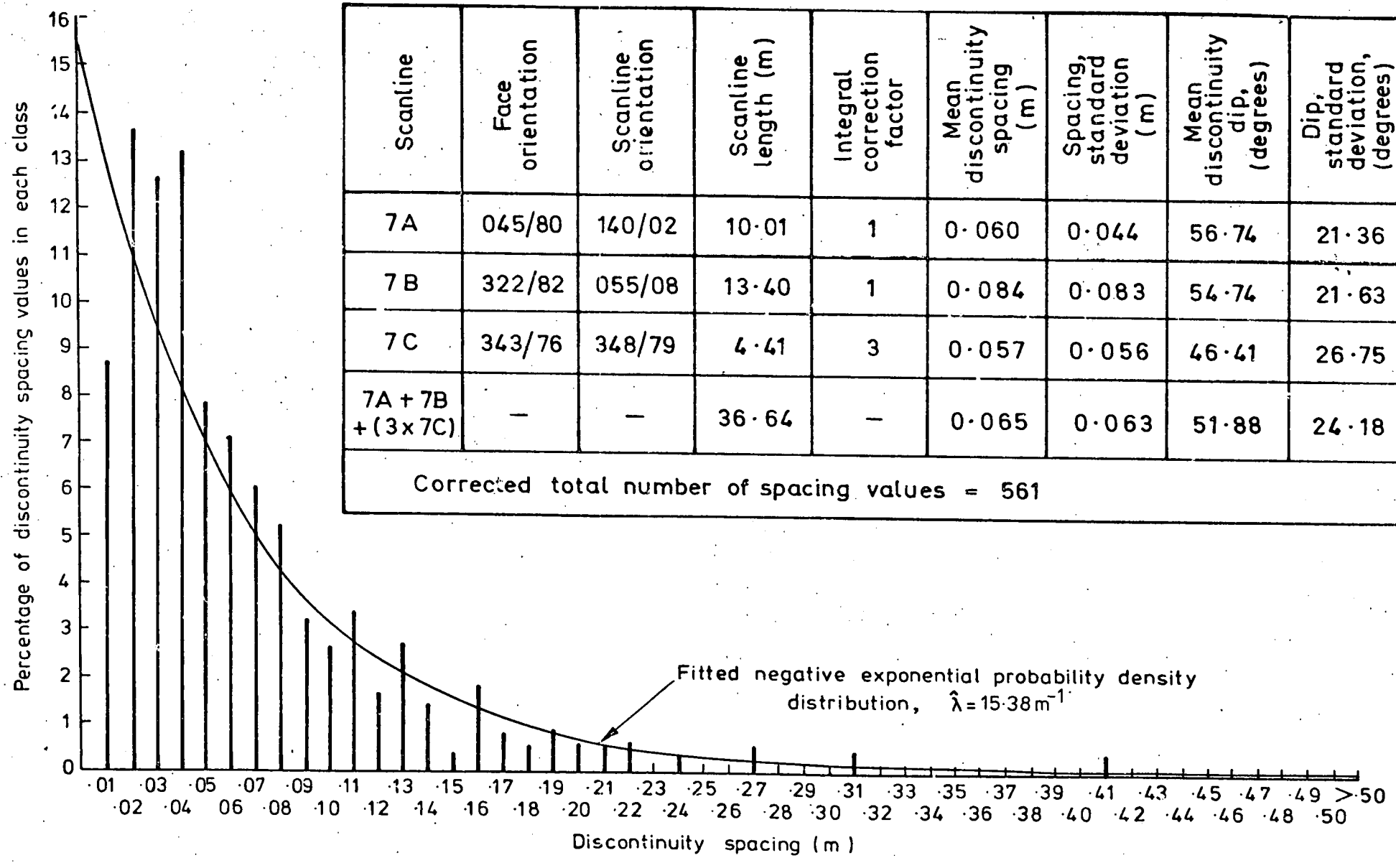

Fig. 2.9 DISCONTINUITY SPACING HISTOGRAM, CHINNOR QUARRY LOCATION 7

Scanline	Face orientation	Scanline orientation	Scanline length (m)	Integral correction factor	Mean discontinuity spacing (m)	Spacing, standard deviation (m)	Mean discontinuity dip, (degrees)	Dip, standard deviation, (degrees)
8A	333/86	240/00	12·50	1	0·083	0·084	62·85	19·82
8B	036/83	129/00	11 30	1	0·063	0·053	64·17	20·58
8C	316/80	315/75	5·35	2	0·084	0·063	57·78	22·13
8A + 8B +(2 x 8C)	–	–	34·50	–	0·075	0·068	62·07	20·81
Corrected total number of spacing values = 457								

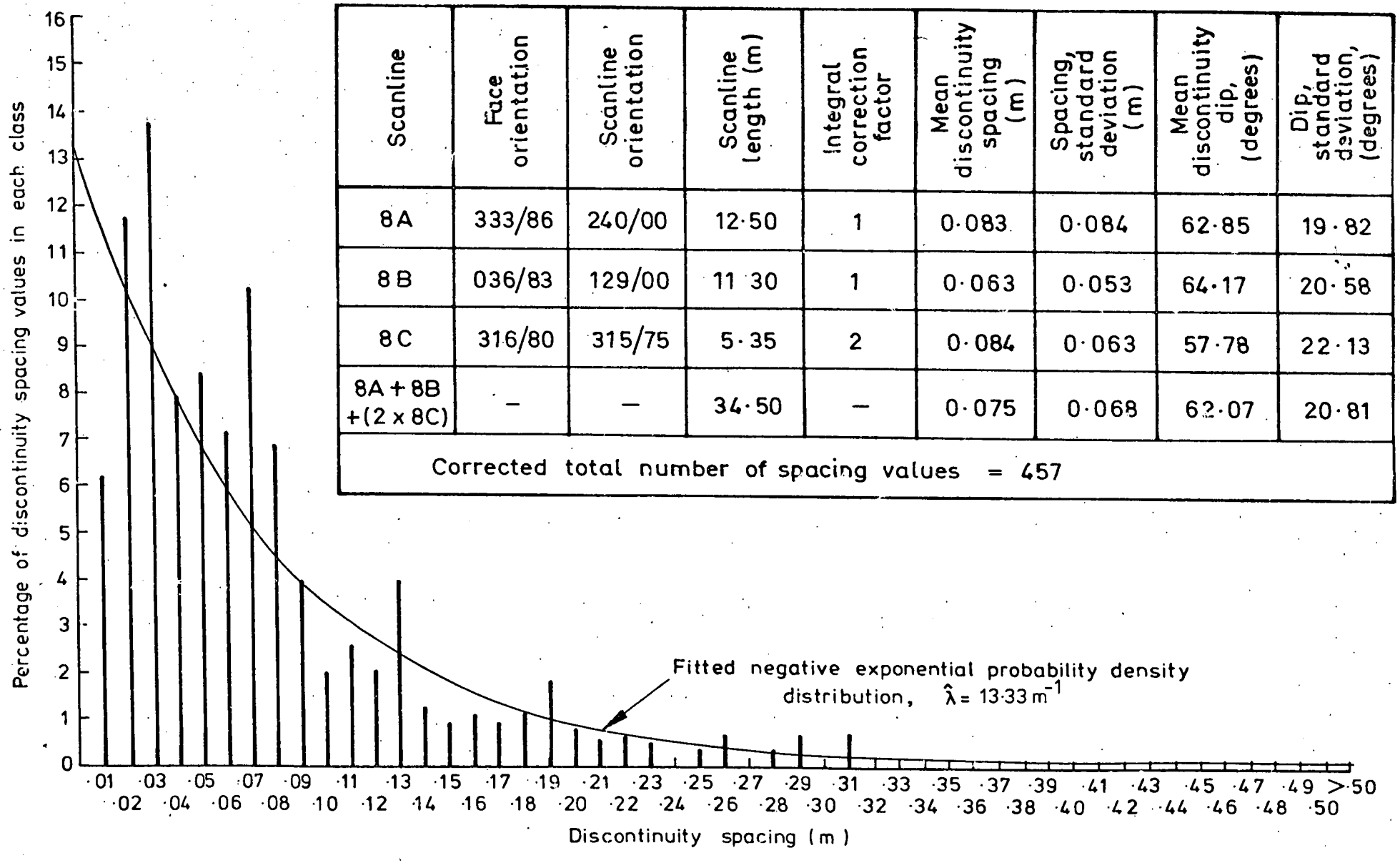

Fig. 2.10 DISCONTINUITY SPACING HISTOGRAM, CHINNOR QUARRY LOCATION 8

Scanline	Face orientation	Scanline orientation	Scanline length (m)	Mean discontinuity spacing (m)	Spacing, standard deviation (m)	Mean discontinuity dip, (degrees)	Dip, standard deviation, (degrees)
9A	039/83	126/02	10·60	0·056	0·049	54·94	21·55
Total number of spacing values = 191							

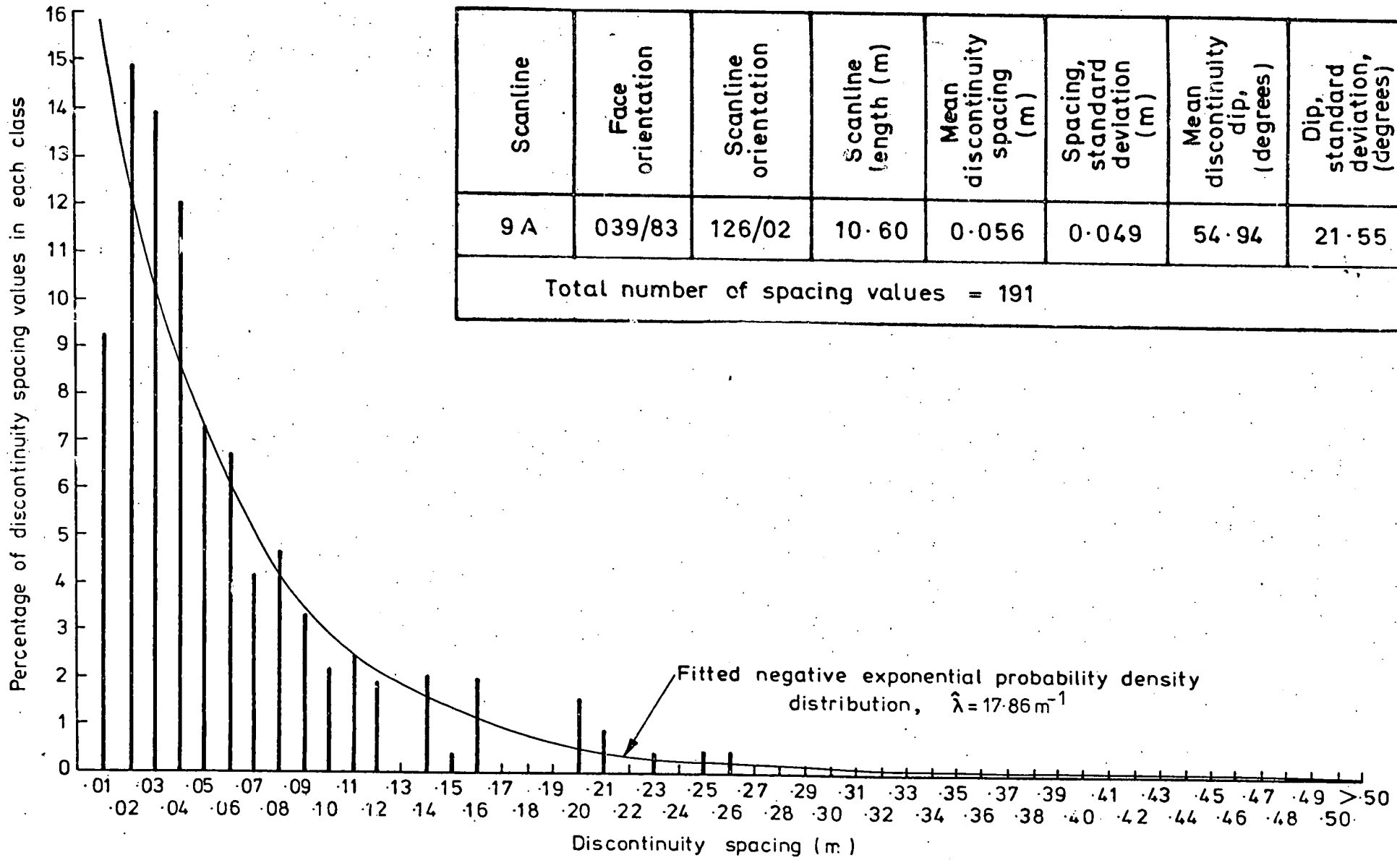

Fig. 2.11 DISCONTINUITY SPACING HISTOGRAM, CHINNOR QUARRY LOCATION 9

Scanline	Face orientation	Scanline orientation	Scanline length (m)	Integral correction factor	Mean discontinuity spacing (m)	Spacing, standard deviation (m)	Mean discontinuity dip, (degrees)	Dip, standard deviation, (degrees)
10 A	196/85	100/00	6·90	1	0·075	0·075	50·97	21·55
10 B	196/85	184/78	3·60	2	0·056	0·050	47·26	27·39
10 C	095/86	189/00	4·90	1	0·060	0·045	58·71	25·91
10A + 10C +(2x10B)	—	—	19·00	—	0·063	0·058	51·49	25·64
Corrected total number of spacing values = 302								

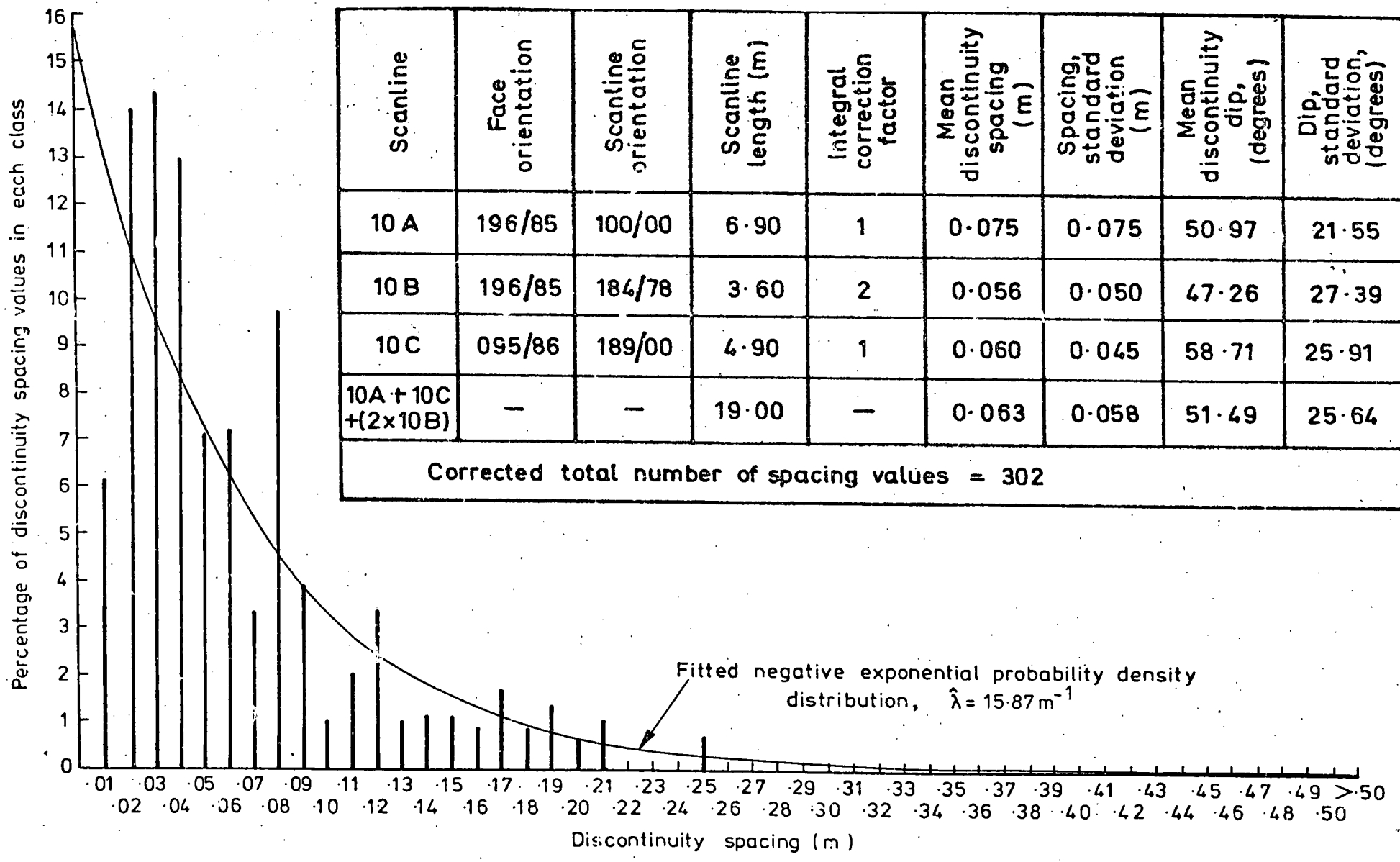

Fig. 2.12 DISCONTINUITY SPACING HISTOGRAM, CHINNOR QUARRY LOCATION 10

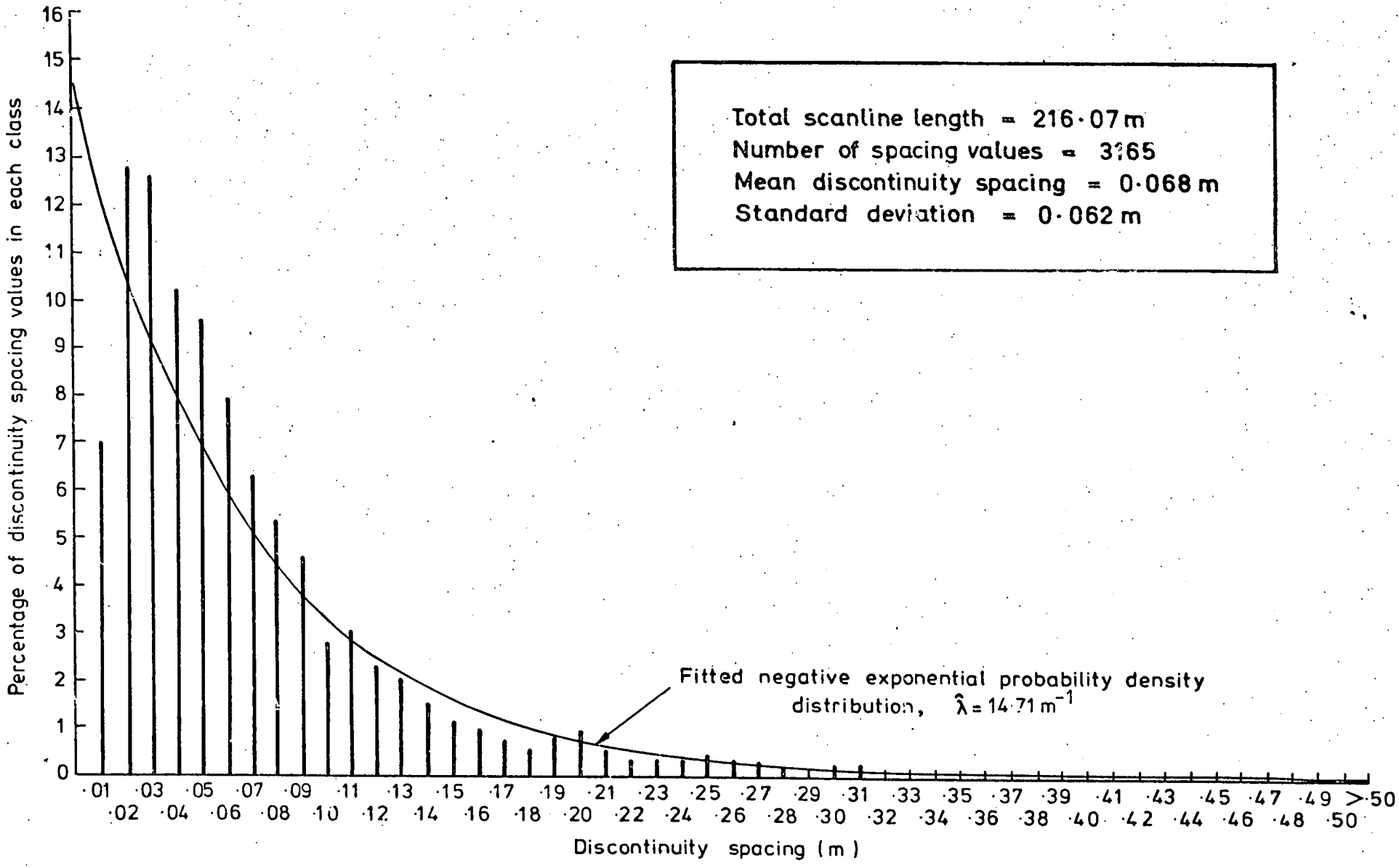

Fig. 2.13 DISCONTINUITY SPACING HISTOGRAM SUM OF ALL SCANLINES AT LOCATIONS 1 TO 10 IN THE CHINNOR QUARRY

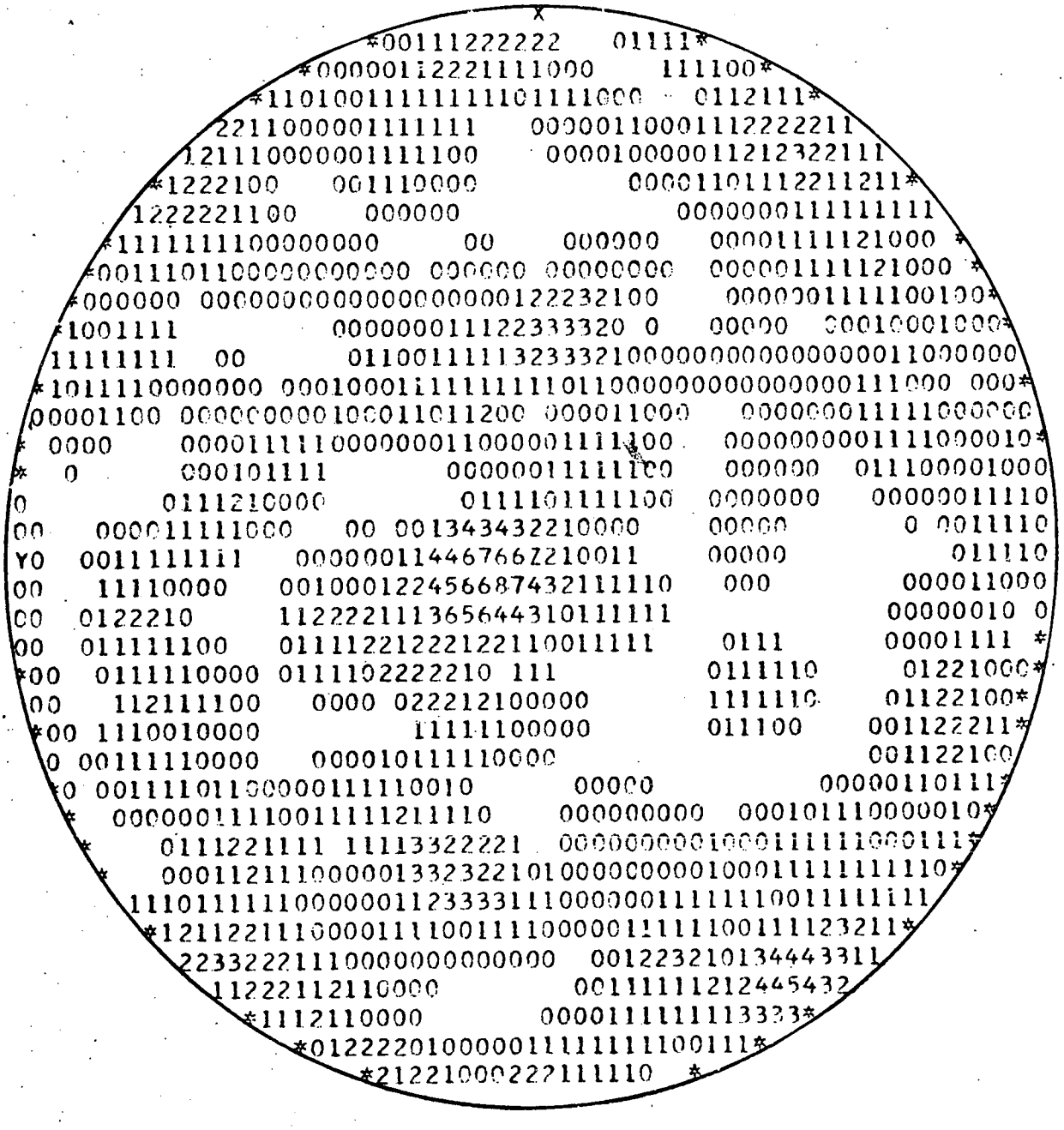

261 readings

Fig. 2.14 UPPER HEMiSPHERE PROJECTION OF DISCONTINUITY ORIENTATION, CHINNOR QUARRY LOCATION 1.

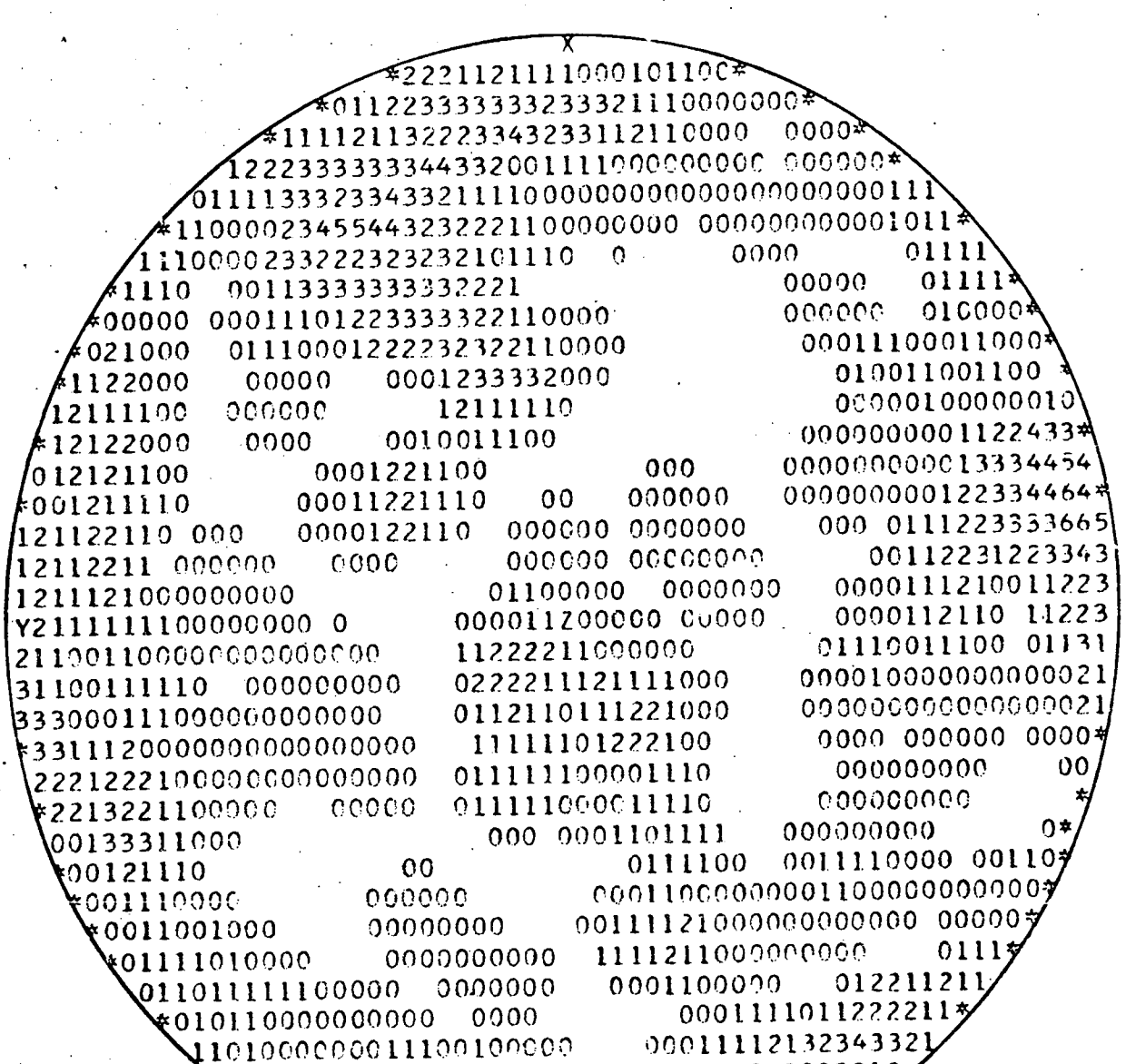

326 readings

Fig.2.15 UPPER HEMISPHERE PROJECTION OF DISCONTINUITY ORIENTATION, CHINNOR QUARRY LOCATION 2.

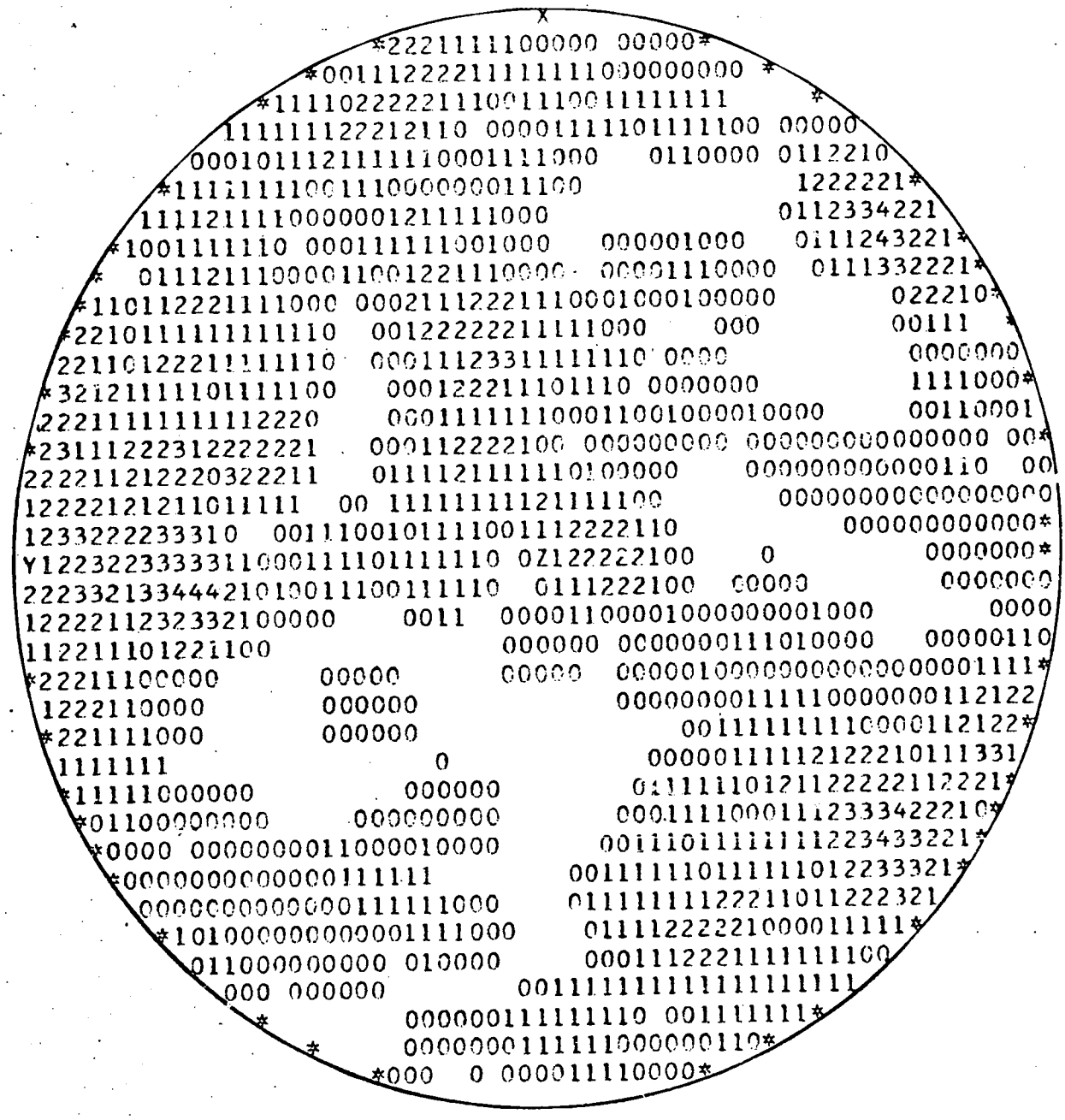

276 readings

Fig. 2.16 UPPER HEMISPHERE PROJECTION OF DISCONTINUITY ORIENTATION, CHINNOR QUARRY LOCATION 3.

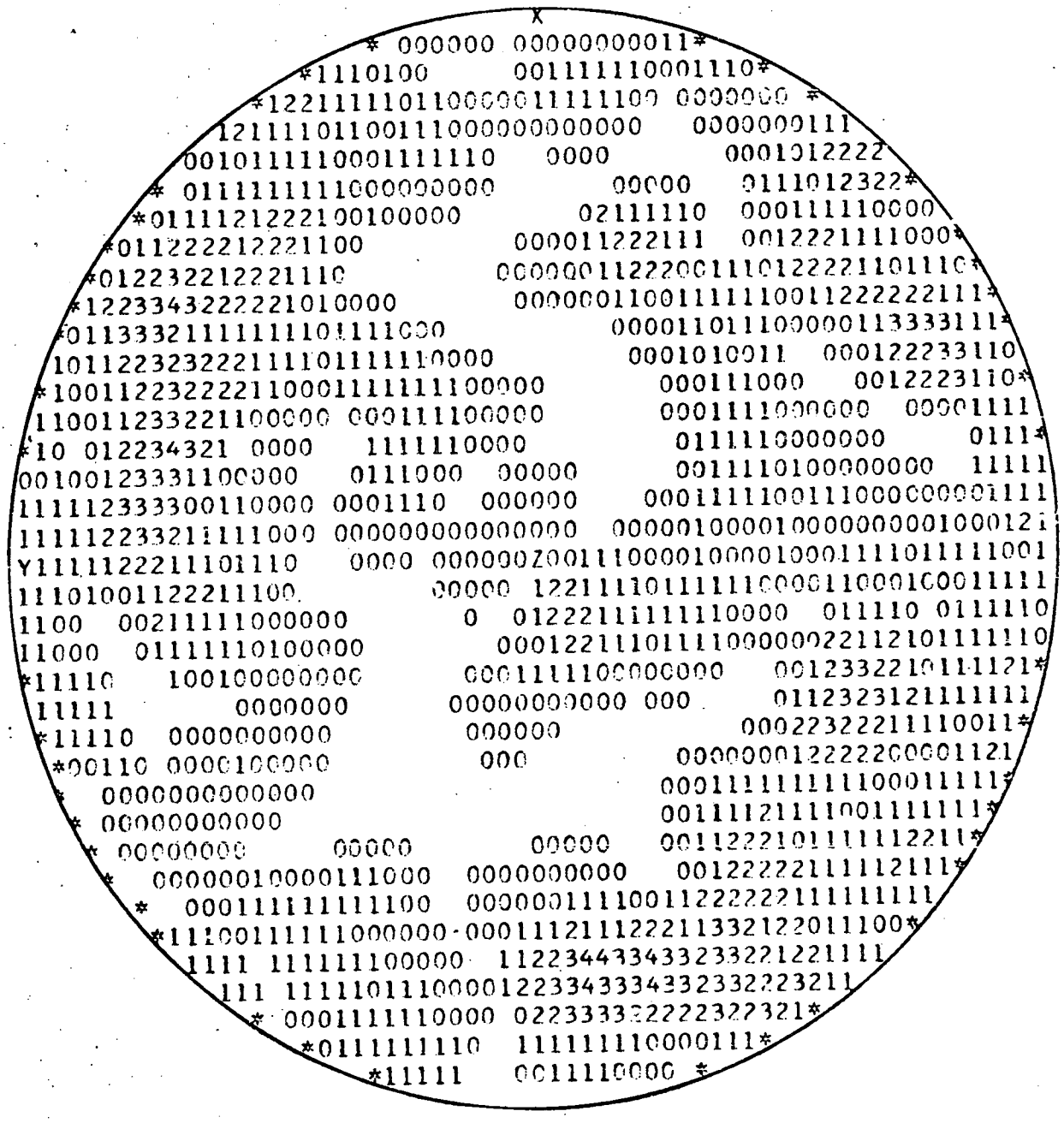

277 readings

Fig. 2.17 UPPER HEMISPHERE PROJECTION OF DISCONTINUITY ORIENTATION, CHINNOR QUARRY LOCATION 4.

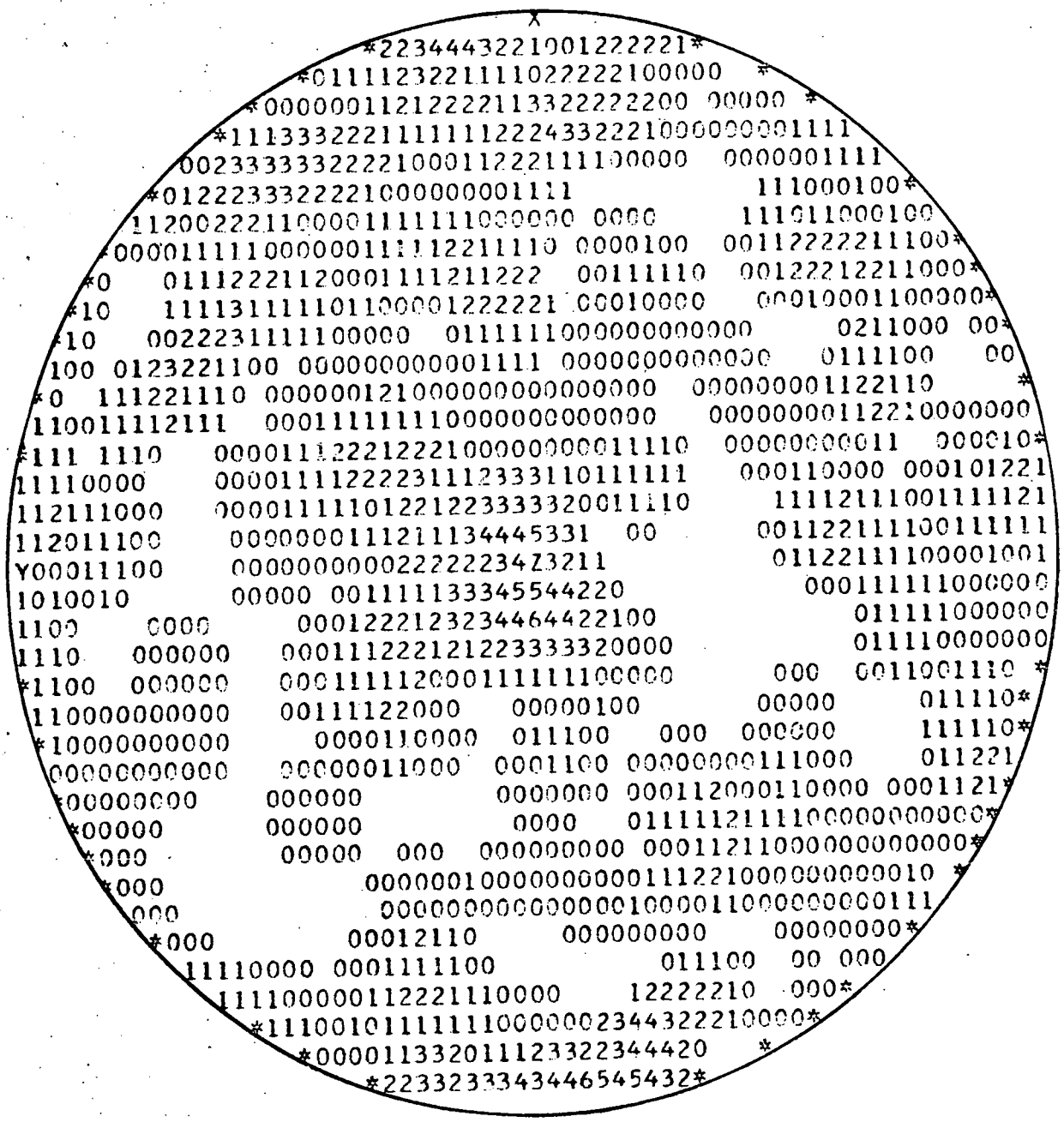

429 readings

Fig.2.18 UPPER HEMISPHERE PROJECTION OF DISCONTINUITY ORIENTATION, CHINNOR QUARRY LOCATION 5..

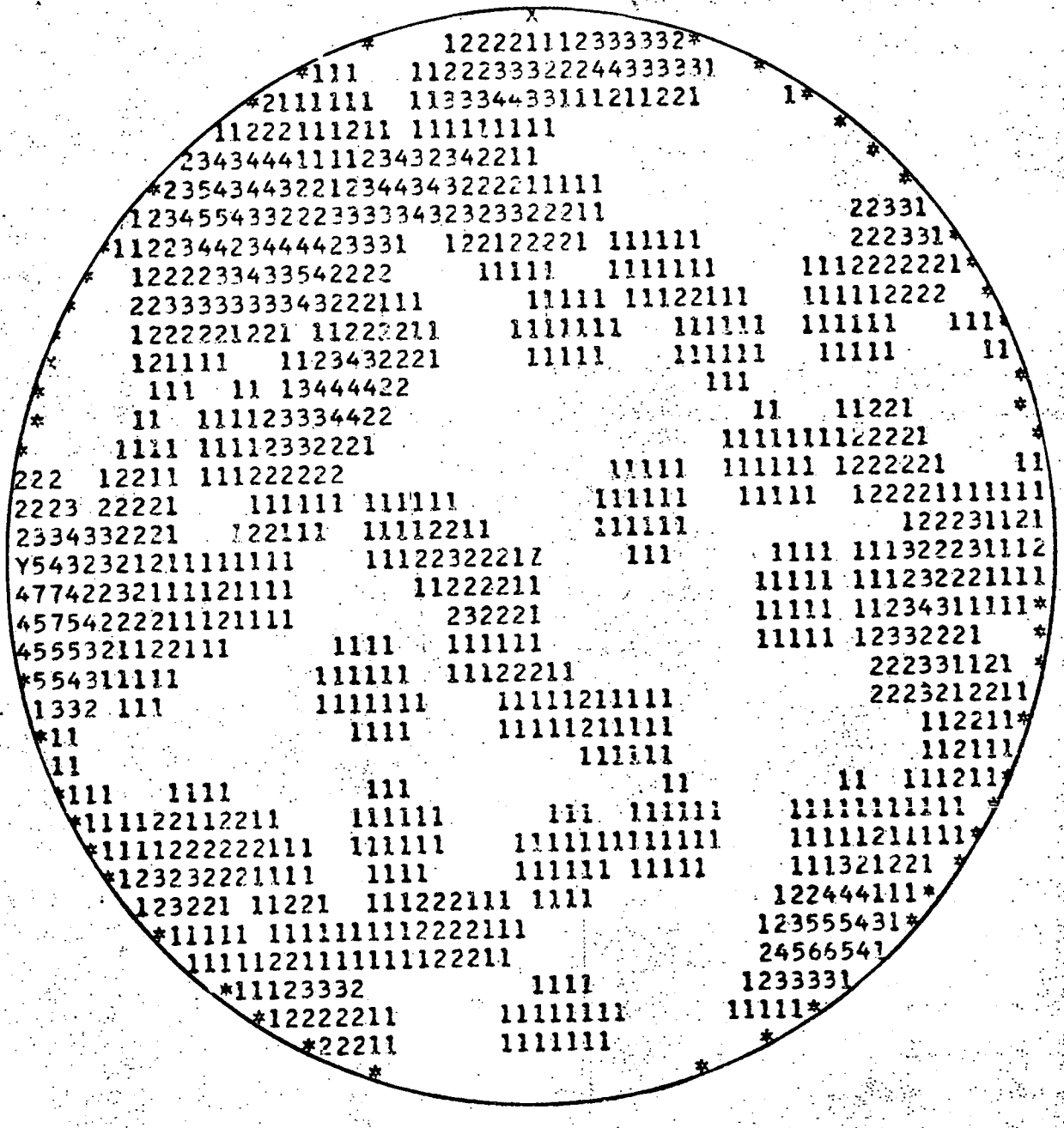

99 readings

Fig. 2.19 UPPER HEMISPHERE PROJECTION OF DISCONTINUITY ORIENTATION, CHINNOR QUARRY LOCATION 6.

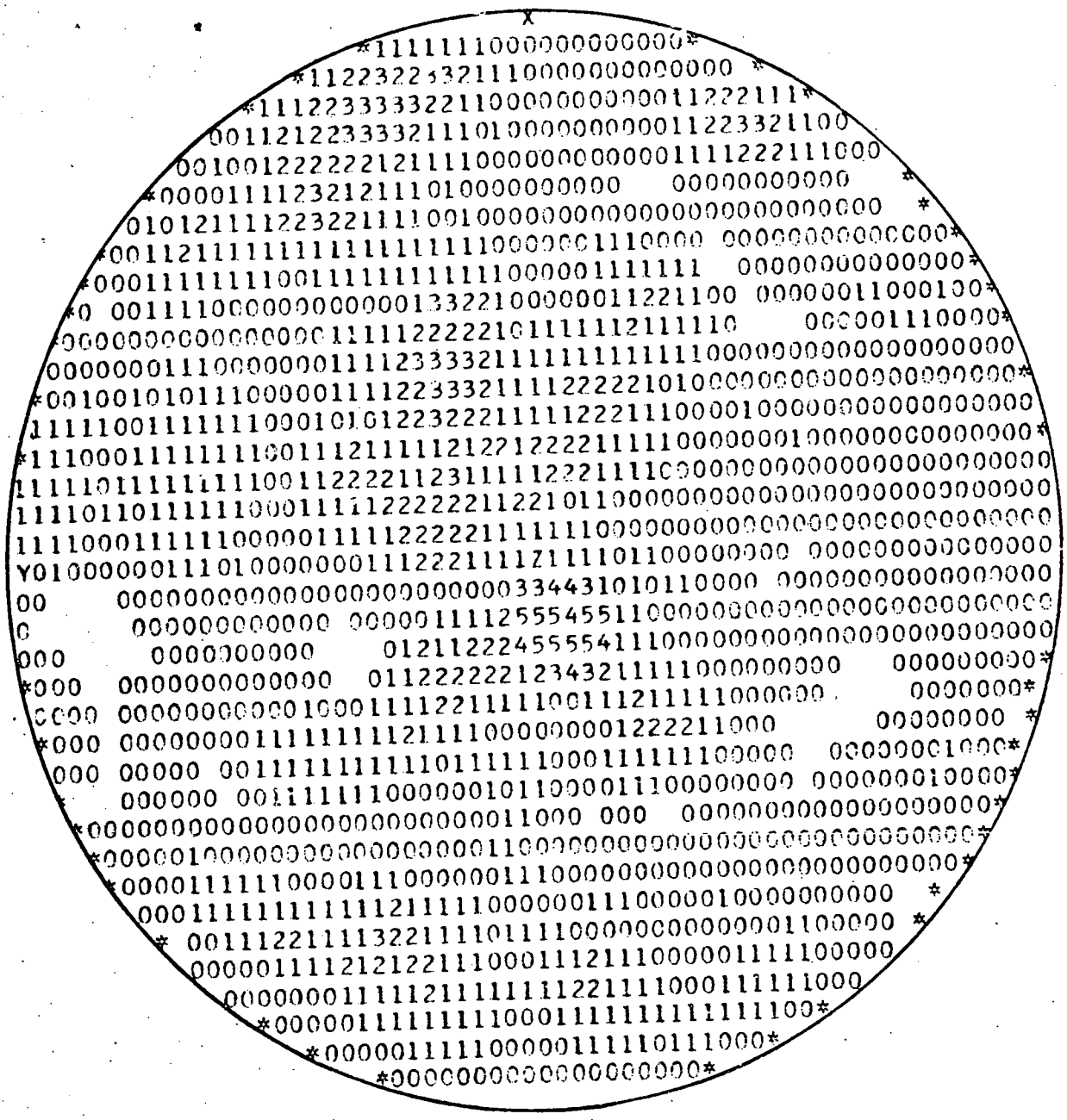

563 readings

Fig.2.20 UPPER HEMISPHERE PROJECTION OF DISCONTINUITY ORIENTATION, CHINNOR QUARRY LOCATION 7.

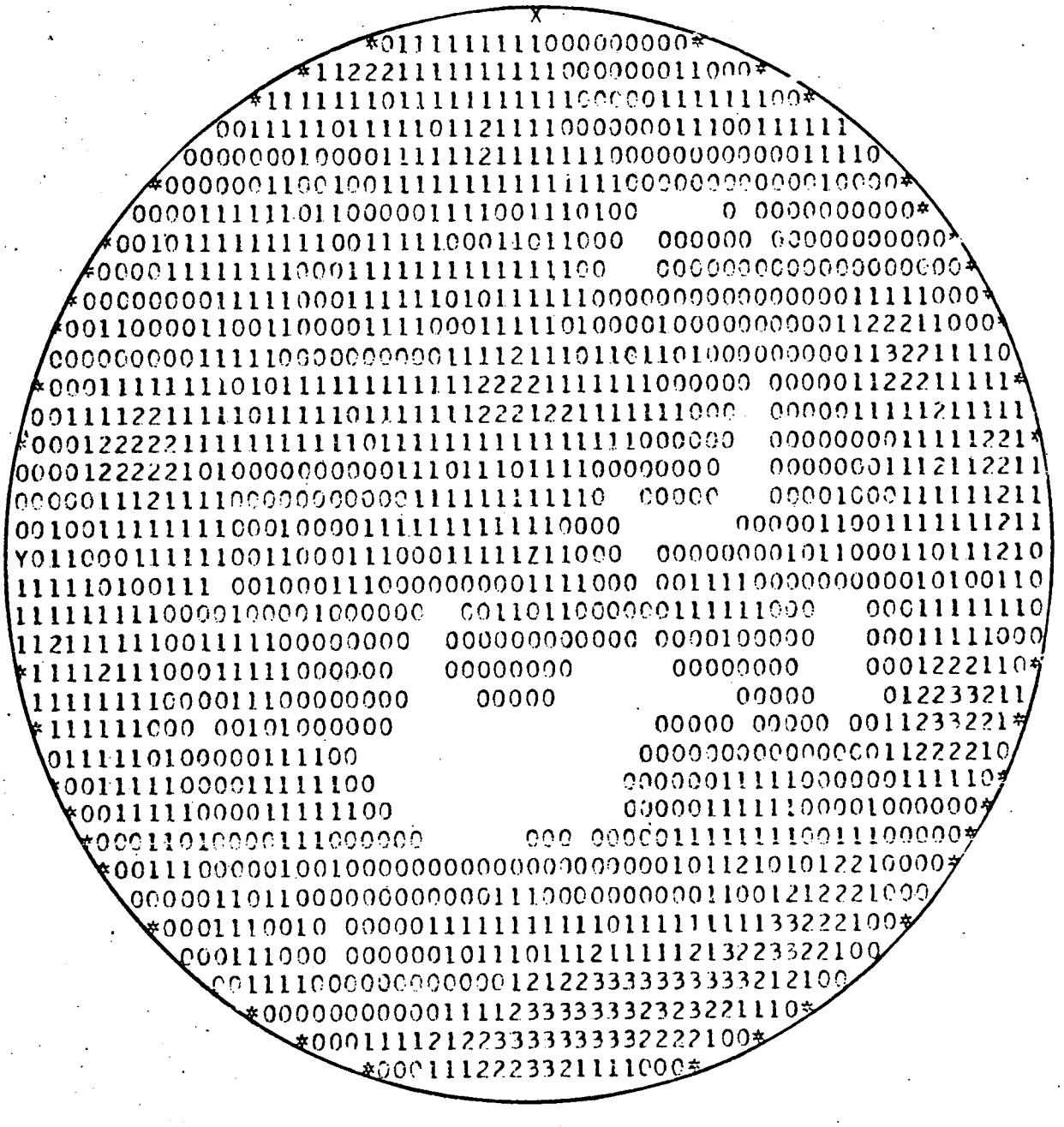

461 readings

Fig. 2.21 UPPER HEMISPHERE PROJECTION OF DISCONTINUITY ORIENTATION, CHINNOR QUARRY LOCATION 8.

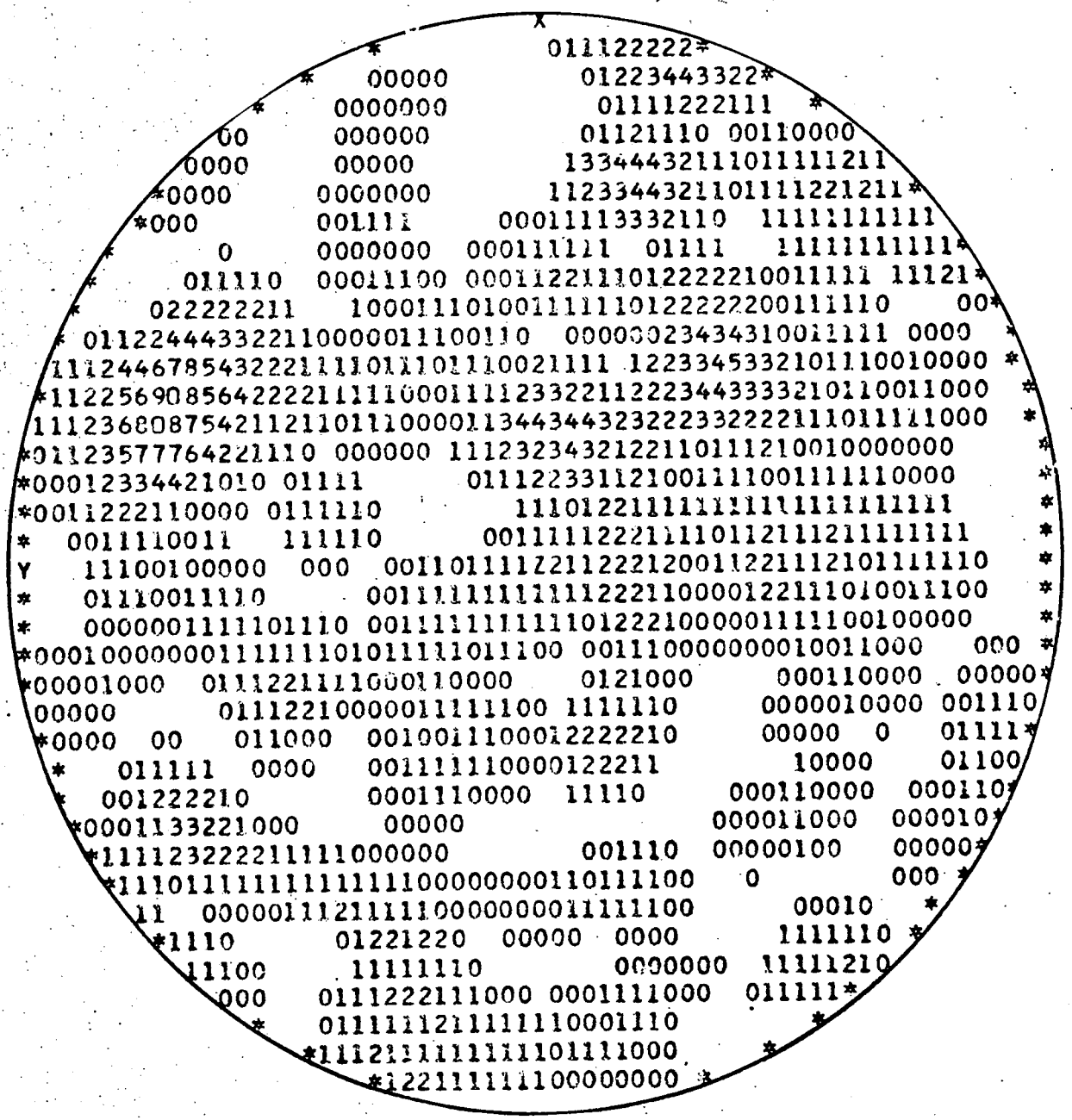

191 readings

Fig. 2.22 UPPER HEMISPHERE PROJECTION OF DISCONTINUITY ORIENTATION, CHINNOR QUARRY LOCATION 9.

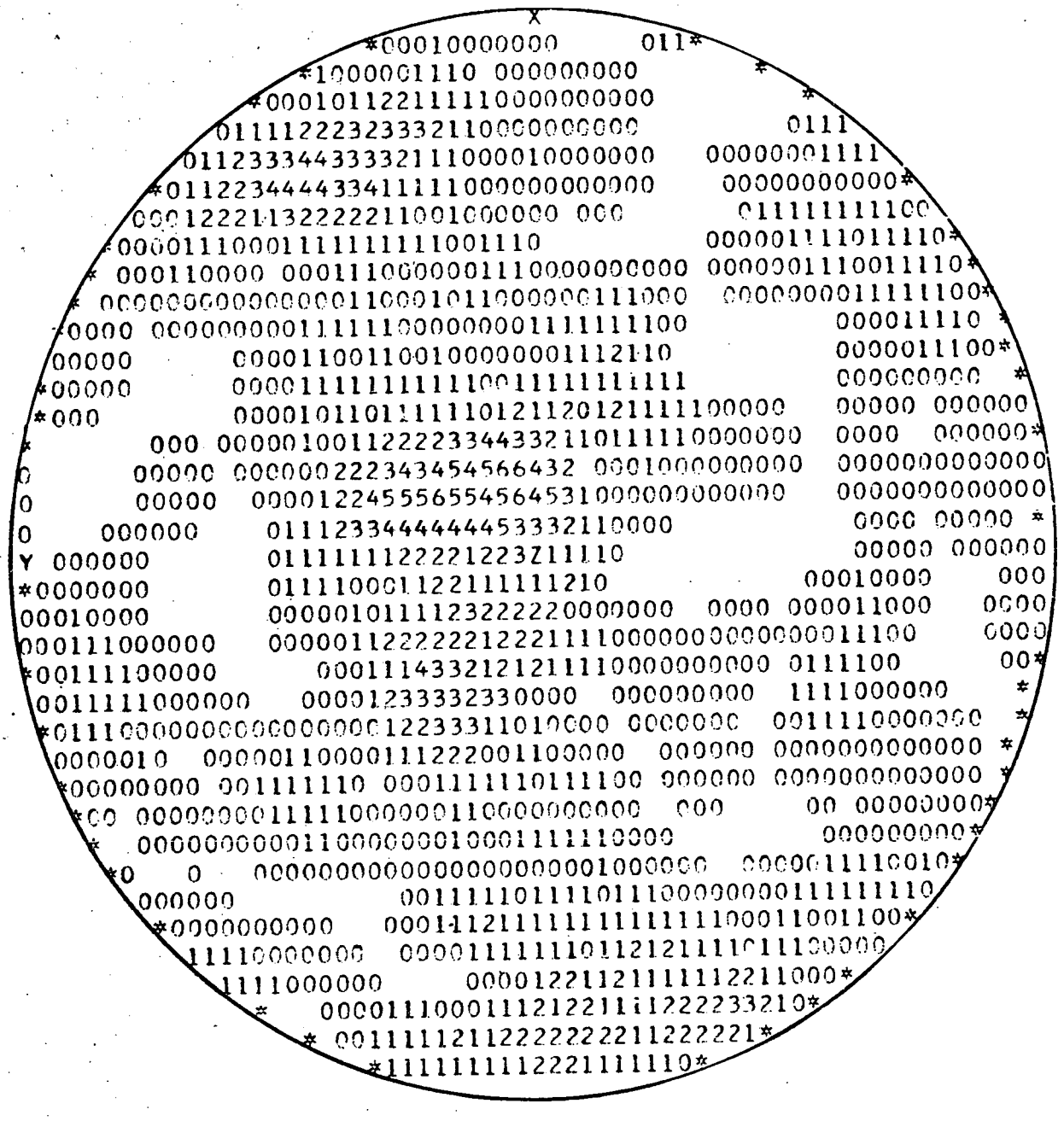

306 readings

Fig. 2.23 UPPER HEMISPHERE PROJECTION OF DISCONTINUITY ORIENTATION, CHINNOR QUARRY LOCATION 10.

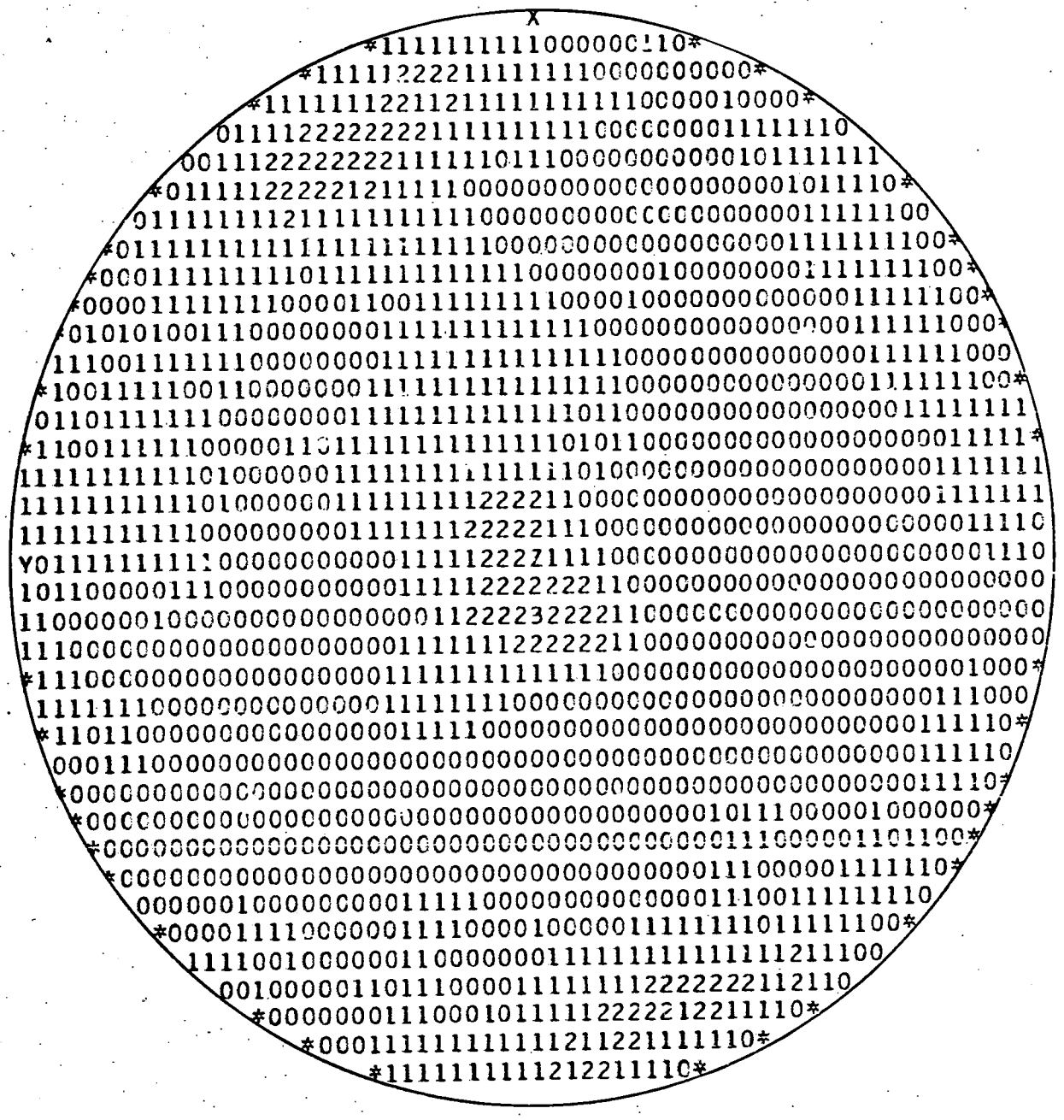

2899 readings

Fig.2.24 UPPER HEMISPHERE PROJECTION OF DISCONTINUITY ORIENTATION, CHINNOR QUARRY LOCATIONS 1,2,3,4,5,7,8 AND 10.

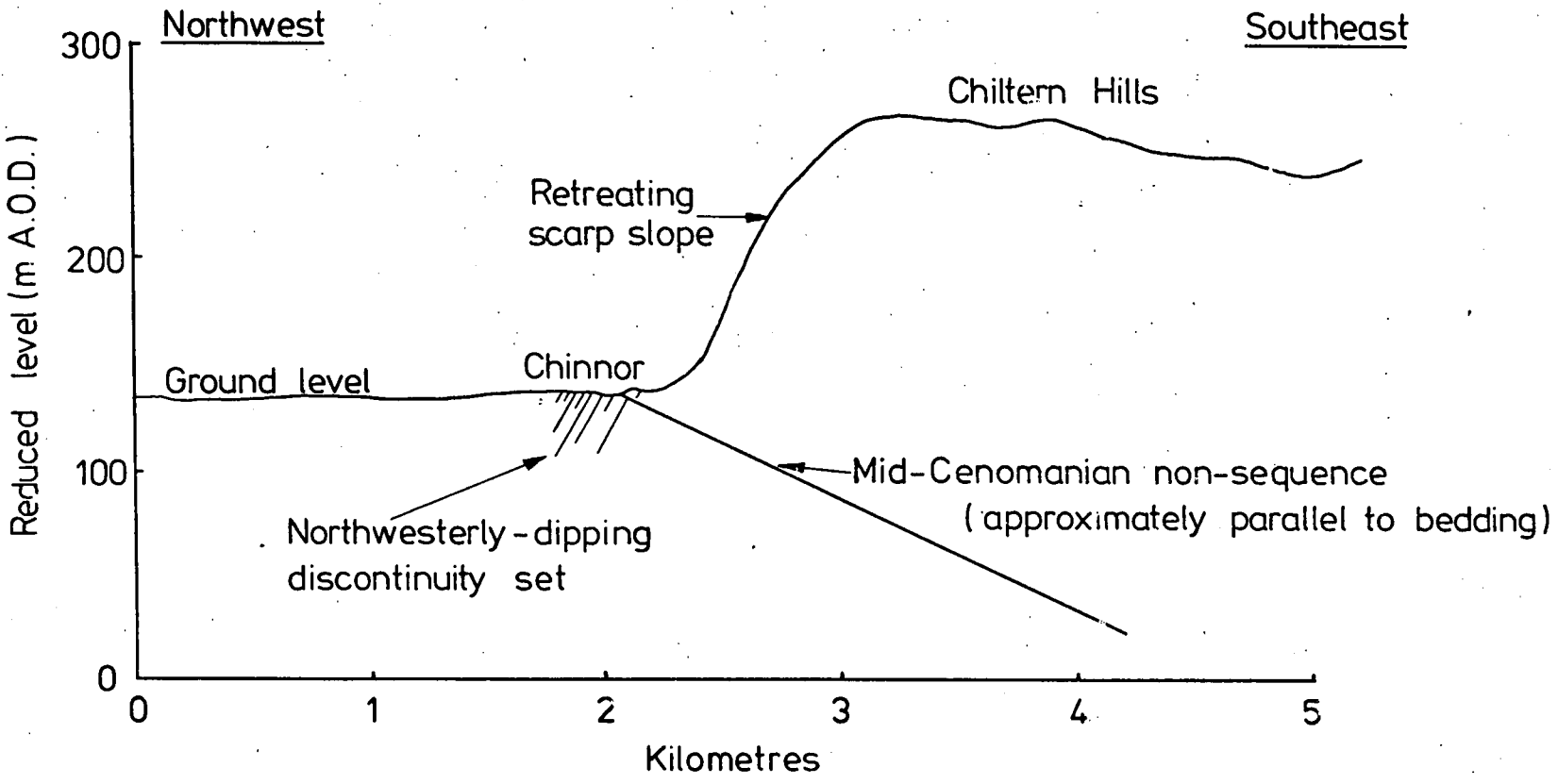

Fig. 2.25 NORTHWEST-SOUTHEAST SECTION ACROSS CHINNOR AREA.

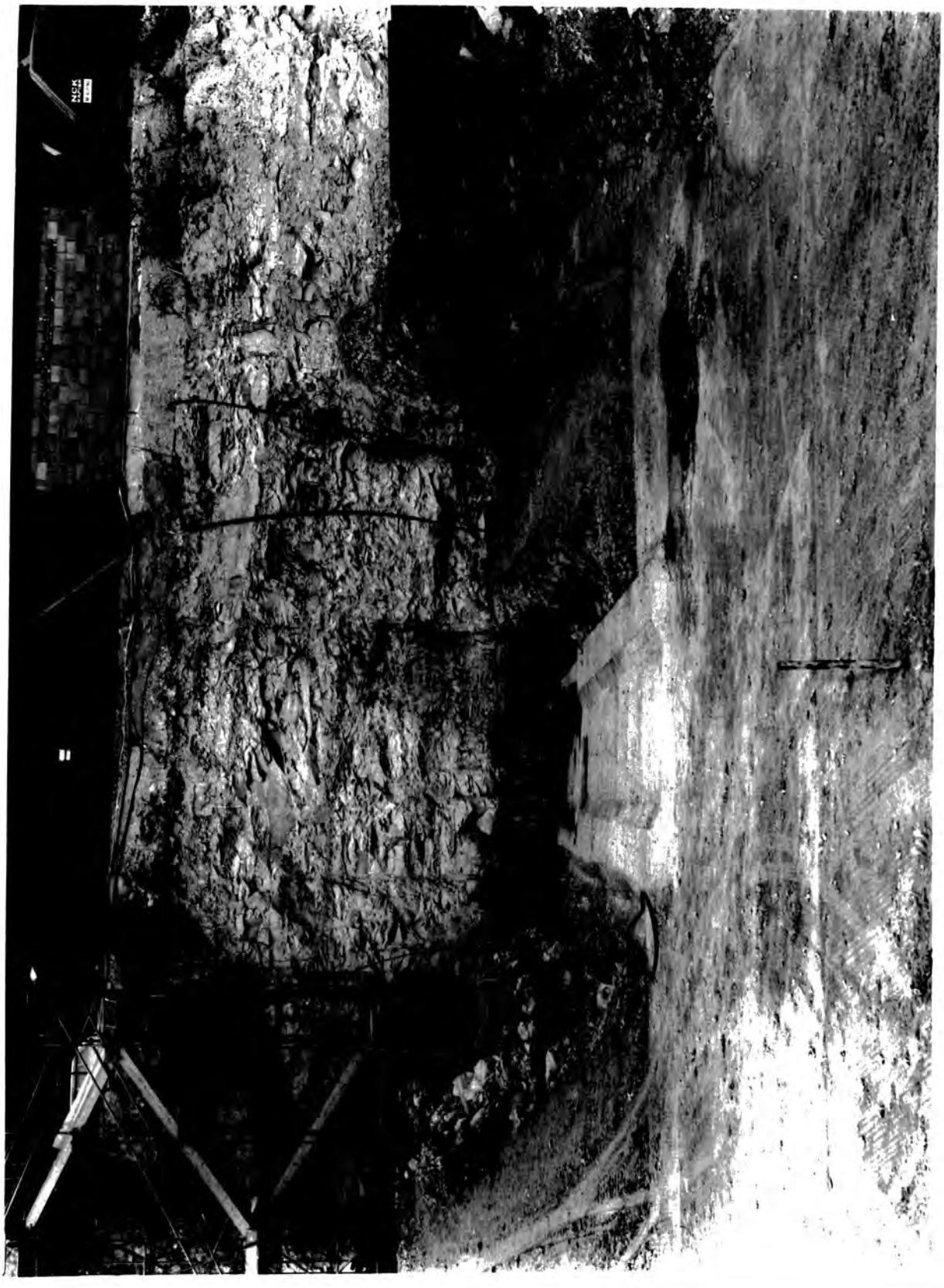

Plate 2.1 DISCONTINUITY SURVEY LOCATION NUMBER 10 — THE TUNNEL PORTAL FACE.

CHAPTER 3

SITE INVESTIGATION AT CHINNOR, UNDERTAKEN IN BOREHOLES AND A 3m DIAMETER SHAFT

3.1 Introduction

A two-stage site investigation programme was undertaken at Chinnor by Soil Mechanics Ltd., the main geotechnical sub-contractors on the Chinnor project. The aim of stage I was to obtain sufficient information concerning chalk properties and ground water level over the whole site to allow finalisation of the tunnel line and level. The stage II site investigation was designed to examine in detail the ground to be encountered during tunnelling. Both stages of the investigation were carried out on samples taken using vertical boreholes, backed up by laboratory and *in situ* testing. Except where stated, all data concerning stages I and II of the investigation were obtained and made available to the author by Soil Mechanics Ltd. Data have, however, been re-arranged, re-plotted and re-evaluated by the author for the particular purpose of this thesis.

In addition to the investigations described above, a 3m diameter vertical shaft 23.4m deep was sunk by the main contractors for TRRL in the Lower Chalk with the shaft wall 4m from the proposed centre line of the 5m diameter tunnel (Figure 3.1). The shaft was sunk for the following reasons:

(1) For direct site investigation purposes.

(2) For assessing site investigation techniques.

(3) To provide a facility for geotechnical experiments.

The shaft was hand-dug using pneumatic rock-breakers and lined with wire mesh supported by 2m rock bolts. The rock bolts were anchored using both mechanical rock anchors and resin grout. Figure 3.2 shows the progress of shaft excavation between August 1973 and January 1974. A photograph of the completed shaft is shown in Plate 3.1. Except where stated all data collection and processing for the shaft were carried out by the author.

3.2 Stage I site investigation

Five boreholes (Numbers 10 - 14) were sunk to a maximum depth of 32.7m using 131mm diameter rotary coring equipment. The location of these boreholes is shown in Figure 1.2. Double tube core barrels were used, containing in most cases a mylar lining designed to reduce disturbance of the cores on extrusion. 100% core recovery was obtained in most cases. Detailed logs of these cores are presented in the Soil Mechanics Ltd. report to the Transport and Road Research Laboratory, Volume I (1974).

Three distinct horizons of chalk were encountered, distinguished on the basis of colour:

1. Light creamy grey chalk, this was only penetrated in borehole 13 to a depth of 9.7m and being the youngest of the three chalk types represents the lower part of the Grey Chalk described in Section 1.5.

2. Light brown grey chalk, a maximum thickness of 25m was penetrated in borehole 14. This represents the upper part of the Chalk Marl described in Section 1.5.

3. Grey blue chalk, all boreholes (except borehole 13) terminated in this material which represents the lower horizons of the Chalk Marl.

The boundary between chalk types 2 and 3 is poorly defined, there being an intermediate banded zone of alternating grey blue and light brown grey chalk. The approximate transition point between types 2 and 3 is indicated in Figure 3.3. In the construction of this Figure the position of boreholes 10 to 14 has been projected laterally along a line normal to the dip direction of the Chalk onto the proposed tunnel line.

Porous pot piezometers were installed in boreholes 10 to 14. The standing water level recorded in these piezometers is shown in Figure 3.3. Water injection tests were carried out in boreholes 10, 11 and 12, a description of these tests and the results being included in Chapter 4.

Point load strength index tests (described in Appendix D) were carried out on selected lengths of core remaining after removal of samples for laboratory testing. The results were reduced to $I_{s\ 50}$ index (the equivalent index for the same material having a tested dimension of 50mm) using standard charts. The variation of point load index (P.L.I.) with depth for each borehole is shown in Figure 3.3. D'Andrea *et al.* (1965) examining data concerning the point load strength index and uniaxial compressive strength of rocks found that there is an approximately linear relation between the two, such that the uniaxial compressive strength is approximately 24 times the point load strength index for a given rock. Comparison between data presented in Figure 3.3 and Table 3.1 confirms in general terms this approximate relation for the Chalk at Chinnor.

3.3 Laboratory testing

Material recovered in boreholes 10 to 14 was tested to obtain:

(a) Indices of rock material properties

(b) Mechanical properties of the rock.

3.3.1. Index tests

Moisture content, specific gravity and bulk density of one hundred and two samples were determined. The results averaged for each borehole, are presented in Table 3.1. The porosity and degree of saturation of each sample was also calculated. Variation of porosity with depth in each borehole is shown in Figures 3.4 and 3.5.

The percentage of calcium carbonate ($CaCO_3$) by weight in the dry material was determined by Soil Mechanics Ltd. using the Collins calcimeter. Using this instrument, an accurate measure is obtained of the volume of carbon dioxide liberated when approximately 1gm of chalk sample is dissolved in a measured amount of hydrochloric acid. This volume of carbon dioxide liberated is used to estimate the calcium carbonate content expressed as a percentage by weight of the original sample. The variation in calcium carbonate percentage with depth in each borehole is shown in Figures 3.4 and 3.5.

3.3.2 Mechanical properties of the rock

Laboratory tests were carried out on intact specimens (which had been sealed to prevent water loss) taken from boreholes 10, 11, 12 and 14. Unconfined compressive strength was measured on twenty-one samples tested at the cored diameter of approximately 100mm. The tensile strength of thirteen of these samples was determined indirectly using the Brazilian disc method. The results of these tests, averaged for each borehole, are shown in Table 3.1.

Table 3.1 Chalk material properties, average values for each borehole, stage I site investigation

Borehole number	Moisture content %	Specific gravity	Bulk density (Mg/m^3)	Unconfined compressive strength (MN/m^2)	Secant modulus (MN/m^2)	Poisson's ratio	Brazil tensile strength (MN/m^2)
10	17.6	2.68	2.11	7.5	3281*	0.30*	0.96*
11	18.4	2.61	2.14	7.2	1114	0.38	0.46
12	20.1	2.64	2.08	3.0	1306*	0.26*	0.47
13	15.4	2.69	2.21				
14	19.6	2.66	2.11	7.8	2030**	0.18**	0.49

Note: * Average of less than five tests

** One test only

Elastic modulus measurements were carried out on nine samples by measuring applied stress and recording related strains using electrical resistance strain gauges. The uniaxial loading cycles were at strain rates of approximately 1×10^{-4} per minute on 100mm diameter samples having an aspect ratio of approximately 2:1. Stress/strain curves for three of the samples from boreholes 11 and 12 are reproduced in Figure 3.6. Moduli, averaged for each borehole in Table 3.1, represent secant moduli taken between stress levels of approximately 0.1 MN/m^2 and 2.0 MN/m^2.

Six samples were instrumented with strain gauges fixed normal to the loading axis, thus allowing a determination of Poisson's ratio. The results, averaged for each borehole, are shown in Table 3.1. Six triaxial permeability tests were carried out in which flow was measured under differential heads of approximately 10 kN/m^2. Permeability of the intact specimens tested ranged from 1.4×10^{-10} m/sec to 2.3×10^{-8} m/sec. These results are discussed in Chapter 4.

3.4 Stage II site investigation

Six boreholes (Numbers 100 to 105) were sunk to a maximum depth of 38m using 131mm diameter rotary coring equipment. The location of these boreholes along the tunnel line is shown in Figure 1.2. Detailed logs of the cores recovered are presented in the Soil Mechanics Ltd. report to the Transport and Road Research Laboratory, Volume II (1975). The results of the core logging indicate a similar zonation of chalk types to that described in Section 3.2.

Point load strength index tests (described in Appendix D) were carried out on core that remained following removal of samples for laboratory testing. The variation of point load index (P.L.I.) with depth for each borehole is plotted in Figure 3.7, which shows a section

along the tunnel line.

Data concerning fracture spacing and Rock Quality Designation (RQD)* were obtained by the author from the core logs. The variation of fracture spacing and RQD with depth in each borehole is plotted in Figure 3.8, again showing a section along the tunnel line.

Further boreholes 100P, 100L, 102P and 102L were sunk to provide a facility for a programme of specialised *in situ* testing. In boreholes 100P and 102P, Menard pressuremeter tests described in Appendix D were carried out. The variation of E_p (the chalk mass deformation modulus obtained from the pressuremeter tests) with depth in each of the boreholes is shown in Figures 3.9 and 3.10. These Figures also include plots of the variation in fracture spacing and RQD with depth as obtained from core logs. Seismic velocity was measured at varying depths in boreholes 100L, 102L and 106L. These measurements are described in Appendix D. The variation of P and S wave velocity with depth in each of these boreholes is summarised in Figues 3.11, 3.12 and 3.13. Figure 3.12 includes a plot of the variation of fracture spacing and RQD with depth in borehole 102L. Boreholes 100L and 106L were not cored.

Laboratory tests were carried out on samples taken from boreholes 100 to 105 following the methods described in Section 3.3. The results of these tests, averaged for each borehole, are summarised in Table 3.2.

3.5 Summary and discussion of site investigation results - stages I and II

The results of the site investigation prove that the Lower Chalk at Chinnor, extending to at least 35m below ground level, can be divided into

* Defined as the percentage of a length of core consisting of intact lengths $\geq$0.1m. Since 100% core recovery was obtained in most cases this is effectively equivalent to the alternative definition of RQD in which the intact core lengths are expressed as a percentage of the borehole length.

Table 3.2 Chalk material properties, average values for each borehole, stage II site investigation

Borehole number	Moisture content %	Specific gravity	Bulk density (Mg/m^3)	Unconfined compressive strength (MN/m^2)	Secant modulus (MN/m^2)	Poisson's ratio	Brazil tensile strength (MN/m^2)
100	17.0	2.63	2.13	6.5			0.67
100P	12.5	2.54	2.10	7.9	1539*	0.23	
101	17.3	2.64	2.14	5.5	1179*	0.22*	0.50
102	19.3*		2.16	8.8	1555	0.35	0.60
102P	12.0	2.56	2.15		1465	0.26	
102L	13.6		2.06		1452		
103	16.5	2.57	2.13	6.8	924*	0.18*	0.62
104	16.0	2.53	2.18	9.8	1015*	0.37*	0.75
105	17.6	2.53	2.05	7.1	1163*	0.22	0.78

Note: * Average of less than five tests

three lithological types: (1) Light creamy grey chalk (youngest) (2) Light brown grey chalk, (3) Grey blue chalk. The point load index strength profiles shown in Figures 3.3 and 3.7 indicate that the mechanical properties of the intact chalk are highly variable on the small scale (1 - 2m). The profiles suggest a slight tendency for strength to increase with depth. Classification of the chalk using the system proposed by Ward *et al.* (1968) indicates that the Chalk at Chinnor is in general Grade III.

The chalk, whilst variable on the small scale, has uniform index and mechanical properties when averaged for each borehole. The average specific gravity lies consistently between 2.5 and 2.6 with a bulk density close to 2.1 Mg/m^3. Unconfined compressive strength averaged for each borehole is commonly between 6 MN/m^2 and 9 MN/m^2, whilst tensile strength is generally between 0.5 MN/m^2 and 1.0 MN/m^2.

Figures 3.4 and 3.5 show that there is a general trend of decreasing calcium carbonate content with depth, reducing by about 10% every 20m. This is often accompanied by a corresponding increase in porosity, resulting from the fact that the increased silica content of chalk with a low $CaCO_3$ content has a higher porosity than pure 'chalk'.

The discontinuous nature of the chalk is emphasised by the values of fracture spacing and RQD obtained from core logging. On the small scale (1 - 2m) discontinuity characteristics, like intact chalk properties, are seen to be very variable, with highly fractured bands developing at all levels. The degree of fracturing generally decreases with depth. Average spacing values range from $\simeq$0.05m (RQD $\simeq$10%) in the weathered zone near the surface to values between 0.1m and 0.2m (RQD $\simeq$ 50%) 10m below ground level. In the grey blue chalk (type 3), average discontinuity spacing values approach 0.3m (RQD $\simeq$ 90%).

Figures 3.8 to 3.10 show that there is a moderately good correlation between RQD and fracture spacing. This relation, summarised in Figure 3.14 for boreholes* 102, 104, 105 and 102L, indicates a broad scatter with a general trend of increasing RQD with increasing mean discontinuity spacing ($\bar{x}$). In addition Figure 3.14 includes the theoretical curve $RQD = 100e^{-0.1\lambda}(0.1\lambda + 1)$, where $\lambda = {}^{1}/_{\bar{x}}$, derived from the negative exponential distribution. The relation between RQD and mean discontinuity spacing is discussed in detail in Chapter 11. It is, however, important to note here that the conclusions in Chapter 11 indicate that the deviation of data points in Figure 3.14, to the lower RQD and higher mean spacing side of the theoretical curve $RQD = 100e^{-0.1\lambda}(0.1\lambda + 1)$, is a result of sampling error arising from two effects:

1. Mean dicontinuity spacing values are artificially high due to the presence of unmeasured closely spaced discontinuities.

2. RQD values are artificially low due to the presence of <u>evenly spaced</u> discontinuities imposed during coring.

Figures 3.9 and 3.10 show the variation in E_p (the mass deformation modulus obtained from pressuremeter tests) and rock quality (fracture spacing and RQD) with depth in boreholes 100P and 102P. It is clear that, in general, low E_p values of between 50 MN/m^2 and 200 MN/m^2 occur in the more fractured horizons within approximately 15m of the ground surface in boreholes 100P and 102P. Larger values of E_p occur at depths exceeding 15m, ranging from 200 MN/m^2 and increasing with depth to values of approximately 1500 MN/m^2 at the base of the boreholes. It is probable that stress release effects led to fracturing and loosening of the chalk

* Data from these four boreholes only were suitable for plotting in this Figure since in only these boreholes did the core lengths over which RQD was calculated exactly correspond with the lengths over which fracture spacing was averaged.

mass in the near surface zone - resulting in the very low mass deformation moduli for this material. This modulus reduction can be expressed in terms of a modulus reduction factor discussed in Chapter 1 and equal to the rock mass deformation modulus divided by the modulus of intact, laboratory size specimens, (Hobbs, 1973). Intact moduli for laboratory samples generally range from 1000 MN/m^2 to 2000 MN/m^2 (Tables 3.1 and 3.2), the average value for samples from borehole 102P being near to 1500 MN/m^2. This value indicates that for borehole 102P, the modulus reduction factor j ranges from approximately 0.05 for rock within 15m of ground surface to values approaching 0.5 at depths of 20m to 27m. At the base of the borehole the j factor is close to unity. The concept of the modulus reduction factor is discussed further in Chapter 8 where the subject is viewed in the light of additional field data obtained from Chalk sites in the UK and theoretical stress analyses of ground behaviour near the Chinnor tunnel.

Figures 3.11, 3.12 and 3.13 show the variation in P and S wave velocity with depth in boreholes 100L, 102L and 106L. Only borehole 102L was cored; it is therefore difficult to evaluate the relation between P and S wave velocity and rock quality. In all three boreholes, P and S wave velocities show a sharp increase at depths of between 18m and 20m. This depth corresponds with the boundary between chalk types 2 and 3, which in turn corresponds with a general increase in fracture spacing. It is likely that this change in lithology and rock quality is responsible for the change in seismic velocities.

3.6 Site investigation in the 3m diameter shaft

3.6.1 Introduction

For direct site investigation purposes, the following chalk properties were studied in the shaft: geological and palaeontological characteristics,

natural moisture content, calcium carbonate content, *in situ* strength index and discontinuity characteristics. For assessing site investigation techniques, the results are compared with those obtained in the adjacent 131mm diameter borehole (No. 100), and the 5m diameter tunnel. A full description of the discontinuity surveys carried out in the tunnel is given in Chapter 5.

As a part of the geotechnical experimental programme, the shaft was rockbolted with mechanical and resin anchored rock-bolts, the heads of which were instrumented with pressure transducers in order to monitor their behaviour during tunnel excavation. Horizontal inclinometer tubes and extensometers, installed in the shaft walls adjacent to the tunnel, were used to monitor ground movement and shaft-tunnel interaction during tunnel excavation. In addition, horizontal movement of the shaft side-walls was monitored using optical plummet techniques, sighting on to targets fixed to the shaft walls. These geotechnical experiments are described in detail in Hudson and McCaul (1975).

The important features of the Lower Chalk encountered during excavation of the shaft may be considered under three headings:

(a) Lithology and palaeontology - including sedimentological and post-diagenetic features.
(b) Intact rock strength and hardness.
(c) Discontinuity characteristics.

3.6.2 Lithology and palaeontology

The Lower Chalk at Chinnor is composed of four main materials:

(1) The remains of coccoliths - the reinforcing plates on the external skeletons of protozoa (coccolithophoridae group).

(2) Calcisphaerulidae (spheres of calcium carbonate), larger protozoa (foraminifera) and other invertebrate skeletal fragments.

(3) Silica, commonly occurring as clay size flakes of the mineral lussatite together with crystalline quartz. Preliminary results of X-ray diffraction (X.R.D.) and X-ray fluorescence (X.R.F.) tests on samples of chalk indicate that there is a negligible (<10%) clay mineral content in the chalk at Chinnor. The fraction commonly, and mistakenly, referred to as 'clay' is silica of clay size present as the mineral lussatite in varying amounts in the samples. The mineral lussatite consists of extended sheets of SiO_4 tetrahedra showing considerable stacking disorder (Calvert, 1974). This structure gives the mineral an 'expanding lattice' potential which may largely explain the 'clayey' behaviour of chalk containing lussatite. The results of the X.R.D. and X.R.F. analyses are discussed further in Appendix E.

(4) Calcite cement, which was precipitated in the sediment during diagenesis. In addition, the following inclusions may be found distributed through the rock mass:

i. Hard siliceous nodules up to 10cm in diameter; these are extremely rare.

ii. Crystalline calcite, occurring as iron stained veins up to 5mm wide.

iii. Two types of iron pyrites have been found: the most common variety is the orthorhombic marcasite occurring as a radiating form within brown nodules up to 20cm long and 5cm in diameter. The cubic or pyritohedron variety is rarer at Chinnor and has been found only in very small quantities in the shaft.

Figure 3.15 shows that the chalk encountered in the shaft may be divided into two main types on the basis of colour. The upper light grey chalk is of a more variable nature than the dark grey chalk, and contains frequent pockets and lenses of soft putty chalk up to 0.5m in diameter, together with iron pyrites, siliceous nodules and crystalline calcite. The dark grey chalk is more homogeneous and characteristically less fissured than the light grey chalk above. These two chalk types correspond with chalk types 2 and 3 discussed in Section 3.2.

The colour change between the light and dark grey chalk is abrupt. However, in areas just above the horizon of the main colour change, sharply defined irregularly-shaped zones of dark grey chalk occur (cf. Section 3.2). This suggests that the colour change is a result of post-diagenetic effects such as variation in chemistry of percolating ground water, rather than syngenetic effects such as variation in the chemistry of the depositional environment which would produce distinctly-layered colour changes.

Hand samples were collected from four positions (90^{o} apart) round the shaft sidewalls at levels 1 metre apart, these samples were tested to determine the natural moisture content and calcium carbonate content. Variations in these properties with depth in the shaft are summarised in Figures 3.16 and 3.17.

A micropalaeontological analysis of samples (S_1 to S_{17} in Figure 3.15) taken from the shaft was performed by D.J. Carter of Imperial College. The results of this analysis (summarised in Figure 3.15) enabled a zonation of the Lower Chalk encountered in the shaft. Evidence provided from the shaft therefore suggests that tunnelling took place largely in zones 9 and 10.

A list of microfossils identified from samples taken in the shaft is included in Appendix F.

3.6.3 Intact rock strength

The *in situ* strength of the chalk in the shaft was estimated (by members of TRRL) using an impact penetrometer along two vertical scanlines on the east and west walls of the shaft.

Rock testing using the impact penetrometer involves firing a hardened steel cone into the rock and measuring the depth of penetration. The cone has an included angle of 5^{o}, is 76mm long and is fired by an explosive charge. The depth of penetration can be used as a direct index, or a strength value can be estimated from a calibration chart. The intact strength values obtained by the impact penetrometer, though related to compressive strength, are not a direct measure of this property but rather a strength index related to rock cutability. For this reason the strength values obtained by the impact penetrometer are termed "penetration strength" rather than "compressive strength". These, and other aspects of the impact penetrometer are discussed in Drew and Hudson (1975).

Impact penetrometer strength measurements were made at 0.2m intervals along the scanlines both in the shaft and at the adjacent tunnel face. The estimated penetration strength profiles for the shaft and the adjacent tunnel face (tunnel chainage 35.9m) are shown in Figure 3.18 (after Priest and Hudson, 1975a), together with a point load index profile obtained from the adjacent borehole 100.

3.6.4 Discontinuity characteristics

Measurement of discontinuity characteristics in the shaft was carried

out using the scanline technique. This technique - as described in Chapter 2 - was slightly modified to allow for the shaft geometry. It was necessary to examine the entire sidewall of the shaft at intervals during excavation, therefore a square scanline technique was adopted for use at the base of the shaft during shaft sinking. The geometry and orientiation of the scanline system used is shown in Figure 3.1. Spacing, orientation and trace length of discontinuities intersecting the projection of the scanline (measuring tape) on the shaft wall were recorded along the square scanlines spaced at approximately 1 metre intervals down the shaft. The vertical levels of the scanlines are shown in Figure 3.15. Following completion of the shaft, two vertical scanlines (on the east and west walls of the shaft) were set up to provide the third dimension in the orthogonal scanline survey. Data from scanline surveys in the shaft are tabulated in Appendix B.

Data from the shaft were processed in the same way as that described for the scanline surveys in the quarry (Chapter 2). Discontinuity spacing histograms for the summed horizontal scanlines and for each of the vertical scanlines are shown in Figures 3.19, 3.20 and 3.21. Additional data concerning each of the vertical scanlines are also shown in these Figures. Data concerning each of the separate horizontal scanlines are listed in Table 3.3. Because measurement of discontinuity spacing was performed along the projection of horizontal square scanlines on the circular shaft-wall it was necessary to multiply the resulting mean spacing by a correction factor $y = \frac{P_s}{P_c}$ where P_s is the perimeter of a square inside a circle of perimeter P_c. The correction factor y was not used when constructing the discontinuity spacing histograms since the distribution would not have been significantly altered by its application.

In order to produce the discontinuity spacing histogram for summed horizontal plus summed vertical scanlines, an integral correction factor

Table 3.3 Discontinuity data from scanlines in the shaft

Scanline depth in shaft (m)	Scanline length (m)	Number of discontinuities measured	Mean discontinuity spacing (m)	Spacing, standard deviation (m)	Corrected mean spacing (m) y = 1.111	Mean discontinuity dip, (degrees)	Dip, standard deviation, (degrees)
1.0	11.30	71	0.159	0.163	0.177	52.53	21.92
1.7	8.62	60	0.144	0.110	0.160	51.03	22.53
2.5	8.95	104	0.086	0.076	0.096	52.47	23.66
3.8	8.52	74	0.115	0.090	0.128	58.16	24.01
5.1	7.55	53	0.142	0.103	0.158	56.78	20.99
6.4	8.49	86	0.099	0.086	0.110	52.00	21.47
7.4	8.34	74	0.113	0.097	0.125	56.32	20.47
8.4	8.40	94	0.089	0.062	0.099	51.83	22.99
9.5	8.35	70	0.119	0.092	0.133	48.15	23.03
10.2	7.90	85	0.093	0.087	0.103	46.79	26.35
11.2	7.98	78	0.102	0.099	0.113	50.77	24.93
12.4	8.02	60	0.134	0.141	0.148	56.59	23.01

Table 3.3 (continued) Discontinuity data from scanlines in the shaft

Scanline depth in shaft (m)	Scanline length (m)	Number of discontinu-ities measured	Mean discontinuity spacing (m)	Spacing, standard deviation (m)	Corrected mean spacing (m) y = 1.111	Mean discontinuity dip, (degrees)	Dip, standard deviation, (degrees)
13.6	8.20	69	0.119	0.115	0.132	55.53	27.46
14.6	7.90	67	0.118	0.110	0.131	55.03	22.91
15.7	7.65	62	0.123	0.087	0.137	57.48	19.22
16.9	7.25	49	0.148	0.151	0.164	58.72	18.30
17.9	8.05	54	0.149	0.144	0.165	59.50	23.25
19.0	8.00	38	0.211	0.147	0.234	47.29	31.66
20.1	8.10	39	0.208	0.127	0.231	51.80	24.60
21.2	8.30	30	0.277	0.177	0.308	54.06	18.64
22.6	8.30	27	0.307	-	0.341	-	-
Vertical, east side	21.85	209	0.105	0.096	-	35.76	23.27
Vertical, west side	22.11	243	0.091	0.080	-	36.08	24.35

was applied to correct for scanline length. The application of this correction factor was described in Chapter 2. The resulting discontinuity spacing histogram, shown in Figure 3.22, therefore gives a largely unbiased 3-dimensional characterisation of the ground through which the shaft was excavated.

In order to obtain an idea of variation of discontinuity characteristics with depth, data from the two vertical scanlines were processed to produce mean spacing values for each 0.5m run of scanline. The resulting profiles, together with the corrected mean spacing values for each of the horizontal scanlines are plotted in Figure 3.23. In addition, this Figure summarises the variation of discontinuity spacing with depth in borehole 100, and at an adjacent tunnel face (tunnel chainage 35.9m). The discontinuity spacing data for borehole 100 were obtained by the author using the scanline technique. All discontinuities cutting the core were measured.

Upper hemisphere equal area projections showing the discontinuity orientation fabrics for each of the horizontal scanlines taken at various levels in the shaft (Appendix Figures G.1 to G.20) serve to indicate the variation of discontinuity orientation characteristics with depth. The construction of the equal area projections is described in Appendix C. Figure 3.24 shows the discontinuity orientation fabric obtained from surveys at an adjacent tunnel face at tunnel chainage 35.9m.

Equal area projections showing the discontinuity orientation fabric measured on the summed horizontal scanlines and on each of the vertical scanlines are presented in Figures 3.25, 3.26 and 3.27. In the construction of the equal area projection for the summed horizontal plus summed vertical scanlines the integral correction factor (discussed in Chapter 2)

correcting for scanline length, was again applied. The resulting projection, shown in Figure 3.28, therefore shows a largely unbiased 3-dimensional discontinuity orientation fabric for the ground encountered during shaft excavation.

3.7 Discussion and comparison of results obtained in the shaft, borehole 100 and the adjacent tunnel face.

Examination of Figure 3.16, showing the variation of moisture content with depth in the shaft, reveals that there is a trend of increasing moisture content with depth, from a value of 7% just below ground level to 24% 14m below ground level (cf. Tables 3.1 and 3.2). Below 118m A.O.D., the average moisture content is constant at 24%. The location of the standing water level at 117m A.O.D. serves to confirm that the "levelling off" of the moisture content profile at this point indicates saturation at 24%. This corresponds reasonably well with the average porosity values of approximately 30% discussed in Section 3.2.

The calcium carbonate profile shown in Figure 3.17, though highly variable, indicates a trend of reducing calcium carbonate content with depth, from 80% at the top of the shaft to 55% near the base. These findings are in general agreement with the results of the Stage I site investigation described earlier. The higher calcium carbonate content and therefore reduced silica content of the younger deposits indicates a changing depositional environment during accumulation of the sequence.

The intact rock strength profiles, shown in Figure 3.18, indicate a highly variable material with estimated penetration strength values ranging from 0.2 MN/m^2 to 12 MN/m^2. The good correlation between the profiles taken from opposite sides of the shaft indicates a tendency

towards horizontal strength layering in the chalk (this was also noted in the tunnel, Chapter 5). In addition, average strength values from the tunnel face agree well with those from the same level on the east side of the shaft and thus tend to confirm this conclusion. It is suggested (Priest and Hudson, 1975a) that the lower average strength values on the west side of the shaft at tunnel level reflect a weakening and disturbance caused by drilling operations during instrumentation.

There is a general increase of intact strength with depth in the shaft and borehole 100, ranging in the shaft from approximately 2 MN/m^2 (penetration strength) 10m below ground level to approximately 5 MN/m^2 23m below ground level. The apparently increased wavelength of variability of the material in borehole 100 (P.L.I. profile) compared with the shaft is a result of a reduced sample frequency in the borehole.

The discontinuity spacing histograms shown in Figures 3.19, 3.20 and 3.21 indicate a broadly similar distribution of discontinuity spacing values for both the vertical and horizontal scanlines. It is clear that for a given scanline or group of scanlines the frequency of occurrence of any given discontinuity spacing value decreases exponentially as the magnitude of the spacing value increases. A similar distribution of discontinuity spacing values was found to apply to discontinuity spacing data from scanline surveys at exposed faces in the Chinnor quarry (Chapter 2). In both cases the distributions follow the negative exponential distribution discussed further in Chapter 11.

Mean spacing values measured on the two vertical scanlines are 0.091m and 0.105m. However, the corrected mean spacing value for the summed horizontal scanlines is 0.140m. The difference in the mean spacing value between the vertical and horizontal scanlines may have resulted from one

or more of the following effects:

(a) The rock sampled on the vertical scanlines may have had a true inherited lower discontinuity spacing than the rock sampled on the horizontal scanlines.

(b) A preponderance of sub-horizontal discontinuities may have led to preferential sampling along vertical scanlines, giving an apparent reduction in mean discontinuity spacing for these scanlines.

(c) Rock weathering and stress release effects between the (earlier) horizontal scanline survey and the later vertical scanline survey may have exposed or emphasised additional discontinuities, leading to an apparently reduced mean discontinuity spacing for the later vertical scanlines. The apparent tendency for discontinuity frequency to increase with time of exposure was noted by Fookes and Denness (1969) and also at survey locations in the Chinnor quarry.

Because large numbers of discontinuities were measured along intersecting vertical and horizontal scanlines there was a large degree of spatial overlap in the surveys. The effect (a) could therefore only be responsible for slight discrepancies between the mean spacing values on the vertical and horizontal scanlines.

The mean discontinuity dip for all scanlines in the shaft, corrected for scanline length, is 46.39^{o}. Therefore, on average, one would expect a similar mean discontinuity spacing value for vertical and horizontal surveys since the discontinuities were inclined equally to both the vertical and horizontal scanlines. The effect (b) may therefore be discounted. It must, however, be pointed out that the preferential sampling

of sub-horizontal discontinuities on vertical scanlines, and sub-vertical discontinuities on horizontal scanlines leads to a lower mean discontinuity dip for the vertical scanlines than the horizontal scanlines. This effect is apparent in Table 3.3.

By elimination of the other effects it becomes clear that the effect (c) is largely responsible for the lower mean discontinuity spacing on the vertical scanlines and that during the time between the two surveys, weathering and stress relief effects in the shaft walls led to the exposure of additional, hitherto mechanically unimportant, discontinuities. It may therefore be concluded that the mean spacing measured on the vertical scanlines is artificially low, and not truly representative of conditions in the rock mass.

The equal area projections in Figures 3.25 to 3.28, showing the orientation fabrics for discontinuities measured in the shaft, reveal that a large proportion of discontinuities encountered on both the vertical and horizontal scanlines show a low dip ($\simeq 15^{o}$) to the west and northwest. For the summed horizontal scanlines (Figure 3.25) this sub-horizontal set is accompanied by a steeply dipping set ($\simeq 70^{o}$) inclined to the south, together with a concentration of discontinuities showing a moderate and steep dip to the northwest and north.

For the vertical scanlines Figures 3.26 and 3.27, the sub-horizontal set is accompanied by more random sets showing a slightly higher dip ($\simeq 40^{o}$) towards the northwest, east and south. The lack of significant concentrations of steeply dipping discontinuities in these projections underlines the effects, discussed earlier, of preferential selection of sub-horizontal discontinuities on vertical scanlines. The additional imposed discontinuities sampled on the vertical scanlines do not appear

as any one significant set on the projections. It is therefore likely that the orientiation fabric of these imposed discontinuities is largely random.

Figure 3.23, showing the variation in discontinuity spacing with depth in the shaft, tunnel and borehole 100, reveals that both in the shaft and borehole 100 there is a general increase in discontinuity spacing with depth, particularly below 113m A.O.D. where the dark grey chalk begins. This tendency, also noted in the results of the Stage II site investigation, is probably a reflection of the geomorphological controls on discontinuity occurrence, discussed in Chapter 2. The discontinuity spacing profiles, though highly variable, show that in general, discontinuity spacing increases from approximately 0.100m near the ground surface to values in excess of 0.250m at depths of 23m. The apparently lower degree of variability in the profile based on horizontal scanlines in the shaft is a result of the greater volume of data per depth increment obtained using the horizontal scanlines.

Table 3.4 summarises the comparison between mean discontinuity spacing values in the tunnel, shaft and borehole 100 at the tunnelling horizon.

It is evident that the best prediction of mean discontinuity spacing for the tunnel was obtained from the shaft. This greater effectiveness of the shaft in predicting tunnel conditions may largely be a result of the close similarity between the excavation geometries and discontinuity survey techniques in the shaft and tunnel. The comparatively low mean discontinuity spacing values for cores taken from borehole 100 probably reflect values artificially lowered by the imposition of evenly spaced

discontinuities during coring*. These rock breakage effects during sampling, discussed previously in connection with Figure 3.14, are analysed further in Chapter 11.

Table 3.4

Comparison between mean discontinuity spacing values in the tunnel, shaft and borehole 100 at the tunnelling horizon.

Tunnel, Chainage 35.9m	Shaft	Borehole 100
Sum of vertical scanlines 0.104m	Vertical scanline, west side 0.091m	0.085m
	Vertical scanline east side 0.105m	
Sum of horizontal scanlines 0.181m	Sum of horizontal scanlines 0.140m	
Sum of vertical plus horizontal scanlines 0.143m	Sum of vertical plus horizontal scanlines (corrected for scanline length) 0.117m	

The pattern of variation of discontinuity orientation characteristics with depth in the shaft is shown in Appendix G. When interpreting the discontinuity orientation fabrics in Appendix G it must be remembered that the measurements were taken along horizontal scanlines, which will have led to a preferential sampling of sub-vertical discontinuities and an associated smaller probability of sampling sub-horizontal discontinuities.

The Figures in Appendix G indicate that the basic orientation patterns shown in Figure 3.28 (which summarises the whole shaft) are developed at each survey level. In addition to this basic pattern, the discontinuity

* Although ideally these imposed fractures should be ignored during RQD logging, in practice it was difficult to discriminate between imposed and inherited discontinuities due to the presence of a putty-chalk smear accumulated during coring.

orientation fabrics for the separate levels contain a more randomly orientated set of discontinuities, the pattern of which varies from level to level. No consistent trends of variation of orientation can be detected. There is, however, a slight tendency for the set of sub-horizontal discontinuities to be better developed in the lower levels of the shaft.

Figure 3.24 shows the discontinuity orientation fabric for the tunnel face at chainage 35.9m. Comparison of this fabric with those in Appendix G reveals that the general patterns of discontinuity orientation found in the tunnel are reflected in the shaft, particularly at the depth of 11.2m.

3.8 Summary and conclusions concerning site investigation, stages I and II

1. The Lower Chalk at Chinnor, extending to at least 35m below ground level, was divided into three lithological types: (1) Light creamy grey chalk (youngest), (2) Light brown grey chalk, (3) Grey blue chalk.

2. The chalk, shown to be highly variable on the small scale, has uniform index and mechanical properties when averaged for each borehole, belonging in the main to Grade III of the Ward *et al.* (1968) chalk classification system.

3. A clear trend of decreasing calcium carbonate content and increasing discontinuity spacing with depth was noted. The increasing discontinuity spacing with depth is probably a reflection of the geomorphological controls on discontinuity occurrence.

4. Discussions, elaborated in Chapter 11, suggest that mean discontinuity spacing values for the boreholes are, in some cases, artificially high due to the presence of unmeasured closely spaced discontinuities. In addition, RQD values are artificially too low due to the presence of evenly spaced discontinuities imposed during coring.

5. Rock mass deformation moduli obtained from pressuremeter testing indicated that chalk within 15m of the ground surface has a modulus 0.05 times that obtained from intact laboratory size specimens. It is probable that this modulus reduction is a direct result of the discontinuous nature of the chalk.

6. Down-hole seismic and pressuremeter testing systems were shown to be of value for *in situ* assessment of chalk quality. In general, these systems served to detect the broader variations of fracture intensity with depth.

3.9 Summary and conclusions concerning rock quality assessment in the 3m diameter shaft

1. A 23.4m deep shaft, 3m in diameter was sunk in Lower Chalk for both site investigation purposes and to provide a facility for geotechnical experiments.

2. A variety of chalk properties was examined:

(a) Lithology and palaeontology.

(b) Moisture content.

(c) Calcium carbonate content.

(d) Intact rock strength index.

(e) Discontinuity characteristics.

3. Two major chalk lithologies were distinguished in the shaft: the upper 'light grey chalk' (chalk type 2 of Section 3.2) and the lower 'dark grey chalk' (chalk type 3 of Section 3.2). Micropalaeontological zoning proved that the shaft passed through parts of zones 9, 10 and 11(ii).

4. *In situ* moisture content was found to increase with depth, from a value of 7% near ground level to a constant value of 24%, coincident with the water table, at a depth of approximately 14m. Average calcium carbonate contents decreased with depth, from a value of 80% near the ground surface to approximately 50% at the bottom of the shaft. Results of X-ray analyses indicate that the non-calcium carbonate component of the chalk at Chinnor consists, in the main, of silica in the form of crystalline quartz and the mineral lussatite.

5. The *in situ* intact rock strength index termed penetration strength was measured down two vertical scanlines set up on the shaft walls. In addition, point load strength index tests were performed on core samples recovered from a nearby borehole. There was a general increase of intact strength with depth both in the shaft and borehole, with penetration strength values in the shaft ranging from approximately 2 MN/m^2, 10m below ground surface, to 5 MN/m^2, 23m below ground surface. Comparison between intact strength profiles indicated a tendency towards horizontal strength layering in the chalk.

6. Discontinuity measurements were made along vertical and horizontal scanlines set up in the shaft. Average discontinuity spacing values for summed scanlines in the shaft ranged from 0.091m to 0.140m. Some

reduction in mean discontinuity spacing as a result of weathering effects in the shaft was experienced.

7. Discontinuity spacing histograms, summarising measurements on vertical and horizontal scanlines, revealed that the distribution of discontinuity spacing values followed the negative exponential distribution. This is discussed further in Chapter 11.

8. In general, discontinuity spacing increased with depth in the shaft, ranging from approximately 0.100m near the ground surface, to values in excess of 0.250m at depths of 23m. Mean discontinuity spacing values in the shaft at tunnelling level were compared with those measured in the tunnel at a face adjacent to the shaft and at tunnelling level in borehole 100. Mean discontinuity spacing values in the adjacent borehole at tunnelling level were found to be lower than in the shaft or tunnel. This may be largely due to rock breakage effects during coring in the borehole.

9. Discontinuity orientation patterns, summarised on equal area projections, were found to consist largely of a sub-horizontal set of discontinuities, a steeper dipping set inclined towards the northwest, together with less consistent sets showing moderate to steep dips towards the north and south. Discontinuity orientation patterns for the shaft at tunnelling level were found to broadly reflect those measured at the adjacent tunnel face.

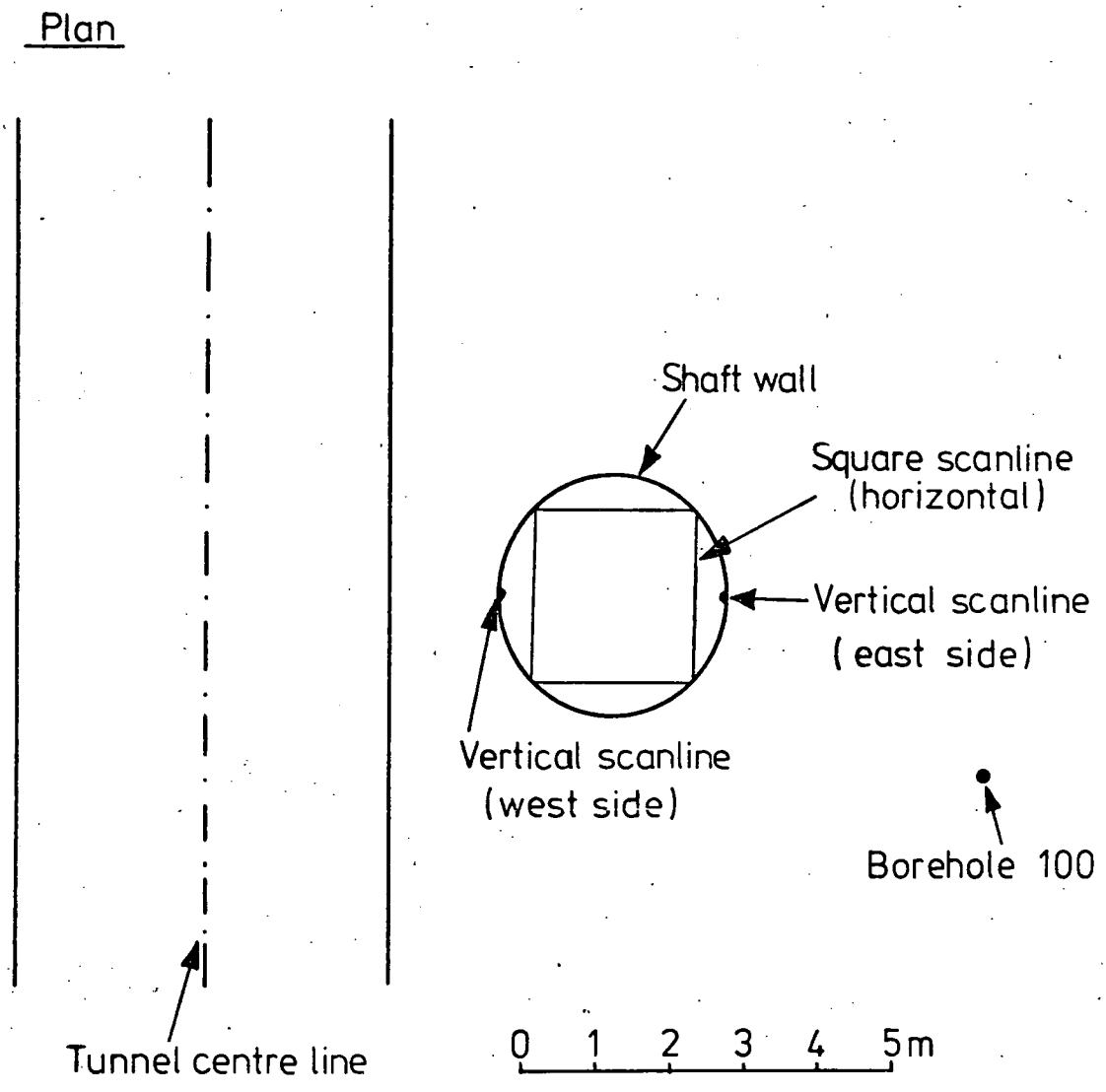

Fig. 3.1 SCANLINE GEOMETRY IN THE SHAFT (PLAN VIEW).

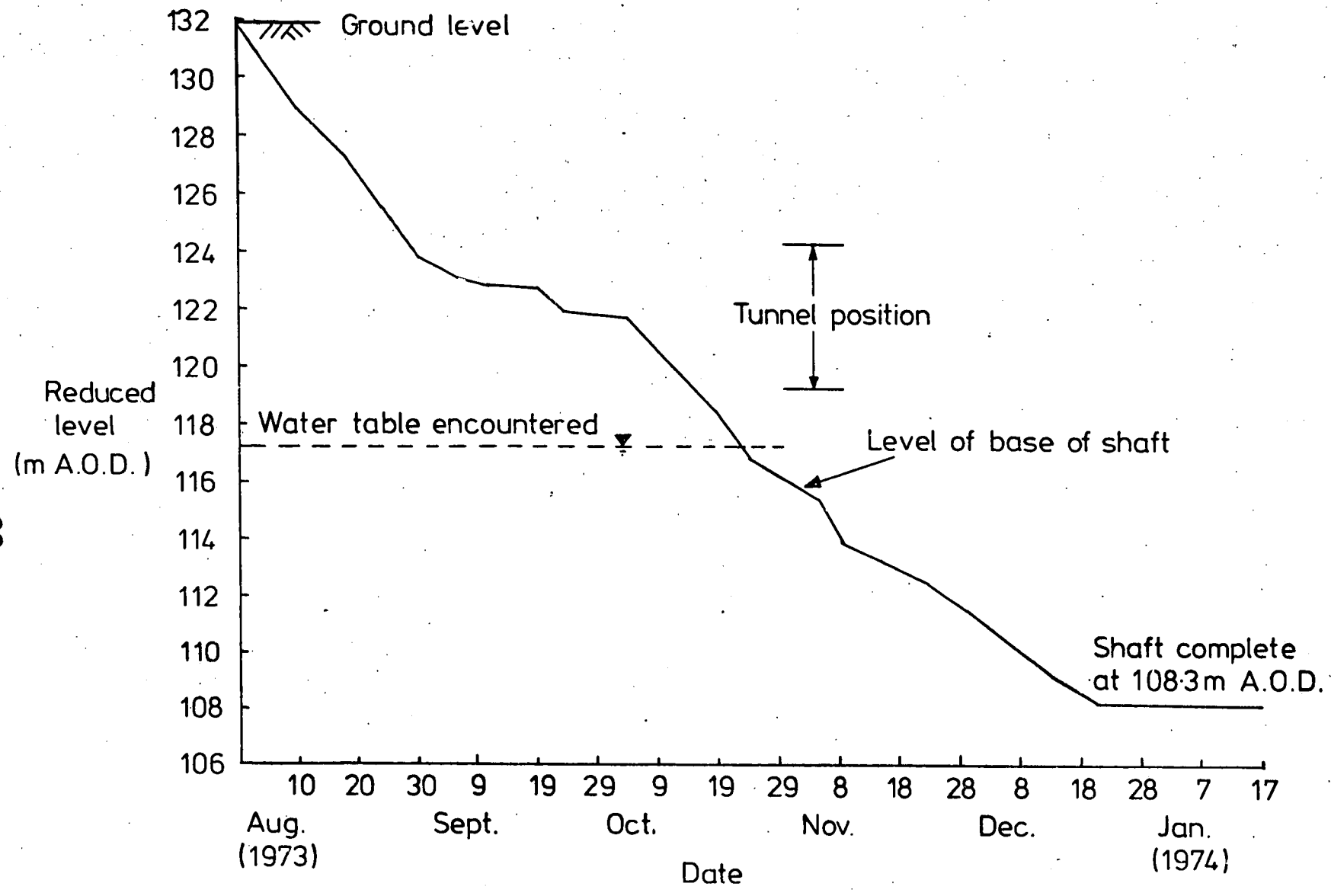

Fig. 3.2 PROGRESS OF SHAFT EXCAVATION.

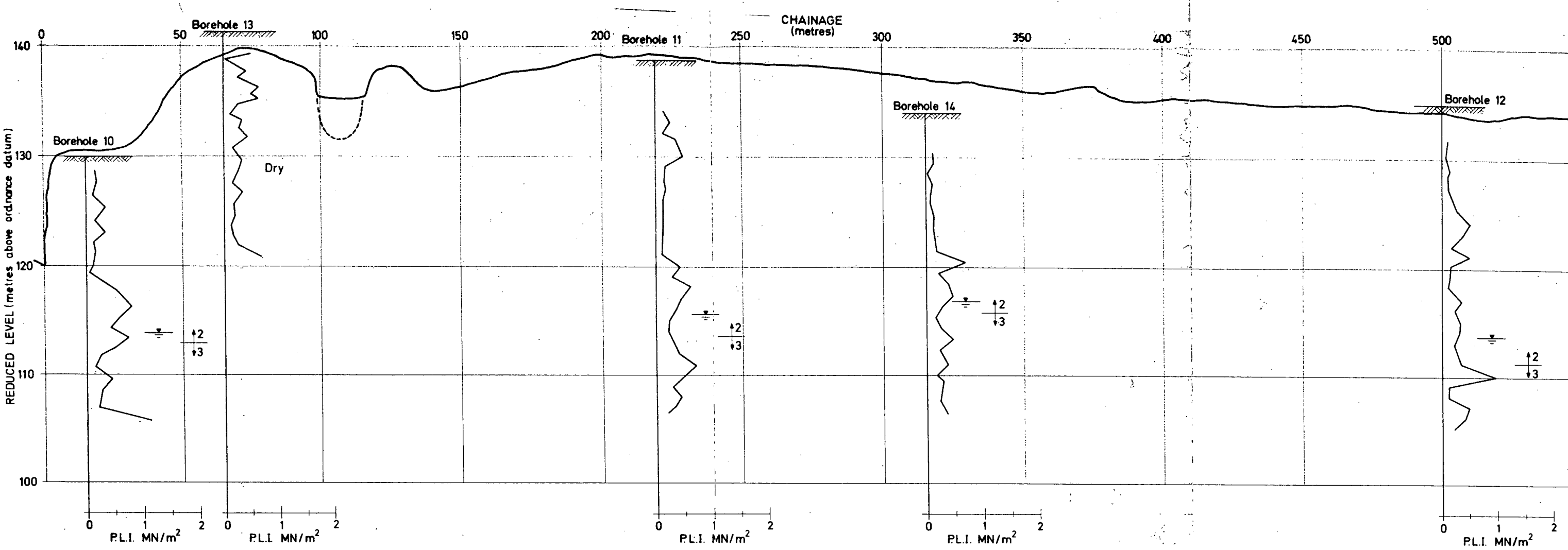

NOTE 2/3 Approximate transition point between chalk types 2 and 3

Standing water level

Fig. 3.3 VARIATION OF POINT LOAD STRENGTH INDEX (P.L.I) WITH DEPTH IN BOREHOLES 10 TO 14. PROJECTED ONTO THE TUNNEL LINE

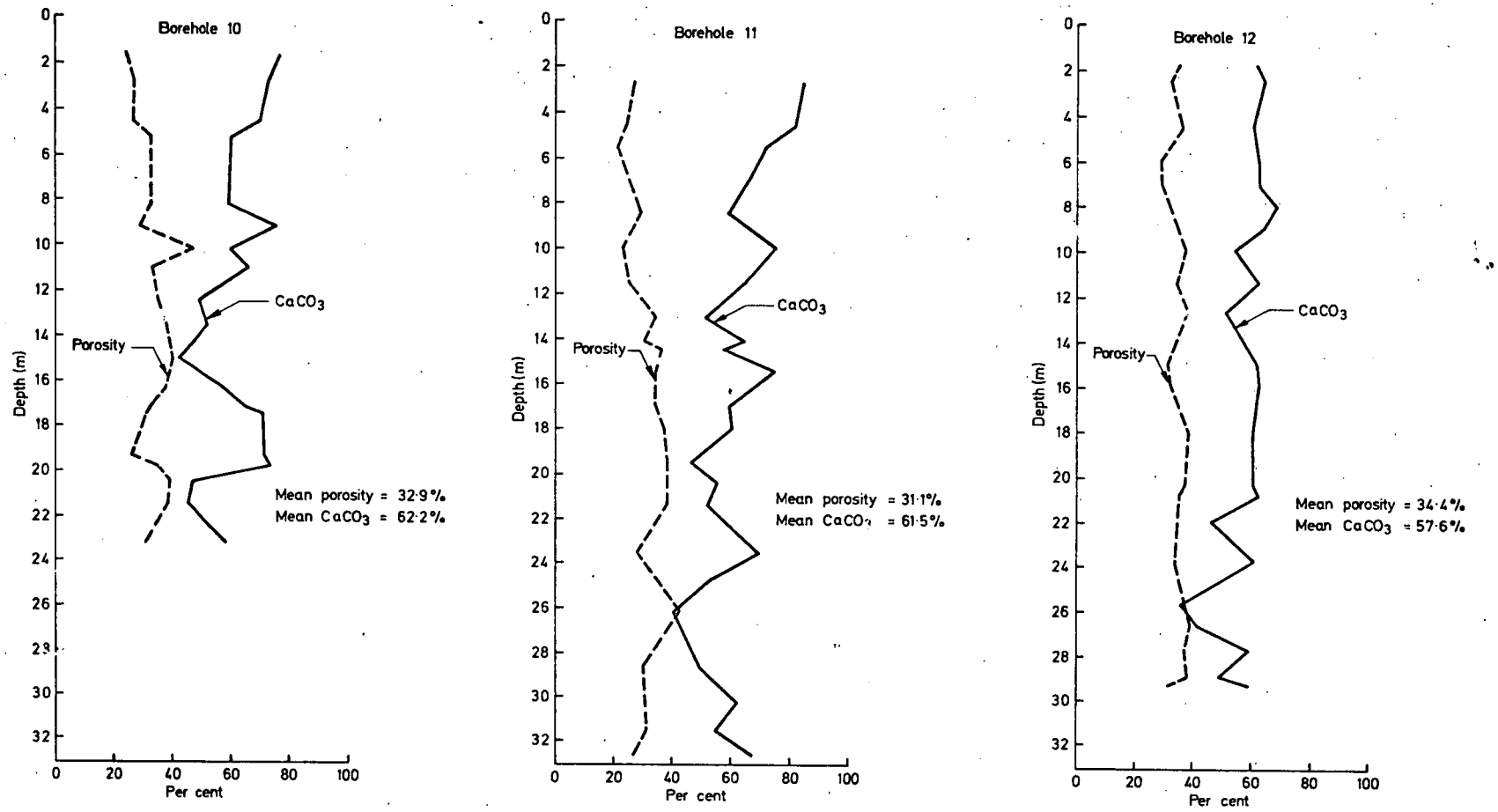

Fig. 3.4 VARIATION OF POROSITY AND CALCIUM CARBONATE ($CaCO_3$) CONTENT WITH DEPTH IN BOREHOLES 10, 11 AND 12

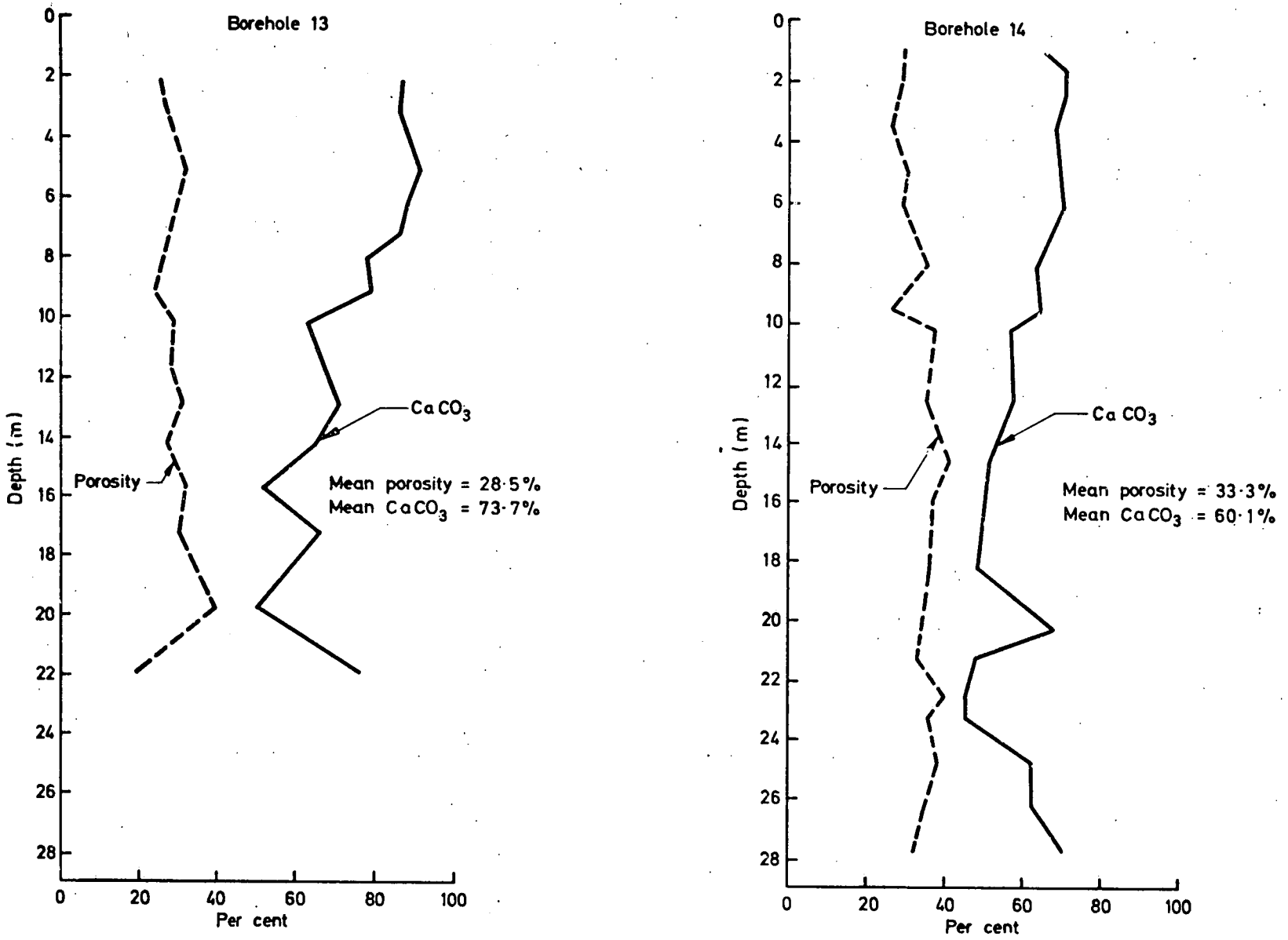

Fig. 3.5 VARIATION OF POROSITY AND CALCIUM CARBONATE ($CaCO_3$) CONTENT WITH DEPTH IN BOREHOLES 13 AND 14

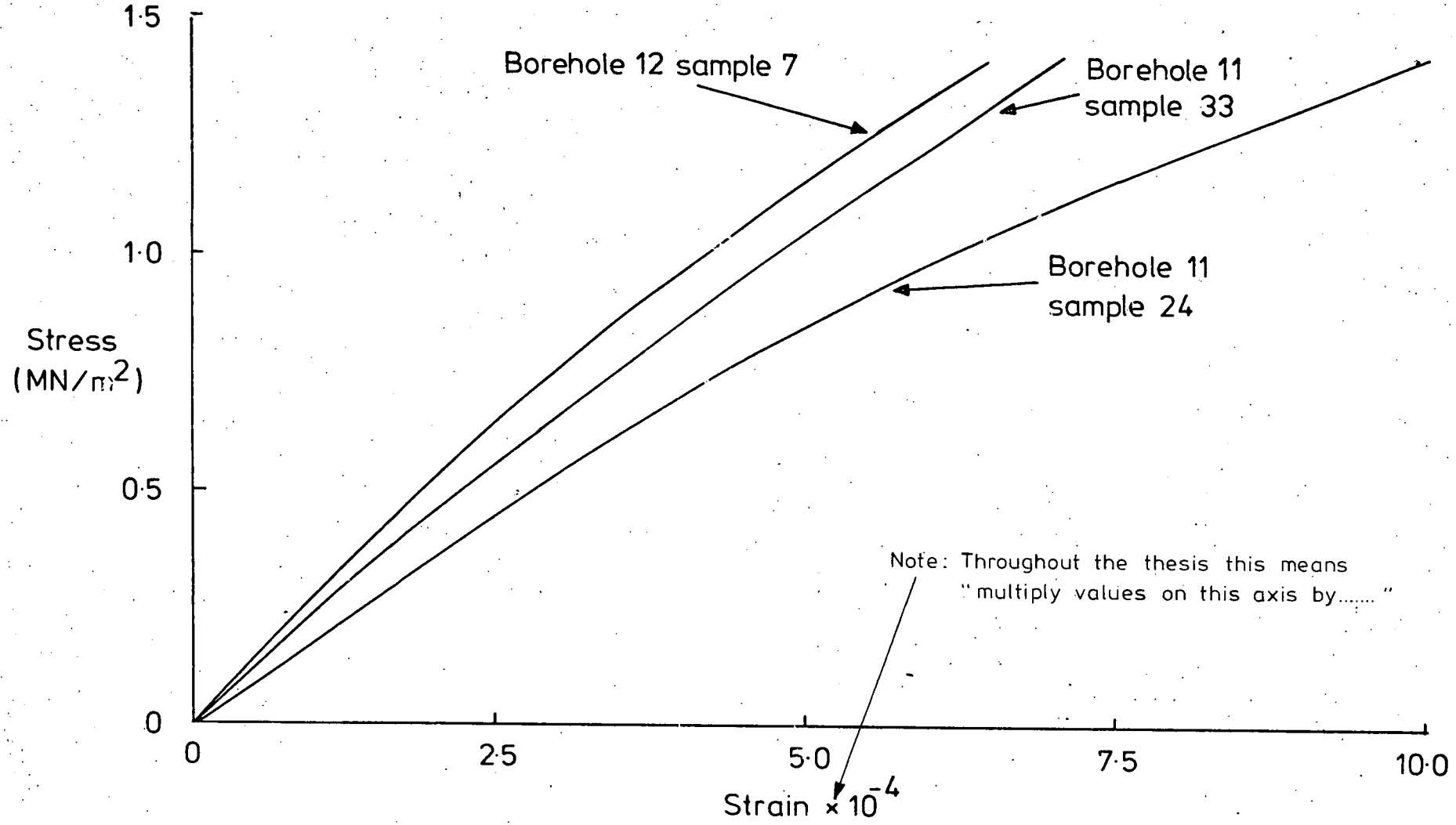

Fig. 3.6 STRESS-STRAIN CURVES FOR SAMPLES FROM BOREHOLES 11 AND 12, FIRST LOADING CYCLE.

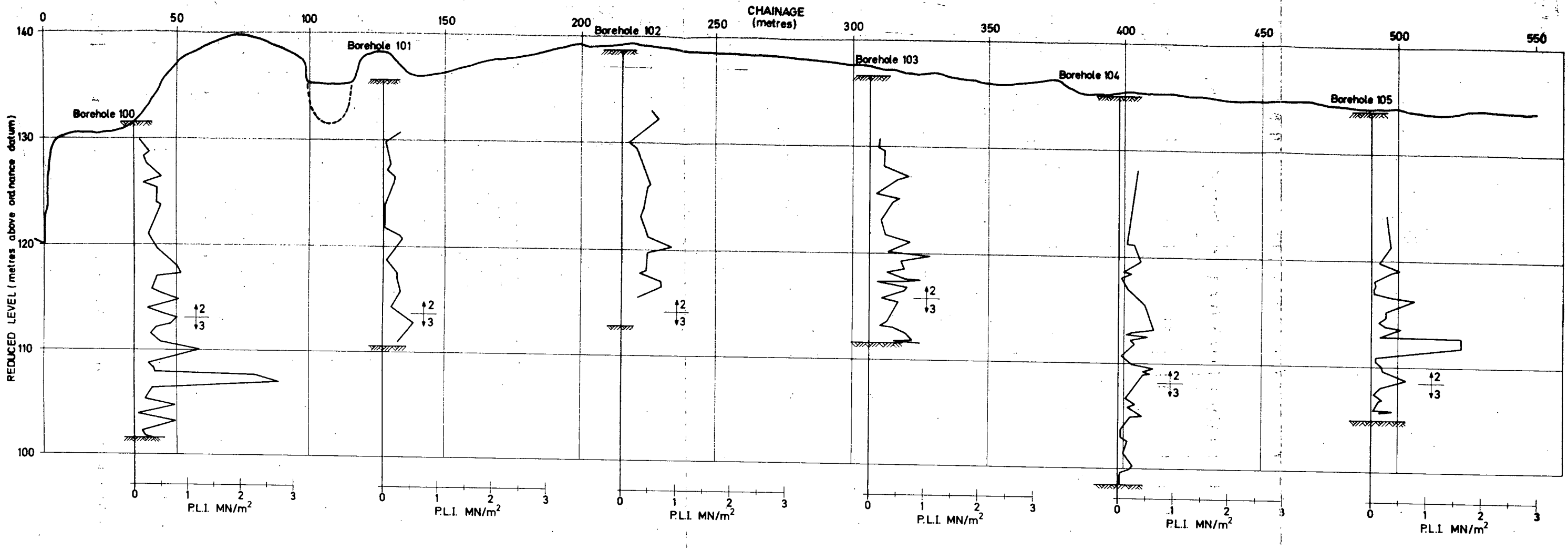

NOTE : 2/3 Approximate transition point between chalk types 2 and 3

Fig 3.7 VARIATION OF POINT LOAD STRENGTH INDEX (P.L.I.) WITH DEPTH IN BOREHOLES 100 TO 105 ALONG THE TUNNEL LINE

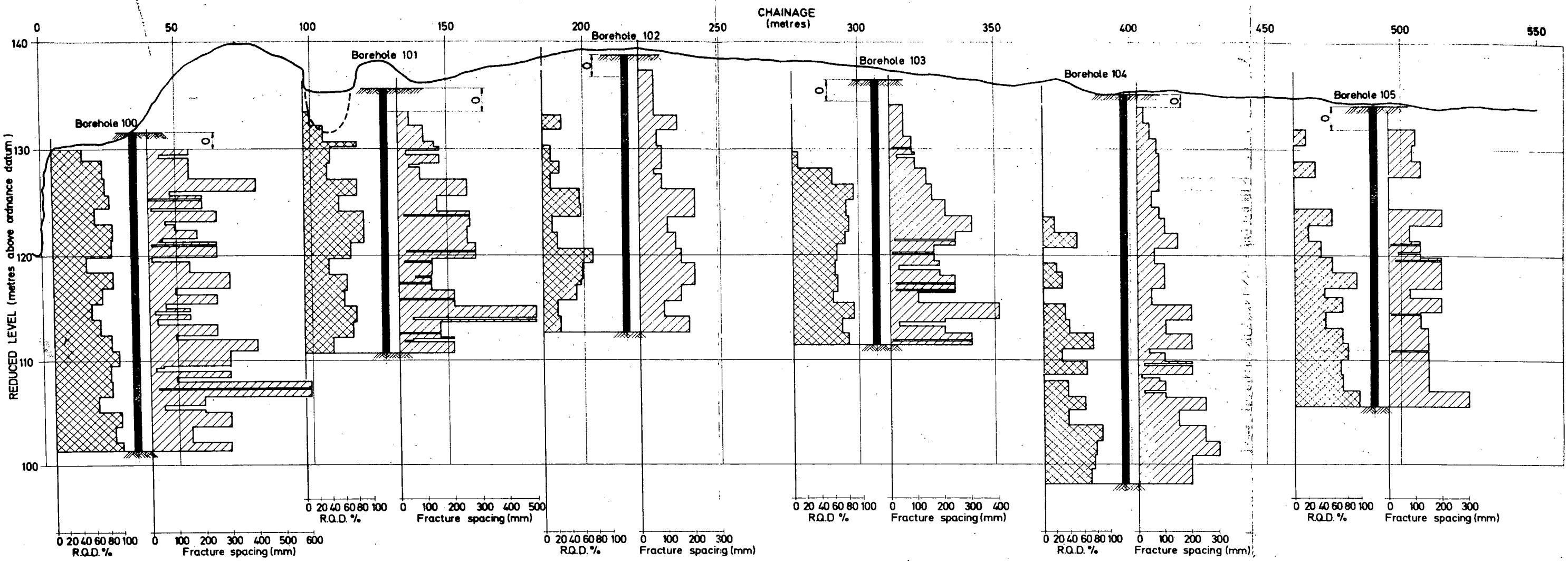

Key :

O = Open hole

Highly fractured zone

Relatively intact core

℄ of borehole

Fig. 3.8 VARIATION OF FRACTURE SPACING AND R.Q.D. WITH DEPTH IN BOREHOLES 100 TO 105

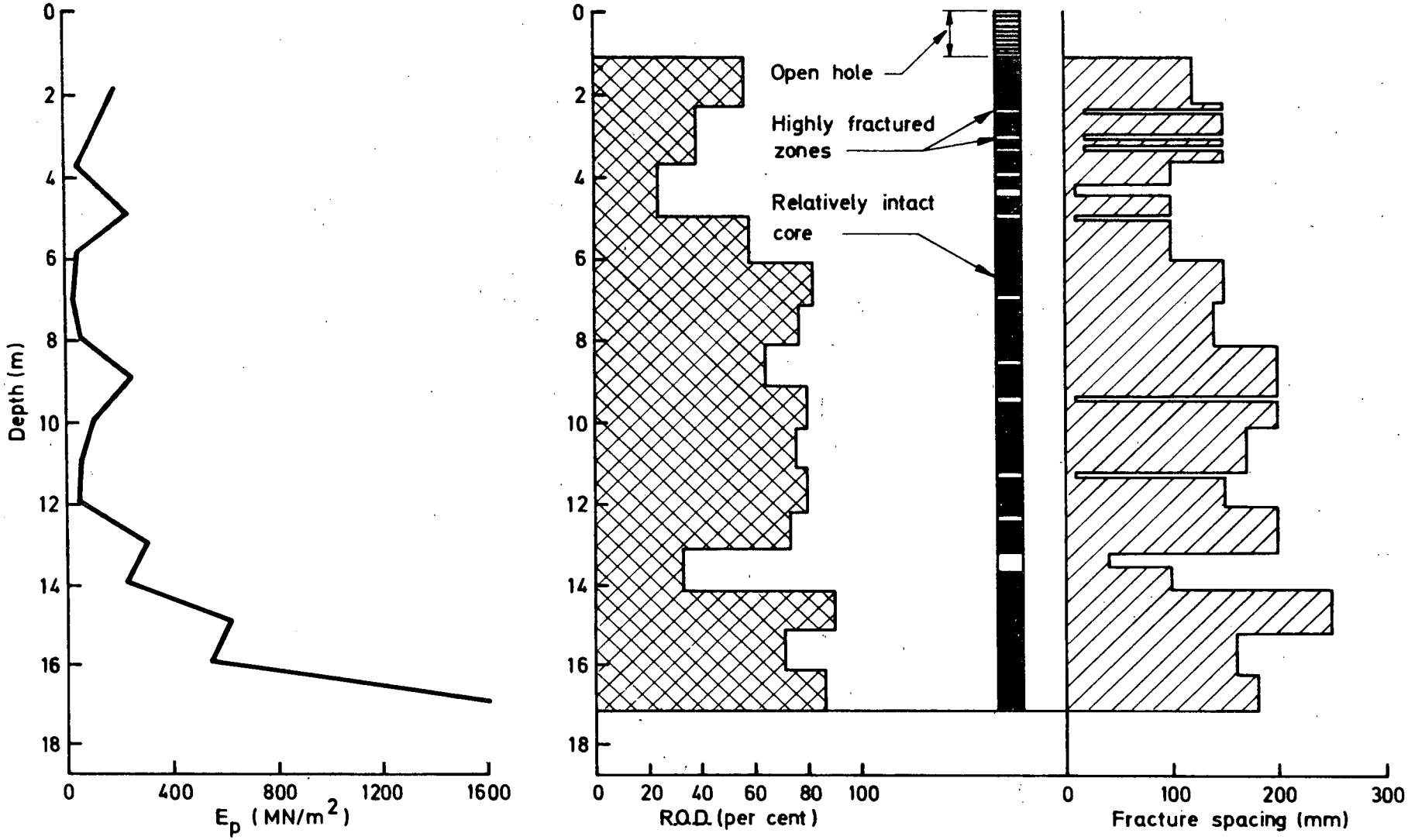

Fig. 3.9 VARIATION OF IN SITU DEFORMATION MODULUS AND ROCK QUALITY WITH DEPTH IN BOREHOLE 100P

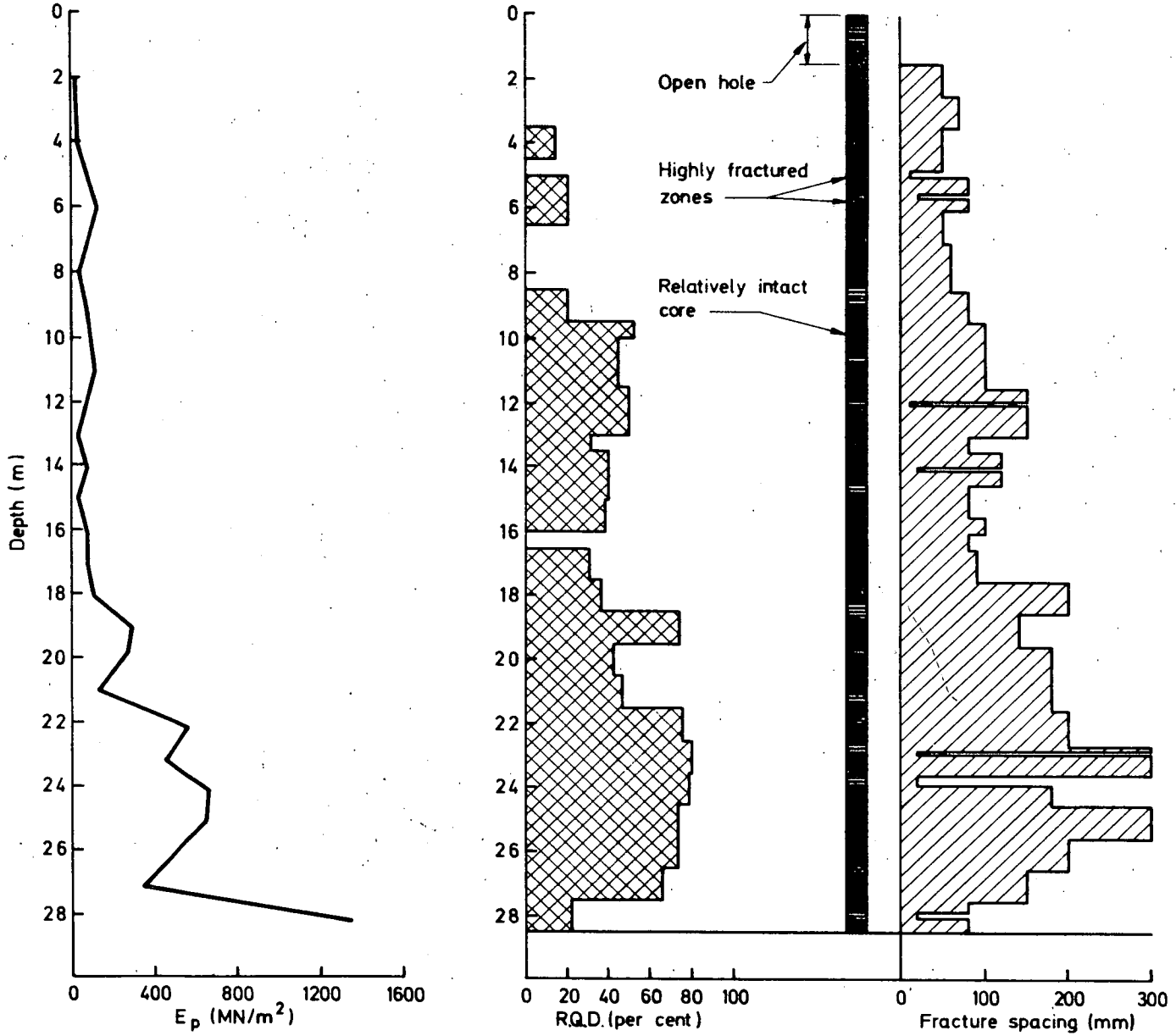

Fig. 3.10 VARIATION OF IN SITU DEFORMATION MODULUS AND ROCK QUALITY WITH DEPTH IN BOREHOLE 102P

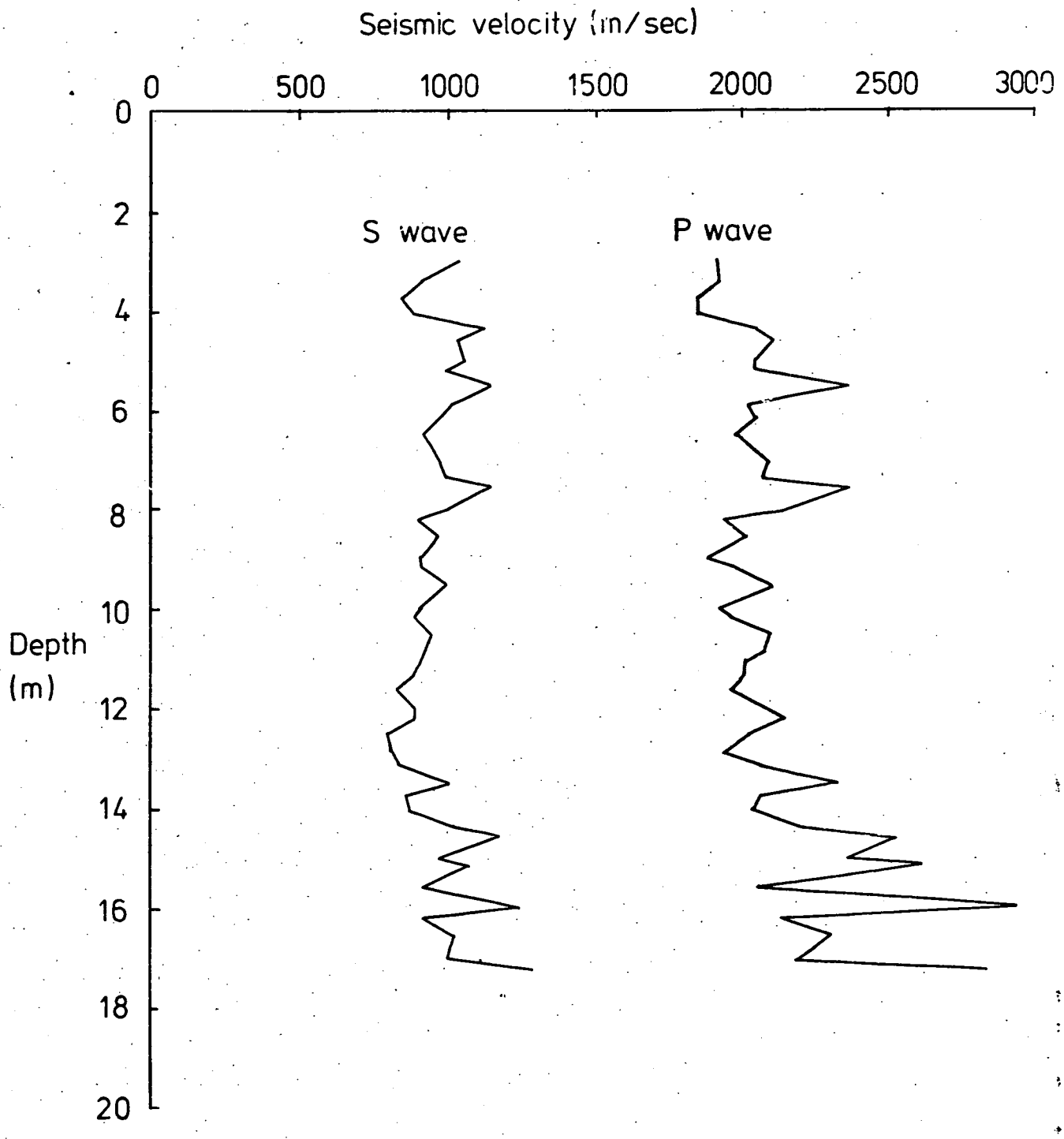

Fig. 3.11 VARIATION OF SEISMIC VELOCITY WITH DEPTH IN BOREHOLE 100L.

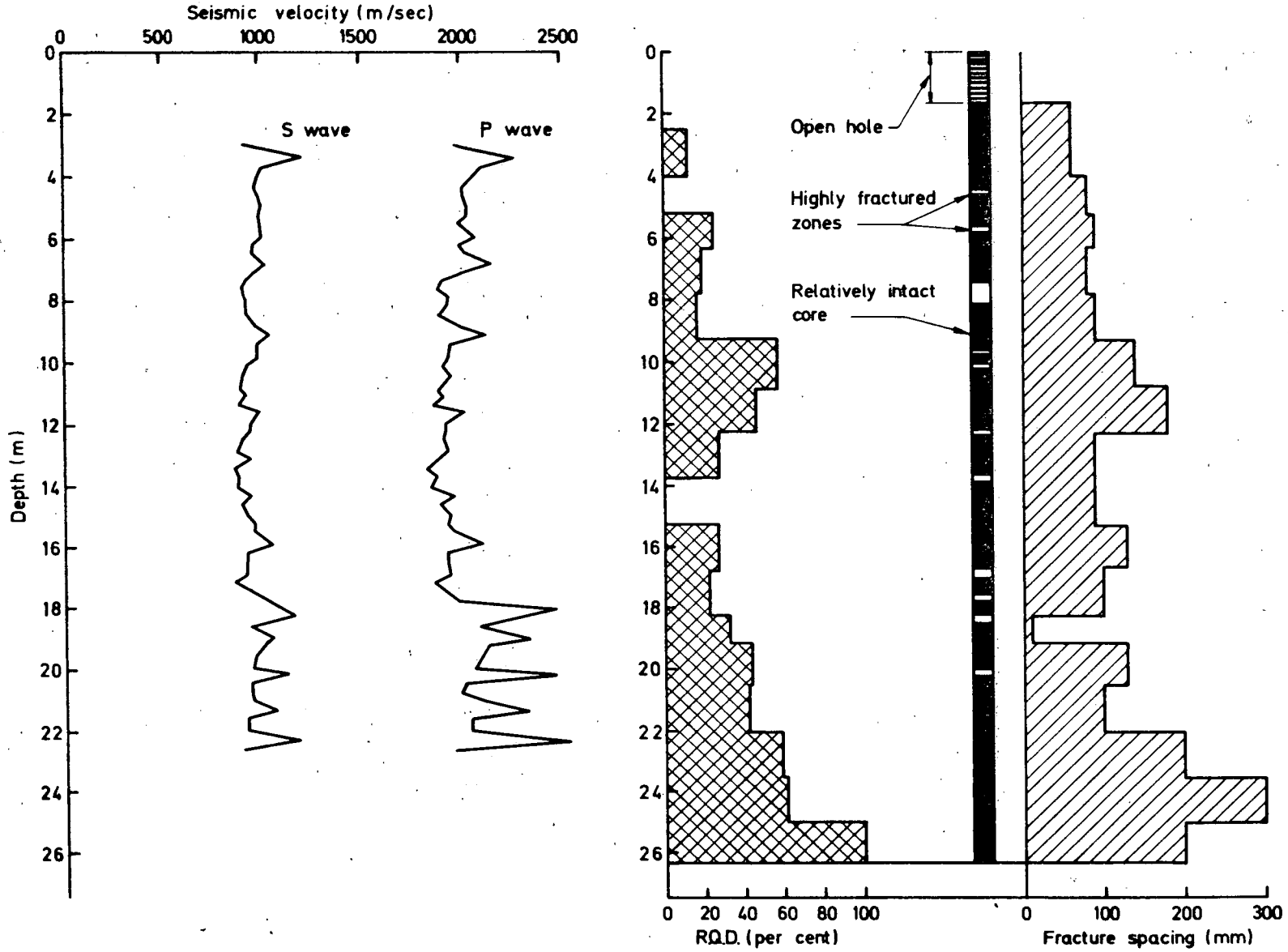

Fig. 3.12 VARIATION OF SEISMIC VELOCITY AND ROCK QUALITY WITH DEPTH IN BOREHOLE 102L

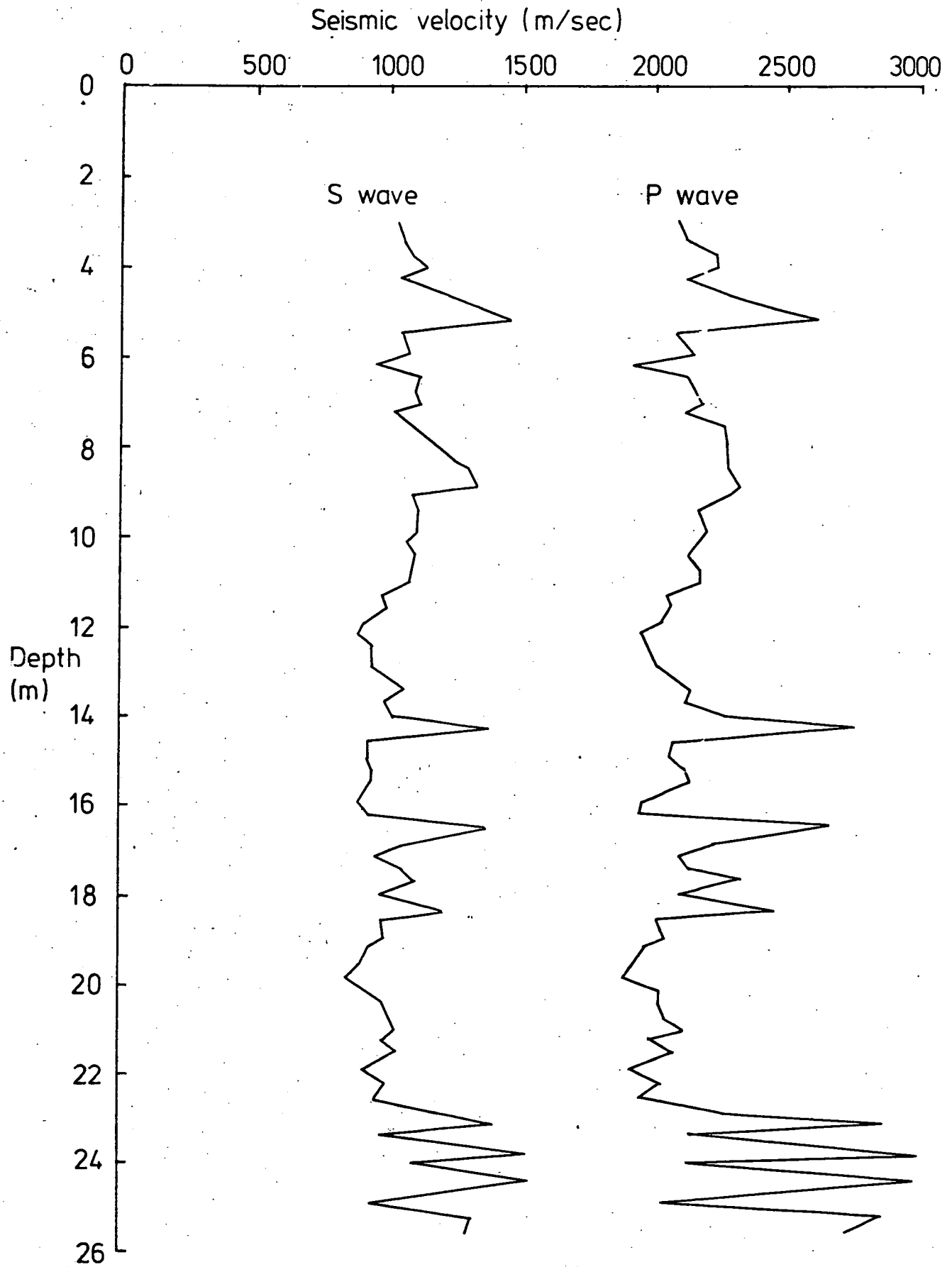

Fig. 3.13 VARIATION OF SEISMIC VELOCITY WITH DEPTH IN BOREHOLE 106 L.

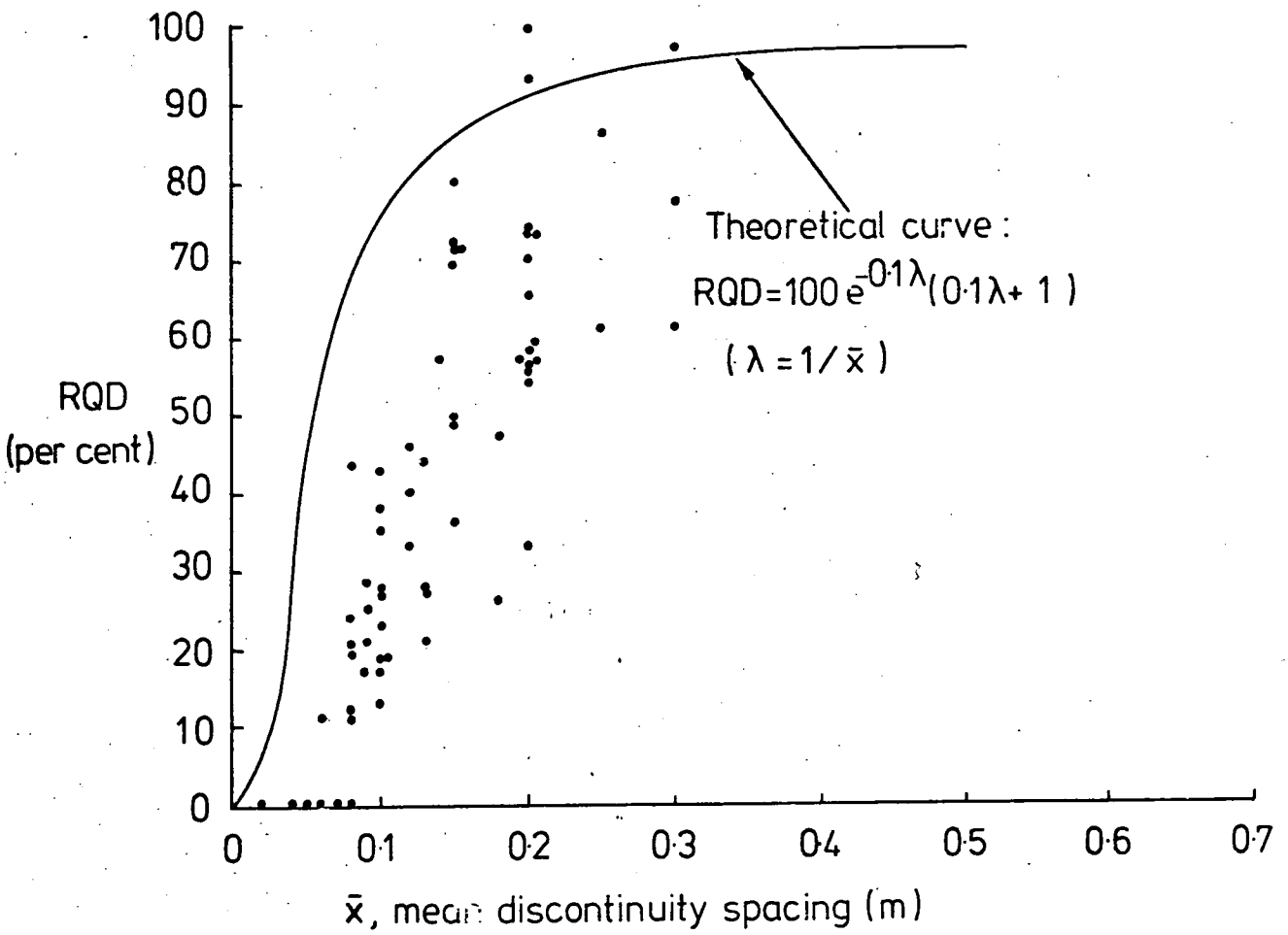

Fig. 3.14 RELATION BETWEEN RQD AND MEAN DISCONTINUITY SPACING FOR BOREHOLES 102,104,105 AND 102L.

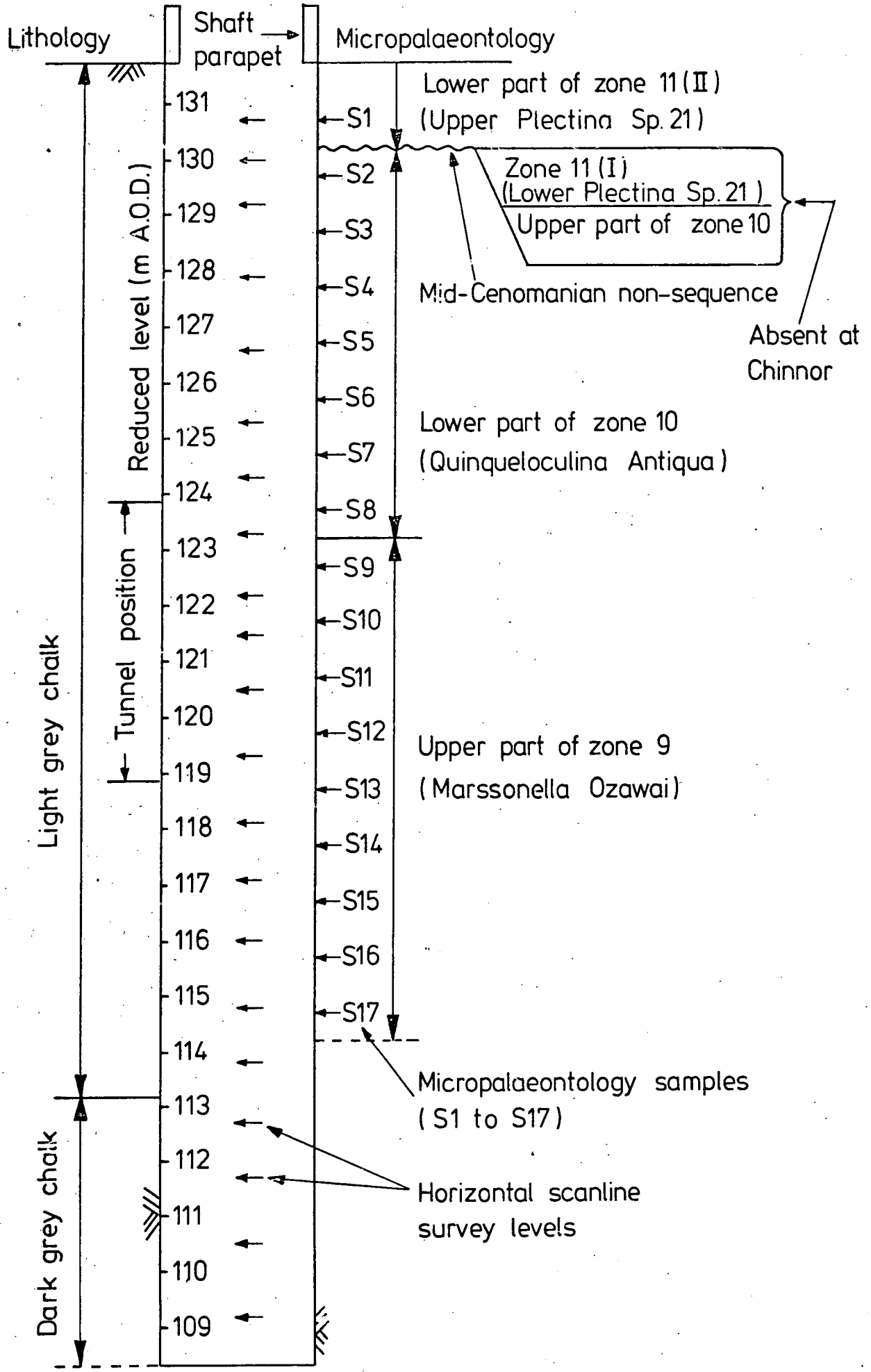

Fig. 3.15 SUMMARY OF THE GEOLOGY IN THE 3m DIAMETER SHAFT.

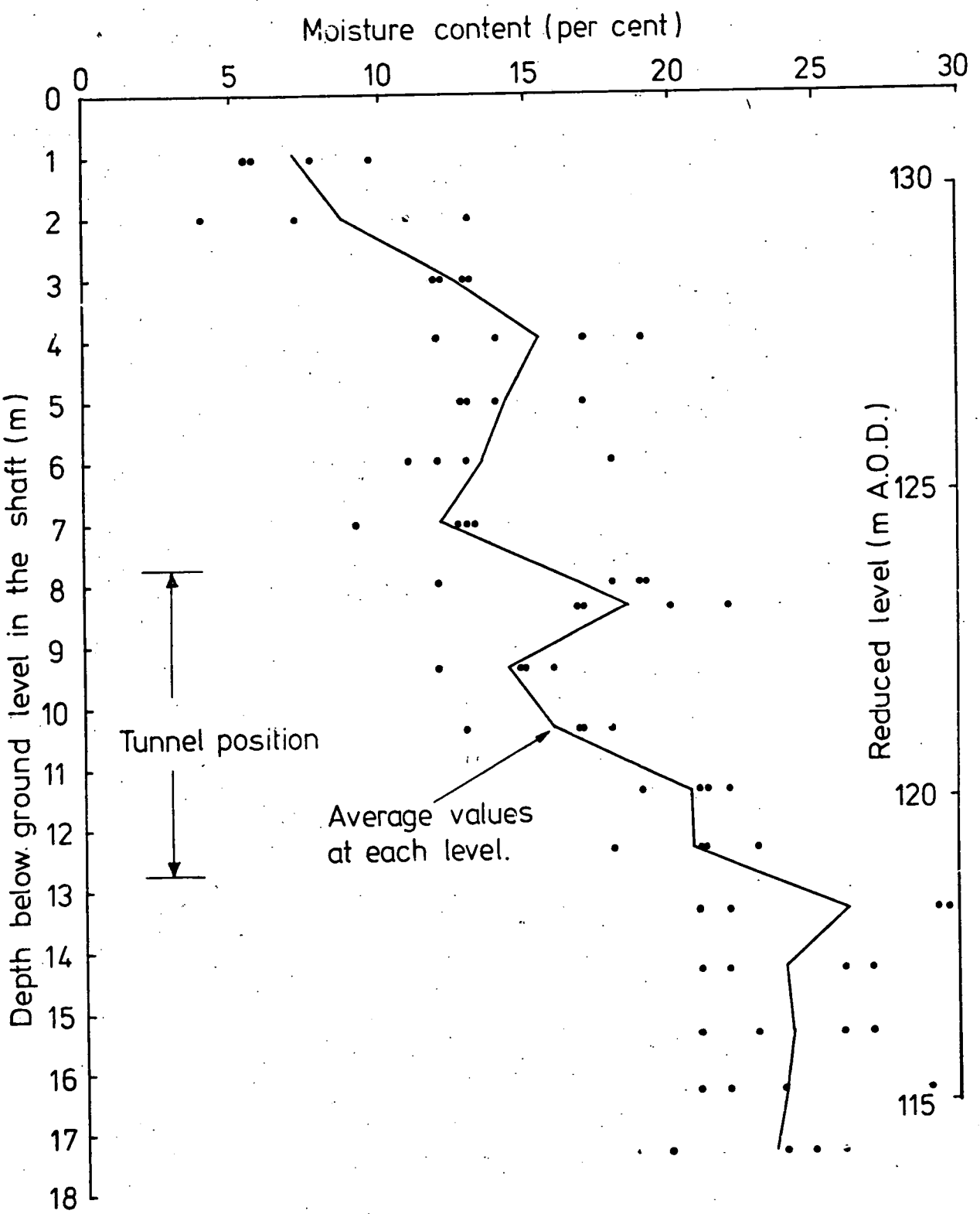

Fig. 3.16 VARIATION OF MOISTURE CONTENT WITH DEPTH IN THE SHAFT.

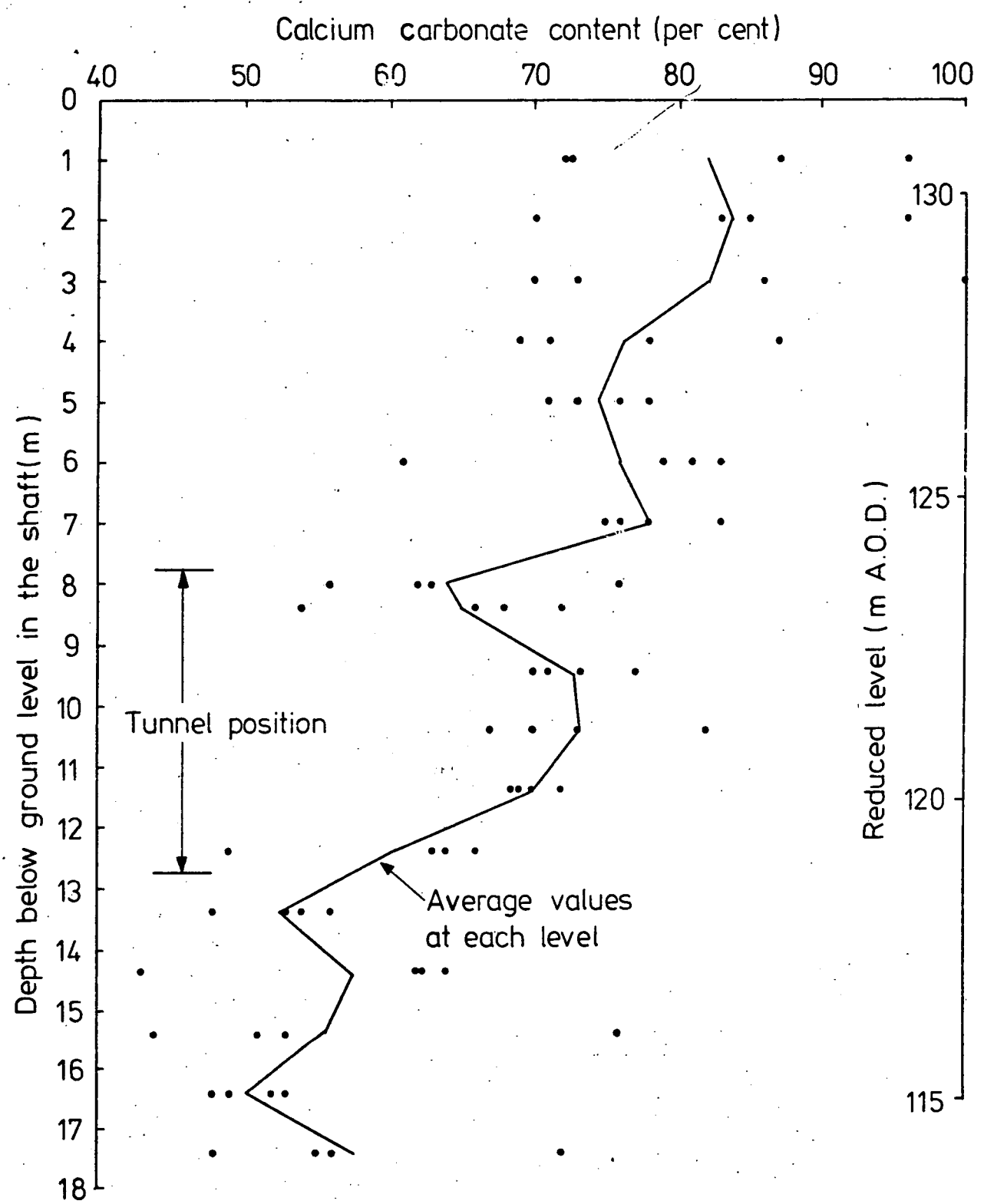

Fig. 3.17 VARIATION OF CALCIUM CARBONATE CONTENT WITH DEPTH IN THE SHAFT.

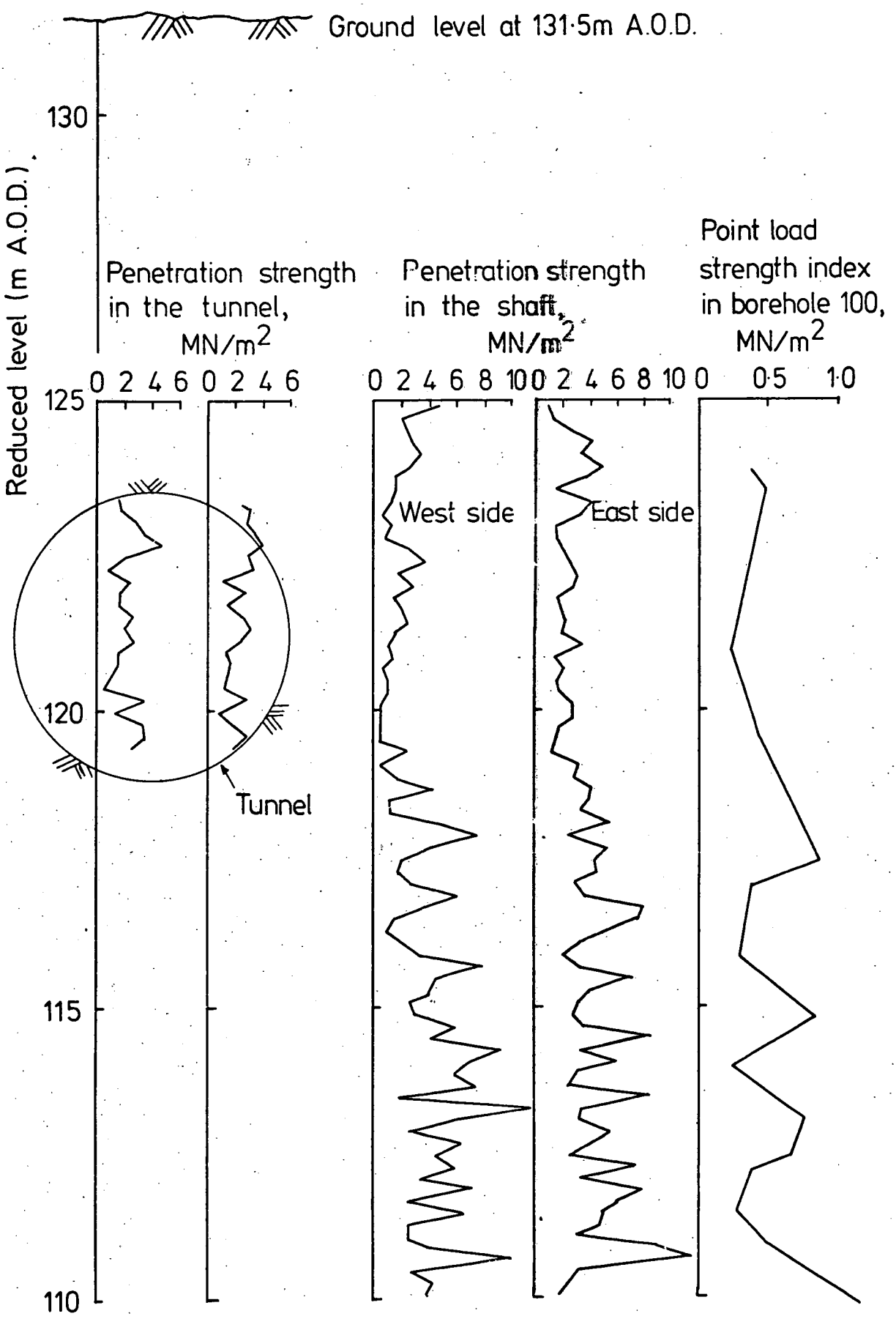

Fig. 3.18 COMARISON BETWEEN PENETRATION STRENGTH PROFILES IN THE SHAFT AND TUNNEL, AND POINT LOAD STRENGTH INDEX IN BOREHOLE 100.

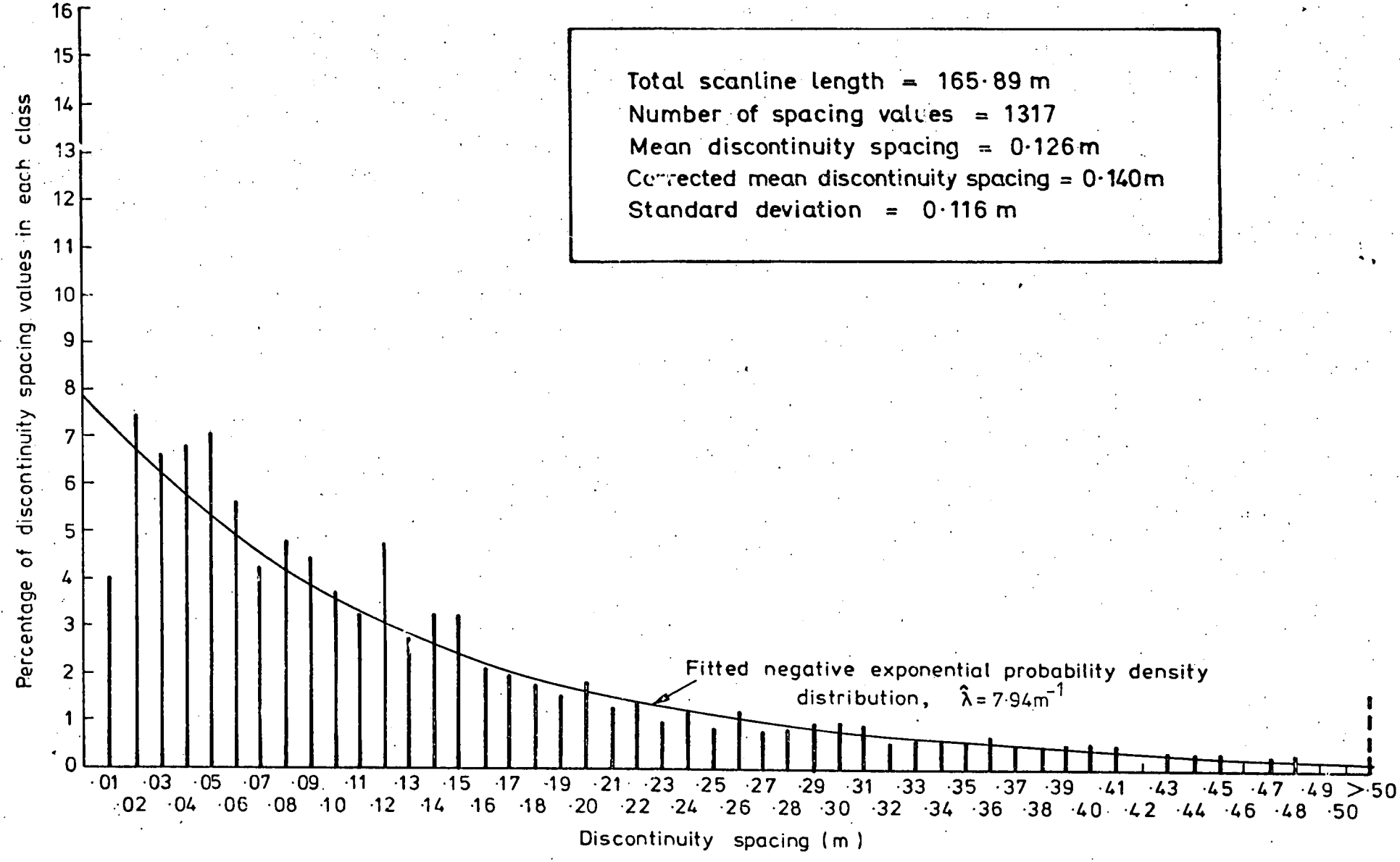

Fig. 3.19 DISCONTINUITY SPACING HISTOGRAM, SUM OF HORIZONTAL SCANLINES IN THE SHAFT

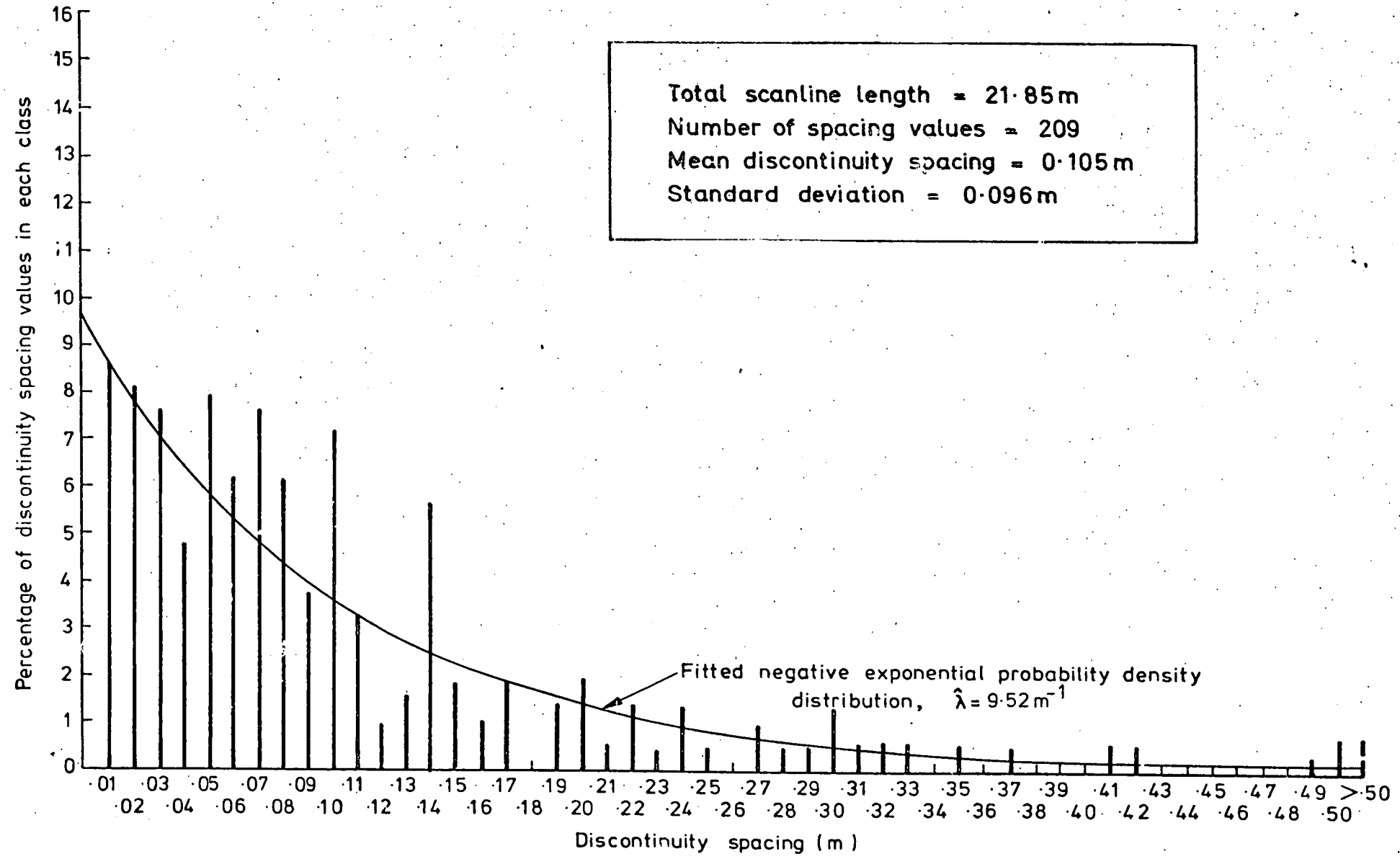

Fig. 3.20 DISCONTINUITY SPACING HISTOGRAM, VERTICAL SCANLINE IN THE SHAFT, EAST SIDE

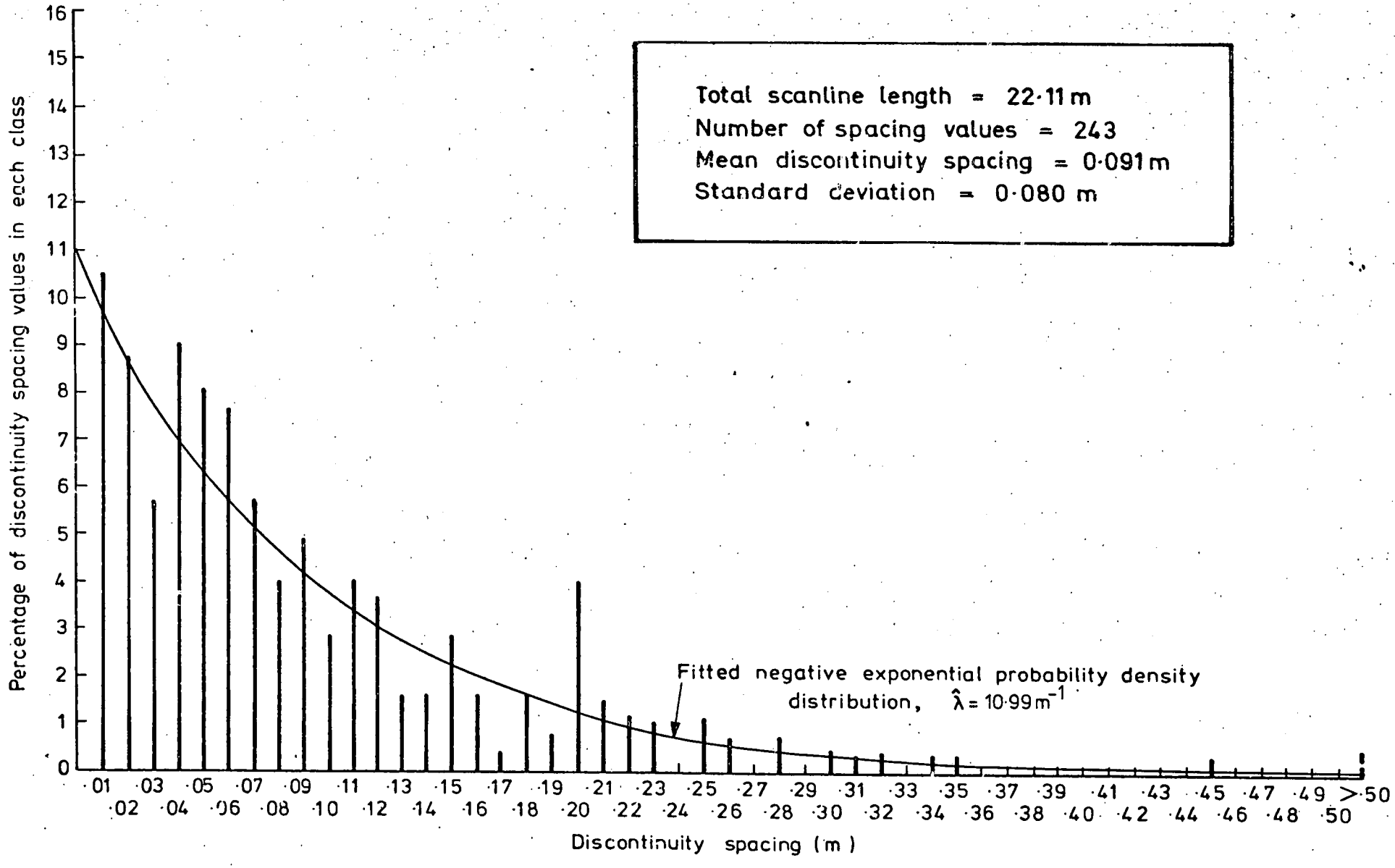

Fig. 3.21 DISCONTINUITY SPACING HISTOGRAM, VERTICAL SCANLINE IN THE SHAFT, WEST SIDE

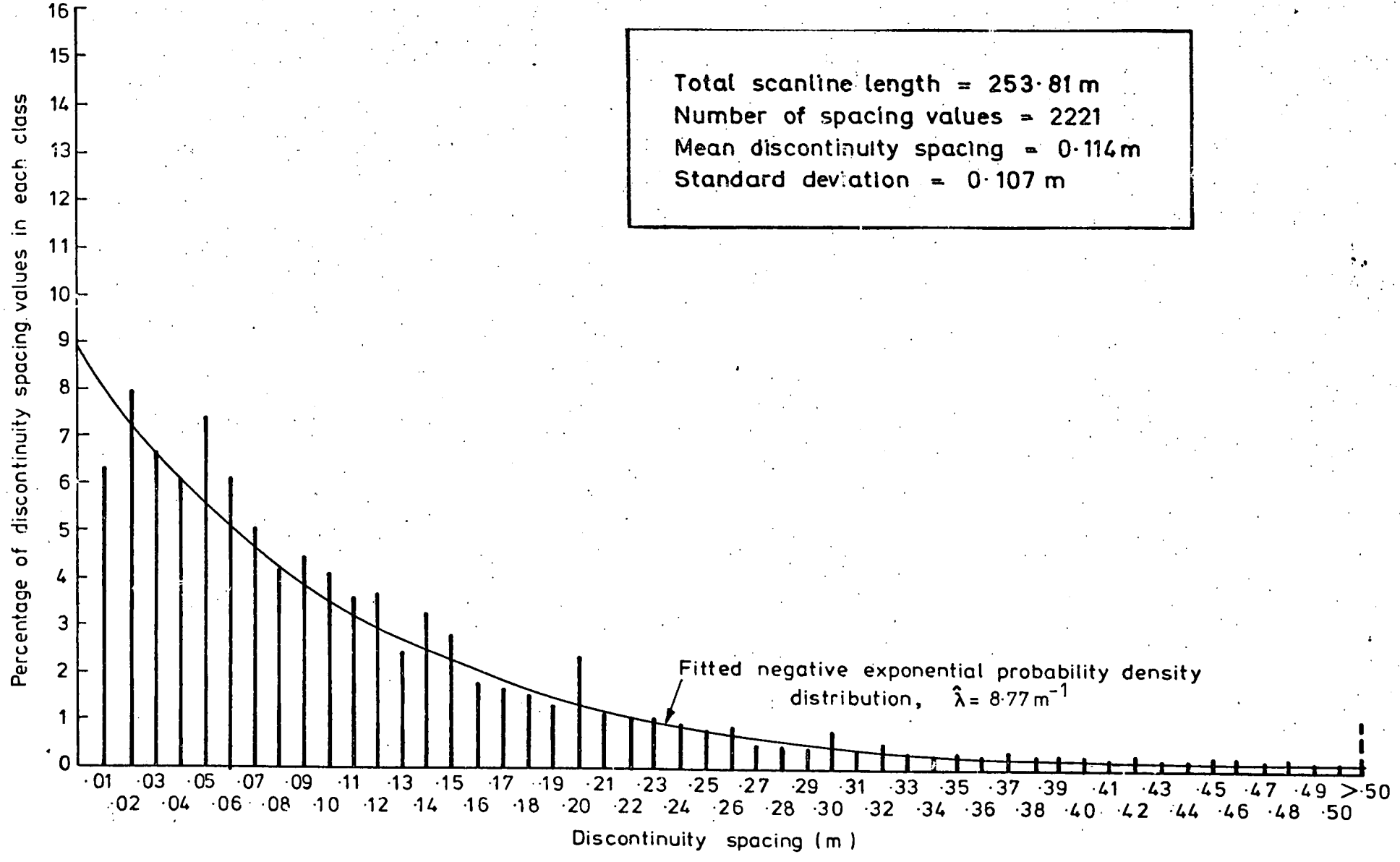

Fig. 3.22 DISCONTINUITY SPACING HISTOGRAM, SUM OF ALL SCANLINES IN THE SHAFT.

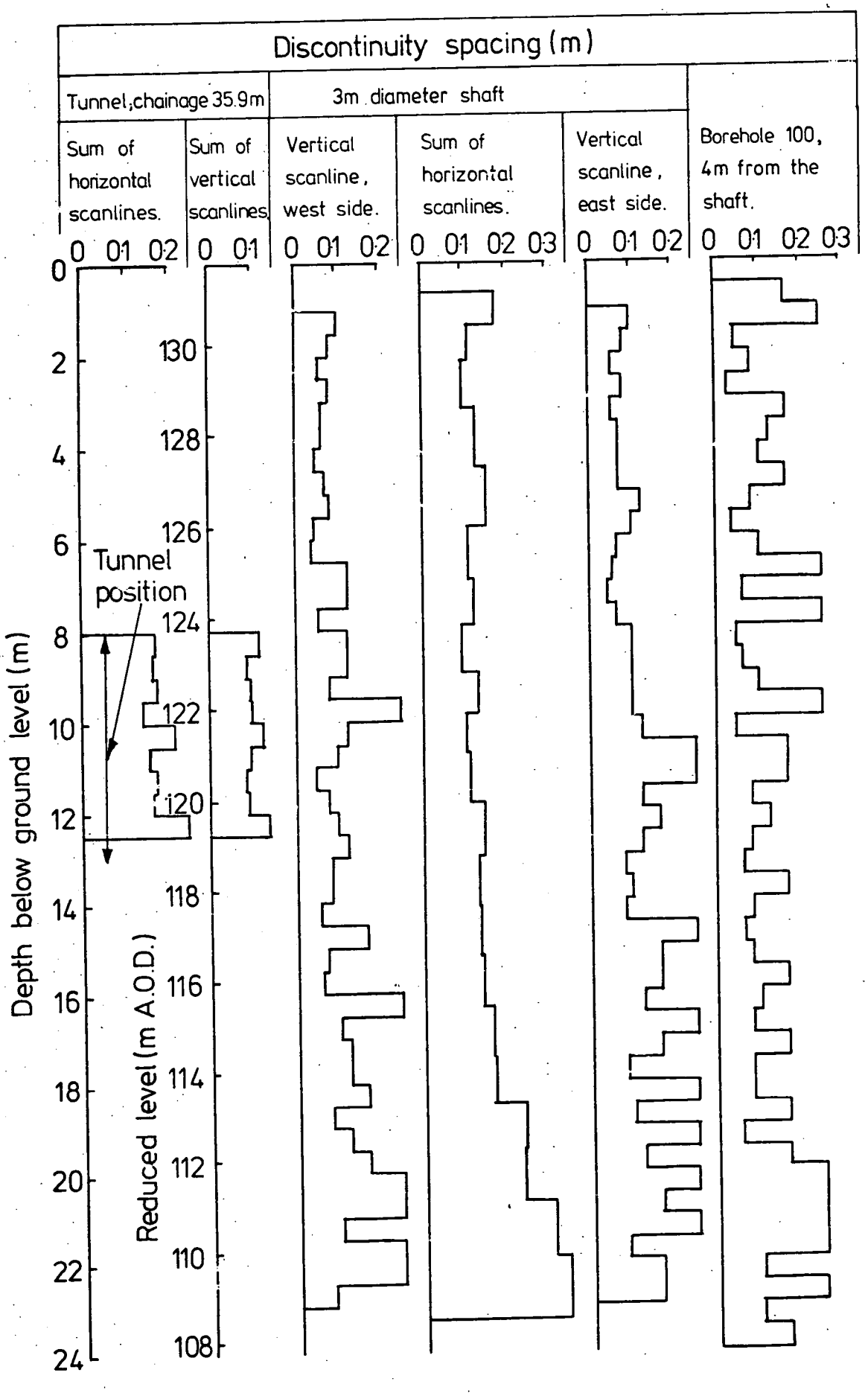

Fig. 3.23 VARIATION OF DISCONTINUITY SPACING WITH DEPTH, IN THE THE TUNNEL, SHAFT AND BOREHOLE 100.

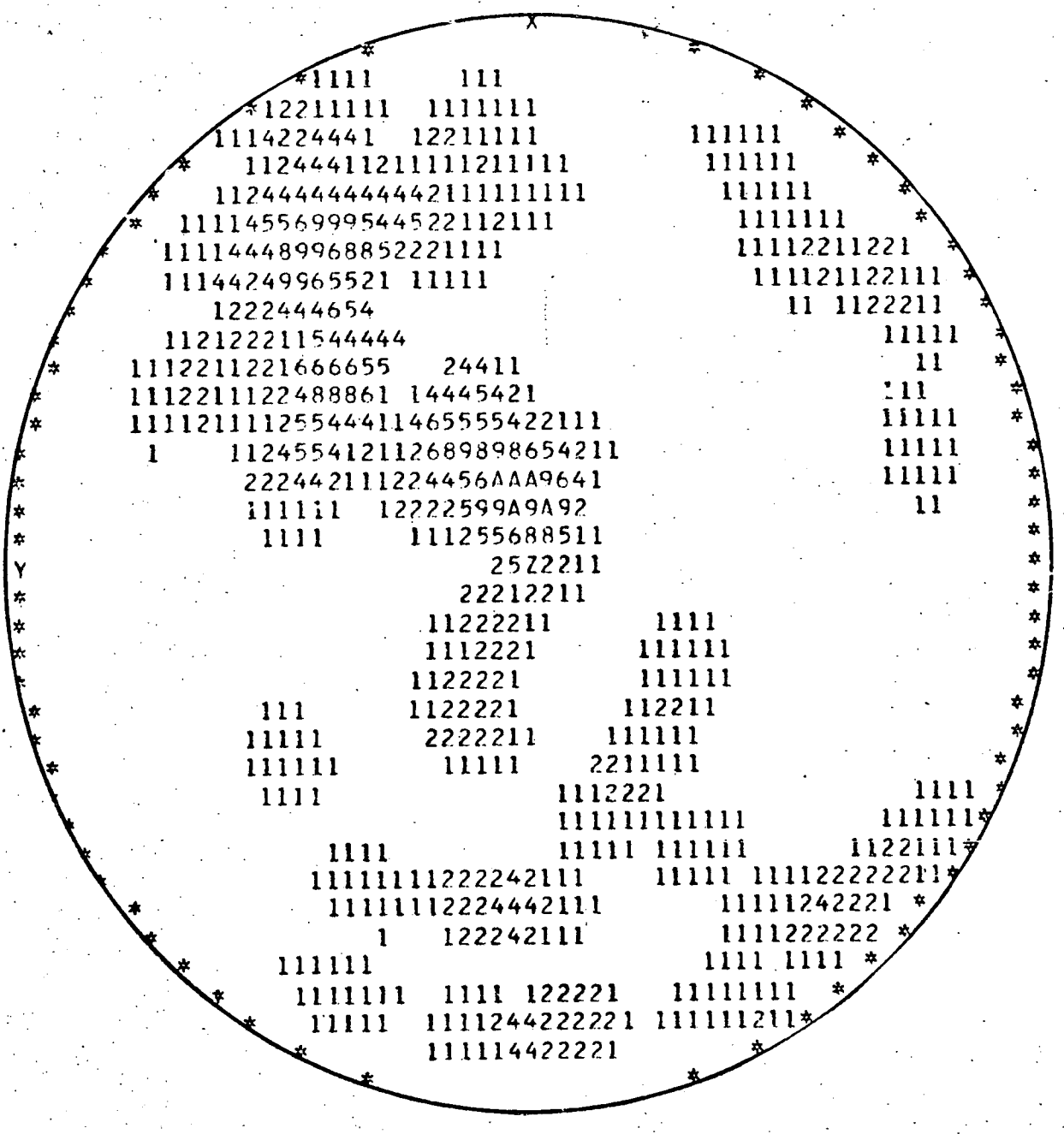

72 readings

Fig. 3.24 UPPER HEMISPHERE PROJECTION OF DISCONTINUITY ORIENTATION, TUNNEL CHAINAGE 35·9m.

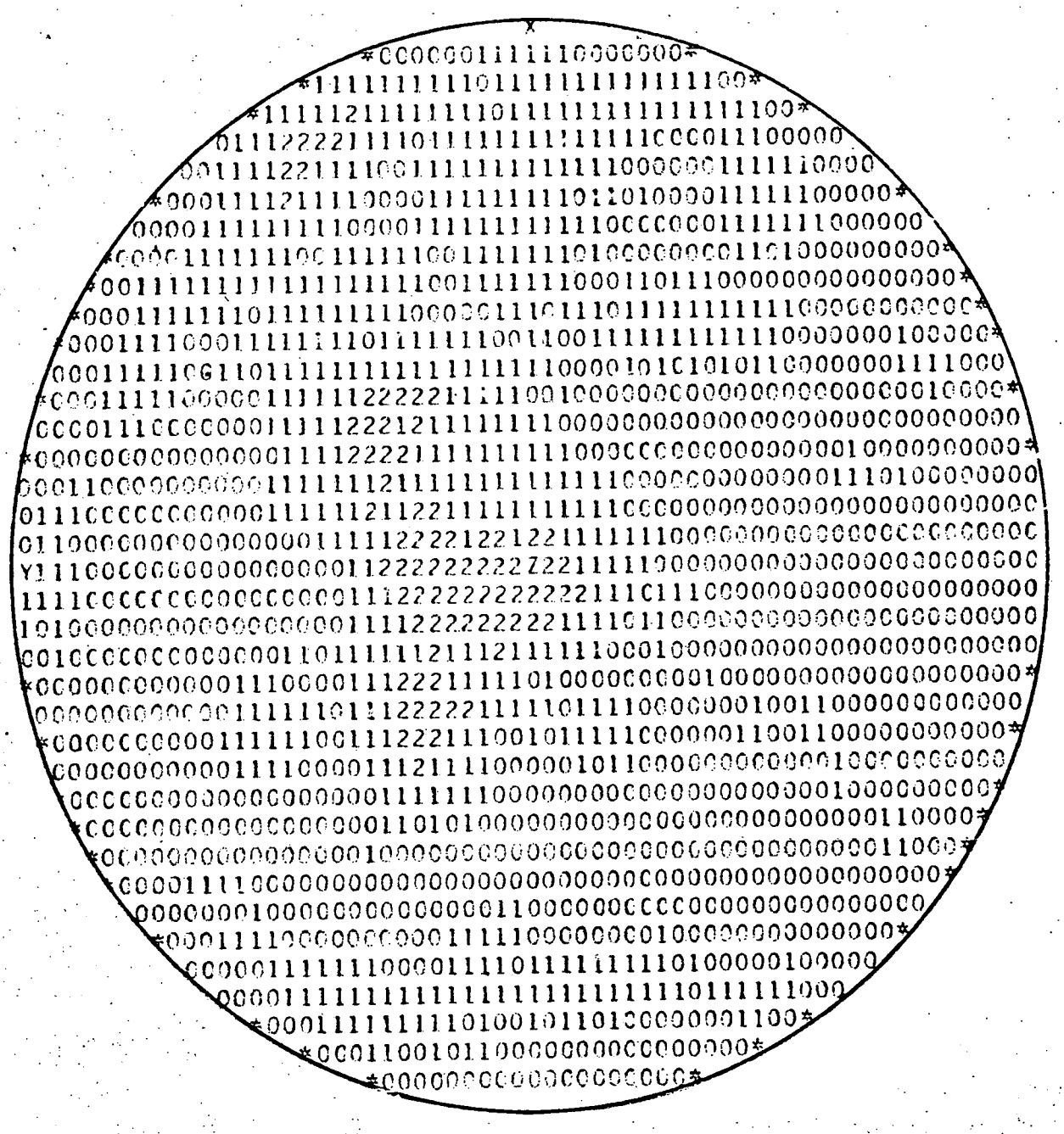

1333 readings

Fig.3.25 UPPER HEMISPHERE PROJECTION OF DISCONTINUITY ORIENTATION, SUM OF HORIZONTAL SCANLINES IN THE SHAFT.

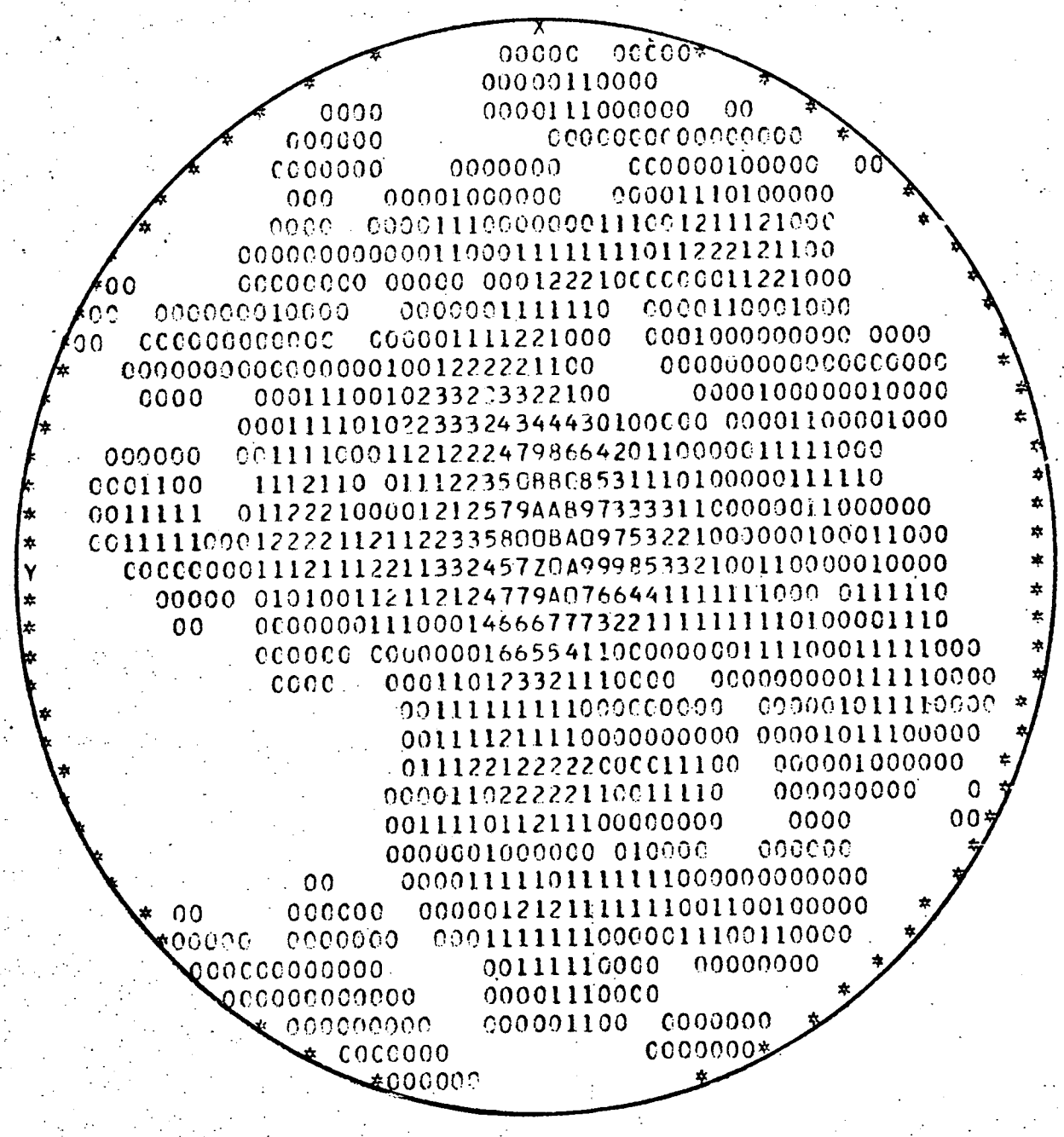

210 readings

Fig. 3.26 UPPER HEMISPHERE PROJECTION OF DISCONTINUITY ORIENTATION, VERTICAL SCANLINE IN THE SHAFT, EAST SIDE.

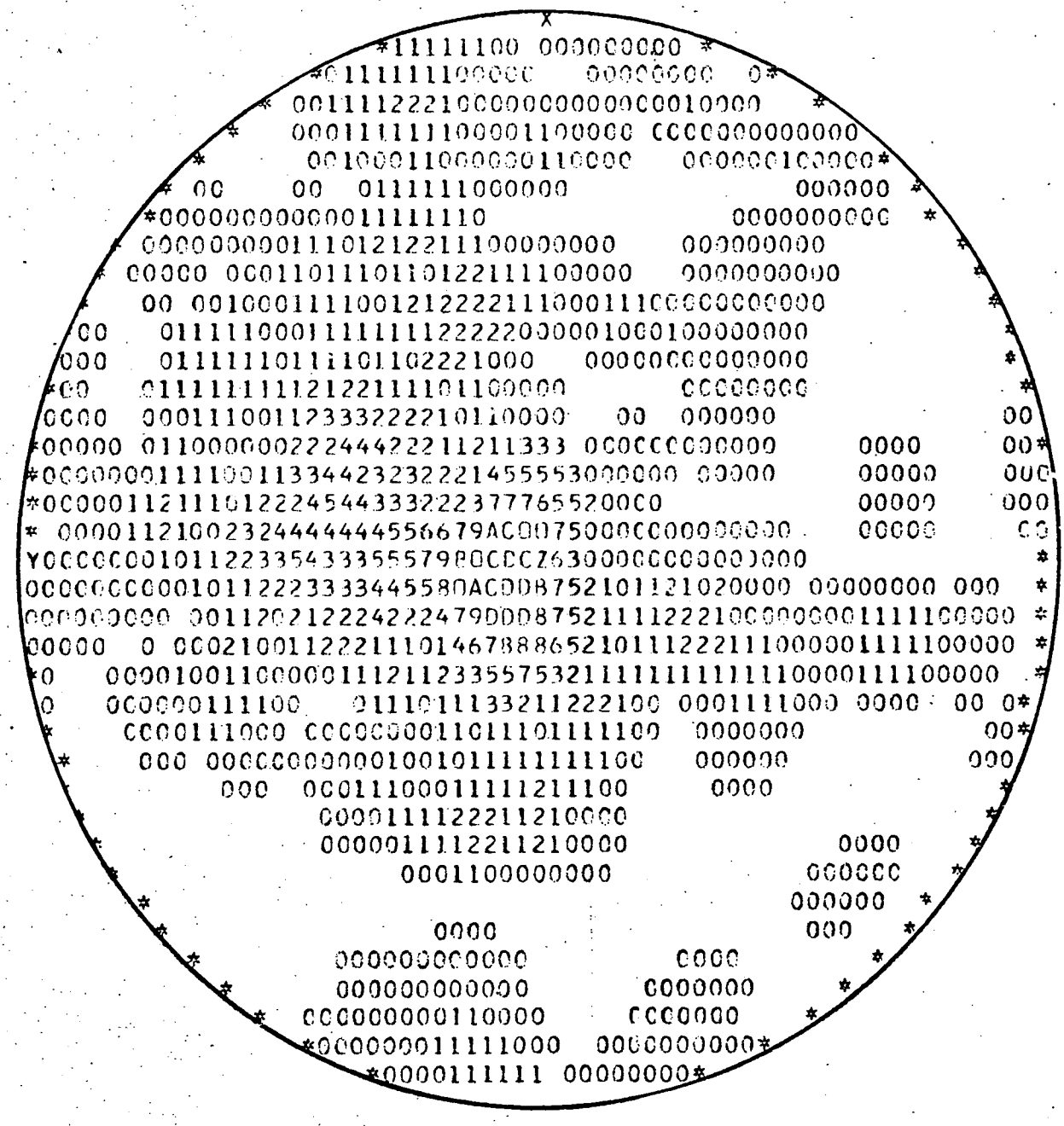

239 readings

Fig.3.27 UPPER HEMISPHERE PROJECTION OF DISCONTINUITY ORIENTATION, VERTICAL SCANLINE IN THE SHAFT, WEST SIDE.

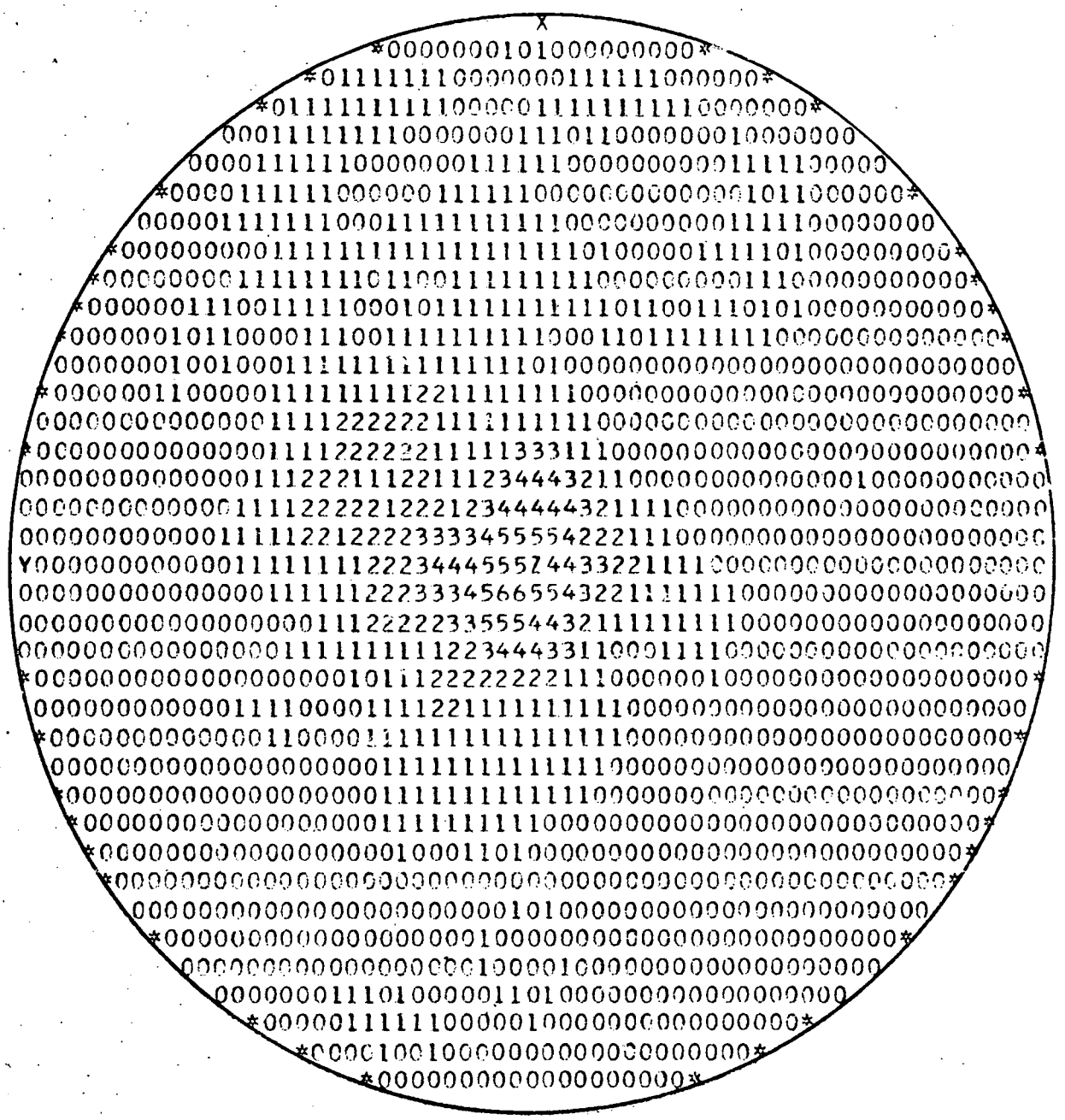

2231 readings

Fig. 3.28 UPPER HEMISPHERE PROJECTION OF DISCONTINUITY ORIENTATION, SUM OF ALL SCANLINES IN THE SHAFT.

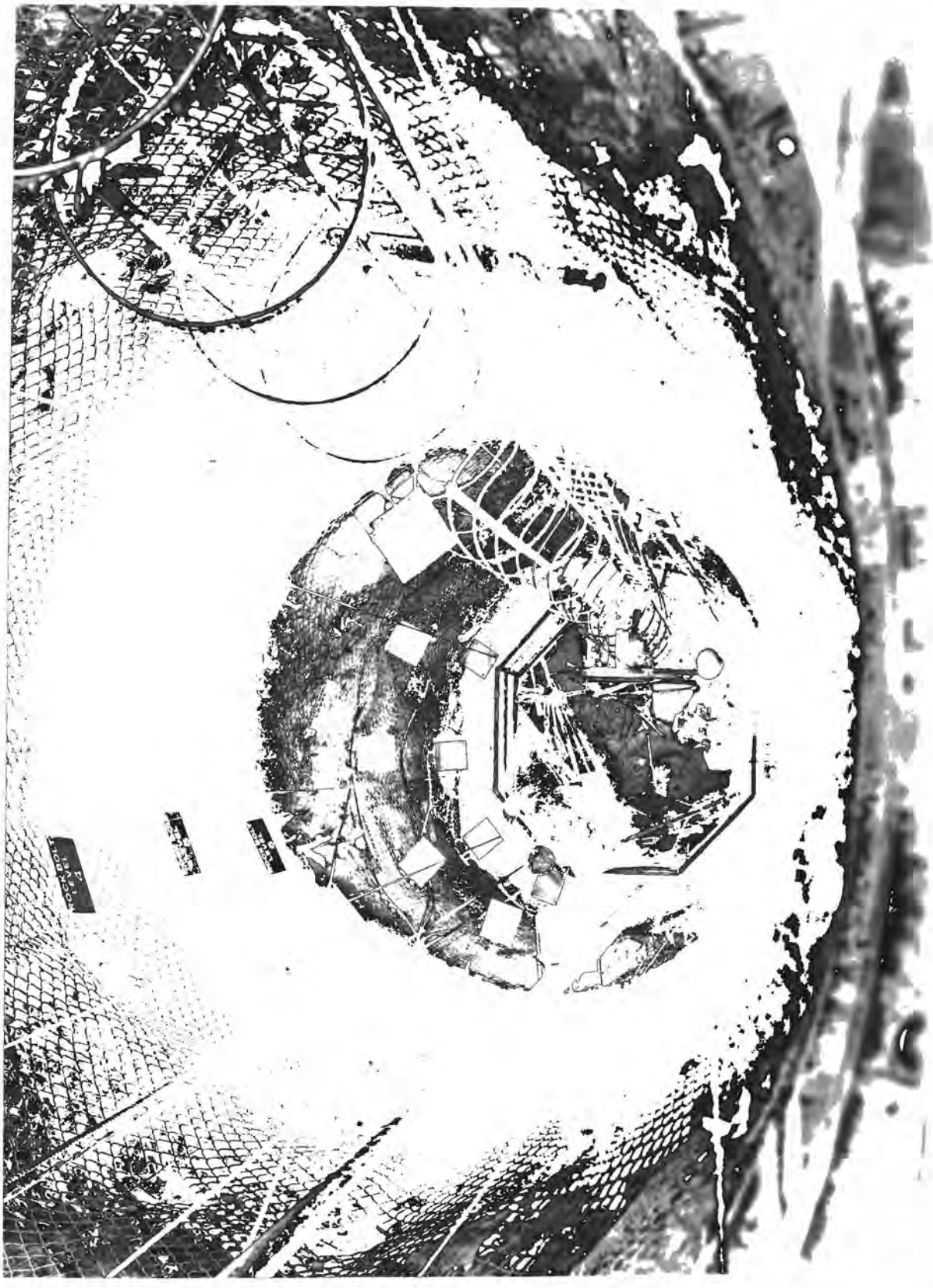

Plate 3.1 THE 3m DIAMETER SHAFT.

CHAPTER 4

HYDROLOGICAL INVESTIGATIONS IN THE 3m DIAMETER SHAFT AND 0.13m DIAMETER BOREHOLES

4.1 Introduction

The general aims of the hydrological investigation were to determine the mass permeability of the chalk near the shaft and hence:

(1) to compare the resulting permeability values with those obtained from boreholes on site,

(2) to use the permeability values determined for predicting water make likely to be encountered in the tunnel.

Ineson (1962) presented a now somewhat dated hydrogeological study of the permeability of the Chalk. He emphasised that the permeability of the Chalk is determined essentially by the effective permeability of the fissures as conduits. He concluded that areas of high permeability are often related to geological or geomorphological conditions likely to increase the amount of fracturing in the Chalk. It is probable that Chinnor, situated at the base of the scarp slope of the Chilterns, presents one such geomorphological situation. Edmunds *et al.*(1973) examining the Middle and Upper Chalk of Berkshire also emphasised the importance of fissure flow in the Chalk, stating that the estimated bulk permeability of the aquifer and its intergranular permeability differ by many orders of magnitude.

Foster (1974) and Foster and Milton (1974), studying the permeability and storage of an unconfined Chalk aquifer in east Yorkshire again

emphasised that the Chalk is a dominantly fissure-flow and fissure-storage formation. They concluded, from the results of a comprehensive hydrological investigation, that permeability in the aquifer under study was localised in two main layers of limited thickness associated with horizontal discontinuities which had experienced preferential solution.

A comprehensive study of the hydrological characteristics of the Lower Chalk in the Strait of Dover was presented by the Channel Tunnel Study Group (1964-1965)*. The results of borehole packer tests, emphasising the importance of fissure flow in controlling permeability in the chalk mass, also indicated that permeability decreased considerably with geological depth. This latter effect, noted for other rocks by Snow (1968), may largely be a result of the reduced fissure apertures at depth. Permeability values, broken down into the three lithological types of the Lower Chalk under the Strait of Dover, are presented in histogram form in Figure 4.1. The three Chalk types in this figure may be taken as comparable to those discussed in Chapter 3.

4.2 Methods of Investigation

4.2.1 Visual inspection

Examination of the side walls of the shaft below the water table proved that flow through discontinuities (fissure flow) was by far the greatest contributor to mass permeability. At some stages of excavation the total inflow for the shaft could be attributed to a dozen or so discontinuities, many of which produced water at rates exceeding $1 m^3/hr$ (220 gph).

* Crown Copyright, referred to here with the permission of the Channel Tunnel Unit, Department of the Environment

4.2.2 Evaluation of steady state flow

When the base of the shaft was excavated below 116m A.O.D., a submersible pump was installed, which maintained a depth of water in the shaft generally less than 0.1m. The output of this pump was measured at intervals between November 1973 and May 1974, thus determining the steady state flow of water into the shaft during this period. The measurements were obtained by monitoring the time taken to fill a container of known volume, taking the average of five repeat tests.

The results of this work are plotted in Figure 4.2. Also plotted in this Figure is a graph of progress of excavation in the shaft over this period, together with weekly rainfall data for the Chinnor area obtained from the Meteorological Office.

4.2.3 Monitoring rest water level regain

During the period November 1973 to February 1974, six tests were undertaken on water level rise in the shaft with the pump switched off. During each test and prior to switching the pump off, the steady state output was determined together with steady state level of water in the shaft and depth of the shaft. After switching the pump off, water levels were recorded at 15 minute intervals for the first hour, then at 30 minute intervals. Readings were taken, when possible, over a period of 48 hours. The final reading was assumed equal to the rest water level for the shaft, being equivalent to the ground water table. The curves resulting from this investigation are shown in Figure 4.3. During the period from November 1973 to May 1974 when the pump was switched off (in addition to the times of the tests described above) the rest water level in the shaft was recorded. The variation in rest water level over the seven month

period is shown in Figure 4.2.

4.2.4 Packer tests in boreholes

Water injection testing by the pumping-in method, described in Appendix D,was carried out by Soil Mechanics Ltd in boreholes 10, 11 and 12, referred to in Chapter 3. The tests were carried out over 3m lengths of borehole as drilling progressed, using the single pneumatic packer system. The results, corrected for static head and head loss through the supply hoses, were presented by Soil Mechanics Ltd in the form of pressure/inflow curves. These curves were then used to calculate the *in situ* mass permeability of the chalk near the boreholes. The results of nineteen tests are presented graphically in Figure 4.4.

4.3 Determination of mass permeability

Using the results obtained in the shaft as described in Section 4.2, two methods were used to obtain values of the mass permeability of ground near the shaft.

4.3.1 Method based on Dupuit's solution

If certain assumptions are made concerning the hydrological properties of the shaft/ground system it is feasible to apply Dupuit's equations for flow through an isotropic medium (derived from solutions of Laplace's equation) to this situation. The assumptions are that the shaft completely penetrates to the base of an isotropic, homogeneous medium, in which there is laminar flow and a co-axial boundary of constant head in an unconfined aquifer. The assumption that the shaft terminates at an impermeable horizon is perhaps invalid in this case. However, visual inspection

revealed that there was no significant influx of water through the base of the shaft. Foster and Milton (1974) confirmed that assumptions of laminar flow in fissured Chalk were valid under hydraulic gradients associated with pumping rates up to approximately $300m^3/hr$. It is therefore concluded that the errors introduced by making the above assumptions are small.

For unconfined flow: if H_1 is the head in an observation well at distance r_1 from the pumping well, H_2 the head at a distance r_2 and Q the constant discharge from the pumping well (Figure 4.5). The permeability, k, of the material is given by:

$$k = \left(\frac{Q}{\pi(H_2^2 - H_1^2)} \right) 2.3 \log_{10} r_2/r_1 \quad \ldots.(4.1)$$

Since there were no functioning observation wells near the shaft, r_2 was taken as equal to the radius of influence of draw-down of the shaft (R in Figure 4.5). H_2 was therefore equal to the draw-down in the shaft, d. Using the shaft as the first observation well, r_1 becomes r_s (radius of the shaft) and H_1 equal to zero.

Therefore:

$$k = \frac{Q}{\pi d^2} 2.3 \log_{10} R/r_s \quad \ldots.(4.2)$$

For each of the six rest water level regain tests two values of Q were used:

a. The steady state discharge from the shaft prior to pumping (Q_s).

b. The flow of water into the shaft during the first 2 metre rise

of water (Q_c), as determined from the appropriate rest water level regain curve.

Three values for R were taken: 1500m, 150m, and 15m, however since k is relatively insensitive to changes in R a reasonably small spread of results was obtained. The values of k determined for each of the tests are shown in Table 4.1.

4.3.2 Method based on Kirkham's solution

Kirkham (1954) calculated a solution for mass permeability of material near a borehole. He showed that if the material below the bottom of a borehole is regarded as impermeable then permeability may be calculated from rest water level regain data:

$$k = 0.617 \frac{r_s}{Sd} \frac{\Delta h}{\Delta t} \qquad \ldots.(4.3)$$

Where: d = depth of the shaft below the water table

r_s = radius of the shaft

Δh = rise of water level in a time Δt

h = average height of the water level above the bottom of the hole during the time Δt (Figure 4.5).

Application of Equation 4.3 is again based on the assumption that the shaft terminates at an impermeable boundary. However, since the same assumption was made when applying Dupuit's equation to this problem, the results of the two analyses will be compatible.

Table 4.1 Permeability values determined from tests in the 3m diameter shaft at Chinnor

A. Dupuit solution, Q_s = steady state flow into the shaft

Date	Q_s (m^3/sec)	d(m)	R(m)	k (m/sec)
8 Nov	5.581×10^{-4}	2.280	1500	23.6×10^{-5}
			150	15.7×10^{-5}
			15	7.9×10^{-5}
17 Nov	5.981×10^{-4}	3.698	1500	9.6×10^{-5}
			150	6.4×10^{-5}
			15	3.2×10^{-5}
23 Nov	5.381×10^{-4}	4.355	1500	6.2×10^{-5}
			150	4.2×10^{-5}
			15	2.1×10^{-5}
1 Dec	5.192×10^{-4}	5.340	1500	4.0×10^{-5}
			150	2.7×10^{-5}
			15	1.3×10^{-5}
7 Dec	10.090×10^{-4}	5.900	1500	6.4×10^{-5}
			150	4.2×10^{-5}
			15	2.1×10^{-5}
8 Feb	45.250×10^{-4}	12.280	1500	6.6×10^{-5}
			150	4.4×10^{-5}
			15	2.2×10^{-5}

Table 4.1 (Continued) Permeability values determined from tests in the 3m diameter shaft at Chinnor

B. Dupuit solution, Q_c = flow derived from curve of rest water level regain in the shaft.

Date	Q_c (m^3/sec)	d(m)	R(m)	k (m/sec)
8 Nov	4.446×10^{-4}	2.280	1500	18.8×10^{-5}
			150	12.5×10^{-5}
			15	6.3×10^{-5}
17 Nov	5.611×10^{-4}	3.698	1500	9.0×10^{-5}
			150	6.0×10^{-5}
			15	3.0×10^{-5}
23 Nov	5.480×10^{-4}	4.355	1500	6.3×10^{-5}
			150	4.2×10^{-5}
			15	2.1×10^{-5}
1 Dec	5.237×10^{-4}	5.340	1500	4.0×10^{-5}
			150	2.7×10^{-5}
			15	1.3×10^{-5}
7 Dec	9.426×10^{-4}	5.900	1500	6.0×10^{-5}
			150	4.0×10^{-5}
			15	2.0×10^{-5}
8 Feb	43.639×10^{-4}	12.280	1500	6.4×10^{-5}
			150	4.2×10^{-5}
			15	2.1×10^{-5}

C. Based on Kirkham's solution

Date	Δt(sec)	d(m)	S	k (m/sec)
8 Nov	31800	2.280	1.20	2.1×10^{-5}
17 Nov	25200	3.698	1.20	1.4×10^{-5}
23 Nov	25800	4.355	1.51	1.1×10^{-5}
1 Dec	27000	5.340	1.70	0.8×10^{-5}
7 Dec	15000	5.900	1.75	1.2×10^{-5}
8 Feb	3240	12.280	2.59	1.8×10^{-5}

In Equation 4.3, S is a geometrical function given by:

$$S = \cos\frac{\pi h}{2d} \cdot \frac{K_2(\pi r_s/2d)}{K_1(\pi r_s/2d)} - \frac{1}{3^2}\cos\frac{3\pi h}{2d} \cdot \frac{K_2(3\pi r_s/2d)}{K_1(3\pi r_s/2d)}$$

$$+ \frac{1}{5^2}\cos\frac{5\pi h}{2d} \cdot \frac{K_2(5\pi r_s/2d)}{K_1(5\pi r_s/2d)} - \ldots \qquad \ldots.(4.4)$$

in which $K_1(\pi r_s/2d)$ and $K_2(\pi r_s/2d)$, etc. are Bessel functions defined by the infinite series:

$$K_1(x) = -\left\{\left[0.5772 + \log_e\frac{x}{2}\right]\left[1 + \frac{x^2}{2^2(1)^2} + \frac{x^4}{2^4(2)^2} + \frac{x^6}{2^6(6)^2} \ldots\right]\right\}$$

$$+ \left\{\frac{1}{(1)^2}\frac{x^2}{2^2}(1)\right\} + \left\{\frac{1}{(2)^2}\frac{x^4}{2^4}(1 + \tfrac{1}{2})\right\}\ldots \qquad \ldots.(4.5a)$$

$$K_2(x) = \left\{\left[0.5772 + \log_e\frac{x}{2}\right]\left[\frac{x}{2} + \frac{x^3}{16} + \frac{x^5}{12(2)^5} + \frac{x^7}{144(2)^7} + \ldots\right]\right\}$$

$$+ \frac{1}{x} - \left\{\frac{x}{2}(1 - \tfrac{1}{2})\right\} - \left\{\tfrac{1}{2}\left(\frac{x}{2}\right)^3(1 + \tfrac{1}{2} - \tfrac{1}{4})\right\} \ldots \qquad \ldots.(4.5b)$$

Solution of these infinite series to obtain the function S is complicated and time consuming. However, Spangler (1951) using values of $K_1(x)$ and $K_2(x)$ tabulated in the British Association Tables (1937) produced a graph giving S values for different $h/_d$ and $r/_d$ ratios (Figure 4.6). In this Figure, r is directly equivalent to r_s in Equations 4.3 and 4.4.

Using Figure 4.6 graphs of S versus $r/_d$ at six specific $h/_d$ ratios were constructed (Figure 4.7). The six $h/_d$ values taken were those appropriate to the six rest water level regain tests performed in the shaft. It was therefore then possible to read off values of the function S relating to each of the tests.

Evaluation of permeability based on Kirkham's solution was performed using the six rest water level regain curves reproduced in Figure 4.3. In Equation 4.3, Δh was taken as the first 2m of rise during the test, and Δt the time required for this 2m rise, h was therefore equal to 1m. The radius of the shaft was assumed to be constant at 1.5m. The values of k produced using this method are listed in Table 4.1.

4.4 Discussion of results, and comparison with values obtained from packer tests in boreholes.

The values of mass permeability k determined using the methods described in 4.2 are summarised in Table 4.1. It is clear that the Dupuit permeability values closest to those determined using Kirkham's solution are those values based on an R (radius of drawdown influence) of 15m, and a Q (rate of flow of water into the shaft) derived from the first part of the rest water level regain curve (Q_c). This latter point is to be expected since the Kirkham solution k values were also derived using the first part of the rest water level regain curve. It is likely, however, that 15m is a rather low estimate for R. The Dupuit values for permeability therefore work out approximately two to three times larger than the values derived using Kirkham's solution. Both these sets of results are compared (in Figure 4.4) with the *in situ* permeability values determined by Soil Mechanics Ltd. In most cases the Soil Mechanics values

are at least half an order of magnitude lower than the values* determined from the shaft. The probable reasons for this discrepancy are as follows:

1. The *in situ* permeability tests were conducted in recently cored boreholes. Visual inspection, and also experience with rock-bolt pullout tests, have proved that holes drilled in the Lower Chalk at Chinnor develop a smear of putty chalk. During a packer test this smear would tend to seal off the borehole and produce a lower value for permeability. In the shaft however, continual pumping, resulting in long term fissure flow will have caused a 'washing out' of discontinuities, producing a slight increase in permeability near the shaft. It is also evident that the method of excavation in the shaft will have obviated the smearing effect.

2. The *in situ* packer tests sampled a 3m length of 131mm diameter borehole. Vertical discontinuity scanlines carried out in various parts of the Chinnor quarry and the shaft reveal an average vertical spacing between discontinuities of approximately 0.15m. It is therefore unlikely that the sample area for the packer test will include more than 20 or 30 intersected discontinuities. It is also apparent from visual inspection in the shaft that only a small percentage of discontinuities actually significantly contribute to the secondary permeability of the ground. It may therefore be concluded that the highly non-homogeneous nature of the secondary permeability in the chalk at Chinnor, caused by the selective 'fissure' flow, will lead to significant discrepancies between permeabilities determined by sampling a 3m length of borehole and those determined by sampling several metres of a 3m diameter shaft.

---

* Excepting those calculated using Kirkham's solution.

Comparison between Figures 4.1 and 4.4 indicates that the packer permeability values obtained under the Strait of Dover are generally between 1 and 2 orders of magnitude less than those obtained at Chinnor. Scanline surveys taken on Lower Chalk exposed in the machine erection chamber of the Channel Tunnel indicate mean discontinuity spacing values of approximately 0.4m (Chapter 11). It is probable that this higher discontinuity spacing under the Channel combined with the greater overburden are responsible for the lower permeability values.

The importance of discontinuities in controlling the magnitude of mass permeability is further emphasised by the results of laboratory permeability tests carried out by Soil Mechanics Ltd. on intact samples and discussed in Chapter 3. Values of permeability for the intact samples, ranging from 1.4×10^{-10} m/sec to 2.3×10^{-8} m/sec, are clearly several orders of magnitude lower than the values of mass permeability obtained in the field. These results serve to confirm for the Lower Chalk at Chinnor the already well established ideas concerning water flow in the Middle and Upper Chalk discussed by Edmunds *et al.* (1972), and Foster and Milton (1974).

4.5 Prediction of water make in the Chinnor tunnel

Two methods were used to predict water make in the tunnel:

1. A direct empirical method, involving direct comparison between the shaft and tunnel.

2. A method using previously-determined permeability values inserted into a standard formula.

4.5.1 Empirical method

A direct empirical approach was adopted as a first approximation to predicting possible water make in the tunnel. For this approach it was assumed that under conditions of constant permeability and aquifer recharge there are two single factors controlling water make in an excavation:

(a) The internal surface area of the excavation below the water table.

(b) The head of water above the base of the excavation, (d and H in Figure 4.5).

In terms of the shaft, therefore, it was assumed that there was a linear relation between d and water make per unit area of shaft wall below the rest water level. Figure 4.8 shows this linear relation plotted from tests carried out in the shaft on 8 February 1974. From this line, water make values per unit area of shaft for six values of d were calculated. These water make values were then applied directly to the inner surface of a metre run of tunnel, assuming H (in Figure 4.5) to be equivalent to d. The resulting predictions of water make per metre run of tunnel, tabulated in Figure 4.8, are plotted graphically in Figure 4.9. These results are presented only as a very rough guide to what water make conditions may be expected in the tunnel, since, although it is safe to assume that similar conditions of permeability and aquifer recharge apply in the shaft and tunnel it is unreasonable to assume strict hydrological compatibility in view of the widely different geometries.

4.5.2 Theoretical method

The Channel Tunnel Study Group (1965) outlined a method for predicting water make in a horizontal tunnel of a given diameter knowing the permeability of the surrounding material and the ground water conditions. They proposed the following relation:

$$Q_t = 2\pi k \frac{H}{\ln\left(\frac{2T}{r_t} - 1\right)} \qquad \ldots.(4.6)$$

where Q_t = water make per unit length of tunnel

H = the distance between the invert level of the tunnel and the free water surface

T = the thickness of ground assumed to have isotropic characteristics of permeability above the tunnel

r_t = radius of the tunnel

At Chinnor the water table is below ground level, therefore T = H and:

$$Q_t = \frac{2\pi k\, H}{2.3 \log_{10}\left(\frac{2H}{r_t} - 1\right)} \qquad \ldots.(4.7)$$

Figure 4.9 shows values of Q_t for varying water table conditions and six values of mass permeability. It is interesting to note that in this Figure the curve determined from Section 4.5.1 (based on direct comparison between the shaft and the tunnel) shows a good correlation with the curve based on the formula proposed by the Channel Tunnel Study Group, assuming a permeability of between 1×10^{-5} m/sec and 2×10^{-5} m/sec.

Actual water make in the tunnel may well be lower than predicted in Figure 4.9 since:

1. Long term pumping will lead to extensive dewatering of the area near the tunnel.

2. Drier summer conditions will mean less water flow directly from the ground surface into the tunnel, and less aquifer recharge.

3. Smearing of the tunnel surface with putty chalk as a result of cutting and movement of the shield and reaction ring will cause blocking of many of the discontinuities, and a reduction in water make.

Evaluation of the predicted values of water make in the light of those actually encountered in the tunnel was impossible since, contrary to the original plans, the tunnel was driven above the water table to avoid the problems of water inflow described above.

4.6 Summary and conclusions

1. An investigation of the hydrological characteristics of the Lower Chalk was carried out in a 3m diameter shaft and 0.13m diameter boreholes. Visual inspection in the shaft indicated that a large part of the water flow came from relatively few discontinuities.

2. A variety of techniques was used to interpret the data obtained from the shaft. Permeability values obtained from the shaft were found to be somewhat larger than those obtained from packer tests in boreholes. It is likely that smearing of putty chalk combined with selective fissure

flow effects produced the lower permeability values in the boreholes.

3. Packer permeability values obtained for the Lower Chalk under the Strait of Dover were found to be between 1 and 2 orders of magnitude less than those obtained at Chinnor. It is probable that the higher discontinuity spacing under the Channel combined with the greater overburden are responsible for the lower permeability values.

4. The importance of discontinuities in controlling the magnitude of mass permeability, emphasised by laboratory tests on intact samples, serves to confirm for the Lower Chalk at Chinnor the already well-established ideas concerning water flow in the Middle and Upper Chalk.

5. Empirical and theoretical methods, used to predict water make in the Chinnor tunnel, were found to give reasonably comparable results. Evaluation of the predicted values of water make in the light of those actually encountered in the tunnel was impossible, since the tunnel remained above the water table.

6. It is concluded that one of the major problems of tunnelling in highly fractured Lower Chalk below the water table could be that of excessive water inflow. The sensitivity of the magnitude of permeability to discontinuity characteristics, in particular discontinuity spacing, suggests that precise evaluation of these properties should form an integral part of any tunnel site investigation.

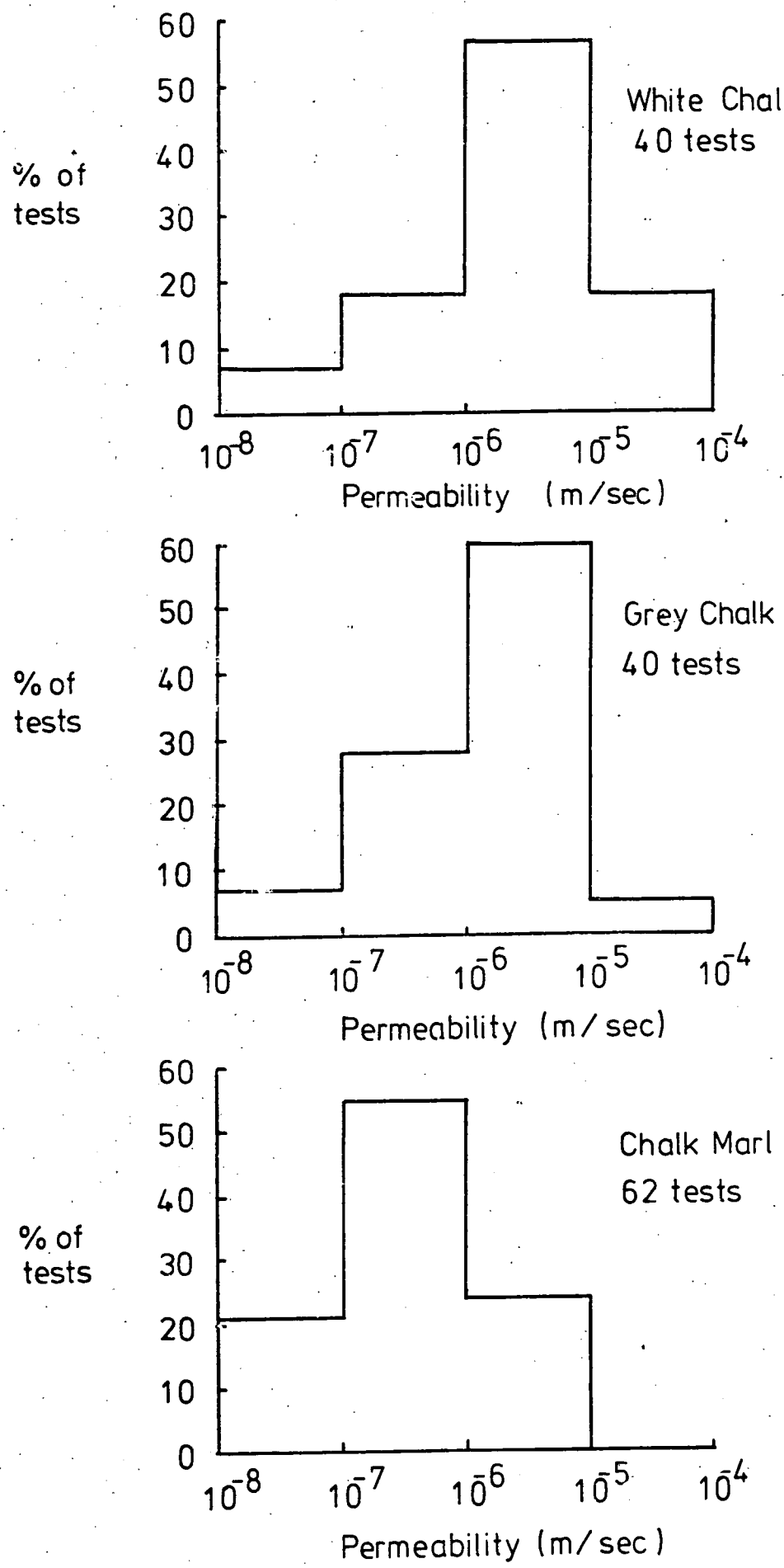

Fig. 4.1 HISTOGRAMS OF ESTIMATED PERMEABILITY VALUES FOR THE LOWER CHALK UNDER THE STRAIT OF DOVER. AFTER, THE CHANNEL TUNNEL STUDY GROUP (1964-'65)

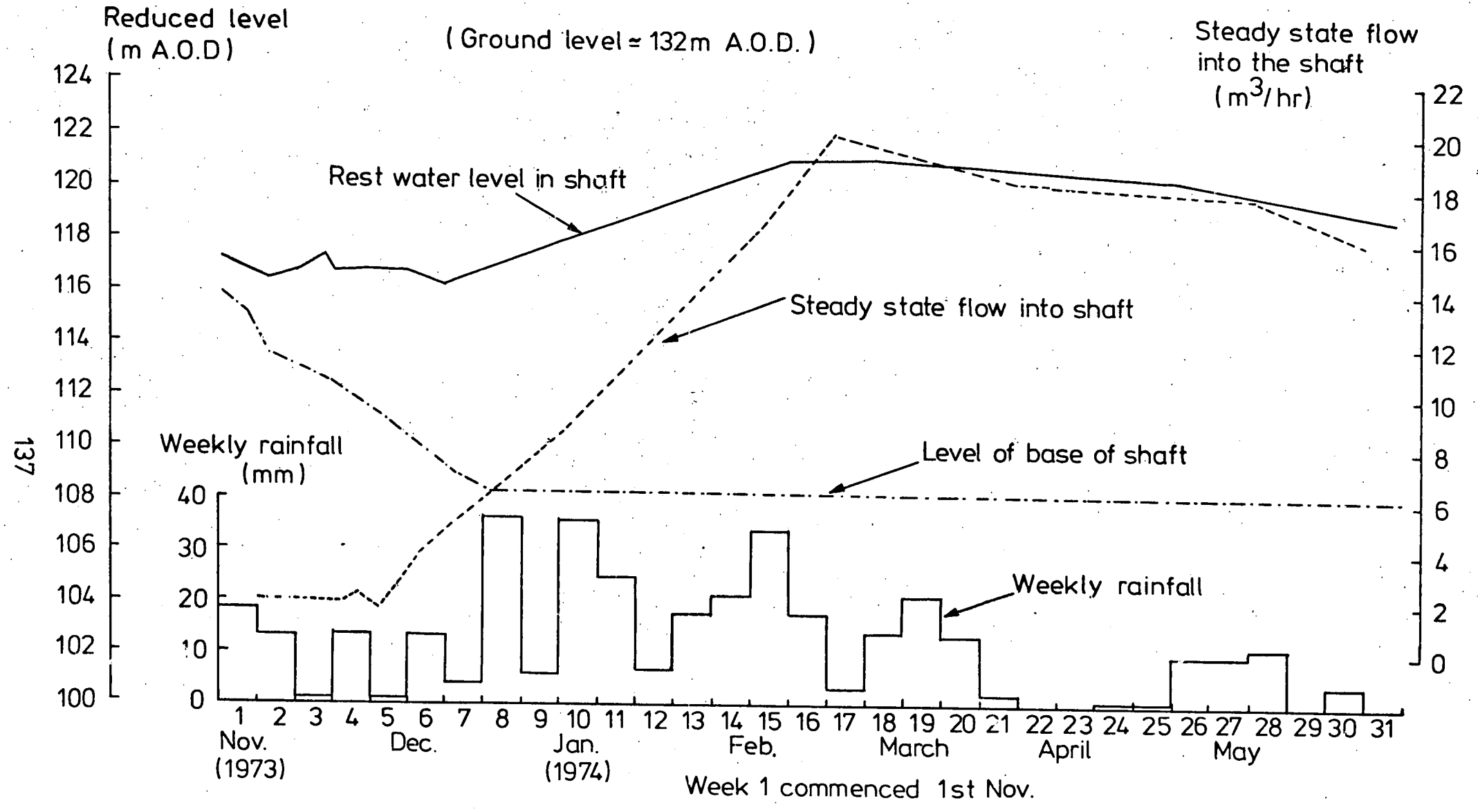

Fig. 4.2 PROGRESS OF SHAFT EXCAVATION, STEADY STATE FLOW INTO SHAFT, REST WATER LEVEL IN SHAFT AND WEEKLY RAINFALL.

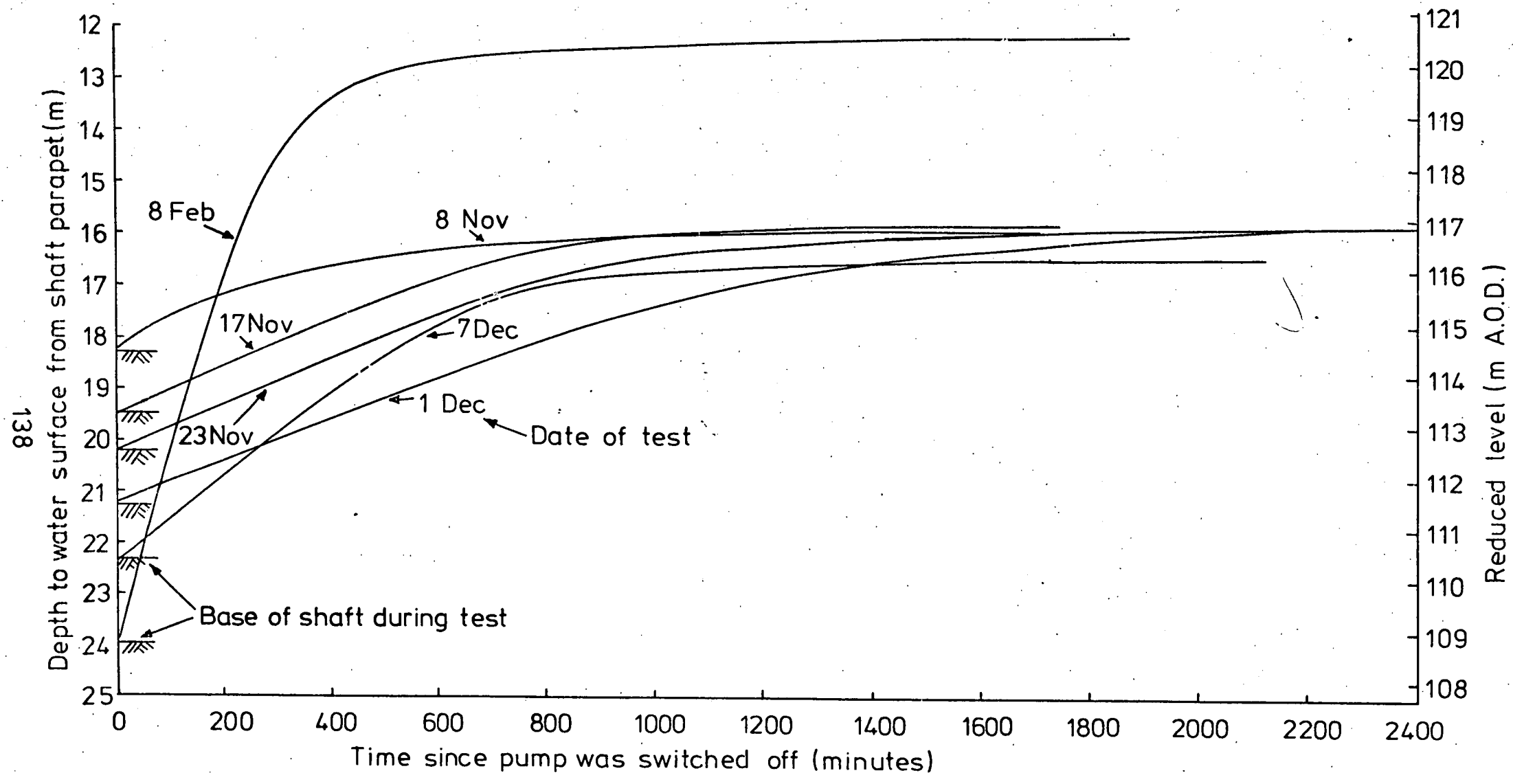

Fig. 4.3 REST WATER LEVEL REGAIN CURVES FOR 3m DIAMETER SHAFT AT CHINNOR.

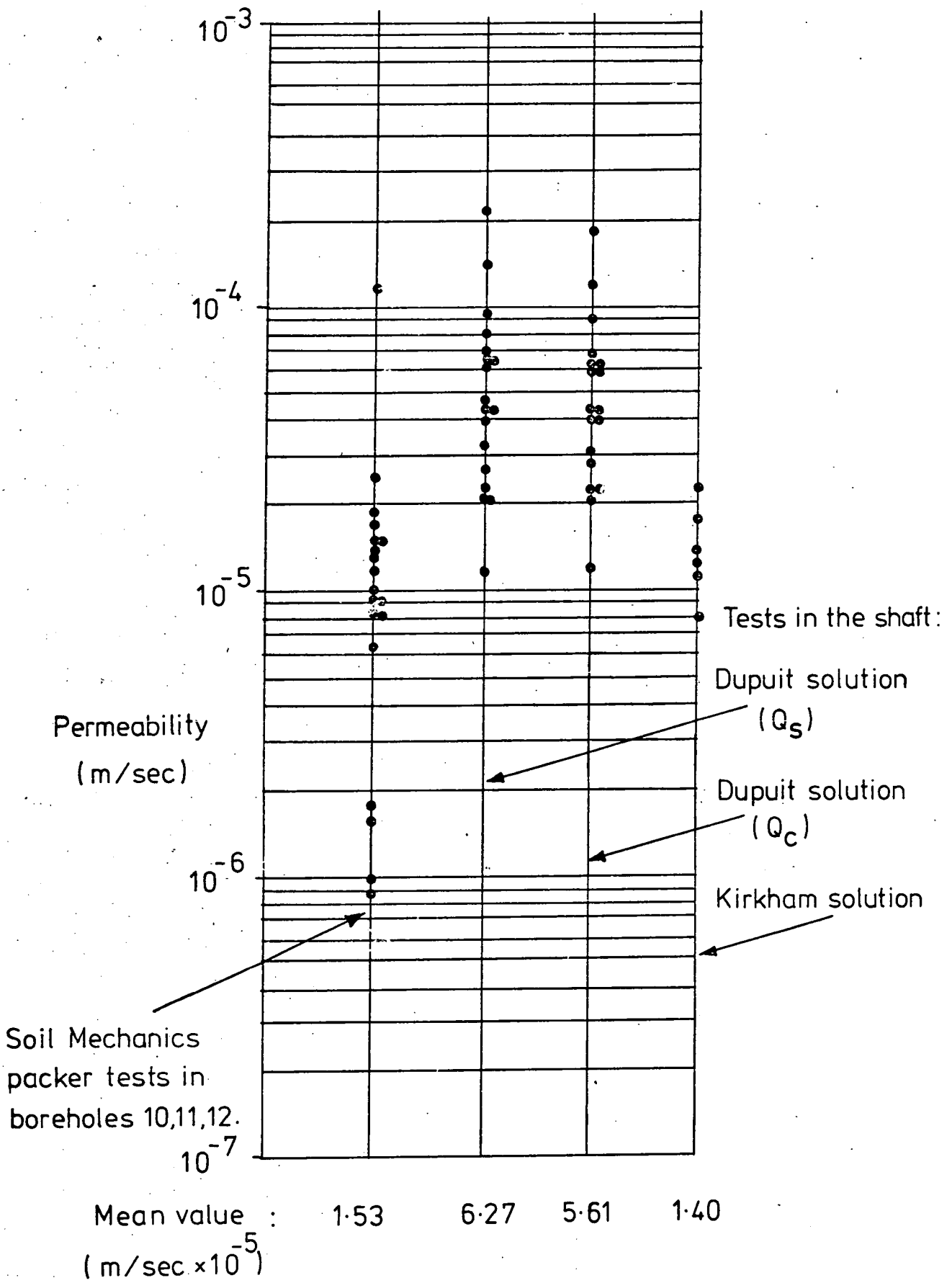

Fig. 4.4 COMPARISON BETWEEN PERMEABILITY VALUES DETERMINED BOTH IN BOREHOLES AND THE SHAFT AT CHINNOR.

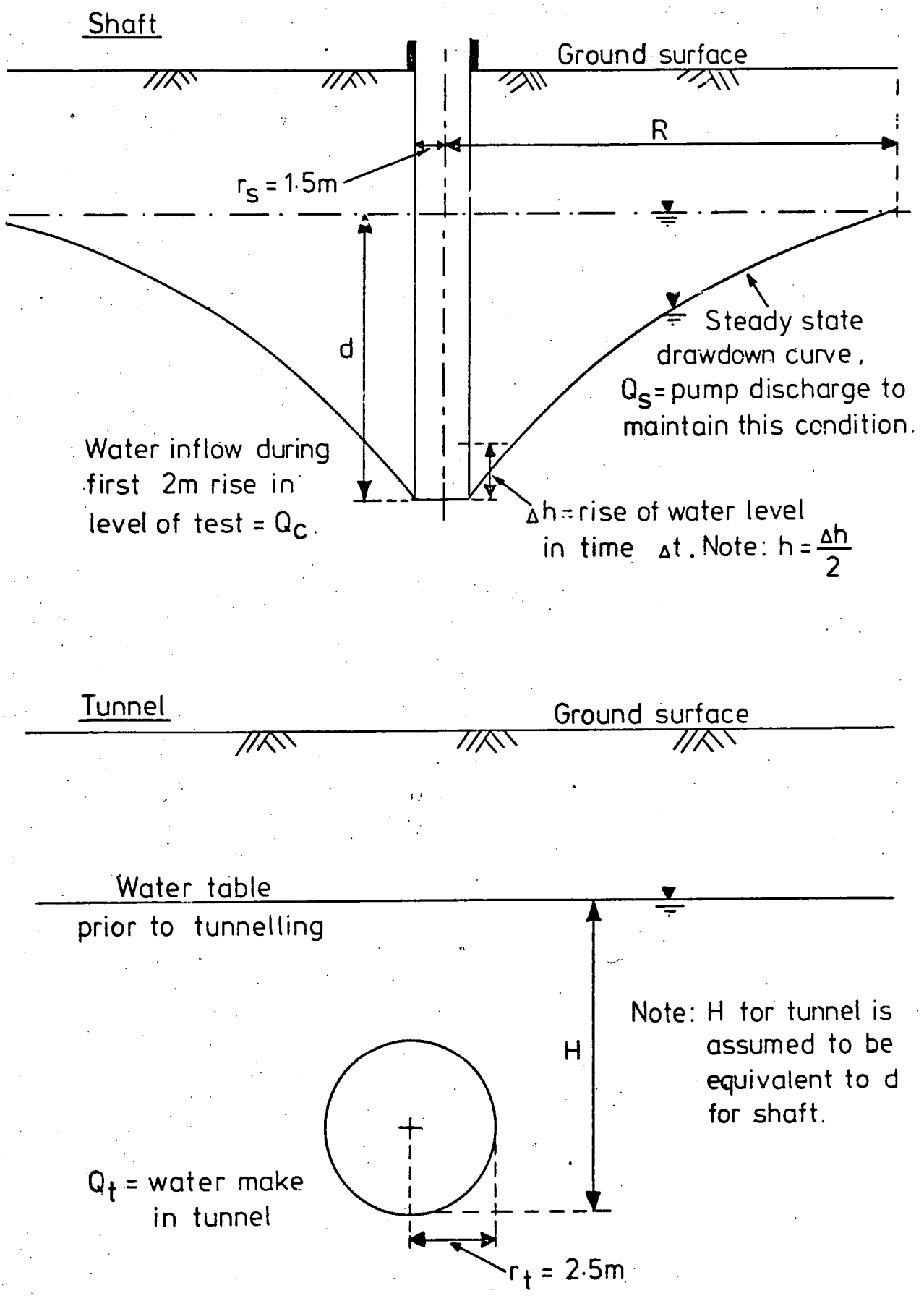

Fig. 4.5 DIAGRAMS SHOWING SYMBOLS USED IN HYDROLOGICAL ANALYSIS OF THE SHAFT AND TUNNEL AT CHINNOR.

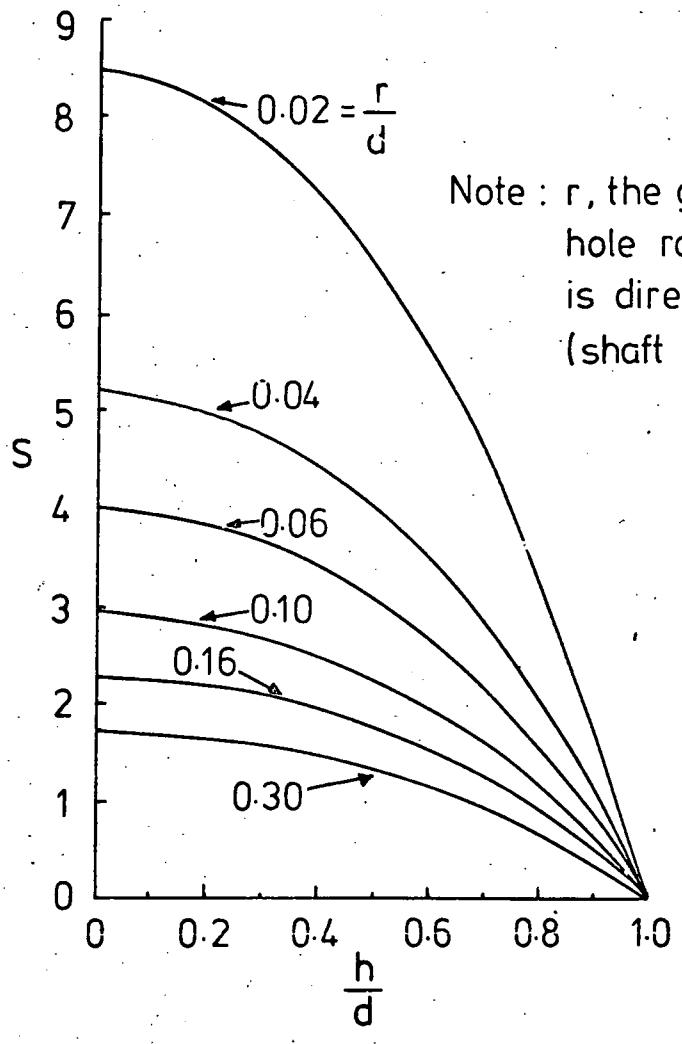

Note : r, the general term for hole radius in this Figure, is directly equivalent to r_s (shaft radius) in Equation 4.3.

Fig. 4.6 VALUES OF S IN EQUATION 4.3 (FROM SPANGLER, 1951)

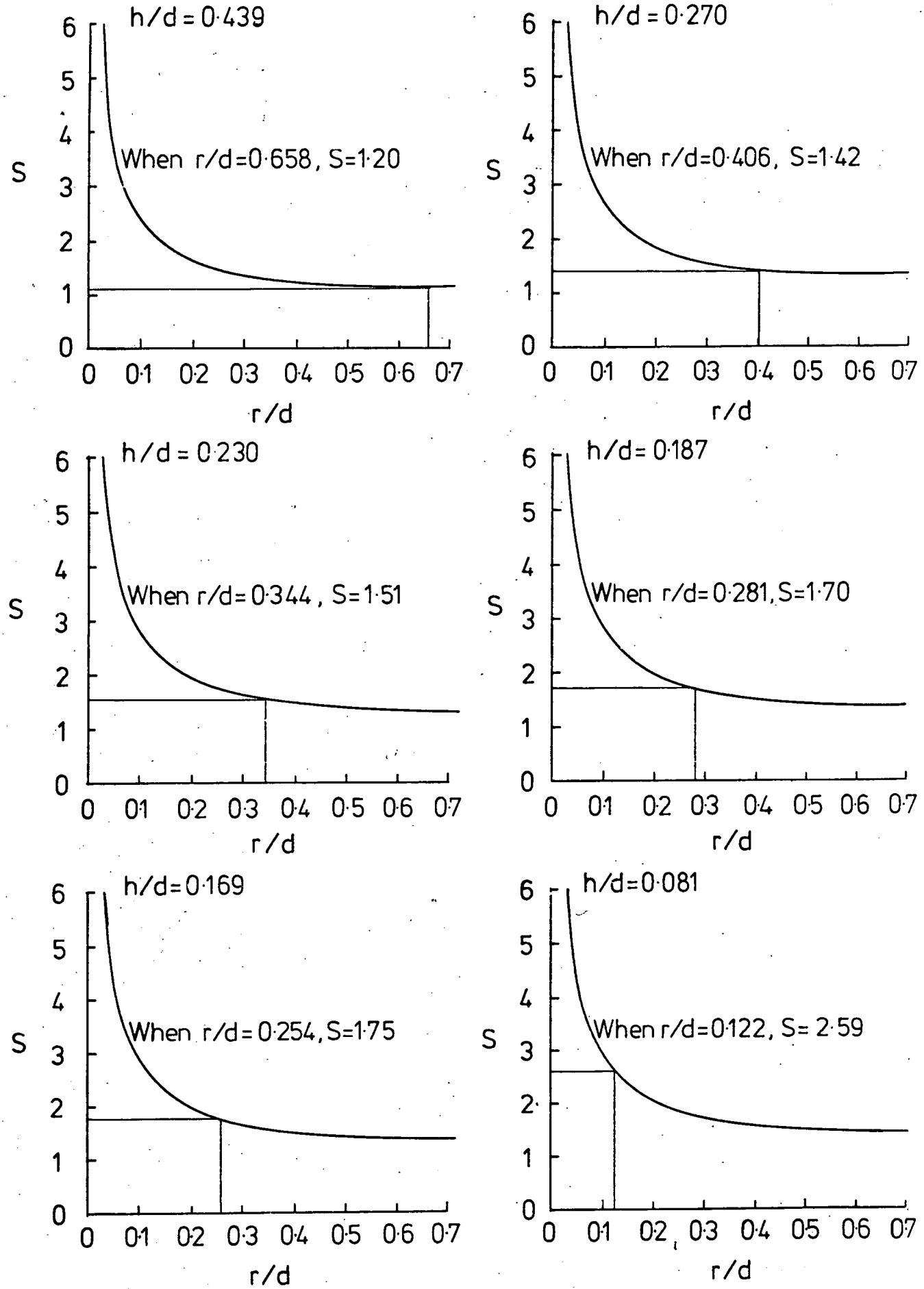

Fig. 4.7 VALUES OF S PLOTTED AGAINST r/d FOR SELECTED VALUES OF h/d.

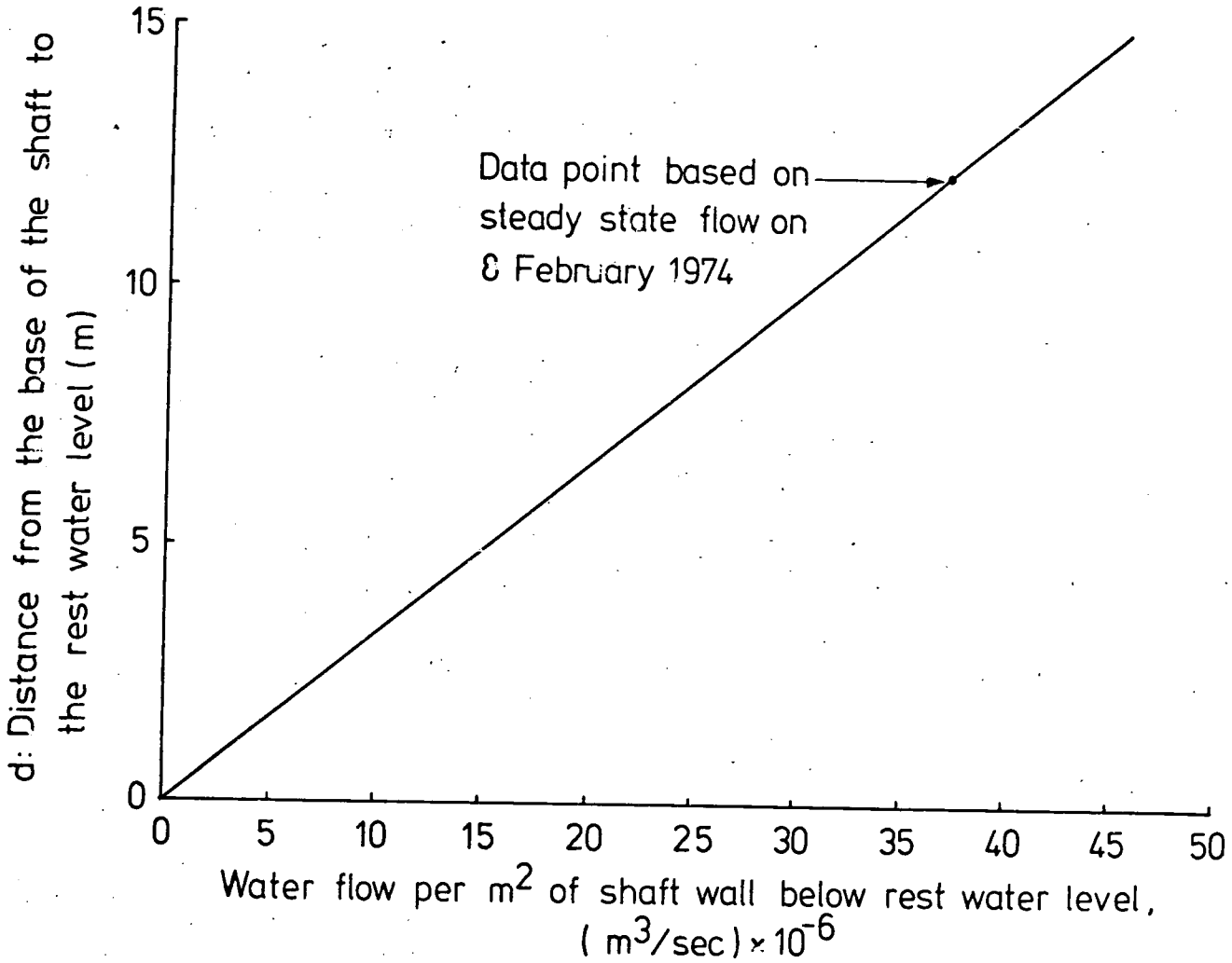

Data calculated assuming a linear relation between d and water flow per unit area in the shaft:

d (m); assumed to be equivalent to H in Figure 4.5	Water flow per m^2 of shaft wall below rest water level. $(m^3/sec) \times 10^{-6}$	Predicted water make per m run of tunnel $(m^3/sec) \times 10^{-4}$
5	14·7	2·31
7	20·5	3·22
9	26·4	4·15
11	32·8	5·15
13	39·2	6·16
15	45·6	7·16

Fig. 4.8 PREDICTION OF WATER MAKE IN THE TUNNEL USING A DIRECT EMPIRICAL METHOD.

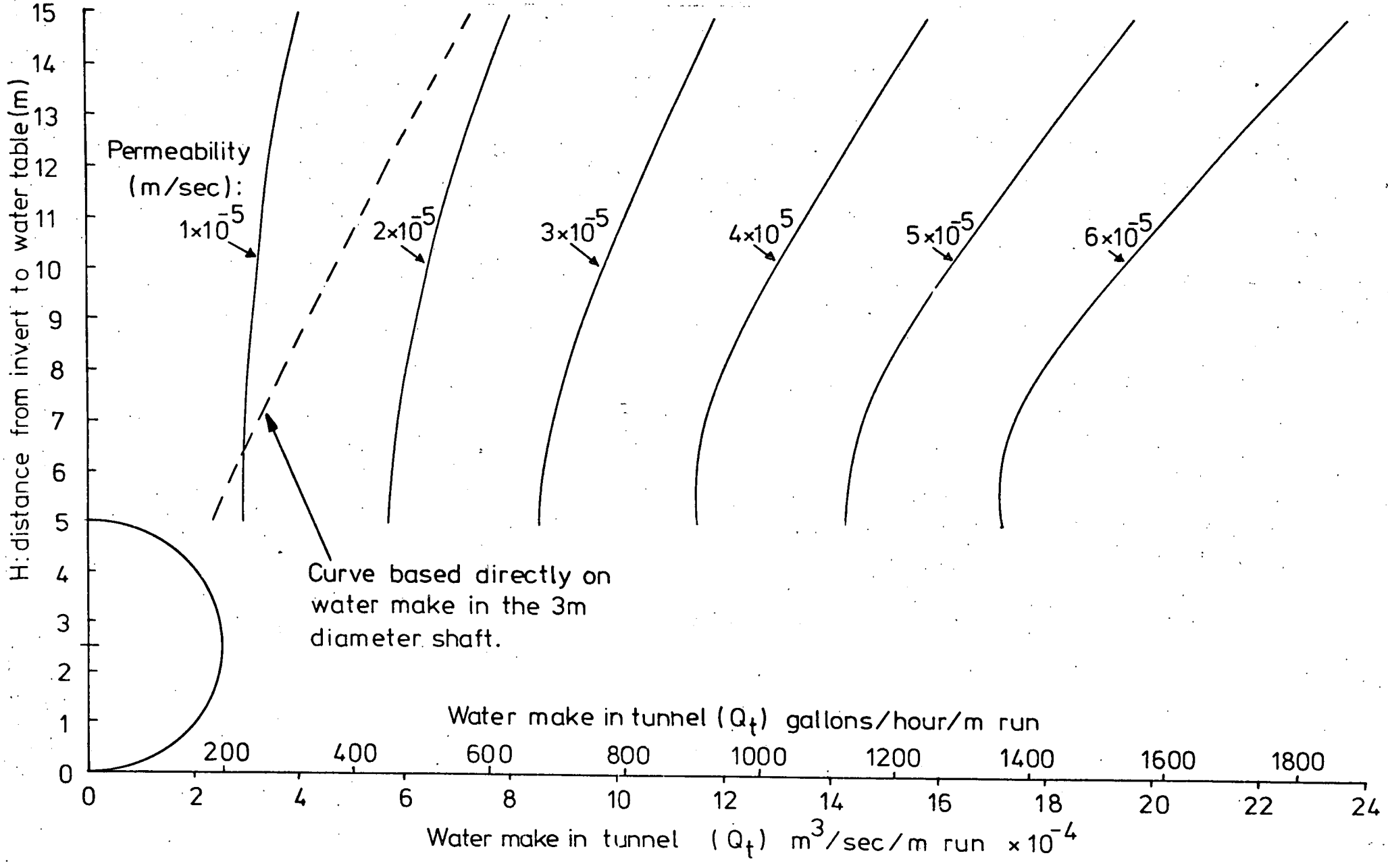

Fig. 4.9 PREDICTIONS OF WATER MAKE IN THE 5m DIAMETER CHINNOR TRIAL TUNNEL.

CHAPTER 5

DETERMINATION OF IN SITU ROCK QUALITY IN THE CHINNOR TRIAL TUNNEL

5.1 Introduction

A large part of the TRRL tunnelling trials at Chinnor was directed towards developing an understanding of the mechanics of cutting rock (Hignett and Boden, 1974). By systematically varying the design of the cutting head, modifying such components as pick width and geometry, depth of cut and pick array, it was hoped to assess those factors most critically affecting tunnelling machine performance. In order that meaningful comparisons between results could be made, it was necessary to monitor any variability in rock conditions, such that variation in machine performance resulting from modification in the cutting head design could be distinguished from that caused by variation in ground conditions.

In addition to the aims described above, it was hoped to examine the detailed results concerning ground conditions encountered during tunnelling in terms of site investigation and ground movement results. In this way an assessment of the effectiveness of site investigation methods used in tunnelling could be obtained, together with a greater insight into the critical factors controlling tunnel stability.

There are two rock properties that are widely accepted as critically influencing cutability and stability in tunnels: (a) the mechanical properties of the intact rock, in particular compressive strength

(Roxborough, 1969) and (b) the discontinuity characteristics of the rock mass (Bieniawski, 1973). In order to achieve the aims outlined above it was therefore necessary to develop an efficient rock indexing technique capable of producing numerical indices classifying these critical properties in the chalk exposed at the tunnel face ahead of the tunnelling machine.

It was necessary that each face survey be completed in approximately three hours to avoid disturbing the scheduled cutting experiments and contractual work in the tunnel. Therefore the most significant constraint on the type of measurement techniques adopted at the tunnel face was the time available for the survey.

5.2 Intact rock strength

It is known that a variety of mechanical properties of intact chalk influence cutability: compressive strength, tensile strength, shear strength and moisture content (Roxborough and Rispin, 1972). Due to lack of available time, however, it is impractical to measure all these properties over a highly variable 5m diameter face by taking core samples. It is therefore desirable to adopt a quick *in situ* method for rock characterisation that gives an index directly related to rock cutability. The mode of action of such an indexing technique would thus, ideally, have to simulate the cutting action of the picks (cf. Roxborough, 1969). Bearing these criteria in mind Drew and Hudson (1975) developed the impact penetrometer. The use of the impact penetrometer for rock quality assessment in the shaft at Chinnor is described in Chapter 3 and Priest and Hudson (1975a). An assessment of the effectiveness of the impact penetrometer compared with existing techniques together with a full description of its use for rock indexing at Chinnor is given in

Drew and Hudson (1975). It is worth reiterating here that the intact strength values obtained by the impact penetrometer, though related to compressive strength, are not a direct measure of this property but rather a strength index related to rock cutability. For this reason the strength values obtained by the impact penetrometer are termed "penetration strength" rather than "compressive strength".

In order to obtain a characterisation of rock quality over the whole face, intact rock penetration strength was measured along scanlines set up at the tunnel face. A variety of scanline geometries was adopted in order to assess the most efficient sample size and geometry for face characterisation purposes. It was found that approximately 100 separate measurements were necessary to give an average estimated penetration strength having a value within 11% of the true value at the 95% confidence level. A total of 12 faces was indexed for intact rock strength during the first 85m of tunnelling. Figure 5.1, plotted using data supplied by TRRL, summarises the variation in average estimated penetration strength at the face over this first 85m.

In order to establish the precise nature of chalk variability over a tunnel face a high density grid of scanlines 0.5m apart was set up on four faces at chainages 11.5m, 12.1m, 18.1m, and 20.4m. Penetrometer readings, taken every 0.5m along the scanlines, were plotted in grid form and contoured in intervals of 2 MN/m^2. The resulting contoured diagrams are shown in Figure 5.2 (Data supplied by TRRL).

5.3 Discussion of intact rock strength results

Examination of Figure 5.1 indicates that during the first 85m of tunnelling, the average penetration strength at the face varied between

1.25 MN/m^2 and 3.25 MN/m^2. In general along the tunnel route there are few dramatic changes in average strength, except near chainage 85m where the drop in penetration strength is probably merely a reflection of the increased water flow.

Figure 5.2 shows that there is considerable variability of intact penetration strength across the 5m diameter face, with a marked tendency towards horizontal strength zoning. It is clear, therefore, that the chalk strength, whilst varying considerably across a single face, has a reasonably constant value along the tunnel when averaged over the whole face (Figure 5.1).

This latter point is important when interpreting the cutting experiment results in the context of the face indexing results. The picks, in moving round the face, will have encountered the same large area of chalk as the scanline survey during the face indexing. The average strength value for the whole face will therefore be a good index of the average conditions encountered during cutting. Indexing by sampling just a small area of the face, using core samples for example, would not have given these benefits.

5.4 Discontinuity characteristics

The relative merits of existing survey techniques that are commonly used when assessing discontinuity characteristics were discussed in Chapter 2. The scanline technique was adopted for use in the Chinnor tunnel because it provided a quick method of obtaining large amounts of numerical data, thus allowing the production of a numerical index representative of conditions at the face. In addition, it was possible to compare directly the data obtained from the scanline surveys with

those from borehole cores, thus making it possible to directly assess site investigation results in terms of actual conditions encountered during tunnelling.

Although a three-dimensional characterisation of the rock mass, along orthogonal scanlines, is desirable (Chapter 2) the availability of only a single face in the tunnel at any one time limited the survey to a series of two-dimensional characterisations. Additional surveys along the tunnel-wall were impossible due to the smearing effects of the tunnelling machine. At each tunnel face (except chainage 76.1m) discontinuity spacing, orientation and trace length were measured along horizontal and vertical diametral scanlines using the methods described in Chapter 2. A photograph illustrating the use of the scanline survey technique at the tunnel face is presented in Plate 5.1.

Discontinuity orientation was measured using a compass-clinometer. However, due to the presence of the tunnel boring machine (that is a large mass of metal), it was impossible to relate azimuth readings to magnetic north; instead azimuth readings were taken relative to the tunnel centre line direction*. The azimuth measurements were assumed accurate to $\pm 5^{o}$ and the dip measurements to $\pm 1^{o}$. Data from scanline surveys in the tunnel are tabulated in Appendix B.

In addition to the vertical and horizontal diametral scanlines, further scanlines on a high density (0.5m) grid were set up on selected faces (at chainages 18.1m, 20.4m, 35.9m) in order to assess the most efficient sample size and geometry for face characterisation purposes. On these additional scanlines, discontinuity spacing only was measured

* The tunnel centre line direction is 010^{o}. It is therefore necessary to add 10^{o} to azimuth readings taken in the tunnel to convert them to geographical readings. This small angle difference can be ignored for purely qualitative assessment of data.

since lack of available time at the tunnel face prevented the measurement of orientation and trace length.

On the basis of measurements taken on the high density grids, the scanline geometries adopted between chainages 55.4m and 85.0m were designed (a) to give a precise index of discontinuity characteristics in the time available at each face, (b) to provide additional data for use when interpreting the results of additional measurements (cutting forces*, intact strength) taken at each face. Figure 5.3 summarises diagrammatically the scanline geometries adopted at each face, a solid line representing a scanline on which discontinuity spacing, orientation and trace length were measured, and a broken line representing a scanline on which discontinuity spacing only was measured. The circular scanlines were set up, using a graduated piece of curved wood, along grooves created by the picks during cutting. In most cases the grooves selected for the circular scanlines were those created by the instrumented picks. By doing this it was hoped to be able to compare discontinuity characteristics at the face with the cutting forces measured on the instrumented picks. This work is described further in Chapter 6.

5.5 Processing and discussion of discontinuity results

The discontinuity measurements taken in the tunnel were processed in a similar way to that described previously in Chapters 2 and 3. The vertical, horizontal and circular scanlines at each face were set up such that there was always an equal proportion of vertical and horizontal scanline sample lengths. By doing this, the use of the correction factor adjusting for scanline length was avoided.

---

* The use of instrumented picks in determining cutting forces at the face is described further in Chapter 6.

Discontinuity spacing data from the high density grids at chainages 18.1m, 20.4m and 35.9m were processed to produce contoured diagrams illustrating the variation in discontinuity spacing across the tunnel face: Each of the 0.5m squares in the grid, defined by the vertical and horizontal scalines, was allocated a mean discontinuity spacing value based on data obtained from the 2m of scanline making up the perimeter of the square, thus applying a form of moving average. Suitable corrections were applied for squares at the edge of the grid. The mean spacing values were then contoured to produce the diagrams shown in Figures 5.4, 5.5 and 5.6.

Discontinuity spacing histograms for the aggregated data obtained at each face during the first 85m of tunnelling are shown in Appendix Figures H.1 to H.17. These Figures include tabulated data concerning scanline length, number of values, mean spacing and standard deviation of spacing. These data, together with mean dip values are summarised for the first 85m of tunnel in Table 5.1. A discontinuity spacing histogram summarising discontinuity spacing data for this first 85m of tunnelling is presented in Figure 5.7.

Figure H.1 to H.17 and 5.7 include a fitted negative exponential probability density distribution, calculated in each case for the appropriate parameter $\hat{\lambda}$ equal to the reciprocal of the mean discontinuity spacing. In general the measured distributions conform well to the fitted negative exponential distributions. These fitted curves and the negative exponential distribution are discussed fully in Chapter 11.

Discontinuity orientation data were processed using the computer program discussed in Chapter 2. The resulting equal area projections are shown in Appendix Figures H.18 to H.31.

Table 5.1 Discontinuity data from scanlines in the tunnel

Tunnel chainage (m)	Total scanline length (m)	Number of discontinuities measured	Mean discontinuity spacing (m)	Spacing standard deviation (m)	Mean discontinuity dip, (degrees)	Dip, standard deviation, (degrees)
9.9	8.12	45	0.180	0.143	48.87	26.84
11.5	9.36	59	0.159	0.156	46.07	25.98
12.1	9.28	73	0.127	0.139	50.60	28.00
14.0	9.42	60	0.157	0.169	37.65	20.65
18.1	68.94	542	0.127	0.112	41.25	24.23
20.4	69.82	561	0.125	0.125	33.31	21.59
35.9	72.50	579	0.125	0.136	48.56	23.98
55.4	27.00	267	0.101	0.099	50.70	21.40
57.5	26.62	344	0.080	0.072	44.40	25.34
60.6	26.70	301	0.089	0.082	51.56	27.45
65.2	37.03	315	0.118	0.134	35.82	22.46
70.2	37.46	461	0.081	0.082	40.65	30.90
72.7	34.69	352	0.099	0.097	51.21	26.51
73.9	17.15	200	0.086	0.094	46.88	23.19
76.1	7.25	97	0.075	0.119	-	-
79.3	36.25	410	0.088	0.112	52.95	20.36
85.0	16.98	218	0.078	0.075	47.36	29.93

Variation of mean discontinuity spacing and dip averaged for each face during the first 85m of tunnelling is summarised in Figure 5.8. It is clear that the maximum variation in mean spacing over this length of tunnel at the 95% confidence level is from 0.05m (lower bound minimum) to 0.22m (upper bound maximum), whilst the minimum variation is from 0.07m (lower bound maximum) to 0.14m (upper bound minimum). Similarly the maximum variation in mean dip at the 95% confidence level is from 27^{o} to 58^{o} whilst the minimum variation is from 39^{o} to 49^{o}.

The contour diagrams of discontinuity spacing at three selected faces in the tunnel (Figures 5.4 to 5.6) show that the variability in mean spacing between zones on a given face is approximately equal to the variability in mean spacing (averaged for each of the indexed faces) during the first 85m of tunnelling. It is apparent, therefore, that the discussions presented in Section 5.3 regarding strength variability are, to a certain extent, applicable to considerations of variation in discontinuity spacing. The mean discontinuity spacing for any given face can only be assumed to give a good index of conditions encountered during excavation of the chalk when obtained from scanlines covering the whole face.

In Chapter 11 a full discussion of discontinuity spacings is presented, in which the significance of variations in mean spacing between samples of varying sizes are examined. In particular, the factors controlling the spatial distribution of discontinuities are analysed by examining histograms (such as those in Appendix Figures H.1 to H.17) in simple mathematical terms.

The precise influence of variations in discontinuity characteristics on the cutability of the rock is difficult to ascertain, since, during

the first 85m of tunnel not only was there variation in discontinuity characteristics and, to a lesser degree, intact strength of the rock but also a systematic variation in the design of the cutting head. The precise influence of the variation of just one parameter is therefore difficult to isolate. In Chapter 6 the cutting characteristics of the discontinuous chalk are examined by analysing in detail the cutting forces, intact strength and discontinuity characteristics common to a small area of rock being excavated by an instrumented pick. Further considerations of the cutting characteristics will therefore be postponed until Chapter 6.

The greatest single influence of discontinuities in the Chinnor tunnel was on ground stability. At several stages during the first 85m of tunnelling severe instability at the face was experienced; exhibited as blocks and wedges parting along sub-veritcal discontinuities and falling out of the face both during and following excavation. During the shoving action and advancement of the reaction ring, instability at the crown and shoulders was often experienced, exhibited as falling rubble with blocks up to 2m across parting along sub-horizontal planes. This instability, particularly noticeable on the left (west) side of the tunnel, is also discussed in Chapter 10. Instability at the crown often led to an overbreak extending 2m above the tunnelling machine (Plate 5.2).

Following the passage of the reaction ring, the tunnel was supported with steel arch sets spaced at 1m intervals and lined with wire mesh. This support system was not back-packed into the over-break and consequently the latter often remained as a cavity above the wire mesh (Plate 5.3). During the period following the installation of the support system degradation at the crown often continued, so leading to the accumulation of rubble on the wire mesh. This degradation continued until the overbreak cavity was filled with rubble or had achieved a stable geometry.

In general, the two discontinuity characteristics that are likely to have controlled stability in the Chinnor tunnel, as indeed in most tunnels through jointed rock, are orientation and spacing. Unfavourable combinations of these two characteristics will have led to instability. The influence of these two characteristics is discussed in the following paragraphs.

Variation in discontinuity orientation characteristics at the face during the first 85m of tunnelling is summarised in Appendix Figures H.18 to H.31. The equal area projections show that at all faces examined there is a set of sub-horizontal discontinuities dipping to the northwest at approximately 15^{o}. At most faces this set is accompanied by a concentration of discontinuities showing a steep dip ($\doteq 70^{o}$) to the northwest and southeast. In addition a more dispersed 'concentration' of discontinuities showing a steep dip to the northeast and southwest is developed at many of the faces examined. At all faces the above mentioned orientation concentrations are accompanied by a more random component of discontinuity orientation. The orientation concentrations described above are developed to a lesser or greater degree at each of the faces examined during the first 85m of tunnelling.

The orientation patterns measured in the tunnel are summarised in Figure 5.9 showing the aggregated readings for the first 85m of tunnel. In general, the orientation patterns correspond well with those plotted from measurements taken in the Chinnor quarry and shaft, summarised in Figures 2.24 and 3.28.

As a result of earlier discussions and experience in the Chinnor tunnel the following specific discontinuity characteristics are thought likely to have controlled stability in the tunnel:

(1) Low mean discontinuity spacing contributed towards overall instability, such that, for a given tunnel diameter, tunnel stability can be regarded as proportional to mean discontinuity spacing.

(2) Preponderance of sub-horizontal discontinuities contributed towards roof instability, such that, the degree of roof stability can be regarded as proportional to mean discontinuity dip.

(3) Preponderance of sub-vertical discontinuities contributed towards wall and face instability, such that the degree of wall and face stability can be regarded as proportional to (90-mean dip).

(4) High variability in discontinuity orientation contributed to overall instability by permitting progressive block loosening and dislocation. Therefore tunnel stability can be regarded as inversely proportional to the variability of discontinuity dip, expressed for convenience in terms of the standard deviation of discontinuity dip.

The components (1) to (4) outlined above can be combined, by multiplication, to produce indices representing the stability characteristics of a given rock mass at a vertical free face (tunnel wall and face) or at a horizontal free face (tunnel roof).

Selecting the components (1), (3) and (4):

$$\text{Wall and face stability index} = \text{mean spacing} \left(\frac{90 - \text{mean dip}}{\text{standard deviation of dip}} \right)$$

Selecting components (1), (2) and (4):

$$\text{Roof stability index} = \text{mean spacing} \left(\frac{\text{mean dip}}{\text{standard deviation of dip}} \right)$$

It must be emphasised that these indices are totally empirical and are adopted here merely as a method of understanding the behaviour of the tunnel in discontinuous ground. These stability indices are plotted against tunnel chainage in Figure 5.10. Areas of tunnel that were actually found to exhibit severe face or roof instability are indicated on this Figure. It is clear that, generally, instability at the face or in the roof was experienced when the appropriate stability index fell below 0.2m. When interpreting this diagram it must be remembered however, that the stability indices were obtained from measurements at the tunnel face whilst the actual instability was developed in rock not directly examined during the discontinuity surveys. The validity of extrapolation of the indices through the rock mass is debatable.

It is important to note that the magnitude of the critical stability index in other tunnels, 0.2m in the case of the 5m diameter tunnel at Chinnor, will depend on a variety of additional factors such as ground water conditions, excavation methods and perhaps most important, excavation size. To acknowledge the importance of excavation size in controlling tunnel stability under a given set of ground conditions it is appropriate to express the critical stability index as a fraction of a tunnel dimension, say, tunnel diameter. The value for Chinnor would therefore be 0.2/5.0 = 0.04.

In this Chapter an empirical approach to considerations of tunnel stability based on measurements taken at the tunnel face has been presented. In Chapters 8 and 10 alternative, more rigorous approaches to the problem of tunnel stability in discontinuous rock are presented.

5.6 Summary and conclusions

1. Intact chalk strength (tested using an impact penetrometer) and discontinuity characteristics were measured along scanlines set up at selected faces during the first 85m of tunnelling at Chinnor. A variety of scanline geometries was adopted.

2. Intact strength, as measured by the impact penetrometer, whilst varying considerably across a single face was found to have a reasonably constant value of between 2 MN/m^2 and 4 MN/m^2 in the first 80m of tunnel when averaged over the whole face. The average strength value for a face is regarded as giving a good index of the average conditions encountered during cutting.

3. Discontinuity spacing histograms, summarising measurements at the tunnel face, revealed that the distribution of discontinuity spacing values followed the negative exponential distribution. This is discussed further in Chapter 11.

4. The variability in mean spacing between zones on a given face was found to be approximately equal to the variability in mean spacing (averaged for each of the indexed faces) during the first 85m of tunnelling. The mean discontinuity spacing for a face is regarded as giving a reasonably good index of the average conditions encountered during cutting.

5. The greatest single influence of discontinuities in the Chinnor tunnel was found to be on ground stability at the face and in the crown both during and after cutting.

6. Orientation data collected from discontinuity measurements at

the face were computer plotted on equal area projections. The orientation patterns were found to reflect those already measured in the Chinnor quarry and the shaft, consisting of a well developed sub-horizontal set of discontinuities inclined to the northwest, accompanied by less well developed steeper dipping sets. A computer analysis of stability in the Chinnor tunnel, utilising orientation data obtained at the face, is presented in Chapter 10.

7. Two empirical tunnel stability indices were devised incorporating data concerning discontinuity orientation and spacing. Examination of conditions actually encountered during tunnelling indicated that tunnel instability was experienced when the appropriate stability index fell below a critical level of, in the case of the 5m diameter tunnel at Chinnor, 0.2m.

8. As a general conclusion it is felt that the problems of ground stability in the Chinnor tunnel were a direct result of the low mean discontinuity spacing compared with tunnel diameter; a situation aggravated by the excavation and support methods. The particular role of discontinuity orientation in controlling the behaviour of the relatively small blocks composing the rock mass can best be expressed in terms of the relation between discontinuity orientation and the orientation of free faces exposed in the tunnel. In this context it is concluded that the highly variable discontinuity orientation patterns encountered at Chinnor suggested no particularly favourable or unfavourable potential tunnel drive directions.

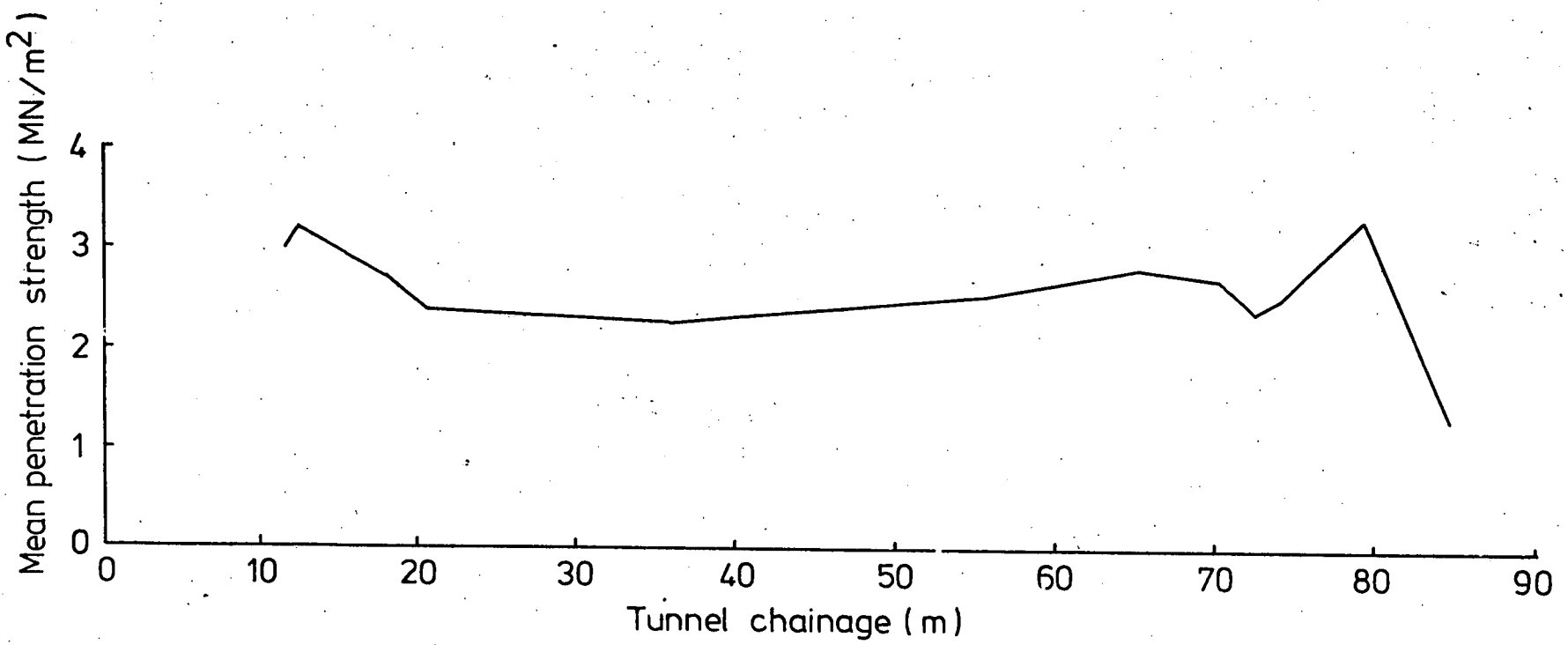

Fig. 5.1 VARIATION OF MEAN PENETRATION STRENGTH AT THE FACE DURING THE FIRST 85m OF TUNNELLING.

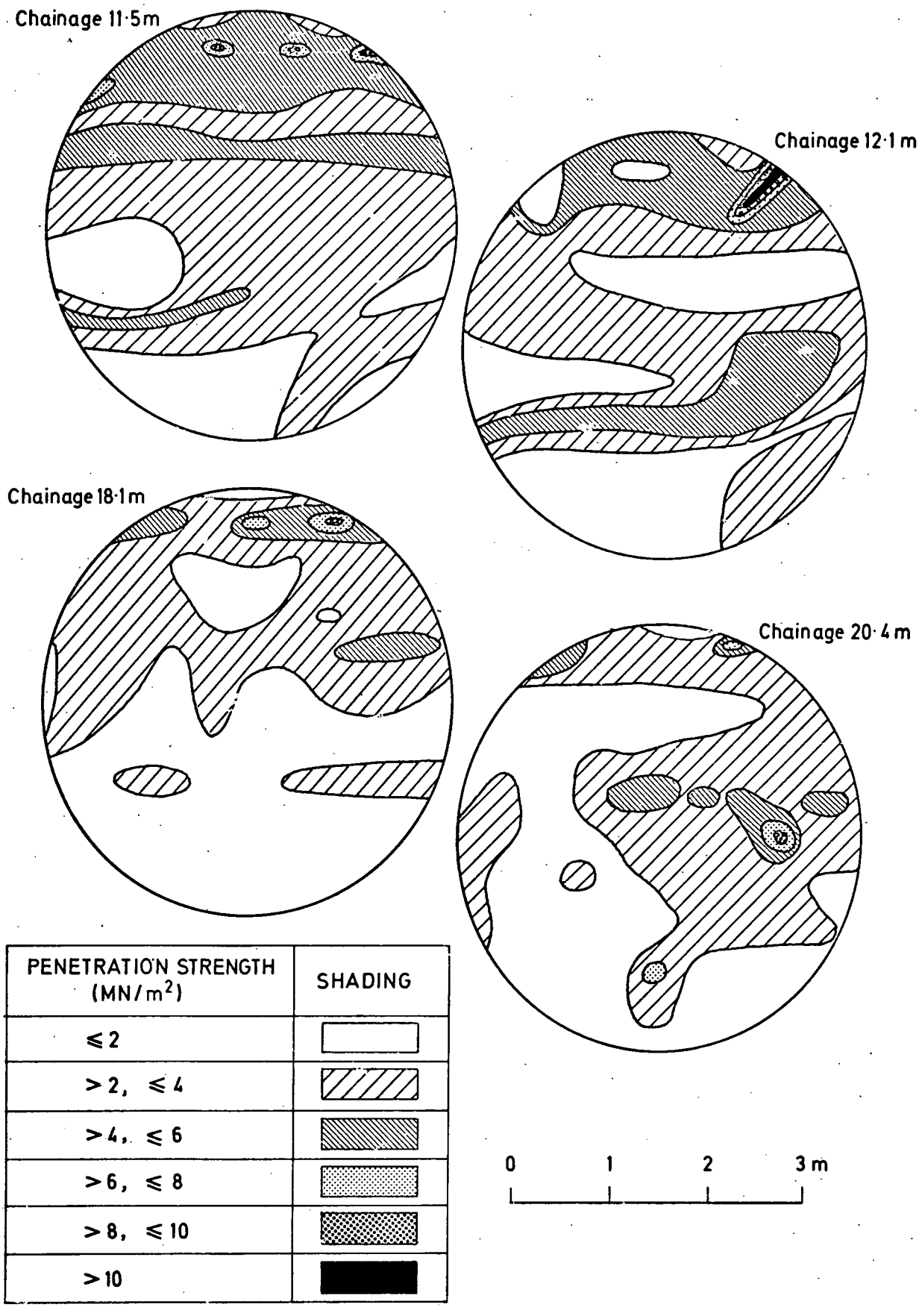

PENETRATION STRENGTH (MN/m^2)	SHADING
≤ 2	
$> 2, \leq 4$	
$> 4, \leq 6$	
$> 6, \leq 8$	
$> 8, \leq 10$	
> 10	

Fig. 5.2 CONTOUR DIAGRAMS OF CHALK STRENGTH VARIATION AT THE TUNNEL FACE, CHAINAGES:- 11·5m, 12·1m, 18·1m AND 20·4m. DATA PROVIDED BY T.R.R.L.

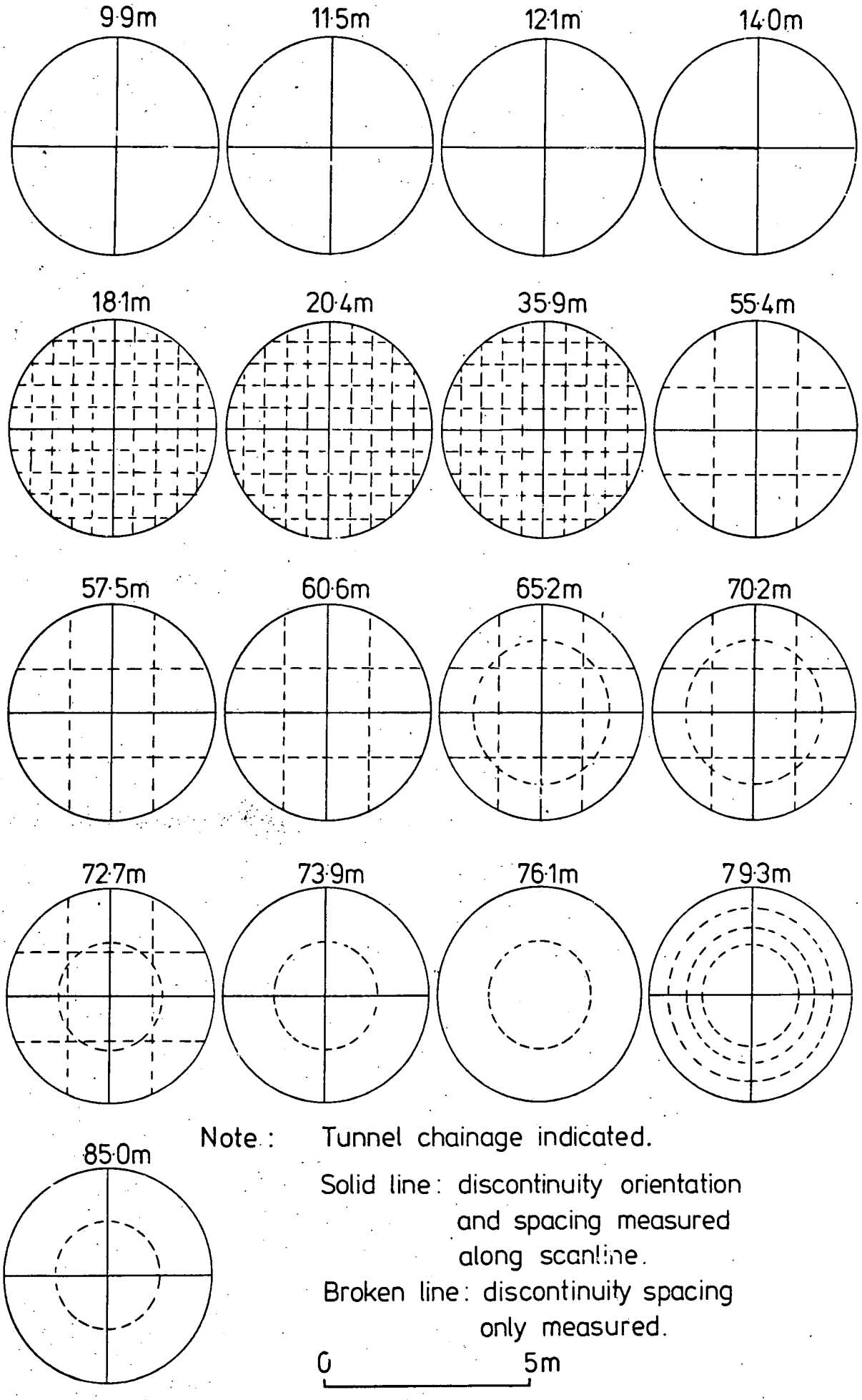

Fig. 5.3 SCANLINE GEOMETRIES ADOPTED AT EACH FACE.

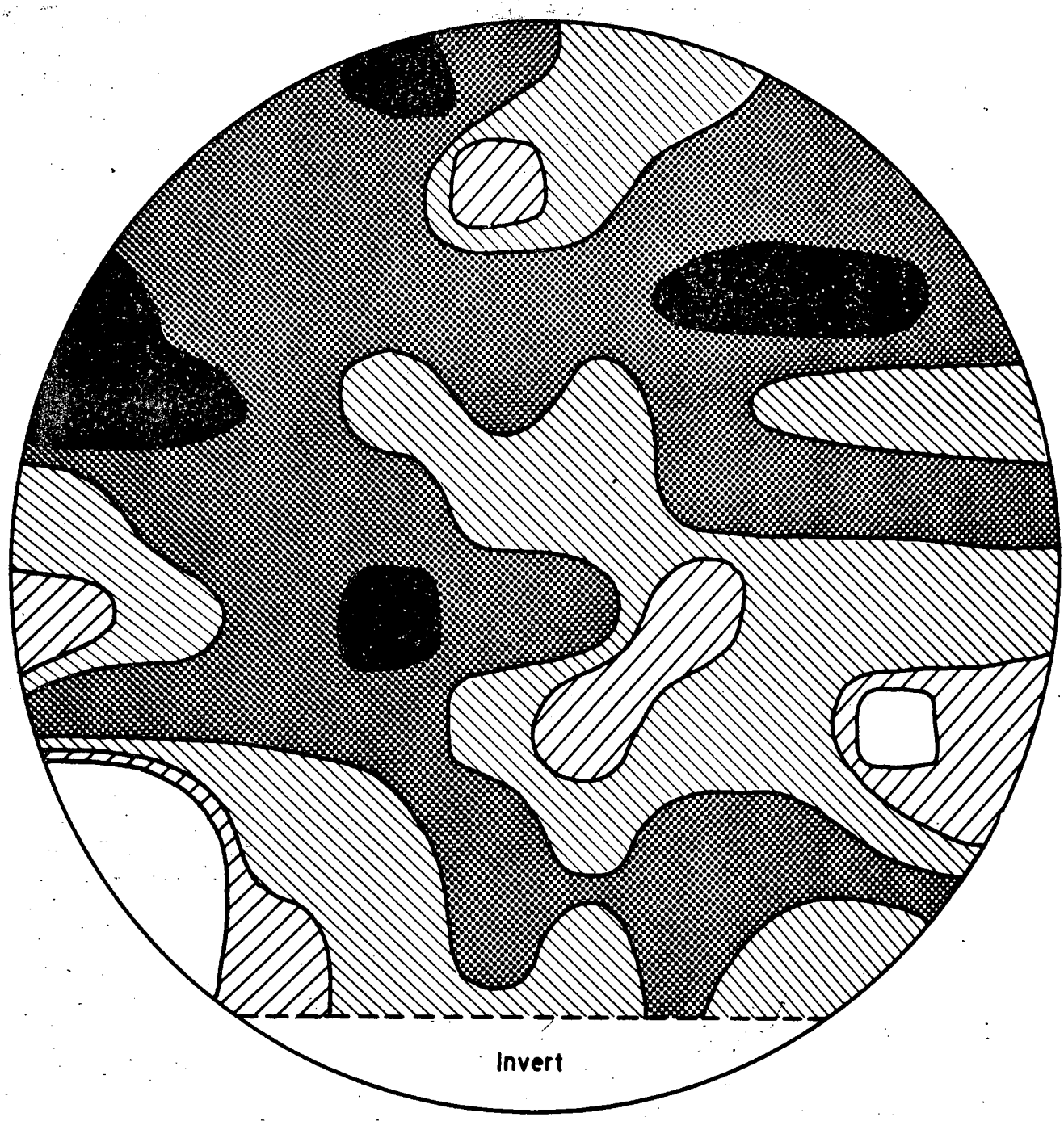

Data obtained from nine vertical and nine horizontal scanlines

DISCONTINUITY SPACING	SHADING
⩽ 0·10 m	
> 0·10 m, ⩽ 0·15 m	
> 0·15 m, ⩽ 0·20 m	
> 0·20 m, ⩽ 0·25 m	
> 0·25 m	

0 1m

Fig. 5.4 DISCONTINUITY SPACING AT THE TUNNEL FACE, CHAINAGE 18.1m

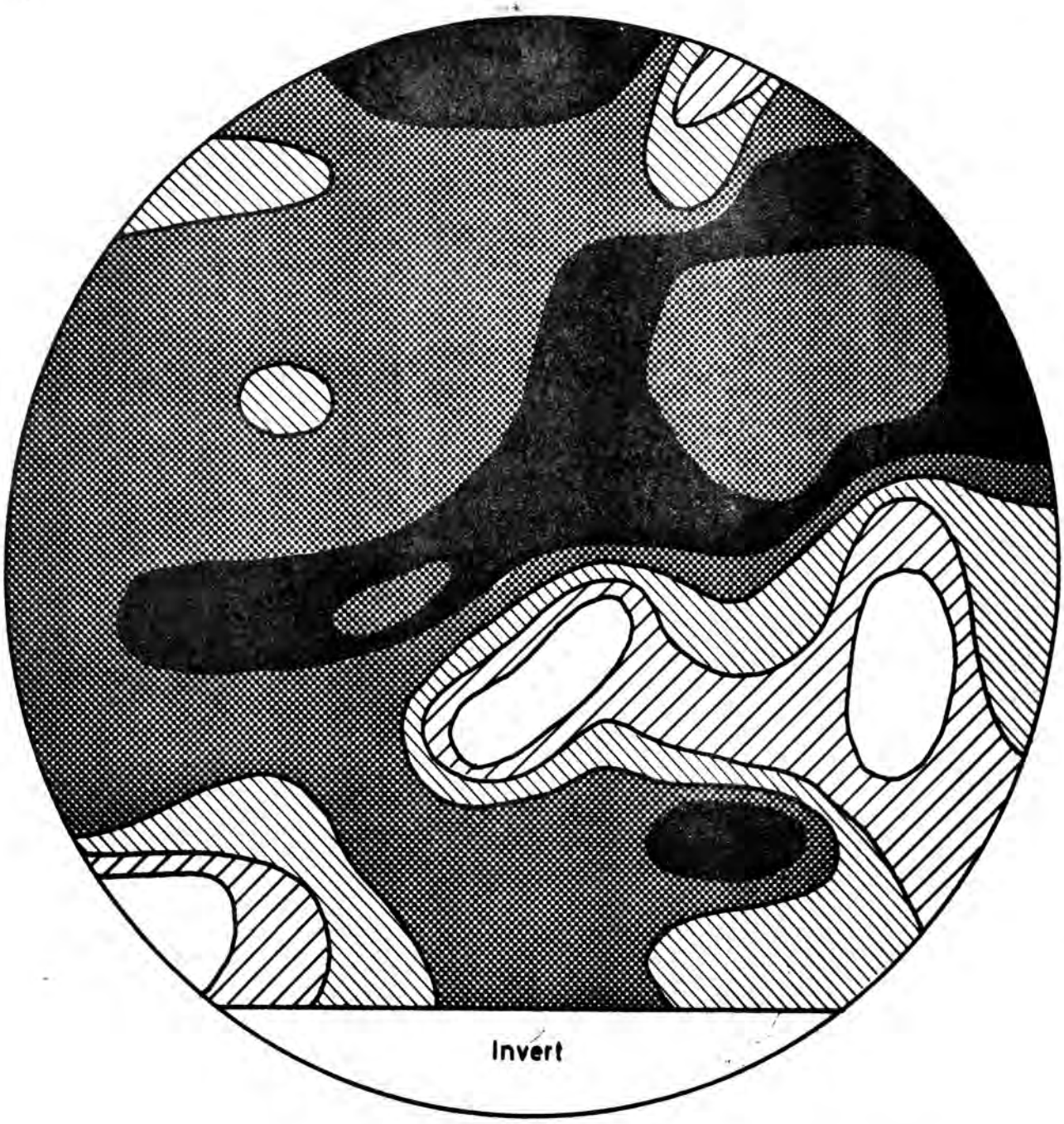

Data obtained from nine vertical and nine horizontal scanlines

DISCONTINUITY SPACING	SHADING
⩽ 0·10 m	
> 0·10 m, ⩽ 0·15 m	
> 0·15 m, ⩽ 0·20m	
> 0·20m, ⩽ 0·25 m	
> 0·25m	

0 1m

Fig. 5.5 DISCONTINUITY SPACING AT THE TUNNEL FACE, CHAINAGE 20.4 m

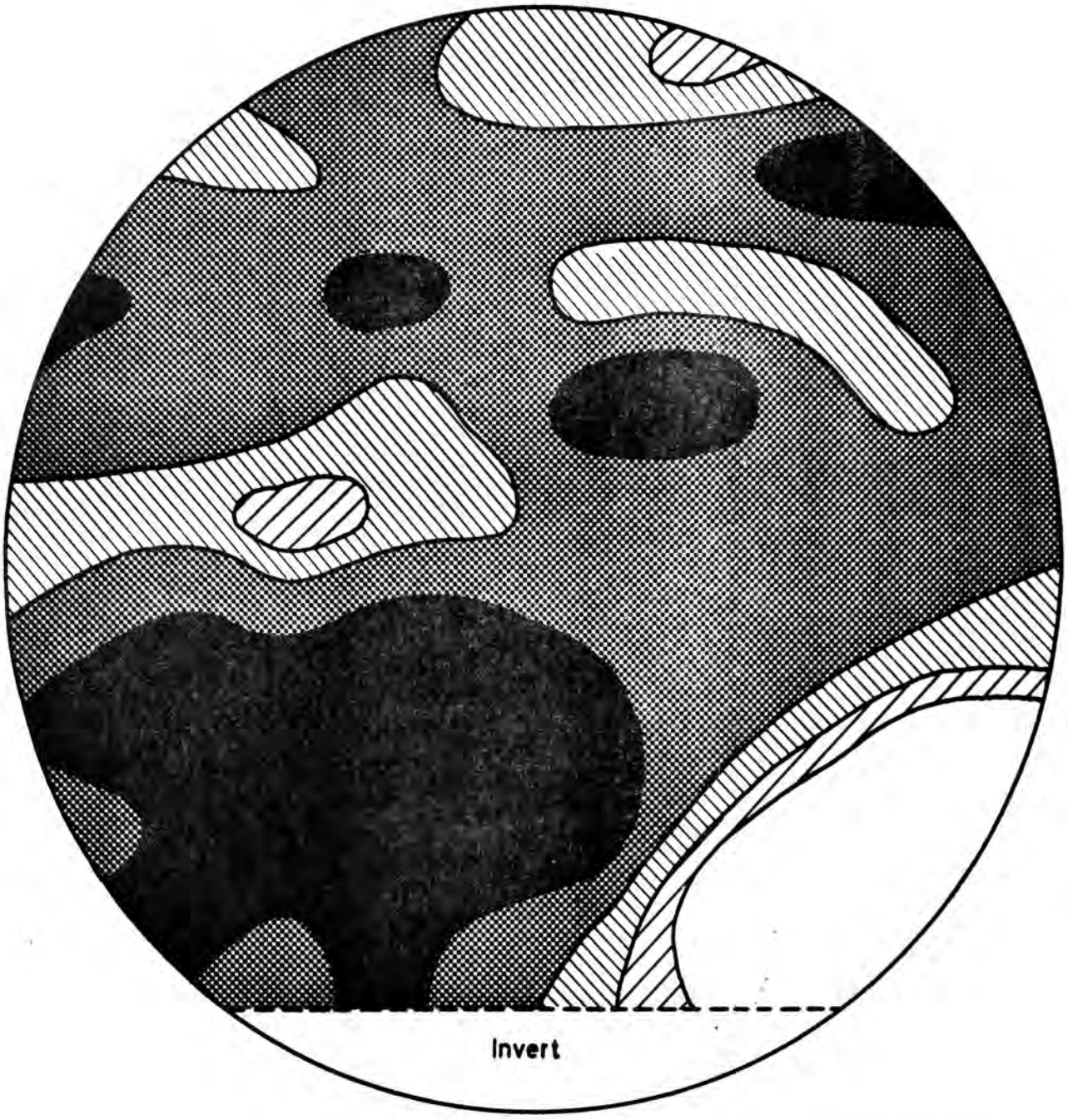

Data obtained from nine vertical and nine horizontal scanlines

DISCONTINUITY SPACING	SHADING
≤ 0·10 m	
> 0·10 m, ≤ 0·15 m	
> 0·15 m, ≤ 0·20m	
> 0·20m, ≤ 0·25m	
> 0·25m	

0 1m

Fig. 5.6 DISCONTINUITY SPACING AT THE TUNNEL FACE, CHAINAGE 35.9m

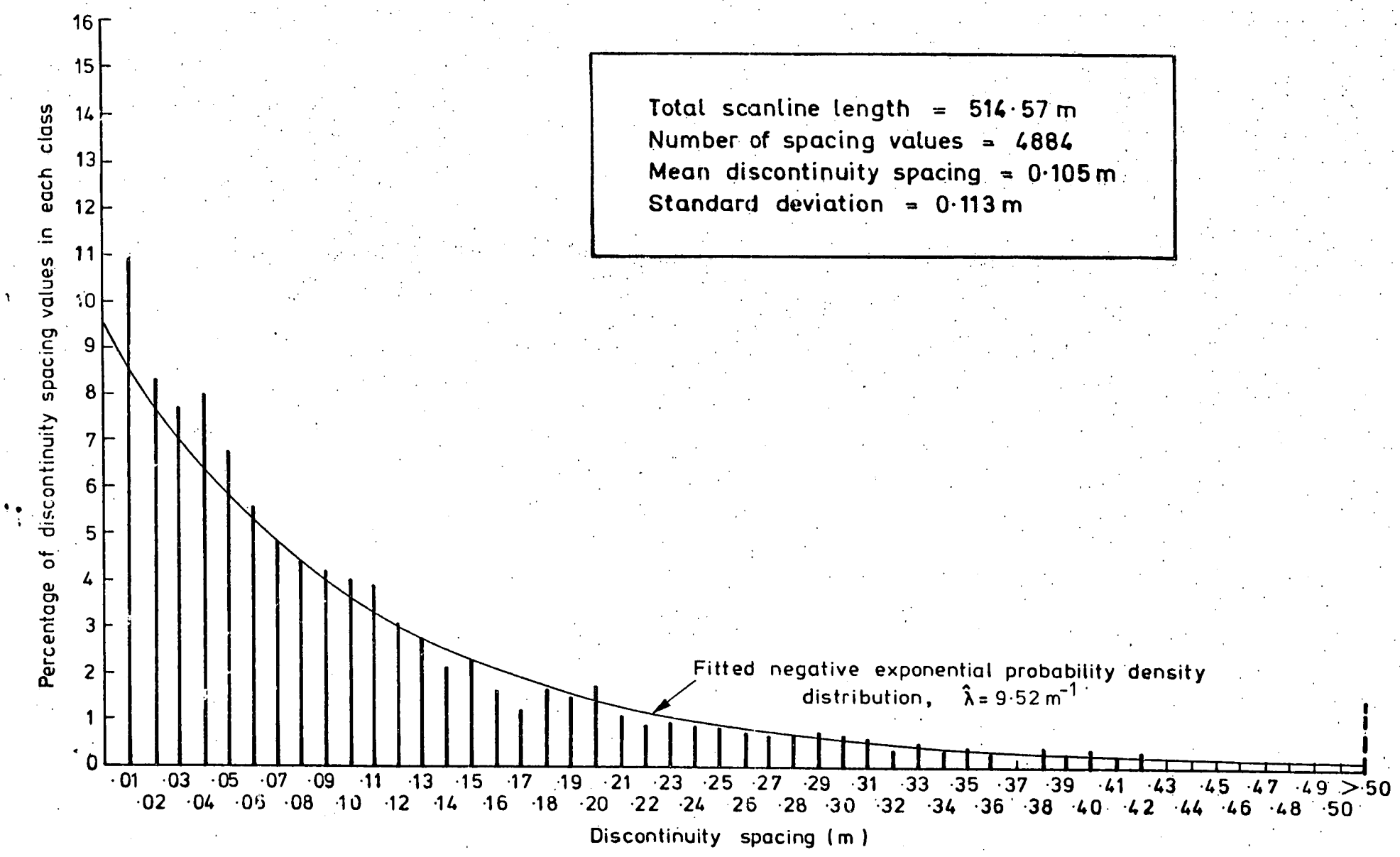

Fig. 5.7 DISCONTINUITY SPACING HISTOGRAM, SUM OF ALL SCANLINES IN THE FIRST 85m OF TUNNEL.

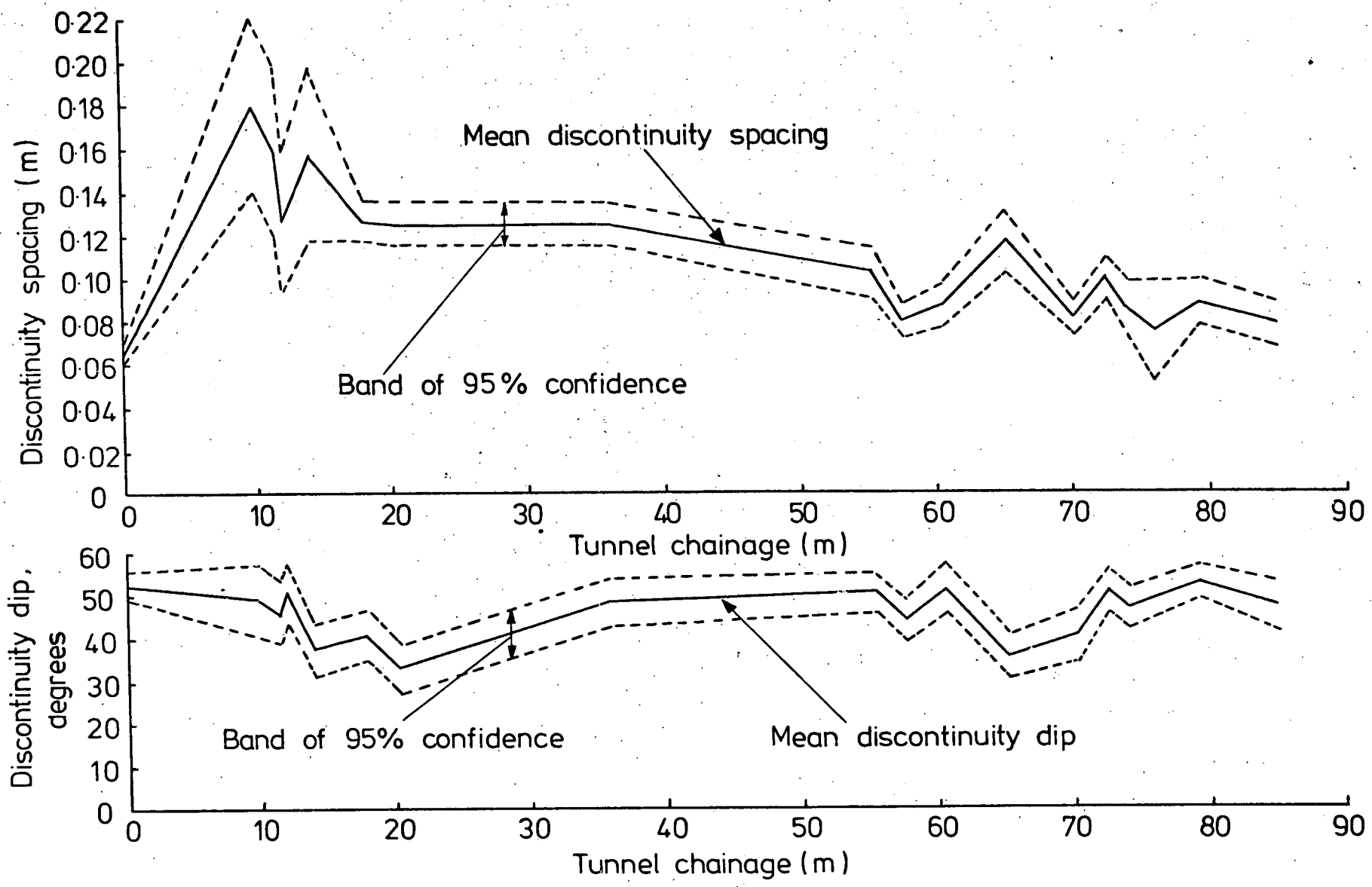

Fig.5.6 VARIATION OF MEAN DISCONTINUITY SPACING AND DIP AT THE FACE DURING THE FIRST 85m OF TUNNELLING.

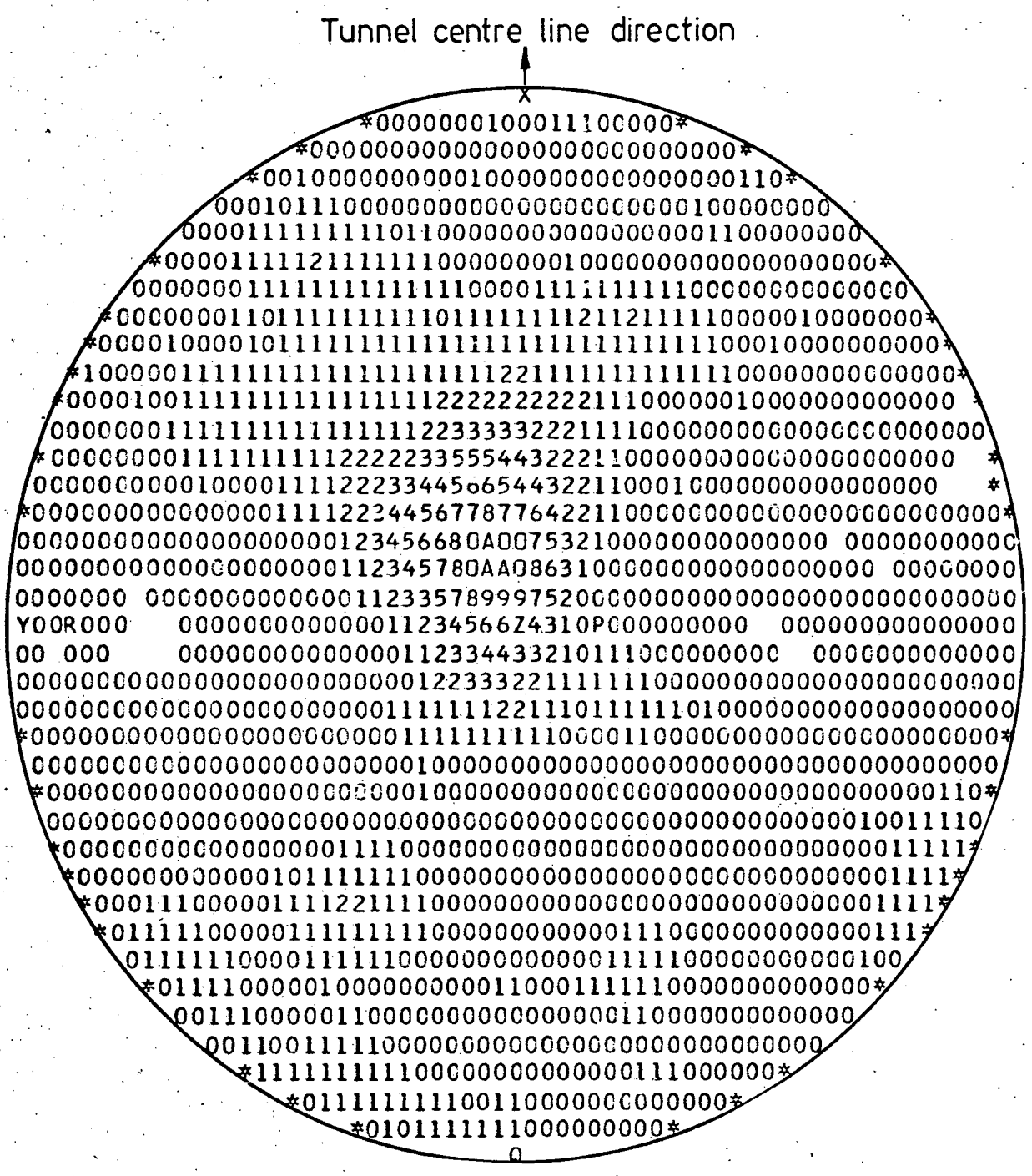

Fig. 5.9 UPPER HEMISPHERE PROJECTION OF DISCONTINUITY ORIENTATION, ALL SCANLINES IN THE FIRST 85m OF TUNNEL.

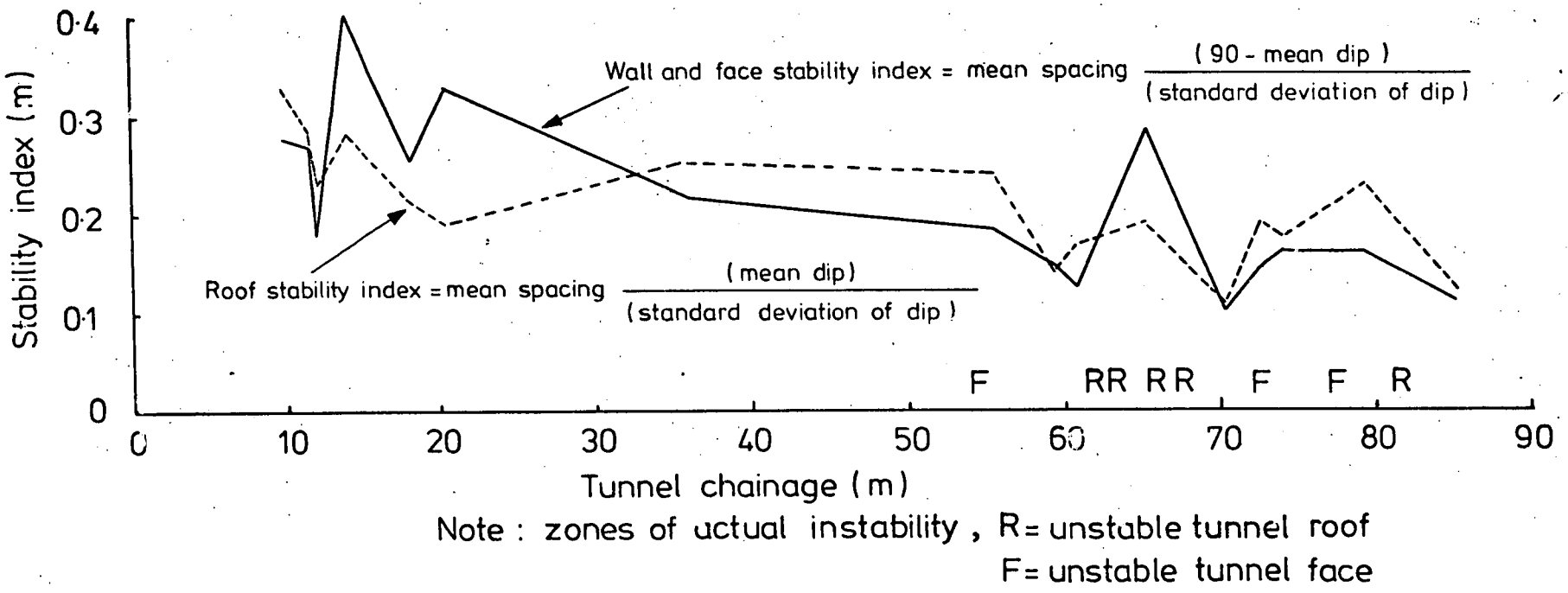

Fig. 5.10 ROOF AND FACE STABILITY ALONG TUNNEL DURING THE FIRST 85m OF TUNNELLING.

Plate 5.1 THE USE OF THE SCANLINE SURVEY TECHNIQUE AT THE TUNNEL FACE.

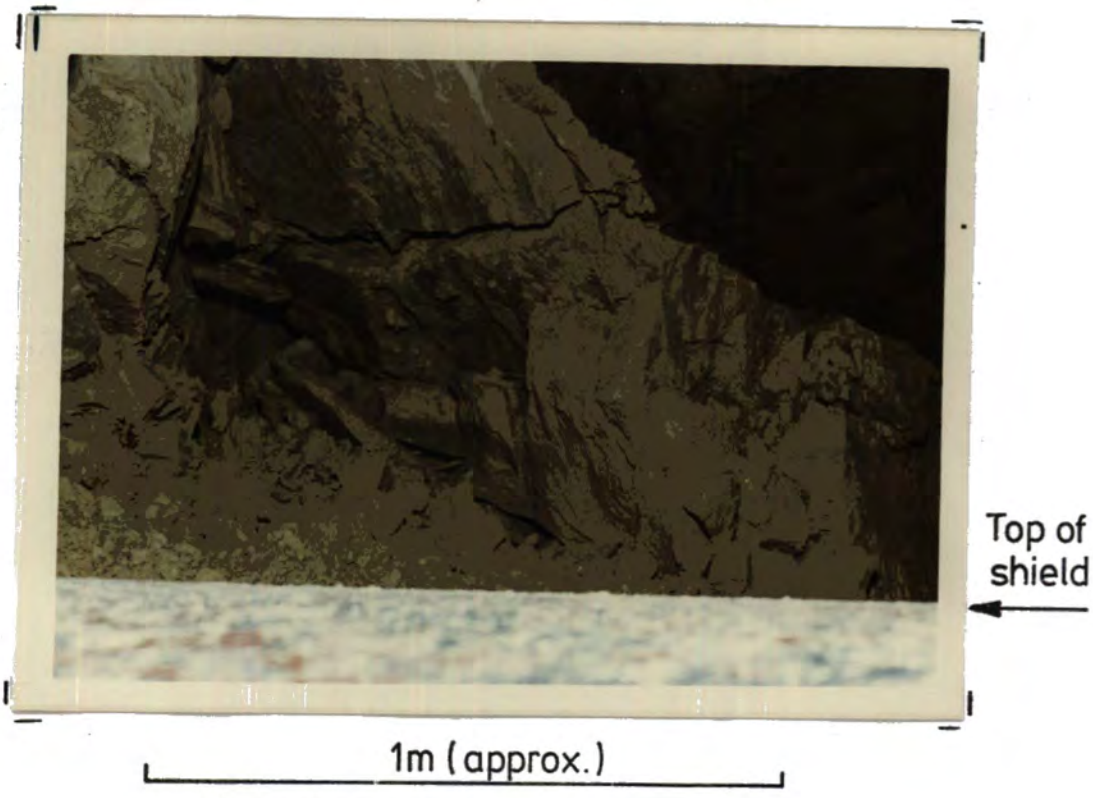

Tunnel face on the left.

Plate 5.2 LOOSENING AND OVERBREAK ABOVE THE TUNNELLING SHIELD.

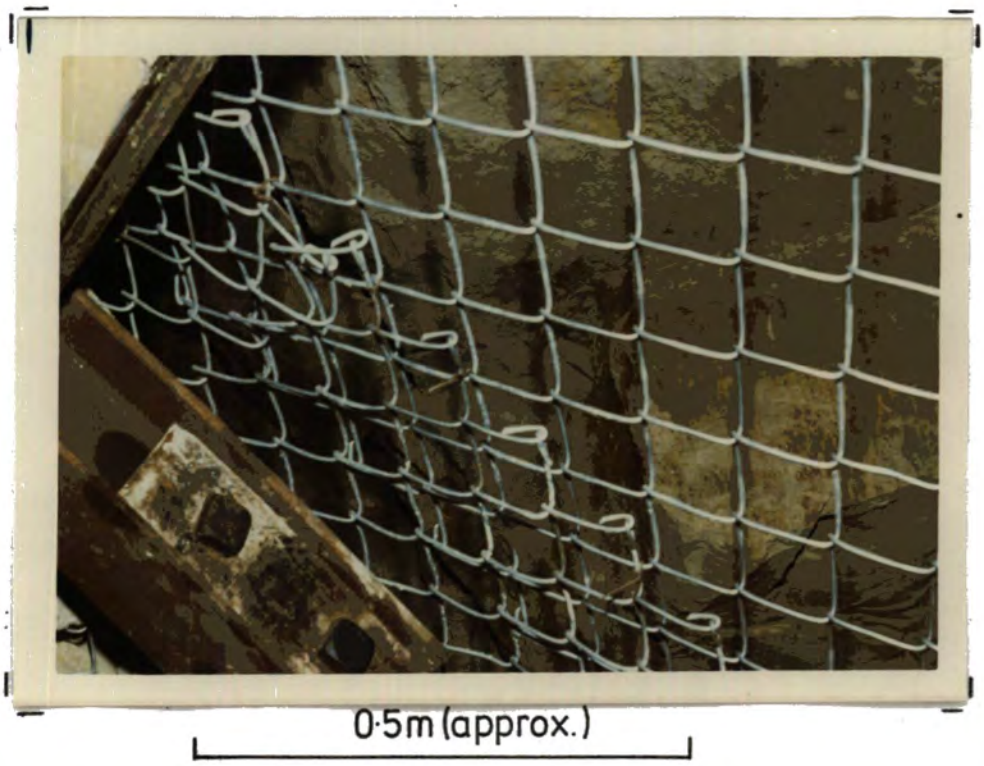

Plate 5.3 OVERBREAK CAVITY BEHIND THE WIRE MESH IN THE CHINNOR TUNNEL.

CHAPTER 6

MECHANICAL CUTTING CHARACTERISTICS OF THE LOWER CHALK AT CHINNOR

6.1 Introduction

In this Chapter the cutting characteristics of the Lower Chalk at Chinnor are examined. This is done by analysing the pick forces, intact strength and discontinuity characteristics common to a small area of rock being excavated by an instrumented pick. It is hoped to develop a preliminary understanding of the factors controlling the rock cutting and in addition assess the effectiveness and validity of the methods used in the examination presented here.

The collection of data concerning the magnitude of forces acting on the instrumented picks attached to the cutting head formed an integral part of the research programme at Chinnor (Hignett and Boden, 1974). Raw data, in the form of light sensitive paper (UV) traces from galvonometric recordings, summarising the variation in pick forces with time during the cutting operations, were made available to the author by TRRL. Data concerning intact rock strength, expressed in terms of penetration strength, were obtained by members of TRRL, using the impact penetrometer (Chapter 3). The discontinuity characteristics of the rock were obtained by the author.

6.2 Pick forces

6.2.1 Data collection

The three orthogonal forces acting on each instrumented pick during cutting: normal force, lateral force and cutting force were measured

using a triaxial dynamometer (Figure 6.1). The system used to monitor these forces during the cutting experiments, described fully in Hignett (1974), is outlined below.

The forces imposed on the pick during the cutting operations are expressed in the dynamometer as deformations of the tool carrying bars. These deformations are measured using an array of 24 strain gauges mounted on the bars. The strain gauges are connected in groups of eight to form three Wheatstone bridges, each of which resolves one of the orthogonal forces. Each bridge produces an output of approximately 10mV for a 0.02 MN applied force. This output is fed into a voltage controlled oscillator, whose output frequency is changed by the voltage from the strain gauge bridges. The output frequencies are then multiplexed into a single signal and transmitted from the cutting head at radio frequency.

The receiving aerial, situated outside the revolving cutting head, is positioned as close as possible to the transmitters to achieve maximum signal strength. The signal is fed into a frequency converter and taken back to the instrumentation cabin by a single coaxial cable. After demultiplexing, the dynamometer signals thus received are recorded on a UV recorder (and/or a data logger) to facilitate analysis.

In order to make detailed analyses of the UV traces it was necessary to calibrate the system. This was done by members of TRRL prior to the cutting experiments by using hydraulic rams to apply known forces to a specially constructed pick shank in the normal, lateral and cutting directions. In addition to this mechanical calibration a further calibration of the telemetry and recorder system was carried out by connecting a test oscillator in place of the strain gauge bridges.

A portion of a UV trace showing a typical recording of dynamometer output relating to cutting force is shown in Figure 6.2.

6.2.2 Analysis of the UV traces

In order to simplify the analysis of the UV traces only the cutting forces are examined here. The analysis is confined to cutting forces since it is likely that the magnitude of these forces will be more sensitive to variations in ground conditions than the magnitudes of either the normal or lateral forces.

It was necessary to extract cutting data, relevant to the face indexing positions, from the large volume of data generated by the routine cutting experiments. Twelve UV traces were examined which gave data on cutting forces for twelve chainage positions grouped in six pairs, each of which bracketed a face indexing (Table 6.1). From each trace a chart length appropriate to one revolution of the cutting head was examined. The trace lengths selected were those which represented the final cut (C_1), monitored immediately before, and the first cut (C_2), monitored immediately after, a face indexing position.

The high frequency (noise) component of each trace was smoothed out, peak to peak, by eye. The magnitude of the cutting force was then sampled from the smoothed trace at intervals representing points spaced at 5^{o} intervals round the instrumented cutting circle. Then, applying the appropriate calibration factor, each trace was redrawn as a graph plotting cutting force in kN against clockwise angle from top dead centre. The twelve resulting graphs, grouped in six pairs of C_1 and C_2 are shown in Figures 6.3 to 6.8. The radius of the cutting circle, either 1.58m or 1.23m, appropriate to the instrumented pick examined is indicated in these Figures.

Table 6.1 Chainages for dynamometer traces and face indexing

Dynamometer trace chainage (m)	Face indexing chainage (m)
64.70	
65.16	65.16
72.47	
72.85	72.65
73.76	
73.86	73.86
75.87	
76.05	76.05
78.91	
79.30	79.30
84.56	
84.95	84.95

6.3 Intact strength

The circular groove created by the instrumented pick immediately prior to the face indexing was tested during the indexing to assess the variation of chalk strength round the groove. The radius of the groove selected depended on the radial position of the instrumented pick which in turn depended on the cutting head geometry adopted at the particular stage of the cutting experiments.

The chalk strength was determined by members of TRRL using the impact penetrometer described in Chapters 3 and 5. Penetrometer measurements were generally taken at 7.5^{o} intervals round the cutting circle, representing approximate sample spacings of between 17cm and 20cm depending on the cutting circle radius. Measurements were taken at five of the six indexing sections dealt with in this Chapter. The penetration strength profiles obtained using the impact penetrometer are plotted in Figures 6.3 to 6.8 showing the variation of penetration strength with clockwise angle from top dead centre round the cutting groove.

6.4 Discontinuity characteristics

Discontinuity spacing values round the instrumented cutting circle were obtained by the author using the circular scanline technique described in Chapter 5. Discontinuity spacing data were averaged over 15^{o} intervals round the circular scanline. This interval represented 0.33m or 0.40m lengths depending on the cutting circle radius. Graphs showing the variation of mean spacing, averaged over the appropriate lengths, round the cutting circle are shown in Figures 6.3 to 6.8.

6.5 Comparison between cutting forces, intact rock strength and discontinuity spacing

The aims of this Chapter, stated in 6.1, are to obtain a preliminary understanding of the factors controlling rock cutting at Chinnor. Bearing this in mind it was felt that visual assessment of the curves in Figures 6.3 to 6.8 would suffice as a preliminary study. The benefits of using more rigorous and exhaustive numerical techniques, though acknowledged here, are thought to be questionable in this context at this stage.

The curves in Figures 6.3 to 6.8 showing the variation of penetration strength and discontinuity spacing round the cutting groove indicate that there is often a high degree of chalk variability over a relatively short distance. This confirms the conclusions of Chapter 5 based on examination of the contour diagrams in Figure 5.2 and Figures 5.4 to 5.6.

The curves in Figures 6.3 to 6.8, relating to the six chainages examined were compared by eye. The pairs of curves compared at each chainage were awarded a 'good', 'fair' or 'poor' rating, depending on their similarity. The results of this comparison are summarised in Table 6.2.

Examination of Table 6.2 indicates that the degree of correlation between each member of a pair of dynamometer traces, C_1 C_2, is variable. At chainages 72.65m and 73.86m the correlation is good, at chainages 76.05m and 79.30m it is fair whilst at chainages 65.16m and 84.95m it is poor. The maximum chainage separation between the members of any pair is approximately 0.5m. It is therefore possible that the ground variability across a given face (discussed earlier) is in some cases also

Table 6.2 Visual correlation matrix for dynamometer traces, penetration strength profiles and discontinuity spacing profiles at selected faces

Indexing chainage (m)	Comparison between curves					
	C_1 C_2	C_1 P	C_1 D	C_2 P	C_2 D	P D
65.16	P	P	P	G	G	G
72.65	G	P	P	P	P	P
73.86	G	P	P	F	F	F
76.05	F	-	P	-	P	-
79.30	F	F	P	F	F	F
84.95	P	F	P	P	F	P

Note:

C_1 = Dynamometer trace prior to indexing.

C_2 = Dynamometer trace after indexing.

P = Penetration strength profile.

D = Discontinuity spacing profile.

G = Good correlation

F = Fair correlation

P = Poor correlation

reflected as variation along the tunnel between adjacent points on consecutive faces, leading to the widely differing pick traces. This ground variability along the tunnel will inevitably lead to discrepancies between the rock indexing profiles and the dynamometer traces. The degree to which the strength or discontinuity profiles correlate with either of the dynamometer traces considered separately will therefore depend largely on ground variability and the proximity of the indexing chainage to either of the dynamometer trace chainages.

Examination of Table 6.2 indicates that, in all cases except one, each indexing was at the same chainage as the second dynamometer trace in the pair (C_2). This reflects the fact that prior to each indexing, approximately 0.3m of tunnel was excavated without the data collection systems in operation in order to 'clean up' the face for the indexing. Instrumented cutting was then resumed almost immediately after the indexing. It is therefore reasonable to expect a better correlation between C_2 and the rock indexing profiles than for C_1. Table 6.2 indicates in qualitative terms that this is generally the case.

The correlations summaried in Table 6.2 suggest that for certain faces there is 'good' or 'fair' correlation between the rock indexing profiles and the cutting force profiles, in other words peaks in cutting force were generated by areas of high penetration strength or high discontinuity spacing. It is also clear that 'good' or 'fair' correlations between cutting force traces and the rock indexing profiles were only obtained when the indexed face chainage was very close to that of the appropriate dynamometer trace, thus largely removing the effects of ground variability. It can, however, be stated that for a given pick geometry and tool array on the cutting head, the results suggest that less energy will be required to cut highly fractured or weaker zones of rock than less fractured or

stronger zones. This conclusion, though intuitively obvious cannot be regarded as a general rule on the basis of the limited data presented in this Chapter. Detailed rock cutting results from the Chinnor tunnelling trials, currently being processed at TRRL, will shed further light on how these factors control rock cutability.

It is interesting to note that in Table 6.2 the correlation between the penetration strength profile and discontinuity spacing profile at a given face is often 'good' or 'fair'. This indicates that the weaker areas of rock tended to fracture more easily; or conversely that the fractured rock tended to give a lower strength reading when measured using the impact penetrometer.

Referring back to the curves in Figures 6.3 to 6.8 and bearing in mind the comments made concerning Table 6.2 it becomes apparent that there is no consistent or systematic relation between cutting force and the indexed rock properties. It is felt that, in addition to the factors discussed earlier, there are a number of possible reasons for the lack of any systematic relation:

(1) Jerky forward movement of the cutting shield may have led to sudden increases in the normal pick force (Figure 6.1), which will have led to corresponding increases in the cutting force, unrelated to variations in rock quality.

(2) Variable surface geometry at the face may have led to peaks and troughs in the measured cutting forces that were unrelated to variations in rock quality. These peaks and troughs may simply have been a reflection of the pick striking large protruding blocks or cavities in the face.

(3) Variations in cutting force may have been partly due to a varying rock property (eg surface friction characteristics) not measured by the impact penetrometer or the scanline surveys.

The conclusions of Chapter 5 (based on the examination of Figures 5.1 and 5.8) concerning the applicability of face indexing results averaged over the whole face are not invalidated by the points raised in this Chapter. Variation in the distribution pattern of rock quality from face to face does not necessarily imply that the rock quality averaged over the whole face is varying significantly. In particular it is important to note that the apparent lack of significant correlation between cutting forces and rock quality on the small scale need not imply any lack of correlation on the large scale over the whole face. In fact recent results (Hignett, 1975) show that cutting characteristics averaged over the whole face correlate well with average strength indices obtained using the penetrometer.

6.6 Summary and conclusions

1. A qualitative comparison between profiles of cutting forces, intact rock penetration strength and discontinuity spacing measured at six faces in the Chinnor tunnel was undertaken.

2. Visual comparison between profiles indicated that for certain faces peaks in cutting force were generated by areas of high penetration strength or high discontinuity spacing.

3. Reasonable correlation between cutting force traces and rock indexing profiles was only obtained when the indexed face chainage was

very close to that of the appropriate dynamometer trace, thus largely removing the effects of rock variability.

4. The lack of any apparent systematic or consistent relation between cutting force and rock quality indicates that there may be a more complicated set of factors causing variations in the cutting force measured at the face.

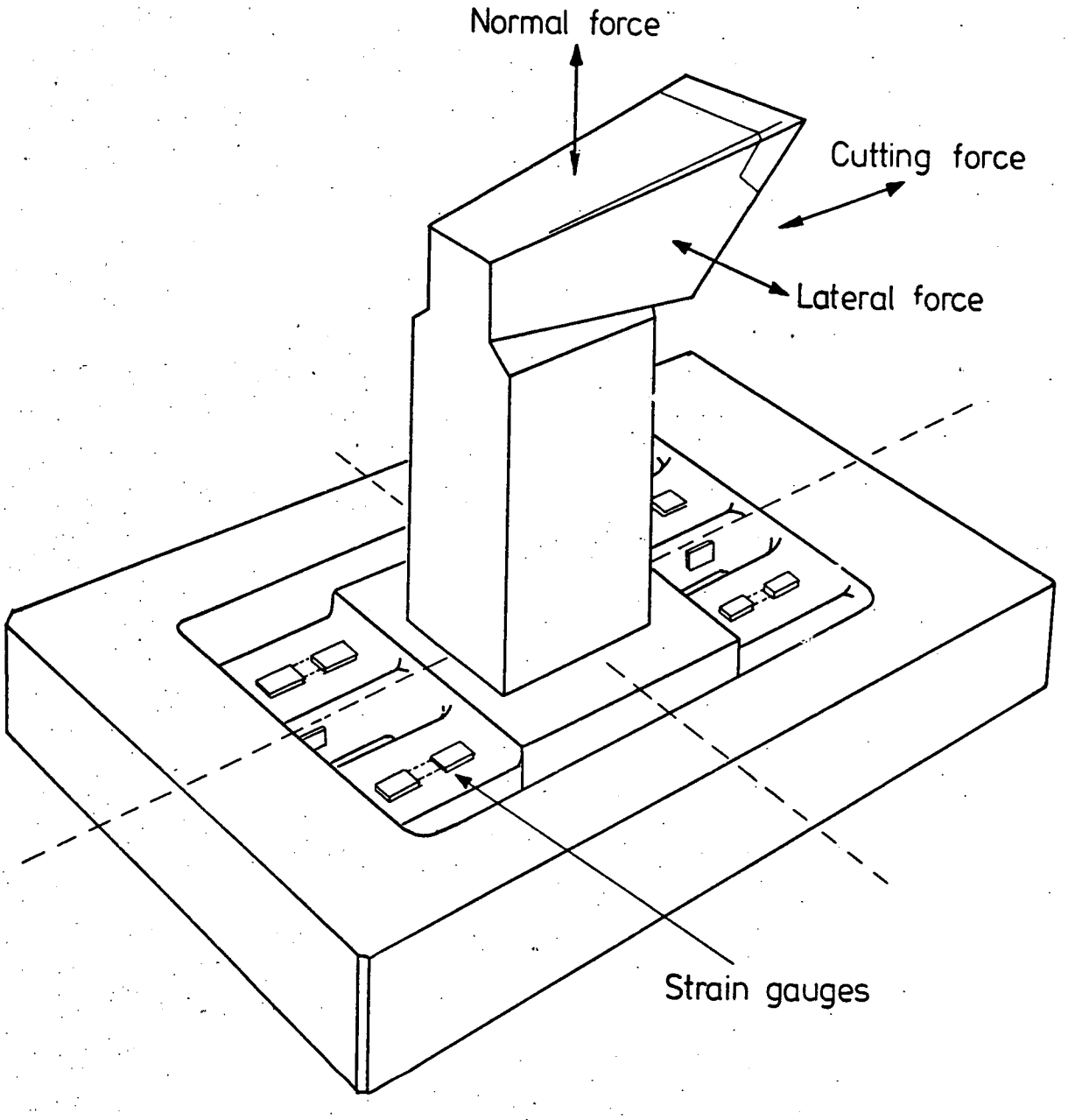

Fig. 6.1 DRAG PICK MOUNTED IN DYNAMOMETER.
(AFTER HIGNETT, 1974)

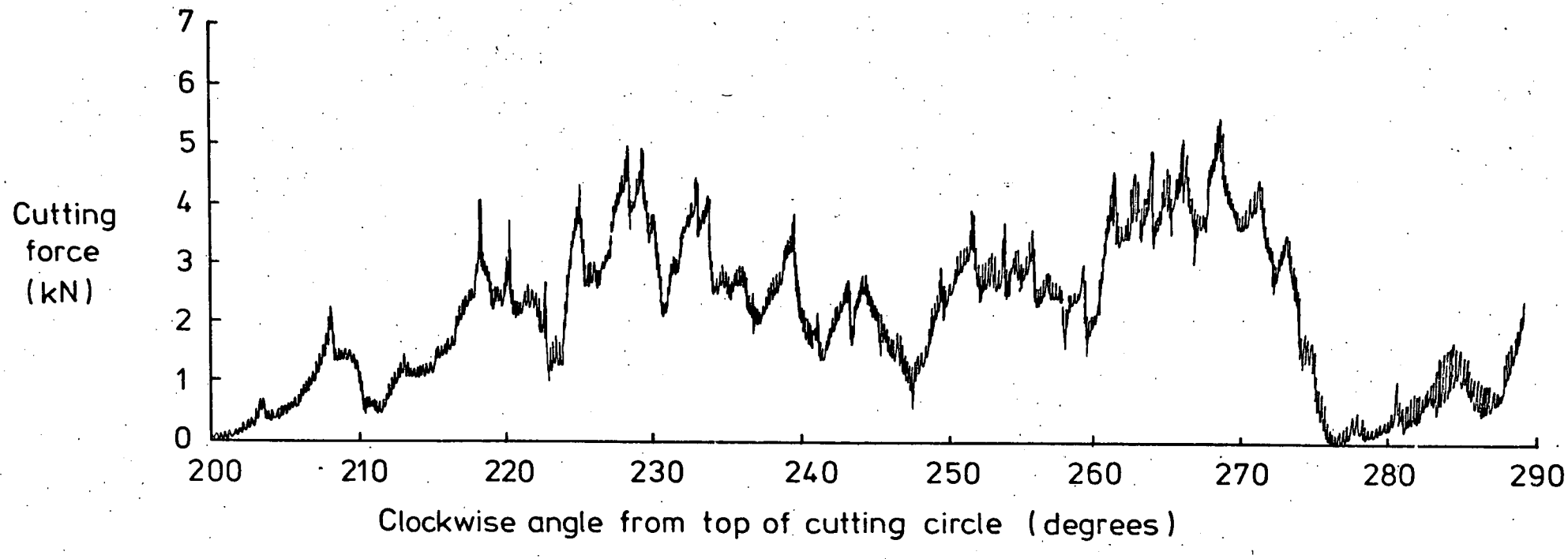

Fig.6.2 SAMPLE OF UV TRACE RECORDING TYPICAL CUTTING FORCE DATA OUTPUT OF A DYNAMOMETER.

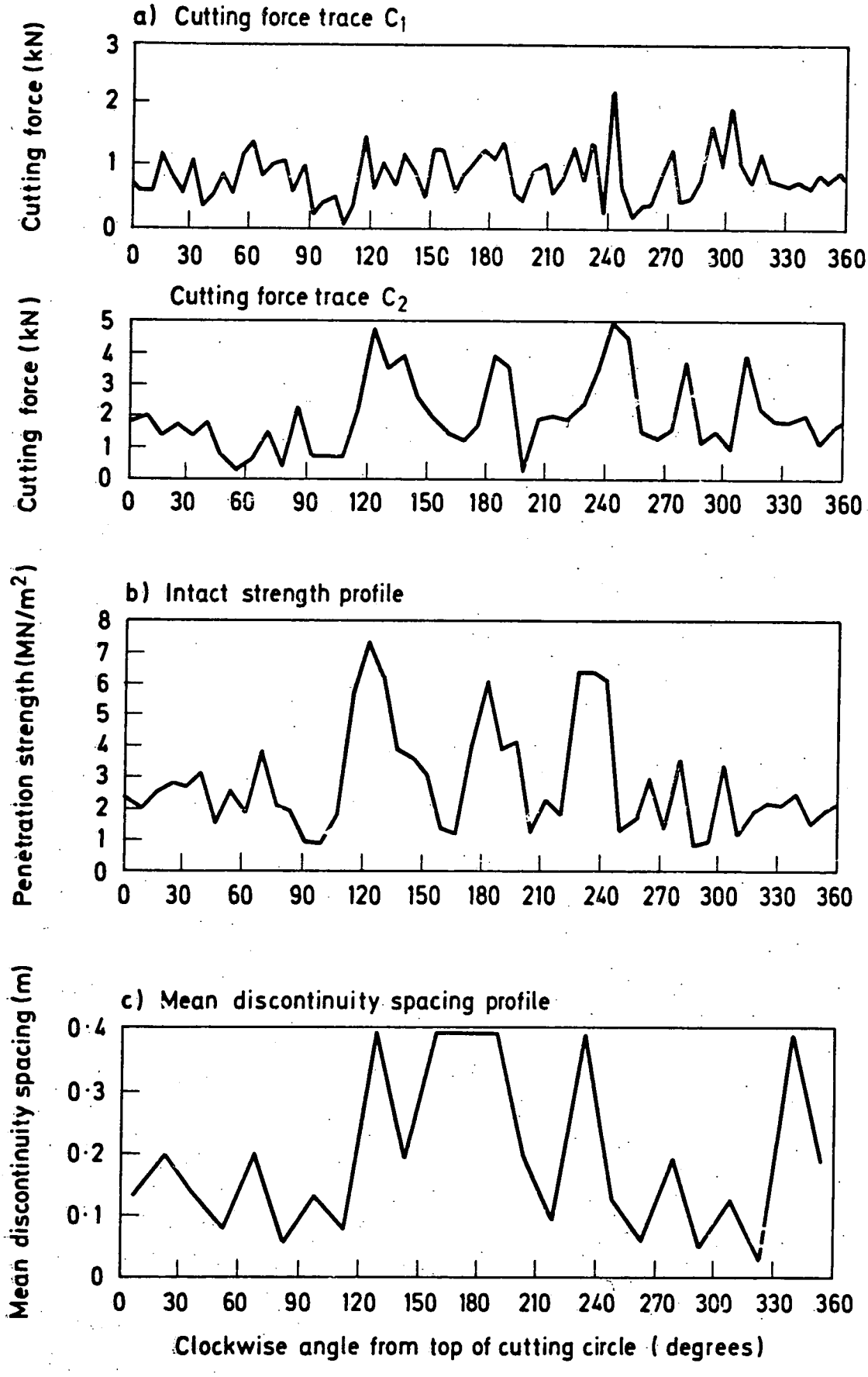

Fig. 6.3 CUTTING FORCE, INTACT STRENGTH AND MEAN DISCONTINUITY SPACING PROFILES AT THE FACE. CHAINAGE 65·2m, CUTTING CIRCLE RADIUS 1·58m

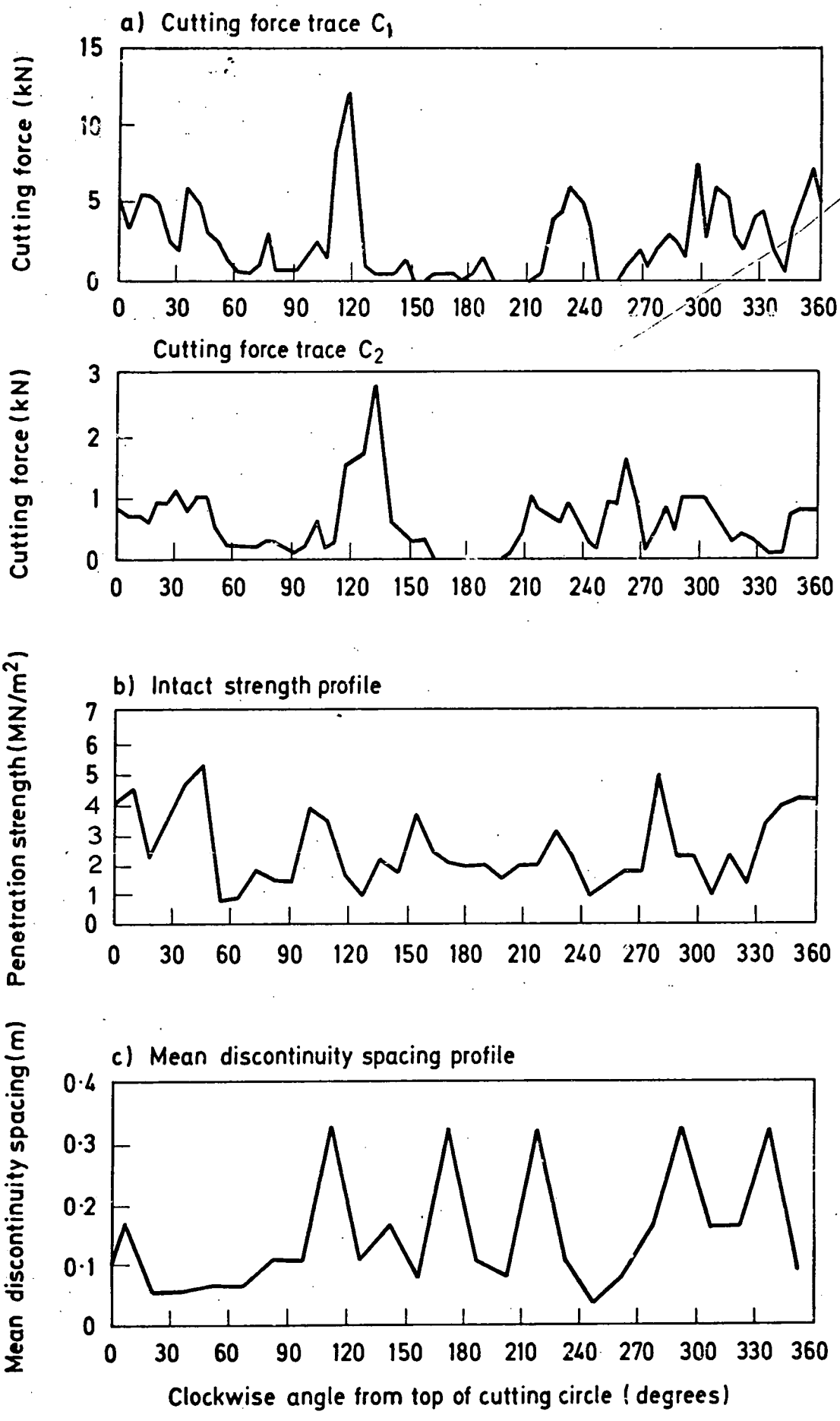

Fig. 6.4 CUTTING FORCE, INTACT STRENGTH AND MEAN DISCONTINUITY SPACING PROFILES AT THE FACE. CHAINAGE 72·7m, CUTTING CIRCLE RADIUS 1·23m

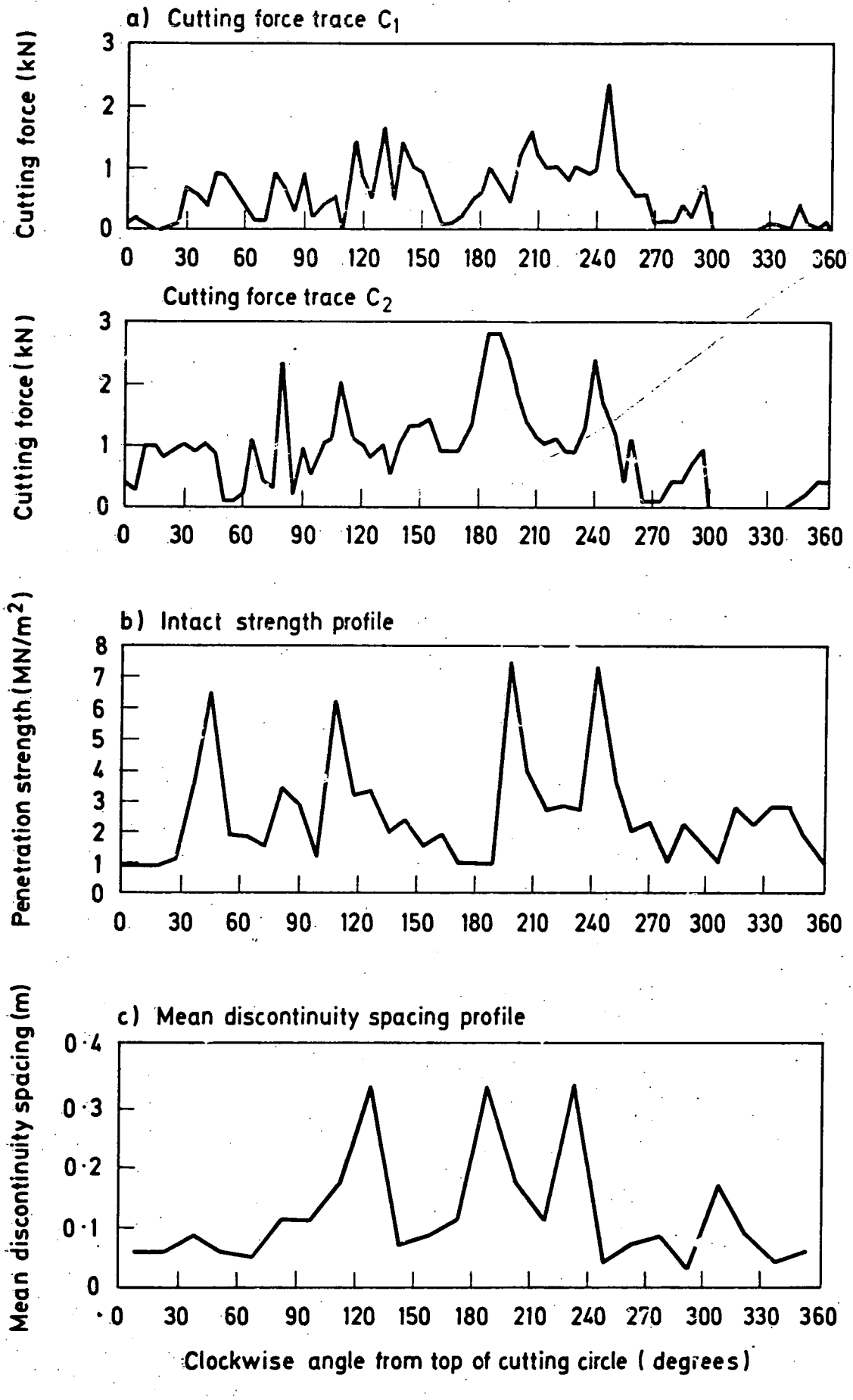

Fig. 6.5 CUTTING FORCE, INTACT STRENGTH AND MEAN DISCONTINUITY SPACING PROFILES AT THE FACE. CHAINAGE 73·8m, CUTTING CIRCLE RADIUS 1·23m

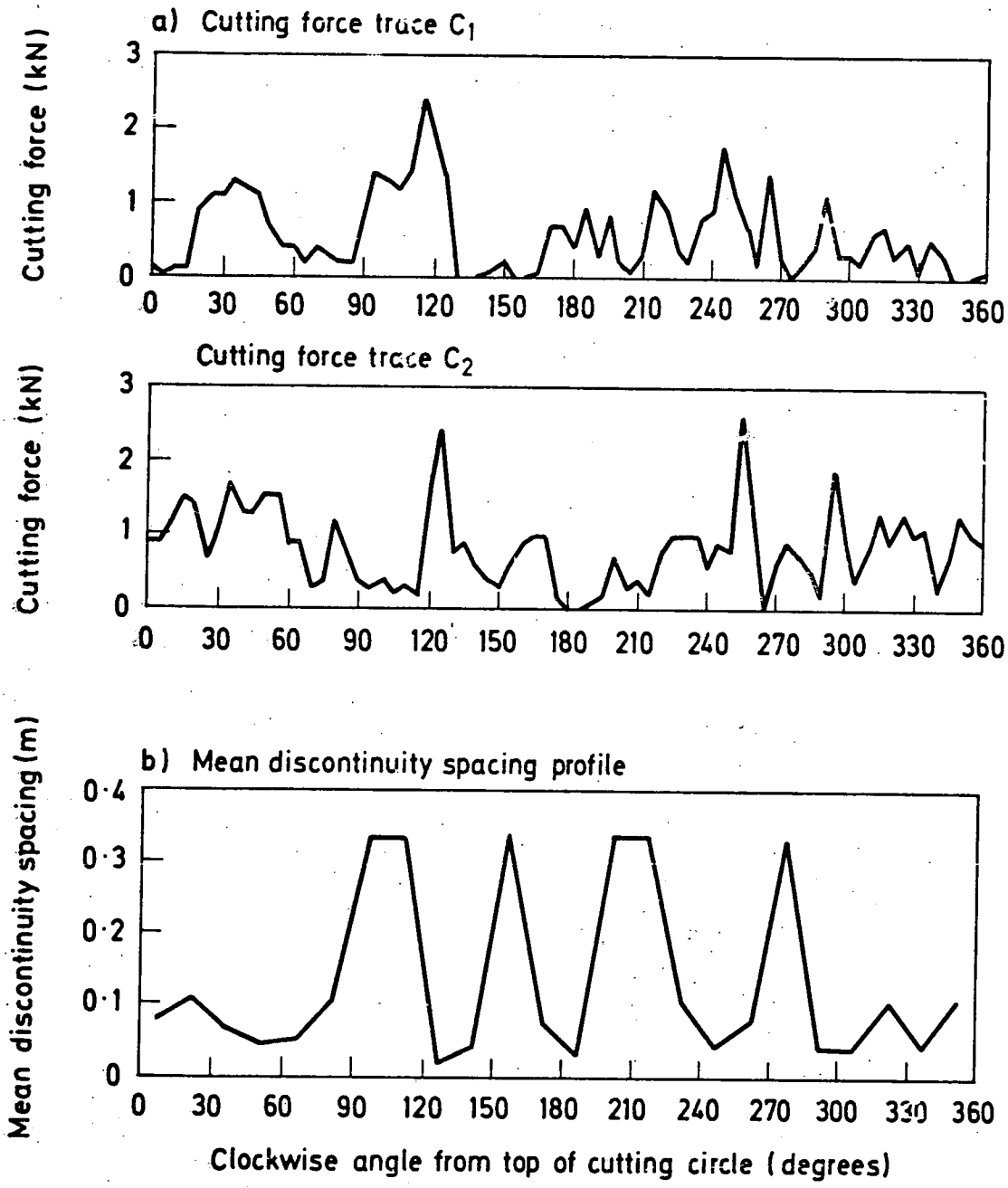

Fig. 6.6 CUTTING FORCE AND MEAN DISCONTINUITY SPACING PROFILES AT THE FACE. CHAINAGE 76·1m, CUTTING CIRCLE RADIUS 1·23m

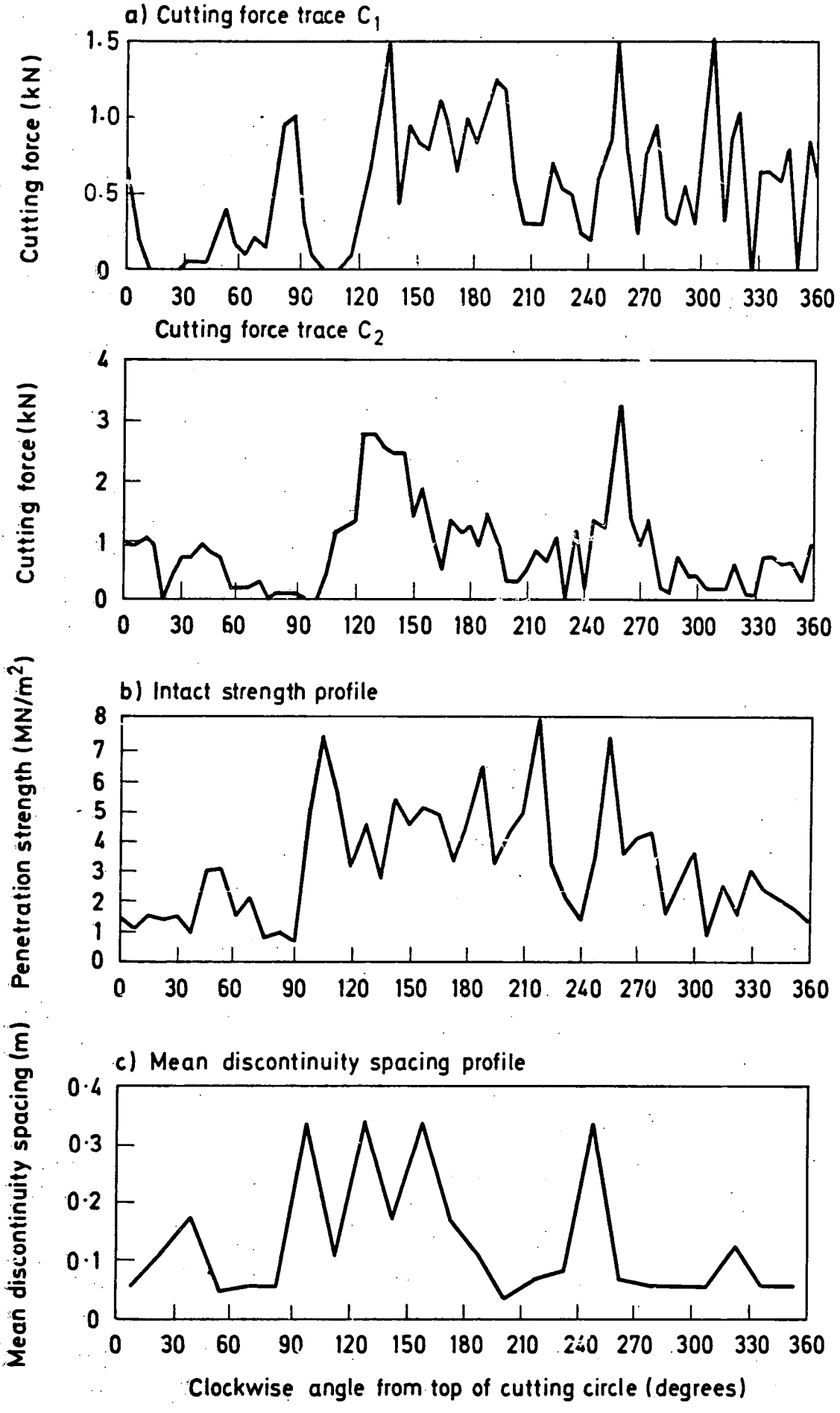

Fig. 6.7 CUTTING FORCE, INTACT STRENGTH AND MEAN DISCONTINUITY SPACING PROFILES AT THE FACE. CHAINAGE 79·3 m, CUTTING CIRCLE RADIUS 1·23 m

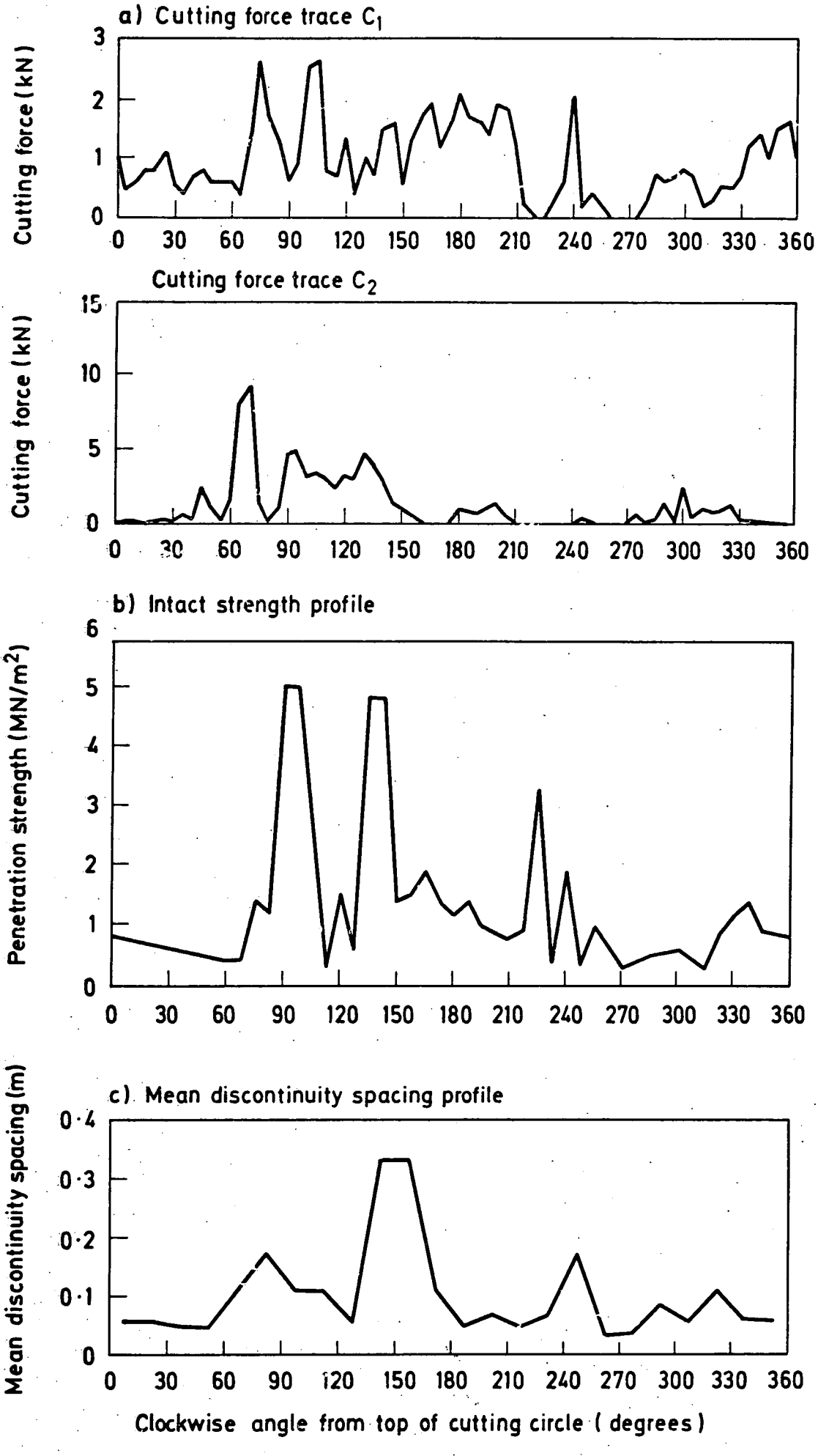

Fig. 6.8 CUTTING FORCE, INTACT STRENGTH AND MEAN DISCONTINUITY SPACING PROFILES AT THE FACE. CHAINAGE 85·0m, CUTTING CIRCLE RADIUS 1·23m

CHAPTER 7

GROUND MOVEMENTS CAUSED BY TUNNELLING AT CHINNOR

7.1 Introduction

A section of the Chinnor tunnel, at a chainage of approximately 20m was instrumented to measure ground movements. The aim of this work was to assess the influence of the tunnelling operations on the ground, and in particular to detect possible disturbances at ground level likely to affect surface structures.

The ground movement measurements were of two types, taken at two locations:

(a) Measurements taken in boreholes and from surface levelling at a chainage of approximately 21m. This work was carried out by members of TRRL.

(b) Measurements taken in a trench excavated across the tunnel line at a chainage of 23m. This work was carried out by the author.

7.2 Ground movement measurements taken in boreholes and from surface levelling

7.2.1. Measurement Techniques

Ground movements resulting from tunnel excavation and reaction ring jacking tests (Section 7.4) were measured in boreholes and by surface

levelling by members of the Transport and Road Research Laboratory. This ground movement measurement programme, together with the results, is described by McCaul *et al.* (1975).

The geometry of the measurement boreholes P1 to P6 is shown in Figure 7.1. Inclinometer tubes were installed in boreholes P4, P5 and P6 and horizontal movement of these tubes was monitored using a digital inclinometer. Magnetic rings were fitted to the outside of the inclinometer tube in borehole P5, vertical movement of these magnetic rings (reflecting vertical ground movement) was montitored using a sensor. Vertical ground movement was also monitored using Whittaker wire extensometers installed in boreholes P1, P2 and P3. The principle of the wire extensometer is explained in Figure 7.2. The movement of the weight (and thus vertical ground movement) was measured to 0.01mm using a micrometer. Vertical movement of the tops of the boreholes was measured using an automatic level fitted with an optical micrometer. Levels were taken relative to a remote concrete bench mark.

Horizontal movement of the tops of borehcles P4, P5 and P6 parallel to the tunnel axis was measured using a theodolite. Lateral horizontal movement at these boreholes was measured using a steel band anchored to the base of a concrete pillar.

Two control boreholes at a location remote from the tunnel were instrumented and monitored in order to eliminate any 'noise' encountered in measurements taken from boreholes P1 to P6. A full discussion of system accuracy is presented in McCaul *et al.* (1975).

7.2.2 Ground movement results

McCaul *et al.* (1975) found that surface movement began when the tunnel was approximately 10m from the borehole section and that 2-3mm of subsidence had occurred when the tunnel passed the boreholes. Subsidence continued until the face had advanced approximately 40m beyond the boreholes. The total surface subsidence at borehole P2 (above the tunnel axis) was 8mm, total surface subsidence at boreholes P1 and P3 was 4.5mm and 7.5mm respectively. The possible detrimental effects of ground movements of this order on surface structures are discussed in Chapter 8.

Vertical and horizontal displacements in the plane normal to the tunnel axis, measured in boreholes P1 to P6 are summarised in Figure 7.3. Graphs showing the variation of downward vertical movement with distance from tunnel axis level in boreholes P1, P2 and P3 are shown in Figure 7.4.

7.3 Measurements taken in a trench excavated across the tunnel line

7.3.1 Measurement procedure

The aim of this series of measurements was to determine directly the ground strain above the tunnel resulting from tunnel excavation. This strain was measured both in intact rock and across discontinuities, thereby giving insight into the part played by discontinuities in controlling ground movement.

The rock was exposed for instrumentation by means of a trench (Figure 7.1). This was excavated across, and at right angles to, the proposed tunnel centre line using an army trencher (Plate 7.1). The trench

was smooth walled, 1.6m deep, 0.6m wide, extending 8m to the right (east) of the centre line of the tunnel and 14m to the left, at chainage 23m (Plate 7.2). 22m was the maximum possible length of the trench at this chainage. The bottom of the trench was 4.5m above the proposed tunnel crown.

Immediately following excavation, the trench was covered with tarpaulin sheets mounted on a frame to keep the rock at a reasonably constant temperature and moisture content. Water accumulating in the trench proved to be a problem, but this water was pumped out at regular intervals to minimise weathering effects. The protective measures described above proved to be successful since, during the eight month period over which measurements were taken, there was little visible degradation of the trench walls.

The trench was instrumented using Demec points. These small metal discs were fixed to the trench walls (Figure 7.5). Variation in the distance between adjacent points was monitored using a Demec gauge (Plate 7.3). The Demec points were fixed to the rock using two methods:

(a) The Demec points were stuck directly to the rock surface using a water resistant resin bonding agent. Before fixing, it was necessary to clean and dry the rock surface to ensure a good bond. This method had the disadvantage that the bond was only as good as the rock underneath, therefore chipping or flaking of the rock surface could produce problems. In fact less than 5% of Demec points fixed in this way were lost.

(b) Nails, 7cm long were fired into the rock at the required position using a nail gun. The Demec points were then fixed to the top

of the nail using 'Araldite'. This method produced a good Demec point/rock bond, but had the disadvantage that close positioning of Demec points was impossible due to possible interference effects resulting from a large nail length compared with Demec point spacing. A Demec point fixed by this method is shown in Plate 7.4.

Three Demec gauge lengths were used: long (nominal span 40cm), medium (nominal span 20cm), short (nominal span 5cm). All short Demec points were fixed using method (a), the long and medium span points were fixed by method (b), though method (a) was used when appropriate (for example close to discontinuities). Three main Demec point configurations were adopted:

(1) Short span across discontinuities. All discontinuities instrumented belonged to the WNW dipping set shown in Figure 2.24. These discontinuities were most common largely because the orientation of the trench (west-east, Figure 7.1) was most favourable for intersecting discontinuities having this orientation. Each discontinuity was instrumented with four Demec points positioned as shown in Figure 7.5(a). The configuration was such that spans x and z would pick up normal movements across the discontinuity (dilation or compression) and span y would pick up movements parallel to the discontinuity. Eight dicontinuities were instrumented in this way.

(2) Long span across discontinuities. Again all discontinuities instrumented belonged to the WNW dipping set shown in Figure 2.24. The Demec point configuration was as shown in Figure 7.5(a) with the nominal span lengths 40cm instead of 5cm. Thirteen discontinuities were instrumented in this way.

(3) Long span across tunnel centre line. A horizontal line of long span Demec points was set up along the sidewall of the trench (Figure 7.5 (b)). This line consisted of 48 x 40cm spans, and served to monitor the gross horizontal strain in the ground 5m above the tunnel crown.

7.3.2 Standardisation and control of readings

The invar bars accompanying each Demec gauge enabled a regular check to be made on the zero readings of the Demec gauges. This was done before and after each series of readings and thus ensured that all measured movements were real movements.

In order to establish the validity of the results a series of control Demec spans was set up:

(1) At the far end of the trench, 14m from the tunnel centre line, six short and six long Demec spans were set up across intact rock. Three of the short and three of the long spans were fixed directly to the rock using the resin bonding agent; the rest were fixed using the nails. This provided a direct comparison between the two fixing methods. The position of these control spans, three diameters from the tunnel, was thought to be largely beyond the range of influence of significant strain effects. The control spans therefore gave an indication of factors causing real span variation that were not directly associated with tunnelling.

(2) At six positions along the trench, medium span Demec points were set up across intact rock. At each of the six positions, one

vertical and one horizontal span was set up. These spans gave an indication of strain effects in the intact rock not associated with movement along discontinuities.

Reading were taken on all control and discontinuity spans approximately once every four days between January 1974 and July 1974. A total of approximately 4300 Demec gauge readings were taken.

7.3.3 Processing of Results

Each Demec gauge reading was taken to a precision of ± one division on the dial gauge, giving a precision of, at the worst, ± 0.002mm to the measurement of each Demec point span. The initial reading for each span (R_0) was taken approximately two days after installation of the Demec points. All subsequent readings R_1, R_2 ..... R_n were processed relative to R_0, giving the deviation from the initial value; $D_1 = R_1 - R_0$, $D_2 = R_2 - R_0$..... $D_n = R_n - R_0$. D_n = positive indicated increase in the span length, D_n = negative indicated decrease in the span length. Each span was allocated a number to facilitate processing and cross-reference, thus $D_{48,12}$ indicated the deviation of the 12th reading on span 48, from the initial reading. It was thus possible to tabulate the D value in matrix form $D_{i,j}$, the above reading being found in row 48 column 12. Specific results matrices refer to specific Demec point configuration types:

Matrix A = short span across discontinuities
B = long span across discontinuities
C = medium span across intact rock, control
D = short control spans
E = long control spans
F = long span series across tunnel centre line.

The columns and rows in these matrices are related to time and position in Appendix Tables I.1 and I.2. Processing of results in each matrix was done using a desk calculator. Matrices A-F are presented in Appendix Tables I.3 to I.8.

Matrices A and B

The results in these matrices refer to movements on discontinuities of two types: normal movement and movement parallel to the discontinuity. Rows containing data on normal movement are designated "N", rows containing data on movement parallel to the discontinuity are designated "P"; the "N" rows and "P" rows are subsequently considered separately. The average absolute deviation for each column j was calculated for the N rows and P rows grouped separately.

$$\text{Average absolute deviation N, P} = \frac{\sum_{i=1}^{n} |D_{i,j}|}{n}$$

where n is the number of rows.

This produced two row matrices $\{N\}$, $\{P\}$ with the column number indicating the time of the readings, and thus chainage of the tunnel. The average deviation values were converted into strain values by applying the appropriate gauge factor listed in Appendix I. The results are plotted in Figures 7.6 and 7.7 as graphs of average absolute 'normal' and 'parallel' strain against tunnel chainage. The position of the trench is indicated in each Figure.

Movement along one discontinuity set only was recorded in matrices A and B, and it was therefore possible to process the results further to give an indication of the general sense of the movement. All positive

normal deviations in each column of each matrix were summed, then expressed as a percentage of the total normal deviation for that column. In this way, the percentage of movement of a dilational nature was determined. In a similar way all positive (Figure 7.8) parallel deviations were summed, then expressed as a percentage of the toal parallel displacement for the appropriate column. The results, plotting percentage against chainage for matrices A and B are shown in Figure 7.8.

Matrices C, D and E

Matrices C, D and E were processed in a similar way to that described above. Averaging column by column produced a row matrix of average absolute deviation for each matrix, with the column number again indicating the time of the readings, and thus chainage of the tunnel. The average deviation values were converted into strain values by applying the appropriate gauge factor. The results are plotted in Figure 7.9 as graphs of average absolute deviation against tunnel chainage. The position of the trench is indicated in this Figure.

Matrix F

Data in this matrix represent a series of readings along a line of Demec points set in the trench wall. Each column of the matrix represents a profile across the tunnel axis. In order to smooth these profiles, and facilitate interpretation, the data were averaged in pairs down each column. This method of moving average smoothing produced a new matrix containing one fewer rows than the original. The deviation values were converted into strain values by applying the appropriate gauge factor.

Columns 14-19 of matrix F represent measurements taken over a 24 hour period during the reaction ring jacking tests and are considered separately in Section 7.4. Five separate columns of the smoothed matrix (Column numbers 7, 13, 20, 24 and 27) were extracted and plotted as profiles to indicate the development of lateral horizontal strain during tunnel advance (Figure 7.10). The initial state is represented by a horizontal straight line, indicating zero strain prior to tunnel excavation.

7.3.4 Discussion of results

Examination of Figures 7.6 and 7.7 reveals that the average absolute normal and parallel strain across the discontinuities that were monitored show a rapid increase as the tunnel approaches to within 5m of the trench. The strain continues to increase as the tunnel passes and only begins to level off when the tunnel face is 40m past the trench. These results are in agreement with those of McCaul *et al.* (1975) described in Section 7.2. The continuation of ground movement following the passage of the tunnel is consistent with other published evidence of clay settlement behind a tunnel face (Hansmire and Cording, 1972; Attewell and Farmer, 1974 a,b) and, for this material, suggests a progressive block loosening and movement following initial disturbance.

Block loosening effects near tunnels in discontinuous ground have been noted by several workers (Terzaghi, 1946; Lang, 1957; 1959). In particular Lang (1959) noted that loosening effects in the rock mass resulted from tension or rotation between blocks leading to crushing or shearing at the corners of blocks. Cecil (1970) presented a comprehensive study of loosening effects near tunnels, based on laboratory model studies and field-work. He concluded that there is a variety of complicated failure mechanisms for loosened rock, but that 'joint' friction and

discontinuity orientation can drastically affect both the mode of failure in a loosening block mass and the stress level at which failure occurs.

The onset of strain effects one diameter ahead of the tunnel at Chinnor is in apparent contradiction with Abel and Lee (1973) who detected stress effects at least two diameters ahead of model tunnels excavated in concrete and elastic acrylic. The late onset of strain effects at Chinnor is largely a result of the shallow tunnel depth.

It is noticeable in Figures 7.6 and 7.7 that shear movement along discontinuities is dominant over normal movement, suggesting a combination of block loosening and rotation. It is evident that strain measured on the short gauge is half as large again as strain measured on the long gauge. This is a result of the fact that both the long and short Demec spans sampled only one major discontinuity. Thus if a similar movement is attributed to all the discontinuities, the larger span will record a lower strain.

The average absolute strain recorded on the long and short control spans remote from the tunnel and shown in Figure 7.9(a) indicates a steady increase in strain uninterrupted by the passage of the tunnel. It is probable, therefore, that the average absolute strain accumulated on these remote spans during the first 65m of tunnelling over a period of 6 months, is attributable to slow and imperceptible degradation of the trench walls, causing a gradual deviation of the span readings from the initial values. This 'drift' is also evident on the first part of the curves in Figures 7.6 and 7.7.

Figure 7.9(b) shows the average absolute strain measured on the medium spans set in intact rock at selected positions along the trench walls. It is evident that there was a small increase in strain when the tunnel

approached to within 5m of the trench. However, following this step-up in strain - and after passage of the tunnel - further deviation may be explained by 'drift' affects. It is clear, therefore, that the response of intact elements of rock to stresses induced by tunnelling is much less than the response of the discontinuities. Furthermore, the response of intact elements is of an essentially 'elastic' nature, there being no further movement after passage of the tunnel face.

Figure 7.8 summarises the type of movement developed on the discontinuities. In general, both long and short gauges reveal that the normal strain is between 80% and 90% compressive. Interpretation of the parallel movement along the discontinuities is not simple. It is clear, however, that there is a sharp increase in positive parallel movement as the tunnel approaches to within 5m of the trench.

Selected horizontal strain profiles across the tunnel line are shown in Figure 7.10. The irregular form of these strain profiles suggests that the horizontal strain resulted from discrete block movements (that is, movement along discontinuities) rather than from purely elastic deformation of the rock mass. However, Figure 7.10 does indicate a zone of horizontal compression directly above the tunnel and a zone of horizontal tension approximately 7m from the centre line. This zone of tensile strain will have tended to exacerbate loosening and dislocation of discontinuities above the tunnel. A third degree polynomial curve was fitted to the final profile F and the result is shown in Figure 7.11.

Figure 7.12, from the Subsidence Engineers Handbook (1966) shows the three principal types of horizontal strain profile that can develop over an area of longwall mining. In this Figure, W is the width of the working

and h is the depth. It is clear that the form of the smoothed strain profile in Figure 7.11 closely approximates that of profile (a) in Figure 7.12 which has a w/h of 0.45 and therefore represents undercomplete (sub-critical) extraction with respect to the critical area. At Chinnor the diameter/depth ratio is approximately unity and therefore also represents a situation of sub-critical extraction. The general similarity between the horizontal strain profiles developed above a mining area and the tunnel at Chinnor indicates that broadly similar subsidence mechanisms operated in the two situations.

A horizontal strain profile similar to that shown in Figure 7.11 has also been obtained from recent measurements taken above a syphon tunnel driven in silty alluvium at Willington Quay on the north bank of the river Tyne (Attewell, 1975). As in Figure 7.11 the transverse strain profiles above the soft ground tunnel were characterised by the development of horizontal compressive strain above the centre line and two zones of horizontal tensile strain at the flanks of the tunnel.

7.4 Reaction Ring jacking tests

7.4.1 Test Programme

The long span series of Demec points across the tunnel centre line was used to monitor ground movement during a programme of reaction ring jacking tests carried out by TRRL on 1 May 1974. The reaction ring of the tunnelling machine was positioned with its centre 2m down chainage (south) from the trench. Additional ground movement measurements were taken in borehole P2, located above the reaction ring centre (Figure 7.1).

Pressurisation of the reaction ring jacks caused the two halves of the reaction ring to move vertically outwards and press against the tunnel crown and invert, applying pressure to the rock.

The sequence of readings taken in the trench is represented by columns 14-19 in matrix F (Appendix I). The time of each reading and the state of the reaction ring are summarised in the following Table (see also Appendix Table I.1).

Table 7.1 Reaction ring jacking test programme

Date and time of reading	1 May 09.15	1 May 12.00	1 May 14.15	1 May 15.35	1 May 16.05		2 May 10.15
State of reaction ring	Relaxed (pre-test)	Pressurised	Relaxed	Pressurised	Relaxed	Eight presurisation/ relaxation cycles	Relaxed
Column number in matrix F	14	15	16	17	18		19

For the plotting of results, and in order to isolate graphically the reaction ring effect, the initial pre-test condition (column 14) was assumed to be one of zero horizontal strain. Columns 15-19 were therefore re-processed in the way described in Section 7.3, taking column 14 as the R_o column. The resulting profiles of deviation values were smoothed by using a moving average, taking the values in pairs, then converted into strain values by applying the appropriate gauge factor. These strain profiles are plotted in Figure 7.13. The initial profile is shown as a horizontal straight line indicating zero strain.

A part of each profile (x) extending symmetrically 6.0m each side of the tunnel centre line, was extracted and processed to determine the nett horizontal strain. This nett horizontal strain for the 12.0m length over the tunnel centre line at each stage of the test programme is shown in Figure 7.13.

Vertical ground movement developing during the reaction ring jacking programme was measured in borehole P2 using Whittaker wire extensometers (described in Section 7.2). The results of these tests have been made available to the author by TRRL. Ground movement measured at four anchor points was registered as a movement of four weights located in the extensometer measuring head. The movement of each weight was monitored consecutively using an LVDT* which provided the x input for an x-y recorder. The hydraulic pressure in the jacks was measured using a pressure transducer which provided the y input. Thus it was possible to monitor ground movement at four positions above the axis, together with reaction ring hydraulic pressure (and therefore vertical ground loading), during the reaction ring jacking sequences. The results of four such jacking cycles are presented in Figure 7.14, showing the relation between vertical pressure imposed on the ground by the reaction ring and upward vertical movement at the four anchor points.

7.4.2 Discussion of results

Figure 7.14 indicates that there was considerable upward movement of the ground above the tunnel during pressurisation of the hydraulic jacks, ranging from 10mm near the tunnel crown to 0.5mm 3m above the crown. Figure 7.14 also shows that the vertical displacements were totally recovered following relaxation of the reaction ring.

---

* Linear variable differential transformer

The upward vertical movements in Figure 7.14 are reflected in Figure 7.13 as horizontal tensile strain above the tunnel during periods of jack pressurisation. The tensile strain partly - but never completely - recovered following relaxation of the reaction ring will have led to considerable opening and loosening of discontinuities. Following the eight pressurisation/relaxation cycles there is considerable permanent dislocation of the ground. This residual strain in the ground is of a highly irregular nature, again implying discrete relative movement and rotation of blocks rather than a smooth elastic response to the high stresses induced by the reaction ring.

The upward vertical pressure on the ground induced by the reaction ring can be estimated by dividing the jacking force by the horizontal sectional area of the reaction ring at axis level. At a jacking force of 7.5MN this vertical ground pressure is approximately $0.5MN/m^2$, whereas the downward vertical ground pressure at the appropriate depth is approximately $0.15MN/m^2$. It is likely, therefore, that the reaction ring reacted against additional ground extending at least one tunnel diameter each side of the tunnel, this load shedding being achieved by the shear strength properties of the chalk. The high shear stresses induced by this load shedding process will therefore have tended to exacerbate ground disturbance above the tunnel and will have led to the permanent dislocations recorded at ground level.

7.5 Summary and conclusions

1. Ground movements were measured during the TRRL tunnelling trials at Chinnor, both over the long-term during the passage of the tunnelling machine, and over the short-term during reaction ring jacking tests.

2. The measurements were taken both in boreholes and in a trench excavated above and across the tunnel line. The depth to tunnel crown was approximately 5m.

3. The total surface settlement above the tunnel centre line was found to be 8mm - total surface settlement above the tunnel springing lines was found to be 4.5mm and 7.5mm on the east and west sides respectively.

4. Following the passage of the tunnel face, significant permanent movements along discontinuities, as monitored in the trench, were observed. Deformation of intact elements of rock was small compared with that observed along discontinuities.

5. Measurements in the boreholes and in the trench indicated that ground movement began when the tunnel was between 1 and 2 diameters away and continued until the face had advanced approximately 8 diameters beyond the instrumented section.

6. The horizontal strain profile, developed as a result of tunnel excavation, indicated a zone of horizontal compression directly above the tunnel and a zone of horizontal tension approximately 7m from the centre line. This strain profile was found to have a similar form both to profiles developed above areas of longwall mining under conditions of incomplete extraction of the critical area, and above a shallow soft ground tunnel.

7. Significant ground movements and permanent dislocation were observed during the reaction ring jacking test programme. Ground disturbance was partly exacerbated by the development of high shear stresses as a result of load shedding above the vertically acting reaction ring. The form of the horizontal strain profile during the jacking tests indicated the

development of a zone of horizontal tensile strain above the tunnel. Following the reaction ring jacking test programme, there was found to be permanent movement and dislocation of the ground above the tunnel.

8. The zones of horizontal tensile strain, developed 7m from the centre line as a result of tunnel excavation and directly above the tunnel as a result of reaction ring pressurisation, will have tended to open and loosen unfavourably orientated discontinuities. These effects will have tended to aggravate the problems of ground instability.

9. It is concluded that there were three significant factors controlling the behaviour of the ground near the Chinnor tunnel:-

(a) Discontinuities present in the chalk provided weakness planes which facilitated block rotation and dislocation in the rock mass.

(b) The vertically-acting reaction ring induced permanent loosening and dislocation of blocks during the tunnelling operations.

(c) Gradual movement of blocks on to the steel arch supports, taking up the overbreak cavity (discussed in Chapter 5) provided a facility for continued ground deformation following the passage of the tunnel face.

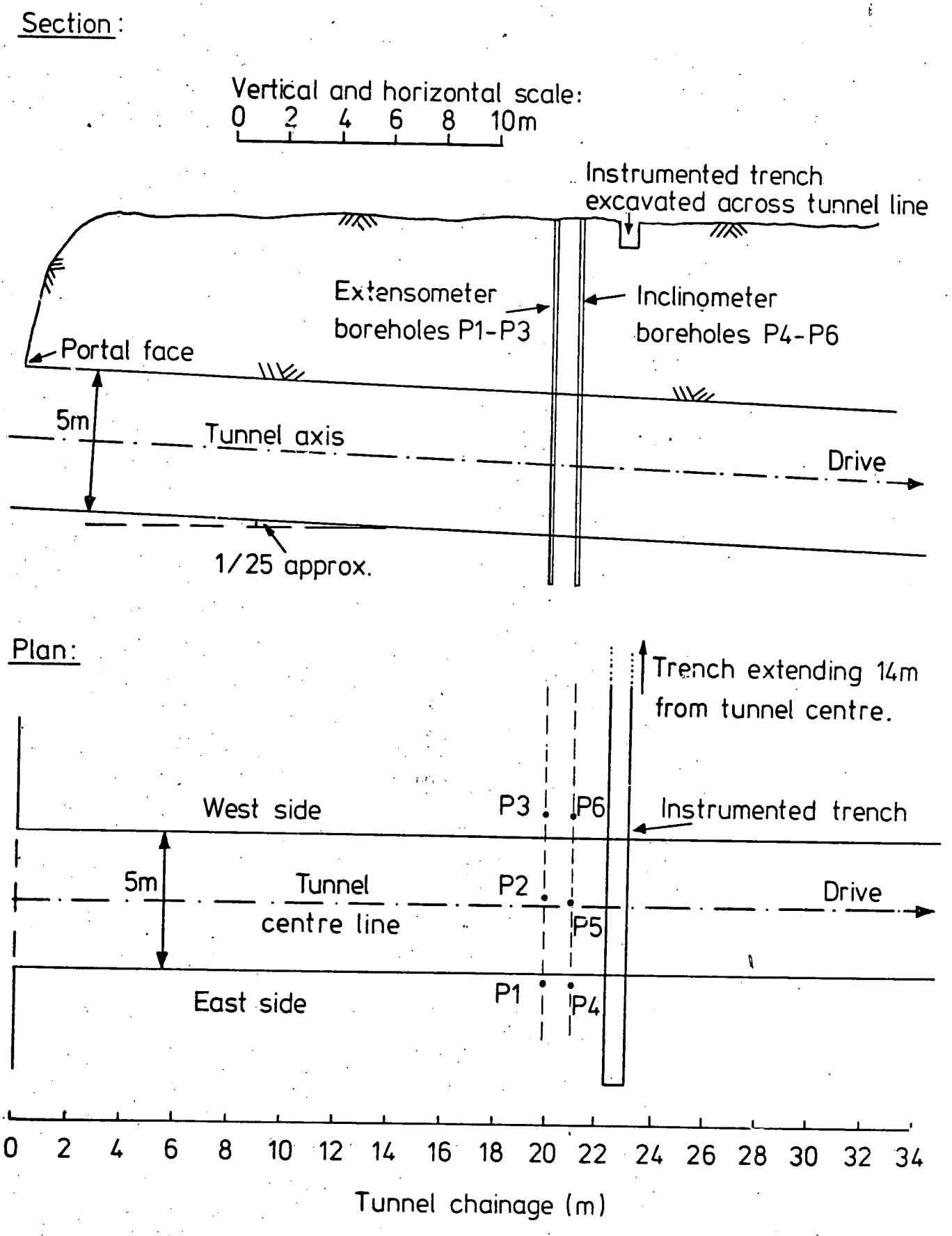

Fig. 7.1 LOCATION OF THE INSTRUMENTED SECTION
(AFTER McCAUL et al., 1975)

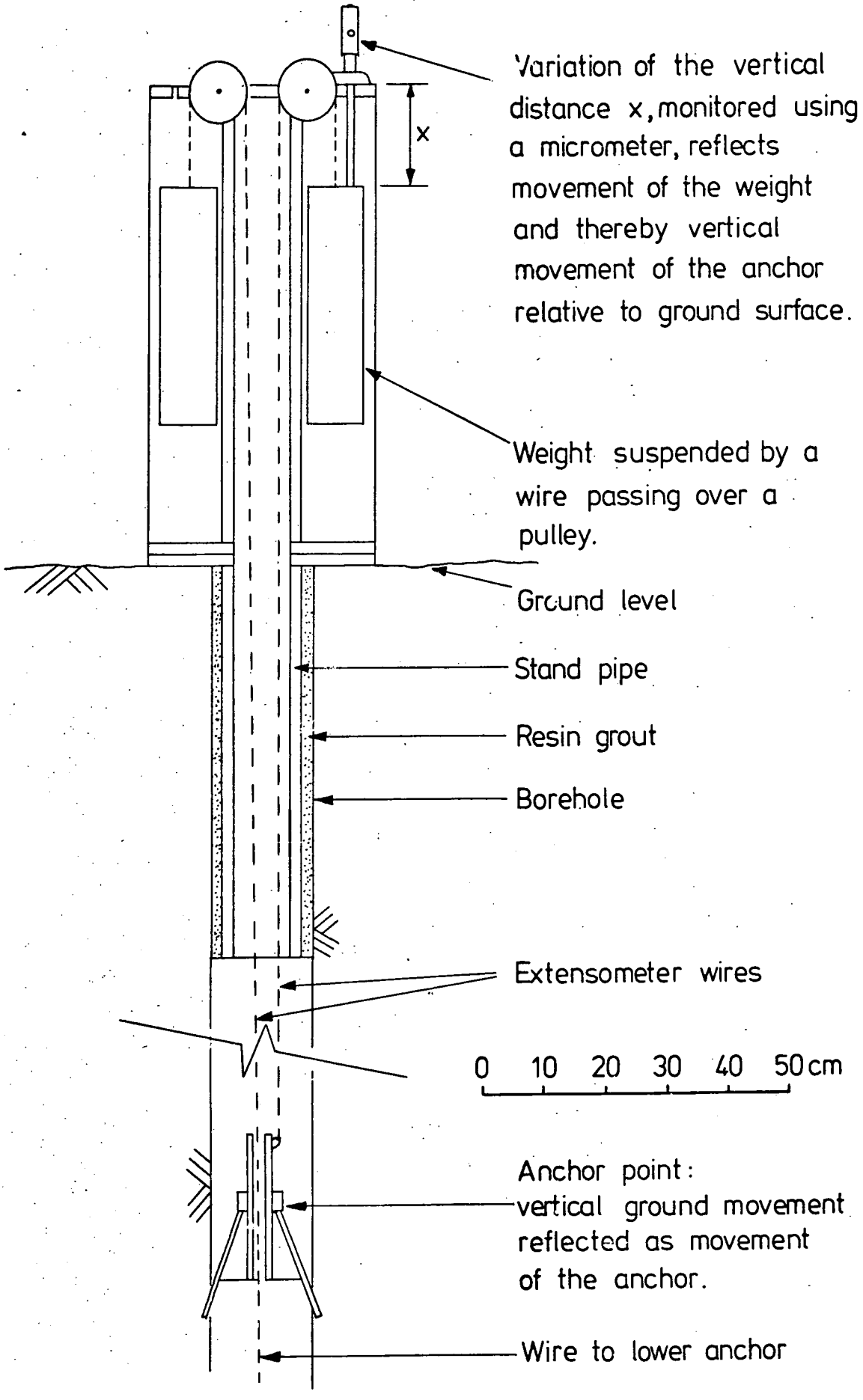

Fig. 7.2 PRINCIPLE OF THE WHITTAKER WIRE EXTENSOMETER

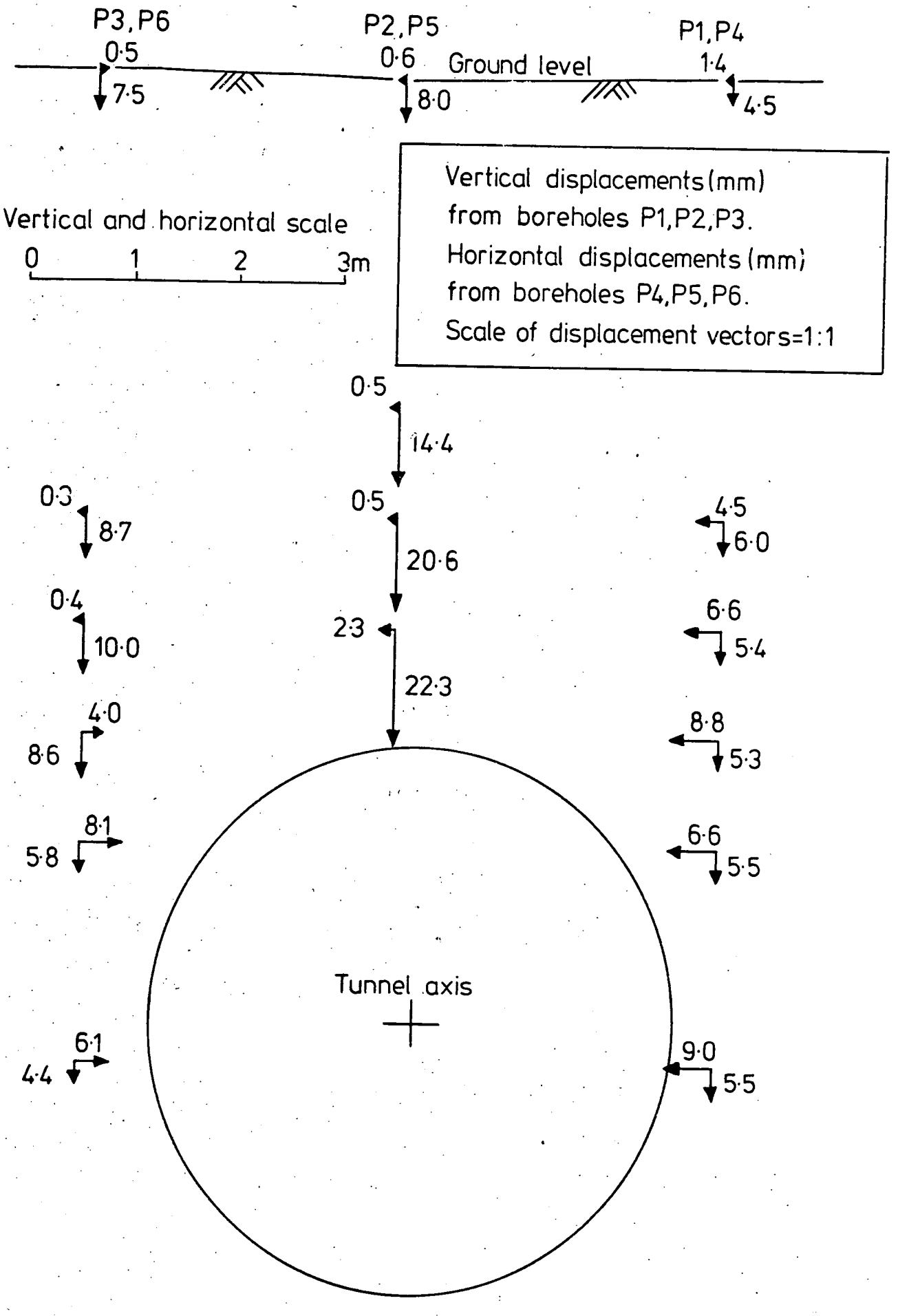

Fig. 7·3 TOTAL VERTICAL AND HORIZONTAL DISPLACEMENTS IN THE PLANE NORMAL TO THE TUNNEL AXIS. (AFTER Mc CAUL et al., 1975)

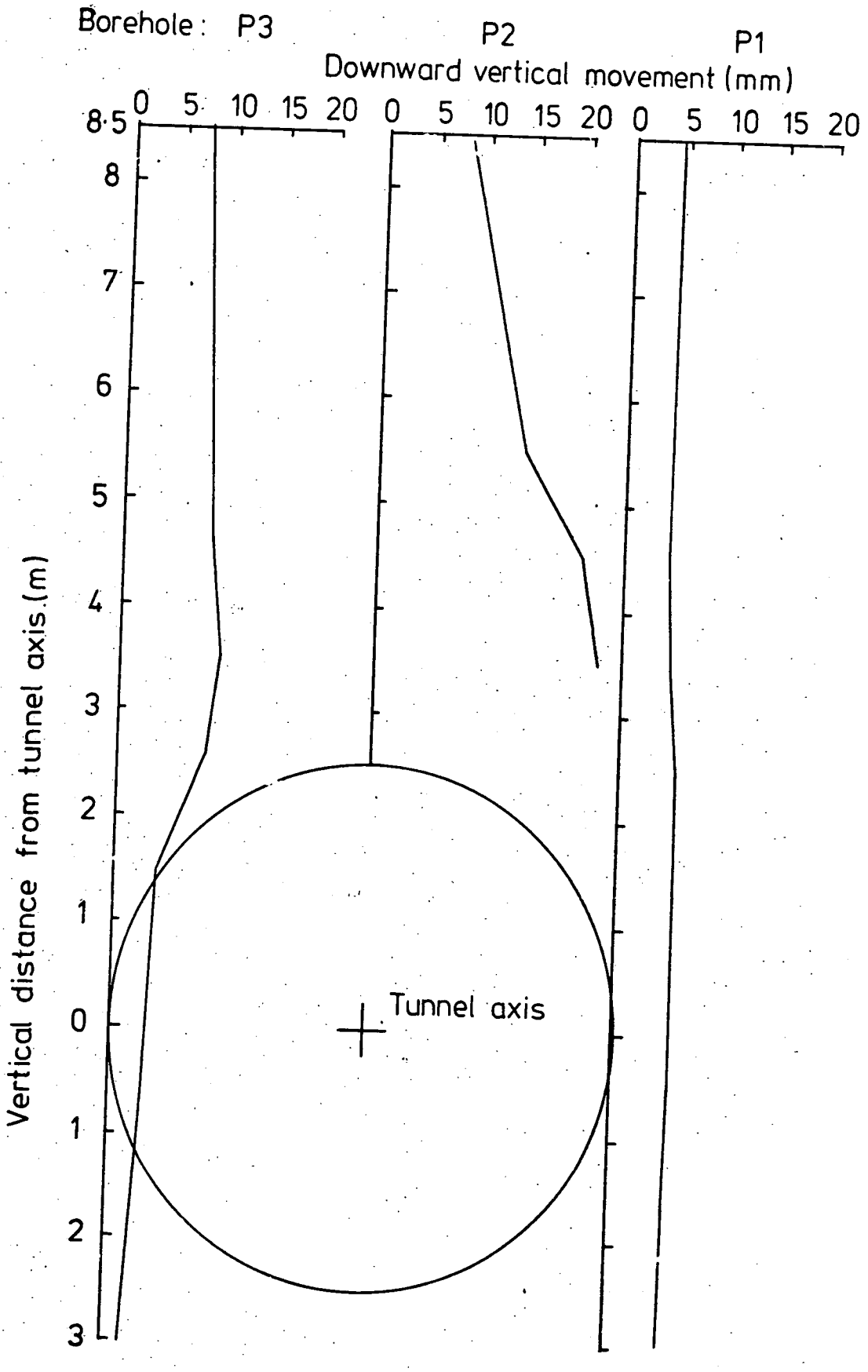

Fig. 7.4 VARIATION OF DOWNWARD VERTICAL MOVEMENT WITH DISTANCE FROM TUNNEL AXIS IN BOREHOLES P1, P2 AND P3.

a. Demec points monitoring movement along a discontinuity

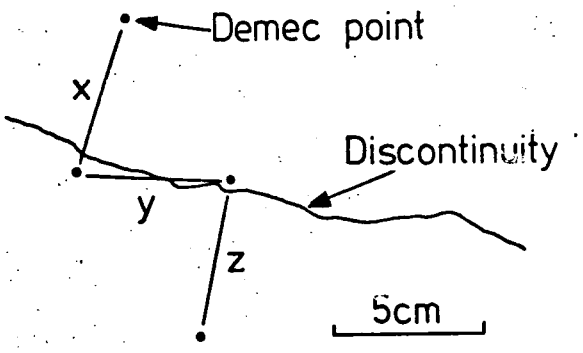

b. Demec points monitoring gross horizontal strain

Section :

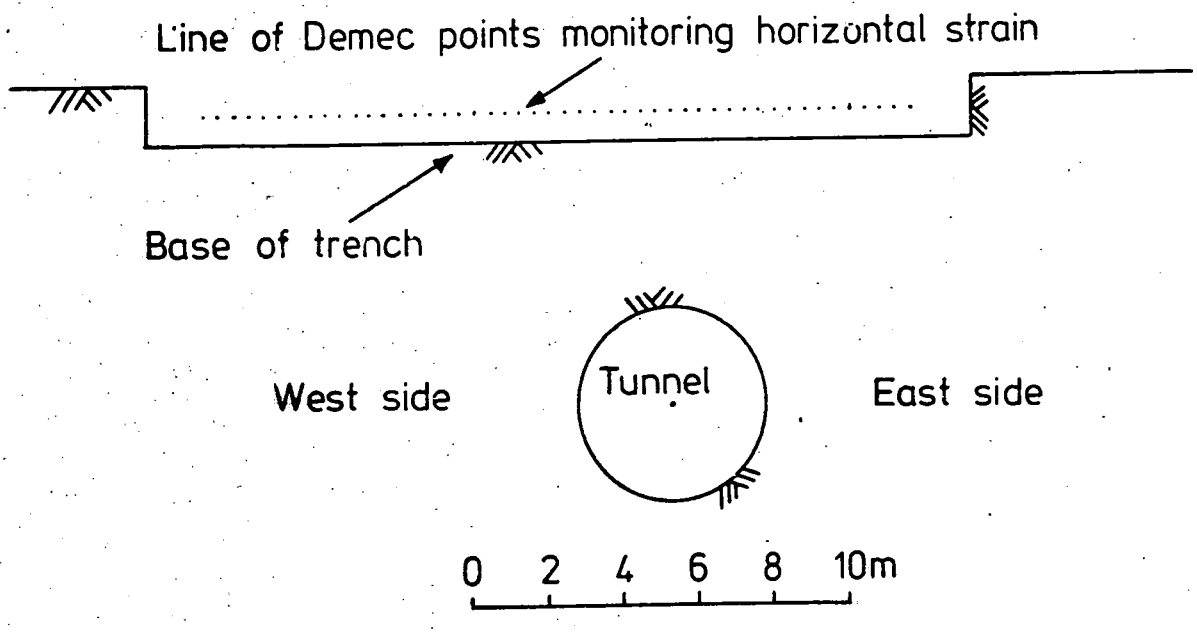

Fig. 7.5 DEMEC POINT CONFIGURATIONS IN THE TRENCH EXCAVATED ACROSS THE TUNNEL LINE

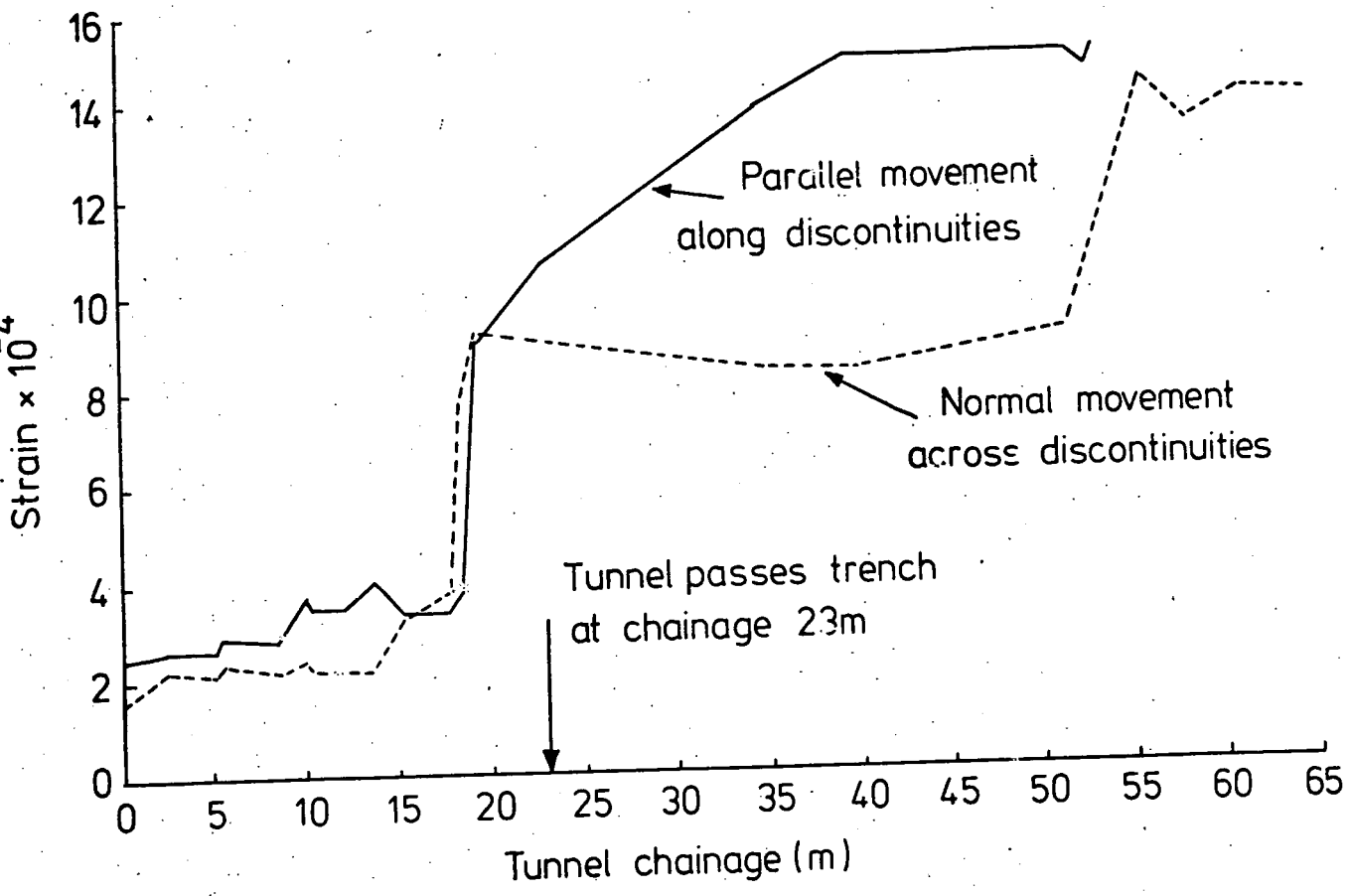

Fig. 7.6 DEVELOPMENT OF AVERAGE ABSOLUTE STRAIN ON SHORT DEMEC SPANS LOCATED ACROSS DISCONTINUITIES.

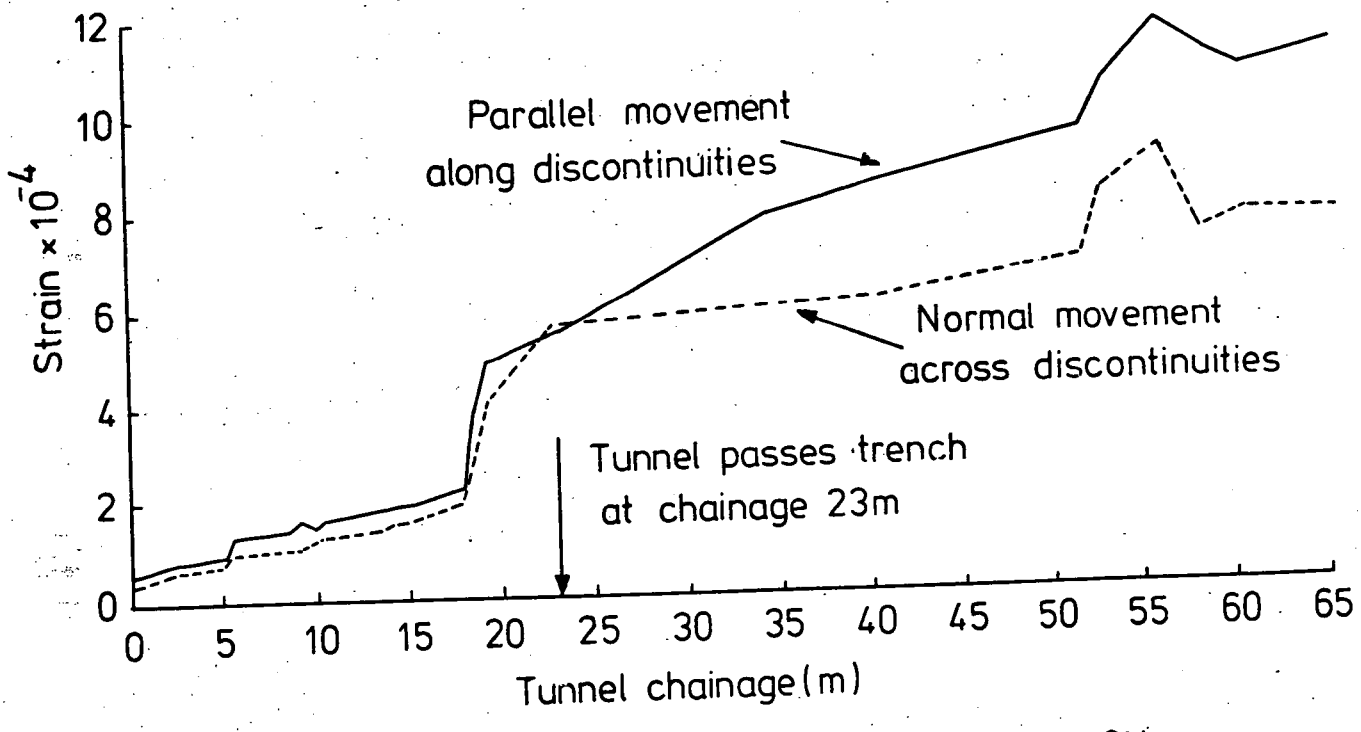

Fig. 7.7 DEVELOPMENT OF AVERAGE ABSOLUTE STRAIN ON LONG DEMEC SPANS LOCATED ACROSS DISCONTINUITIES.

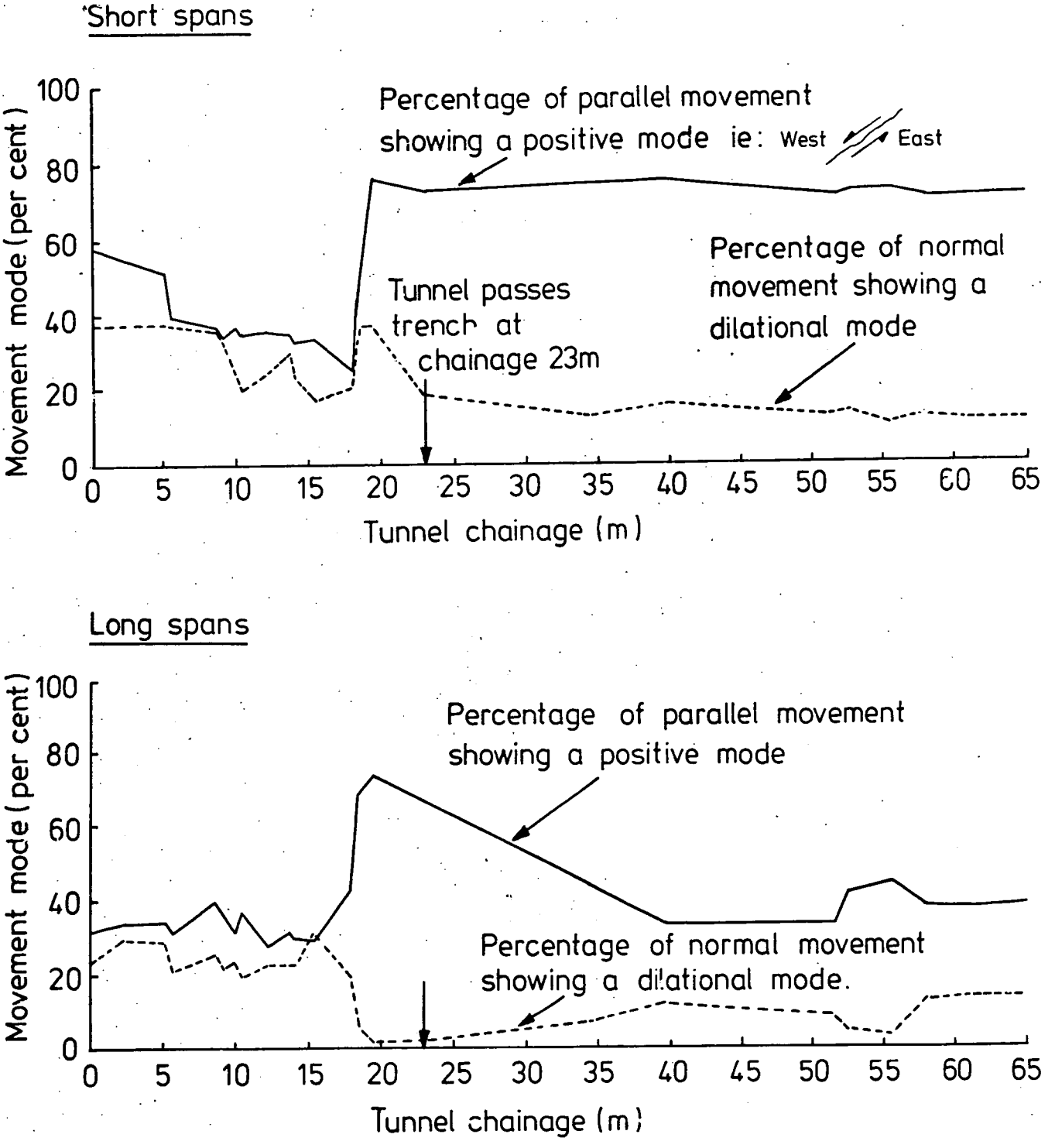

Fig. 7.8 MODE OF MOVEMENT ALONG DISCONTINUITIES MONITORED IN THE TRENCH.

a. Long and short Demec spans across intact elements of rock remote from the tunnel.

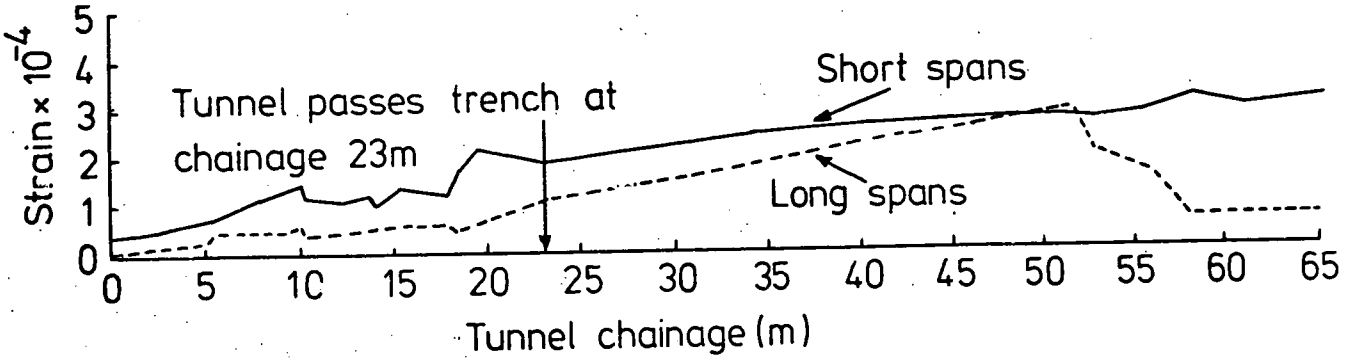

b. Medium Demec spans across intact elements of rock above the tunnel.

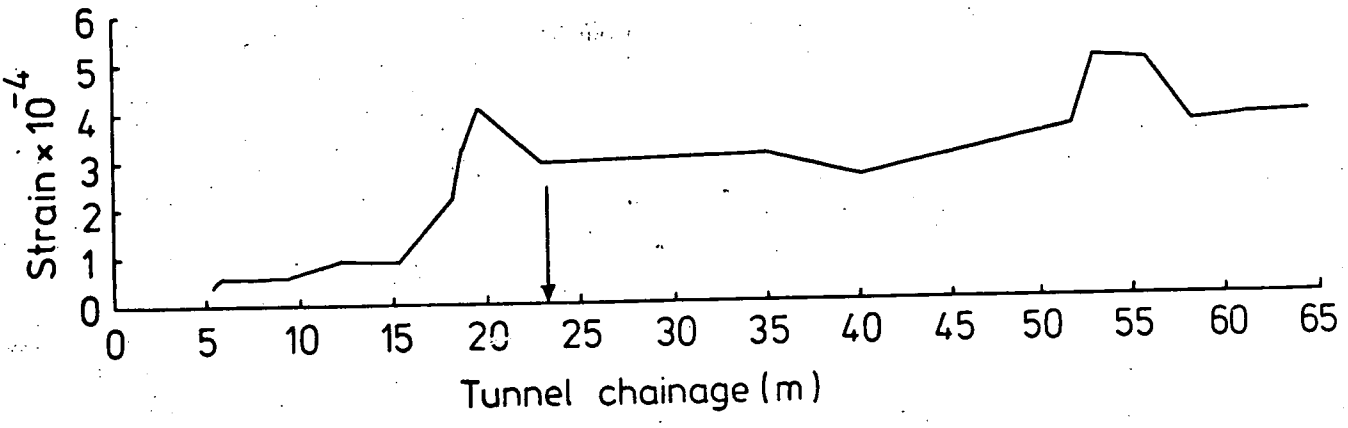

Fig. 7.9 DEVELOPMENT OF AVERAGE ABSOLUTE STRAIN ON CONTROL DEMEC SPANS.

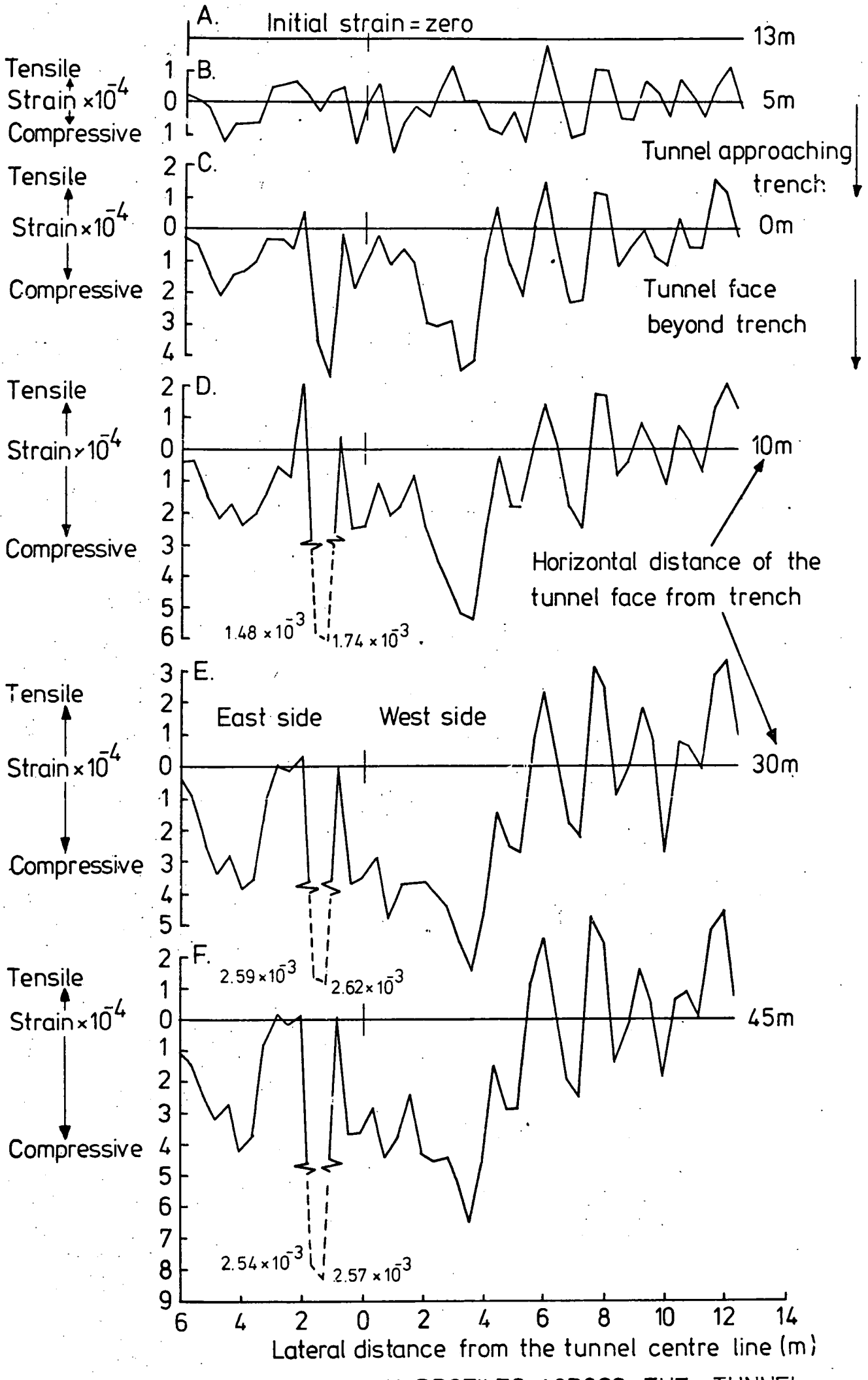

Fig. 7.10 HORIZONTAL STRAIN PROFILES ACROSS THE TUNNEL LINE, AT SIX STAGES DURING TUNNEL ADVANCE.

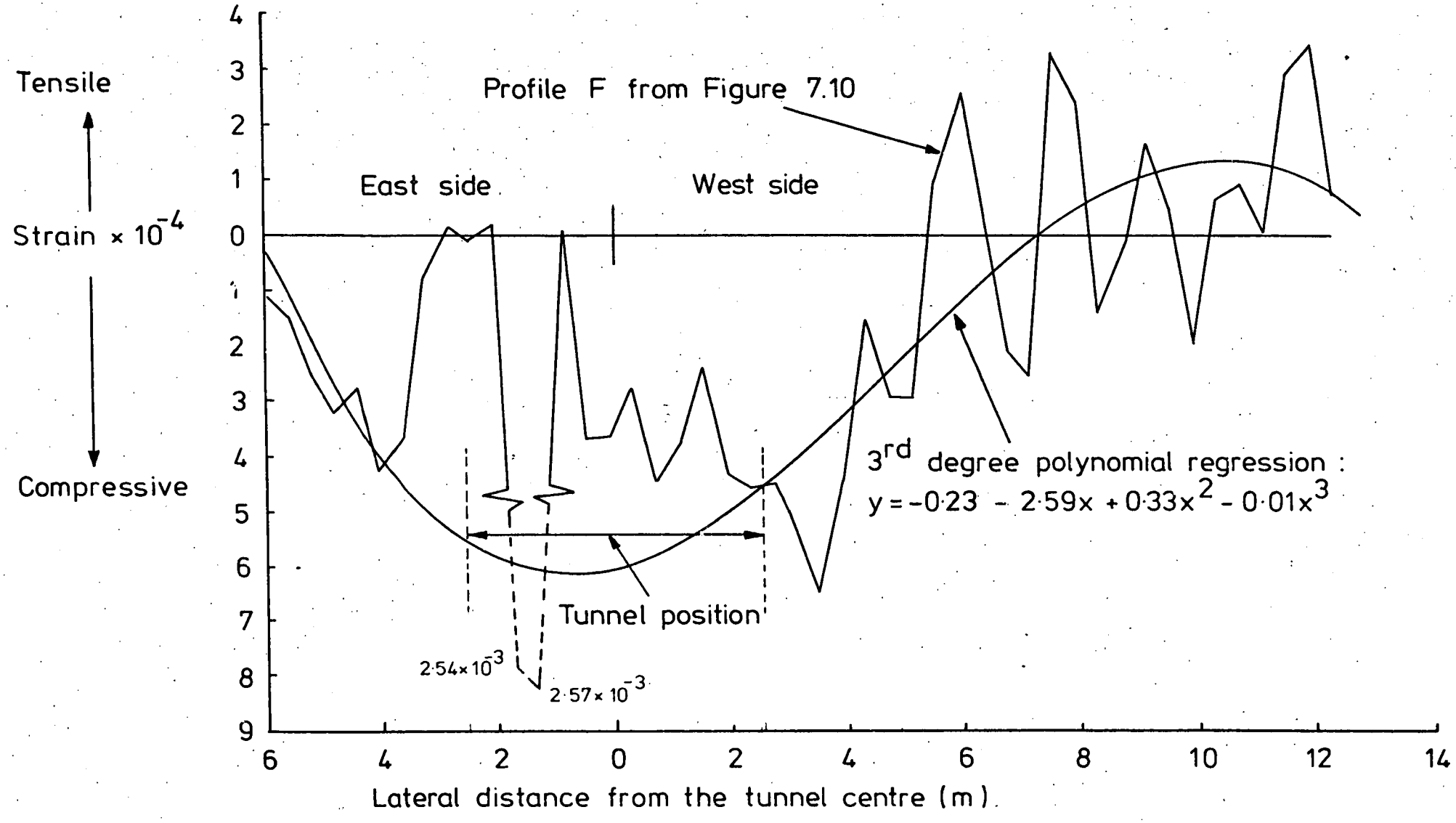

Fig. 7.11 THIRD DEGREE POLYNOMIAL REGRESSION ON THE FINAL HORIZONTAL STRAIN PROFILE ACROSS THE TUNNEL LINE.

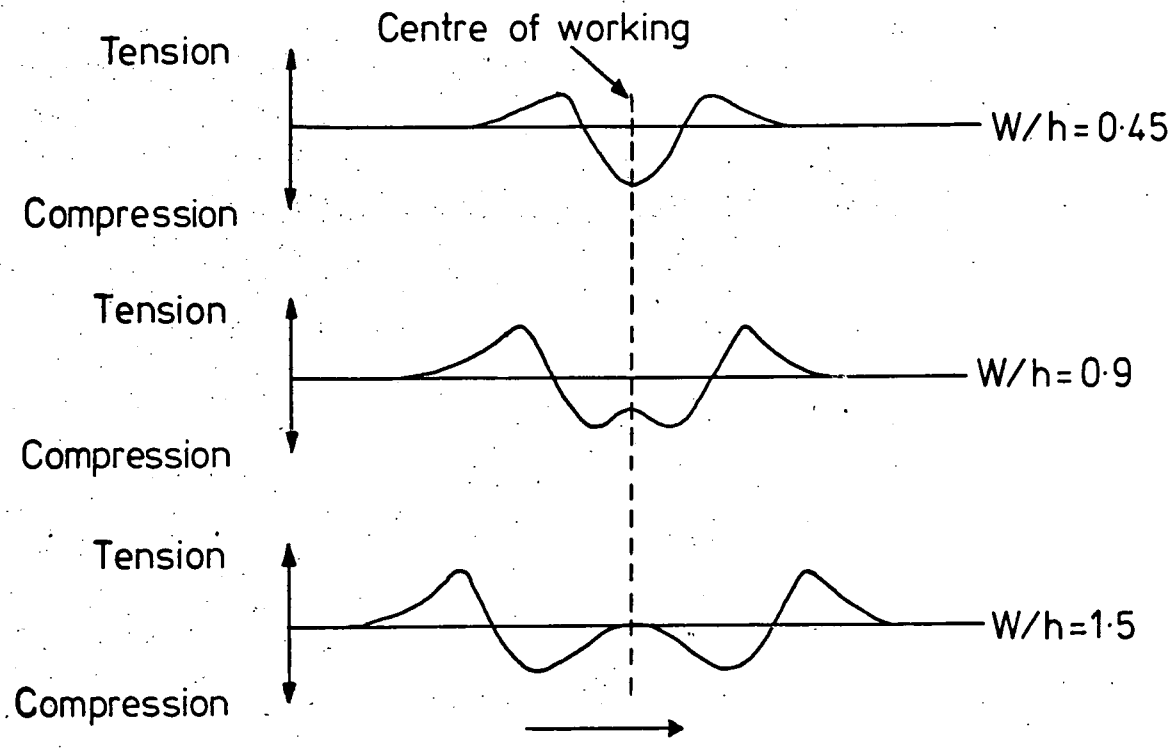

Note: W = width of working
h = depth of working

Fig. 7.12 PRINCIPLE TYPES OF HORIZONTAL STRAIN PROFILE THAT CAN DEVELOP OVER AN AREA OF LONGWALL MINING, (FROM THE SUBSIDENCE ENGINEERS HANDBOOK; NATIONAL COAL BOARD, 1966).

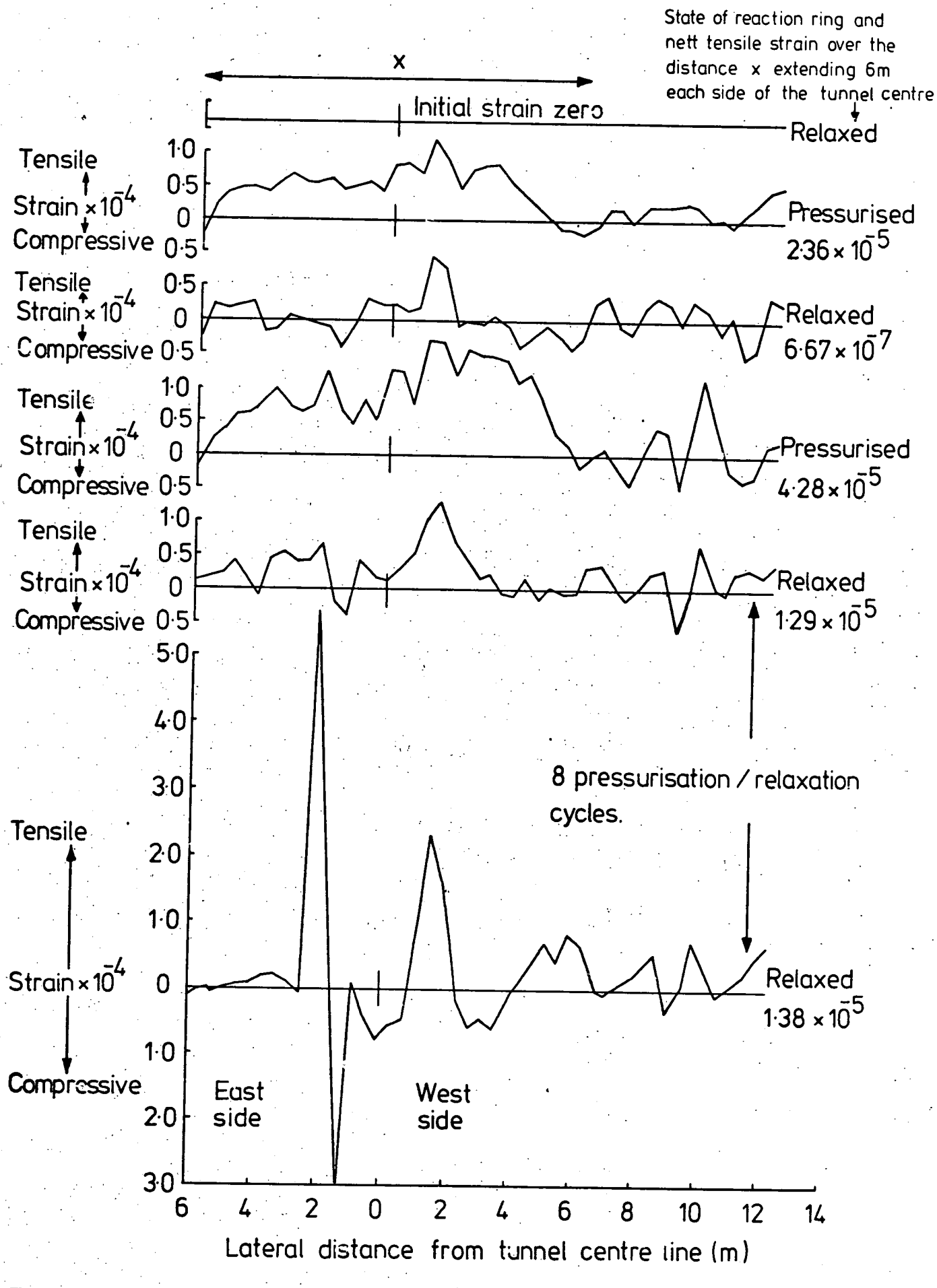

Fig. 7.13 HORIZONTAL STRAIN PROFILES ACROSS THE TUNNEL LINE DURING REACTION RING JACKING TESTS.

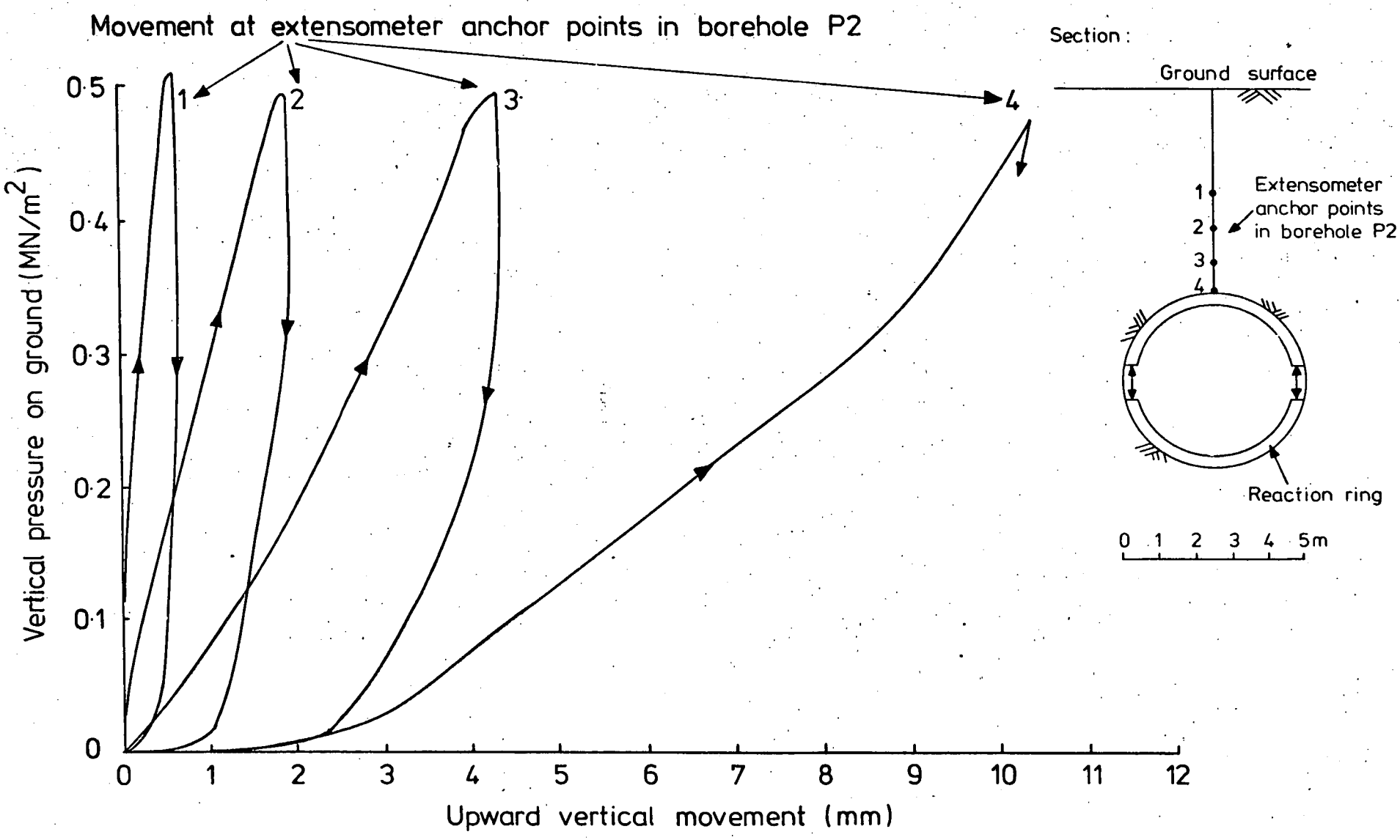

Fig. 7.14 RELATION BETWEEN VERTICAL PRESSURE IMPOSED ON THE GROUND BY THE REACTION RING AND UPWARD VERTICAL MOVEMENT AT FOUR ANCHOR POINTS.

Plate 7.1 TRENCH BEING EXCAVATED USING AN ARMY TRENCHER.

Plate 7.2 COMPLETED TRENCH, EXCAVATED ACROSS THE TUNNEL LINE.

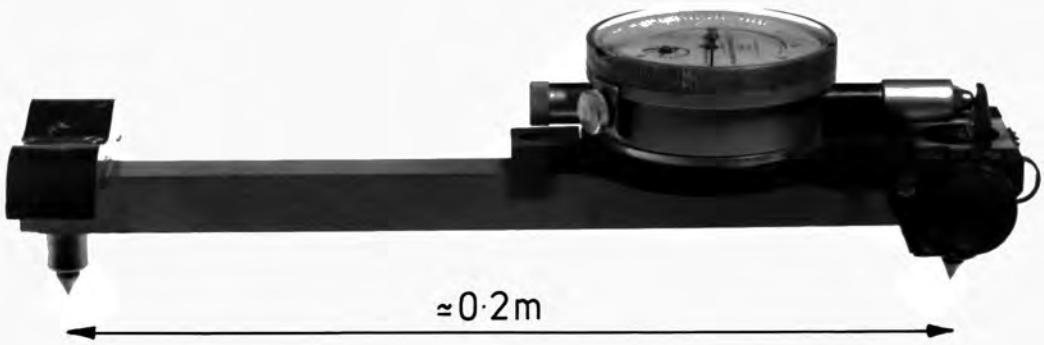

Plate 7.3 THE DEMEC STRAIN GAUGE

Plate 7.4 DEMEC POINT FIXED TO A 7cm NAIL EMBEDDED IN THE TRENCH SIDEWALL.

CHAPTER 8

A THEORETICAL DETERMINATION OF GROUND STRESS AND MOVEMENT NEAR A 5m DIAMETER TUNNEL IN LOWER CHALK

8.1 Introduction

Finite element methods were used to model the tunnelling situation at Chinnor, taking depths to axis of 7.5m and 17.5m. Chalk material properties such as bulk density, Young's modulus and Poisson's ratio were obtained from tests on intact core samples recovered during the preliminary site investigation programme at Chinnor.

By systematically varying the applied K_o factor (the coefficient of lateral earth pressure at rest) and Young's modulus it was hoped to model realistically the situation at Chinnor and assess the parameters most significantly controlling ground behaviour. A full description of the computing techniques adopted in the finite element analysis is given in Appendix J. In all analyses, the plane strain option of the finite element program was used.

8.2 Summary of input data

A mesh was drawn up (Figure 8.1) modelling the right-hand half (ie the east side) of the single tunnel system plus ground surface. The mesh was designed such that, by adding or removing elements it was possible to model a variety of tunnel depths. In the analyses two depths were modelled: 7.5m to axis ('shallow') and 17.5m to axis ('deep').

The chalk, for the purposes of this analysis, was assumed to be homogeneous with a multi-linear elastic stress-strain curve (Figure 8.2).

The curve in Figure 8.2 was determined from laboratory tests on two 100mm diameter intact chalk samples, carried out by Soil Mechanics Ltd. The bulk density of the chalk was taken as 2.1 Mg/m^3 with a Poisson's ratio of 0.3, again determined from laboratory tests on intact samples.

Because the real tunnel was driven above the water table, hydrostatic stress effects and pore water pressure were not considered; consequently, in the analysis total stress is effective stress.

A range of eight K_c factors was selected: 0.1, 0.2, 0.3, 0.4, 0.5, 0.6, 0.8 and 1.0. The K_o factor is defined as the horizontal effective stress at any one point, divided by the vertical effective stress. K_o is used in the finite element program to calculate horizontal stress from the vertical gravitational load for a given element (Appendix J).

The multi-linear stress-strain curve obtained from intact material was used in the analyses involving the permutation of K_o for the shallow and deep tunnels. Seven more multi-linear stress-strain curves were produced, each having an incrementally lower Young's modulus (Figure 8.3), expressed in terms of a J_a factor, equal to the reduced (input) deformation modulus divided by the intact deformation modulus obtained from laboratory tests. A K_c factor of 0.4 was then adopted for further analyses, on the shallow tunnel only, involving the permutation of this J_a factor using the eight stress-strain curves. The permutations described above are summarised in the following Tables:

Table 8.1

Permutation of K_o

(shallow plus deep)

K_o	J_a
0.1	1.0
0.2	
0.3	
0.4	
0.5	
0.6	
0.8	
1.0	

Table 8.2

Permutation of J_a

(shallow only)

K_o	J_a
0.4	1.0
	0.8
	0.6
	0.4
	0.2
	0.1
	0.07
	0.05

In the permutation of Young's modulus a K_o factor of 0.4 was selected on the basis of the known value for Poisson's ratio for the chalk, equal to approximately 0.3. The relation adopted (Coates, 1970) K_o equal to $\nu/(1-\nu)$, where ν is Poisson's ratio, therefore indicates a K_o of approximately 0.4.

8.3 Permutation of K_o

Permutation of the eight K_o values for the shallow and deep tunnels produced sixteen sets of computer output. Details of nodal movement and element stresses were extracted from this output and plotted for the various K_o values.

Figures 8.4 and 8.5 show the variation of theoretical downward vertical movement, resulting from tunnel excavation, with distance above the tunnel crown for the shallow and deep tunnels respectively, for the full range of K_o factors. Figures 8.6 and 8.7 show the variation with K_o of the change in vertical and horizontal internal tunnel diameters for the shallow

and deep tunnels. The change in internal diameter considered is: that change in diameter from the nominal value assumed to follow hypothetical instantaneous excavation.

Radial and tangential stress magnitudes for elements bounding the tunnel, the centroids of which were approximately 0.3m from the tunnel surface, were extracted from the listed computer output. Using data from the K_o = 0.4 and K_o = 1.0 outputs, polar-plots were constructed showing the variation in average radial and tangential stress round the annulus of rock near the tunnel. The construction of these diagrams is explained in Figure 8.8. Figures 8.9 to 8.12 show the resulting polar-plots for the shallow and deep tunnels at K_o values of 0.4 and 1.0.

Elements at three positions round the tunnel (crown, axis level, invert) were selected to illustrate the relation between radial stress, tangential stress and K_o Figures 8.13 and 8.14 show the variation in stress with K_o at these selected positions for the shallow and deep tunnels respectively.

Data from the K_o = 0.4 and K_o = 1.0 outputs for the shallow and deep tunnels were used to construct graphs showing the variation in stress with distance from the tunnel. Figures 8.15 to 8.18 are the resulting plots showing the variation in radial, tangential and principal stresses with distance from the tunnel, horizontally at axis level and vertically above the crown.

8.4 Discussion of results of K_o permutation

Figures 8.4 and 8.5 indicate that the theoretical downward vertical movement above the tunnel increases as the distance from the crown

decreases. In addition it is apparent that for a given K_o value, settlement above the shallow tunnel is greater than that above the deep tunnel. This latter point suggests that for the shallow situation, where the tunnel diameter is large compared with the depth, the ground above the tunnel behaves like a flexible bending beam responding to gravitational loading and gives relatively high settlement values. For the deep situation the 'beam' is thicker and consequently stiffer, giving less settlement. If the ground above the shallow tunnel is to be regarded as behaving like a bending beam, it is reasonable to expect the development of compressive horizontal stress (and consequently strain) at ground surface above the tunnel crown, and tensile horizontal stress at the tunnel crown. The former of these conclusions is confirmed from a theoretical standpoint in Figure 8.27 (discussed in Section 8.6). The development of tensile horizontal stress (that is tangential stress) at the tunnel crown conflicts with an additional effect (Figures 8.9 to 8.12) which predicts the development of high compressive tangential stresses near the tunnel surface, consequently any bending beam stress effects near the tunnel are masked by the stress redistribution caused by tunnel excavation.

Figures 8.4 and 8.5 indicate that downward vertical movement at any given point above the tunnel crown decreases with increasing K_o, that is, increasing lateral stress. This effect is better illustrated in Figures 8.6 and 8.7 which show that at low K_o values the deformed tunnel cross-section is of elliptical form with the major axis horizontal. As the K_o value approaches unity the deformed tunnel cross-section approaches a circular shape, with the decrease in vertical and horizontal diameters having the same value. The behaviour of the tunnel in response to vertical and horizontal loading may therefore be regarded as analogous to that of a proving ring under biaxial loading (Figure 8.19). An increase in the x diameter and decrease in the y diameter is induced by external compressive

loading in the y direction which is several times greater than that in the x direction, and by analogy equivalent to a low K_0 factor. As the x loading increases, and again by analogy K_0 increases, the x diameter decreases, until, when the x loading equals the y loading (equivalent to a K_0 of unity) the decrease in x and y diameters is the same.

Figures 8.13 and 8.14, summarising the variation with K_0 of radial and tangential stress at selected points near the tunnel, illustrate the behaviour of the rock in response to lateral loading. Before discussing the lateral loading effects it is important to note that at any given position and K_0 value the stresses developed near the shallow tunnel have a very similar value to those developed near the deep tunnel. In other words, at these relatively shallow depths the amount of overburden has little effect on the magnitude of stresses developed near the tunnel.

Figures 8.13 and 8.14 indicate that at crown and invert tangential stress increases linearly with increasing K_0. At axis level tangential stress decreases linearly with increasing K_0. The material at axis level, however, is not as sensitive to changes in K_0 as the material at crown and invert. The greater sensitivity of material at crown and invert to changes in K_0 is a result of the fact that tangential stress at these points is directly affected by changes in lateral stress (since tangential stress is a lateral stress at crown and invert). However, the response of material at axis level is an indirect result of changes in lateral stress, since the tangential stress is vertical at this point.

Figures 8.9 to 8.12 show that the radial stress in the rock near to, and approximately 0.3m from the tunnel surface is approximately an order of magnitude less than the corresponding tangential stress, for K_0 values

exceeding 0.3. This is a result of the fact that load shedding near the tunnel leads to the development of high compressive stress parallel to the free surface, whilst compressive stress normal to the free surface is inhibited. This effect is clearly illustrated in Figures 8.15 to 8.18 which show the variation in stress with distance from the tunnel. In all cases, at between 3m and 5m from the tunnel surface the magnitude of the tangential stress begins to increase and radial stress to decrease with decreasing distance from the tunnel, to achieve respective maxima and minima approximately 0.3m from the tunnel surface. The high tangential stresses near the tunnel surface illustrate the arching effects which serve to transfer rock loads round the excavated cavity (Széchy, 1970).

Figures 8.9 to 8.12 reveal that the three positions (crown, axis level and invert) selected in Figures 8.13 and 8.14 represent points of maximum and minimum stress near the tunnel. In all cases, except at high K_o values, the maximum compressive tangential stress is developed at axis level and ranges from approximately 0.8 MN/m^2 at K_o = 0.1 to 0.6 MN/m^2 at K_o = 1.0. At crown and invert small tensile tangential stresses are developed at K_o values below 0.3, but never exceed 0.3 MN/m^2.

The rock within 0.3m of the tunnel surface may be assumed to be in a state of unconfined compression, with the tangential stress ($\simeq\sigma_1$) providing the compressive pressure and the radial stress ($\simeq\sigma_2$) approximating to zero. Average unconfined compressive strength values for the Lower Chalk at Chinnor range from 3.0 MN/m^2 to 10.0 MN/m^2 whilst average tensile strength values range from 0.6 MN/m^2 to 1.0 MN/m^2 (Chapter 3). Therefore it is clear that there is a factor of safety at least 2 (but commonly more than 5) against compressive or tensile failure of the intact rock near the unlined tunnel at Chinnor. It is apparent, therefore, that considerations of intact rock strength are of minor importance when

examining the stability of this tunnel for even the most unfavourable K_o factors. For a jointed rock, however, with essentially zero tensile strength one would expect considerable tensile failure of the rock mass near the tunnel crown. The comments in Chapter 5 confirm that this did in fact occur.

8.5 Permutation of J_a

Permutation of the eight J_a factors for the shallow tunnel (7.5m depth to axis) produced eight sets of computer output. The factor J_a has been defined earlier as the input deformation modulus divided by the intact modulus obtained from laboratory tests. Details of nodal movement and element stresses were extracted from the output and plotted for the various J_a values.

Elements at three positions round the tunnel (crown, axis level, invert) were selected to illustrate the relation between radial stress, tangential stress and J_a at a K_o of 0.4. Figure 8.20 shows the variation in stress with J_a at these selected positions for the shallow tunnel.

Using the plotting facility of the computer it was possible to produce a diagrammatic representation of the variation in the magnitude and direction of the two principal stresses over a selected area of the mesh. Figures 8.21 and 8.22 show the resulting plots for J_a factors of 0.07 and 1.00. In these plots the magnitudes and directions of the major and minor principal stresses are indicated by the length and direction of the stress trajectory lines. Tensile principal stress trajectories are designated with an 'arrow head'.

Variation of downward vertical movement with J_a at two positions above the tunnel crown is illustrated in Figures 8.23 and 8.24: Figure 8.23

for a point at ground level and Figure 8.24 for a point 3m above the tunnel crown. The actual movements observed at these points during the ground movement measurement programme (Chapter 7) are also presented in these Figures.

A J_a factor of 0.07 was selected to illustrate the variation of downward vertical movement with vertical distance from the tunnel. Figure 8.25 shows downward vertical movement above the crown, and Figure 8.26 upward and downward vertical movement above (and below) the springing lines. The actual movements measured at these points near the tunnel (Chapter 7) are also presented in these Figures.

J_a factors of 0.07, 0.10 and 0.2 were selected to illustrate theoretical horizontal strain profiles across the tunnel line at ground level. The resulting plots are shown in Figure 8.27. In addition, Figure 8.27 includes the actual smoothed horizontal strain profile obtained from measurements taken in the trench above the tunnel and presented previously in Figure 7.11.

8.6 Discussion of results of J_a permutation

In this Section, a discussion of the theoretical results only is presented. The actual ground movements, presented in Figures 8.23 to 8.27 will be discussed in the light of the theoretical results, and additional experimental results in the next Section.

It is clear from Figures 8.20, 8.21 and 8.22 that, at any given position, variation of J_a has a negligible effect on ground stress. This is due to the fact that the two factors controlling the magnitude of stress in any given element of rock, gravitational loading and externally applied

loading, are not significantly affected by variation of the J_a factor. It is apparent, therefore, from previous discussions that the factors most significantly influencing the ultimate magnitude of ground stress in a given element of rock near the tunnel at Chinnor are the applied K_o factor and position in relation to the tunnel.

Figures 8.23 and 8.24 indicate that ground movement is significantly affected by the magnitude of the applied J_a factor. It is clear that downward vertical movement increases in a non-linear manner with decreasing J_a, such that below a J_a of 0.2 there is a 'take off point' where movement increases very rapidly with decreasing J_a. The J_a factor is an index of the material 'stiffness' fed into the computer, the lower the J_a factor the lower the stiffness. The larger movements at lower J_a factors reflect the greater deformability of the less stiff material.

Figures 8.25 and 8.26, show the variation in vertical ground movement with vertical distance from the tunnel. Figure 8.25 reiterates the effects already noted in Figures 8.4 and 8.5. However, in Figure 8.25 the ground movements are much larger. Figure 8.26 indicates a tendency towards upward vertical movement of material located below the tunnel.

Figure 8.27 showing horizontal strain profiles across the tunnel line indicates the development of a compressive zone directly above the tunnel with a tensile zone approximately 7m from the tunnel centre line. It is clear that the amount of strain developed increases with decreasing J_a.

8.7 Ground movements caused by tunnelling in discontinuous rock at Chinnor

In this Section the experimental results concerning ground movements near the Chinnor tunnel (discussed in Chapter 7) are compared with the

theoretical results obtained using finite element analysis discussed earlier.

It is clear from Figures 8.23 and 8.24 that total ground movements resulting from tunnelling at Chinnor are between 8 and 15 times the settlements predicted by adopting a J_a factor equal to unity. Such a large difference was to have been expected in view of the discontinuous nature of the chalk. The magnitude of the actual ground movements can be explained in terms of theoretical multi-linear elastic stress analysis by adopting a deformation modulus that is 5-7% of the intact modulus, ie a J_a factor between 0.05 and 0.07.

Figure 8.25 indicates that if actual and theoretical movements are matched at ground surface, actual settlement increases more rapidly with depth than theoretical settlement based on the assumptions outlined in Section 8.2. This suggests the development of a loosened zone (exhibiting greater settlement) near the tunnel. This loosened zone is not evident in Figure 8.26 which summarises settlement above the tunnel springing lines and which therefore suggests that the loosening is confined to the area above the tunnel crown.

The horizontal strain profiles shown in Figure 8.27 imply that at ground surface theoretical analyses involving multi-linear elastic solutions provide a good approximation to the real situation when a modulus reduction factor of between 0.07 and 0.20 is selected. It is likely, therefore, that loosening and movement along discontinuity surfaces - processes which are dominantly responsible for the overall reduction in the deformation modulus - do not cause significant modification of the overall horizontal strain profile at ground surface. The form of the horizontal strain profile actually developed at Chinnor was discussed in Chapter 7.

The incorporation of the J_a factor into the finite element analysis may therefore be regarded as an acknowledgement of the discontinuous behaviour of the ground near the tunnel at Chinnor. This discontinuous behaviour is largely a result of the three effects listed in 7.5 (conclusion 9) and summarised below:

(a) Discontinuities provided a facility for block rotation and dislocation.

(b) The vertically acting reaction ring exacerbated the problems of ground stability near the tunnel.

(c) Movement of ground into the overbreak cavity provided a facility for continued ground deformation following the passage of the tunnelling machine.

It is clear that the J_a factor used in this Chapter is directly analagous to the j factor of Hobbs (1973, 1974) defined in Chapter 1 (page 3). The term 'J_a' is used here to describe the variable parameter fed into the finite element computer program thus avoiding confusion with the factor 'j' adopted by Hobbs to describe the quality of a rock mass.

Hobbs (1974) commented that the j value is stress dependent, such that when analysing the behaviour of foundations, fractures at depth will be 'stiffer' than similar fractures near the surface. This effect results from the fact that the higher stresses at depth tend to 'tighten up' the fractures, thus inhibiting the effects of shearing and dislocation responsible for the modulus reduction. This effect is clearly demonstrated in Figures 8.23 to 8.27, where a modulus reduction factor of 0.05 is required to match actual and theoretical movements in the loosened zone

near the tunnel, whereas modulus reduction factors of between 0.07 and 0.10 are required in the less disturbed chalk near the ground surface. The sensitivity of the modulus reduction factor to variations in ground conditions was previously noted in Section 3.5, where the results of pressuremeter tests indicated modulus reduction factors of approximately 0.05 near the ground surface but values approaching 0.5 at depths exceeding 20m.

Hobbs (1974) examined the relation between fracture frequency and the j factor at four Chalk sites in the UK using results from large diameter plate loading tests and pressuremeter tests. His results are presented in Figure 8.28, together with data obtained from Chinnor. In addition Hobbs, (1974) examined the relation between j and fracture frequency in terms of theoretical analyses carried out by Walsh and Brace (1966) who assessed the modification of elastic constants caused by the effects of cracks and pores in rock. The resulting relation between j and fracture frequency for cubical and layered fracture patterns is shown in Figure 8.29 together with the experimental results from Chinnor.

It is clear from Figures 8.28 and 8.29 that, in general, for the fracture spacings in the Chalk at Chinnor the modulus reduction factors predicted by Walsh and Brace (1966) and by Hobbs (1974) are slightly large. The best prediction of the modulus reduction factor is given in Figure 8.29 for open cubical fractures. The more drastic reduction in modulus required to model the behaviour of the Chalk at Chinnor is largely a result of the ground loosening and dislocation effects discussed in Section 7.5 (conclusion 9).

The problems of tunnelling at shallow depths in discontinuous chalk outlined in this Chapter have a variety of structural and geotechnical

implications:

(1) The maximum observed settlement (δ_{max}) at ground surface above the tunnel centre line was 8mm. The minimum observed settlement (δ_{min}) at ground surface measured at the top of borehole P1 at a lateral distance (l) of 2.5m from the tunnel centre line was 4.5mm. Considering differential settlement above the tunnel at Chinnor:

$$\delta_{diff} = \frac{\delta_{max} - \delta_{min}}{l} = 0.0014$$

Sowers (1962) used a similar equation in a scheme for evaluating the maximum differential settlement allowable for a variety of surface structures. He suggested that values of δ_{diff} exceeding 0.001 were likely to cause damage to one storey brick buildings, high continuous brick walls and also cracking in plaster. For reinforced-concrete or steel frame buildings, values of δ_{diff} up to 0.002 were tolerable.

(2) The loosening and movement along discontinuity surfaces near the tunnel will have greatly increased the mass permeability of the chalk in these regions. These effects would have serious repercussions for a tunnel beneath the water table, since under these conditions water inflow would be greatly increased with the tunnel acting as a 'drain'. Grouting or other costly remedial measures would be required to reduce the water inflow.

It is likely that many of the problems of overbreak and falling blocks in the Chinnor tunnel, exacerbated by the use of a vertically acting reaction ring, could have been reduced by the use of a horizontally-acting reaction ring. In this way reaction would be obtained from the tunnel walls, thereby minimising the loosening effects above the tunnel caused by ground lifting and load shedding. This horizontally-acting reaction ring would

have to incorporate a partial external shield at the crown to minimise the effects of instability in this region aggravated by the tensile tangential stresses that could be set up by the reaction ring.

8.8 Summary and conclusions

(1) The tunnelling situation at Chinnor was modelled using finite element methods, taking depths to axis of 7.5m and 17.5m. Chalk material properties were obtained from tests on intact core samples.

(2) Permutation of the K_o factor (the coefficient of lateral stress at rest) and J_a factor (the modulus reduction factor) produced a range of theoretical results.

(3) Downward vertical movement above the tunnel crown was found to increase with decreasing distance from the tunnel. Greater movements were calculated for the shallow tunnel. The effect of K_o on ground movement near the tunnel was found to be analogous to the behaviour of a proving ring under biaxial loading. Low lateral loading produced a decrease in the vertical diameter and an increase in the horizontal diameter.

(4) At the relatively shallow depths modelled, the amount of overburden was found to have little effect on the magnitude of stresses developed near the tunnel. At crown and invert, tangential stress was found to increase linearly with increasing K_o. At axis level, tangential stress decreased linearly with increasing K_o. At a distance of 0.3m from the tunnel surface, tangential stress was found to be an order of magnitude greater than radial stress due to stress concentration effects near the excavation.

(5) Considerations of maximum compressive and tensile stresses in the light of known average compressive and tensile strengths of the chalk indicated a factor of safety of at least 2 against failure of the intact rock near the tunnel. Consequently, considerations of intact rock strength were proved to be of minor importance when examining the stability of the tunnel at Chinnor.

(6) It was found that whilst variation of J_a had a negligible effect on ground stress, ground movement near the tunnel increased in a non-linear manner with decreasing J_a.

(7) Theoretical horizontal strain profiles across the tunnel line indicated the development of a compressive zone directly above the tunnel and a tensile zone approximately 7m from the centre line.

(8) Measured total ground settlements were found to be between 8 and 15 times the settlements predicted by a finite element analysis adopting $J_a = 1$. Modulus reduction factors of between 0.05 and 0.07 were required to match actual and theoretical settlements at selected distances from the tunnel crown. Modulus reduction factors of between 0.07 and 0.20 were required to match actual and theoretical horizontal strain profiles at ground surface.

(9) Variation of actual settlement, and the J_a factor required to model this settlement, with height above the tunnel indicated the development of a zone of progressively loosened rock above the tunnel crown. It is suggested that the need for a modulus reduction factor to model the behaviour of the ground near the tunnel at Chinnor is a result of loosening and dislocation along discontinuities, stimulated by the tunnelling operations.

(10) Comparison between modulus reduction factors at Chinnor and those derived from plate loading tests on chalk indicates that for a given discontinuity spacing, there is a more drastic modulus reduction in the case of the tunnel. It is probable that the need for a smaller modulus reduction factor to model the behaviour of the tunnel is a result of the ground loosening effects stimulated by tunnel excavation.

(11) It is likely that the ground disturbance caused by tunnelling in discontinuous rock at shallow depth using the methods adopted at Chinnor could cause appreciable damage to weak or sensitive surface structures. For a tunnel below the water table serious water in-flow problems could be encountered as a result of increased permeability caused by loosening effects. It is suggested that many of the problems of overbreak and falling blocks in the tunnel at Chinnor could have been reduced by the use of a horizontally acting reaction ring.

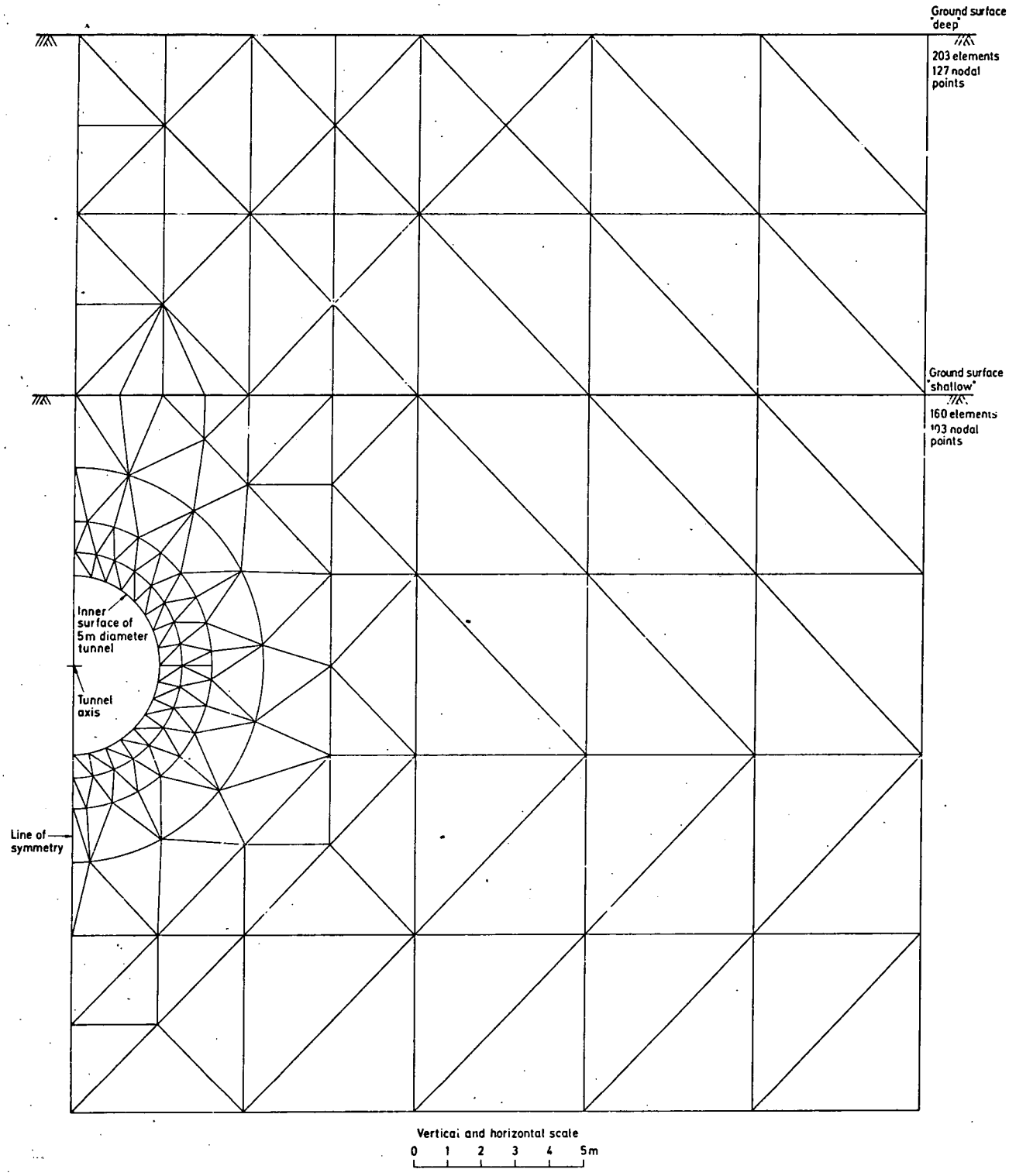

Fig. 8.1 FINITE ELEMENT ANALYSIS, SIMPLEX TRIANGULAR MESH

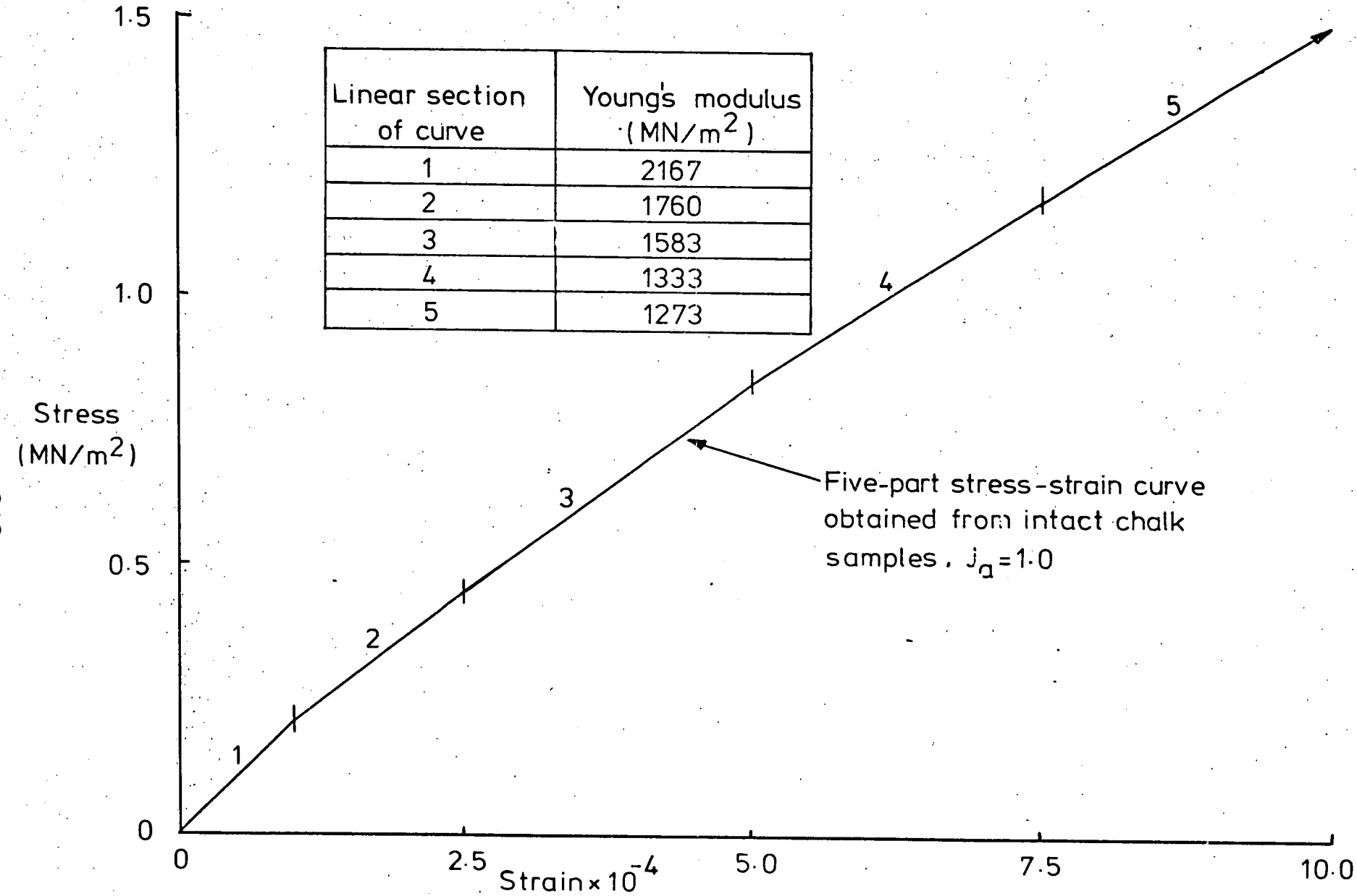

Linear section of curve	Young's modulus (MN/m^2)
1	2167
2	1760
3	1583
4	1333
5	1273

Fig. 8.2 MULTI-LINEAR STRESS-STRAIN CURVE OBTAINED FROM LABORATORY TESTS ON INTACT CHALK SAMPLES, Nos. 24 AND 33, BOREHOLE 11.

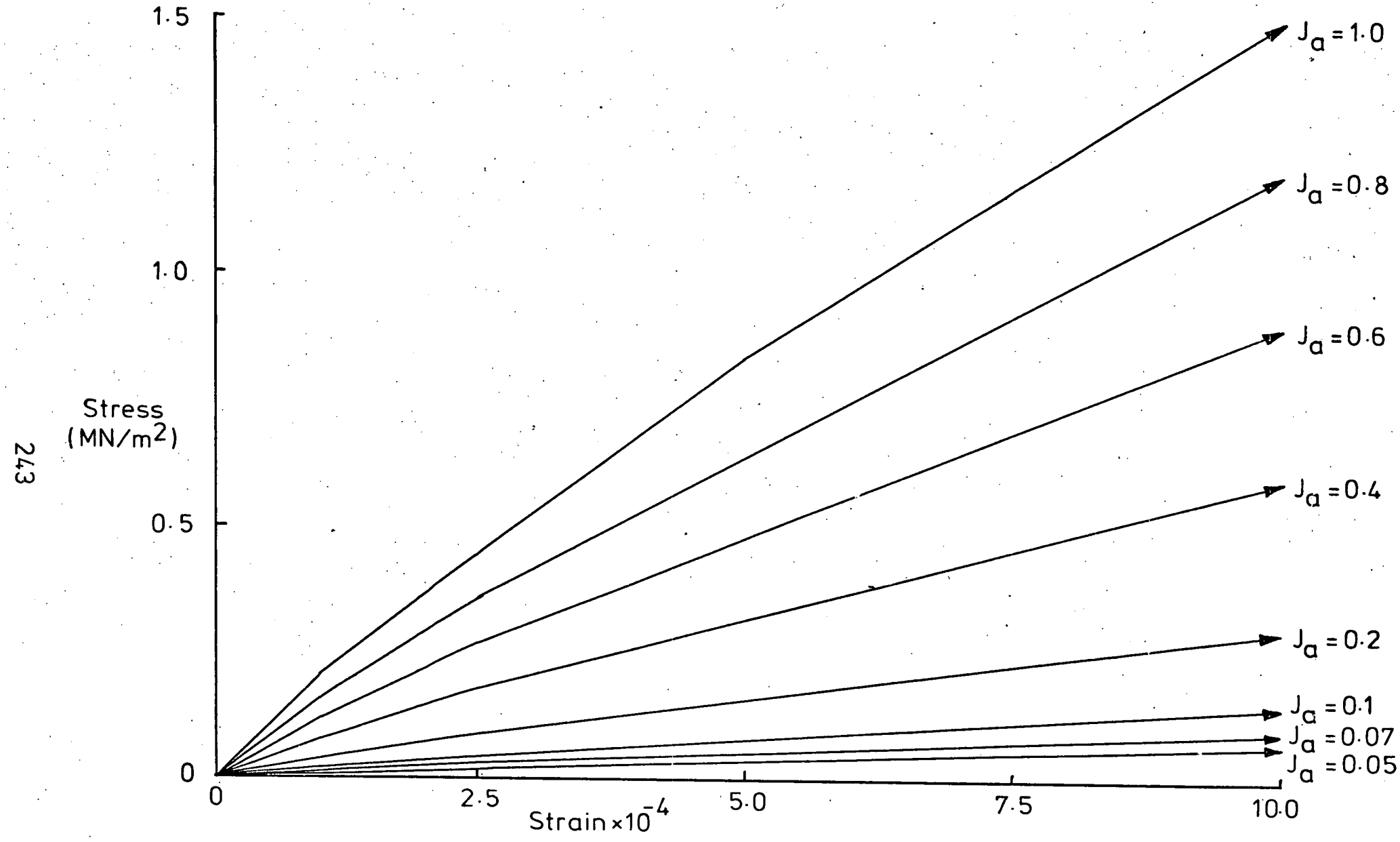

Fig. 8.3 STRESS-STRAIN CURVES FOR J_a FACTORS OF 0.05 TO 1.0

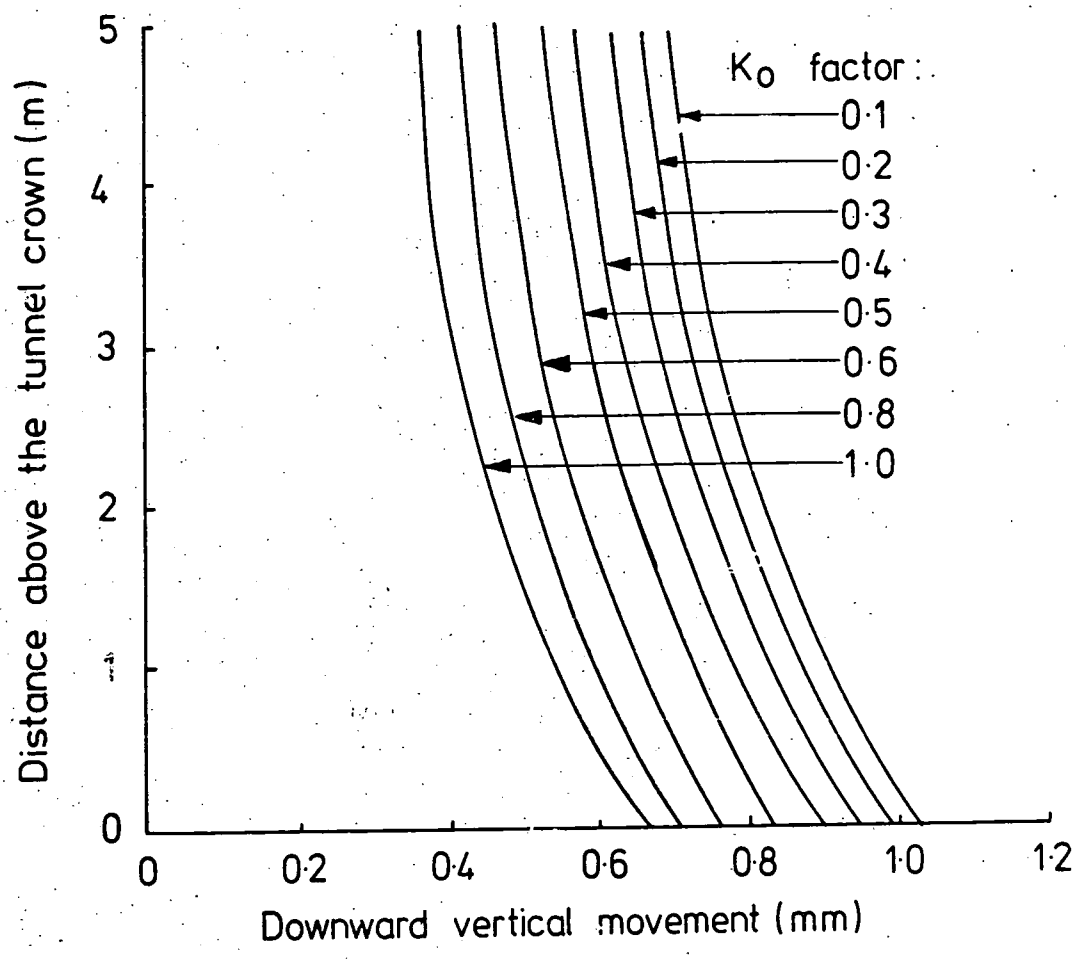

Fig. 8.4 VARIATION OF THEORETICAL DOWNWARD VERTICAL MOVEMENT WITH DISTANCE ABOVE THE TUNNEL CROWN. SHALLOW, K_o FACTORS 0·1 TO 1·0.

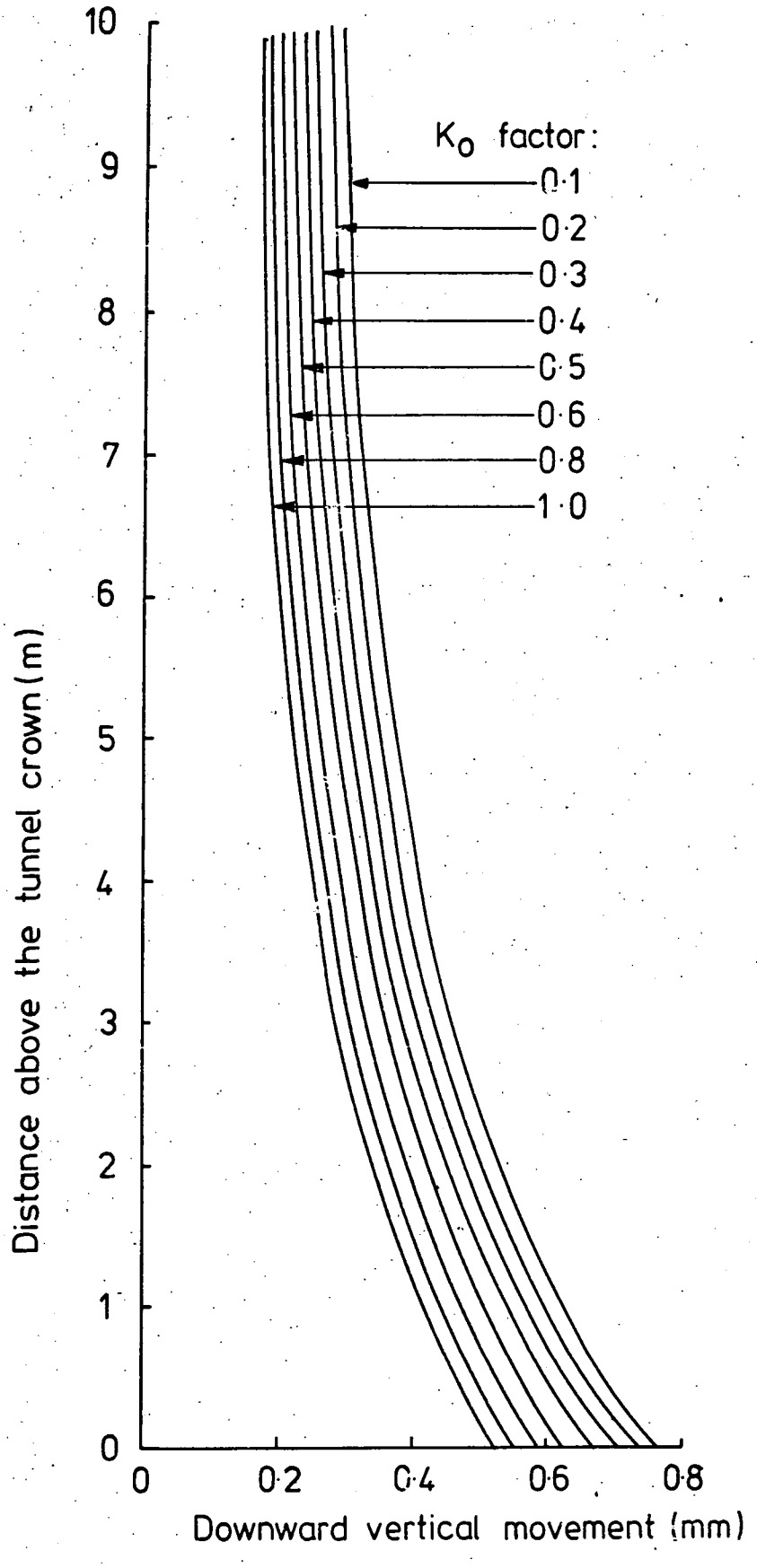

Fig. 8.5 VARIATION OF THEORETICAL DOWNWARD VERTICAL MOVEMENT WITH DISTANCE ABOVE THE TUNNEL CROWN. DEEP, K_o FACTORS 0·1 TO 1·0

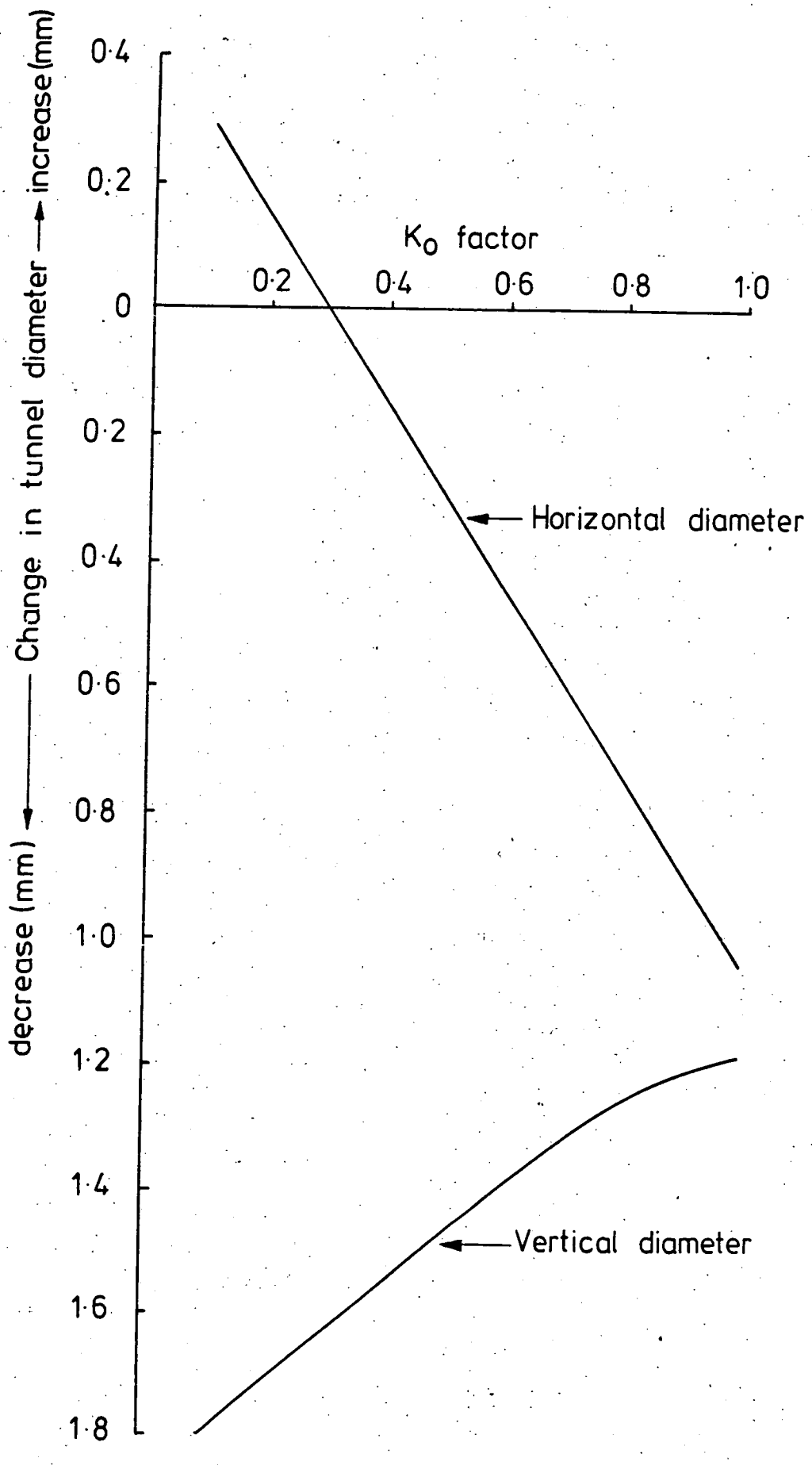

Fig. 8.6 THEORETICAL CHANGE IN HORIZONTAL AND VERTICAL TUNNEL DIAMETERS FOLLOWING EXCAVATION, AS A FUNCTION OF K_o. SHALLOW TUNNEL.

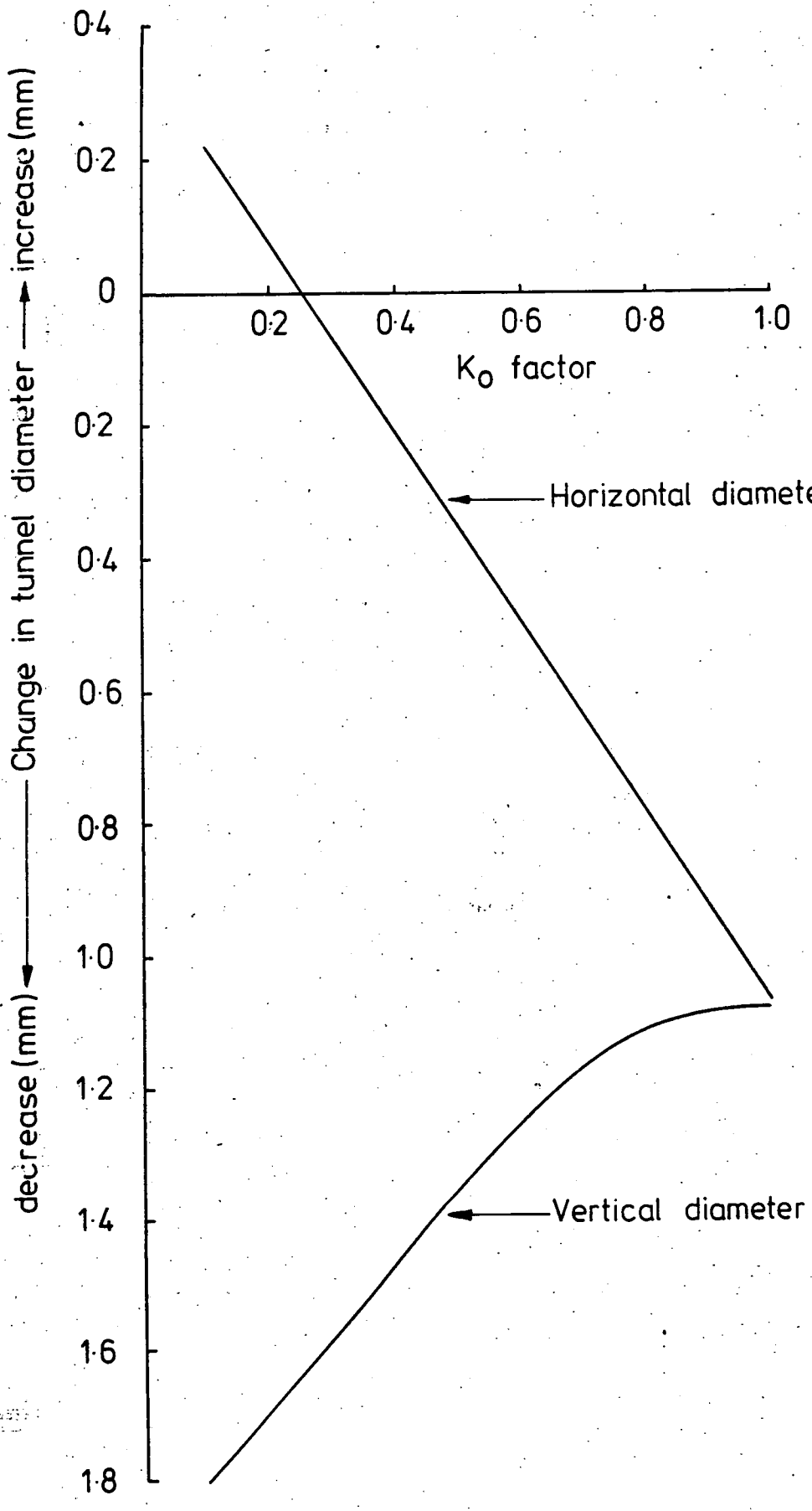

Fig. 8.7 THEORETICAL CHANGE IN HORIZONTAL AND VERTICAL TUNNEL DIAMETERS FOLLOWING TUNNEL EXCAVATION, AS A FUNCTION OF K_o. DEEP TUNNEL.

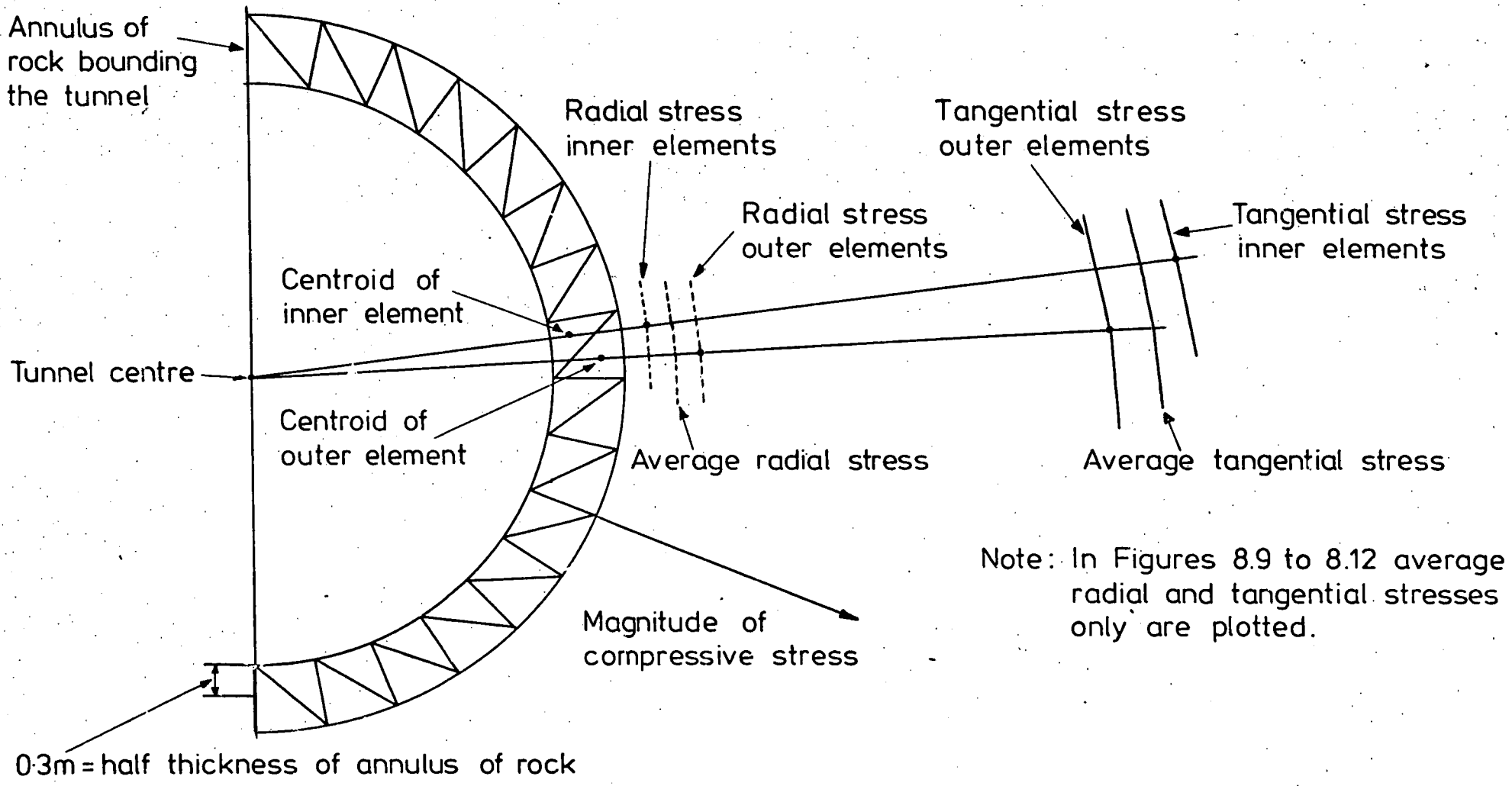

Note: In Figures 8.9 to 8.12 average radial and tangential stresses only are plotted.

Fig. 8.8 EXPLANATION OF THE METHOD USED IN THE CONSTRUCTION OF DIAGRAMS SHOWING THE VARIATION OF THEORETICAL RADIAL AND TANGENTIAL STRESS ROUND THE ANNULUS OF ROCK BOUNDING THE CHINNOR TUNNEL.

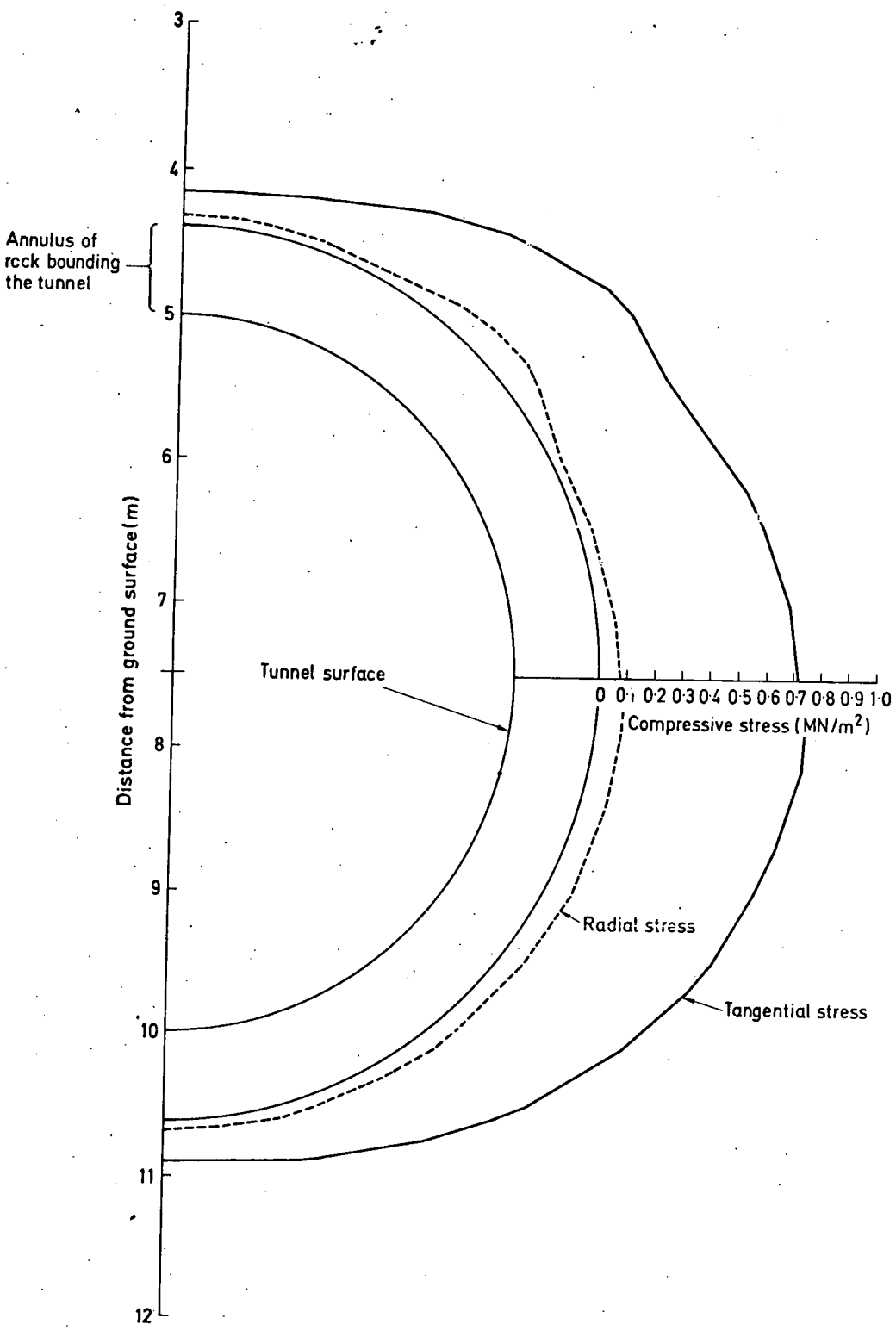

Fig. 8.9 VARIATION IN THEORETICAL RADIAL AND TANGENTIAL STRESS MAGNITUDES ROUND THE ANNULUS OF ROCK 0·3 m FROM THE TUNNEL SURFACE, $K_0 = 0{\cdot}4$, SHALLOW

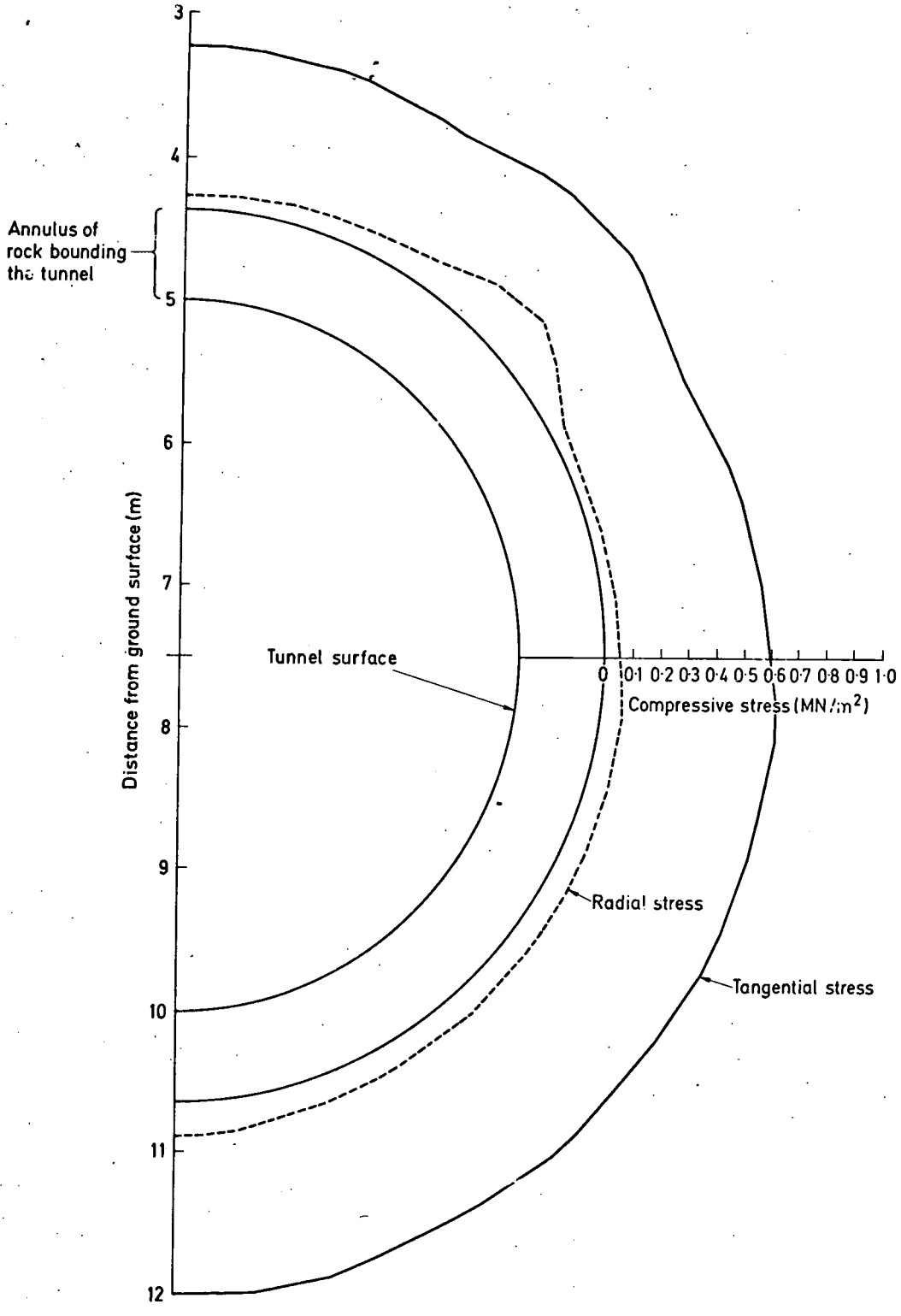

Fig. 8.10 VARIATION IN THEORETICAL RADIAL AND TANGENTIAL STRESS MAGNITUDES ROUND THE ANNULUS OF ROCK 0·3m FROM THE TUNNEL SURFACE, $K_0 = 1·0$, SHALLOW

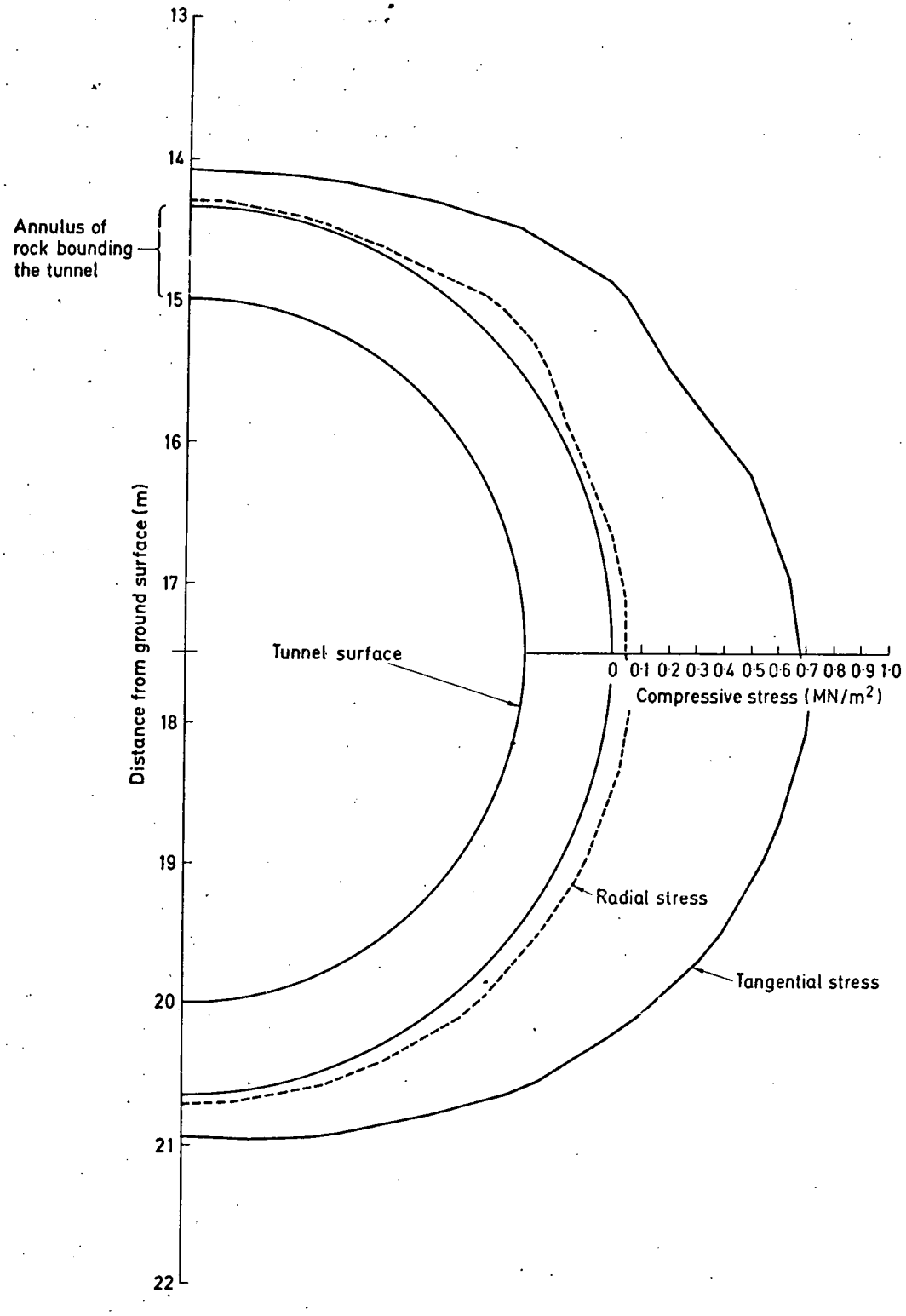

Fig. 8.11 VARIATION IN THEORETICAL RADIAL AND TANGENTIAL STRESS MAGNITUDES ROUND THE ANNULUS OF ROCK 0·3m FROM THE TUNNEL SURFACE, $K_0 = 0{\cdot}4$, DEEP

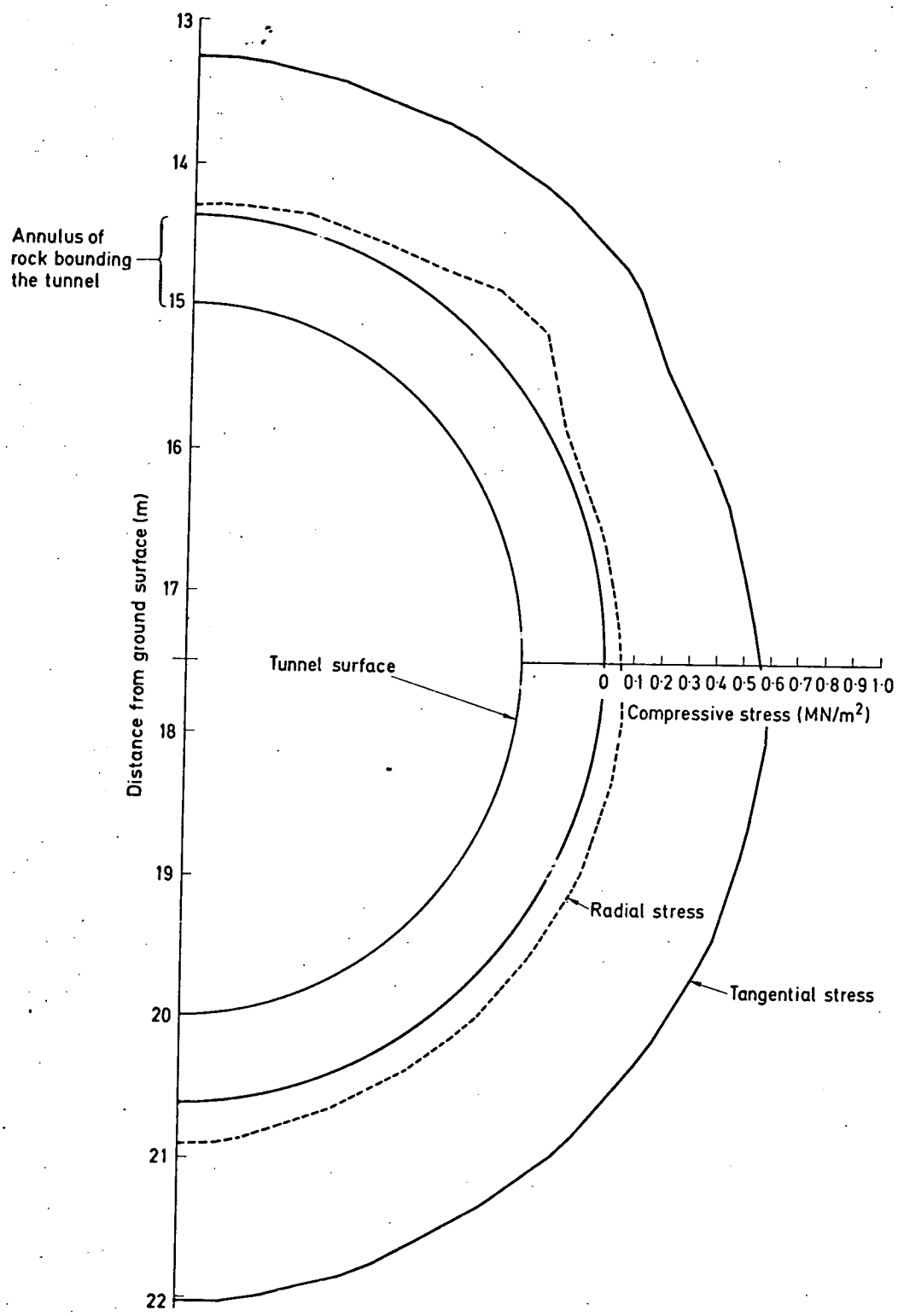

Fig. 8.12 VARIATION IN THEORETICAL RADIAL AND TANGENTIAL STRESS MAGNITUDES ROUND THE ANNULUS OF ROCK 0·3m FROM THE TUNNEL SURFACE, $K_0 = 1·0$, DEEP

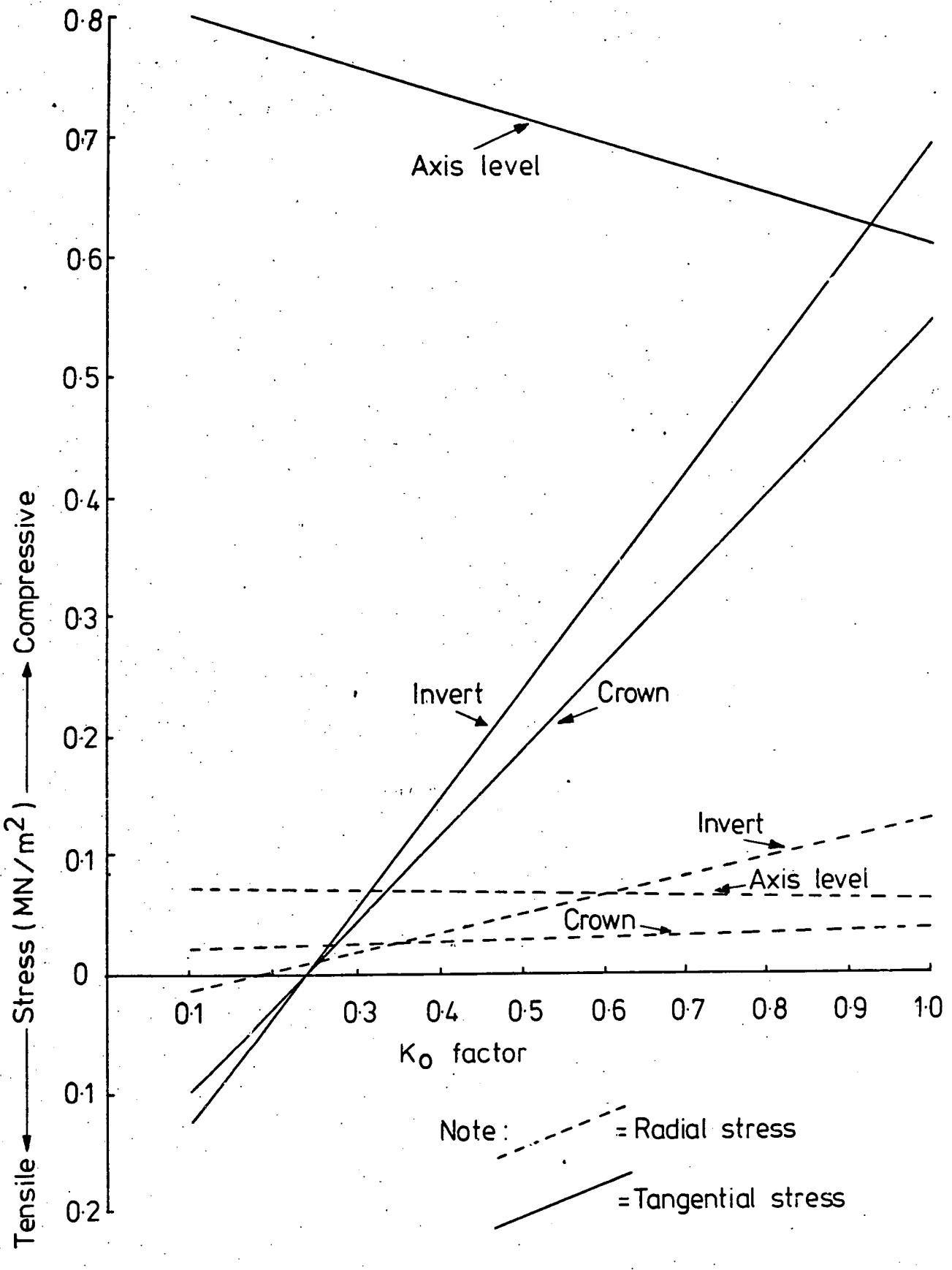

Fig. 8.13 VARIATION OF THEORETICAL RADIAL AND TANGENTIAL STRESS WITH K_o AT SELECTED POSITIONS ROUND THE ANNULUS OF ROCK BOUNDING THE TUNNEL. SHALLOW.

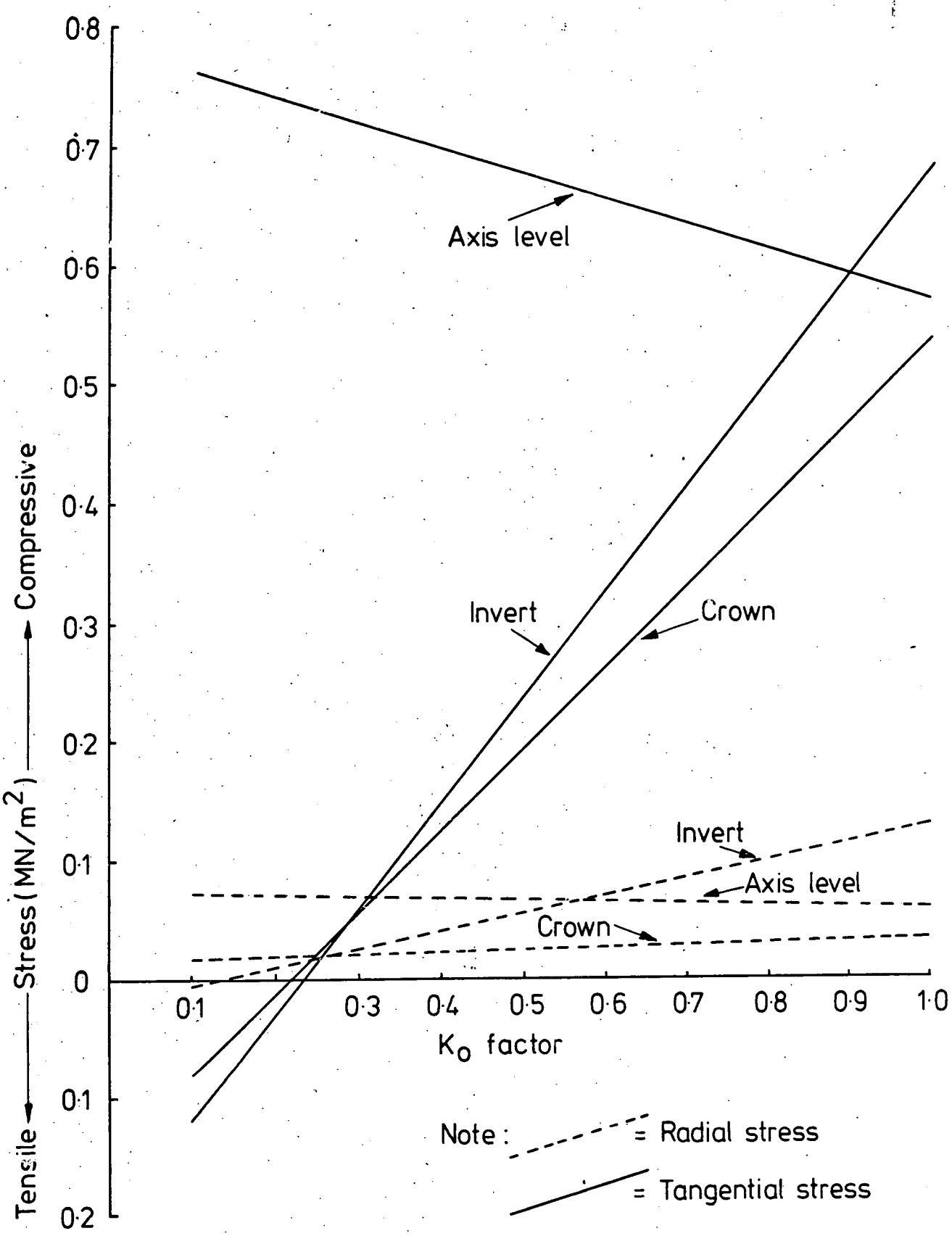

Fig. 8.14 VARIATION OF THEORETICAL RADIAL AND TANGENTIAL STRESS WITH K_0 AT SELECTED POSITIONS ROUND THE ANNULUS OF ROCK BOUNDING THE TUNNEL. DEEP.

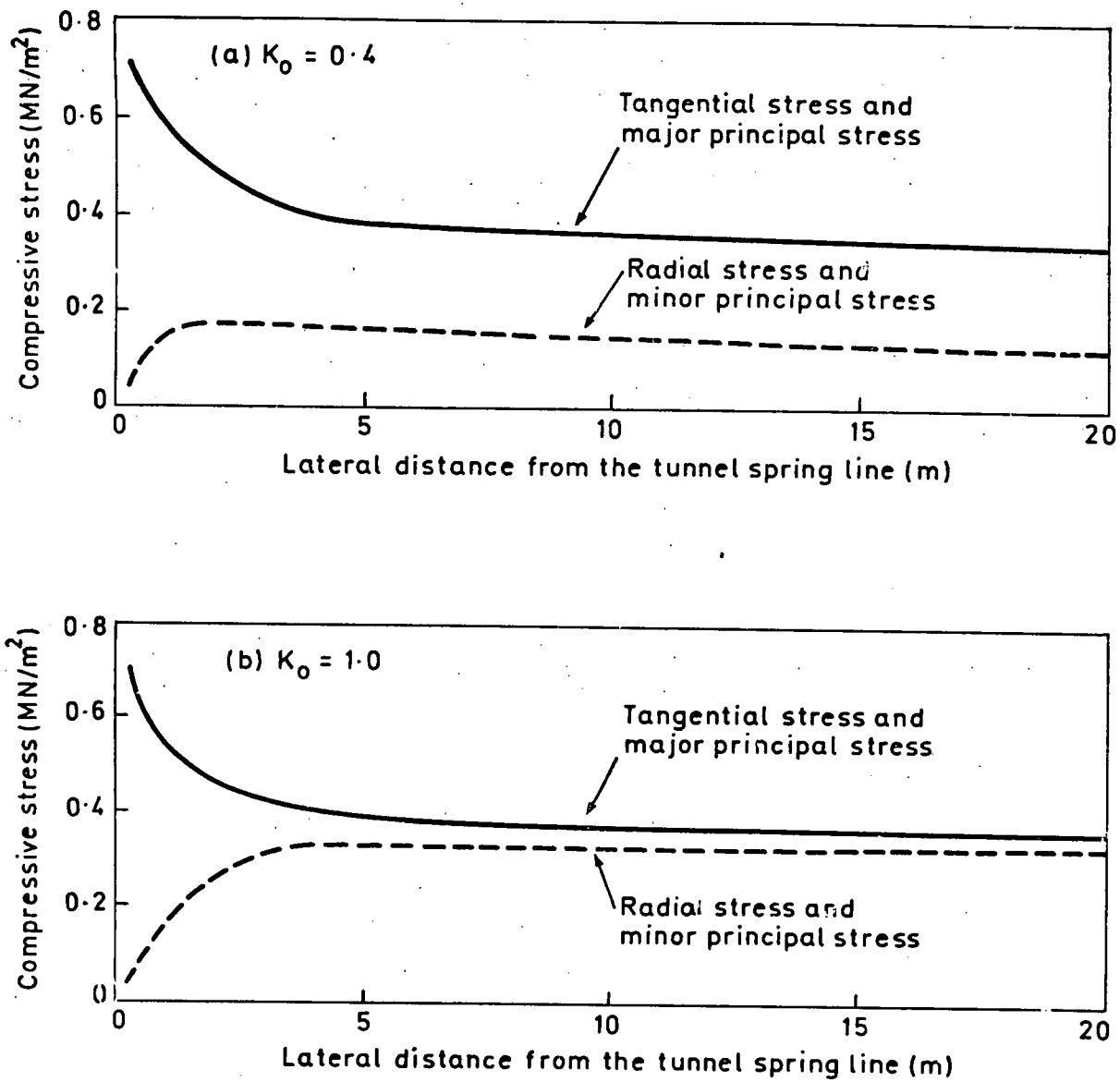

Fig. 8·15 VARIATION IN THEORETICAL STRESS MAGNITUDES WITH LATERAL DISTANCE FROM THE TUNNEL SPRING LINE. SHALLOW

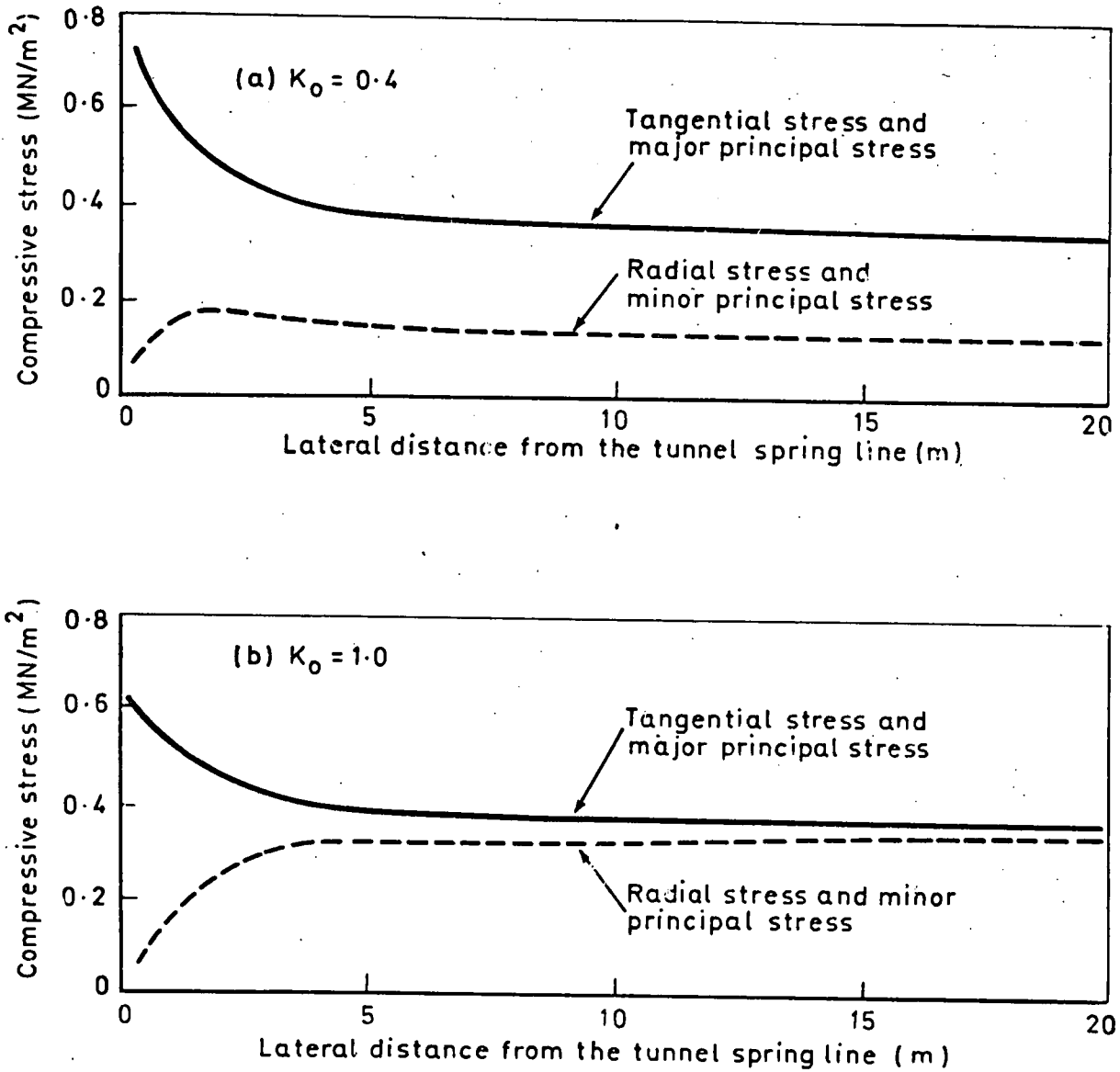

Fig 8·16 VARIATION IN THEORETICAL STRESS MAGNITUDES WITH LATERAL DISTANCE FROM THE TUNNEL SPRING LINE. DEEP

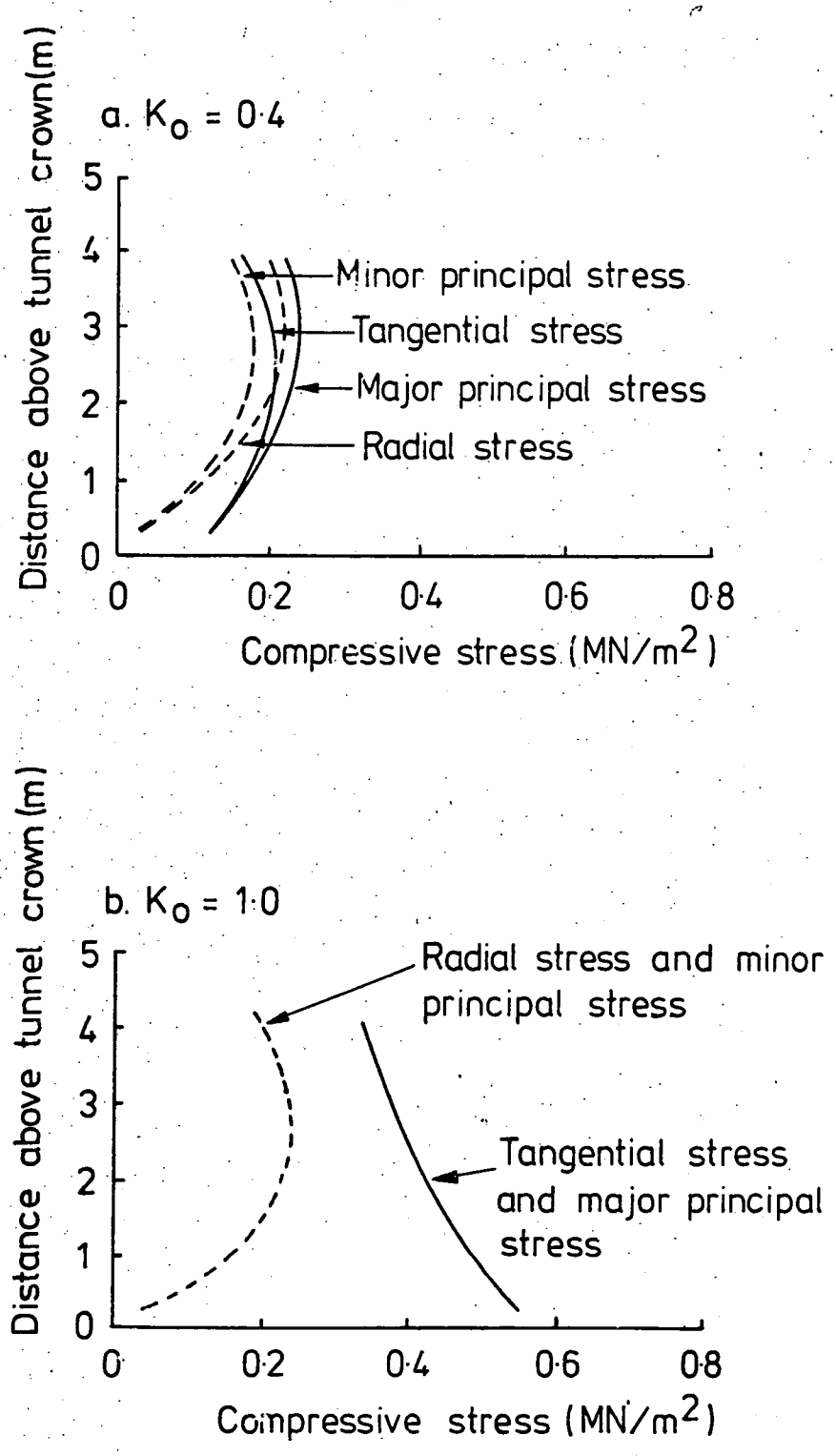

Fig. 8.17 VARIATION OF THEORETICAL STRESS MAGNITUDES WITH DISTANCE ABOVE THE TUNNEL CROWN. SHALLOW TUNNEL.

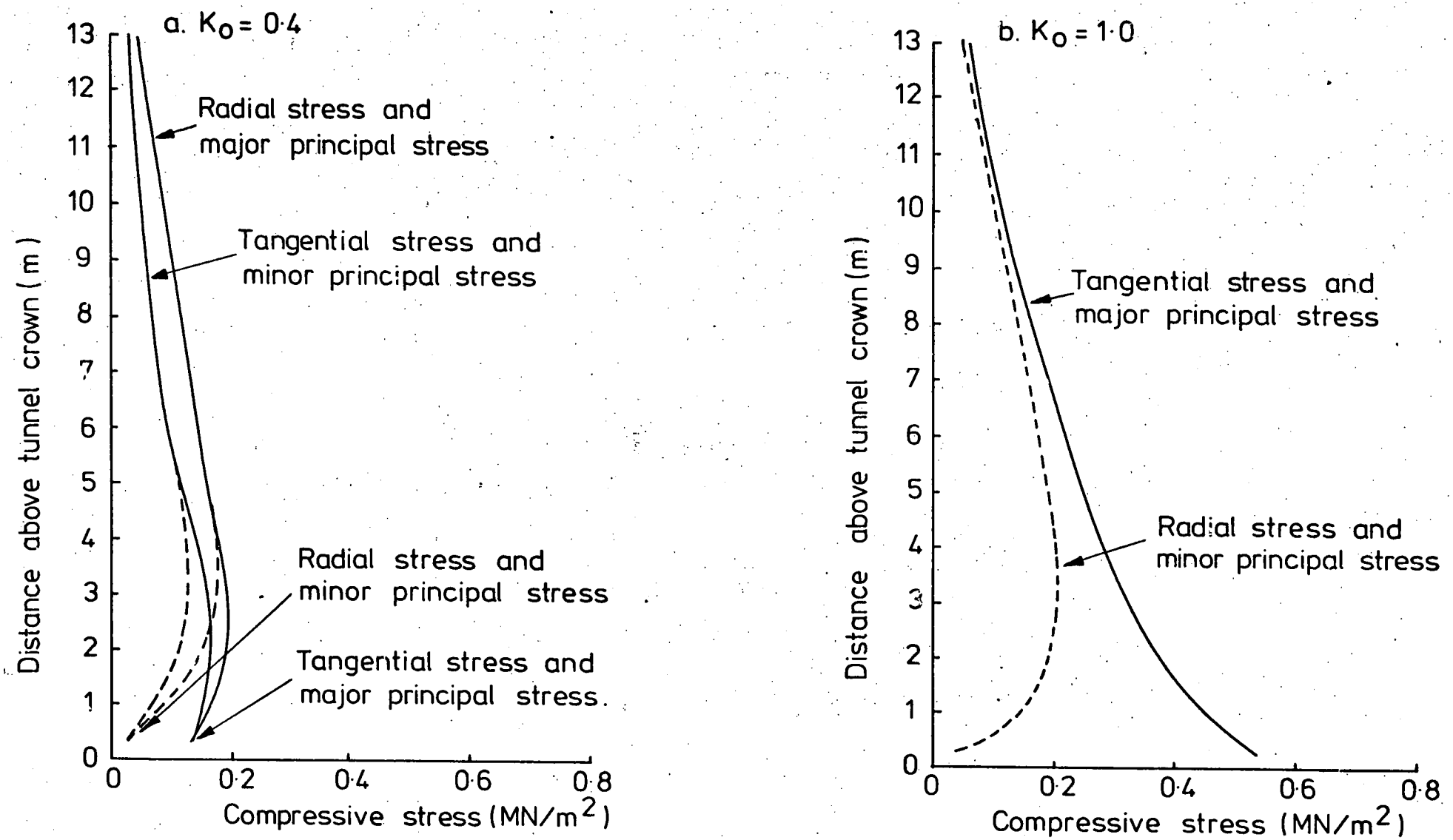

Fig. 8.18 VARIATION OF THEORETICAL STRESS MAGNITUDES WITH DISTANCE ABOVE THE TUNNEL CROWN. DEEP TUNNEL.

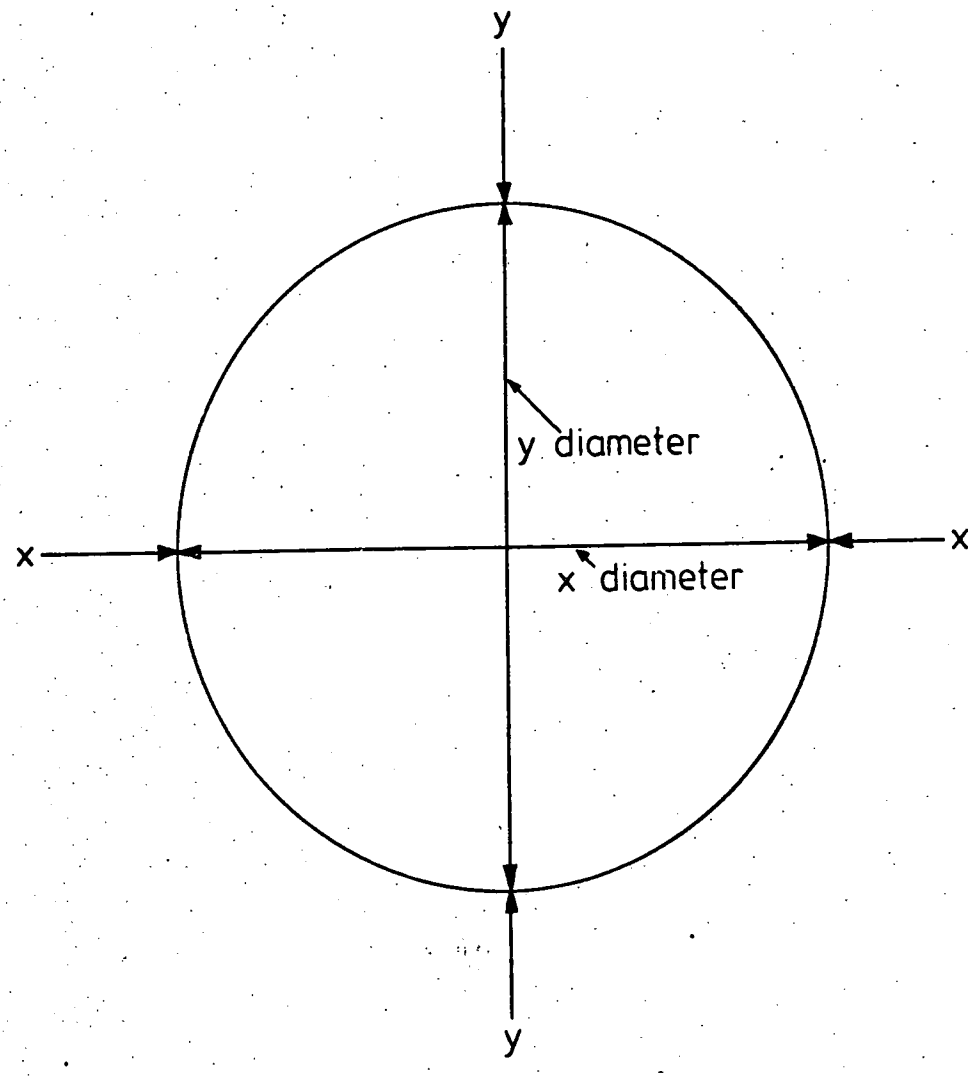

a. If y loading > x loading (equivalent to a low K_o)
∴ x diameter > y diameter.

b. If x loading > y loading (equivalent to a high K_o)
∴ y diameter > x diameter.

Fig. 8.19 BEHAVIOUR OF A PROVING RING UNDER BIAXIAL LOADING.

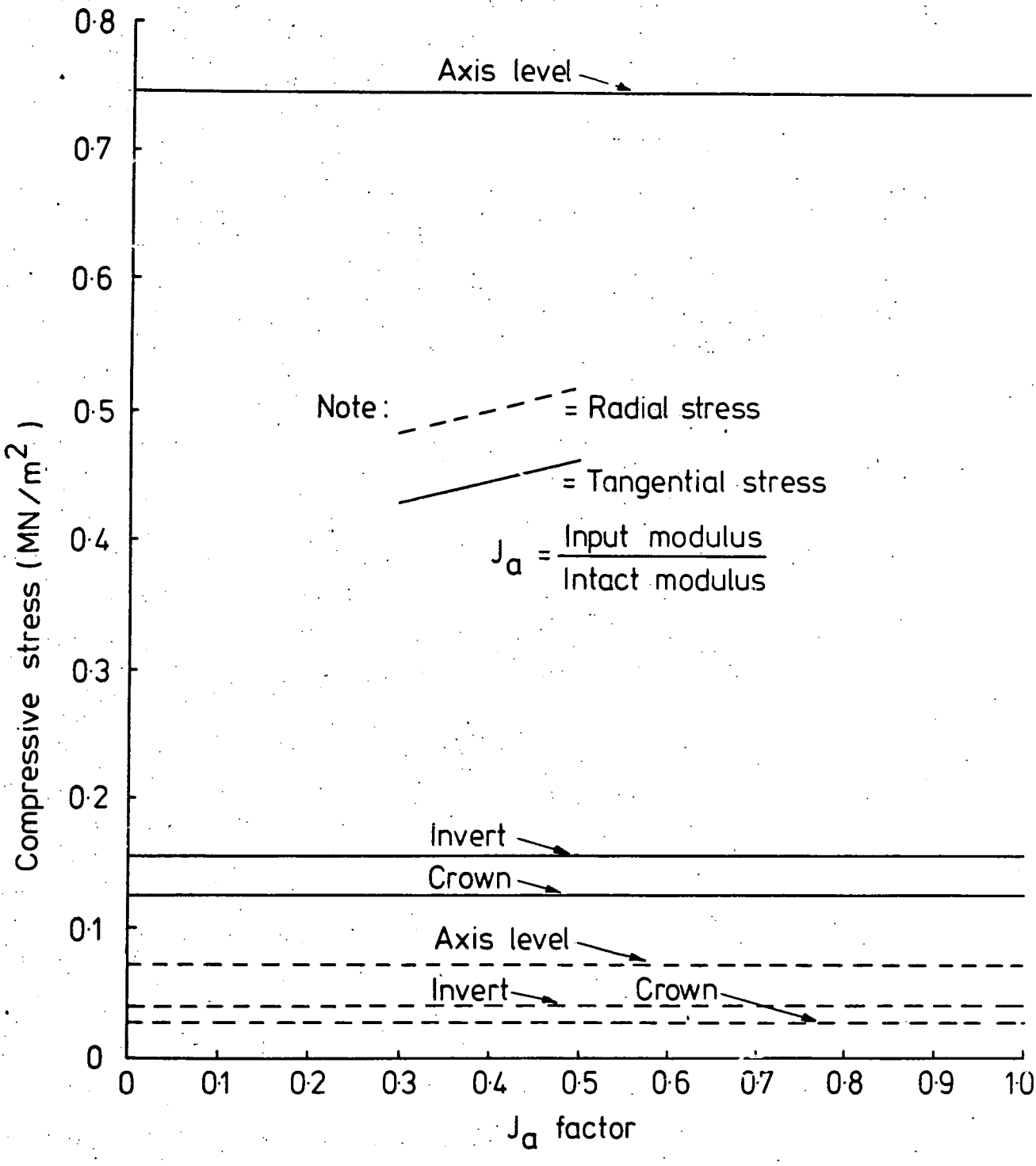

Fig. 8.20 VARIATION IN THEORETICAL RADIAL AND TANGENTIAL STRESS WITH J_a AT SELECTED POSITIONS ROUND THE ANNULUS OF ROCK BOUNDING THE TUNNEL.
$K_o = 0{\cdot}4$. SHALLOW.

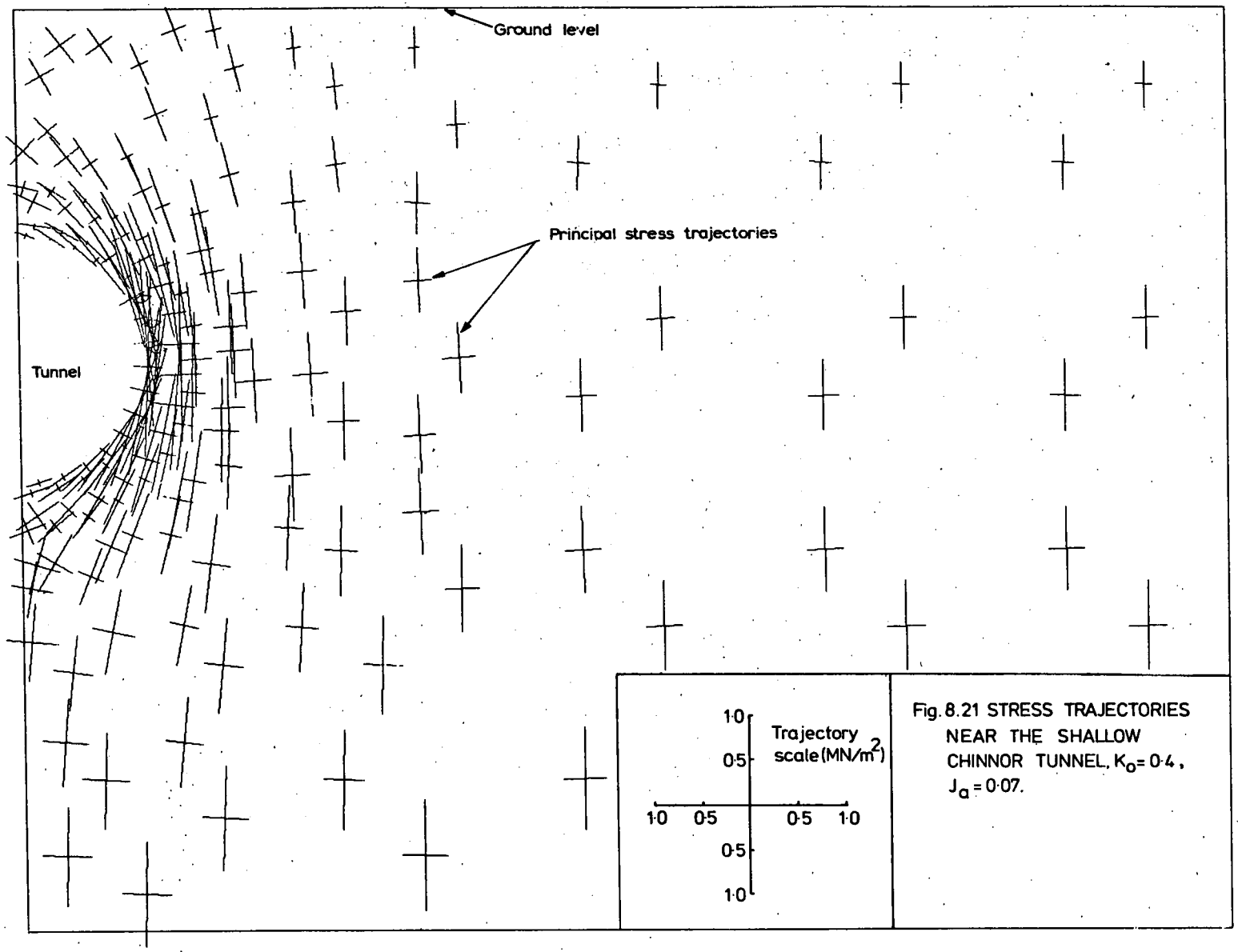

Fig. 8.21 STRESS TRAJECTORIES NEAR THE SHALLOW CHINNOR TUNNEL, $K_o = 0{\cdot}4$, $J_a = 0{\cdot}07$.

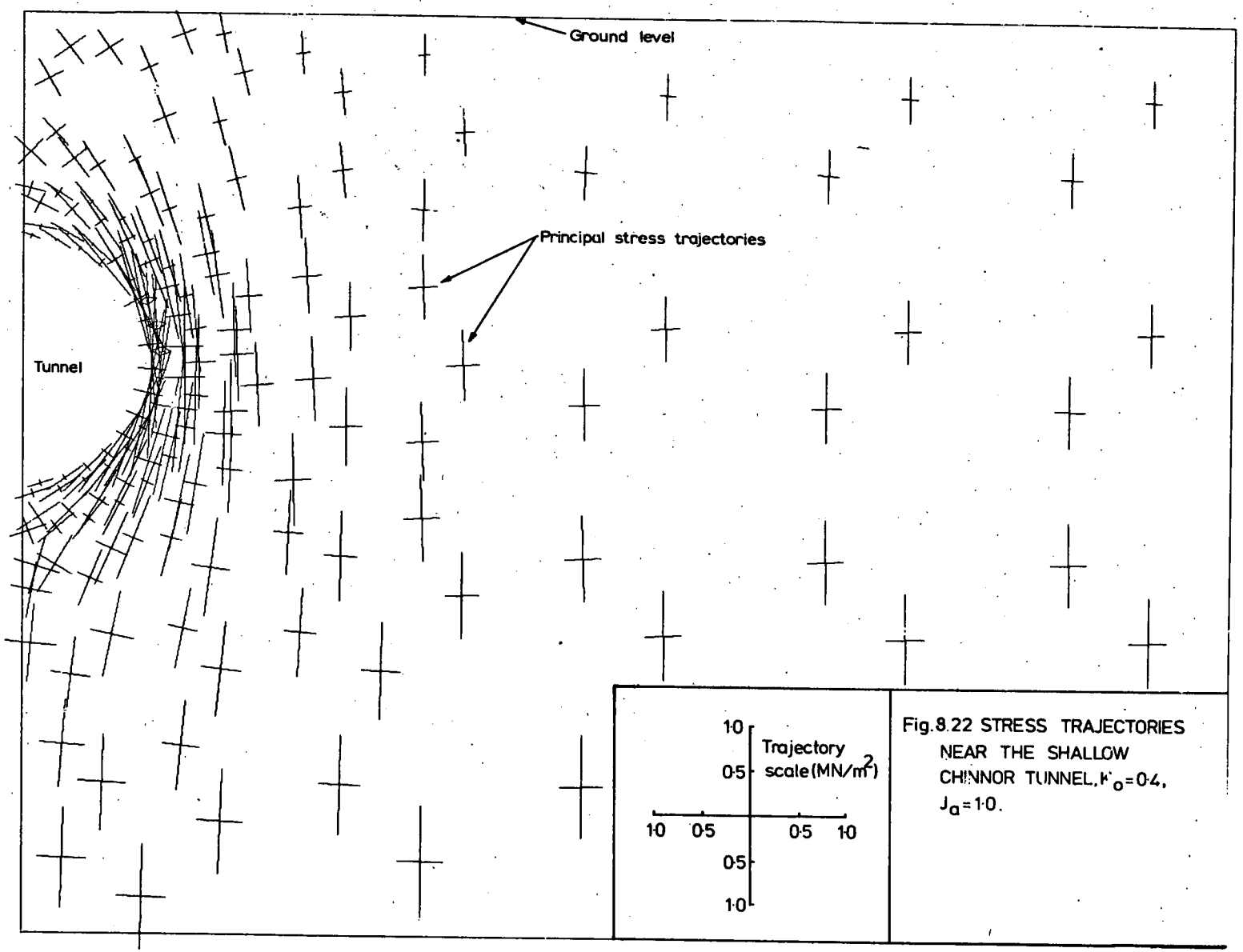

Fig. 8.22 STRESS TRAJECTORIES NEAR THE SHALLOW CHINNOR TUNNEL, $K'_o = 0.4$, $J_a = 1.0$.

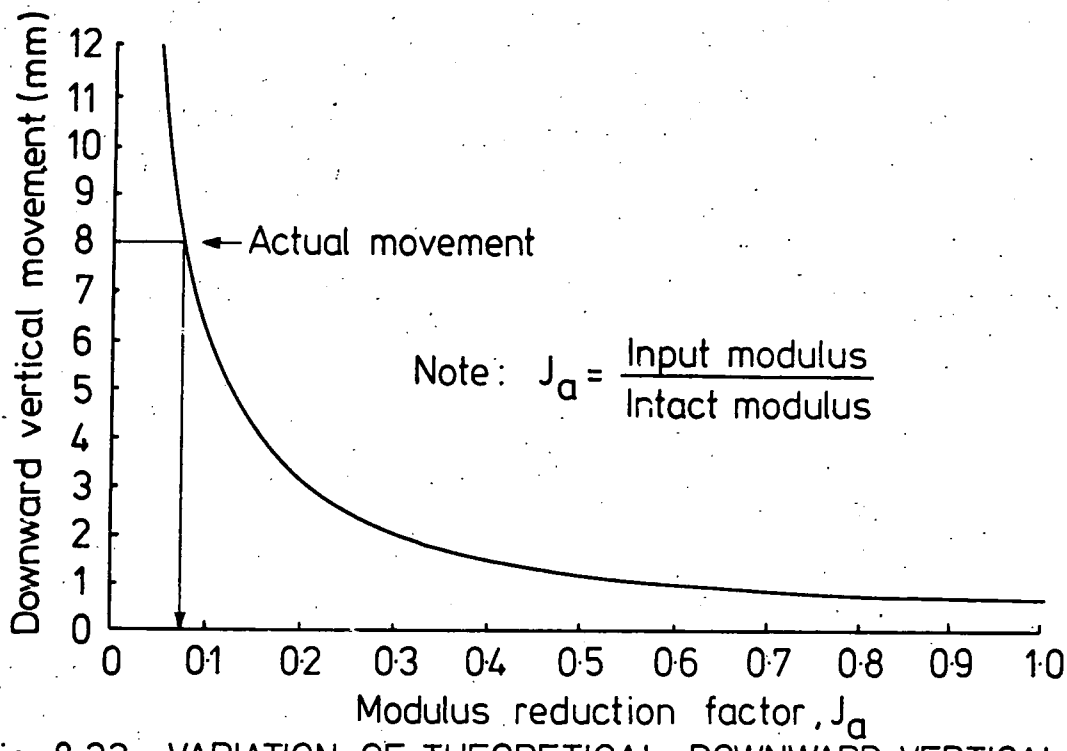

Fig. 8.23 VARIATION OF THEORETICAL DOWNWARD VERTICAL MOVEMENT AT GROUND LEVEL WITH CHANGES IN THE MODULUS REDUCTION FACTOR J_a.

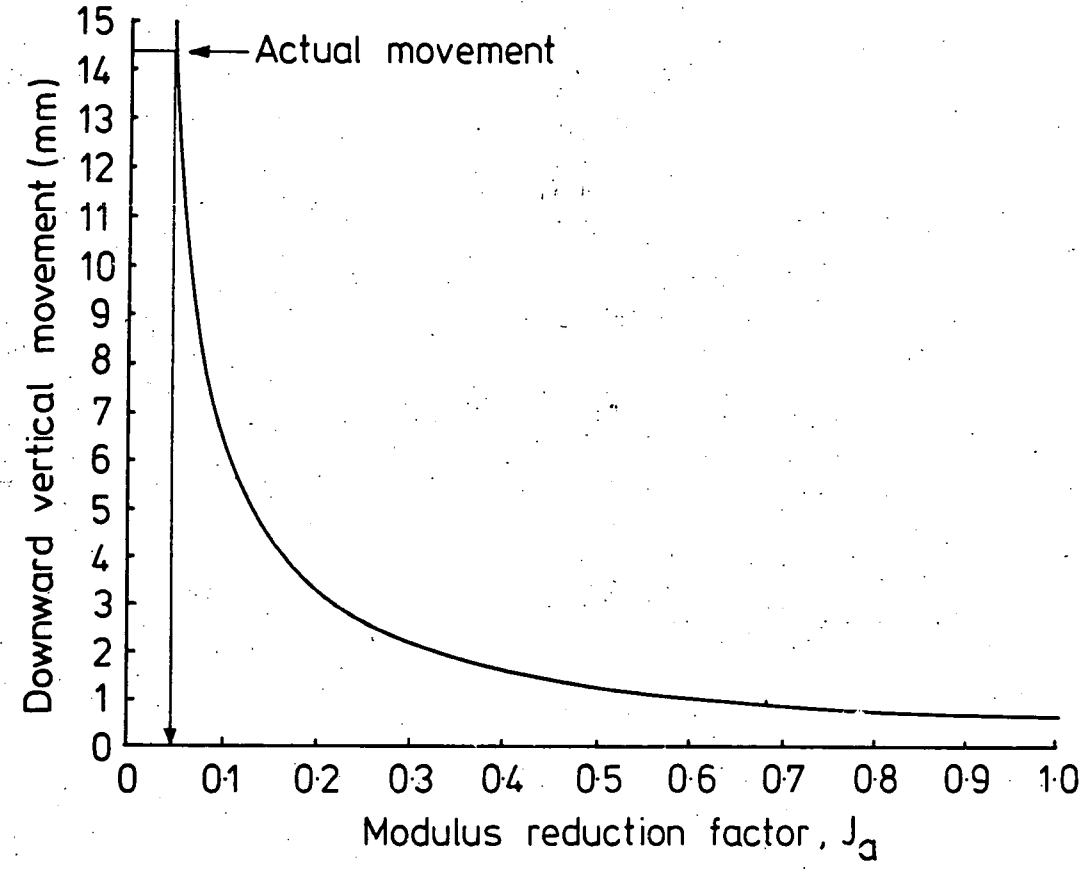

Fig. 8.24 VARIATION OF THEORETICAL DOWNWARD VERTICAL MOVEMENT 3m ABOVE THE TUNNEL CROWN WITH CHANGES IN THE MODULUS REDUCTION FACTOR J_a.

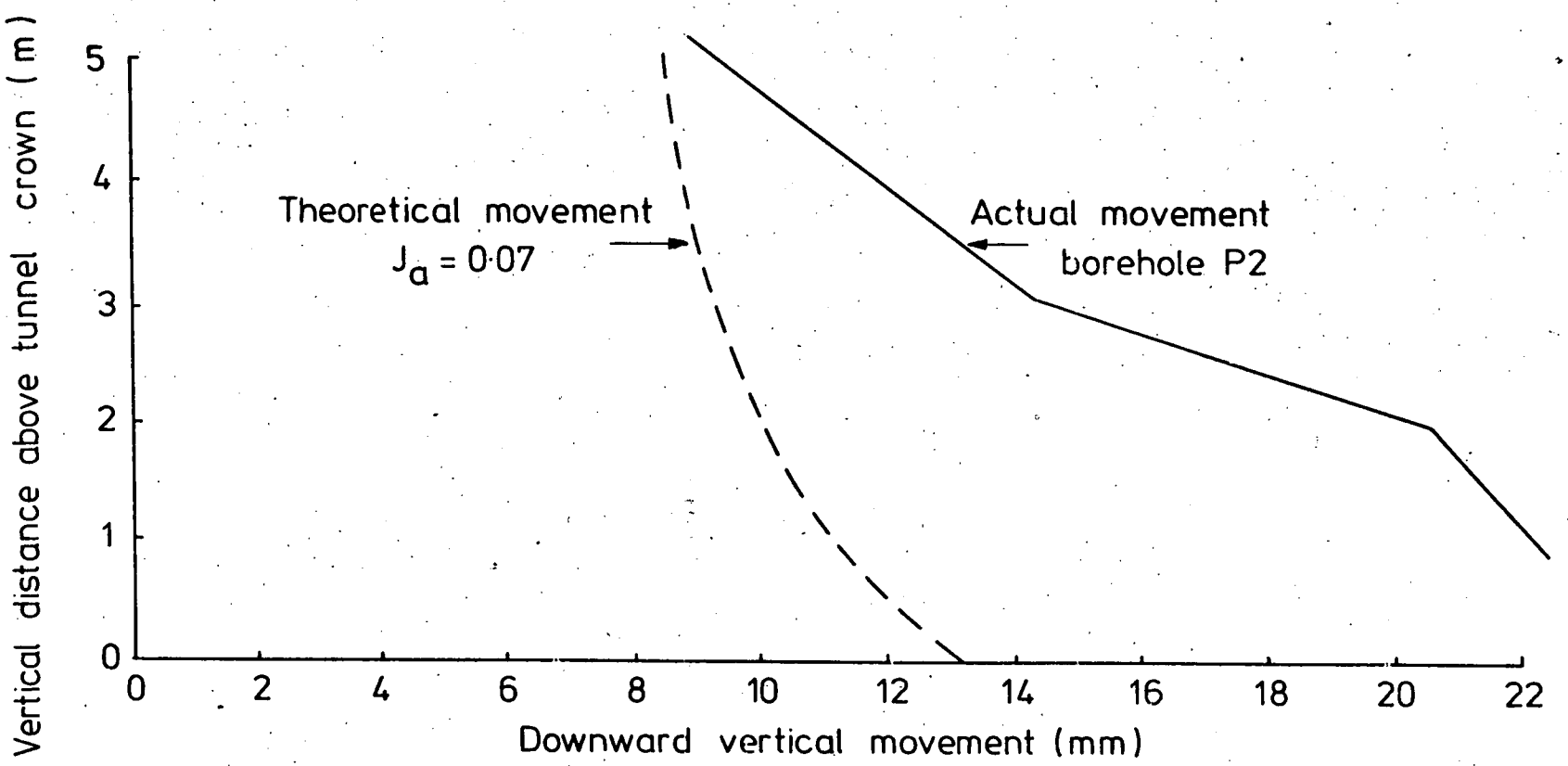

Fig. 8.25 ACTUAL AND THEORETICAL VARIATION IN DOWNWARD VERTICAL MOVEMENT WITH DISTANCE ABOVE THE TUNNEL CROWN. SHALLOW.

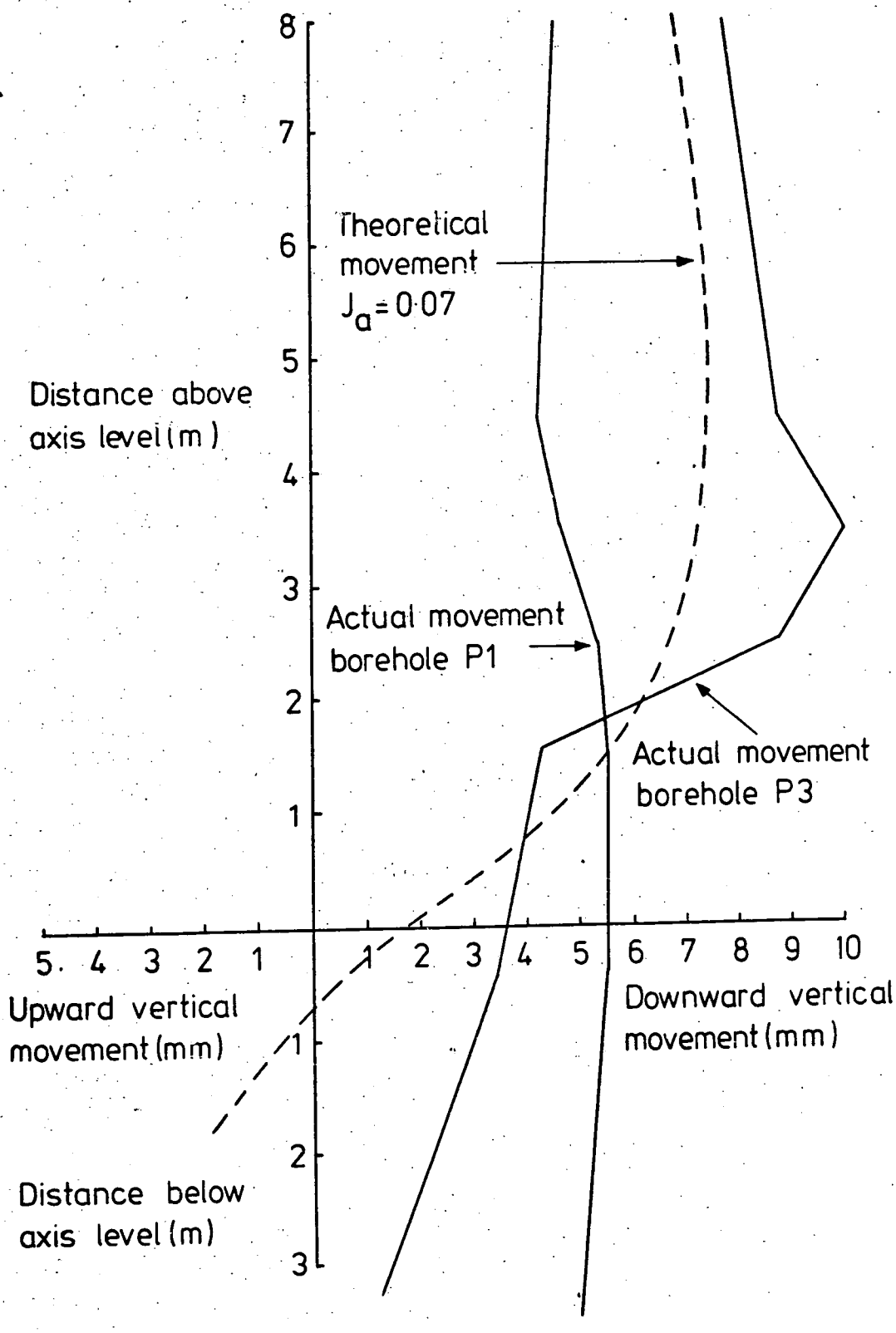

Fig. 8.26 ACTUAL AND THEORETICAL VERTICAL MOVEMENT ALONG VERTICAL LINES INTERSECTING THE TUNNEL AT AXIS LEVEL. SHALLOW.

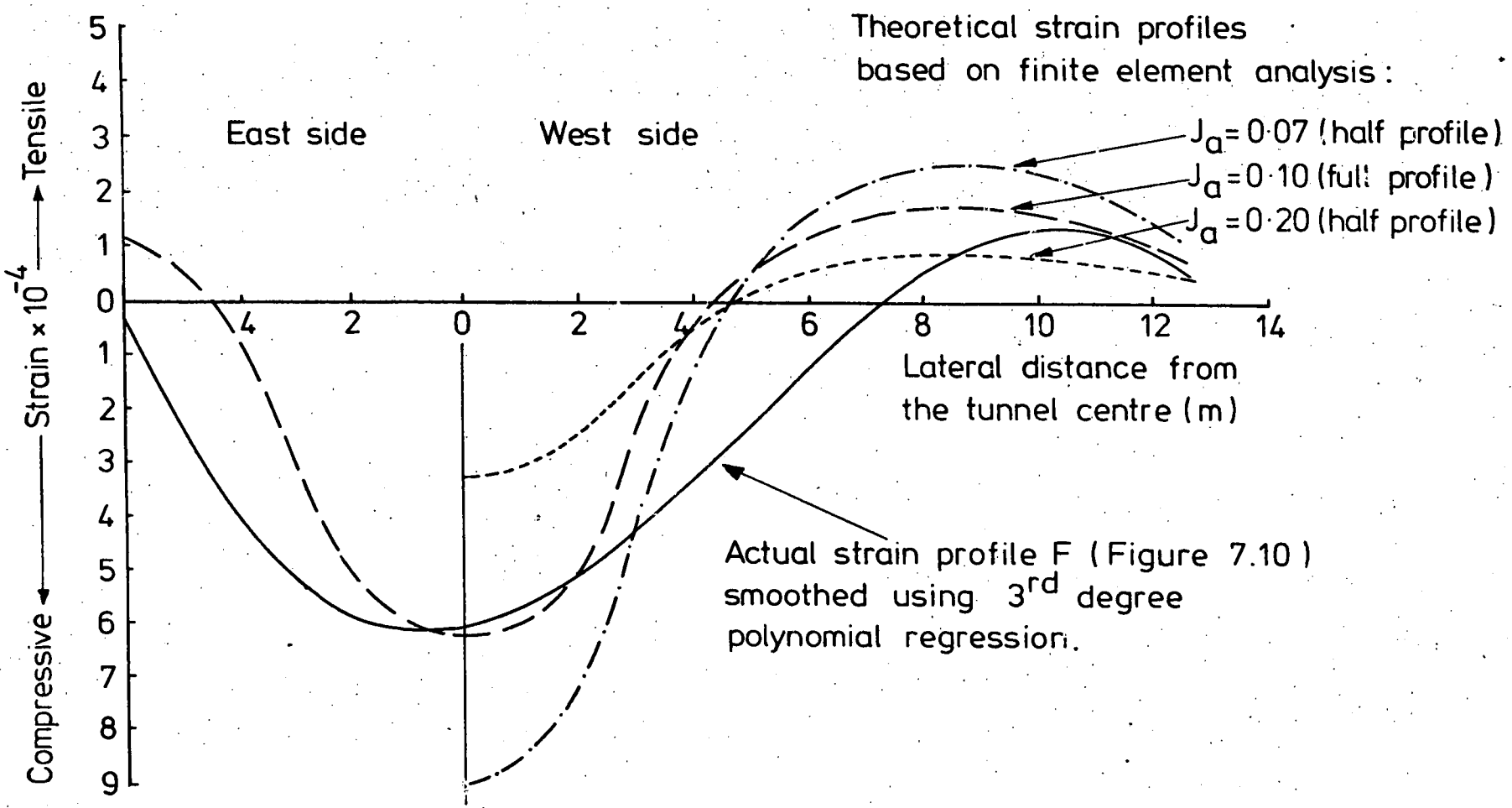

Fig. 8.27 COMPARISON BETWEEN ACTUAL AND THEORETICAL HORIZONTAL STRAIN PROFILES ACROSS THE TUNNEL LINE.

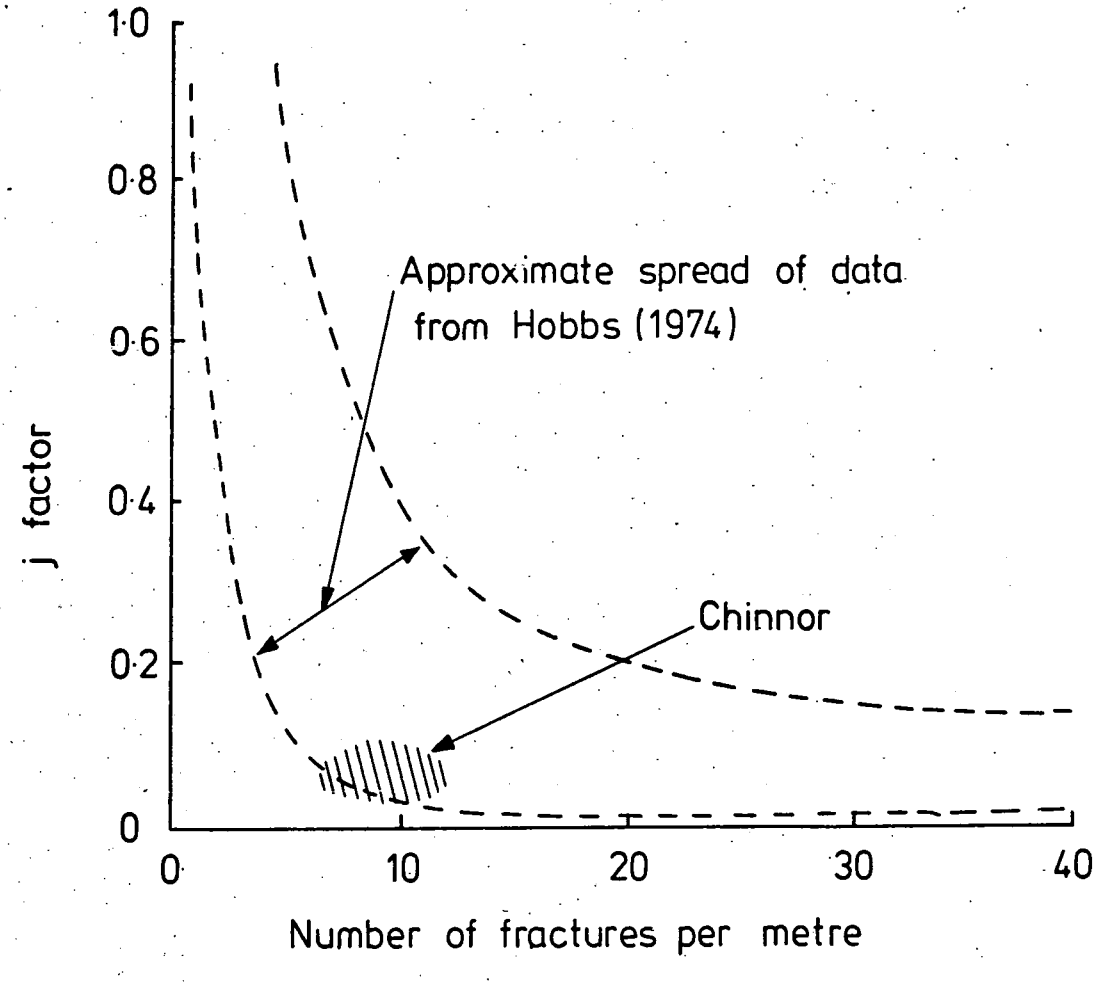

Fig. 8.28 RELATION BETWEEN ROCK MASS FACTOR j AND FRACTURE FREQUENCY FOR CHALK SITES IN THE UK (AFTER HOBBS, 1974)

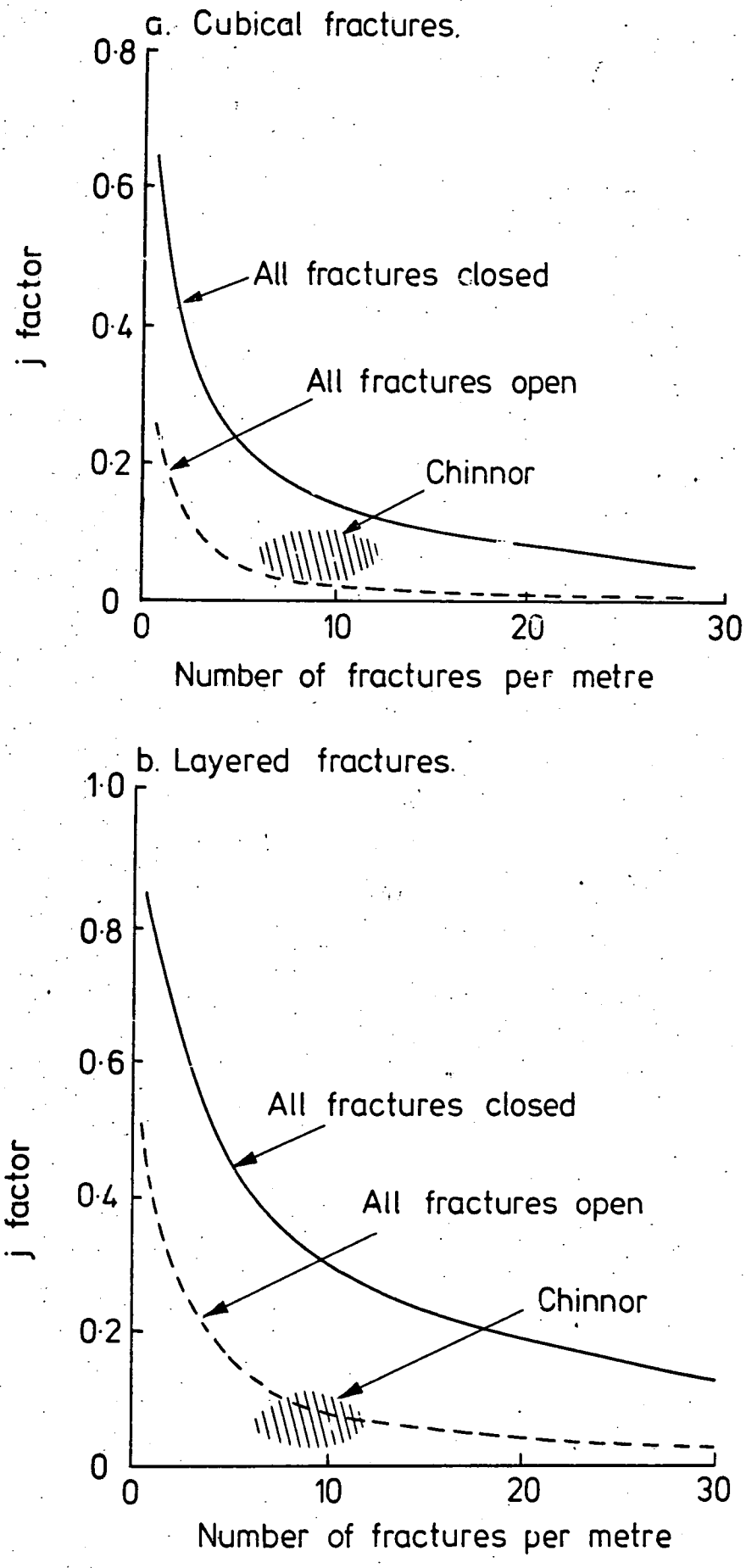

Fig. 8.29 RELATION BETWEEN ROCK MASS FACTOR j AND FRACTURE FREQUENCY (AFTER HOBBS, 1974)

CHAPTER 9

DETERMINATION OF THE SHEAR STRENGTH CHARACTERISTICS OF DISCONTINUITY SURFACES IN THE LOWER CHALK AT CHINNOR

9.1 Introduction

A series of field shear box tests was undertaken to determine shear strength characteristics of discontinuities sampled in cores recovered during the site investigation programme at Chinnor. This work was directed towards two broad aims: (1) To obtain a value for cohesion and the angle of shearing resistance of discontinuity surfaces for use in stability calculations. (2) To examine the influence of discontinuity geometry, calcium carbonate content and moisture content on the shear strength of the discontinuity surfaces.

Stressing and deformation of discontinuous rock, for example following tunnel excavation, may be accompanied by shearing along discontinuity surfaces. This shearing is controlled by the shear strength (τ) mobilised between the discontinuity surfaces. The maximum shear strength (τ_{max}) mobilised is influenced by three factors:

(1) The cohesion (c') between the discontinuity surfaces (derived from effective stress parameters).

(2) The effective normal stress (σ'_n) acting across the discontinuity surfaces (controlled by ground stress conditions).

(3) The effective angle of shearing resistance (ϕ') of the surfaces.

For simple sliding $\tau_{max} = c' + \sigma'_n \tan \phi'$

The principle of the shear box test is to apply a known normal pressure to a discontinuity in a sample housed in a cement block, the maximum shear resistance of the surface being then measured. This is repeated for several values of σ'_n allowing a determination of c' and ϕ'.

A number of workers have examined the use of direct shear tests in determining the shear strength characteristics of rock discontinuities (Locher, 1968; Romero, 1968; Hoek, 1970). Romero (1968), underlining one of the major problems concerning the direct shear test, questioned the validity of applying shear strength parameters obtained from a small area of discontinuity to much greater areas in the rock mass. Patton (1966) commented on the influence of joint roughness on shear strength. He concluded that it is often possible to allow for joint roughness by increasing the friction angle of the joint surface by an amount ϕ_r, equal to the average angle between the undulations on the joint surface and the direction of sliding.

Boyd (1975) provides a detailed analysis of the effects of surface roughness on the shear strength characteristics of discontinuity surfaces. He concluded that the following Equation

$$(\tau/\sigma_c) = K(\sigma_n/\sigma_c)^x \qquad 2/3 \leq x \leq 1 \qquad \ldots\ (9.1)$$

adequately represented the shear failure of rough discontinuity surfaces in hard rock where: τ is the average shear stress on the surface

σ_n is the average normal stress on the surface

σ_c is the uniaxial compressive strength of the rock

K,x are constants

Boyd concluded that for many naturally occurring geological surfaces x lies between 0.8 and 0.9 and K between approximate limits of 0.6 and 0.8. The implication of Equation 9.1 is that there is a straight line relation between $\ln(\tau/\sigma_c)$ and $\ln(\sigma_n/\sigma_c)$, with K and x the parameters of the line. Boyd also concluded that Equation 9.1 could be expressed in terms of the angle of shearing resistance of the sliding surfaces, incorporating the roughness factor (ϕ_r) of Patton (1966).

9.2 Testing procedure

The apparatus that was used (the Hoek portable shear box) is shown in Plate 9.1. A 100mm diameter core containing a suitable discontinuity was selected and trimmed. Then the two surfaces of the discontinuity were traced onto graph paper to allow determination of the surface area (A). The two halves of the sample were bound together with wire and set in the lower half of the mould with the supporting screws intruding approximately 5mm. A stiff mix of Ciment Fondu* cement was used to house the sample, taking care to position the discontinuity surface in the plane of shearing. When the cement was set, the mould was inverted and placed over its partner, allowing completion of the second half of the sample housing (Plates 9.2 and 9.3).

After allowing a day for hardening, the wires were cut and the sample was ready for testing. Before testing, however, it was necessary to obtain an indication of the geometry of the discontinuity surface. The method proposed by Patton (1966), involving the measurement of the average angle between the undulations on the discontinuity surface and the direction of sliding, was found to be a highly subjective and largely impractical procedure.

---

* Manufactured by Ciments Lafarge S.A.

Fookes and Denness (1969) suggested a scheme for classifying discontinuity surfaces, based on measurements of the degree of curvature, combined with various purely descriptive terms which related the surface roughness of the discontinuity to an appropriate sandpaper grade. It was found however that the Fookes and Denness system did not cover in sufficient detail the discontinuity geometries encountered at Chinnor. Therefore, since the aim was to produce a numerical index of discontinuity geometries tested in the shear box, it was necessary to develop a new system.

Discontinuity geometry was assessed in terms of two indices, first a curvature index (CI) for deviations from planar geometry having a wavelength greater than 50mm; second a roughness index (RI) for deviations from planar geometry having a wavelength less than 50mm. Discontinuity surfaces having deviations from planar geometry greater than 18mm were unsuitable for testing in the shear box, 18mm therefore provided the upper limit for both the deviation indices. The range from 0 - 18mm was then split into 6 increments, the lowest increment being given the index 0 and the highest the index 5. The classification is summarised in Table 9.1 and correlated with the Fookes and Denness classification. For each shear box sample the curvature and roughness indices were assessed in terms of the maximum deviations measurable, then summed to produce a deviation index (DI) ranging from 0 - 10, characterising the discontinuity geometry. The values of RI and CI for each sample are listed in Tables 9.2 and 9.3.

Half of the twenty-four samples prepared were soaked in water for 24 hours prior to testing to produce the 'wet' sample condition. For testing, each sample was placed carefully in the testing apparatus and a normal force of 2kN was applied. The dial gauge was zeroed, then shearing was commenced. The shearing was maintained at rates of less than 1mm per minute such that, in the case of the 'wet' tests, the build-up of excess

Table 9.1 Indices of discontinuity surface geometry

Maximum deviation from a planar surface, (mm)	RI: deviations with wavelength < 50mm	CI: deviations with wavelength > 50mm	Curvature classification based on Fookes and Denness (1969) (for 100mm diam. sample)
> 0 ≤ 3	0	0	Planar $\left(\frac{L}{R} \leq \frac{\pi}{8}\right)$ *
> 3 ≤ 6	1	1	
> 6 ≤ 9	2	2	Semi-curved $\left(\frac{\pi}{4} > \frac{L}{R} > \frac{\pi}{8}\right)$
> 9 ≤ 12	3	3	
>12 ≤ 15	4	4	Curved $\left(\frac{L}{R} \geq \frac{\pi}{4}\right)$
>15 ≤ 18	5	5	

* Note:

L = Length of discontinuity

R = Radius of curvature

pore water pressure was inhibited. For the first 2mm of displacement the shearing force (indicated by hydraulic pressure in the shearing ram) was noted every 0.2mm; after this it was recorded every 0.5mm up to a maximum displacement of 10mm, or until a constant value of shearing force was reached. The normal force was maintained constant throughout the test. The principle of the shear box test is summarised diagrammatically in Figure 9.1.

Following each test, the apparatus was returned to zero displacement and then the test was repeated for values of normal force equal to 4kN, 6kN, 8kN and 10kN (first cycle tests). The whole series of tests was then repeated (second cycle tests) for the same sample, during which maximum shear stress only was recorded. Twenty-four samples were tested, 12 'dry' (moisture content less than 2%) and 12 'wet' (moisture content approximately 18%). Two calcium carbonate determinations were done on each sample. Moisture content and calcium carbonate content values for the samples are listed in Tables 9.2 and 9.3.

9.3 Processing and interpretation of results

The normal stress (σ'_n) acting on each discontinuity surface was calculated by dividing the normal force by the area of the discontinuity sample. Similarly, the shear stress (τ) was calculated by dividing the shearing force by the discontinuity area.

Graphs plotting shear stress (τ, ordinate) versus displacement (abcissa) were then constructed to determine τ_{max} for each of the tests at the various values of normal force. An example of one set of curves typical of those obtained is shown in Figure 9.2. The curves in this Figure show that there is little difference between the peak and

Table 9.2 Shear box test results, dry samples

Sample	A (cm^2)	RI	CI	c'_p (MN/m^2)	ϕ'_p	c'_{ult} (MN/m^2)	ϕ'_{ult}	Mean $CaCO_3$%	Mean moisture content %
BH100 4m	83	1	2	0.07	30^o	0.0	30^o	70.8	< 2
BH100 15m	77	2	2	0.0	35^o	0.0	25^o	47.4	
BH100 17.6m	116	2	1	0.05	42^o	0.0	41^o	46.3	
BH100 29.8m	76	1	4	0.0	27^o	0.0	26^o	64.1	
BH101 4m	65	2	2	0.05	37^o	0.0	33^o	77.5	
BH101 5.5m	60	2	3	0.04	32^o	0.0	30^o	71.0	
BH101 12.8m	104	1	4	0.08	31^o	0.0	33^o	66.0	
BH101 18.2m	87	5	4	0.04	56^o	0.0	47^o	47.2	
BH101 19.2m	53	3	4	0.17	39^o	0.05	36^o	48.5	
BH101 21.5m	70	4	2	0.24	23^o	0.0	30^o	67.3	
BH101 22.6m	96	1	5	0.07	27^o	0.0	27^o	55.9	
BH101 22.8m	88	1	5	0.02	31^o	0.0	29^o	56.7	
Mean c'_p =0.07 MN/m^2 St.Dev.=0.07 MN/m^2 Mean ϕ'_p =34.2^o St.Dev.=8.7^o						Mean c'_{ult} 0.0 MN/m^2 St.Dev.=0.01 MN/m^2 Mean ϕ'_{ult} 32.3^o St.Dev.=6.4^o			

Table 9.3 Shear box test results, wet samples

Sample	A (cm^2)	RI	CI	c'_p (MN/m^2)	ϕ'_p	c'_{ult} (MN/m^2)	ϕ'_{ult}	Mean $CaCO_3$ %	Mean moisture content %
BH100 4.2m	74	1	2	0.0	28^o	0.0	26^o	75.4	13.5
BH100 7.7m	93	2	3	0.03	31^o	0.0	31^o	67.5	18.0
BH101 3.7m	76	2	3	0.01	33^o	0.0	32^o	77.0	14.7
BH101 7.6m	75	1	2	0.05	22^o	0.01	22^o	70.2	17.9
BH101 15m	76	1	1	0.0	28^o	0.0	25^o	61.3	25.0
BH102 6m	68	4	3	0.11	35^o	0.04	37^o	75.5	13.9
BH102 18.8m	103	3	3	0.03	34^o	0.0	34^o	54.4	21.0
BH104 17.9m	77	1	1	0.02	17^o	0.01	15^o	65.5	18.7
BH104 18.2m	75	1	0	0.07	15^o	0.0	15^o	58.2	20.8
BH105 3m	75	2	2	0.09	24^o	0.0	23^o	74.1	16.0
BH105 20.3m	74	2	3	0.08	23^o	0.02	20^o	49.3	19.7
Road cutting sample	74	1	1	0.02	31^o	0.0	31^o	81.8	16.2
Mean c'_p =0.04 MN/m^2 St.Dev.=0.04 MN/m^2 Mean ϕ'_p =26.8^o St.Dev.=6.6^o						Mean c'_{ult} =0.01 MN/m^2 St.Dev.=0.01 MN/m^2 Mean ϕ'_{ult} =25.9^o St.Dev.=7.2^o			

residual strengths. This is often the case with weak rocks and soils (Hoek,1970).

Graphs of τ_{max} (ordinate) versus σ'_n (abcissa) were then constructed for each series of tests, the two series of tests for each sample being plotted on one graph. The resulting graphs are shown in Appendix K, Figures K.1 to K.24. Examination of these Figures reveals that in general for both 'wet' and 'dry' samples there is a linear relation between τ_{max} and σ'_n. The slope of this line gave values of ϕ'_p for the first cycle tests and ϕ'_{ult} for the second cycle tests. τ_{max} at $\sigma'_n = 0$ for the first cycle tests was recorded as c'_p, and τ_{max} at $\sigma'_n = 0$ for the second cycle tests as c'_{ult} (Figure 9.3). The ϕ' and c' values for each of the samples are listed in Tables 9.2 and 9.3. It is clear from the Tables that values of c'_p and c'_{ult} are generally close to zero in all cases. Mean ϕ'_p values are 26.8^o for the wet samples and 34.2^o for the dry samples, whilst mean ϕ'_{ult} values are 25.9^o for the wet samples and 32.3^o for the dry samples. These ϕ' values are somewhat lower than the 35^o to 41^o range quoted by Hoek (1970) for the peak friction angles of discontinuities in chalk. The lower friction angles at Chinnor probably reflect the lower calcium carbonate content of the chalk in this region. This effect is discussed later.

The existence of a straight line relation between τ_{max} and σ'_n in Appendix Figures K.1 to K.24 implies that there cannot be a straight line relation between $\ln(\tau/\sigma_c)$ and $\ln(\sigma_n/\sigma_c)$ for this material. Consequently, the applicability of Equation 9.1 for this material is debatable. This does not, however, invalidate the general conclusions of Boyd (1975) since:

(1) Preliminary tests by Boyd (1975) indicated that the Hoek portable shear box was not sufficiently sensitive for tests on plaster (a material

of comparable strength to chalk). The tests described in this Chapter, therefore, do not allow a precise evaluation of the applicability of Equation 9.1 to the softer, weaker rocks such as chalk.

(2) The development of a putty chalk smear on the discontinuity surfaces may have modified the mode of shear failure, producing the straight line relation between τ and σ'_n instead of the curve predicted by Equation 9.1.

The wide spread of ϕ' values for the discontinuity surfaces tested (Tables 9.2 and 9.3) indicates that surface geometry critically influences the shear strength characteristics.

Figure 9.4 showing graphs plotting DI against ϕ'_p and ϕ'_{ult}, indicates that there is a general trend for ϕ'_p and ϕ'_{ult} to increase with DI (ie increased roughness) such that these friction angles increase by approximately 3^o when DI increases by 1. This effect is particularly noticeable for the 'wet' tests, which may be partly attributed to the fact that the lubricated wet discontinuities rely mainly on large scale (wavelength and amplitude > 5mm) deviations from planar geometry for mobilsation of shear strength. The increased friction angles for the 'rougher' discontinuity surfaces reflects the fact that at all but the very lowest values of σ'_n shearing along the discontinuity surfaces involves shearing through intact elements of chalk. For the rougher discontinuity surfaces, shearing through intact elements may represent a major part of the shearing mechanism.

Examination of Tables 9.2 and 9.3 which summarise the results of the shear box tests indicates that, in general, there is little difference between ϕ'_p and ϕ'_{ult}, even though for all tests ϕ'_{ult} was determined

from samples having experienced shear displacements in excess of 50mm. This tendency for little or no fall-off from peak shear strengths can also be seen in Figure 9.2 (discussed on page 274) and may be attributed to the fact that the Lower Chalk falls in the weaker range of rocks.

ϕ'_p and ϕ'_{ult} values obtained from 'wet' tests are 20 - 25% lower than values obtained from 'dry' tests. This is largely due to the development of a lubricating wet putty chalk smear between the discontinuity surfaces during shearing in the wet tests. As mentioned earlier for all tests c'_p and c'_{ult} are small, and in most cases $c'_{ult} = 0$; this reflects the fact that there was no significant fill or binding agent between the discontinuity surfaces prior to testing.

Figure 9.5 summarises the relation between ϕ'_p, ϕ'_{ult}, calcium carbonate content and moisture content. In general there is no significant relation between ϕ'_p, ϕ'_{ult} and calcium carbonate content. However, the 'wet' sample results show a tendency towards increasing ϕ'_p and ϕ'_{ult} with increasing calcium carbonate content. This may be partly due to the lower silica* content at higher calcium carbonate percentages inhibiting the development of a lubricating putty chalk smear. Figures 9.5(e) and (f) reveal a slight tendency for ϕ'_p and ϕ'_{ult} to decrease with increasing moisture content. This tends to confirm the results of the comparative tests between 'wet' and 'dry' samples, where the reducing ϕ'_p and ϕ'_{ult} values may be explained by the development of a lubricating wet clay smear.

9.4 Summary and conclusions

(1) The shear strength characteristics of twenty-four discontinuity surfaces sampled in the Lower Chalk were tested using the Hoek field shear

---

* This silica (of clay size) is composed mainly of the mineral lussatite which behaves in many respects as a soft clay (Chapter 3).

box. Half of the samples were tested in a dry state and half at a moisture content of approximately 18%. An arbitrary numerical index was used to describe the geometry of the discontinuity surfaces.

(2) For all samples tested there was found to be an approximately linear relation between maximum shear strength and normal stress. Values of cohesion were found to be near to zero in all cases. Mean ϕ'_p values were 26.8^0 for the wet samples and 34.2^0 for the dry samples, whilst mean ϕ'_{ult} values were 25.9^0 for the wet samples and 32.3^0 for the dry samples.

(3) ϕ' was found to decrease with increasing moisture content, an effect largely caused by the development of a lubricating putty chalk smear during shearing.

(4) For all samples ϕ' was found to increase with increasing roughness as represented by the arbitrary roughness index. This critical influence of discontinuity roughness on the shear strength is widely acknowledged in the literature.

(5) It is concluded that for stability analyses the peak shear strength characteristics obtained from wet tests are the most applicable, the average values from twelve tests being $c'_p = 0.04\ MN/m^2$, $\phi'_p = 26.8^0$.

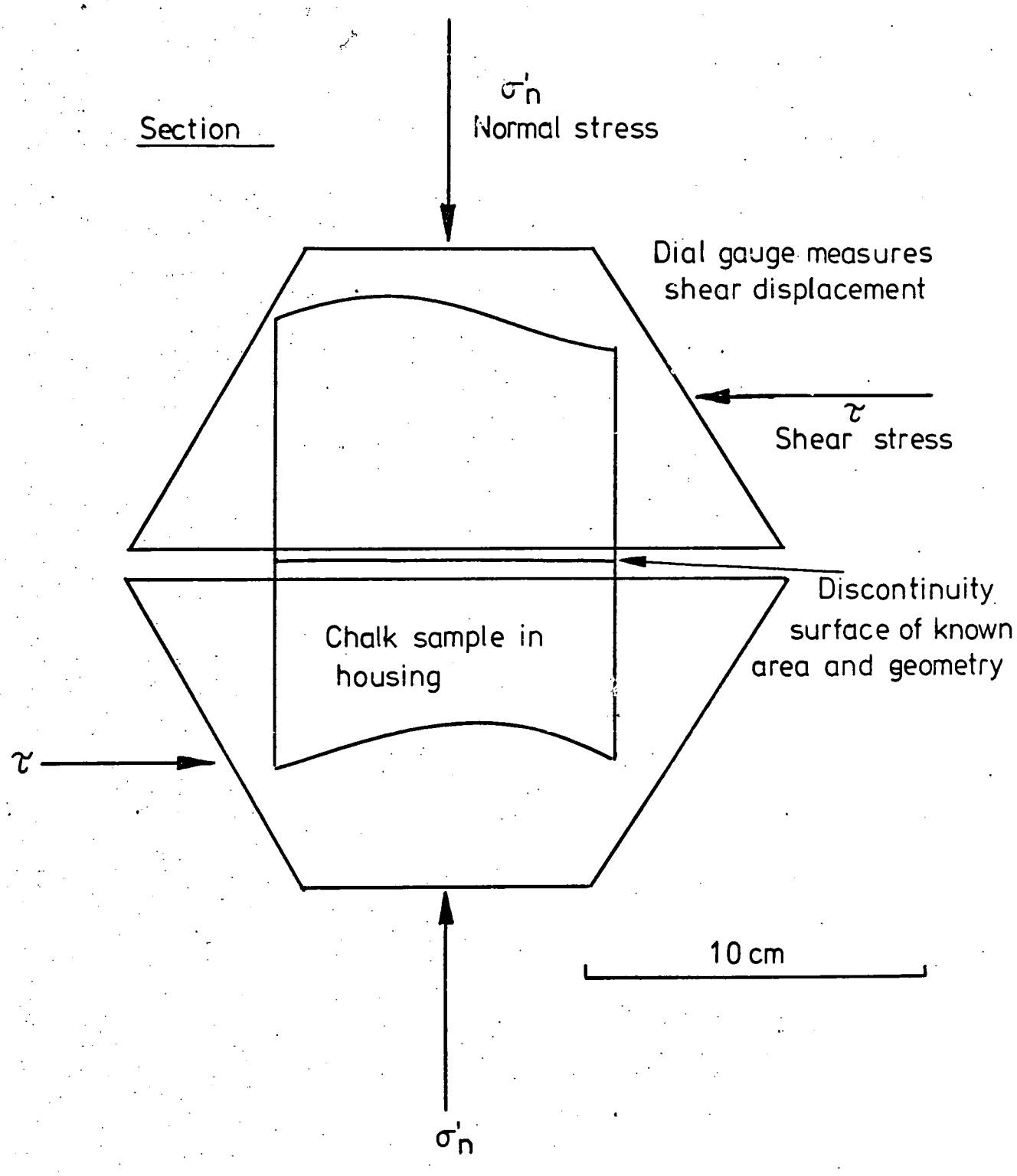

Fig. 9.1 PRINCIPLE OF THE SHEAR BOX TEST USED TO EVALUATE THE SHEAR STRENGTH OF DISCONTINUITY SURFACES.

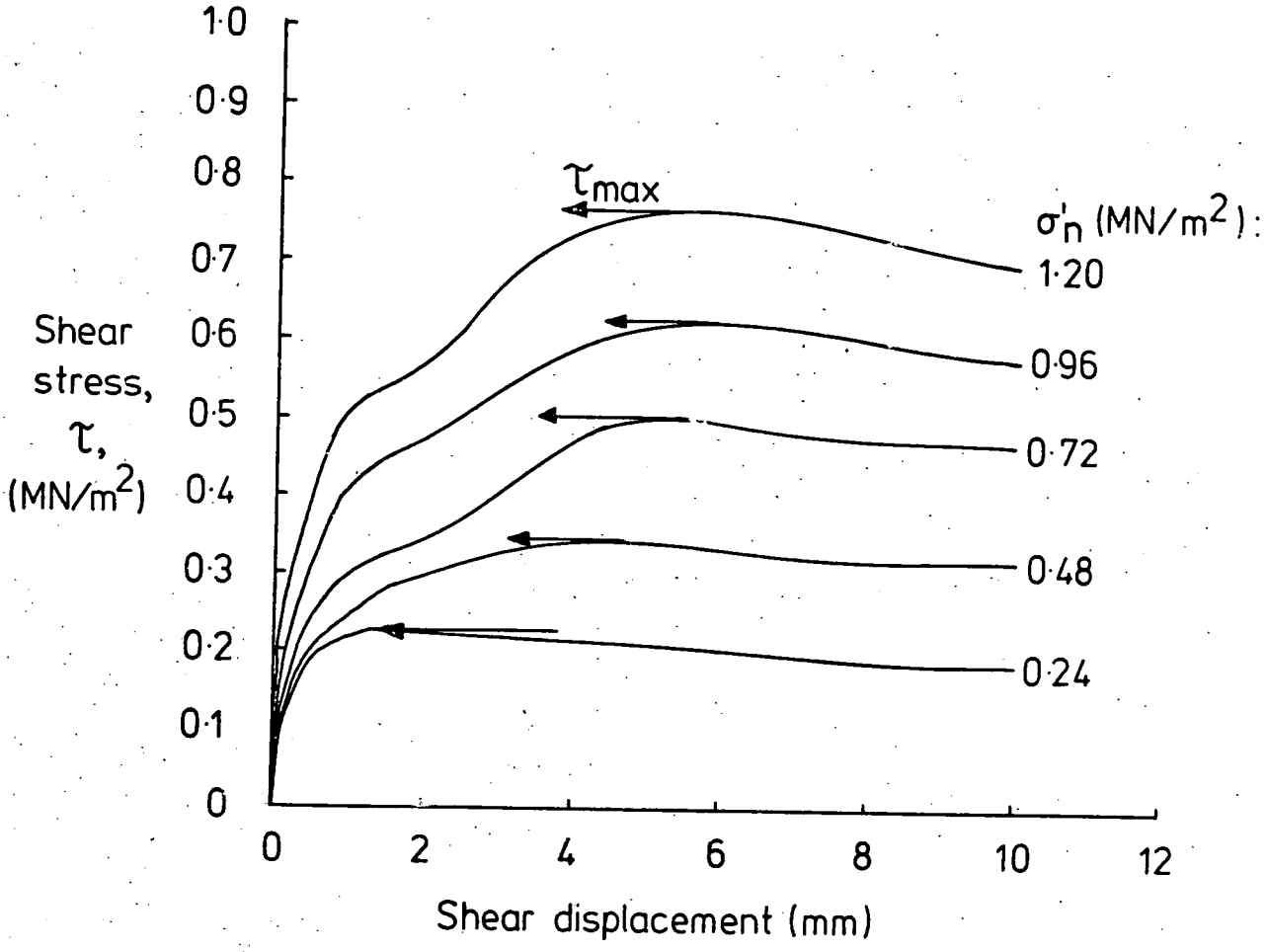

Fig. 9.2 SHEAR BOX TEST, TYPICAL SHEAR STRESS-DISPLACEMENT CURVES, FIRST CYCLE TESTS, SAMPLE: BOREHOLE 100 DEPTH 4m .

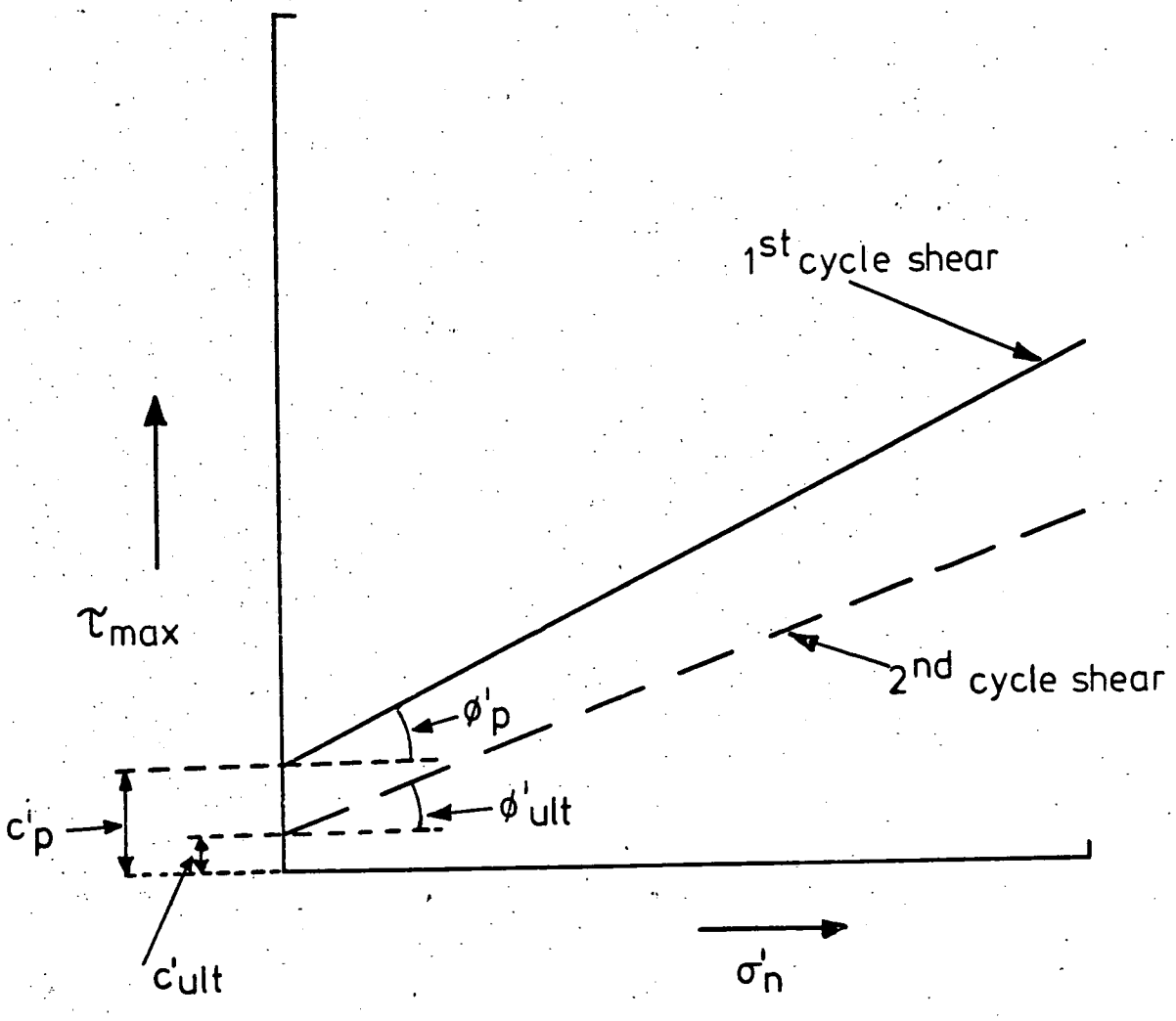

Fig. 9.3 SHEAR STRENGTH PARAMETERS DERIVED FROM SHEAR BOX TESTS ON DISCONTINUITIES.

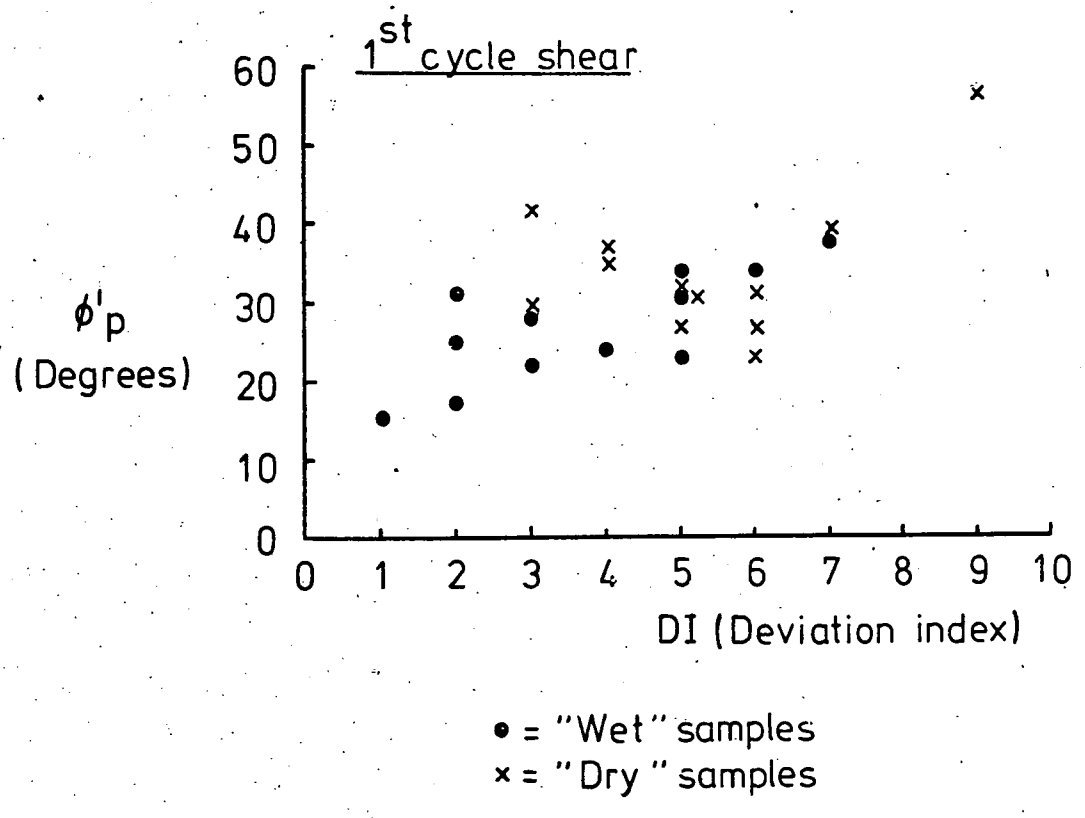

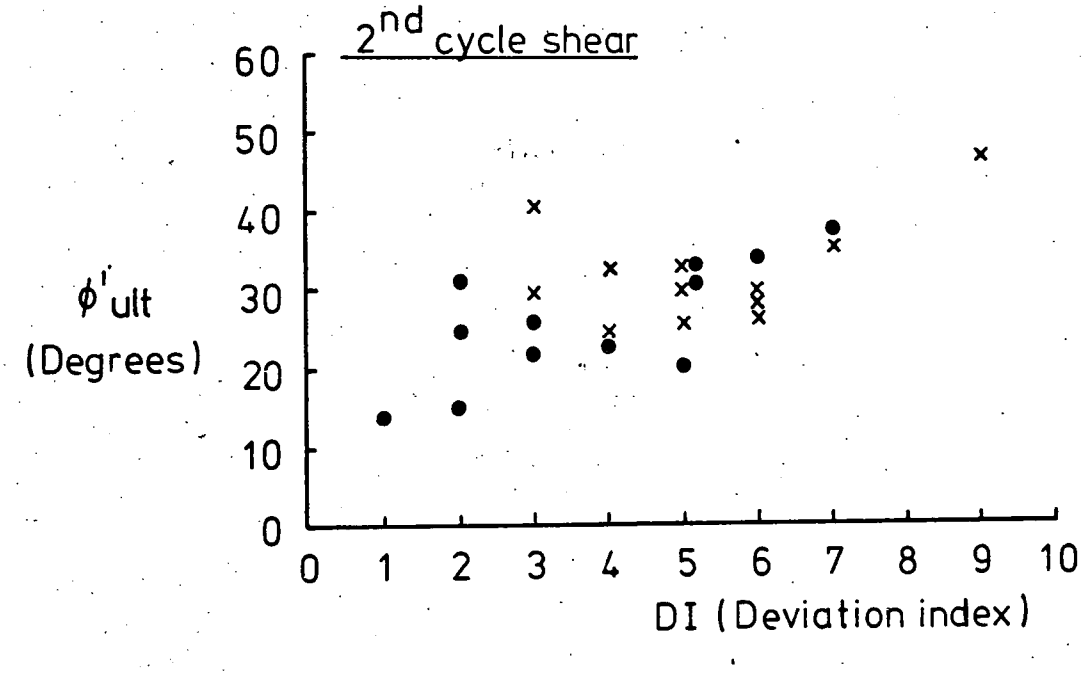

Fig. 9.4 CORRELATION BETWEEN DEVIATION INDEX (DI) ϕ'_p AND ϕ'_{ult} FOR DISCONTINUITY SURFACES.

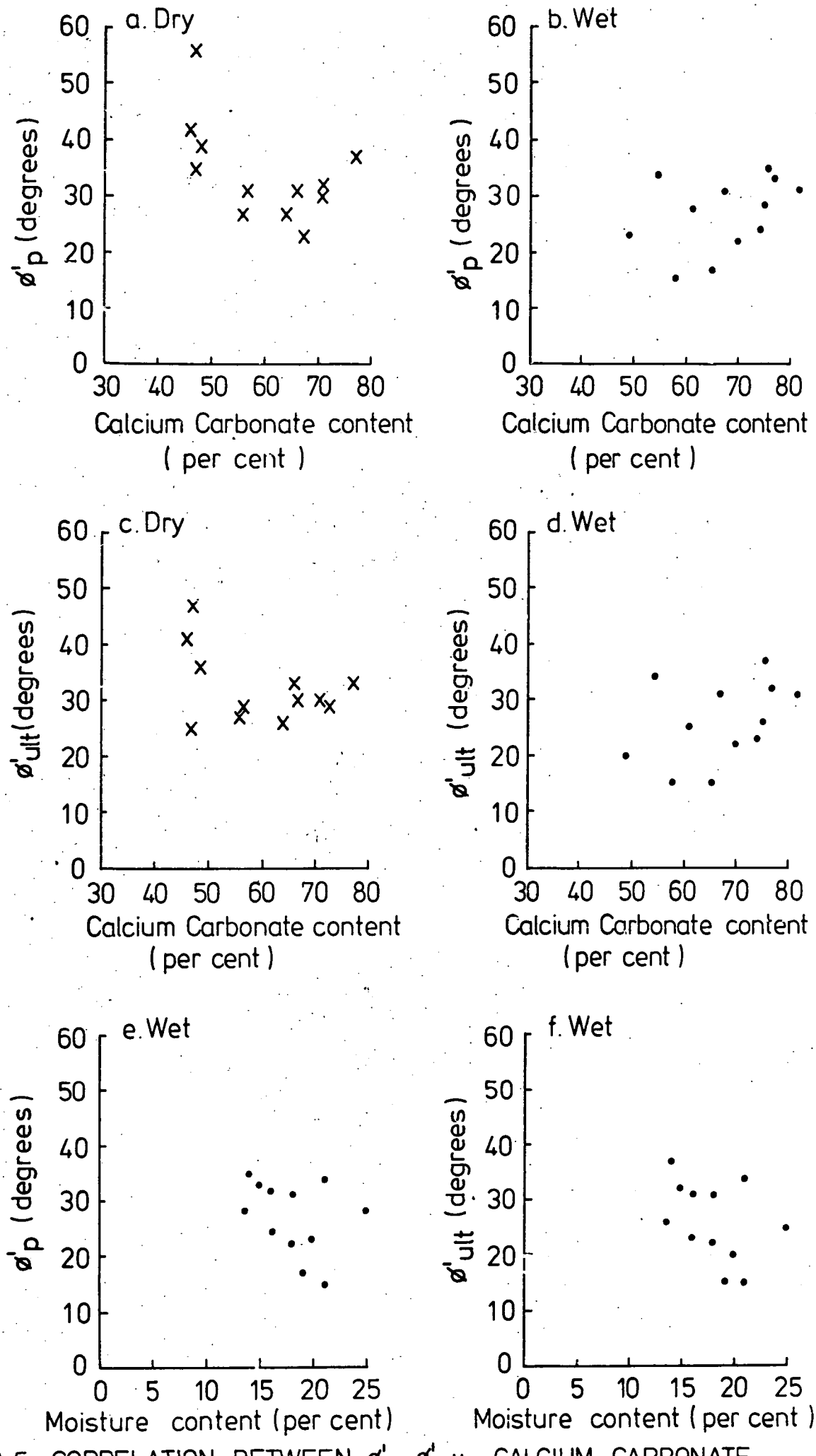

Fig. 9.5 CORRELATION BETWEEN ϕ'_p, ϕ'_{ult}, CALCIUM CARBONATE CONTENT AND MOISTURE CONTENT FOR DISCONTINUITIES.

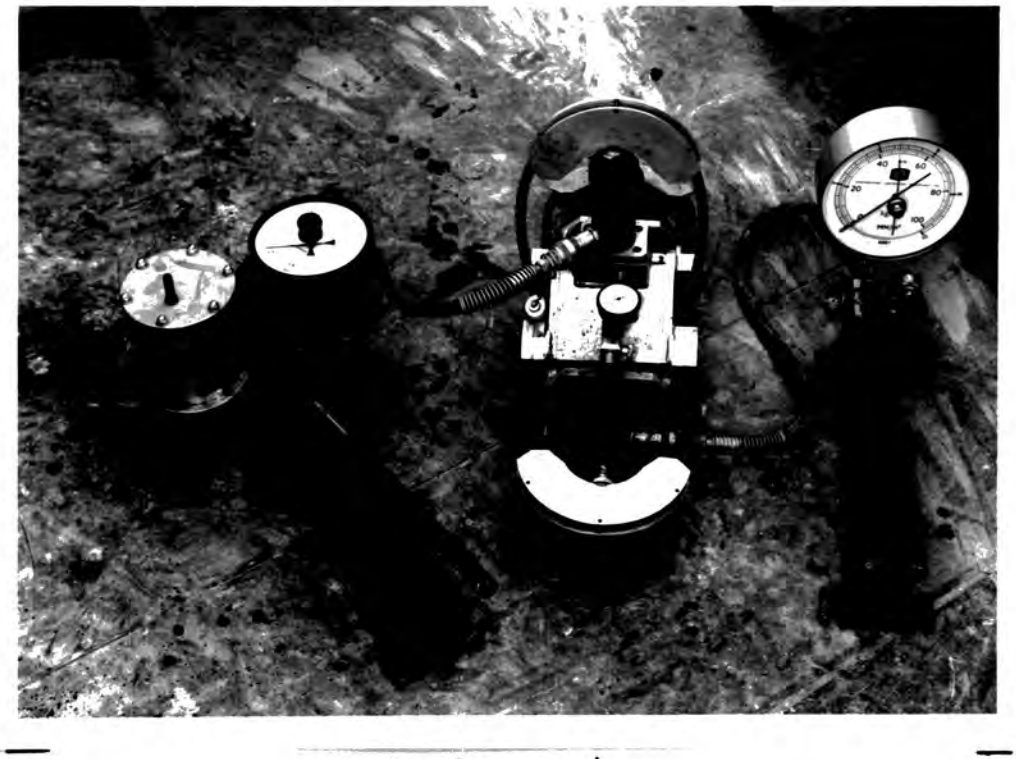

Plate 9.1 THE HOEK PORTABLE SHEAR BOX

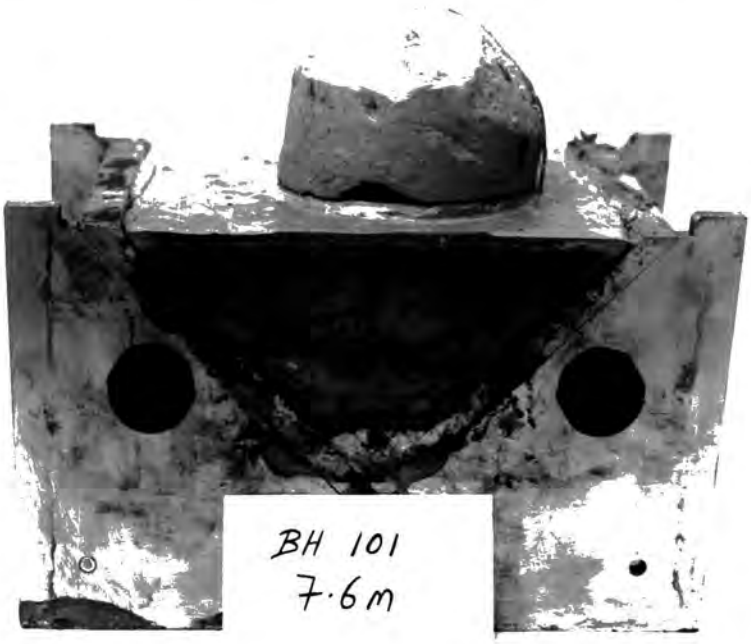

0·2m (approx.)

Plate 9.2 SAMPLE PRIOR TO TESTING AWAITING THE SECOND HALF OF THE SAMPLE HOUSING.

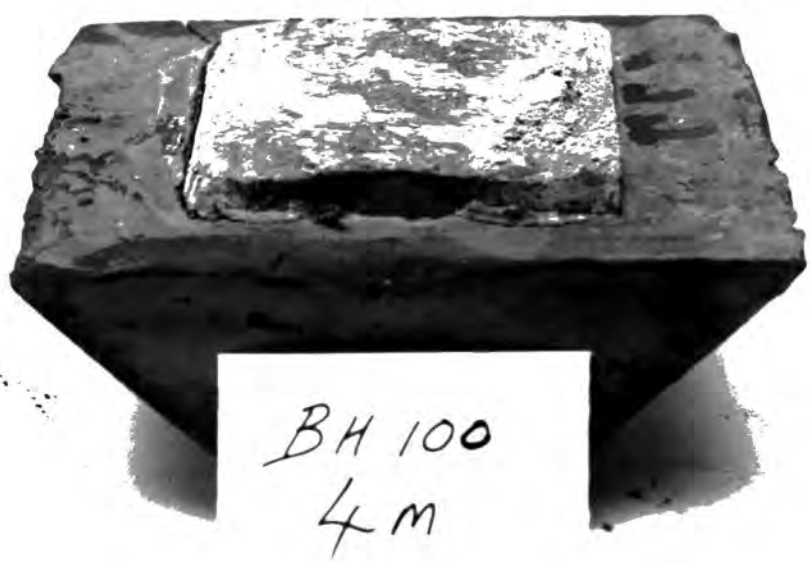

0·2m (approx.)

Plate 9.3 DISCONTINUITY SURFACE AFTER TESTING.

CHAPTER 10

AN ANALYSIS OF THE STABILITY OF THE GROUND NEAR THE CHINNOR TUNNEL USING EXPERIMENTAL AND THEORETICAL DATA

10.1 Introduction

In this Chapter, experimental data and theoretical data are combined in an analysis of ground stability near the Chinnor tunnel, using a computer program on file at the University of Durham (Attewell and Woodman; 1971). Using this program, discontinuity orientation zones of potential instability based on a Coulomb-Navier-Mohr criterion of failure are delimited on equal area projections. Additional processing yields indices of discontinuity stability based on a shear strain energy criterion.

The data required for the analysis fall under three headings:

(1) Discontinuity orientation density distribution fabrics obtained from measurements taken at the tunnel face and summarised in Figure 10.1.

(2) Theoretical stress magnitudes near the Chinnor tunnel calculated using the finite element analysis techniques described in Chapter 8 and Appendix J.

(3) Shear strength characteristics of discontinuity surfaces in the Lower Chalk at Chinnor determined using a shear box and described in Chapter 9.

10.2 Summary of computing technique

The data described in Section 10.1 were fed into the computer program, written by Attewell and Woodman (1971). A part of the computing facility

of this program was used in Chapters 2, 3 and 5 for plotting and contouring discontinuity orientation data. This part of the program is described in Appendix C. An additional facility of the program caters for the incorporation of stress configurations and discontinuity shear strength characteristics to allow the computation of stability within the discontinuum. The theoretical basis for this part of the program is outlined below:

It is assumed that shear movement takes place along a discontinuity, leading to localised sliding and general instability, when the shear stress along it exceeds a limiting value $|\tau|$ given by the following well-known equation.

$$|\tau| = \sigma'_n \tan \phi' + c'$$

where ϕ' and c' are the effective shear strength parameters of the discontinuity and σ'_n is the resolved effective stress acting normal to the discontinuity. For ground below the water table $\sigma'_n = (\sigma_n - u)$ where σ_n is the total normal stress and u is the water pressure. For essentially dry ground above the water table $\sigma'_n = \sigma_n$.

The principal stresses, $\sigma_1 > \sigma_2 > \sigma_3$ acting in the discontinuum are referred to orthogonal axes x, y, z. The direction cosines of the normals to the discontinuities, related to these axes are taken as l, m, n. It is then possible to calculate σ'_n and τ for every element on the projection using the following standard Equations:

$$\sigma'_n = \sigma_n = l^2\sigma_1 + m^2\sigma_2 + n^2\sigma_3 \quad \text{(when } u = 0\text{)}$$

$$\tau^2 = l^2\sigma_1^2 + m^2\sigma_2^2 + n^2\sigma_3^2 - \sigma_n^2$$

The locus of $|\tau| = \sigma'_n \tan \phi' + c'$ is printed on the equal area projection to indicate orientation zones of potential instability. The degree to which orientation zones of potential instability coincide with measured concentrations of discontinuity orientation reflects the stability of the rock mass under consideration. An indication of total mass stability can be obtained using the strain energy failure criterion described fully in Attewell and Woodman (1971) and outlined briefly below:

For a cohesionless discontinuity surface sliding will take place when

$$|\tau| - \sigma'_n \tan \phi' > 0$$

$(|\tau| - \sigma'_n \tan \phi')$ is defined as the shear stress (τ') available for the promotion of sliding. When $\tau' > 0$ for a particular discontinuity surface the consequent sliding induces a corresponding shear strain energy. The total shear strain energy for all zones of potential instability can be calculated by integrating over the appropriate areas of the projection. This shear strain energy along discontinuity surfaces is essentially the energy that would have been stored as deformation of the intact rock had the material been a continuum. However, since the mass is discontinuous considerations of energy stored as a result of deformation of intact rock (Jaeger and Cook, 1969, page 116) are inapplicable. The findings of Chapter 7 concerning ground movement near the Chinnor tunnel confirm this conclusion since the greatest proportion of ground deformation was found to develop along discontinuity surfaces.

The total shear strain energy for the measured (anisotropic) discontinuity orientation density distribution is represented by an index "A". The hypothetical total shear strain energy for an isotropic discontinuity

orientation density distribution is also calculated and represented by the index "I". When A > 0, there is shear movement potential along one or more discontinuities. "I" is an arbitrary datum factor which permits the comparison of A/I or I/A for different fabrics. Thus A/I is a 'danger' index in that the greater it is, the higher the possibility of shear failure. Conversely I/A is a 'safety' index, such that when I/A exceeds unity it may be assumed that the measured orientation distribution tends to favour stability under the given stress conditions.

10.3 Summary of input data

A single discontinuity orientation density distribution fabric was used in the analysis. The fabric used, previously presented in Figure 10.1, represents 1082 aggregated discontinuity orientation measurements taken at freshly exposed faces during the first 85m of tunnelling at Chinnor. It was felt, therefore, that this fabric would give a reasonably good representation of the actual inherited discontinuity orientation patterns near the tunnel. It is important to reiterate that discontinuity azimuth directions were taken relative to the tunnel axis direction, the latter representing the 'north-south' line on the equal area projection.

Stress magnitudes near the Chinnor tunnel were calculated using finite element analysis techniques described in Chapter 8 and Appendix J. Stress magnitudes from two analyses were used: the first adopting a K_o factor of 0.4 and a J_a factor (modulus reduction factor) of 1.0, and the second adopting a K_o factor of 0.4 and a J_a factor of 0.07. Principal stress magnitudes at the centroids of six elements at selected positions near the tunnel were extracted from the computer output. The locations of the centroids of the elements selected are shown in Figure 10.2. The finite element analysis, being two-dimensional, gave the magnitudes and directions

of the major and minor principal stresses in the plane normal to the tunnel axis only. The magnitude of the intermediate principal stress, acting parallel to the tunnel axis, was estimated from the following plane strain relation:

$$\sigma_2 = \nu (\sigma_1 + \sigma_3)$$

where ν (Poisson's ratio) was assumed to be 0.5. The use of a Poisson's ratio of 0.5 is a reasonable approximation in the light of the discontinuous character of the material, for which Poisson's ratio values of 0.3 were appropriate when dealing with intact samples in the laboratory. Work in Chapters 7 and 8 has proved that the discontinuous chalk did not behave in a strictly elastic manner, therefore the term "Poisson's ratio", though convenient, should strictly be replaced by the term "deformation ratio".

The finite element analysis only considered the right-hand half, that is the east side of the symmetrical tunnelling situation. Therefore in order to assess the behaviour of the three dimensional discontinuum, which contained an asymmetrical discontinuity orientation fabric, it was necessary to consider stress magnitudes and directions in both the right and left halves of the plane section normal to the tunnel axis. It was not necessary to repeat the finite element analysis to obtain these data for the left half (ie west side) of the system, since it was simply a matter of producing a mirror image of the stress patterns for the right half. This was done by interchanging the azimuthal directions of σ_1 and σ_3, that is adding 180^0 to each, leaving the stress magnitudes unchanged.

The magnitudes of σ_1, σ_2 and σ_3 at the six points selected, for J_a factors of 1.0 and 0.07, are listed for the right-hand side of the system in Table 10.1. In addition, Table 10.1 contains data concerning the

Table 10.1 Summary of input data for computation of the stability of the discontinuous rock mass near the Chinnor tunnel. Data for right-hand side

Note:
*- These columns are interchanged to give data for the left-hand side

Element	σ_1 MN/m^2	σ_2 MN/m^2	σ_3 MN/m^2	σ_2/σ_1	σ_3/σ_1	c'/σ_1	$\alpha(\sigma_1)$ Degrees	$\beta(\sigma_1)$ Degrees *	$\alpha(\sigma_3)$ Degrees	$\beta(\sigma_3)$ Degrees *	Tan ϕ'
33	0.1347	0.1030	0.0714	0.7649	0.5298	0.2968	71	270	19	90	
41	0.3851	0.2187	0.0523	0.5679	0.1357	0.1039	21	270	69	90	
49	0.5049	0.3344	0.1640	0.6625	0.3250	0.0792	0	270	90	90	0.5051
92	0.2288	0.1943	0.1598	0.8491	0.6982	0.1748	30	270	60	90	
97	0.3461	0.2255	0.1049	0.6516	0.3032	0.1156	13	270	77	90	
101	0.4457	0.3104	0.1752	0.6965	0.3930	0.0897	2	270	88	90	
33	0.1575	0.1187	0.0799	0.7535	0.5071	0.2540	73	270	17	90	
41	0.3877	0.2208	0.0540	0.5695	0.1393	0.1032	21	270	69	90	
49	0.5069	0.3369	0.1669	0.6647	0.3294	0.0789	1	270	89	90	0.5051
92	0.2284	0.1949	0.1615	0.8536	0.7072	0.1751	28	270	62	90	
97	0.3442	0.2229	0.1017	0.6477	0.2954	0.1162	13	270	77	90	
101	0.4457	0.3110	0.1763	0.6978	0.3956	0.0897	3	270	87	90	

orientation of σ_1 and σ_3 expressed as tilt from the vertical (α) and azimuth, that is, the angle (β) between this tilt direction and the tunnel axis direction. In order to facilitate computation, each of the stress magnitudes is re-expressed as a fraction of σ_1 in Table 10.1.

Shear strength parameters for the discontinuity surfaces at Chinnor were determined using methods described in Chapter 9. The strength parameters selected for use in this analysis are those representing peak strength along 'wet' discontinuity surfaces. It was felt that these conditions reflected as nearly as possible those obtaining in the rock mass near the tunnel at Chinnor. The shear strength parameters selected represent the mean of twelve separate tests giving $c'_p = 0.04$ MN/m^2, $\phi'_p = 26.8^o$. In order to facilitate computation c', (ie c'_p) was expressed as a fraction of σ_1 and ϕ' (ie ϕ'_p) as tan ϕ' in Table 10.1.

Using the data tabulated in Table 10.1 and the discontinuity orientation fabric mentioned earlier a series of computer analyses was undertaken using the program on file at the University of Durham. Analyses for six separate points, at two J_a factors, for the left and right halves were completed. This gave a total of 24 analyses.

10.4 Discussion of results

Examination of the output for the 24 analyses proved that orientation zones of potential instability were only developed in the four analyses pertaining to element 41, approximately 1m into the rock from the left and right tunnel shoulders. These four equal area projections are shown in Figures 10.3 to 10.6. On these projections σ_1, σ_2 and σ_3 are denoted by P, Q and R respectively. The tunnel centre line direction is also denoted on each Figure.

The orientation zones of potential instability in Figures 10.3 to 10.6 are located by taking those orientation zones, demarcated by the loci of crosses, that do not contain a principal stress axis. It is clear that at element 41 on the right-hand (east) side of the tunnel (for both J_a factors) potential instability is developed on discontinuities dipping at approximately 45^0 to the right or approximately 80^0 to the left. On the left-hand side of the tunnel, potential instability is developed on discontinuities dipping at approximately 45^0 to the left or approximately 80^0 to the right. In other words the mirror imaged stress configurations produced mirror imaged orientation zones of instability. These results agree with the findings of Cording and Mahar (1974) who found that discontinuities having a strike* direction within 25^0 of the tunnel centre line direction caused greatest stability problems.

The principal stress values listed in Table 10.1 indicate that variation of the J_a factor has little effect on the magnitude of stress at any given point near the tunnel. This effect, discussed earlier in Chapter 8, explains the close similarity between Figures 10.3 and 10.5, and Figures 10.4 and 10.6. Values of I/A obtained from analyses relating to Figures 10.3 to 10.6 are tabulated below.

Table 10.2 I/A values near the Chinnor tunnel

		Element 41	
		Left	Right
J_a = 1.0	I/A	1.9984	2.7674
J_a = 0.07	I/A	2.0116	2.7795

The values of I/A in this Table show that the discontinuity orientation density distribution measured in the Chinnor tunnel in general favours

---

* The horizontal direction at 90^0 to the direction of maximum dip.

stability with respect to sliding along discontinuity surfaces. This is because the orientation zones of potential instability do not in general coincide with concentrations of measured discontinuity orientation. The left-hand side of the tunnel, however, is less favourable for stability than the right (ie has a lower I/A index) since the zone of potential instability dipping at 45^{o} to the left in Figures 10.3 and 10.5 cuts the lower part of a concentration of discontinuity orientation. This does not occur on the right side of the tunnel. Inspection of the tunnel during periods of face indexing indicated that in many cases more severe instability was experienced on the left (west) side of the tunnel than on the right side. In fact ground movement results presented in Chapter 7 show that significantly larger ground settlement was observed in borehole P3 on the left side of the tunnel, than in borehole P1 on the right.

The lack of any apparent instability at elements 33, 49, 92, 97 and 101 suggests that at these points the stresses resulting from tunnel excavation were not sufficient to induce sliding along discontinuities. The conclusions of Chapter 7, however, indicate that considerable deformation of the discontinuum resulted from tunnel excavation. This discrepancy could have resulted from one of the following:

(1) The input data for the analyses in this Chapter may not have been representative of true ground conditions.

(2) The actual mode of deformation of the rock mass, in particular movement along discontinuities, may not have corresponded with the assumptions inherent in the analyses presented in this Chapter.

This latter point can be considered in the light of the conclusions presented in Chapter 8. The loosening of the rock mass, induced by tunnel

excavation and reaction ring jacking, may well have reduced the normal stresses acting across discontinuities and thereby facilitated sliding and dislocation within the discontinuum. This effect is not allowed for in the analyses presented here since at all times the discontinuum is regarded as remaining 'tight'. Tensile normal stresses acting across discontinuities, which near to the tunnel led to overbreak and instability at the crown, are not regarded in the analysis as contributing to instability since only a shear mode of failure is catered for.

10.5 Summary and conclusions

1. Experimental data and theoretical data were combined in an analysis of ground stability at six locations near the Chinnor tunnel.

2. Orientation zones of potential instability were developed under the stress configurations at only two points, approximately 1m into the rock from the left and right tunnel shoulders.

3. Potential instability near the right shoulder was developed on discontinuities dipping at approximately 45^{o} to the right or approximately 80^{o} to the left. The stress configurations on the left side of the tunnel, being a mirror image of those on the right, produced mirror-imaged orientation zones of instability.

4. In general, the discontinuity orientation density distribution measured in the Chinnor tunnel was found to favour stability with respect to sliding along discontinuity surfaces. The left-hand side of the tunnel, however, was found to be less favourable for stability than the right. Ground movement measurements and inspection of the tunnel indicated that the left side of the tunnel was in many cases more prone to instability

than the right.

5. The discrepancies between predicted instability and measured instability suggest that the actual mode of deformation of the rock mass, in particular movement along discontinuities, may not have corresponded with the assumptions inherent in the analyses presented in this Chapter.

6. It is concluded that the analyses presented here, whilst giving a picture of instability in terms of discontinuity orientation trends cannot be relied on to give detailed information concerning the behaviour of the ground. This is because loosening effects caused by the tunnelling operations, not accommodated for in the analyses, can significantly reduce the compressive normal stress acting across discontinuities and thereby reduce the stability of the discontinuum. In addition, tensile normal stresses acting across discontinuities, which near the tunnel led to overbreak and instability at the crown and consequent general loosening of the rock mass, are not regarded in the analyses as contributing to instability since only a shear mode of failure is catered for.

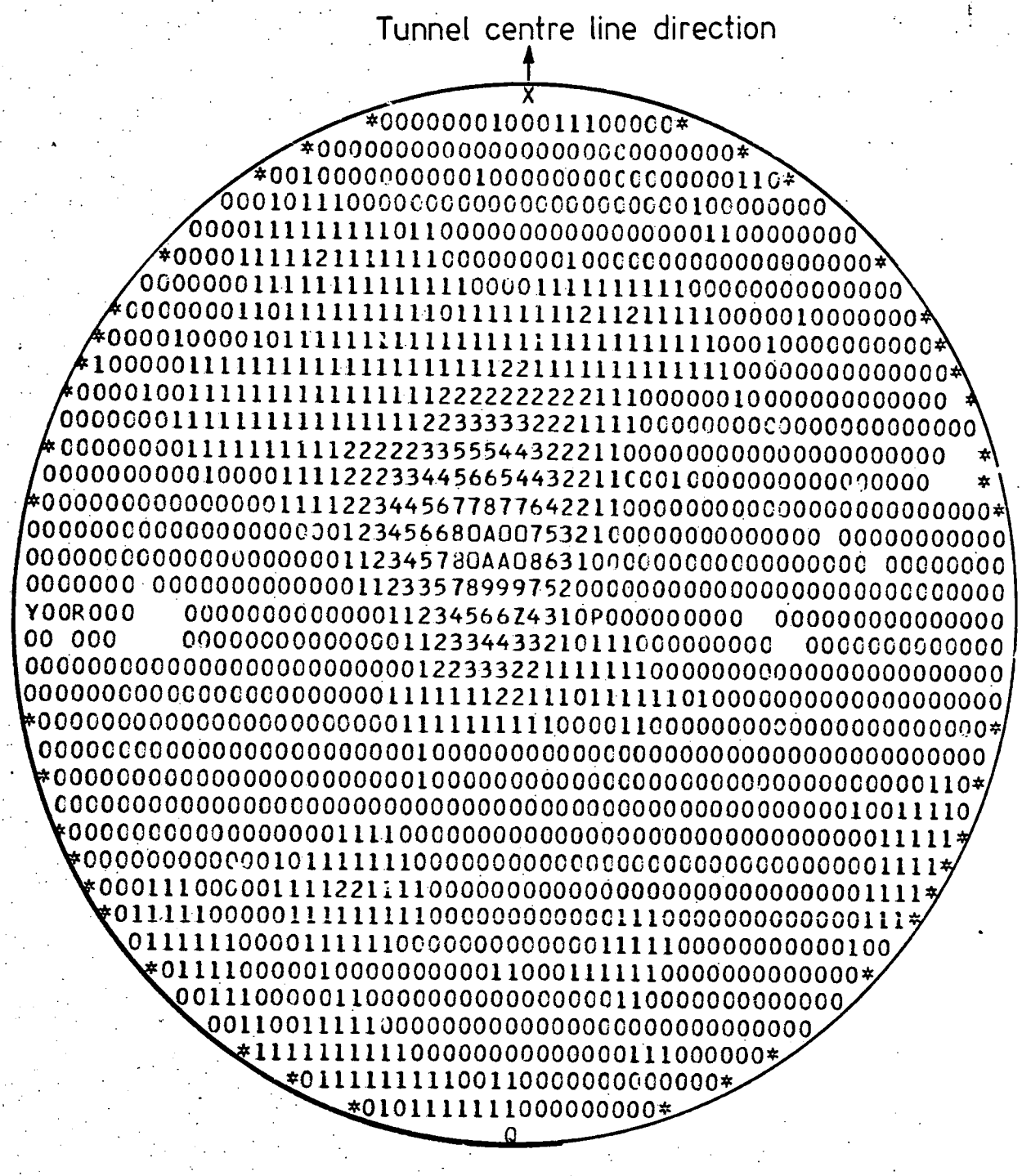

1082 readings

Fig.10.1 UPPER HEMISPHERE PROJECTION OF DISCONTINUITY ORIENTATION, ALL SCANLINES IN THE FIRST 85m OF TUNNEL.

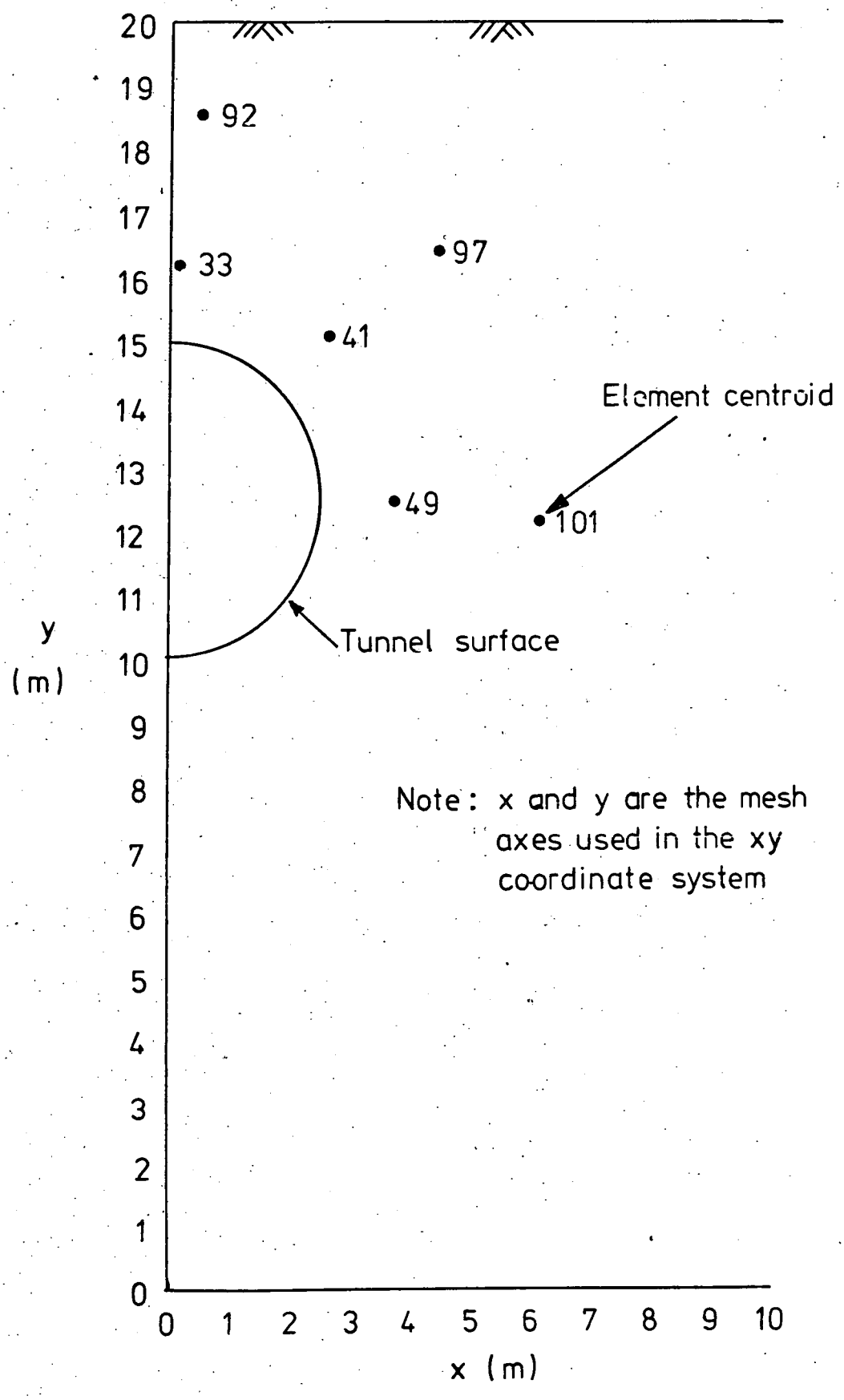

Fig. 10.2 LOCATIONS OF ELEMENT CENTROIDS USED IN THE TUNNEL STABILITY ANALYSIS.

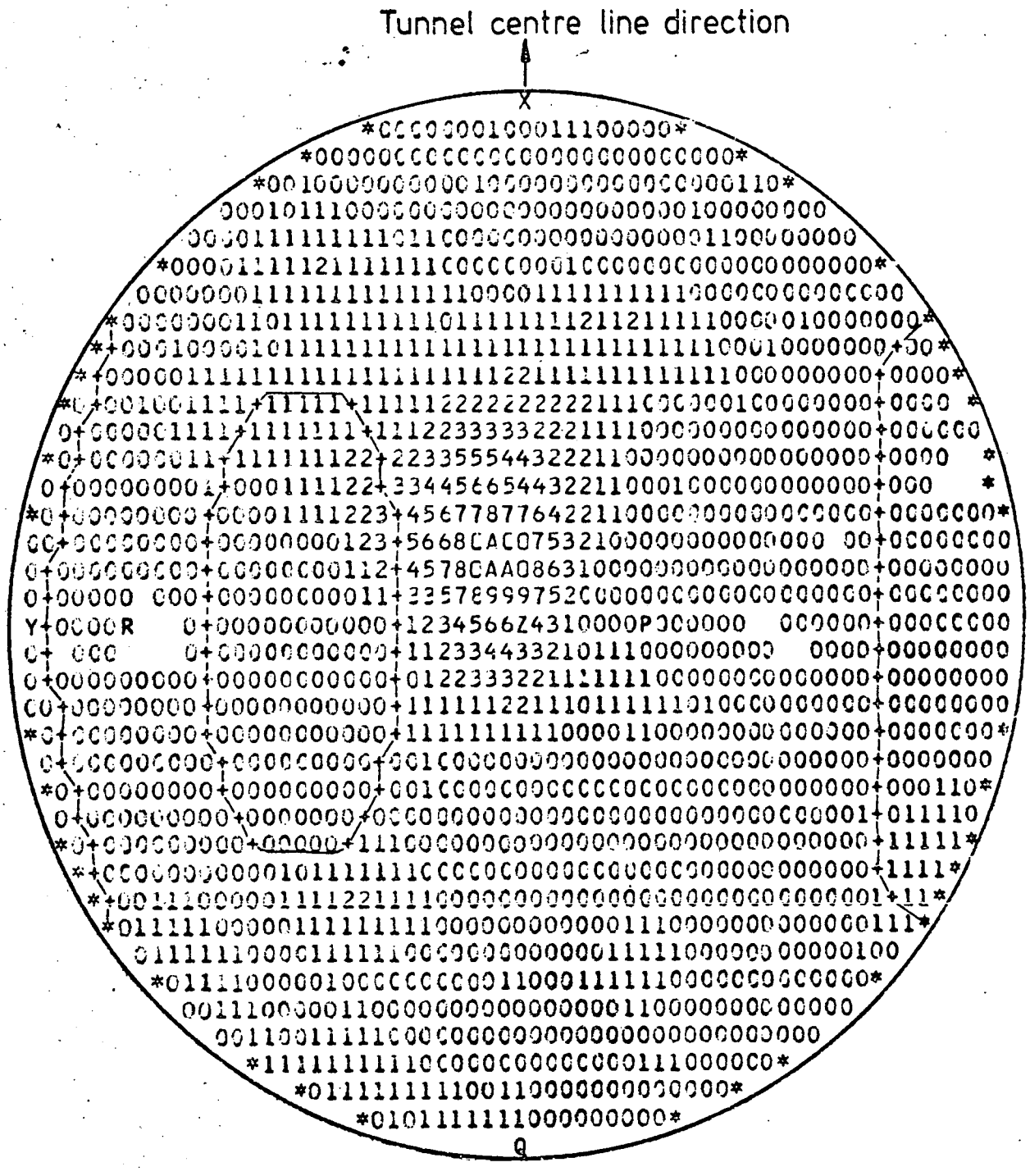

Fig. 10.3 UPPER HEMISPHERE PROJECTION OF ORIENTATION ZONES OF POTENTIALLY UNSTABLE DISCONTINUITIES, ELEMENT 41, LEFT, $J_a = 1{\cdot}0$.

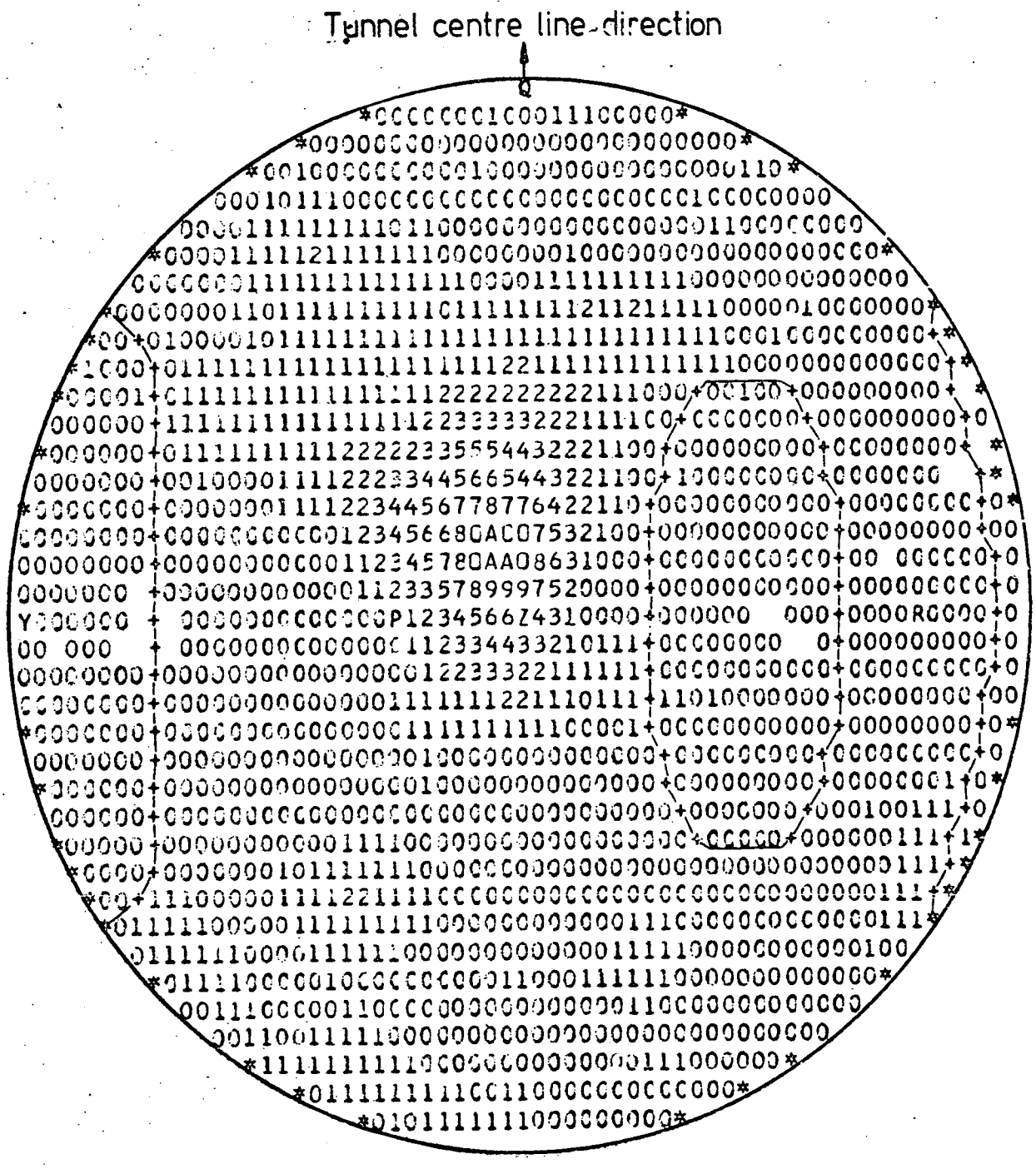

Fig. 10.4 UPPER HEMISPHERE PROJECTION OF ORIENTATION ZONES OF POTENTIALLY UNSTABLE DISCONTINUITIES, ELEMENT 41, RIGHT, $J_a = 1{\cdot}0$.

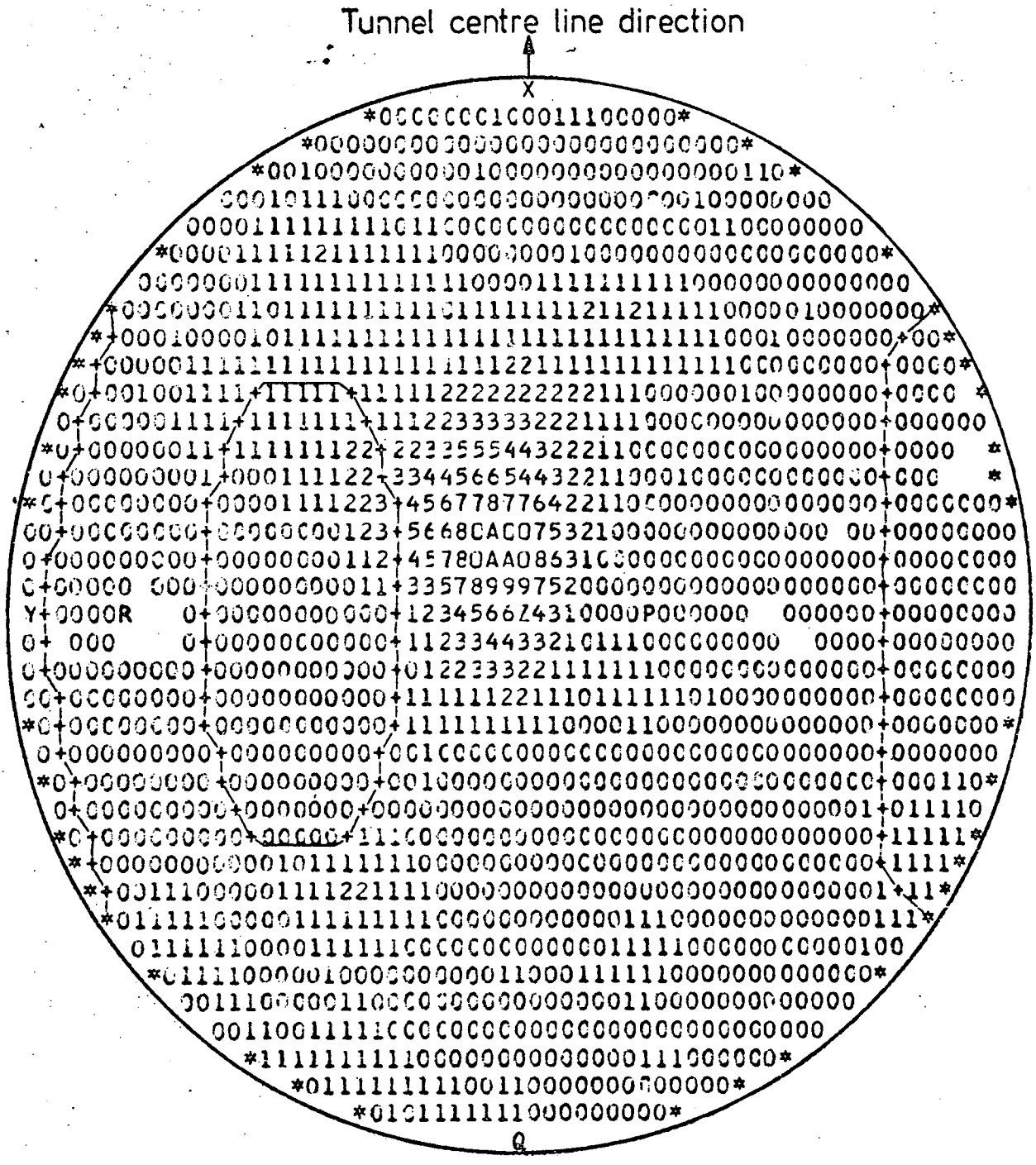

Fig. 10.5 UPPER HEMISPHERE PROJECTION OF ORIENTATION ZONES OF POTENTIALLY UNSTABLE DISCONTINUITIES, ELEMENT 41, LEFT, $J_a = 0{\cdot}07$.

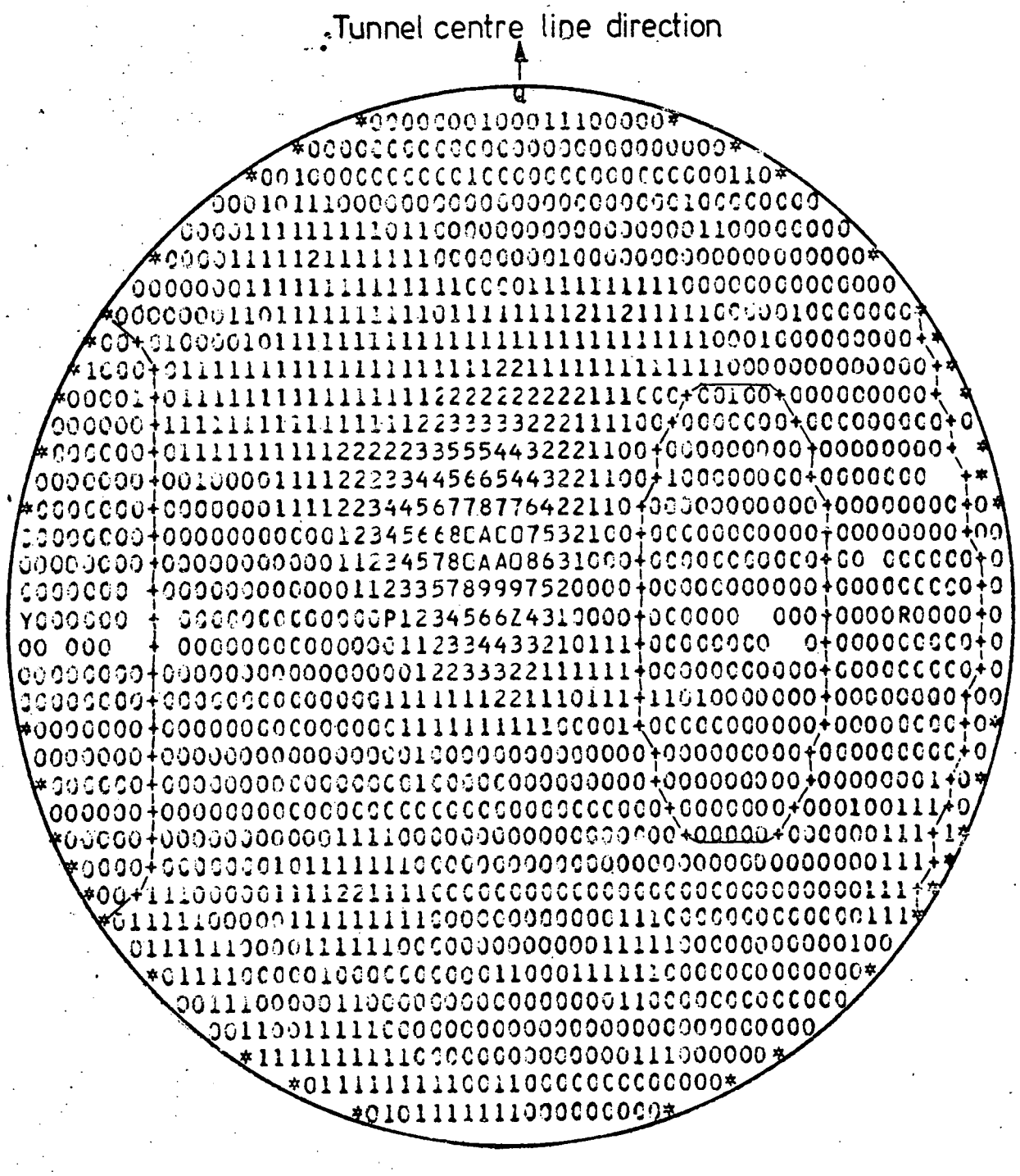

Fig. 10.6 UPPER HEMISPHERE PROJECTION OF ORIENTATION ZONES OF POTENTIALLY UNSTABLE DISCONTINUITIES, ELEMENT 41, RIGHT, $J_a = 0{\cdot}07$.

CHAPTER 11

DISCONTINUITY SPACINGS IN ROCK*

11.1 Introduction

11.1.1 Aims of this Chapter

Detailed discontinuity surveys undertaken at Chinnor were described in Chapters 2, 3 and 5. Additional surveys were undertaken by the author in tunnels at two other locations: The Kielder Experimental Tunnel, Rogerley Quarry, Co. Durham, and the Channel Tunnel machine erection chamber, Kent. At all survey locations, in addition to other measurements, a large amount of data concerning discontinuity spacings was obtained. Examination of the literature (Chapter 1), and experience at Chinnor has proved that the spacing of discontinuities in a rock mass critically controls the behaviour of ground in response to tunnel excavation.

The purpose of this chapter is to present a theoretical approach to discontinuity spacings and RQD (Rock Quality Designation) based on the statistical distributions of spacing values that could occur along scanlines and to compare these results with experimental data obtained in the field discontinuity surveys.

In the theoretical section of this Chapter, the influence of spacing distributions on the RQD value is explained, and the sensitivity of the RQD value to mean discontinuity spacing is illustrated. In the experimental

---

* The work described in this Chapter was done jointly by the author and Dr J. A. Hudson of the Transport and Road Research Laboratory, Crowthorne, Berks. Much of this work is to be published as a joint paper (Priest and Hudson, 1975b)

section, data obtained by the author are presented for the three different tunnel locations together with additional published data on discontinuity spacings. These results are compared with the theoretical values.

Finally, the usefulness of this interpretation of discontinuity spacings and the geotechnical implications are discussed.

11.1.2 Indices of discontinuity intensity

The form of the index adopted to describe discontinuity intensity is often influenced by the nature of the exposure and the survey technique (Chapter 1). Skempton *et al.*(1969) described discontinuity intensity in the London Clay in terms of the number of discontinuities per unit volume of material. The values were obtained by dissecting blocks of clay. Using a similar technique on Cretaceous sediments in south east England, Fookes and Denness (1969) expressed intensity as discontinuity area per unit volume. Piteau (1970) used a scanline survey technique on rock faces and expressed discontinuity intensity as the number of discontinuities per unit distance normal to the strike of a set of sub-parallel discontinuities.

The results of a scanline survey or the quality of rock cores recovered during a site investigation programme can be described using the method proposed by Deere (1964). The Rock Quality Designation (RQD) is the proportion of scanline or borehole core that consists of intact lengths that are 0.1m (4 ins) or longer. To calculate the RQD value, these intact lengths are summed and expressed as a percentage of the total length:

$$RQD = 100\sum_{i=1}^{n} x_i/L \qquad \ldots\ (11.1)$$

where x_i is the value of the i^{th} length $\geq$ 0.1m

n is the number of intact lengths $\geq$ 0.1m

L is the length of scanline or borehole along which the RQD value is required.

Thus, the RQD can be calculated for various sections or the complete length of the scanline or borehole.

Deere *et al.* (1967) suggested that a scanline, which can be used to measure discontinuity intensity at a face, may be regarded as directly analogous to a borehole core since the RQD can be found in both cases. This is important because it allows site investigation results to be compared with conditions actually experienced during excavation, and is one of the main reasons why the scanline survey technique was adopted for the work described in this thesis.

11.2 Theoretical approach

11.2.1 Possible spacing distributions

The discontinuity spacings will be considered with reference to the distances between points where discontinuities intersect a straight line through the rock mass - shown in Figure 11.1(a). This is equivalent to the scanline or measuring tape that is used for field determinations of discontinuity spacing or to a thin borehole core. The spacing values x_i for i=1 to n, are shown in Figure 11.1(b). The discontinuity intersection points can be evenly spaced, clustered, random or some combination of these.

If the discontinuities are fairly evenly spaced with a normal distribution of spacing values having a relatively low standard deviation, the frequency distribution shown in Figure 11.1(c) will be appropriate. This type of distribution will occur in, say, a uniform columnar jointed basalt or evenly bedded sandstone with the magnitude of the standard deviation reflecting the uniformity of jointing and bedding respectively.

In the case of clustered discontinuities, a high frequency of low spacing values occurs within clusters and a low frequency of high spacing values occurs between clusters. This frequency distribution is shown in Figure 11.1(d). Clustering can develop as a result of spalling near a free face due to stress or weathering effects. In addition, cyclic variation in lithology such as alternating layers of sandstone and highly fractured siltstone could produce this distribution.

For randomly positioned discontinuities, the discontinuity/scanline intersection points are here defined as random if the position of each intersection point does not depend on the position of any others. In other words, there is no interaction between discontinuities. This could occur in a homogeneous rock mass where the formation of discontinuities has not been dominated by lithological or structural variability. In Appendix L, from standard statistical theory it is shown that if each small segment of scanline has an equal but small chance of containing a discontinuity intersection point, the randomly positioned points are a Poisson process and the associated discontinuity spacings follow a negative exponential distribution of similar form to that shown in Figure 11.1(e).

The negative exponential distribution is mathematically expressed as

$$f(x) = \lambda e^{-\lambda x} \qquad \ldots\ldots (11.2)$$

where f(x) is the frequency of a discontinuity spacing x and λ is the average number of discontinuities per metre.

This is a one parameter (λ) distribution with the mean and standard deviation both equal to $1/\lambda$.

In a geologically complex rock mass with a varied mechanical history, it is likely that a combination of the evenly spaced, clustered and random distributions will be present. This will result in the type of distribution shown in Figure 11.1(f) which will be similar to the negative exponential distribution. If, however, the mean spacing of the superimposed random distribution is large compared with that of the evenly spaced distribution, the latter will be largely unaffected and consequently dominate. In all other combinations, the clusters are largely unaffected whilst the even spacing values are broken up by superimposed random discontinuity patterns. It is important to note that the orientation of discontinuities, relative to that of the scanline, in general controls the number of discontinuities intersected per unit length and not the overall pattern of the discontinuity spacing distribution.

11.2.2 Influence of spacing distributions on the Rock Quality Designation

The Rock Quality Designation is the summed percentage of the scanline or borehole core length that consists of intact lengths over 0.1m. Theoretical RQDs can therefore be determined directly from distribution curves similar to those in Figure 11.1 by considering the frequency of spacing values above the 0.1m threshold value. This leads to the concept of maximum and minimum values of RQD for the clustered and evenly spaced distributions and a relation between discontinuity frequency and RQD for

the random distribution.

The maximum possible value for the RQD at any mean discontinuity spacing is always close to 100% because:

(a) if the mean discontinuity spacing is less than 0.1m, an RQD value close to 100% is obtained when the discontinuities are very clustered with large intact lengths between the clusters;

(b) if the mean discontinuity spacing is greater than 0.1m, an RQD value close to 100% can be obtained either by clustering or even spacing.

The minimum possible value for the RQD is zero for an average spacing less than 0.1m if the discontinuities are evenly spaced. When the average spacing is greater than 0.1m, the minimum RQD occurs when all but one of the spacing values are just below 0.1m with one high remaining spacing value. This leads to the linear relation derived below, between the minimum possible RQD value (RQD_{min}) and the discontinuity frequency.

The total number of discontinuities in a scanline = λL

Where λ = mean number of discontinuities/metre

L = scanline length

Thus, neglecting end effects, there are ($\lambda L - 1$) spacing values just below 0.1m and the rejected length of scanline is approximately 0.1 ($\lambda L - 1$) giving, from Equation 11.1

$$RQD_{min} \simeq 100 [L - 0.1 (\lambda L - 1)] / L$$

$$\simeq 100 [1 - 0.1\lambda + (0.1/L)]$$

For a scanline which is long compared with the 0.1m threshold value, the term 0.1/L can be ignored and

$$RQD_{min} \simeq 100\ (1 - 0.1\lambda) \quad \text{for } \lambda < 10m^{-1} \qquad \ldots\ldots (11.3)$$

This relation is plotted in Figure 11.2 in terms of RQD_{min} versus mean dicontinuity spacing ($1/\lambda$).

To calculate the RQD value for rock having <u>random</u> discontinuity positions, the percentage of scanline length containing intact lengths greater than 0.1m is found by integrating the spacing values from 0.1m to L for the negative exponential distribution as shown in Figure 11.1. The relation between RQD and discontinuity frequency for this case is derived below:

The probability of discontinuity spacings occurring between x and x + dx is given by f(x) dx.

where x is a spacing value

dx is an increment of spacing

f(x) is the probability density distribution of x.

For a long total length of scanline, L, the total number of discontinuities is λL. Thus, the number of intact lengths between x and x + dx is $\lambda L\ f(x)dx$ and the length of these is $\lambda L x f(x)dx$. From the definition of RQD (Equation 11.1) for the continuous case, the theoretical RQD (RQD*) with an arbitrary threshold value, t, is given by:

$$RQD^*_t = 100 \int_t^L \lambda L x f(x) dx / L$$

and with a negative exponential distribution of spacing values (Equation 11.2)

$$f(x) = \lambda e^{-\lambda x} \quad \text{therefore}$$

$$RQD^*_t = 100\lambda^2 \int_t^L x e^{-\lambda x} \, dx$$

For a long scanline, terms containing $e^{-\lambda L}$ can be ignored and

$$\underline{RQD^*_t = 100 e^{-\lambda t}(\lambda t + 1)} \qquad \ldots\ldots (11.4)$$

For the conventional RQD, with a threshold value of t = 0.1m the theoretical value is

$$\underline{RQD^* = 100 e^{-0.1\lambda}(0.1\lambda + 1)} \qquad \ldots\ldots (11.5)$$

The relation given in Equation 11.5 is also plotted in Figure 11.2. Note that Equations 11.4 and 11.5 only apply if the discontinuity spacing values follow a negative exponential distribution.

11.2.3 Variation of RQD with the threshold value

In the conventional RQD, the percentage of scanline consisting of lengths above 0.1m gives the RQD value. However, it is possible to examine the magnitude of the RQD value for a variety of threshold values, t.

By the same arguments presented earlier the maximum RQD value remains close to 100% and the minimum is found by substituting t for 0.1 in Equation 11.3. The intermediate case for the negative exponential distribution of discontinuity spacing values is the suite of curves generated by Equation 11.4 for various values of t. These are shown in Figure 11.3 with RQD_t^* plotted against the mean discontinuity spacing, $1/\lambda$.

The curves in Figure 11.3 show that, with the negative exponential assumption, the conventional RQD (threshold value 0.1m) is sensitive for mean discontinuity spacings between zero and approximately 0.3m; above 0.3m, the RQD is always above 95%. The RQD value can be made more sensitive for high mean discontinuity spacing values by increasing the threshold value.

From scanline measurements made in a rock mass with a mean discontinuity spacing of 0.3m, the conventional RQD is 95% - ie 95% of the scanline consists of intact lengths greater than 0.1m. From Equation 11.4 however, the percentage of scanline consisting of intact lengths above any required threshold can be found. For example, from the vertical line in Figure 11.3, 16% of the scanline consists of intact lengths greater than 1m, when the conventional RQD = 95%.

11.2.4 Precision of the discontinuity frequency and RQD estimates

Assuming a negative exponential distribution of spacing values, it is possible to study the effect of scanline length on the precision of the discontinuity frequency (λ) estimate. A short scanline, say 10 times the mean discontinuity spacing, might give a bad estimate of λ and hence the RQD value will not be a good representation of the rock mass. In fact, widely different RQD values measured over metre or two metre lengths

of a borehole can simply be a reflection of the random positioning of the discontinuities.

The method for studying the precision of the λ estimate is explained in Appendix L.

Examination of Table L.2 reveals that if, say, 50 discontinuities are measured along a scanline length (L) of 5m, the true λ (ie $\frac{\lambda L}{5}$) is within $7.79m^{-1}$ and $12.66m^{-1}$ at the 90% confidence level. The estimated λ of $10m^{-1}$ (ie 50/5) gives the RQD* as 74% from Equation 11.5 but, from the $\hat{\lambda}$ variation† at the 90% confidence level, the true RQD varies between 82% and 64%. This is summarised in Figure 11.4, where the effect of the sample length on the RQD* error band is shown. For the specific case of 5 discontinuities per metre encountered in sample lengths ranging from 1m to 10m, the RQD* error band varies from 98% - 72% to 84% - 87% respectively.

An alternative approach is to determine the probability of estimating the discontinuity frequency (λ) to within ±20% or ±10% for different sample lengths; graphs of the resulting probabilities are shown in Figure 11.5. For example if the sample length is 50 times the mean discontinuity spacing, the estimated λ will lie within ±20% of the true λ,86 times out of 100.

11.3 Field discontinuity surveys, experimental results

In all the field surveys carried out by the author discontinuity characteristics were measured along scanlines set up on exposed faces, following the methods described in Chapters 2, 3 and 5.

---

† λ is the true population parameter; $\hat{\lambda}$ is the estimate obtained by sampling.

11.3.1 Chinnor

A total of ten thousand discontinuity spacing values were processed for a total scanline length of approximately 1000m taken at exposed faces in the Chinnor quarry, in the 3m diameter shaft and in the 5m diameter tunnel (Chapters 2, 3 and 5). Figures 2.3 to 2.12 and 3.19 to 3.21 show discontinuity spacing histograms for measurements taken at exposed faces in the Chinnor quarry and in the shaft. Appendix Figures H.1 to H.17 show spacing histograms for measurments taken at selected faces during the first 85m of tunnelling. The Figures referred to above all include a fitted negative exponential probability density distribution calculated in each case for the appropriate parameter $\hat{\lambda}$ equal to the reciprocal of the mean discontinuity spacing at each survey location. Tables 2.1, 3.3 and 5.1 list, amongst other data, values of mean spacing and standard deviation together with total scanline length and number of observed values at each survey location.

Figures 2.13, 3.22, and 5.7, show summary discontinuity spacing histograms for measurements taken in the quarry, shaft and tunnel respectively. The probability density distributions corresponding to Figures 2.13, 3.22, and 5.7 are replotted on a logarithmic scale in Figures 11.6, 11.7 and 11.8. The fitted negative exponential probability density distribution is a straight line (cf Equation 11.2):

$$\ln f(x) = \ln\hat{\lambda} - \hat{\lambda}x$$

Examination of Figures 11.6, 11.7 and 11.8 shows that there is close agreement between the theoretical and measured distributions for the shaft and tunnel. In addition, for each location (Tables 3.3 and 5.1) the value of the mean spacing is approximately equal to the standard deviation; this

is a theoretical characteristic of the negative exponential distribution and serves to confirm the conclusions drawn above based on visual comparison.

Figures 2.13 and 11.6 (quarry scanlines) indicate a slight deviation from the negative exponential form, in particular the frequency of low discontinuity spacings is less than that predicted by the negative exponential distribution. Examination of Table 2.1, however, indicates that there is still reasonably good agreement between mean spacing and standard deviation values for the quarry scanlines.

11.3.2 Kielder Experimental Tunnel

The Kielder Experimental Tunnel, Rogerley Quarry, Co. Durham, was excavated in rocks belonging to the Carboniferous Limestone sequence. The tunnel was driven at three levels: in sandstone, limestone and mudstone horizons. During tunnel excavation a detailed assessment of rock quality at selected faces in the sandstone and mudstone horizons was undertaken by the author. A part of this rock quality assessment included an examination of rock discontinuity characteristics, using measurement techniques described earlier. Raw data concerning discontinuity characteristics measured in the Kielder Experimental Tunnel are presented in Appendix B. A more detailed description of the work in the Kielder Experimental tunnel is presented in Priest and Hudson (1975c).

Discontinuity spacing histograms for the sandstone and mudstone horizons are presented in Figures 11.9 and 11.10 together with the corresponding negative exponential probability density distributions plotted for the appropriate value of mean discontinuity spacing. Figures 11.9 and 11.10 show that there is good agreement between the theoretical and measured distributions. In addition, for each distribu-

tion there is close agreement between the mean spacing and standard deviation. This serves to verify the applicability of the negative exponential distribution in describing the real discontinuity spacing distribution for these Carboniferous rocks. It is important to note that Figures 11.9 and 11.10 illustrate that the negative exponential distribution is equally applicable for the highly fractured mudstone as the less fractured sandstone.

In the section dealing with the theoretical approach it was stated that a feature of the negative exponential distribution is that the mean spacing is equal to the standard deviation. Figure 11.11 is a graph plotting the mean discontinuity spacing against the standard deviation of the spacing for separate survey locations at Chinnor and Rogerley Quarry. The data have been divided into two groups based on the sample size: < 200 values and > 200 values. The straight line in Figure 11.11 indicates the idealised relation for which the mean discontinuity spacing is equal to the standard deviation. It is clear from this Figure that the experimental results conform well to the theoretical line, particularly for the larger samples where sampling error is minimised, and the freshly exposed sample locations where weathering is minimised. It is worth noting that in other distributions, for example the normal distribution, the mean and standard deviation are totally independent.

11.3.3 Channel Tunnel

Excavation of the machine erection chamber during Phase II of the Channel Tunnel construction programme provided an additional facility for examining *in situ* Lower Chalk. Assessment of discontinuity characteristics was carried out using the scanline techniques described earlier.

Raw data concerning discontinuity characteristics measured in the Channel Tunnel are presented in Appendix B. Figure 11.12 shows a histogram of discontinuity spacing values, for a 0.05m class interval. The fitted negative exponential probability density distribution indicates a reasonably good comparison between actual and theoretical distributions considering the small sample size.

11.3.4 Published data

Mahtab *et al.*(1973) presented a detailed study of the discontinuity characteristics of a variety of igneous rocks examined in the San Manuel copper mine, Arizona. Discontinuity spacings were measured as the normal distance between two discontinuity planes. A series of histograms illustrating the discontinuity spacing frequency distributions for the three rock types examined is presented in Figure 11.13.

McGown *et al.*(1974) working on glacial till at Hurlford, Ayrshire, measured discontinuity characteristics using the cavity technique. This technique, described in Fookes and Denness (1969), was modified slightly for use at Hurlford. Figure 11.14 presents discontinuity spacing histograms for measurements taken at two depths in the till.

Examination of Figures 11.13 and 11.14 indicates that the discontinuity spacing frequency distributions follow a general negative exponential form since, in most cases, the low discontinuity spacings are the most frequent. In addition, the frequency of discontinuity spacing values tends to decrease in an exponential form with increasing spacing.

In view of the data presented in this Section, it is felt that the negative exponential probability density distribution provides a good

approximation to the distribution of discontinuity spacings measured on unweathered rocks in the field. The fact that, for all rocks examined, the distribution of discontinuity spacing values follows the negative exponential distribution indicates that the occurrence of discontinuities along a scanline may be a Poisson process. In other words, for all rocks examined, the discontinuities were probably randomly positioned along the scanlines.

The applicability of the negative exponential has, to date, only been verified at a few locations for a limited range of rock types. It is hoped that, in the future, further work will shed light on the validity of wider application of the negative exponential distribution.

11.4 Discussion

11.4.1 Validity of the negative exponential discontinuity spacing distribution assumption

The validity of the negative exponential distribution, verified earlier for the available experimental data, indicates that Equation 11.5 can be used to calculate the RQD for a rock, given the mean discontinuity spacing ($1/\lambda$).

Table 11.1 summarises values of RQD, calculated from individual discontinuity spacing measurements using Equation 11.1 and RQD* calculated from theory using Equation 11.5 for the measurement locations discussed earlier. This Table, presented graphically in Figure 11.15 demonstrates the close agreement between RQD and RQD* for the measurements taken at fresh exposures. The RQD values obtained from surveys in the Chinnor quarry deviate slightly from the straight line and serve to indicate the

Table 11.1 Comparison between measured and theoretical RQD

Rock formation, location	Lithology	Scanline configuration	Measured RQD % (from Equation 11.1)	Theoretical RQD* % (from Equation 11.5)	Average number of discontinuities per metre, $\hat{\lambda}$ (m^{-1})
Lower Chalk, Chinnor quarry	Chalk	Location No. = 1	38	53	15.9
		2	37	52	16.1
		3	44	55	15.2
		4	51	60	13.7
		Horizontal 5	46	55	15.2
		plus 6	78	83	7.5
		vertical 7	48	55	15.4
		scanlines 8	52	62	13.3
		9	40	47	17.9
		10	43	53	15.9
Lower Chalk Chinnor shaft	Chalk	Horizontal scanlines	79	81	7.9
		Vertical scanline, west	67	70	11.0
		Vertical scanline, east	70	75	9.5
Lower Chalk Chinnor tunnel	Chalk	Chainage = 9.9m	91	89	5.6
		11.5m	87	87	6.3
		12.1m	80	81	7.9
		14.0m	83	87	6.4
		18.1m	82	81	7.9
		20.4m	78	81	8.0
		Horizontal 35.9m	78	81	8.0
		plus 55.4m	72	74	9.9
		vertical 57.5m	60	64	12.5
		scanlines 60.5m	66	69	11.3
		for each 65.2m	79	79	8.5
		face 70.2m	64	65	12.3
		72.7m	71	73	10.1
		73.9m	64	68	11.7
		79.3m	65	69	11.3
		85.0m	63	63	12.8
Carboniferous Limestone, Rogerley tunnel	Sandstone	Vertical plus horizontal scanlines	83	82	7.8
	Limestone	Vertical plus Horizontal scanlines	100	98	2.0
	Mudstone	Vertical plus	12	12	37.0
		horizontal	32	31	23.8
		scanlines at	14	16	32.5
		selected faces	22	26	26.3
Lower Chalk, Channel Tunnel	Chalk	Vertical plus horizontal scanlines	99	99	1.2
			88	90	5.3

influence of weathering on the applicability of Equation 11.5.

The closeness of the agreement between the measured and theoretical RQD values is not a confirmation of Equation 11.5 but a measure of how closely the discontinuity spacing values follow the negative exponential distribution in each location. The implication is that a value of RQD, accurate to within 5%, could have been obtained at each of the freshly exposed locations by simply counting the discontinuities and calculating the discontinuity frequency, $\hat{\lambda}$.

Figure 11.16 shows a graph of Equation 11.5 relating RQD* to λ together with the experimental data points presented earlier. It is clear from this Figure that between values of $\lambda = 6m^{-1}$ and $\lambda = 16m^{-1}$ the relation between λ and RQD* is approximately linear. The curve in Figure 11.16 has an inflection point P at $\lambda = 10m^{-1}$; at this point the curve has a slope equal to $\frac{d\ RQD^*}{d\ \lambda}\Big|_{\lambda=10} = -10e^{-1} = -3.68m$. The straight line drawn through P, tangential to the curve defined by Equation 11.5 is therefore described by

$$RQD^* = -3.68\lambda + 110.4$$

This line, shown in Figure 11.16, gives a good approximation of RQD between values of $\lambda = 6m^{-1}$ and $\lambda = 16m^{-1}$. Bieniawski (1973), by reference to Deere *et al.* (1967) suggested that the relation between "fracture frequency" (ie λ) and RQD is linear; this statement is generally in agreement with Figure 11.16 within the stated range of λ.

11.4.2 Imposed discontinuities

The aims of a discontinuity survey are to assess the true discontinuity characteristics of a rock mass by measuring the characteristics of a sample

of the mass. It is possible, however, that the sample contains extra discontinuities not found in the rock mass. These imposed discontinuities will therefore lead to a bias in the estimate of rock mass discontinuity characteristics.

In Chapter 2 the effects of weathering on discontinuity frequency were discussed. Comparison between mean spacing values listed in Tables 2.1, 3.3 and 5.1 tends to confirm the conclusions of Chapter 2 that mean discontinuity spacing is reduced by exposure and weathering of the Lower Chalk at Chinnor.

It is clear from Figure 11.16 that, for the scanlines taken on weathered faces in the Chinnor quarry, Equation 11.5 predicts an RQD* larger than the measured value. The effect causing RQD to be < RQD* (in particular for $\lambda \geq 10m^{-1}$) is a tendency for the discontinuities to be more evenly spaced than predicted by the negative exponential distribution. It is therefore clear that weathering effects serve not only to reduce the mean spacing but also to produce a more evenly spaced discontinuity pattern than that of the negative exponential distribution.

In many engineering situations data concerning discontinuity spacing are obtained from borehole cores. There is therefore a possibility that additional discontinuities may have been introduced by the sampling process - ie drilling the borehole, (Jaeger and Cook, 1969).

Figure 11.17 summarises data presented by Deere *et al.*(1967) from cores and scanlines in a variety of rock types. Figures 11.17 a to d show the comparison between RQD* and the measured values of Deere *et al.* broken down into the four rock types and plotted against fracture frequency. A similar type of graph (Figure 3.14) summarises this relation for data obtained

from cores at Chinnor, this time plotting RQD against discontinuity spacing. These Figures indicate that for a given $\hat{\lambda}$, Equation 11.5 predicts an RQD* larger than the measured value. As mentioned above, the effect causing RQD to be < RQD* (in particular for $\lambda \geqslant 10m^{-1}$) is a tendency for the discontinuities to be more evenly spaced than predicted by the negative exponential distribution.

Most of the data in Figures 11.17 and 3.14 relate to borehole core; it is probable, therefore, that the process of rotary drilling added a more evenly spaced component of discontinuities in the recovered core. Lengths of intact core can snap in the centre during drilling; this, together with the phenomenon of discing can lead not only to an artificially lowered RQD but also to an artificially imposed discontinuity spacing distribution.

The effects outlined above, also noticed during the site investigation at Chinnor (Chapter 3), should be borne in mind when interpreting results concerning rock quality obtained from weathered exposures and boreholes. The advantage of scanline surveys taken on freshly exposed faces is that a largely unbiased estimate of rock mass discontinuity characteristics can be obtained.

11.4.3 Geotechnical implications

The RQD, commonly adopted as a rock quality index is here regarded as having two major drawbacks when viewed in the light of the theoretical approach:

(a) Calculating RQD is a time-consuming process which, when applied to borehole cores, can give results unrepresentative of the rock mass.

(b) The conventional RQD is insensitive to variations in rock quality when the average discontinuity spacing exceeds 0.3m. For example, for a large excavation, transition from 'favourable' to 'unfavourable' conditions may be represented by variations in RQD of only 3%, from 98% to 95%.

RQD has, however, an advantage over simple indices which express, say, an average discontinuity frequency per metre ($\hat{\lambda}$) in that it makes statements about the distribution of block sizes. If the negative exponential distribution is accepted as valid, from a simple knowledge of $\hat{\lambda}$ additional data concerning RQD can be calculated if required. Moreover a two-tier RQD index can be produced by adopting a pair of threshold values t, say 0.1m and 1.0m. The selection of the second threshold value, 1.0m, ensures sensitivity of the two-tier RQD for mean spacing values up to 2.5m for use when considering particularly large excavations. The suggested rock quality index would therefore be, for example $\hat{\lambda} = 3.3m^{-1}$, $RQD^*_{0.1} = 95\%$, $RQD^*_{1.0} = 16\%$. which gives information on discontinuity frequency, percentage of rock containing spacing values greater than 0.1m and percentage of rock containing spacing values greater than 1.0m.

Acceptance of the negative exponential distribution allows caluclations to be made concerning the precision of the discontinuity frequency estimates made from any given scanline. In this way, it is possible to determine the minimum scanline length, expressed as a multiple of the mean discontinuity spacing, required to produce a rock quality index at a specified precision. For example, if the sample length is 50 times the mean discontinuity spacing. the estimated λ will lie within $\pm 20\%$ of the true λ, 86 times out of 100.

These ideas can be extended to considerations of rock cutability, previously discussed in Chapter 6. A pick revolving in a cutting head may

be regarded as following a spiral scanline through the rock. Thus a pick at a radius of 1m will trace out a scanline in excess of 20m during a machine advance of 0.1m. Consequently cutting data averaged over this distance will represent a good statistical sample of discontinuity characteristics in the rock and therefore adequately reflect average conditions at the face evaluated using extensive scanline surveys.

A knowledge that the distribution of discontinuity spacings follows a negative exponential form can be of use in rockbolt design. Rockbolt design criteria may embody requirements that the bolt should be of sufficient length to penetrate, say, the third joint block back. The probability of intersecting three joint blocks for a given rockbolt length can be calculated directly from the statistical theory.

To estimate ground permeability, packer tests are often carried out during site investigation. The rate of water flow into the ground from a sealed length of borehole, under a given head of water, is measured (Chapter 4). The primary permeability of many rocks is relatively low, and the majority of water flow occurs through the discontinuities (Foster and Milton, 1974). Therefore the permeability estimate obtained from a given length of borehole, L, isolated between packers will be a function of the number (and type) of discontinuities intersected in that length. In particular, the applicability of the permeability estimate to considerations of permeability in the rock mass will depend on how accurately the discontinuity pattern isolated in the borehole reflects that of the rock mass. Thus, a similar approach to that used when considering the effect of borehole length on the precision of the λ (mean number of discontinuities per metre) estimate can be used to determine optimal packer permeability test lengths.

Snow (1968; 1970) described a method for determining discontinuity frequency from the proportion of zero discharge packer permeability tests that occur. He made the basic assumption that the occurrence of open discontinuities in a given length of borehole, L, obeys the Poisson process. During a series of tests some of the packer test lengths will contain no discontinuities and thus give a zero discharge. The probability of this occurring, P_o, is given by Equation L.3, substituting L for x, with k (the number of events in a given interval) equal to zero

$$P_o = e^{-\lambda L} \qquad \ldots\ldots 11.6$$

This summarises, in equation form, the graphical techniques described by Snow (1968).

From a knowledge of P_o and L, λ can be calculated:

$$\lambda = (-\ln P_o)/L \qquad \ldots\ldots 11.7$$

Snow also described a method for determining discontinuity porosity (fracture porosity) to enable prediction of grout volumes required to treat the rock. The discontinuity porosity was calculated using the following Equation:

$$\text{Discontinuity porosity, } \theta = 5.45\left(k'/\Delta^2\right)^{\frac{1}{3}} \qquad \ldots\ldots 11.8$$

where k' is the intrinsic permeability of the rock mass and Δ is the mean spacing of the discontinuity set intersected by the borehole.

The discontinuity opening, assuming all discontinuities have the same value, r_o, was found from

$$r_o = \theta\Delta/3 \qquad \ldots\ldots 11.9$$

Therefore, by indirect methods (ie proportion of zero discharge packer permeability tests), it is possible to assess discontinuity geometry, and hence gain insight into the nature of the mass permeability, storativity and rock deformability.

In order to determine Δ from the mean discontinuity spacing, Snow applied a correction factor (f). By assuming a cubical arrangement of discontinuity sets, a value f = 1.25 was selected. From Equation 11.7

$$\Delta = \frac{1.25L}{(-\ln P_o)} \qquad \ldots\ldots 11.10$$

However, measurements of discontinuity orientation (Chapters 2, 3 and 5) have revealed that there is no definite cubical arrangement of discontinuity sets at Chinnor, therefore the correction factor, f, is invalid for the particular case of the Lower Chalk at Chinnor. In the determination of discontinuity porosity for grouting purposes, it is necessary to select an appropriate packer spacing, L, such that a proportion, P_o, of all tests gives a zero discharge. The correct packer spacing can be determined from an estimate of the mean discontinuity spacing (or RQD, cf. Equation 11.5) using Equation 11.7.

Snow (1970) tested the relation in Equation 11.6 using the logs of TV camera surveys taken in boreholes through granite. He found that there was a greater average discontinuity frequency with the fixed sample length (10ft) used in the TV survey than predicted by Equation 11.6. He attributed this to the presence of occasional swarms of close-spaced fractures.

For the methods described above to be applicable to measuring discontinuity characteristics, the rock must satisfy the following requirements:

1. The intergranular permeability (primary permeability) must be small compared with the discontinuity permeability (secondary permeability).

2. The rock should have no large solution cavities or contain discontinuities with openings in excess of 1.5mm since assumptions of laminar flow along discontinuities will not be valid for such cavities (Chapter 4).

3. The discontinuities should be water saturated before packer permeability testing and the rock should be rigid and inert to the testing fluid.

4. The discontinuity spacing distribution in the borehole should obey the negative exponential distribution, ie the occurrence of discontinuities in a given test length must obey the Poisson process.

The Lower Chalk at Chinnor meets the above requirements and therefore the methods outlined above for determining discontinuity characteristics are applicable to this specific case. In particular, it should be noted that the assumptions made by Snow concerning the distribution of discontinuities are verified for the particular rocks examined.

11.5 Summary and conclusions

1. The possible discontinuity spacings along a straight line through a rock mass were considered. The effects of evenly spaced, clustered and randomly positioned discontinuities were examined, from a theoretical standpoint.

2. It was found that, unless there is a large predominance of evenly spaced discontinuities, any combination of evenly spaced, clustered and

randomly positioned discontinuities will lead to a negative exponential form of frequency versus spacing value curve. Analysis of the field results obtained from scanline measurements indicated that a negative exponential distribution of discontinuity spacing values is a good approximation for all available data. The only exceptions are data obtained from weathered exposures, data obtained from borehole core (discontinuities superimposed by drilling) and histograms constructed from a small number of measurements (sampling error).

3. Using the negative exponential distribution of discontinuity spacing values, a relation was established between the theoretical Rock Quality Designation (RQD*) and the average number of discontinuities per metre:

$$RQD^* = 100e^{0.1\lambda}(0.1\lambda + 1)$$

With this formula it was possible to compare the theoretical RQD, obtained from the discontinuity frequency alone, with the actual RQD calculated from the individual spacing values. This was done for all measurement locations on freshly exposed rock. The maximum error was 5% indicating that the RQD could have been found to within 5% simply by counting the number of discontinuities along the scanline and using the formula. In addition, the formula shows that the conventional RQD with a threshold value of 0.1m is insensitive when the mean discontinuity spacing is above 0.3m.

4. It is recommended that discontinuity spacing data obtained from scanlines be presented in the following form:

(a) $\hat{\lambda}$ - the mean number of discontinuities per metre, or $\bar{x}$ the mean discontinuity spacing ($\bar{x} = {}^{1}/\hat{\lambda}$).

Since RQD is a commonly used method of expressing discontinuity spacing data in site investigation, a two-tier RQD may be used:

(b) $RQD_{0.1}$ - the conventional RQD

(c) $RQD_{1.0}$ - the RQD with a threshold value of 1.0m.†

If the theory outlined earlier is applicable, (b) and (c) can be calculated directly from (a).

5. It was found that to estimate the number of discontinuities per metre to within a reasonable precision required a scanline at least fifty times the mean discontinuity spacing. Thus, if there are about five discontinuities every metre, the scanline must be at least ten metres long. Moreover, at least two hundred measurement values were generally required before negative exponential distribution form became clear on a histogram. One of the features of this distribution is that theoretically the mean and standard deviation are equal : this was found to be the case to within 20% for the nineteen measurement locations where greater than two hundred readings were taken.

6. Sampling factors are considered to be relevant to packer permeability tests where water flow occurs essentially through the discontinuities. Very large variations of water flow should be expected if the test lengths are only of the order of ten times the mean discontinuity

---

† A threshold value of 1.0m is recommended for general use; however any value can be used to suit particular conditions.

spacing, implying that correlation of permeability values from borehole to borehole should not then be attempted.

7. Following Snow (1968; 1970) a method for determining mean discontinuity frequency and discontinuity porosity for grouting purposes from the proportion of zero discharge test lengths was examined. It is concluded that the methods described are applicable to the Lower Chalk at Chinnor.

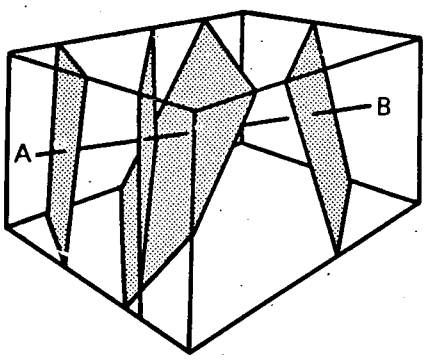

(a) Discontinuity intersection points along a straight line (AB) through the rock mass

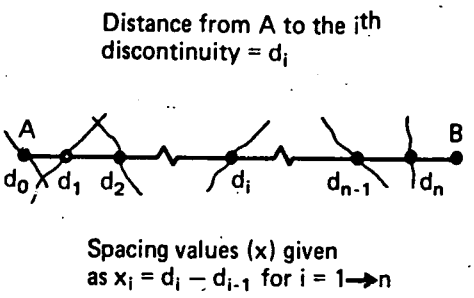

(b) Scanline (measuring tape) on exposed rock face

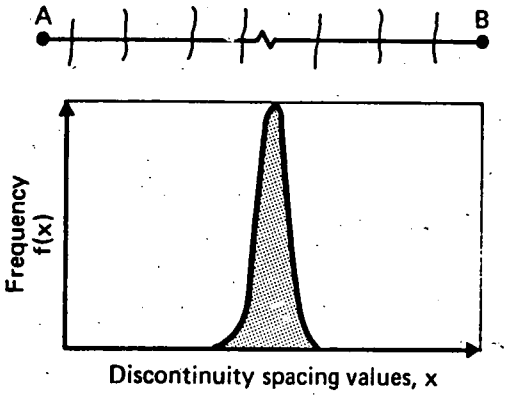

(c) Fairly evenly spaced distribution

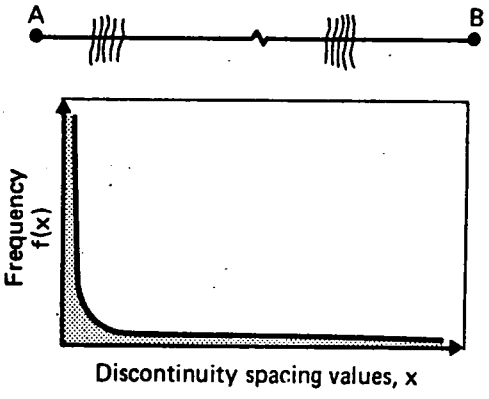

(d) Clustered distribution

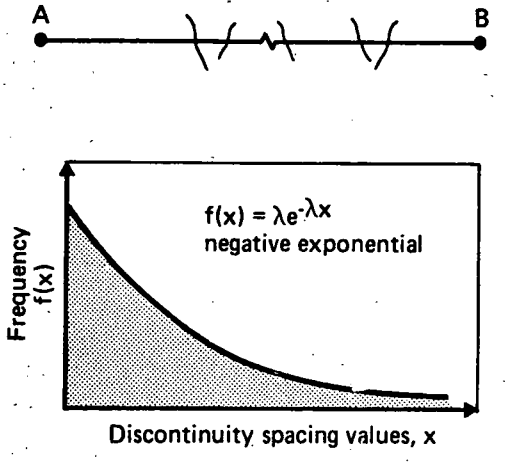

(e) Random distribution

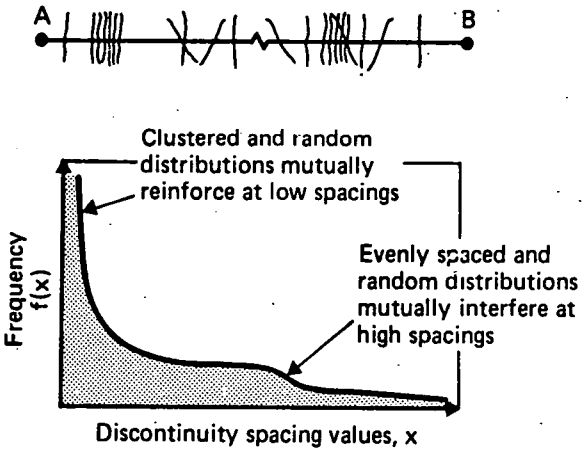

(f) Combination of distributions

Fig. II.1 THEORETICAL DISCONTINUITY SPACING DISTRIBUTIONS

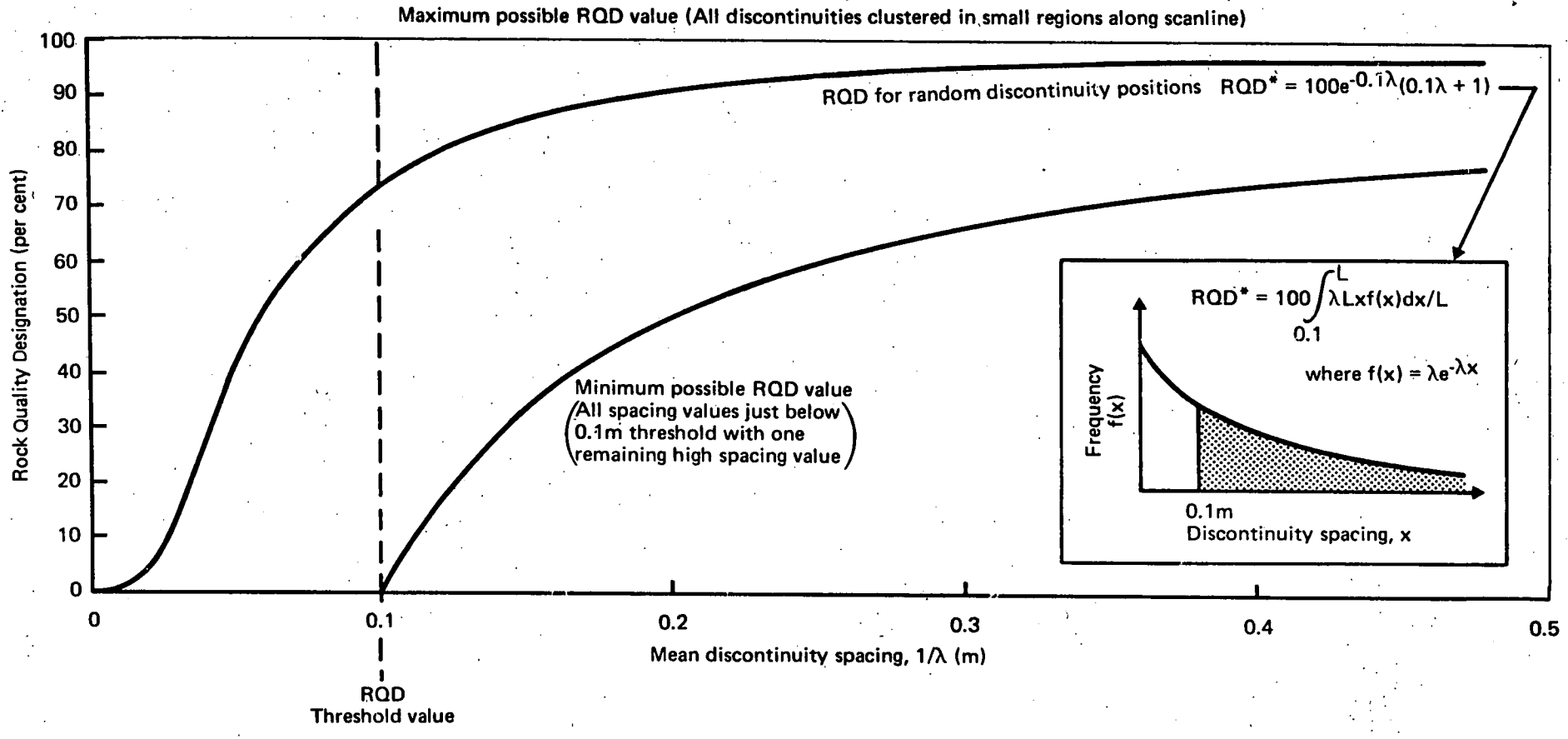

Fig. II.2 MAXIMUM AND MINIMUM POSSIBLE RQD VALUES AND RQD VERSUS MEAN DISCONTINUITY SPACING FOR RANDOMLY POSITIONED DISCONTINUITIES

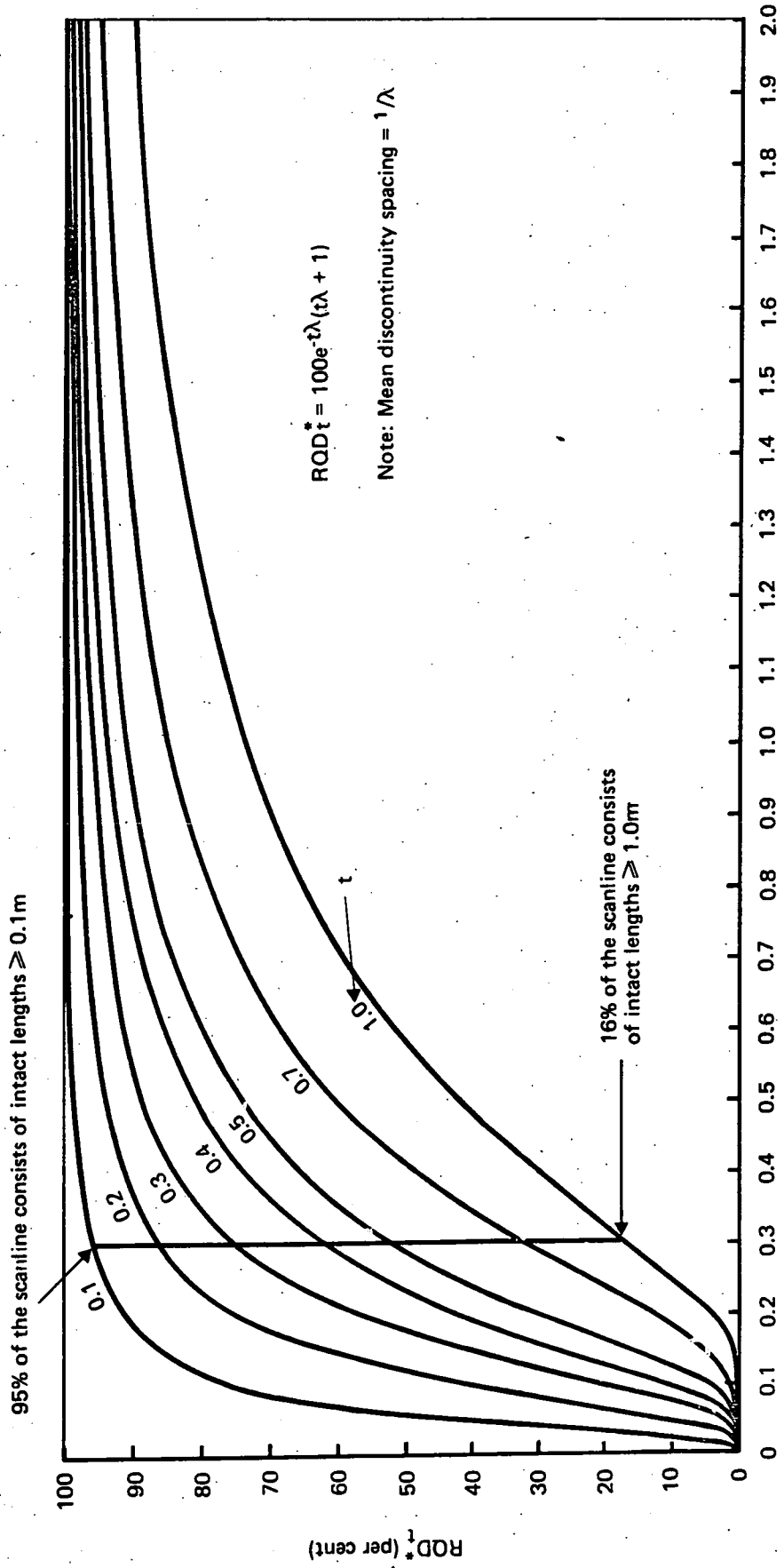

Fig. II.3 VARIATION OF RQD WITH MEAN DISCONTINUITY SPACING FOR A RANGE OF RQD THRESHOLD VALUES t

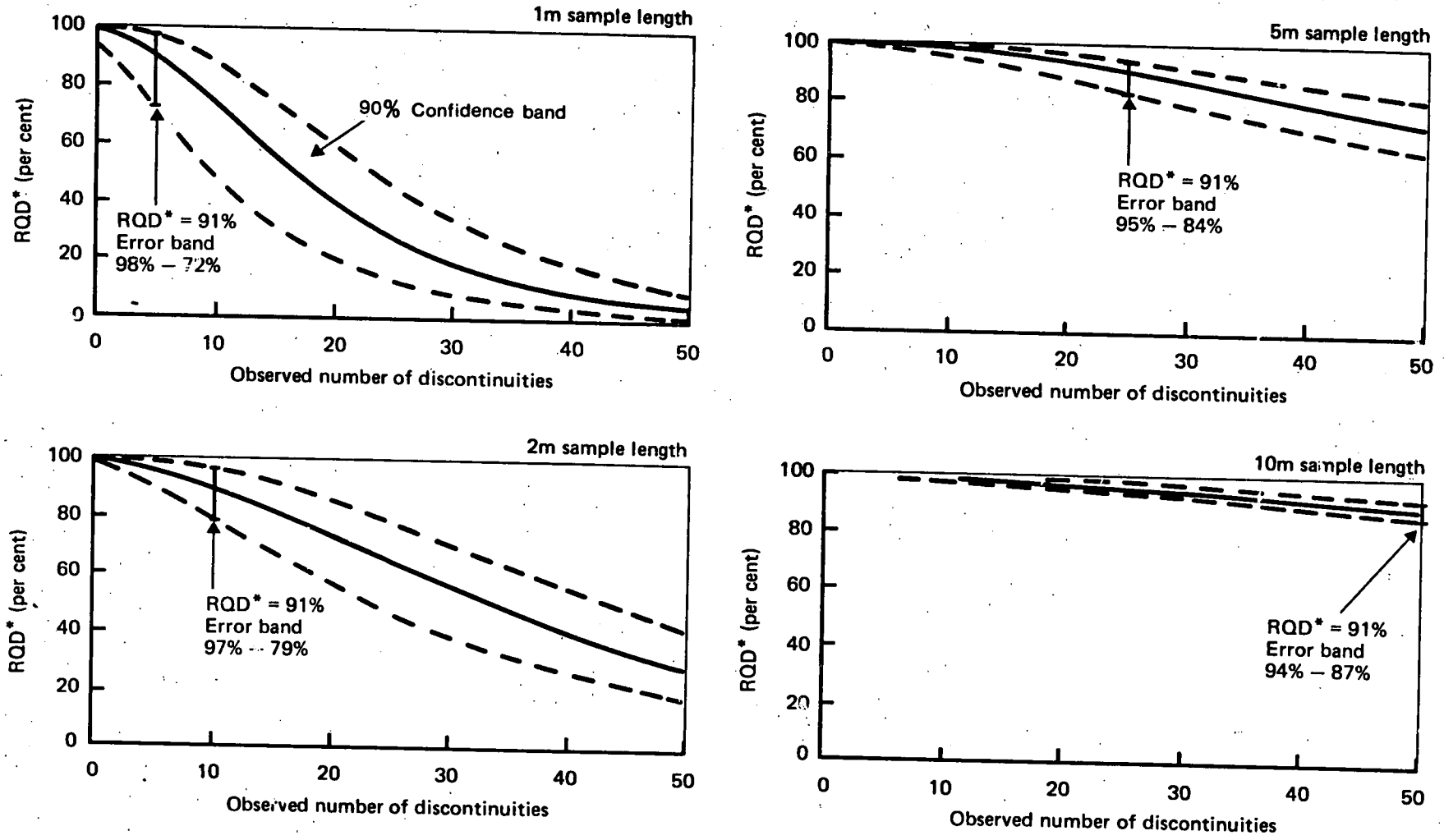

Fig. 11.4 EFFECT OF SAMPLE LENGTH ON THE RQD* ERROR BAND (90% CONFIDENCE BAND)

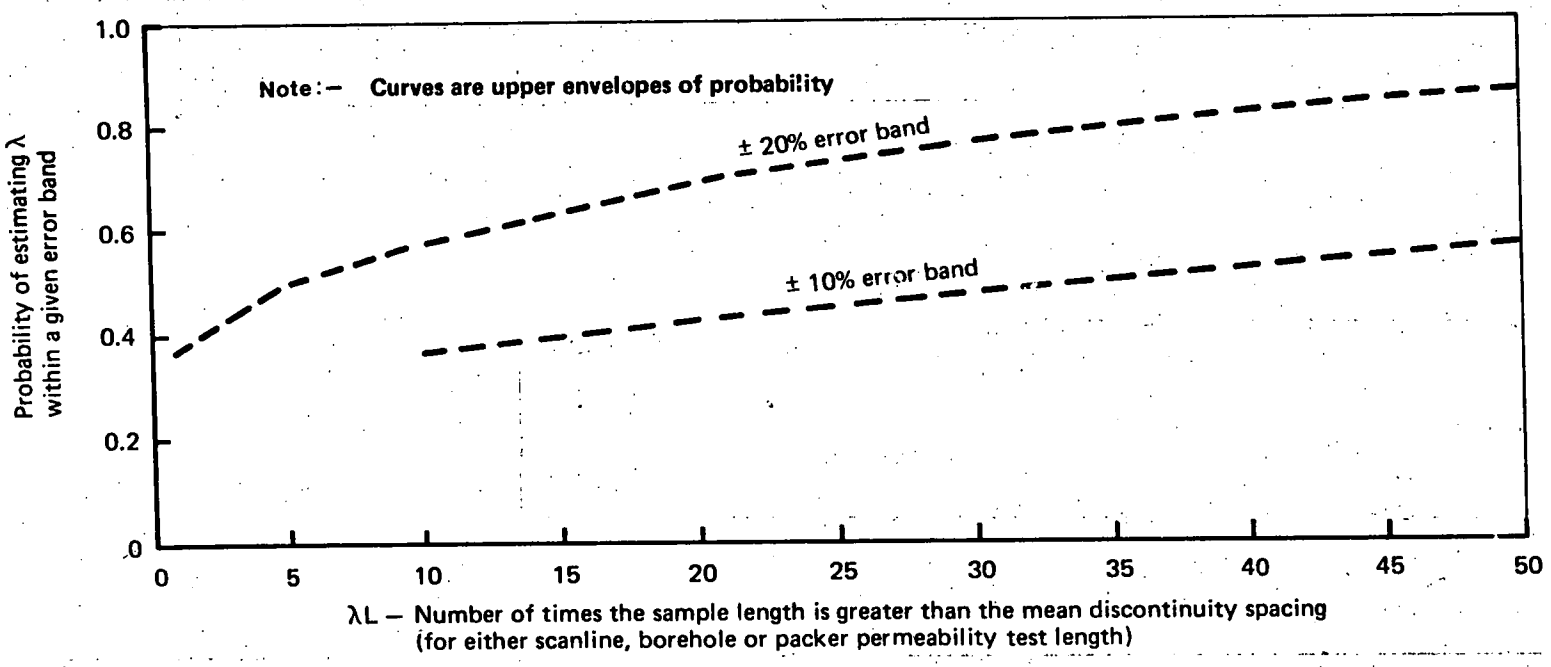

Fig. II.5 PROBABILITIES OF ESTIMATING THE DISCONTINUITY FREQUENCY (λ) TO WITHIN ±20% OR ±10% FOR DIFFERENT SAMPLE LENGTHS, FROM EQUATION L.9

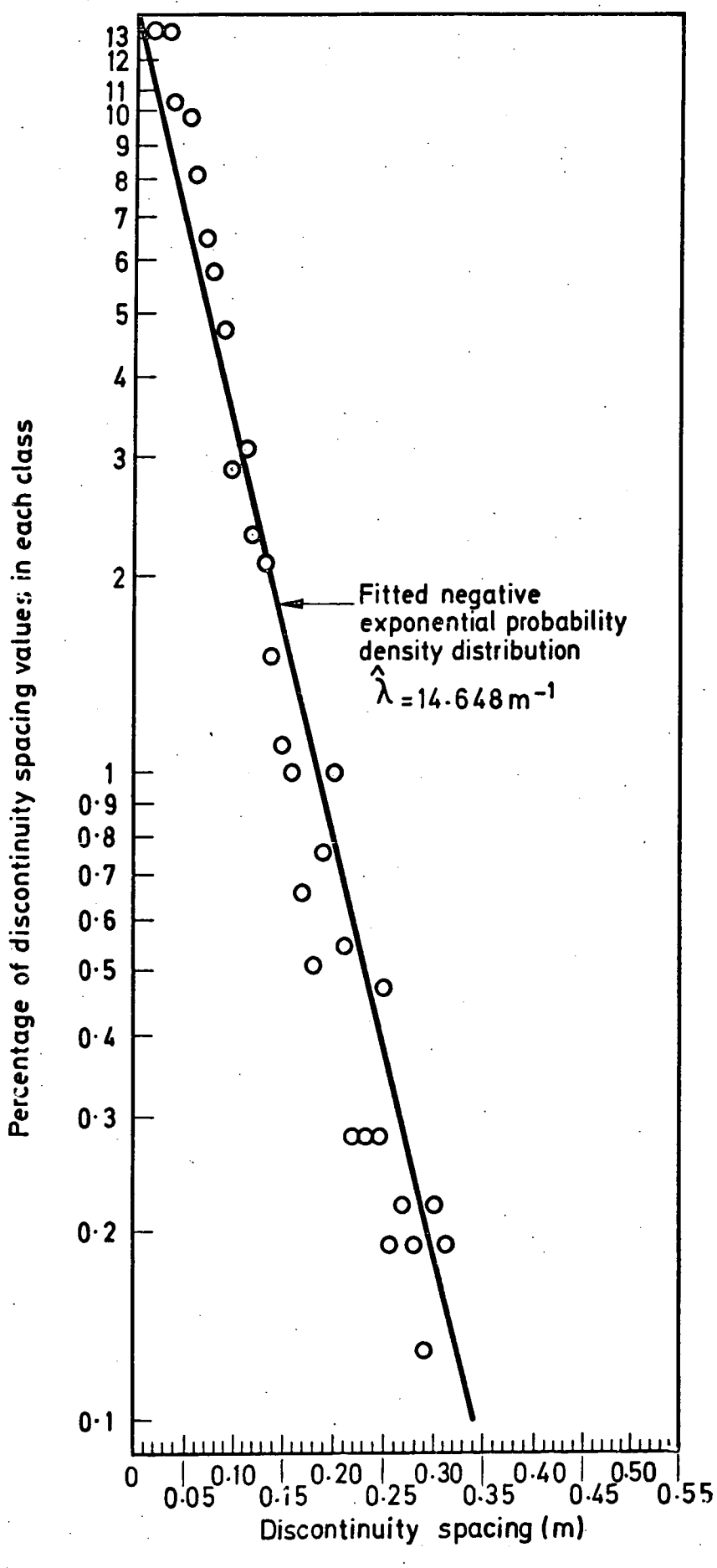

Fig. 11.6 SAMPLE PROBABILITY DENSITY DISTRIBUTION OF DISCONTINUITY SPACING VALUES, PLOTTED ON A LOGARITHMIC SCALE. SUM OF ALL SCANLINES IN THE CHINNOR QUARRY

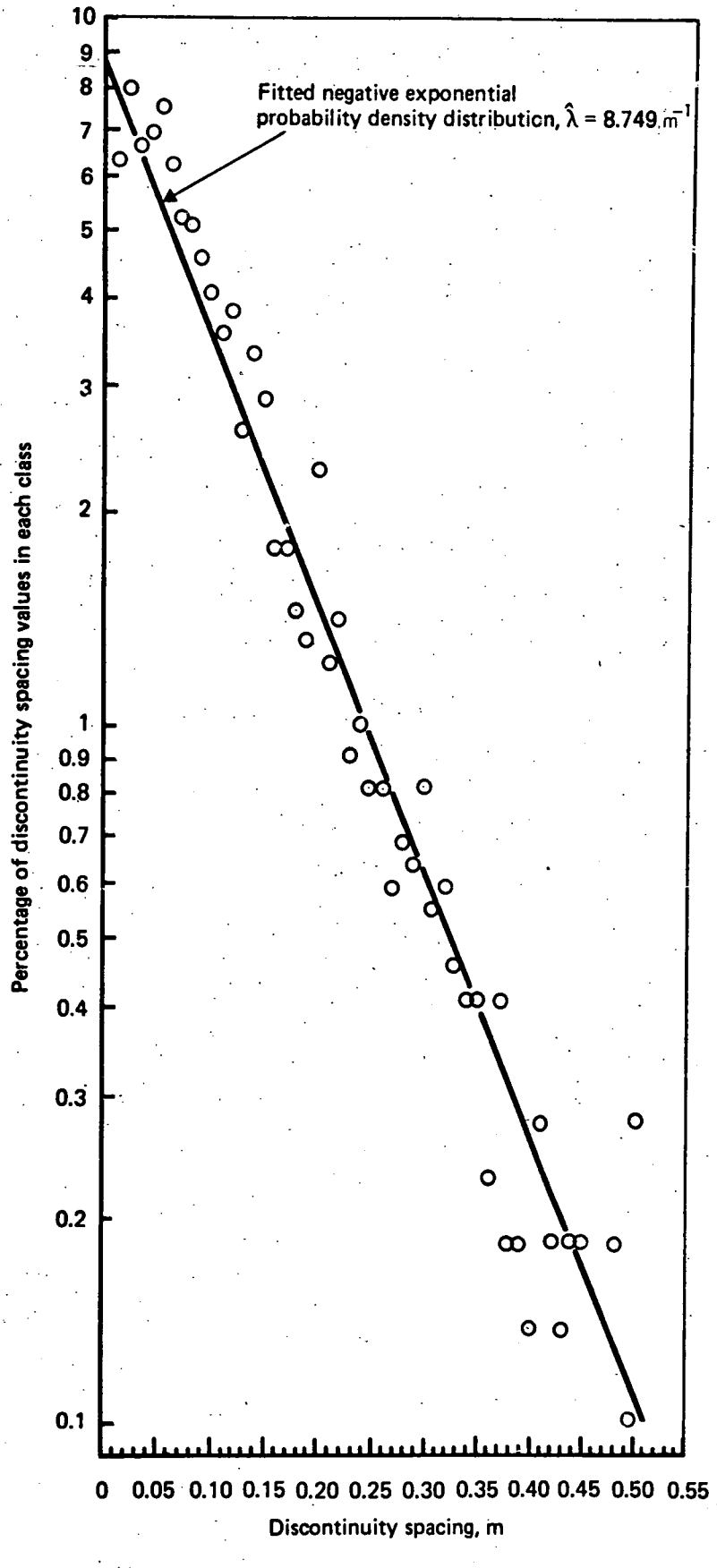

Fig. 11.7 SAMPLE PROBABILITY DENSITY DISTRIBUTION OF DISCONTINUITY SPACING VALUES, PLOTTED ON A LOGARITHMIC SCALE. SUM OF ALL SCANLINES IN THE 3m DIAMETER SHAFT.

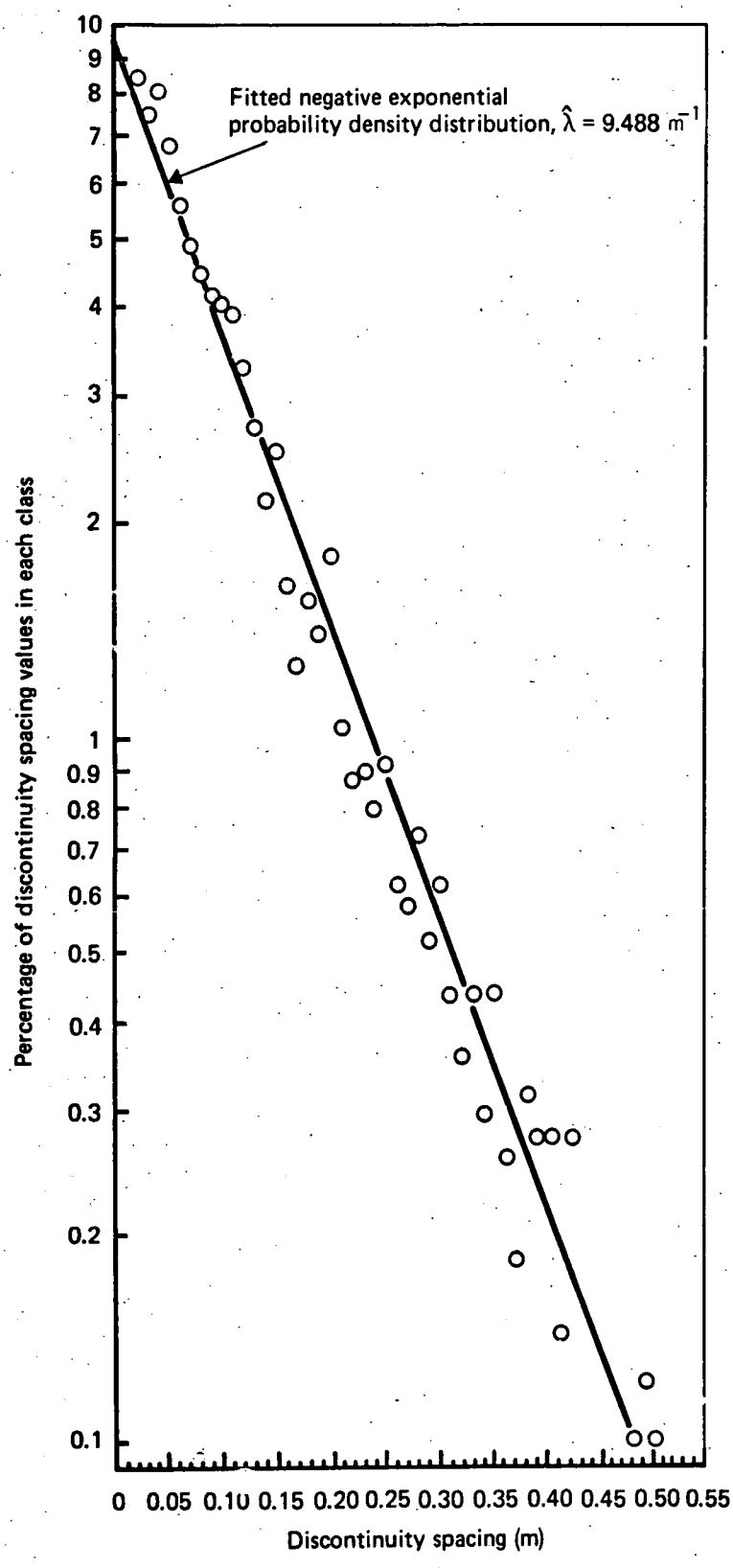

Fig. 11.8 SAMPLE PROBABILITY DENSITY DISTRIBUTION OF DISCONTINUITY SPACING VALUES, PLOTTED ON A LOGARITHMIC SCALE. SUM OF ALL SCANLINES IN FIRST 85m OF TUNNEL.

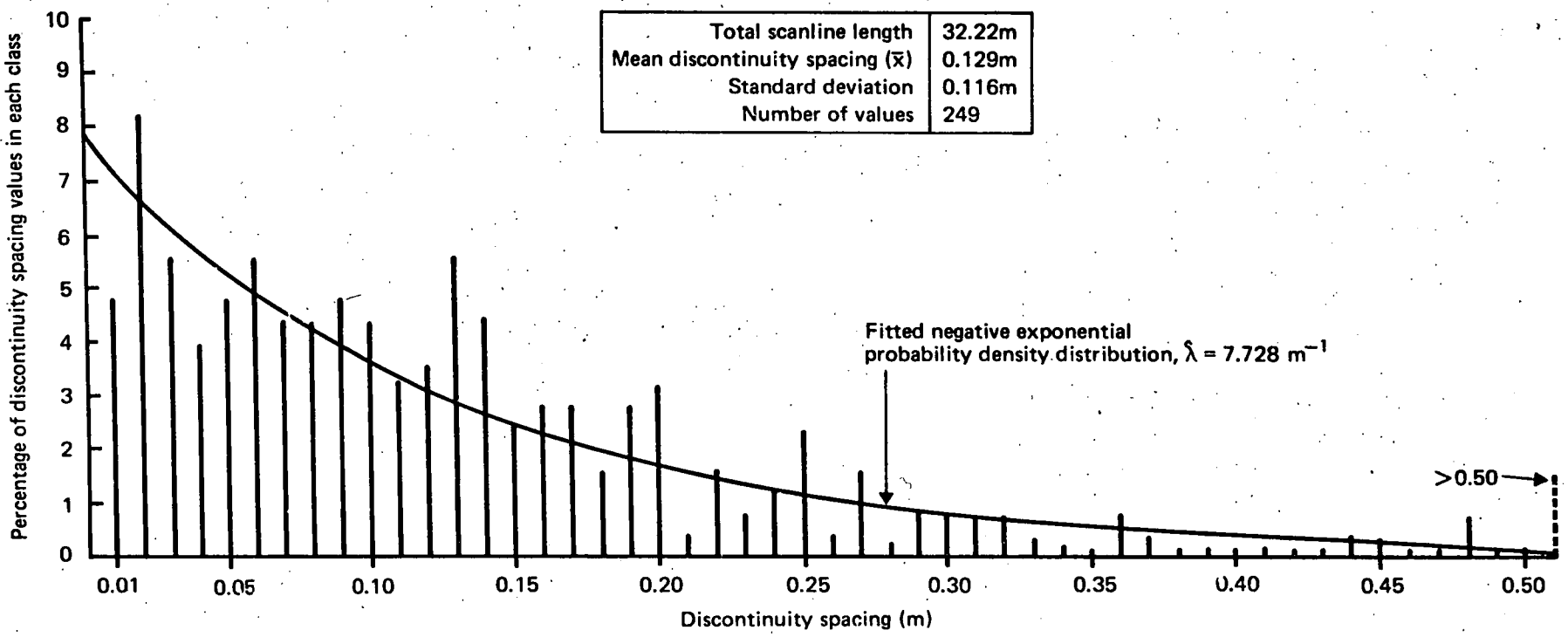

Fig.II.9 DISCONTINUITY SPACING HISTOGRAM, ROGERLEY QUARRY TUNNEL, SUM OF ALL SCANLINES IN THE SANDSTONE

Total scanline length	60.73m
Mean discontinuity spacing ($\bar{x}$)	0.033m
Standard deviation	0.032m
Number of values	1828

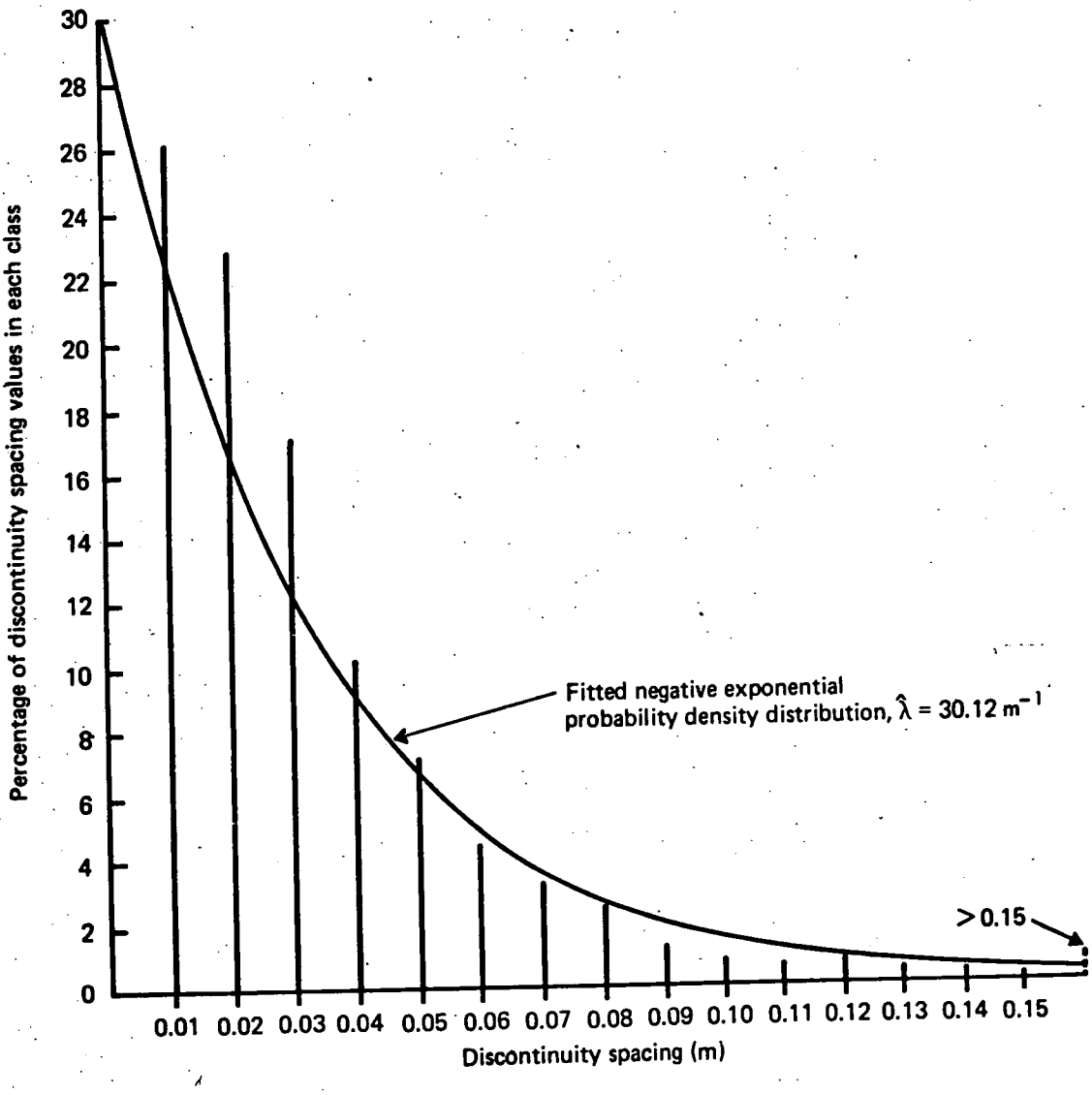

Fig. 11.10 DISCONTINUITY SPACING HISTOGRAM, ROGERLEY QUARRY TUNNEL, SUM OF ALL SCANLINES IN THE MUDSTONE

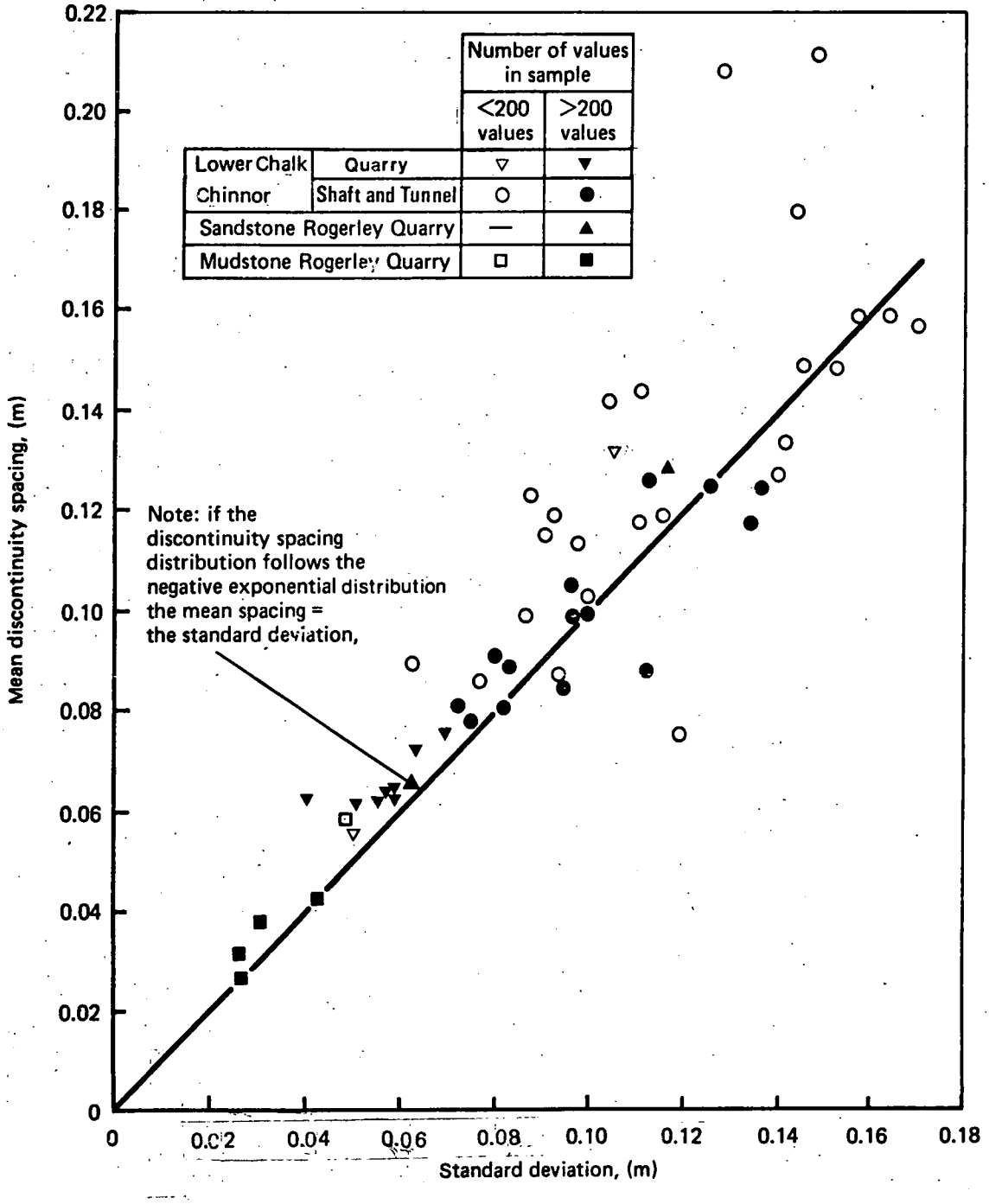

Fig 11.11 MEAN DISCONTINUITY SPACING AND STANDARD DEVIATION MEASURED AT CHINNOR, AND IN THE EXPERIMENTAL TUNNEL, ROGERLEY QUARRY

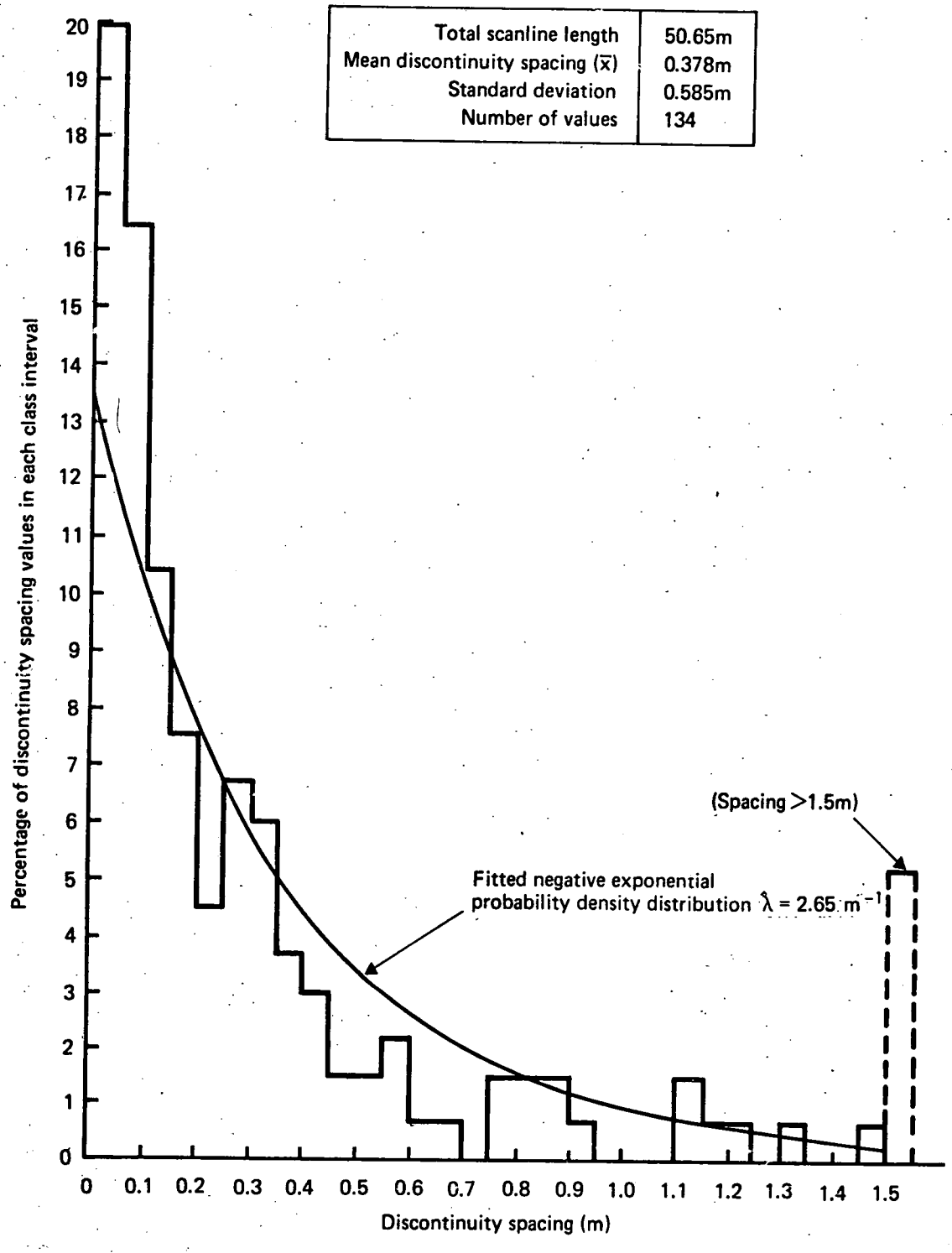

Fig. II.12 DISCONTINUITY SPACING HISTOGRAM CHANNEL TUNNEL LOWER CHALK, SUM OF VERTICAL AND HORIZONTAL SCANLINES IN THE MACHINE ERECTION CHAMBER

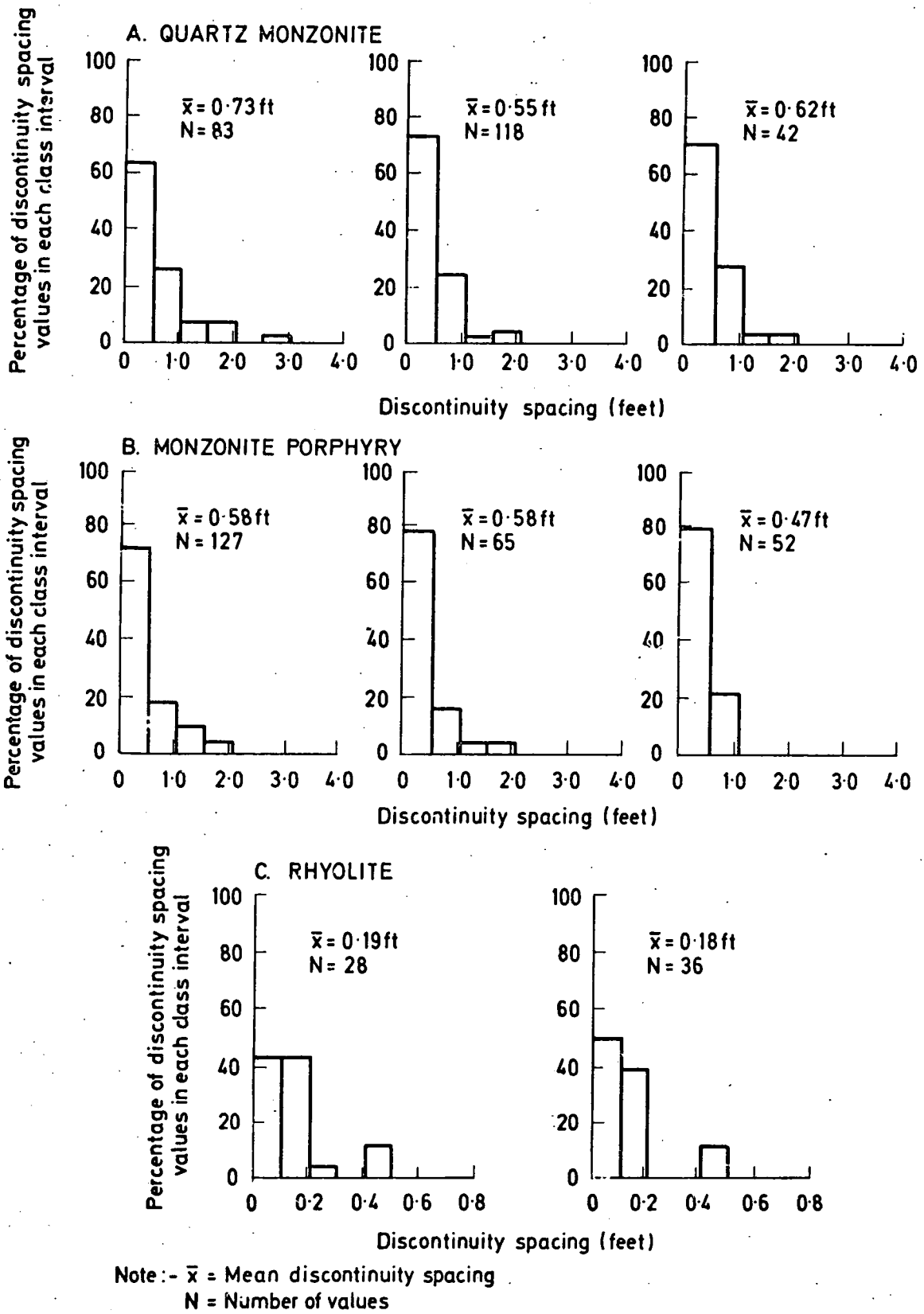

Fig. 11.13 DISCONTINUITY SPACING HISTOGRAMS OF THREE PROMINENT FRACTURE SETS IN THE SAN MANUEL COPPER MINE, ARIZONA (AFTER MAHTAB et al., 1973)

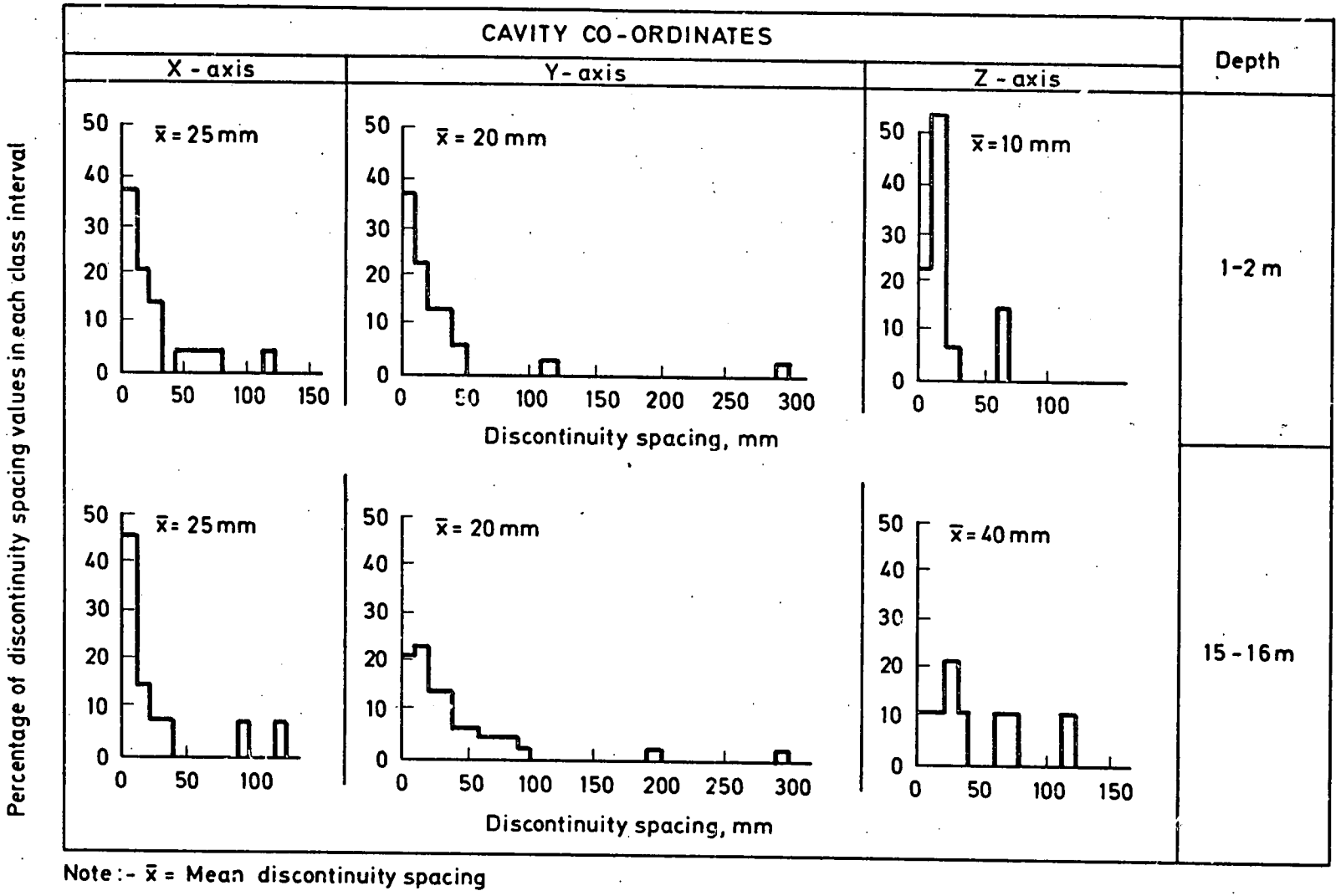

Fig. 11.14 DISCONTINUITY SPACING HISTOGRAMS; MEASUREMENTS TAKEN USING THE CAVITY TECHNIQUE IN GLACIAL TILL AT HURLFORD, AYRSHIRE (AFTER McGOWN et al. 1974)

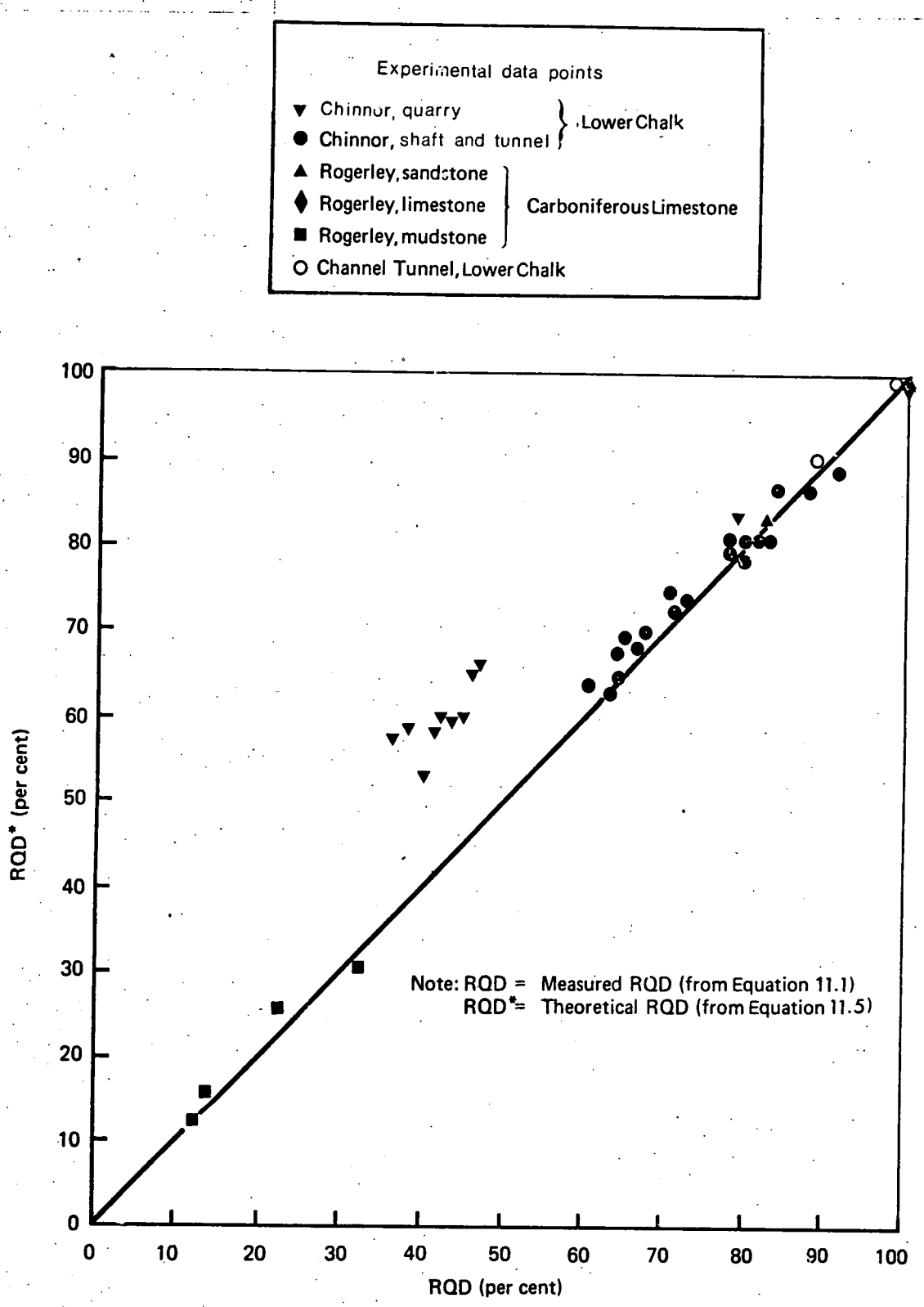

Fig. 11.15 COMPARISON BETWEEN MEASURED AND THEORETICAL RQD

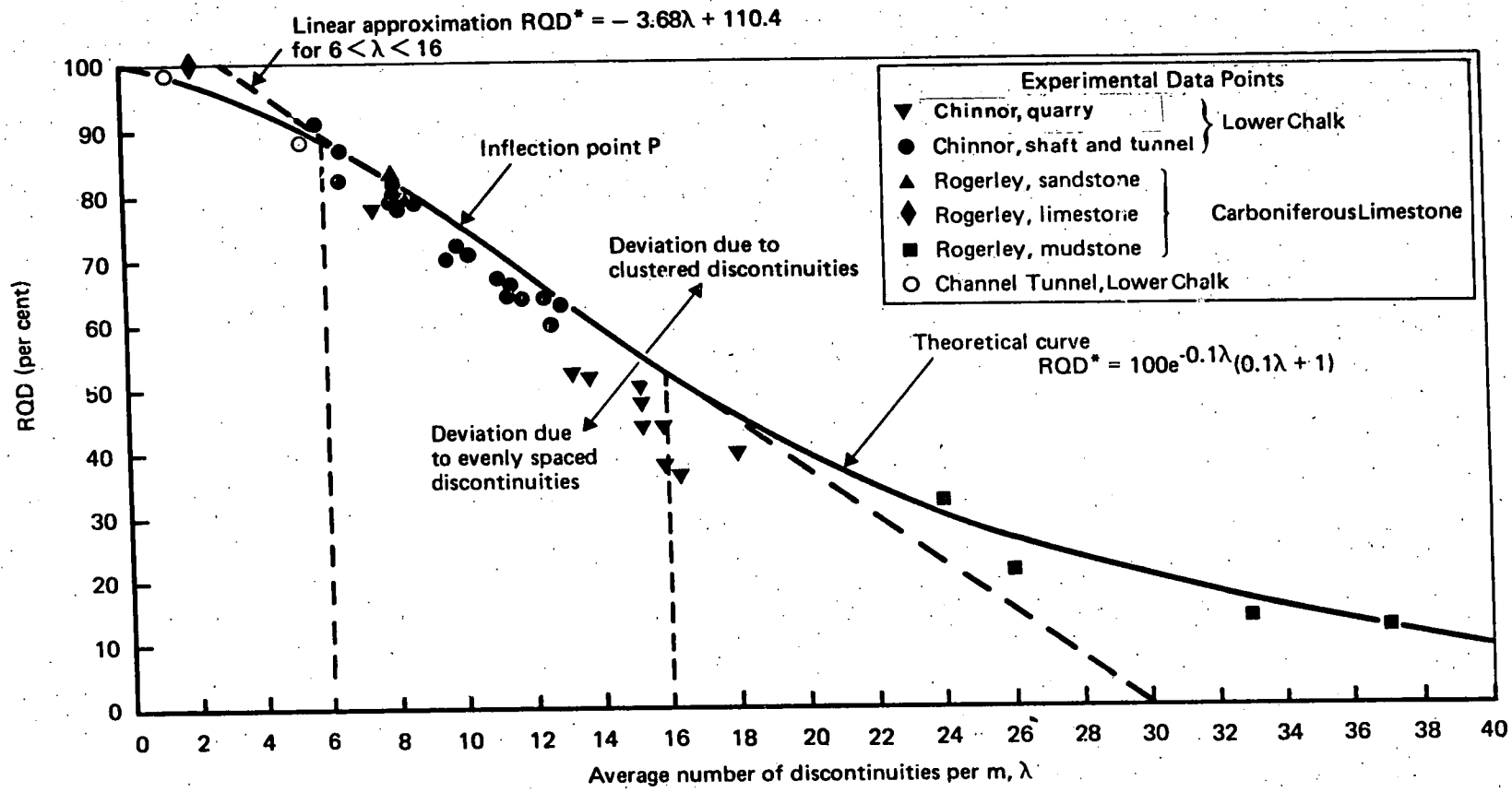

Fig. 11.16 RELATION BETWEEN RQD AND MEAN DISCONTINUITY FREQUENCY (λ)

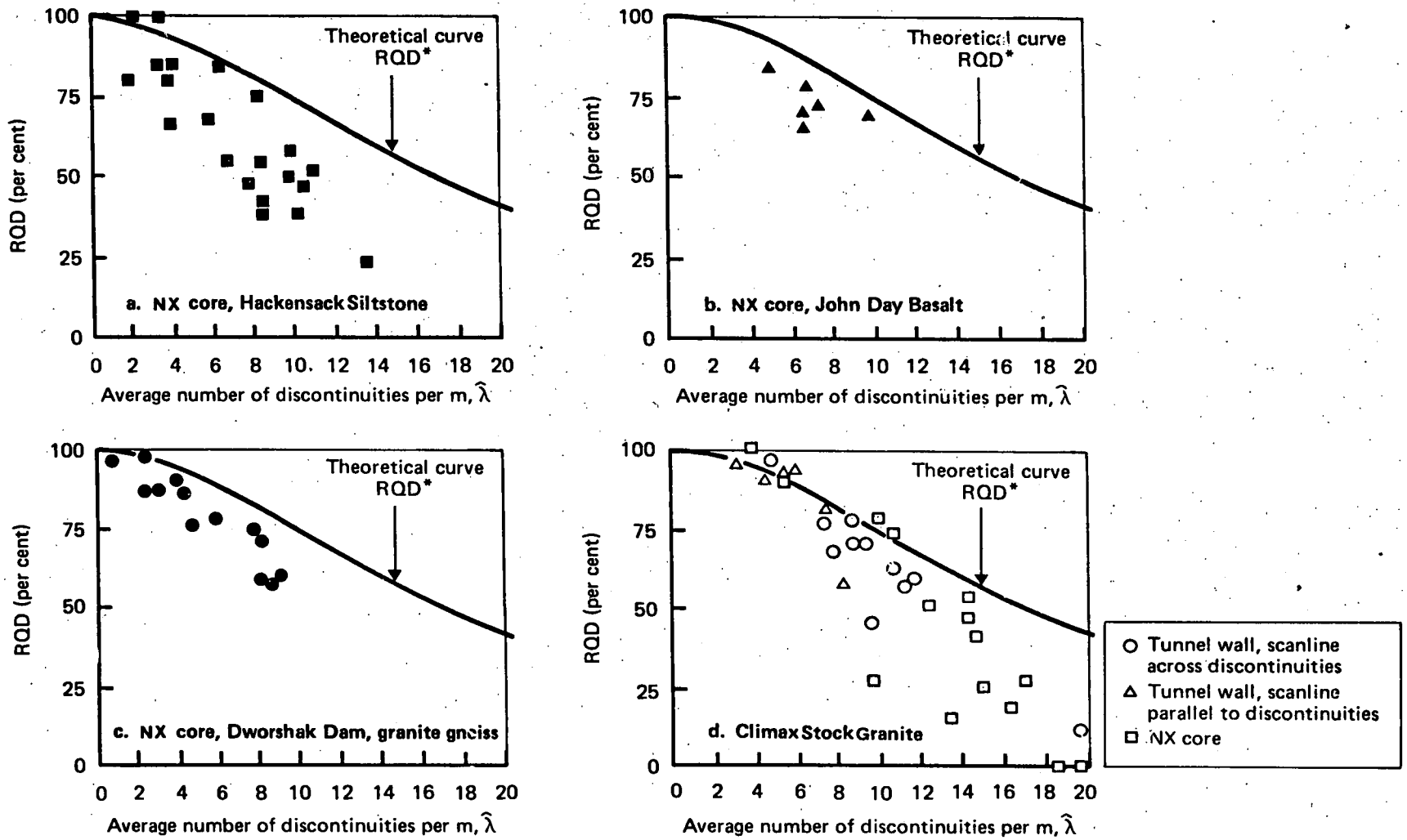

Fig. 11.17 COMPARISON BETWEEN MEASURED AND THEORETICAL RQD (RQD VALUES FROM DEERE et al.,1967)

CHAPTER 12

SUMMARY AND CONCLUSIONS, SUGGESTIONS FOR FURTHER WORK

The work described in Chapters 2 to 11 is summarised schematically in Figure 12.1. In this Figure the three main areas of study outlined in Chapter 1 are represented by the circles numbered 1, 2 and 3. The three peripheral areas of study outlined in Chapter 1 are represented by the circles numbered I, II and III. The conclusions concerning Chapters 2 to 11 will be considered in terms of these six areas of study.

12.1 Area of study 1. Evaluation of discontinuity characteristics of the chalk

Scanlines taken in orthogonal directions were found to be a quick and effective method of obtaining a largely unbiased sample of the chalk discontinuity characteristics. Where orthogonal scanlines were not of equal lengths, scanline length correction factors were applied to reduce the possibility of the introduction of bias.

Discontinuity intensity, expressed in terms of mean discontinuity spacing was found to vary with the degree of weathering. Mean spacing values in the tunnel and shaft were generally greater than 0.10m. Mean spacing values on weathered faces in the Chinnor quarry were commonly less than 0.08m. Discontinuity spacing values obtained from borehole cores were often lower than those obtained from scanlines. The apparently increased fracturing suggested by borehole cores, due to rock breakage effects during coring, underlines the problems of evaluating

the true discontinuity characteristics using boreholes. Scanline surveys in the shaft were found to predict accurately conditions actually encountered during tunnelling.

Discontinuity orientation patterns were analysed using a computer program on file at the University of Durham. At all survey locations a concentration of discontinuities dipping towards the northwest (at angles of dip ranging from 30^{o} to 70^{o}) was detected. At many locations this concentration was accompanied by poorly developed more steeply dipping concentrations dipping towards the southeast, southwest and northeast. In many cases there was a well developed sub-horizontal set of discontinuities accompanied by a more random element of discontinuity orientation.

To summarise, the chalk at Chinnor is highly fractured - cut into blocks by discontinuities of variable orientation. The chalk therefore represents a material highly susceptible to block dislocation and loosening.

Instability at the face and crown was commonly experienced during tunnel excavation; in many cases an overbeak exceeding 1.5m developed. The problems of instability in the discontinuous chalk, largely due to the effects outlined in the previous paragraph, were examined in terms of tunnel stability indices. Examination of conditions actually encountered during tunnelling indicated that tunnel instability was experienced when the appropriate stability index fell below a critical level of, in the case of the 5m diameter tunnel at Chinnor, 0.2m.

12.2 Area of study 2. Geotechnical aspects of tunnelling in discontinuous rock

In the previous Section, the discontinuous nature of the chalk was examined. In addition, the contribution of the discontinuities to problems of instability in the tunnel was noted.

Theoretical finite element stress analyses proved that considerations of intact rock strength are of minor importance when examining the stability of the tunnel at Chinnor. The analyses also showed that theoretical stress magnitudes near to the tunnel are largely influenced by the applied K_o factor, whilst theoretical ground movements are mainly controlled by the deformation modulus modelled in the analyses. The deformation modulus is expressed in terms of a modulus reduction factor (J_a) equal to the input modulus divided by the intact modulus obtained from laboratory tests. Total ground settlements actually measured at Chinnor were found to be between 8 and 15 times the settlements predicted by a finite element analysis adopting $J_a = 1.0$. Modulus reduction factors of between 0.05 and 0.07 were required to match actual and theoretical settlements at selected distances from the tunnel crown. Modulus reduction factors of between 0.07 and 0.20 were required to match actual and theoretical horizontal strain profiles at the ground surface.

Following passage of the tunnel face, significant permanent movements along discontinuities, as monitored in a trench excavated across the tunnel line, were observed. Deformation of intact elements of rock was small compared with that observed along discontinuities. It

is suggested that the need for a modulus reduction factor to model the behaviour of the ground near the tunnel at Chinnor is a result of loosening and dislocation along discontinuities, stimulated by the tunnelling operations.

It is likely that the ground disturbance caused by tunnelling in discontinuous rock at shallow depths using the methods adopted at Chinnor could cause appreciable damage to weak or sensitive surface structures. For a tunnel below the water table serious water in-flow problems could be encountered as a result of increased permeability caused by the block loosening effects.

12.3 Area of study 3. Discontinuity spacings in rock

Examination of the literature (Chapter 1) and experience at Chinnor have proved that the spacing of discontinuities in a rock mass, and in particular the relation between discontinuity spacing and tunnel diameter, critically control the behaviour of ground in response to tunnel excavation. By considering the possible distributions of discontinuity spacings along a straight line through a rock mass the characteristics of evenly spaced, clustered and randomly positioned discontinuities were examined from a theoretical standpoint. Analysis of field results obtained from scanline measurements indicated that a negative exponential distribution of discontinuity spacing values is a good approximation for all available data.

Using the negative exponential distribution of discontinuity spacing values a relation was established between the theoretical Rock

Quality Designation (RQD*) and the average number of discontinuities per metre (λ):

$$RQD^* = 100\, e^{-0.1\lambda}(0.1\lambda + 1)$$

The theoretical approach underlines the limitations of the conventional RQD. To overcome these limitations a two-tier RQD is advocated in which two threshold values are adopted: 0.1m - the conventional RQD used in the above Equation, and 1.0m - substituted for 0.1 in the above Equation. If desired, however, rock quality can be summarised in terms of the single parameter λ.

The theoretical examination of discontinuity spacings allows a rigourous approach to be adopted when considering sample size in discontinuity surveys. It was found that to estimate the number of discontinuities per metre to within a reasonable precision requires a scanline at least fifty times the mean discontinuity spacing. Theoretical considerations of sampling factors in terms of the negative exponential distribution can be extended for use in the fields of packer permeability testing and rock-bolting.

Conclusions concerning the three peripheral areas of study (I, II and III) outlined in Figure 12.1 were presented at the ends of Chapters 4, 6, 9 and 10.

12.4 Suggestions for further work

The work described in this thesis is essentially a detailed case history that should only be viewed in the broader context of tunnel

engineering. It is hoped, however, that some of the research methods adopted at Chinnor will provide useful guidelines for further work. In particular it is recommended that discontinuity surveys, adopting the scanline technique, be undertaken to test the wider applicability of the negative exponential distribution to other rocks. This work could help to establish a firmer experimental basis for the concept of the theoretical RQD.

It is also felt that examination of the concept of the rock mass modulus reduction factor, in terms of rock quality and ground stress configurations, will provide a fruitful line of research. The use of large scale *in situ* tests in fractured ground, using flat-jacks, could form an integral part of a research programme along these lines. When considering the modulus reduction factor in the context of tunnelling it is important to evaluate the control exerted by the excavation and support methods on ground behaviour, and thereby to examine the relation between the modulus reduction factor, ground properties and tunnelling methods. Research techniques used and proved effective at Chinnor could be adopted in this work.

Ultimately it is desirable to collect a body of data concerning the behaviour of tunnels constructed in a variety of ground conditions, and thereby evaluate the various geotechnical aspects of tunnelling in discontinuous rock. In this way excavation and support techniques adopted in tunnel construction could be designed to suit known ground conditions and expected ground behaviour. It is clear that an important part of any such system is the evaluation of ground conditions prior to

tunnel excavation. It is recommended that the orthogonal scanline survey technique be adopted to obtain an unbiased three-dimensional characterisation of discontinuity properties to establish in numerical terms the relation between discontinuity intensity and excavation size. The results of the scanline surveys, conducted on exposed faces or in shafts, should be considered in terms of the theoretical approaches described in Chapter 11 and used to calibrate the results of any site investigation programme based on borehole sampling along the tunnel route.

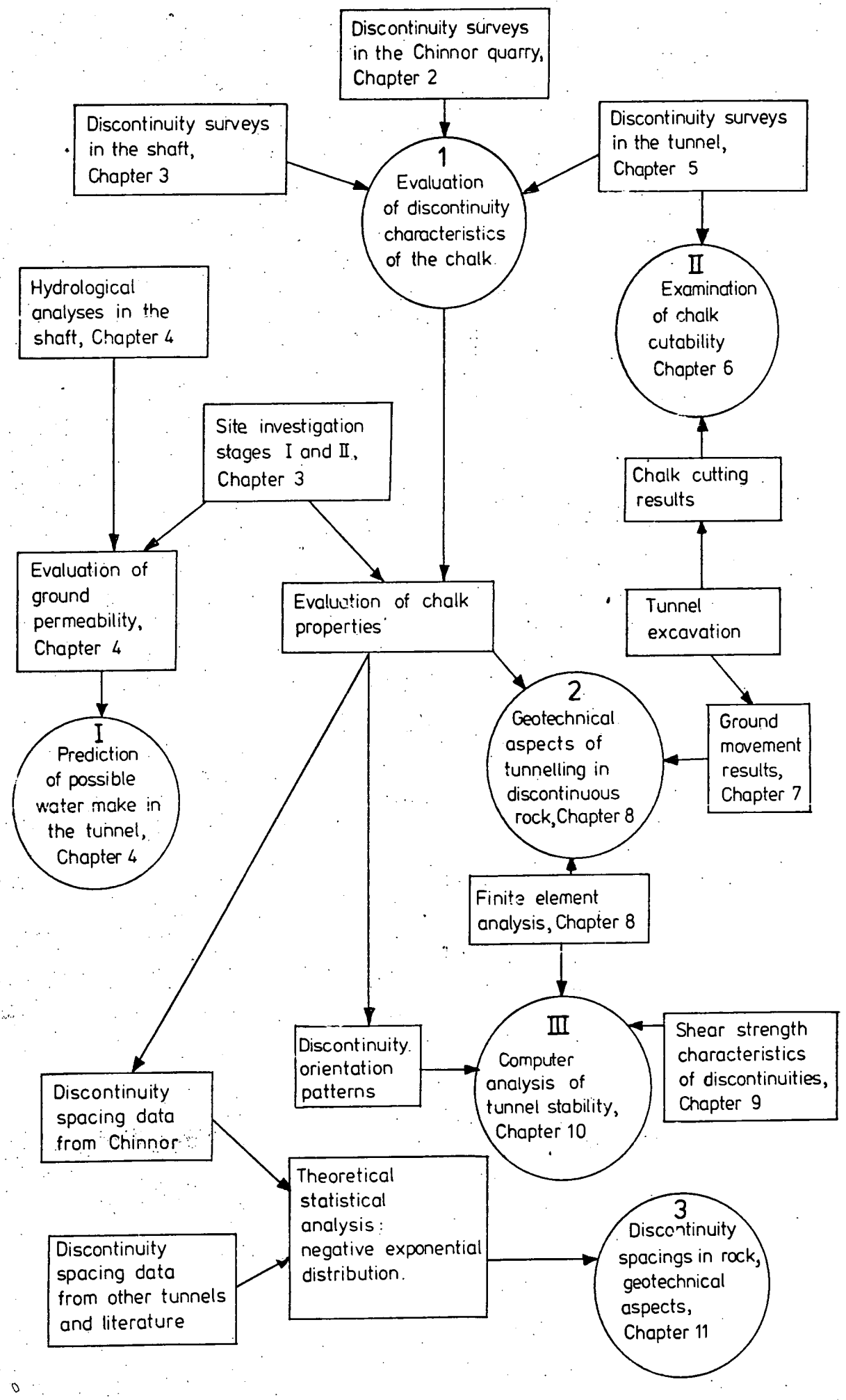

Fig. 12.1 SUMMARY OF WORK IN CHAPTERS 2 TO 11

LIST OF REFERENCES

Abel, J.F. and Lee, F.T.	1973	Stress changes ahead of an advancing tunnel. Int. J. Rock Mech, Min. Sci. & Geomech. Abstr. v. 10, pp 673-697.
Attewell, P.B.	1975	Personal communication
Attewell, P.B. and Farmer, I.W.	1974 a	Ground deformation resulting from shield tunnelling in London Clay. Canadian Geotechnical Journal, v.11, No.3, pp 380-395.
Attewell, P.B. and Farmer, I.W.	1974 b	Ground disturbance caused by shield tunnelling in a stiff, overconsolidated clay, Engineering Geology, v.8, pp 361-381
Attewell, P.B. and Woodman, J.P.	1971	Stability of discontinuous rock masses under polyaxial stress systems. 13th Symposium on Rock Mechanics. Stability of Rock Slopes. ASCE. pp 665-683.
Bartlett, J.V., Biggart, A.R. and Triggs, R.L.	1973	The bentonite tunnelling machine. Proc. Inst. Civ. Eng., Part 1 Design and Construction, v.54, Paper 7670, pp 605-624.
Barton, N., Lien, R. and Lunde, J.	1974	Analysis of rock mass quality and support practice in tunnelling, and a guide for estimating support requirements. Norwegian Geotechnical Institute. Internal report, 74 p.
Bieniawski, Z.T.	1971	Mechanics of jointed rock masses. CSIR Report MEG 998, 42 p.
Bieniawski, Z.T.	1973	Engineering classification of jointed rock masses, The Civil Engineer in South Africa v.15, No. 12, pp 335-343.
Boyd, J.M.	1975	Analysis of surface roughness - Part 1, Imperial College of Science and Technology, Research report No. 30 47 p.
Braybrooke, J.C.	1966	The Strength effects and measurement of discontinuities in rock masses, M.Sc. Dissertation, University of London.
British Association Mathematical Tables,	1937	Bessel Functions of Orders Zero and Unity v.6, Part 1, University Press, Cambridge.

Broch, E. and Franklin, J.A. 1972 The point load test Int. J. Rock Mech. Min. Sci, & Geomech. Abstr. v.9, pp 669-697.

Bruckshaw, J.M., Goguel, J., Harding, H.J.B. and Malcor, R. 1961 The work of the Channel Tunnel Study Group, 1958-1960. Proc. Inst. Civ. Engs. v.18, pp 149-178.

Calvert, S.E. 1974 Deposition and diagenesis of silica in marine sediments. Spec. Publs. Int. Ass. Sediment. v.1, pp 273-299

Cecil, O.S. 1970 Correlations of rock bolt-shotcrete support and rock quality parameters in Scandinavian tunnels. Ph.D. thesis, University of Illinois, Urbana.

Channel Tunnel Study Group 1965 Site Investigations in the Strait of Dover, 4 volumes, 6 appendices.

Coates, D.F. 1964 Classification of rocks for rock mechanics, Int. J. Rock Mech. Min. Sci., v.1 pp 421-429

Coates, D.F. 1970 Rock Mechanics Principles Mines Branch Monograph 874, Department of Energy, Mines and Resources. Ottawa. 363p.

Cording, E.J. and Mahar, J.W. 1974 The effect of natural geologic discontinuities on behaviour of rock in tunnels. Proc. 2nd, North American Rapid Excavation and Tunnelling Conference, AIME v.1, Chapter 12, pp 107-133

D'Andrea, D.V., Fischer, R.L. and Fogelson, D.E. 1965 Prediction of compressive strength from other rock properties. U.S. Bureau of Mines Report of Investigations 6702. 23p.

Deere, D.U. 1964 Technical description of rock cores for engineering purposes, Rock. Mech. Eng. Geol. v.1, pp 17-22

Deere, D.U. 1968 Geological Considerations, in Rock Mechanics in Engineering Practice Eds. Stagg, K.G. and Zienkiewicz, O.C., John Wiley and Sons, London. pp 1-20.

Deere, D.U., Hendron, A.J., Patton, F.D. and Cording, E.J. 1967 Design of surface and near surface construction in rock, in Failure and Breakage of Rock, Ed. C. Fairhurst, AIME, New York, pp 237-302.

Deere, D.U., Peck, R.B., Monsees, J.E. and Schmidt, B. 1969 Design of tunnel liners and support systems - Final Report to Office of High Speed Ground Transportation, US Dept of Transportation, Contract No. 3-0152.

Edmunds, W.M., Lovelock, P.E.R. and Gray, D.A. 1973 Interstitial water chemistry and aquifer properties in the Upper and Middle Chalk of Berkshire, England. Journal of Hydrology v.19 pp 21-31

Einstein, H.H., Bruhn, R.W. and Hirschfeld, R.C. 1970 Mechanics of jointed rock-experimental and theoretical studies. MIT Research Report R70-62, Interim Report to Office of High Speed Ground Transportation US Dept of Transportation. 116p.

Einstein, H.H. and Hirschfeld, R.C. 1973 Model studies on Mechanics of jointed rock. Journal of the Soil Mechanics and Foundations Division, ASCE, No. SM 3, Proc. Paper 9610, pp 229-248.

Fairhurst, C. 1969 Foreword in Fundamentals of Rock Mechanics, Jaeger, J.C. and Cook, N.G.W. Publ. Methuen, London. 513 p.

Fookes, P.G. and Dennes:, B. 1969 Observational studies on fissure patterns in Cretaceous sediments of south-east England, Géotechnique, v.19, No. 4, pp 493-497.

Foster, S.S.D. 1974 Groundwater storage - riverflow relations in a Chalk catchment, Journal of Hydrology, v.23, pp 299-311.

Foster, S.S.D. and Milton, V.A. 1974 The permeability and storage of an unconfined Chalk aquifer Hydrological Sciences Bulletin, v.19, No. 4, pp 485-500.

Franklin, J.A. 1970 Observations and tests for engineering description and mapping of rocks, Proc. 2nd Congress of ISRM, Belgrade, v.1, paper 1-3. pp 11-16.

Garwood, F. 1936 Fiducial limits for the Poisson distribution. Biometrika, v.28, Parts 3 and 4, pp 437-442.

Goodman, R.E. 1970 The deformability of joints. In Determination of the *In Situ* Modulus of Deformation of Rock, ASTM, Special Technical Publication, No. 477, pp 174-196.

Goodman, R.E. and Duncan, J.M. 1969 The role of structure and solid mechanics in the design of surface and underground excavations in rock. Proc. Int. Symp. on Structures, Solid Mech. and Engng. Design, Southampton. Paper No. 112, John Wiley and Sons, London.

Hansmire, W.H. and Cording, E.J. 1972 Performance of a soft ground tunnel on the Washington Metro. Proc. 1st North American Rapid Excavation and Tunnelling Conference, AIME, v.1, Chapter 23 pp 371-389.

Heuzé, F.E., Goodman, R.E. and Bornstein, A. 1971 Numerical analyses of deformability tests in jointed rock - "joint perturbation" and "no tension", finite element solutions. Rock Mechanics v.3, pp 13-24.

Higginbottom, I.E. 1966 The engineering geology of Chalk. Proceedings of the Symposium: Chalk in earthworks and foundations. Institution of Civil Engineers. Session A, paper 1, pp 1-13.

Hignett, H.J. 1974 Laboratory and pilot scale studies related to the design of tunnel boring machines, M.Sc Thesis, University of Newcastle upon Tyne. 101p.

Hignett, H.J. 1975 Personal communication.

Hignett, H.J. and Boden, J.B. 1974 Chinnor tunnelling trials - background and progress. Tunnels and Tunnelling v.6, No. 6 pp 65-70.

Hobbs, N.B. 1973 Effects of non-linearity on the prediction of settlements of foundations on rock. Q. Jl. Engng. Geol v.6 pp 153-158.

Hobbs, N.B. 1974 The prediction of settlement of structures on rock (with particular reference to the Chalk and Trias). Conference on Settlement of Structures, Session 4 - Rocks. 38p.

Hoek, E. 1970 Estimating the stability of excavated slopes in opencast mines. Trans. Inst. Min. Metall. Section A. v.79, No.767, pp 109-132.

Hoek, E. and Bray, J.W. 1974 Rock Slope Engineering publ. Inst. Min. Metall., London, 309p.

Hoek, E., Bray, J.W. and Boyd, J.M. 1973 The stability of a rock slope containing a wedge resting on two intersecting discontinuities. Q.Jl. Engng. Geol. v.6, pp 1-55.

Hudson, J.A. and Drew, S.D. 1975 An impact penetrometer for assessing the cutability of soft rocks. In preparation.

Hudson, J.A., and McCaul, C.	1975	Influence of tunnel excavation on an adjacent shaft in chalk. In preparation.
Ineson, J.	1962	A hydrogeological study of the permeability of the Chalk, Journ. Instn. of Water Engrs. v. 16 pp 449-463.
Jaeger, J.C. and Cook, N.G.W.,	1969	Fundamentals of Rock Mechanics, publ. Methuen, London 513p.
Jennings, J.E.	1968	A preliminary theory for the stability of rock slopes based on wedge theory and using results of joint surveys, University of the Witwatersrand, Internal Report (un-published).
John, M.	1971	Properties and classification of rock with reference to tunnelling. CSIR Report MEG 1020, 54p.
Kirkham, D.	1954	Measurment of the hydraulic conductivity of soil in place. ASTM. Special Technical Publication No. 163. pp 80-97.
Lang, T.A.	1957	Rock behaviour and rock bolt support in large excavations, Symposium on Underground power plants, ASCE, October Convention, New York.
Lang, T.A.	1959	Underground experience in the Snowy Mountains - Australia, in Proceedings of the Second Protective Construction Symposium (Deep Underground Construction), RAND Corporation, Santa Monica, 988p.
Lauffer, H.	1960	Die Neuere entwicklung der stollenbautechnik, Osterr. Ingenieur Zeitschrift, v.3, pp 13-24.
Lindley, D.V.	1965	Introduction to Probability and statistics; Part 1 - Probability. publ. Cambridge University Press. 259p.
Locher, H.G.	1970	Some results of direct shear tests on rock discontinuities. Proc. Int. Symp. on Rock Mech. Madrid. pp 171-173.

Mahtab, M.A., Bolstad, D.D. and Kendorski, F.S. 1973 Analysis of the geometry of fractures in San Manuel Copper Mine, Arizona. U.S. Department of the Interior, Bureau of Mines RI7715, 24p.

McCaul, C., Morgan, J.M. and Boden, J.B. 1975 Ground movement around an experimental tunnel in Chalk. In preparation.

McGown, A., Saldivar-Sali, A. and Radwan, M. 1974 Fissure patterns and slope failures in till at Hurlford, Ayrshire, Q. Jl. Engng. Geol. v.7, pp 1-26.

National Coal Board 1966 Subsidence Engineers Handbook, N.C.B. Production Department, Doncaster.

Obert, L. and Rich, C. 1971 Classification of rock for engineering purposes. Proceedings of the First Australia - New Zealand Conference on Geomechanics, Melbourne, v.1 pp. 435-441.

O'Reilly, M.P. and Munton, A.P. 1972 Prospects of urban highways in tunnels. Proceedings of the Transportation Engineering Conference. Institution of Civil Engineers, London. paper 7, pp 69-83.

Patton, F.D. 1966 Multiple modes of shear failure in rock. Proc. 1st Congress Int. Soc. Rock Mech., Lisbon, v.1 pp 509-513.

Pearson, E.S. and Hartley, H.O. 1954 Biometrika Tables for Statisticians, Vol I. Cambridge University Press.

Piteau, D.R. 1970 Geological factors significant to the stability of slopes cut in rock. Proceedings of the Open Pit Mining Symposium. S. Afr. Inst. Min. Metall. pp 33-53.

Piteau, D.R. 1973 Characterizing and extrapolating rock joint properties in engineering practice, Rock Mechanics. Suppl. 2, pp 5-31.

Priest, S.D. and Hudson, J.A. 1975 a Shafts for site investigation: a case study in Chalk. In preparation.

Priest, S.D. and Hudson, J.A. 1975 b Discontinuity spacings in rock. In press.

Priest, S.D. and Hudson, J.A. 1975 c Rock quality in the Kielder Experimental Tunnel, Co. Durham. In press.

Proctor, R.J. 1971 Mapping geological conditions in tunnels. Bulletin of the Association of Engineering Geologists, v.8, No.1, pp 1-43.

Roberts, R.G. 1970 Finite element analysis of tunnel stability. M.Sc. Dissertation, Advanced Course in Engineering Geology, University of Durham.

Robertson, A. Mac G. 1974 Joints and gouge materials - their importance and testing. Tunnelling in Rock Ch. 8, Ed. Bieniawski Z.T. Pretoria. 468p.

Romero, S.U. 1968 *In situ* direct shear tests on irregular surface joints filled with clayey material. Proc. Int. Symp. on Rock Mech. Madrid, pp 189-194.

Roxborough, F.F. 1969 Rock cutting research for the design and operation of tunnelling machines, Tunnels and Tunnelling, v.1, No. 3 pp 125-128.

Roxborough, F.F. and Rispin, A. 1972 The mechanical cutting characteristics of the Lower Chalk. Report to the Transport and Road Research Laboratory (D.O.E.) 196p.

Roxborough, F.F. and Rispin, A. 1973 The mechanical cutting characteristics of the Lower Chalk, Tunnels and Tunnelling v.5, No.1 pp 45-67.

Sapegin, D.D. and Karpov, N.M. 1969 Determination of the deformability characteristics of a fissured rock massiff considered as a medium composed of blocks. Izvestiya Vniig Energiya. v.89, pp 63-69.

Singh, B. 1973 Continuum characterization of jointed rock masses. Int. J. Rock Mech. Min. Sci. & Geomech. Abstr. v.10, pp 311-335.

Skempton, A.W., Schuster, R.L. and Petley, D.J. 1969 Joints and fissures in the London Clay at Wraysbury and Edgware. Géotechnique, v.19, No. 2 pp 205-217.

Snow, D.T. 1968 Rock fracture spacings, openings and porosities. Journal of the Soil Mechanics and Foundations Division, ASCE, v.94 SM1 Proc. Paper 5736, pp 73-91.

Snow, D.T.	1970	The frequency and apertures of fractures in rock. Int. J. Rock Mech. Min. Sci. v.7 pp 23-40.
Sowers, G.F.	1962	Foundation Engineering, Ed. Leonards, G.A., McGraw-Hill, New York, 525p.
Spangler, M.G.	1951	Soil Engineering, International Textbook Co., Scranton, Pa., Chapter 10. pp 124-141.
Széchy, K.	1970	The Art of Tunnelling. Akadémiai Kiadó. Budapest. 891p.
Terzaghi, K.	1946	Rock defects and loads on tunnel supports in: Rock Tunnelling with Steel Supports by Proctor, R.V. and White T.L. The Commercial Shearing and Stamping Co., Youngstown, Ohio. pp 19-99.
Terzaghi, R.D.	1965	Sources of error in joint surveys. Géotechnique. v.15. No.3, pp 287-304.
Timoshenko, S. and Goodier, J.	1951	Theory of Elasticity, publ. McGraw-Hill, New York. 567p.
Trollope, D.H.	1968	The mechanics of discontinua or elastic mechanics in rock problems, in Rock Mechanics in Engineering Practice. Eds. Stagg, K.G. and Zienkiewicz, O.C. Ch.9. pp 275-320.
Walsh, J.B. and Brace, W.F.	1966	Elasticity of rock: a review of some recent theoretical studies. Rock Mech. and Engng. Geol. v.4 No. 4 pp 283-297.
Ward, W.H., Burland, J.B. and Gallois, R.W.	1968	Geotechnical assessment of a site at Mundford, Norfolk, for a large proton accelerator. Géotechnique, v.18 No.4 pp 399-431.
Watkins, M.D.	1971	Terminology for describing the spacing of discontinuities of rock masses. Q. Jl. Engng. Geol. v.3. pp 193-195.
Wickham, G.E., Tiedemann, H.R., and Skinner, E.H.	1972	Support determinations based on geologic predictions. Proc. 1st. North American Rapid Excavation and Tunnelling Conference, AIME, v.1. Chapter 7 pp 43-64.

Zienkiewicz, O.C. and Cheung, Y.K. 1967 The Finite Element Method in Structural and Continuum Mechanics, McGraw-Hill, New York, 272p.

Zienkiewicz, O.C., Valliapan, S. and Kind, I.P. 1968 Stress analysis of rock as a "no tension" material. Géotechnique, v.18, No. 1, pp 56-66.

APPENDIX A

SPECIFICATIONS OF THE TUNNELLING MACHINE USED AT CHINNOR (EXTRACTED FROM HIGNETT AND BODEN, 1974)

The machine cutting head rotates inside the leading edge of a shield which has a front cutting edge similar to that of a normal shield. The cutting head collects the spoil and discharges it into the hopper of the primary conveyor positioned in the upper part of the machine. The spoil is then transported by secondary and tertiary conveyors to the tip.

The head is driven by four radial piston hydraulic motors directly coupled to drive pinions which engage a pin wheel attached to the cutting head. Hydraulic fluid at a maximum working pressure of 20 MN/m^2 is supplied to these motors by four axial piston variable delivery pumps, each driven by a 149 kW (200hp) electric motor. The maximum continuous digging torque of the cutting head is 84 tonne-metres with a speed of rotation which is variable up to 7rpm; rotation of the head is reversible.

Advance and retraction of the machine is achieved by 16 double-acting 178mm diameter hydraulic rams housed within the shield and linked to the thrust reaction ring. Steering is achieved both by these peripheral thrust rams and by two 254mm diameter hydraulic rams operating radially between the tail of the machine and the horizontal steering beam. The hydraulic fluid is supplied to both elements of the advance and steering systems at a maximum working pressure of 20 MN/m^2. The maximum forward thrust available is about 850 tonnes for a total forward movement of 1.1m.

The reaction ring is in two parts and is expanded vertically against the roof and floor of the tunnel by eight 254mm diameter rams. These rams are supplied with hydraulic fluid to produce a pressure of 7 MN/m^2 at a supply rate of 45 litres/min and 20 MN/m^2 at 4 litres/min giving a maximum expansion force of about 850 tonnes.

The total installed electric power of the machine is 644 kW. The machine head weighs 84.5 tonnes, the reaction ring 27 tonnes and the weight of the total unit including sledges, conveyors and electrical and hydraulic equipment is of the order of 150 tonnes.

APPENDIX B

RAW DATA FROM DISCONTINUITY SCANLINE SURVEYS

Data tabulated in this Appendix are raw data concerning discontinuity characteristics sampled using the scanline survey technique at the following locations: Chinnor quarry, Chinnor shaft, Chinnor tunnel, Kielder Experimental Tunnel and Channel Tunnel. Discontinuity survey techniques adopted at these locations are described in Chapters 2, 3, 5 and 11.

The tabulated data, described more fully in Chapter 2, include:

(a) The distance (D) along the scanline of the intersection point between the discontinuity under consideration and the scanline.

(b) Discontinuity orientation, recorded as the geographical azimuth (000^{o} to 360^{o}, counting in clockwise rotation) of the direction of maximum discontinuity dip and the amount (00^{o} to 90^{o}) of this maximum dip.

(c) Trace length of the discontinuity, extending to the right (L_1) and left (L_2) sides of the scanline tape facing the zero end.

Azimuth directions for discontinuities measured in the Chinnor tunnel and the Channel Tunnel were taken relative to the tunnel centre line direction such that the recorded 000^{o} (or 360^{o}) azimuth is the

tunnel drive direction. For the Chinnor tunnel the drive direction was 010^{o} geographical azimuth; for the Channel Tunnel the drive direction was approximately 116^{o} geographical azimuth. Measurements of azimuth direction in the Chinnor quarry, Chinnor shaft and the Kielder Experimental Tunnel were taken relative to geographical north.

SCANLINE 1A

Scanline Orientation 037/00
Face Orientation 130/80

D (m)	Orientation	L_1 (m)	L_2 (m)	D (m)	Orientation	L_1 (m)	L_2 (m)
0.00	288/80	1.40	0.15	3.40	211/47	0.01	0.30
0.25	195/52	0.20	0.10	3.50	321/82	0.05	0.22
0.30	298/42	0.05	0.15	3.65	225/62	0.61	0.32
0.37	046/70	0.05	0.05	3.70	149/76	0.17	0.30
0.45	230/67	0.05	0.60	3.80	248/56	0.06	1.00
0.52	224/72	0.10	0.10	3.82	148/87	0.09	0.52
0.63	227/66	0.17	1.53	3.88	242/58	0.30	0.13
0.68	207/42	0.10	0.10	3.92	220/64	0.08	0.23
0.80	120/44	0.20	0.14	4.00	136/88	0.11	0.51
1.00	019/66	0.90	2.00	4.07	204/61	0.23	0.05
1.10	191/61	0.30	0.40	4.20	109/74	0.20	0.12
1.25	166/71	0.10	0.20	4.40	089/80	0.10	0.37
1.30	347/42	0.20	0.30	4.50	218/76	2.00	0.97
1.35	294/72	0.10	0.40				
1.45	083/85	0.25	0.10				
1.50	111/74	0.21	0.10				
1.54	258/34	0.09	0.03				
1.60	113/70	0.14	0.07				
1.80	292/85	0.18	0.04				
1.88	181/57	0.36	0.56				
1.93	119/42	0.09	0.03				
1.95	319/80	0.01	0.41				
1.98	203/56	0.01	0.10				
2.02	222/85	0.01	0.09				
2.08	218/83	0.01	0.07				
2.20	314/82	0.16	0.08				
2.29	044/71	0.80	0.55				
2.35	077/64	0.10	0.25				
2.40	312/77	0.14	0.10				
2.55	344/66	2.00	1.40				
2.60	263/66	2.00	0.21				
2.64	036/84	0.02	0.05				
2.65	041/79	0.02	0.05				
2.66	049/68	0.04	0.07				
2.67	032/81	0.05	0.06				
2.69	042/88	0.06	0.09				
2.70	065/86	0.08	0.10				
2.74	029/77	0.11	0.16				
2.75	033/65	0.15	0.11				
2.80	131/67	0.30	0.05				
2.89	253/60	0.46	0.30				
3.00	352/81	0.09	0.32				
3.07	096/76	0.01	0.11				
3.12	200/68	0.01	0.16				
3.15	341/61	0.02	0.25				
3.22	225/74	0.28	0.21				
3.25	314/68	0.02	0.28				

SCANLINE 1B

Scanline Orientation 350/08
Face Orientation 074/78

D (m)	Orientation	L_1 (m)	L_2 (m)	D (m)	Orientation	L_1 (m)	L_2 (m)
0.01	029/76	0.10	0.18	3.50	112/74	0.10	0.15
0.10	335/15	0.01	0.05	3.60	122/16	0.04	0.01
0.13	008/70	0.65	0.90	3.68	045/76	0.03	0.08
0.25	105/79	0.44	0.30	3.75	163/75	0.37	0.13
0.30	007/70	0.60	1.00	3.77	146/78	0.01	0.12
0.40	242/76	0.01	0.10	3.78	222/08	0.01	0.02
0.47	120/82	0.12	0.08	3.80	045/90	0.05	0.01
0.48	114/87	0.01	0.10	3.90	038/16	0.01	0.02
0.50	050/46	0.07	0.07	3.99	356/80	0.01	0.09
0.56	129/88	0.60	0.70	4.06	116/67	0.10	0.11
0.63	210/80	0.08	0.25	4.09	344/10	0.01	0.02
0.70	058/66	0.05	0.09	4.10	132/82	0.20	0.01
0.80	049/18	0.04	0.01	4.12	044/90	0.02	0.09
0.85	027/66	0.14	0.16	4.20	326/46	1.02	0.25
0.95	297/76	0.16	0.40	4.23	027/80	0.03	0.01
1.00	086/76	0.06	0.16	4.27	114/70	0.07	0.15
1.10	210/75	0.40	0.20	4.30	336/76	0.09	0.71
1.20	186/85	0.17	0.13	4.37	152/66	0.33	0.15
1.25	070/60	0.07	0.06	4.40	256/66	0.01	0.07
1.35	312/82	1.35	1.10	4.50	038/68	0.05	0.07
1.40	086/34	0.01	0.04	4.60	071/40	0.14	0.11
1.50	315/66	0.23	0.80	4.69	124/90	0.06	0.08
1.55	339/70	0.01	0.07	4.70	089/90	0.01	0.06
1.57	300/05	0.01	0.02	4.76	140/85	0.12	0.09
1.70	071/63	0.08	0.10	4.80	031/85	0.08	0.13
1.71	334/67	0.10	0.08	4.85	162/66	0.22	0.15
1.79	134/83	0.03	0.13	4.90	080/78	0.32	0.13
1.82	173/80	0.26	0.31	5.00	163/43	0.02	0.18
1.90	157/61	0.01	0.06	5.10	106/80	0.40	0.10
1.93	044/20	0.03	0.01	5.15	263/28	0.08	0.05
2.00	206/28	0.02	0.35	5.28	310/83	2.00	0.41
2.10	075/90	0.05	0.07	5.35	225/58	0.13	0.15
2.30	131/70	1.40	0.20	5.36	062/52	0.01	0.21
2.45	294/74	0.23	0.08	5.38	142/76	0.04	0.23
2.55	238/21	0.05	0.07	5.50	323/56	0.06	0.31
2.57	173/55	2.00	1.00	5.60	040/57	0.17	0.12
2.64	037/36	0.01	0.05	5.70	294/56	1.05	0.02
2.73	000/77	0.10	1.20	5.73	154/52	0.38	0.15
2.80	158/65	0.05	0.14	5.75	076/08	0.02	0.01
2.90	025/20	0.03	0.02				
3.00	059/75	0.02	0.18				
3.10	043/88	0.01	0.16				
3.15	344/28	0.11	0.03				
3.20	317/84	0.42	0.73				
3.25	054/80	0.52	0.43				
3.35	032/79	0.61	0.32				
3.40	099/68	0.06	0.09				
3.44	186/86	0.06	0.23				

SCANLINE 1C

Scanline Orientation 165/70
Face Orientation 165/70

D (m)	Orientation	L_1 (m)	L_2 (m)	D (m)	Orientation	L_1 (m)	L_2 (m)
0.00	258/08	0.23	0.10	2.50	174/84	0.03	0.22
0.05	204/30	0.21	0.09	2.57	342/31	0.19	0.14
0.07	212/78	0.03	0.12	2.59	330/28	0.11	0.09
0.10	260/13	0.24	0.16	2.70	120/16	0.18	0.07
0.18	265/08	0.43	0.12	2.80	144/79	0.01	0.31
0.20	260/10	0.40	0.10	2.87	287/43	0.06	0.08
0.22	198/90	0.25	0.17	2.90	346/75	0.04	0.06
0.28	242/22	0.12	0.17	2.95	273/53	0.08	0.25
0.35	271/15	0.09	0.22	3.00	142/60	0.23	0.21
0.40	229/08	0.24	0.18				
0.45	185/52	0.08	0.16				
0.50	245/10	0.09	0.20				
0.60	193/48	0.11	0.12				
0.65	005/36	0.18	0.07				
0.72	217/25	0.47	0.15				
0.75	354/84	0.06	0.05				
0.80	005/34	0.51	0.02				
0.85	011/36	0.43	0.10				
0.90	016/47	0.35	0.12				
0.95	148/82	0.04	0.08				
1.00	180/24	0.08	0.01				
1.05	210/10	0.12	0.08				
1.08	161/90	0.09	0.11				
1.15	232/03	0.36	0.11				
1.20	269/67	0.34	0.50				
1.25	244/71	0.03	0.64				
1.28	035/33	0.11	0.01				
1.35	182/10	0.02	0.07				
1.40	218/46	0.14	0.03				
1.42	007/30	0.20	0.07				
1.50	163/74	0.12	0.09				
1.60	177/90	0.16	0.08				
1.65	243/34	0.23	0.30				
1.70	194/50	0.03	0.18				
1.77	314/34	0.21	0.05				
1.80	200/82	0.06	0.04				
1.85	152/82	0.02	0.28				
1.88	249/36	0.21	0.07				
1.95	228/22	0.06	0.15				
2.00	150/90	0.08	0.13				
2.03	200/48	0.18	0.06				
2.09	277/52	0.56	0.25				
2.10	307/01	0.23	0.06				
2.20	195/90	0.07	0.03				
2.22	258/69	0.22	0.01				
2.25	146/85	0.03	0.07				
2.40	212/88	0.01	0.15				
2.41	120/40	0.05	0.06				

SCANLINE 2A

Scanline Orientation 218/05
Face Orientation 128/84

D (m)	Orientation	L_1 (m)	L_2 (m)	D (m)	Orientation	L_1 (m)	L_2 (m)
0.00	133/88	0.14	0.12	2.69	156/65	0.12	0.08
0.15	216/75	0.03	0.15	2.76	098/60	0.41	0.15
0.20	132/62	0.02	0.12	2.85	047/84	0.05	0.10
0.24	238/84	0.08	0.11	2.86	222/87	0.04	0.12
0.25	234/75	0.08	0.33	2.87	224/83	0.03	0.14
0.27	346/68	0.17	0.13	2.91	167/25	0.04	0.12
0.31	011/81	0.13	0.17	2.94	347/76	0.21	0.07
0.36	159/89	0.09	0.16	3.07	090/48	0.02	0.18
0.41	344/41	0.19	0.22	3.09	025/68	0.06	0.11
0.44	332/50	0.06	0.22	3.15	299/34	0.02	0.03
0.51	331/52	0.01	0.21	3.18	356/79	0.65	0.23
0.60	263/85	0.19	0.19	3.22	324/84	0.42	1.20
0.71	143/87	0.18	0.31	3.25	235/82	0.47	0.86
0.75	235/36	0.05	0.26	3.31	297/36	0.08	0.11
0.78	043/22	0.14	0.21	3.42	073/80	0.24	0.18
0.90	057/60	0.18	0.29	3.47	296/34	0.14	0.07
0.95	200/82	0.12	0.28	3.54	225/71	0.22	0.16
0.98	294/80	0.12	0.17	3.57	249/50	0.25	0.19
1.00	153/19	0.01	0.02	3.65	331/71	0.09	0.14
1.01	251/76	1.03	0.35	3.67	058/21	0.07	0.06
1.08	185/71	0.12	0.21	3.75	201/79	0.05	0.03
1.10	285/88	0.06	0.22	3.76	275/72	0.17	0.26
1.15	147/25	0.01	0.03	3.79	064/46	0.12	0.18
1.20	169/90	0.14	0.13	3.85	218/72	0.21	0.31
1.24	290/79	0.01	0.25	3.88	001/64	0.04	0.29
1.27	147/88	0.04	0.16	3.90	160/80	0.08	0.02
1.34	332/77	0.23	0.34	3.92	101/66	0.20	0.03
1.35	215/12	0.01	0.05	3.94	271/47	0.01	0.21
1.50	131/90	0.22	0.40	3.98	328/54	0.01	0.23
1.70	120/88	0.11	0.28	4.03	081/61	0.14	0.17
1.75	225/84	0.27	0.30	4.05	335/50	0.41	0.23
1.80	213/10	0.04	0.02	4.10	064/55	0.03	0.01
1.83	285/83	0.08	0.32	4.16	338/52	0.31	0.26
1.88	356/79	0.07	0.08	4.24	340/49	0.20	0.19
1.90	274/88	0.53	0.24	4.26	241/79	0.10	0.06
2.01	199/25	0.02	0.14	4.30	336/48	0.32	0.21
2.12	349/64	0.18	0.28	4.32	127/66	0.10	0.01
2.20	277/78	0.01	0.17	4.38	276/55	0.08	0.08
2.26	276/79	0.18	0.34	4.40	334/54	0.13	0.08
2.34	191/53	0.02	0.14	4.46	091/80	0.01	0.31
2.36	001/53	0.02	0.04	4.50	334/60	0.05	0.18
2.50	013/80	0.05	0.53	4.56	072/70	0.18	0.04
2.51	332/44	0.04	0.02	4.62	158/78	0.12	0.05
2.55	129/05	0.03	0.05	4.65	277/79	0.09	0.11
2.56	128/11	0.12	0.01	4.72	007/62	0.03	0.06
2.58	141/15	0.08	0.10	4.78	265/67	0.57	0.34
2.65	152/41	0.05	0.07	4.84	272/72	0.13	0.09

SCANLINE 2A (cont.)

D (m)	Orientation	L_1 (m)	L_2 (m)	D (m)	Orientation	L_1 (m)	L_2 (m)
4.85	261/73	0.22	0.40	8.50	079/83	0.31	0.01
4.91	195/10	0.10	0.02	8.53	111/62	0.03	0.19
4.95	015/76	0.05	0.27	8.54	190/90	0.05	0.23
5.01	351/10	0.02	0.08	8.56	074/63	0.01	0.29
5.05	263/64	0.18	0.16	8.59	182/89	0.06	0.07
5.10	155/56	0.12	0.09	8.63	250/73	0.01	0.11
5.13	206/68	0.25	0.16	8.66	223/72	0.08	0.09
5.20	165/72	0.23	0.33	8.70	034/80	0.02	0.11
5.35	248/81	0.31	0.51	8.75	117/90	0.12	0.25
5.55	148/76	0.12	0.87	8.82	274/55	0.41	0.29
5.80	144/67	0.20	0.96	9.00	166/90	0.15	0.43
6.10	156/73	0.06	0.58	9.14	136/88	0.07	0.25
6.20	359/40	0.60	0.35	9.21	044/86	0.29	0.45
6.25	264/66	0.15	0.08	9.22	043/87	0.30	0.42
6.26	207/48	0.18	0.09	9.27	131/90	0.01	0.08
6.30	190/76	0.03	0.18	9.32	207/89	0.23	0.44
6.35	082/68	0.42	0.06	9.37	081/58	0.01	0.03
6.41	247/61	0.15	0.16	9.40	298/75	0.10	0.24
6.44	131/54	0.01	0.18	9.51	173/74	0.13	0.23
6.51	336/42	0.01	0.19	9.55	176/72	0.07	0.18
6.56	126/54	0.11	0.02	9.59	082/60	0.08	0.18
6.58	307/54	0.01	0.13	9.65	154/71	0.09	0.13
6.60	052/83	0.03	0.07	9.72	185/68	0.01	0.15
6.66	316/58	0.02	0.17	9.76	123/54	0.12	0.10
6.70	238/74	0.77	0.52	9.82	131/90	0.22	0.21
6.81	161/72	0.08	0.09	9.92	335/81	0.03	0.07
6.90	166/79	0.14	0.21	10.00	123/82	0.32	0.20
7.07	256/35	0.39	0.43	10.40	122/84	0.31	0.07
7.15	149/80	0.14	0.45	10.52	094/84	0.06	0.40
7.20	249/46	0.11	0.41	10.62	342/82	0.03	0.15
7.24	162/90	0.03	0.24	10.65	305/83	0.10	0.03
7.30	077/24	0.03	0.10	10.70	289/70	0.01	0.21
7.31	256/63	0.21	0.23				
7.40	356/60	0.02	0.25				
7.49	050/88	0.07	0.12				
7.51	126/20	0.11	0.14				
7.60	323/78	0.34	0.15				
7.80	074/76	0.38	0.40				
7.85	330/70	0.31	0.24				
7.95	321/80	0.53	0.33				
8.00	075/72	0.12	0.16				
8.08	140/56	0.03	0.09				
8.11	198/89	0.01	0.02				
8.12	181/74	0.01	0.01				
8.15	097/80	0.02	0.03				
8.26	156/72	0.09	0.15				
8.35	087/88	0.28	0.01				
8.38	146/88	0.29	0.03				
8.42	058/82	0.12	0.08				
8.47	339/76	0.18	0.07				

SCANLINE 2B

Scanline Orientation 126/68
Face Orientation 125/76

D (m)	Orientation	L_1 (m)	L_2 (m)	D (m)	Orientation	L_1 (m)	L_2 (m)
0.24	198/22	0.07	0.09	3.08	312/27	0.14	0.29
0.28	293/82	0.04	0.03	3.14	325/66	0.04	0.09
0.41	282/71	0.04	0.18				
0.46	166/46	0.02	0.13				
0.53	347/89	0.08	0.06				
0.63	273/90	0.03	0.07				
0.65	044/62	0.01	0.04				
0.71	104/45	0.06	0.09				
0.75	001/75	0.02	0.01				
0.78	196/70	0.01	0.22				
0.93	331/75	0.02	0.07				
0.96	076/76	0.05	0.12				
1.02	347/76	0.09	0.05				
1.09	143/16	0.07	0.02				
1.12	077/82	0.05	0.19				
1.21	263/88	0.25	0.36				
1.29	343/64	0.05	0.07				
1.44	075/86	0.04	0.07				
1.47	345/42	0.01	0.01				
1.57	164/51	0.02	0.04				
1.59	077/84	0.03	0.07				
1.65	349/76	0.01	0.04				
1.73	257/90	0.09	0.47				
1.78	357/78	0.02	0.03				
1.83	152/33	0.05	0.17				
1.87	334/71	0.25	0.17				
1.90	077/70	0.19	0.28				
1.94	330/55	0.37	0.17				
1.98	151/83	0.07	0.14				
2.02	251/76	0.15	0.22				
2.09	059/72	0.04	0.07				
2.11	246/72	0.04	0.08				
2.14	006/77	0.04	0.07				
2.15	142/78	0.05	0.07				
2.17	252/09	0.14	0.19				
2.19	316/66	0.14	0.09				
2.24	088/82	0.13	0.07				
2.41	138/82	0.39	0.09				
2.55	226/13	0.07	0.01				
2.64	328/82	0.14	0.16				
2.70	337/68	0.02	0.04				
2.72	087/60	0.04	0.09				
2.82	328/65	0.43	0.11				
2.92	256/89	0.02	0.29				
2.99	348/56	0.07	0.04				
3.01	346/32	0.14	0.13				
3.02	308/30	0.74	0.12				
3.04	342/34	0.76	0.02				

SCANLINE 3A

Scanline Orientation 224/04
Face Orientation 307/80

D (m)	Orientation	L_1 (m)	L_2 (m)	D (m)	Orientation	L_1 (m)	L_2 (m)
0.00	313/71	0.03	0.21	2.93	162/54	0.15	0.01
0.19	039/82	0.15	0.20	3.00	273/76	0.59	0.20
0.25	256/86	0.09	0.07	3.04	130/61	0.02	0.07
0.34	251/72	0.01	0.03	3.15	120/28	0.42	0.44
0.40	313/86	0.33	0.35	3.20	127/67	0.06	0.04
0.47	262/83	0.09	0.04	3.32	344/78	2.00	0.14
0.54	327/80	0.25	0.32	3.40	106/73	0.02	0.07
0.65	349/90	0.05	0.15	3.49	143/60	0.03	0.08
0.71	260/17	0.02	0.04	3.52	141/50	0.08	0.09
0.74	329/73	0.05	0.14	3.61	348/77	0.11	0.14
0.80	263/57	0.07	0.07	3.64	299/78	0.09	0.01
0.84	134/86	0.01	0.25	3.72	110/11	0.42	0.39
0.88	041/87	1.20	0.35	3.76	155/75	0.15	0.01
0.95	271/60	0.04	0.07	3.84	269/83	0.01	0.24
1.03	345/25	0.03	0.09	3.86	312/74	0.05	0.14
1.06	339/78	0.19	0.24	3.95	325/18	0.09	0.11
1.10	089/80	0.04	0.26	4.02	317/74	0.09	0.23
1.14	044/22	0.07	0.05	4.06	017/86	0.04	0.09
1.19	351/90	0.01	0.33	4.07	131/25	0.06	0.01
1.20	298/20	0.06	0.24	4.12	338/72	0.08	0.13
1.22	162/56	0.01	0.12	4.23	220/78	0.05	0.15
1.30	151/60	0.15	0.01	4.25	102/90	0.11	0.03
1.45	330/89	0.17	0.01	4.26	087/71	0.07	0.05
1.50	273/70	0.14	0.07	4.27	044/72	0.01	0.30
1.58	176/82	0.04	0.03	4.30	149/71	0.08	0.03
1.59	052/82	0.23	0.08	4.31	052/81	0.09	0.02
1.60	269/68	0.05	0.03	4.34	296/78	0.12	0.01
1.62	343/63	0.02	0.03	4.36	019/08	0.14	0.08
1.70	291/84	0.34	0.09	4.38	272/72	0.03	0.24
1.73	089/10	0.30	0.06	4.40	000/82	0.11	0.01
1.75	093/11	0.24	0.12	4.41	289/87	0.08	0.03
1.78	091/13	0.08	0.13	4.46	065/75	0.09	0.03
1.80	113/62	0.15	0.03	4.48	161/88	0.01	0.13
1.91	283/86	0.01	0.24	4.49	263/59	0.11	0.02
2.05	124/52	0.06	0.15	4.50	072/88	0.12	0.05
2.10	129/60	0.11	0.34	4.61	354/42	0.15	0.01
2.14	125/81	0.03	0.07	4.66	313/56	0.01	0.22
2.33	133/88	0.02	0.17	4.72	079/58	0.06	0.01
2.50	096/18	0.33	0.42	4.79	046/06	0.45	0.89
2.54	306/50	0.01	0.04	4.82	255/78	0.02	0.15
2.55	291/68	0.04	0.07	5.00	190/78	0.03	0.16
2.60	284/80	0.05	0.16	5.06	121/39	0.07	0.18
2.71	122/78	0.07	0.06	5.14	267/81	0.06	0.25
2.75	155/65	0.02	0.01	5.27	216/62	0.07	0.19
2.78	155/64	0.08	0.13	5.32	353/59	0.03	0.11
2.80	131/75	0.11	0.08	5.45	290/48	0.05	0.16
2.91	080/11	0.41	0.28	5.75	005/76	0.04	0.04

SCANLINE 3A (cont.)

D (m)	Orientation	L_1 (m)	L_2 (m)	D (m)	Orientation	L_1 (m)	L_2 (m)
5.81	277/85	0.10	0.06	7.79	131/90	0.15	0.09
5.83	251/86	0.03	0.01	7.80	044/76	0.23	0.01
5.85	126/59	0.04	0.06	7.82	210/74	0.01	0.06
5.90	153/81	0.02	0.15	8.00	128/78	0.16	0.08
5.94	267/81	0.02	0.17	8.20	339/25	0.03	0.07
6.01	108/50	0.05	0.23	8.28	349/86	0.08	0.07
6.05	261/75	0.08	0.09	8.30	194/60	0.31	0.18
6.14	133/78	0.06	0.11	8.35	295/63	0.06	0.10
6.16	241/80	0.12	0.06	8.47	270/88	0.03	0.15
6.17	247/81	0.05	0.07	8.50	286/68	0.18	0.07
6.20	149/86	0.08	0.04	8.65	355/77	0.01	0.28
6.23	251/68	0.06	0.03	8.73	164/65	0.03	0.06
6.25	126/76	0.05	0.09	8.77	350/36	0.04	0.08
6.29	269/76	0.11	1.20	8.78	056/82	2.00	1.11
6.35	123/68	0.24	0.08	8.82	278/88	0.02	0.92
6.37	014/34	0.01	0.12	8.85	331/78	0.29	0.01
6.45	283/76	0.21	0.52	8.90	262/83	0.01	0.17
6.51	175/76	0.13	0.08	8.95	284/79	0.25	0.03
6.55	120/62	0.23	0.11	8.96	330/60	0.01	0.08
6.62	167/53	0.11	0.06	9.04	247/84	0.06	0.31
6.67	112/89	0.20	0.02	9.11	053/84	0.07	0.22
6.73	005/75	0.16	0.02	9.16	243/78	0.03	0.06
6.77	128/80	0.13	0.01	9.20	144/79	0.10	0.62
6.82	119/85	0.07	0.06				
6.91	113/83	0.09	0.03				
6.99	040/12	0.19	0.53				
7.00	040/90	0.16	0.01				
7.05	128/86	0.15	0.01				
7.22	330/89	0.16	0.03				
7.27	039/82	0.07	0.07				
7.29	231/67	0.03	0.04				
7.31	158/82	0.05	0.06				
7.33	068/44	0.02	0.04				
7.35	137/84	0.10	0.07				
7.36	231/88	0.11	0.10				
7.38	226/82	0.07	0.01				
7.40	079/55	0.16	0.12				
7.48	129/72	0.01	0.05				
7.50	272/76	0.02	0.03				
7.53	359/90	0.01	0.03				
7.54	258/86	0.02	0.01				
7.56	347/14	0.05	0.03				
7.60	268/67	0.01	0.07				
7.62	254/90	0.01	0.03				
7.68	262/50	0.04	0.07				
7.70	200/41	0.25	0.01				
7.72	045/81	0.16	0.09				
7.74	042/79	0.15	0.01				
7.76	050/81	0.05	0.45				

SCANLINE 3B

Scanline Orientation 307/77
Face Orientation 308/73

D (m)	Orientation	L_1 (m)	L_2 (m)
0.00	152/44	0.03	0.07
0.09	022/48	0.01	0.05
0.12	143/42	0.03	0.07
0.17	353/36	0.01	0.04
0.22	035/52	0.05	0.04
0.27	159/70	0.01	0.05
0.34	303/72	0.37	0.29
0.57	292/50	0.19	0.16
0.66	341/34	0.07	0.19
0.86	265/14	0.86	0.09
0.91	289/45	0.15	0.27
0.97	176/73	0.05	0.39
1.01	323/11	0.04	0.12
1.06	279/63	0.15	0.22
1.07	022/74	0.03	0.02
1.11	282/58	0.07	0.19
1.14	264/60	0.15	0.37
1.19	047/36	0.05	0.06
1.24	266/60	0.15	0.01
1.27	289/47	0.15	0.33
1.30	125/48	0.07	0.01
1.37	305/55	0.07	0.13
1.39	330/38	0.12	0.03
1.55	000/65	0.03	0.05
1.60	103/38	0.03	0.07
1.66	016/74	0.07	0.03
1.68	261/56	0.05	0.09
1.72	341/41	0.27	0.41
1.75	268/36	0.19	0.24
1.81	209/54	0.06	0.09
1.84	268/54	0.18	0.33
1.89	339/73	0.04	0.28
1.94	316/78	0.15	0.19
1.99	344/82	0.01	0.04
2.01	144/62	0.07	0.09
2.07	287/64	0.33	0.29
2.13	045/74	0.18	0.39
2.22	177/12	2.00	0.29
2.27	306/66	0.15	0.29
2.31	232/36	0.29	0.17
2.34	106/83	0.17	0.29
2.43	202/60	0.07	0.09
2.56	308/25	0.26	0.18
2.63	295/90	0.19	0.17
2.84	124/66	0.19	0.23
2.97	073/72	0.15	0.25
3.03	113/79	0.16	0.93
3.08	287/88	0.12	0.15
3.17	014/28	0.22	0.29
3.36	343/24	0.87	0.43
3.47	332/52	0.19	0.36
3.75	343/51	1.07	1.97
4.22	055/80	0.11	0.06
4.39	272/30	0.01	0.04
4.55	132/72	0.18	0.24

SCANLINE 4A

Scanline Orientation 211/05
Face Orientation 107/79

D (m)	Orientation	L_1 (m)	L_2 (m)
0.00	325/84	0.15	0.62
0.02	338/82	0.16	0.54
0.13	088/47	0.45	0.15
0.21	262/90	0.03	0.42
0.30	045/83	0.06	0.11
0.34	355/08	0.01	0.09
0.41	006/78	0.18	0.31
0.54	055/64	0.68	0.53
0.91	341/76	0.28	0.09
1.01	225/74	0.11	0.19
1.05	238/64	0.07	0.29
1.13	123/61	0.01	0.21
1.16	317/67	0.36	0.13
1.24	059/66	0.47	0.37
1.40	138/53	0.52	0.83
1.55	236/50	0.12	0.08
1.60	108/66	0.28	0.31
1.69	156/65	0.09	0.23
1.70	111/78	0.07	0.17
1.84	345/62	1.04	0.06
1.86	198/68	0.25	0.13
1.88	324/80	0.01	0.06
1.91	278/67	0.01	0.05
1.94	067/33	0.02	0.17
1.95	152/87	0.03	0.11
1.97	036/83	0.06	0.14
2.00	334/90	0.04	0.31
2.09	107/29	0.19	0.16
2.14	075/87	0.01	0.32
2.20	143/89	0.17	0.35
2.24	144/86	0.03	0.19
2.26	132/50	0.14	0.06
2.30	058/37	0.01	0.30
2.36	004/82	0.03	0.07
2.38	088/47	0.04	0.06
2.46	050/36	0.01	0.18
2.53	238/79	0.02	0.14
2.56	219/90	0.25	0.17
2.57	143/46	0.03	0.13
2.59	271/85	0.19	0.07
2.61	318/46	0.06	0.17
2.67	116/26	0.03	0.07
2.70	085/32	0.12	0.05
2.76	134/76	0.01	0.36
2.81	262/60	0.06	0.16
2.83	003/44	0.02	0.14
2.88	270/50	0.13	0.35
2.89	014/47	0.04	0.03
2.92	335/82	0.02	0.06
2.95	067/37	0.05	0.12
2.98	270/66	0.01	0.03
3.03	209/64	0.13	0.17
3.05	216/72	0.17	0.14
3.07	247/38	0.04	0.06
3.12	305/55	0.02	0.07
3.16	273/72	0.09	0.16
3.20	235/57	0.07	0.13
3.26	290/60	0.03	0.19
3.30	108/90	0.09	0.01
3.31	159/66	0.13	0.11
3.36	053/73	0.17	0.14
3.44	288/69	0.15	0.21
3.49	306/80	0.01	0.03
3.59	184/54	0.06	0.11
3.62	286/68	0.01	0.14
3.68	070/31	0.05	0.08
3.79	038/49	0.06	0.10
3.82	257/46	0.01	0.31
3.94	134/72	0.13	0.49
3.97	304/71	0.09	0.13
4.03	197/89	0.24	0.07
4.11	073/86	0.14	0.19
4.22	309/78	0.07	0.18
4.30	101/78	0.14	0.12
4.41	288/62	0.03	0.48
4.50	148/62	0.06	0.10
4.72	114/54	0.02	0.20
5.10	291/66	0.19	0.38
5.20	117/70	0.08	0.07
5.32	173/88	0.06	0.09
5.41	256/81	0.09	0.12
5.45	301/47	0.24	0.36
5.46	145/85	0.10	0.32
5.60	142/26	0.16	0.15
5.61	149/90	0.01	0.02
5.64	280/58	0.13	0.49
5.70	020/52	0.04	0.44
5.86	175/50	0.15	0.36
5.87	007/74	0.19	0.17
5.89	145/52	0.01	0.06
5.92	090/86	0.23	0.21
6.02	193/74	0.02	0.09
6.03	005/70	0.05	0.05
6.05	204/84	0.15	0.03
6.06	063/82	0.11	0.22
6.14	141/52	0.13	0.33

SCANLINE 4A (cont.)

D (m)	Orientation	L_1 (m)	L_2 (m)
6.22	113/50	0.09	0.24
6.25	268/89	0.19	0.18
6.31	300/81	0.01	0.02
6.35	150/18	0.07	0.09
6.37	312/79	0.03	0.06
6.41	097/20	0.06	0.14
6.50	309/66	0.24	0.37
6.56	054/43	0.13	0.41
6.64	323/73	0.04	0.30
6.74	175/82	0.05	0.17
6.78	292/67	0.09	0.18
6.80	165/75	0.02	0.04
6.86	179/67	0.04	0.01
6.90	103/33	0.06	0.06
0.97	168/63	0.03	0.19
7.08	096/75	0.03	0.07
7.10	342/62	0.01	0.71
7.19	135/84	0.05	0.11
7.23	118/55	0.01	0.04
7.35	275/67	0.05	0.52
7.37	088/20	0.06	0.02
7.40	026/80	0.29	0.34
7.55	103/90	0.14	0.19
7.61	127/86	0.51	0.32
7.71	295/61	0.02	0.13
7.80	107/60	0.10	1.30
7.95	282/65	0.01	0.16
8.02	115/55	0.06	0.14
8.04	117/90	0.25	0.13
8.07	016/86	0.33	0.11
8.15	087/77	0.25	0.16
8.24	347/69	0.14	0.01
8.31	106/87	0.32	0.03
8.43	115/60	0.30	1.30
8.80	113/61	0.15	0.19
9.01	108/69	0.42	0.30
9.05	280/65	0.03	0.20
9.06	217/70	0.01	0.15
9.14	099/78	0.06	0.12
9.21	259/50	0.29	0.16
9.30	292/77	0.23	0.19
9.54	038/77	0.06	0.39
9.72	301/68	0.15	0.26
9.81	202/75	0.04	0.06
9.91	342/23	0.64	0.27
10.00	092/73	0.14	0.07
10.08	266/10	0.05	0.19
10.21	115/90	0.08	0.16
10.23	350/72	0.02	0.02
10.33	156/88	0.09	0.03
10.35	098/89	0.10	0.07
10.62	124/84	0.01	0.08
10.63	047/85	0.02	0.06
10.65	159/82	0.14	0.09
10.66	271/54	0.01	0.03
10.69	113/49	0.13	0.07
10.70	330/31	0.02	0.16

SCANLINE 4B

Scanline Orientation 120/80
Face Orientation 119/76

D (m)	Orientation	L_1 (m)	L_2 (m)
0.11	123/58	0.09	0.10
0.23	325/71	0.13	0.22
0.39	098/55	0.03	0.05
0.44	063/75	0.02	0.03
0.49	307/57	0.05	0.16
0.52	295/60	0.16	0.32
0.57	134/08	0.07	0.05
0.62	168/12	0.03	0.04
0.64	170/68	0.07	0.04
0.72	146/68	1.40	0.22
0.76	158/66	0.11	0.25
0.90	151/78	0.04	0.19
0.92	321/40	0.13	0.02
0.95	126/12	0.10	0.04
0.97	106/56	0.13	0.21
0.99	178/64	0.13	0.18
1.06	211/74	0.02	0.04
1.08	150/79	0.07	0.01
1.11	039/68	0.01	0.01
1.14	311/72	0.02	0.03
1.19	207/56	0.04	0.09
1.23	325/63	0.15	0.27
1.28	146/64	0.04	0.17
1.41	130/76	0.18	0.13
1.64	306/78	0.22	0.43
1.84	197/84	0.03	0.05
1.87	192/24	0.03	0.07
1.95	120/84	0.08	0.09
1.97	021/56	0.07	0.52
2.02	285/25	0.07	0.06
2.07	066/72	0.09	0.25
2.10	175/78	0.03	0.25
2.15	300/72	0.04	0.06
2.20	073/52	0.03	0.06
2.33	179/68	0.04	0.36
2.41	299/78	0.08	0.10
2.49	317/60	0.03	0.14
2.58	029/42	0.01	0.07
2.62	273/79	0.25	0.31
2.82	079/83	0.12	0.07
2.95	085/62	0.17	0.01
2.99	318/31	0.14	2.00
3.12	140/62	0.08	2.00
3.20	301/24	0.20	0.33
3.50	162/74	0.15	0.80
3.54	046/69	0.03	0.07
3.58	178/06	0.09	0.24
3.62	048/68	0.03	0.07
3.64	270/61	0.09	0.06
3.76	040/90	0.03	0.02
3.90	040/87	0.07	0.04
4.01	017/52	0.08	0.04
4.03	257/57	0.03	0.04
4.09	043/54	0.03	0.09
4.21	167/70	0.93	0.47
4.23	251/81	0.04	0.06
4.45	167/59	0.05	0.09
4.48	062/73	0.01	0.04
4.54	280/44	0.02	0.09
4.57	158/73	0.24	0.16
4.68	062/81	0.11	0.14
4.80	276/66	0.05	0.05

SCANLINE 5A

Scanline Orientation 263/07
Face Orientation 000/82

D (m)	Orientation	L_1 (m)	L_2 (m)	D (m)	Orientation	L_1 (m)	L_2 (m)
0.00	347/75	0.42	0.21	4.60	261/12	0.22	0.34
0.40	280/88	0.48	0.38	4.74	250/18	0.29	0.01
0.45	350/76	0.28	0.16	4.75	030/80	0.13	0.07
0.80	291/27	0.03	0.12	4.77	332/84	0.01	0.06
0.88	284/26	0.01	0.32	4.79	246/62	0.03	0.07
0.94	088/87	0.07	0.19	4.82	167/84	0.02	0.03
1.10	002/78	0.24	0.18	4.90	170/23	0.29	0.15
1.24	107/77	0.06	0.13	5.10	031/78	0.05	0.09
1.29	303/43	0.06	0.58	5.21	310/35	0.12	0.28
1.34	358/65	0.17	0.13	5.30	319/53	0.11	0.17
1.45	314/20	0.17	0.12	5.31	310/70	0.25	0.37
1.47	187/86	0.03	0.19	5.40	322/52	1.20	0.41
1.51	316/70	0.41	0.07	5.65	182/50	0.06	0.03
1.54	082/76	0.05	0.22	5.71	085/83	0.07	0.05
1.60	325/28	0.12	0.19	5.74	200/68	0.11	0.19
1.80	279/87	0.03	0.08	5.82	286/47	0.25	0.31
1.92	231/90	0.10	0.06	5.85	270/27	0.37	0.24
1.95	179/83	0.38	0.14	5.92	025/45	0.06	0.12
1.96	046/43	0.02	0.29	6.11	147/40	0.03	0.01
2.00	272/42	0.51	0.09	6.12	041/62	0.02	0.01
2.30	165/80	0.11	0.19	6.18	308/30	1.32	0.14
2.41	021/25	0.03	0.06	6.22	088/72	0.13	0.01
2.44	245/75	0.07	0.18	6.24	003/66	0.01	0.17
2.49	294/22	0.08	0.11	6.30	174/48	0.01	0.11
2.52	125/77	0.09	0.02	6.42	342/24	0.03	0.06
2.59	047/22	0.11	0.09	6.53	223/53	0.08	0.06
2.65	182/87	0.14	0.01	6.59	319/42	0.06	0.09
2.71	171/88	0.03	0.33	6.67	092/70	0.01	0.01
2.75	330/54	0.11	0.03	6.74	242/85	0.15	0.01
2.79	346/43	0.05	0.18	6.75	329/73	0.09	0.16
3.12	310/68	0.03	0.01	6.80	169/52	0.01	0.19
3.22	354/58	0.06	0.16	6.92	189/14	0.16	0.07
3.40	338/81	0.09	0.22	6.93	084/68	0.18	0.01
3.44	259/08	0.16	0.12	7.00	055/77	0.05	0.01
3.48	082/77	0.02	0.18	7.05	337/61	0.04	0.01
3.51	260/86	0.19	0.06	7.11	291/72	0.48	0.18
3.53	346/71	0.13	0.07	7.24	234/90	0.08	0.06
3.60	255/60	0.09	0.05	7.26	178/83	0.01	0.05
3.62	184/80	0.04	0.19	7.30	173/17	0.12	0.09
3.69	003/05	0.36	0.08	7.35	328/83	0.02	0.15
3.77	263/90	0.02	0.25	7.60	225/15	0.19	0.09
3.82	350/72	0.09	0.23	7.80	181/77	0.17	0.01
3.95	079/75	0.02	0.04	7.82	131/74	0.23	0.02
4.00	357/80	0.05	0.07	7.93	086/48	0.06	0.28
4.11	016/16	0.03	0.18	8.00	232/09	0.07	0.19
4.15	356/52	0.01	0.25	8.26	151/90	0.33	0.15
4.21	318/60	1.20	0.06	8.31	325/46	0.02	0.09
4.32	349/49	0.25	0.19	8.50	344/83	0.07	0.02
4.45	321/64	0.41	0.20	8.52	333/66	0.02	0.03

SCANLINE 5A (cont.)

D (m)	Orientation	L_1 (m)	L_2 (m)	D (m)	Orientation	L_1 (m)	L_2 (m)
8.57	245/72	0.01	0.03	13.30	348/11	0.25	0.16
8.62	068/56	0.01	0.26	13.49	263/90	0.37	0.04
8.65	336/25	0.08	0.02	13.50	085/54	0.03	0.22
8.68	344/83	0.05	0.32				
8.69	057/43	0.02	0.16				
8.82	357/90	0.01	0.07				
8.85	356/71	0.16	0.11				
9.00	185/78	0.28	0.03				
9.04	101/60	0.38	1.83				
9.34	354/69	0.39	0.24				
9.36	284/36	0.11	0.14				
9.41	000/72	0.06	0.12				
9.90	333/68	0.14	0.07				
9.92	139/75	0.29	0.02				
10.02	303/21	0.08	0.15				
10.43	274/69	0.09	0.08				
10.45	233/21	0.14	0.02				
10.50	025/36	0.22	0.19				
10.53	066/43	0.04	0.09				
10.54	296/63	0.01	0.12				
10.58	340/55	0.07	0.15				
10.63	246/34	0.01	0.23				
10.69	333/73	0.14	0.06				
10.77	241/90	0.17	0.46				
10.82	121/49	0.09	0.15				
10.83	143/58	0.05	0.26				
10.95	015/72	0.16	0.13				
11.07	136/90	0.11	0.39				
11.20	194/72	0.09	0.13				
11.32	219/90	0.06	0.06				
11.34	314/30	0.28	0.24				
11.41	243/38	0.16	0.14				
11.68	021/37	0.01	0.22				
11.71	314/68	0.02	0.07				
11.73	137/60	0.01	0.05				
11.84	306/61	0.03	0.09				
11.97	210/83	0.06	0.32				
11.98	129/60	0.05	0.87				
12.02	274/90	0.02	0.26				
12.12	119/87	0.11	0.14				
12.19	140/60	0.05	0.22				
12.24	002/70	0.13	0.06				
12.36	255/84	0.36	0.02				
12.47	240/23	0.52	0.18				
12.52	354/37	0.11	0.04				
12.55	087/60	0.03	0.01				
12.60	093/80	0.02	0.02				
12.65	183/90	0.59	0.17				
12.90	081/79	0.07	0.23				
12.92	283/22	0.47	0.02				
13.00	182/74	0.13	0.25				

SCANLINE 5B

Scanline Orientation 172/70
Face Orientation 200/70

D (m)	Orientation	L_1 (m)	L_2 (m)
0.00	171/82	0.07	0.15
0.07	343/06	0.03	0.16
0.12	351/44	0.24	0.03
0.22	001/65	0.21	0.02
0.33	240/28	0.14	0.02
0.39	340/53	0.09	0.01
0.44	258/90	0.06	0.23
0.53	175/89	0.07	0.01
0.55	183/10	0.04	0.02
0.60	086/55	0.19	0.22
0.61	007/74	0.03	0.01
0.63	215/31	0.11	0.07
0.70	324/76	0.19	0.06
0.73	298/62	0.07	0.01
0.79	083/45	0.14	0.08
0.82	197/77	0.03	0.15
0.84	305/68	0.12	0.32
0.86	040/68	0.08	0.07
0.87	354/09	0.16	0.05
0.90	008/74	0.18	0.06
0.91	317/78	0.04	0.24
1.00	131/10	0.19	0.09
1.06	014/86	0.38	0.11
1.18	119/04	0.29	0.14
1.22	279/84	0.11	0.12
1.32	226/38	0.02	0.14
1.40	100/64	0.07	0.16
1.49	272/76	0.06	0.14
1.51	189/88	0.36	0.06
1.54	290/70	0.06	0.09
1.55	154/10	0.14	0.01
1.62	164/77	0.22	0.04
1.66	049/69	0.03	0.04
1.69	156/58	0.01	0.07
1.72	314/57	0.11	1.30
1.81	111/79	0.10	0.07
1.85	139/20	0.44	0.09
1.90	214/90	0.18	0.16
2.02	179/87	0.15	0.09
2.08	310/90	0.06	0.10
2.15	308/30	0.19	0.24
2.24	292/36	0.28	0.12
2.25	047/76	0.09	0.11
2.34	249/20	0.03	0.01
2.36	055/21	0.24	0.06
2.42	195/87	0.25	0.16
2.47	290/16	0.25	0.31
2.53	194/66	0.29	0.38
2.67	202/05	0.18	0.07
2.68	355/37	0.06	0.07
2.69	265/06	0.11	0.05
2.73	176/33	0.18	0.01
2.74	135/52	0.06	0.02
2.75	330/10	0.15	0.22
2.76	324/80	0.11	0.31
2.90	159/75	0.23	0.21
3.04	337/72	0.37	0.19
3.24	018/50	0.28	0.24
3.32	214/12	0.53	0.09
3.38	149/50	0.16	0.04
3.40	064/62	0.39	0.22
3.41	199/54	0.01	0.15
3.43	170/82	0.14	0.01
3.50	169/89	0.04	0.13
3.54	345/87	0.01	0.11
3.56	115/90	0.15	0.22
3.57	331/75	0.02	0.06
3.60	064/66	0.09	0.12
3.65	352/82	0.19	0.14

SCANLINE 6A

Scanline Orientation 210/02
Face Orientation 300/75

D (m)	Orientation	L_1 (m)	L_2 (m)
0.00	224/83	0.19	0.83
0.01	312/62	0.35	0.49
0.35	086/68	0.14	0.28
0.40	067/19	0.08	0.13
0.54	123/80	0.02	0.15
0.61	042/46	0.04	0.29
0.75	318/62	0.38	0.02
0.84	198/62	0.33	0.01
0.90	320/78	0.45	0.02
0.92	014/85	0.09	0.02
1.00	313/85	0.33	0.16
1.11	232/70	0.29	0.04
1.15	233/33	0.05	0.03
1.22	274/67	0.03	0.16
1.31	136/80	0.49	0.04
1.34	318/89	0.56	0.27
1.35	230/90	0.02	0.04
1.45	305/73	0.19	1.24
1.71	132/67	0.32	1.35
1.82	291/51	0.64	0.38
2.04	141/77	0.93	0.18
2.20	284/40	0.09	0.14
2.39	052/80	0.06	0.34
2.45	274/86	0.23	0.33
2.47	343/60	1.54	0.15
2.52	144/83	0.11	1.28
2.72	142/76	0.09	0.16
3.00	003/77	0.43	0.22
3.11	009/35	1.52	0.13
3.25	302/68	0.34	0.41
3.50	210/72	1.53	1.24
3.75	223/66	0.15	0.58
4.10	099/43	0.35	0.16
4.16	309/43	0.16	0.23
4.19	052/79	0.09	0.11
4.30	142/81	2.00	0.15
4.52	091/81	0.84	0.23
4.60	300/40	0.63	0.34
5.14	054/65	0.32	0.16
5.40	150/85	0.62	0.43
5.52	316/60	0.08	0.06
5.70	175/47	0.76	0.15
5.79	260/82	0.06	0.16
5.94	356/70	0.35	0.18
6.04	306/39	0.07	0.23
6.14	013/82	0.04	0.25
6.18	273/85	0.08	0.14
6.22	178/22	0.32	0.16
6.31	325/40	0.24	0.07
6.52	152/30	0.18	0.06
6.60	233/79	0.07	0.07
6.78	191/59	0.09	0.19
6.82	318/39	0.12	0.17
6.85	025/50	1.96	0.03
7.00	320/77	0.29	0.16
7.10	074/58	2.00	1.40
7.23	266/75	0.06	0.41
7.34	070/41	0.09	0.16
7.42	337/61	0.33	0.26
7.51	076/62	0.24	0.23
7.72	265/58	0.13	0.48
8.00	262/58	0.13	0.48
8.24	332/82	0.18	0.39
8.50	204/83	0.46	0.29
8.54	096/59	0.16	0.09
8.60	322/80	0.43	0.22
8.85	243/90	0.13	0.15
8.91	208/48	0.05	0.07
9.00	325/54	0.62	0.14
9.15	350/57	0.44	0.29
9.30	258/68	0.63	0.12
9.65	356/79	0.75	0.45
10.20	282/66	0.95	0.65
11.30	261/81	0.31	0.04
11.50	334/68	0.19	0.17
11.56	177/75	0.03	0.18
11.62	269/78	0.24	0.26
11.65	258/85	0.12	0.03
11.71	262/85	0.04	0.03
11.80	353/79	0.12	0.16
11.92	264/88	0.09	0.32
12.00	013/85	0.11	0.34
12.12	326/56	0.03	0.19
12.15	208/15	0.30	0.34
12.18	342/64	0.69	0.01
12.20	153/48	0.11	0.03
12.24	110/84	0.01	0.10
12.30	092/70	0.34	0.01
12.41	237/07	0.43	0.17
12.44	321/70	0.02	0.01
12.52	310/77	0.09	0.04
12.60	209/83	0.32	0.07
12.84	108/75	0.37	0.16
12.92	283/20	0.24	0.06
13.13	265/45	0.13	0.36
13.50	105/65	0.53	0.24

SCANLINE 6A (cont.)

D (m)	Orientation	L_1 (m)	L_2 (m)
13.63	357/50	0.37	0.40
13.75	105/66	0.24	0.27
14.00	003/55	0.30	1.66

SCANLINE 7A

Scanline Orientation 140/02
Face Orientation 045/80

D (m)	Orientation	L_1 (m)	L_2 (m)
0.00	061/60	0.15	0.08
0.19	311/83	0.04	0.07
0.21	279/57	0.08	0.03
0.24	098/60	0.02	0.08
0.31	061/77	0.11	0.06
0.33	334/80	0.54	0.63
0.37	096/84	0.12	0.06
0.42	343/61	0.69	1.33
0.50	320/63	0.02	0.08
0.52	279/65	0.04	0.01
0.58	148/89	0.03	0.05
0.63	227/58	0.01	0.08
0.67	335/71	0.52	1.20
0.72	228/42	0.09	0.11
0.79	132/74	0.02	0.18
0.83	248/52	0.03	0.07
0.84	329/53	0.08	0.13
0.90	248/67	0.03	0.07
0.94	334/77	0.32	0.58
1.00	355/79	0.44	0.18
1.10	292/73	0.56	0.38
1.13	041/62	0.11	0.03
1.14	291/51	0.13	0.07
1.15	326/56	0.18	0.01
1.20	217/80	0.09	0.02
1.22	314/81	0.48	0.17
1.30	035/87	0.08	0.11
1.38	326/71	0.44	0.39
1.42	192/69	0.12	0.08
1.51	344/40	0.04	0.18
1.53	067/43	0.14	0.03
1.55	184/69	0.01	0.05
1.59	067/80	0.08	0.11
1.65	234/90	0.16	0.08
1.73	280/16	0.25	0.25
1.90	307/74	0.52	0.64
1.94	292/78	0.06	0.08
1.95	308/82	0.29	0.33
2.00	076/49	0.05	0.07
2.04	261/41	0.02	0.19
2.14	022/71	0.04	0.12
2.20	158/90	0.05	0.19
2.22	336/67	0.18	1.22
2.24	095/66	0.02	0.08
2.30	356/78	0.02	0.05
2.34	239/73	0.01	0.04
2.35	089/20	0.03	0.03
2.41	124/87	0.29	0.04
2.45	102/45	0.07	0.03
2.49	224/78	0.04	0.02
2.51	331/71	1.83	0.27
2.57	127/67	0.03	0.01
2.65	113/44	0.05	0.13
2.67	069/7-	0.06	0.12
2.70	273/22	0.03	0.14
2.74	146/55	0.22	0.14
2.76	210/77	0.02	0.01
2.80	162/04	0.18	0.08
2.85	075/59	0.02	0.07
2.92	286/54	0.13	0.09
2.98	000/16	0.09	0.07
3.05	325/70	1.04	1.37
3.10	021/74	0.06	0.04
3.16	135/40	0.08	0.03
3.30	002/69	0.02	0.07
3.32	209/63	0.04	0.09
3.41	303/34	0.02	0.32
3.52	012/86	0.09	0.14
3.61	031/21	0.49	0.26
3.85	102/28	0.17	0.23
3.93	280/76	0.08	0.07
4.06	205/58	0.03	0.22
4.11	280/33	0.64	0.09
4.13	342/72	0.39	0.11
4.16	331/85	0.03	0.44
4.19	354/35	0.07	0.08
4.22	323/83	0.45	0.62
4.29	172/66	0.02	0.07
4.32	029/31	0.04	0.07
4.38	169/75	0.06	0.08
4.41	163/82	0.08	0.04
4.53	287/27	0.05	0.11
4.61	221/50	0.02	0.19
4.66	035/44	0.01	0.27
4.75	328/64	0.13	0.13
4.85	322/72	0.04	0.07
4.94	217/55	0.20	0.24
4.96	069/15	0.05	0.02
4.98	065/79	0.08	0.19
5.05	288/81	0.47	0.34

SCANLINE 7A (cont.)

D (m)	Orientation	L_1 (m)	L_2 (m)
5.08	303/15	0.09	0.68
5.16	329/20	0.14	0.09
5.25	338/37	0.07	0.14
5.26	174/70	0.04	0.06
5.37	253/47	0.03	0.08
5.44	323/69	0.05	0.11
5.47	154/62	0.48	0.50
5.50	049/74	0.12	0.08
5.63	186/30	0.22	0.16
5.79	293/32	0.02	0.04
5.80	201/83	0.07	0.06
5.84	275/76	0.04	0.29
5.88	340/75	0.26	0.69
5.94	064/34	0.15	0.04
5.99	041/25	0.12	0.05
6.00	295/54	0.17	0.09
6.03	223/52	0.09	0.14
6.09	298/68	0.29	0.20
6.12	345/85	0.15	0.42
6.17	335/66	0.14	0.64
6.27	035/42	0.08	0.17
6.29	251/55	0.03	0.12
6.31	006/65	0.36	0.09
6.44	098/49	0.34	0.08
6.60	270/40	0.30	0.37
6.62	319/50	0.01	0.38
6.75	335/68	0.06	1.05
6.76	237/53	0.07	0.18
6.82	031/76	0.01	0.08
6.86	115/40	0.02	0.09
6.91	316/66	0.08	0.33
6.94	076/48	0.05	0.07
7.16	274/54	0.03	0.22
7.22	042/64	0.16	0.13
7.24	180/86	0.32	0.64
7.27	040/22	0.09	0.14
7.30	341/85	0.33	0.96
7.43	011/33	0.05	0.22
7.45	208/58	0.02	0.01
7.56	290/55	0.17	0.09
7.57	032/30	0.02	0.04
7.61	297/60	0.24	0.15
7.62	324/70	0.28	0.32
7.75	000/20	0.13	0.19
7.80	208/77	0.03	0.04
7.91	255/22	0.07	0.02
7.94	151/15	0.13	0.08
8.00	263/52	0.06	0.11
8.12	344/60	0.13	0.08
8.32	200/60	0.05	0.12
8.41	344/20	0.06	0.15
8.45	341/36	0.14	0.19
8.56	008/29	0.09	0.10
8.66	061/52	0.06	0.34
8.74	354/61	0.38	0.24
8.78	088/78	0.13	0.28
8.94	339/25	0.09	0.06
9.00	190/76	0.03	0.03
9.01	349/32	0.02	0.11
9.03	278/50	0.36	0.07
9.06	042/35	0.06	0.02
9.11	308/82	0.79	0.52
9.16	005/27	0.04	0.03
9.24	068/17	0.08	0.04
9.32	345/44	0.01	0.03
9.34	301/38	0.18	0.14
9.37	015/10	0.09	0.14
9.41	193/80	0.14	0.07
9.50	346/35	0.07	0.13
9.54	168/65	0.02	0.01
9.61	070/84	0.05	0.01
9.66	115/72	0.29	0.43
9.69	221/67	0.03	0.04
9.70	020/30	0.06	0.09
9.71	341/43	0.04	0.06
9.84	304/48	0.14	0.19
9.85	209/14	0.06	0.04
9.92	347/82	0.27	0.24
10.00	224/73	0.15	0.29

SCANLINE 7B

Scanline Orientation 055/08
Face Orientation 322/82

D (m)	Orientation	L_1 (m)	L_2 (m)	D (m)	Orientation	L_1 (m)	L_2 (m)
0.00	148/77	0.18	0.09	4.70	275/70	0.13	0.02
0.22	153/79	0.23	0 07	4.71	093/59	0.05	0.03
0.35	014/29	0.14	0.05	4.73	238/44	0.02	0.02
0.51	172/68	0.44	0.08	4.75	033/41	0.09	0.11
0.56	219/33	0.01	0.28	4.79	268/62	0.19	0.21
0.64	223/33	0.04	0.09	4.95	351/75	0.45	0.62
0.71	202/69	0.01	0.06	5.22	349/76	0.35	0.29
0.77	215/71	0.03	0.38	5.35	277/57	0.16	0.04
0.81	228/70	0.09	0.06	5.44	347/72	0.16	0.13
0.87	166/81	0.15	0.22	5.51	278/66	0.04	0.06
0.92	165/48	0.06	0.07	5.56	356/61	0.05	0.03
1.04	339/86	0.15	0.10	5.62	114/20	0.07	0.04
1.06	213/22	0.24	0.18	5.64	274/86	0.12	0.09
1.14	253/85	0.06	0.32	5.66	355/52	0.13	0.07
1.19	178/66	0.19	0.11	5.71	282/63	0.03	0.05
1.21	218/32	0.08	0.09	5.79	172/30	0.29	0.07
1.26	204/62	0.01	0.18	5.87	348/82	0.04	0.06
1.29	040/69	0.08	0.11	6.02	175/30	0.04	0.03
1.38	097/83	0.06	0.07	6.09	306/38	0.07	0.02
1.41	338/47	0.02	0.04	6.14	094/72	0.01	0.11
1.45	198/77	0.09	0.31	6.22	159/34	0.08	0.03
1.50	224/05	0.22	0.83	6.26	349/45	0.02	0.01
1.54	200/63	0.07	0.09	6.30	340/36	0.19	0.15
1.68	346/75	0.02	0.24	6.34	135/48	0.04	0.06
1.82	053/39	0.29	0.42	6.51	084/72	0.07	0.19
1.84	347/68	0.02	0.11	6.60	359/30	0.14	0.09
1.93	321/80	1.04	0.32	6.72	163/77	0.04	0.13
2.02	031/40	0.07	0.14	6.75	082/05	0.18	0.03
2.20	122/83	0.15	0.72	6.79	312/44	0.38	0.20
2.31	327/84	1.07	0.22	6.84	214/54	0.13	0.07
2.42	079/37	0.78	0.33	6.90	072/31	0.05	0.08
2.97	318/90	0.42	0.21	6.93	076/13	0.19	0.24
3.14	136/64	0.19	0.22	6.94	210/71	0.05	0.03
3.55	144/82	0.36	0.49	7.00	330/38	0.35	0.14
3.84	109/72	0.53	0.24	7.16	200/53	0.19	0.11
4.00	032/84	0.06	0.06	7.24	269/40	0.12	0.04
4.01	080/86	0.03	0.09	7.30	204/59	0.11	0.02
4.03	157/09	0.01	0.24	7.33	064/28	0.19	0.14
4.16	327/25	0.11	0.19	7.42	222/73	0.07	0.11
4.24	337/42	0.09	0.14	7.45	293/37	0.05	0.03
4.33	196/66	0.07	0.08	7.52	206/39	0.05	0.02
4.41	292/13	0.34	0.02	7.55	083/52	0.01	0.07
4.45	308/76	0.03	0.04	7.57	340/30	0.06	0.02
4.51	218/68	0.15	0.07	7.60	202/66	0.01	0.06
4.52	219/40	0.03	0.19	7.63	187/79	0.03	0.02
4.55	210/79	0.05	0.07	7.71	019/42	0.05	0.01
4.62	290/49	0.35	0.29	7.73	204/34	0.01	0.04
4.66	172/76	0.04	0.03	7.75	220/73	0.04	0.03
4.67	323/18	0.19	0.08	7.81	223/77	0.11	0.02

SCANLINE 7B (cont.)

D (m)	Orientation	L_1 (m)	L_2 (m)	D (m)	Orientation	L_1 (m)	L_2 (m)
7.86	276/55	0.08	0.03	12.02	221/78	0.06	0.04
7.89	351/48	0.07	0.02	12.14	336/71	1.22	0.24
7.93	075/69	0.05	0.03	12.33	278/80	1.31	0.49
7.97	340/53	0.02	0.03	12.50	357/64	1.28	0.15
8.00	162/18	0.01	0.04	12.61	133/38	0.93	0.24
8.05	126/64	0.15	0.09	12.84	118/70	0.14	0.13
8.06	289/88	0.04	0.19	13.04	341/36	0.14	0.08
8.09	008/72	0.07	0.38	13.22	249/65	0.15	0.09
8.10	037/32	0.02	0.01	13.25	149/35	0.02	0.06
8.17	322/33	0.10	0.11	13.39	007/47	0.23	0.18
8.20	141/50	0.09	0.13	13.50	321/44	0.15	0.01
8.23	158/57	0.05	0.02				
8.34	022/53	0.01	0.29				
8.39	307/60	0.04	0.02				
8.41	147/37	0.02	0.04				
8.46	276/37	0.04	0.09				
8.50	021/45	0.08	0.07				
8.56	148/72	0.01	0.03				
8.60	261/19	0.08	0.06				
8.65	317/05	0.19	0.05				
8.69	291/53	0.06	0.12				
8.76	293/77	0.18	0.03				
8.80	010/52	0.36	0.14				
8.83	106/78	0.06	0.03				
8.84	231/48	0.01	0.17				
8.87	340/24	0.05	0.05				
8.90	184/48	0.07	0.03				
8.94	327/72	0.09	0.15				
9.15	275/82	0.48	0.30				
9.17	276/47	0.01	0.12				
9.22	203/62	0.04	0.06				
9.34	316/73	0.10	0.28				
9.38	037/77	0.01	0.08				
9.42	276/23	0.09	0.03				
9.44	039/72	0.02	0.08				
9.47	306/62	0.09	0.03				
9.56	189/28	0.15	0.09				
9.64	310/73	0.25	0.18				
9.81	278/62	0.64	0.29				
10.05	265/25	0.10	0.09				
10.11	230/19	0.19	0.09				
10.15	285/60	0.11	0.14				
10.40	344/66	0.39	0.35				
10.64	327/67	1.24	0.42				
11.03	289/82	0.16	0.33				
11.44	029/68	0.11	0.10				
11.50	308/83	0.16	0.33				
11.60	187/27	0.30	0.10				
11.73	320/20	0.18	0.13				
11.86	327/82	0.11	0.09				
11.91	215/25	0.44	0.11				

SCANLINE 7C

Scanline Orientation 348/79
Face Orientation 343/76

D (m)	Orientation	L_1 (m)	L_2 (m)	D (m)	Orientation	L_1 (m)	L_2 (m)
0.03	172/61	0.05	0.19	2.80	307/08	0.05	0.07
0.04	018/33	0.19	0.29	2.85	175/82	0.01	0.12
0.15	323/62	0.29	0.15	2.91	197/61	0.04	0.19
0.22	140/33	0.27	0.16	2.96	194/75	0.13	0.29
0.28	134/32	0.04	0.05	3.17	026/77	0.15	0.23
0.36	150/34	0.19	0.22	3.31	038/24	0.84	0.37
0.39	150/19	0.07	0.17	3.35	189/15	0.07	0.07
0.41	321/40	0.07	0.09	3.47	025/75	0.39	0.38
0.44	159/12	0.67	0.62	3.51	219/20	1.40	2.00
0.47	162/10	0.64	0.69	3.61	060/66	0.01	0.03
0.51	017/20	0.01	0.04	3.67	311/74	0.07	0.06
0.55	028/85	0.03	0.07	3.68	210/70	0.14	0.19
0.58	292/64	0.02	0.04	3.70	022/48	0.13	0.12
0.59	159/13	0.25	0.27	3.74	054/76	0.03	0.19
0.61	162/09	0.32	0.24	3.77	020/16	0.19	0.23
0.68	332/75	2.00	0.49	3.78	290/15	0.13	0.17
0.84	336/85	2.00	0.50	3.79	057/48	0.01	0.07
1.15	341/80	2.00	0.45	3.81	222/28	0.15	0.09
1.34	150/79	0.24	0.39	3.85	225/40	0.06	0.09
1.61	151/69	0.24	0.29	3.94	345/84	0.19	0.47
1.64	279/84	0.02	0.03	4.02	143/17	0.16	0.19
1.71	158/80	0.36	0.25	4.09	343/47	0.16	0.17
1.72	181/65	0.22	0.19	4.10	231/48	0.03	0.07
1.79	198/10	0.22	0.39	4.17	334/35	0.02	0.07
1.84	158/10	0.02	0.17	4.20	290/18	0.04	0.07
1.88	275/86	0.14	0.29	4.21	118/82	0.14	0.01
1.90	356/85	0.04	0.22	4.24	221/27	0.46	0.38
1.96	152/10	0.14	0.33	4.25	344/77	0.36	0.42
1.99	024/80	0.10	0.11	4.36	032/82	0.01	0.02
2.01	130/07	0.02	0.18	4.40	332/58	0.03	0.18
2.09	332/29	0.44	0.62				
2.21	307/25	0.57	0.06				
2.24	000/15	0.16	0.22				
2.35	330/24	0.16	0.18				
2.39	201/73	0.02	0.04				
2.41	232/82	0.04	0.06				
2.44	329/31	0.04	0.06				
2.47	164/52	0.04	0.07				
2.49	294/33	0.06	0.07				
2.50	192/35	0.04	0.06				
2.51	143/20	0.16	0.01				
2.53	287/31	0.16	0.02				
2.56	187/52	0.01	0.39				
2.58	029/45	0.18	0.39				
2.60	017/11	0.39	0.25				
2.64	170/71	0.12	0.29				
2.74	180/44	0.55	0.39				
2.78	105/22	0.19	0.15				

SCANLINE 8A

Scanline Orientation 240/00
Face Orientation 333/86

D (m)	Orientation	L_1 (m)	L_2 (m)	D (m)	Orientation	L_1 (m)	L_2 (m)
0.00	017/78	0.04	0.39	4.74	236/66	0.13	0.12
0.21	287/67	0.74	0.93	4.81	216/76	0.09	0.24
0.44	029/25	0.07	0.05	4.84	180/77	0.05	0.03
0.50	193/89	0.15	0.06	4.86	355/75	0.18	0.16
0.61	181/14	0.19	0.04	4.89	308/05	0.10	0.11
0.70	063/80	0.16	0.24	4.92	083/85	0.13	0.22
0.74	356/80	0.13	0.14	5.05	034/87	0.17	0.48
0.81	019/70	0.06	0.48	5.11	058/67	0.09	0.13
0.87	039/42	0.14	0.13	5.19	251/53	0.32	0.19
0.90	264/85	0.04	0.26	5.34	022/20	0.18	0.16
1.00	070/66	0.29	0.17	5.36	056/87	0.09	0.09
1.01	193/86	0.05	0.15	5.61	287/68	0.04	0.07
1.04	139/40	0.03	0.10	5.75	244/73	0.09	0.13
1.22	061/67	0.16	0.19	5.77	173/80	0.19	0.17
1.35	000/61	0.07	0.05	5.79	354/84	0.18	0.07
1.44	306/58	0.18	0.33	6.01	210/80	0.32	0.31
1.57	088/66	0.30	0.42	6.12	120/66	0.01	0.24
1.62	289/46	0.05	0.13	6.19	230/75	0.13	0.17
1.65	135/51	0.01	0.03	6.26	060/69	0.10	0.14
1.90	300/48	0.22	0.62	6.31	327/26	0.04	0.18
2.35	180/86	0.30	0.24	6.34	204/80	0.07	0.13
2.36	082/66	0.07	0.05	6.41	114/69	0.04	0.16
2.44	145/79	0.14	0.09	6.50	320/49	0.08	0.13
2.47	274/46	0.13	0.38	6.56	333/87	0.05	0.02
2.54	041/72	0.14	0.49	6.62	233/55	0.07	0.79
2.81	153/80	0.03	0.28	6.64	002/42	0.06	0.36
3.00	166/79	0.04	0.46	6.93	099/72	0.34	0.72
3.06	111/84	0.07	0.04	7.10	205/15	0.40	0.62
3.19	346/90	0.03	0.04	7.13	063/53	0.15	0.07
3.20	330/74	0.06	0.14	7.16	349/40	0.08	0.35
3.25	292/83	0.01	0.07	7.21	220/72	0.03	0.65
3.31	177/78	0.01	0.01	7.25	020/78	0.04	0.09
3.35	195/60	0.02	0.14	7.31	294/55	0.03	0.13
3.42	298/32	0.05	0.07	7.34	188/68	0.06	0.37
3.50	188/54	0.01	0.22	7.40	000/90	0.15	0.06
3.61	093/78	0.24	0.39	7.51	255/43	0.04	0.09
3.92	319/27	0.16	0.14	7.55	017/26	0.09	0.17
4.00	356/25	0.12	0.06	7.60	153/80	0.11	0.06
4.06	198/77	0.02	0.15	7.62	315/70	0.41	0.01
4.12	309/14	0.07	0.03	7.74	031/85	0.03	0.07
4.16	217/78	0.04	0.06	7.76	116/80	0.12	0.38
4.18	200/67	0.36	0.17	7.90	287/72	0.03	0.26
4.21	348/61	0.04	0.23	7.98	276/77	0.02	0.15
4.26	262/79	0.13	0.08	8.01	147/54	0.05	0.07
4.40	094/37	0.02	0.10	8.14	230/44	0.36	0.42
4.48	234/36	0.04	0.03	8.19	324/62	0.08	0.07
4.50	003/45	0.18	0.07	8.20	280/20	0.23	0.36
4.63	007/24	0.07	0.03	8.24	156/76	0.07	0.07
4.70	199/82	0.06	0.14	8.31	110/84	0.01	0.22

SCANLINE 8A (cont.)

D (m)	Orientation	L_1 (m)	L_2 (m)	D (m)	Orientation	L_1 (m)	L_2 (m)
8.34	314/72	0.01	0.15	12.61	331/46	0.09	0.03
8.36	175/83	0.07	0.24	12.65	124/74	0.14	0.16
8.38	274/30	0.01	0.07	12.75	224/80	0.17	0.13
8.46	258/70	0.09	0.93	12.82	298/10	0.32	0.19
8.59	244/50	0.06	0.31	12.91	140/58	0.01	0.28
8.90	154/80	2.00	2.00	13.00	334/61	0.09	0.03
9.09	258/68	0.01	0.34	13.13	251/87	0.35	0.08
9.60	246/72	0.51	0.65	13.20	246/66	0.32	0.18
9.89	039/34	0.07	0.16	13.26	250/79	0.47	0.01
9.91	157/82	1.22	0.46	13.39	295/64	0.19	0.12
9.94	175/66	0.03	0.07	13.42	186/77	0.13	0.08
10.30	098/38	0.09	0.04	13.45	070/89	0.07	0.72
10.35	338/89	0.36	0.32	13.47	076/87	0.13	0.24
10.51	089/54	0.16	0.01	13.50	286/65	0.49	0.66
10.56	248/31	0.10	0.07				
10.58	084/48	0.56	0.37				
10.60	011/62	0.03	0.17				
10.61	255/73	0.02	0.15				
10.70	159/50	0.09	0.11				
10.72	328/35	0.06	0.05				
10.85	287/56	0.14	0.06				
10.96	087/48	0.09	0.12				
10.97	305/42	0.07	0.02				
10.98	163/80	0.02	0.03				
11.00	080/48	0.02	0.16				
11.02	287/55	0.19	0.05				
11.03	308/61	0.02	0.41				
11.08	139/58	0.04	0.02				
11.27	130/76	0.03	0.07				
11.32	321/63	0.04	0.09				
11.37	252/64	0.33	0.63				
11.41	274/45	0.19	0.24				
11.52	008/54	0.49	0.09				
11.53	105/74	0.01	0.07				
11.57	276/56	0.02	0.04				
11.62	230/64	0.09	0.11				
11.65	345/90	0.15	0.12				
11.73	229/76	0.50	0.36				
11.75	033/54	0.07	0.12				
11.86	254/80	2.00	0.95				
11.93	296/64	0.51	0.62				
12.25	319/58	0.07	0.07				
12.26	046/82	0.18	0.24				
12.29	237/78	0.14	0.06				
12.34	234/83	0.05	0.04				
12.38	305/40	0.03	0.14				
12.41	177/51	0.23	0.20				
12.42	034/47	0.19	0.36				
12.45	036/83	0.03	0.05				
12.52	177/55	0.18	0.14				
12.53	032/89	0.14	0.12				

SCANLINE 8B

Scanline Orientation 129/00
Face Orientation 036/83

D (m)	Orientation	L_1 (m)	L_2 (m)	D (m)	Orientation	L_1 (m)	L_2 (m)
0.00	268/72	0.24	0.19	2.61	297/60	0.02	0.09
0.03	052/26	0.18	0.03	2.68	166/76	0.01	0.03
0.10	009/68	0.05	0.17	2.73	042/31	0.08	0.06
0.18	280/66	0.07	0.18	2.80	278/68	0.35	0.09
0.27	262/80	0.01	0.48	2.81	185/84	0.12	0.08
0.31	032/74	0.04	0.01	2.82	096/07	0.15	0.04
0.35	085/85	0.01	0.27	2.84	236/55	0.02	0.07
0.45	323/79	0.07	0.06	2.85	102/64	0.28	0.01
0.50	345/67	0.04	0.16	2.88	248/47	0.03	0.06
0.56	280/84	0.09	0.13	2.96	353/81	0.29	0.10
0.59	174/79	0.02	0.14	2.99	023/39	0.04	0.01
0.62	077/84	0.18	0.19	3.01	261/32	0.04	0.06
0.67	288/80	0.13	0.07	3.17	107/80	0.38	0.02
0.69	040/82	0.12	0.08	3.22	150/45	0.18	0.06
0.70	108/77	0.09	0.13	3.24	274/56	0.05	0.07
0.74	255/80	0.03	0.02	3.30	356/57	0.14	0.13
0.76	063/76	0.12	0.05	3.37	214/60	0.07	0.03
0.78	025/69	0.06	0.17	3.45	079/74	0.39	0.16
0.79	311/89	0.04	0.04	3.53	341/80	0.42	0.07
0.84	323/35	0.01	0.03	3.59	045/04	0.05	0.04
0.85	086/80	0.04	0.09	3.61	274/15	0.09	0.10
0.89	200/63	0.05	0.09	3.64	145/80	0.03	0.06
0.90	304/78	0.07	0.06	3.70	156/61	0.22	0.19
0.94	329/38	0.14	0.22	3.71	037/90	0.02	0.04
1.01	131/83	0.16	0.13	3.81	174/74	0.06	0.92
1.09	326/68	0.04	0.03	3.90	090/87	0.17	0.35
1.25	062/72	0.25	0.54	3.91	091/84	0.16	0.33
1.31	184/72	0.07	0.09	3.93	358/69	0.04	0.02
1.32	058/72	0.16	0.01	4.00	192/77	0.03	0.22
1.61	316/66	0.03	0.05	4.06	099/27	0.08	0.06
1.69	321/75	0.18	0.36	4.09	169/74	0.23	0.15
1.76	335/47	0.08	0.08	4.17	290/24	0.16	0.09
1.84	304/12	0.14	0.19	4.37	035/85	0.18	0.38
1.93	331/26	0.32	0.01	4.56	304/07	0.30	0.15
2.01	154/73	0.09	0.19	4.72	246/82	0.38	0.19
2.02	056/73	0.35	0.02	4.74	110/72	0.59	1.25
2.06	256/68	0.05	0.09	4.77	006/77	0.18	0.29
2.09	323/67	0.18	0.07	4.81	026/88	0.13	0.13
2.18	258/88	0.17	0.04	4.84	340/53	0.17	0.42
2.20	356/71	0.10	0.02	4.93	351/66	0.08	0.16
2.26	061/54	0.31	0.04	4.97	173/76	0.03	0.04
2.28	136/82	0.53	0.18	5.00	238/60	0.38	0.17
2.31	043/47	0.02	0.03	5.14	261/76	0.09	0.03
2.46	071/80	0.04	0.07	5.15	058/26	0.04	0.03
2.47	178/66	0.09	0.09	5.21	110/78	0.02	0.68
2.52	351/25	0.07	0.06	5.24	340/29	0.07	0.18
2.59	353/60	0.38	0.12	5.38	249/50	0.03	0.08

SCANLINE 8B (cont.)

D (m)	Orientation	L_1 (m)	L_2 (m)	D (m)	Orientation	L_1 (m)	L_2 (m)
5.45	002/38	0.02	0.20	9.64	145/82	0.13	0.19
5.57	274/57	0.05	0.09	9.70	183/83	0.02	0.22
5.59	333/88	0.24	0.19	9.71	141/77	0.01	0.13
5.65	105/69	0.23	0.07	9.77	254/60	0.03	0.02
5.67	006/58	0.04	0.03	9.84	008/57	0.03	0.04
5.74	081/67	0.02	0.06	9.90	110/28	0.06	0.03
5.87	004/41	0.09	0.04	9.94	301/47	0.01	0.23
5.89	165/65	0.17	0.20	10.00	330/50	0.13	0.17
5.92	345/19	0.02	0.01	10.12	242/76	0.04	0.18
6.04	091/80	0.36	0.32	10.23	000/70	0.13	0.28
6.23	234/58	0.08	0.06	10.32	065/73	0.02	0.02
6.25	331/82	0.14	0.07	10.33	164/67	0.02	0.07
6.30	312/33	0.17	0.14	10.41	175/71	0.03	0.08
6.34	188/83	0.07	0.09	10.45	066/50	0.10	0.09
6.56	224/52	0.08	0.13	10.46	158/69	0.04	0.06
6.68	101/84	0.22	0.59	10.48	081/47	0.03	0.04
6.81	102/76	0.25	0.54	10.54	173/85	0.10	0.13
6.85	357/52	0.28	0.04	10.57	114/72	0.11	0.07
6.80	346/71	0.18	0.38	10.65	034/80	0.12	0.04
7.31	325/08	0.30	0.22	10.73	349/83	0.02	0.02
7.39	024/85	0.01	0.25	10.81	237/72	0.05	0.03
7.46	318/73	0.06	0.14	10.90	070/65	0.03	0.35
7.54	246/79	0.03	0.24	10.94	267/77	0.03	0.08
7.59	344/81	0.02	0.29	11.00	072/78	0.05	0.06
7.62	257/05	0.24	0.20	11.10	339/80	0.02	0.19
7.67	075/81	0.01	0.36	11.14	065/68	0.11	0.03
7.74	344/62	0.01	0.03	11.21	000/35	0.24	0.25
7.76	184/90	0.02	0.14	11.23	159/82	0.03	0.06
7.90	067/86	0.04	0.12	11.27	342/87	0.06	0.07
7.94	257/80	0.03	0.27	11.30	070/84	0.12	0.22
8.10	058/73	0.02	0.06				
8.13	322/40	0.04	0.45				
8.19	185/62	0.06	0.13				
8.37	084/76	0.03	0.14				
8.43	112/40	0.01	0.03				
8.50	207/53	0.13	0.19				
8.54	106/28	0.25	0.14				
8.71	284/71	0.01	0.29				
8.74	126/52	0.37	0.14				
8.81	018/26	0.15	0.07				
8.90	270/58	0.19	0.07				
8.93	011/80	0.16	0.04				
8.97	218/75	0.01	0.02				
9.02	048/34	0.26	0.09				
9.10	178/61	0.03	0.49				
9.11	280/80	0.03	0.27				
9.16	304/80	0.39	0.22				
9.21	163/78	0.02	0.04				
9.26	215/76	0.23	0.07				
9.33	123/87	0.27	0.01				
9.42	140/54	0.01	0.17				
9.52	005/60	0.15	0.17				

SCANLINE 8C

Scanline Orientation 315/75
Face Orientation 316/80

D (m)	Orientation	L_1 (m)	L_2 (m)	D (m)	Orientation	L_1 (m)	L_2 (m)
0.00	309/59	0.36	0.24	4.41	265/22	0.18	0.22
0.14	311/76	0.49	0.07	4.49	049/58	0.01	0.16
0.28	293/80	0.24	0.16	4.52	268/61	0.04	0.16
0.34	180/04	0.25	0.64	4.58	172/70	0.14	0.16
0.36	084/76	0.07	0.04	4.65	145/56	0.29	0.18
0.39	159/70	0.01	0.04	4.68	333/48	0.19	0.22
0.47	184/80	0.05	0.17	4.71	226/53	0.02	0.07
0.59	298/42	0.16	0.17	4.75	135/55	0.02	0.07
0.61	357/74	0.01	0.18	4.80	113/73	0.04	0.06
0.63	176/78	0.04	0.09	4.85	188/56	0.19	0.08
0.66	109/32	0.04	0.16				
0.77	072/65	0.19	0.23				
0.87	169/75	0.04	0.07				
1.07	019/08	0.15	0.22				
1.09	160/77	0.01	0.19				
1.13	094/64	0.18	0.32				
1.17	354/29	0.16	0.34				
1.22	133/70	0.45	0.93				
1.32	252/48	0.19	0.36				
1.39	111/76	0.64	0.39				
1.57	109/82	0.43	0.29				
1.64	344/28	0.42	0.06				
1.69	170/64	0.02	0.01				
1.82	226/48	0.32	0.39				
1.88	182/78	0.03	0.02				
1.95	162/80	0.14	0.23				
2.02	129/73	0.04	0.06				
2.21	024/36	0.02	0.06				
2.24	148/77	0.04	0.06				
2.41	267/84	0.03	0.06				
2.52	082/64	0.04	0.07				
2.61	021/17	0.09	0.14				
2.64	324/90	0.01	0.04				
2.69	356/23	0.09	0.17				
2.72	140/76	0.19	0.15				
2.74	310/28	0.07	0.09				
2.77	338/68	0.39	0.42				
2.85	150/72	2.00	1.24				
3.13	140/78	0.14	0.36				
3.32	129/13	2.00	1.47				
3.39	147/67	0.04	0.07				
3.46	217/64	0.04	0.02				
3.54	318/18	0.07	0.19				
3.56	345/48	0.07	0.16				
3.62	285/68	0.16	0.24				
3.88	356/41	0.19	0.18				
3.91	281/68	0.17	0.14				
4.14	265/36	0.22	0.19				
4.26	336/85	0.39	0.47				

SCANLINE 9A

Scanline Orientation 126/02
Face Orientation 039/83

D (m)	Orientation	L_1 (m)	L_2 (m)	D (m)	Orientation	L_1 (m)	L_2 (m)
0.00	014/41	0.04	0.03	2.42	014/26	0.22	0.14
0.01	220/87	0.05	0.07	2.48	220/08	0.04	0.07
0.03	236/72	0.01	0.02	2.50	053/90	0.03	0.05
0.15	283/71	0.24	1.23	2.53	112/85	0.03	0.29
0.17	080/50	0.05	0.03	2.58	357/46	0.05	0.02
0.21	209/59	0.04	0.02	2.62	331/55	0.07	0.18
0.24	349/28	0.09	0.04	2.66	079/31	0.14	0.07
0.28	317/32	0.04	0.03	2.68	266/52	0.04	0.07
0.30	185/79	0.15	0.23	2.71	231/30	0.05	0.06
0.34	343/23	0.06	0.03	2.73	011/20	0.03	0.03
0.45	288/66	0.03	0.06	2.75	046/32	0.11	0.07
0.47	059/55	0.10	0.07	2.83	085/54	0.04	0.06
0.50	291/65	0.24	0.53	2.90	295/63	0.18	0.17
0.53	199/78	0.18	0.23	2.93	069/22	0.02	0.03
0.56	029/20	0.03	0.06	2.97	291/59	0.15	0.16
0.64	083/10	0.18	0.03	3.01	048/65	0.18	0.12
0.84	291/62	0.31	0.58	3.20	011/60	0.02	0.46
0.85	102/14	0.09	0.06	3.31	295/51	0.19	0.24
0.90	020/62	0.28	0.07	3.34	215/20	0.06	0.03
1.09	018/86	1.50	0.36	3.36	039/34	0.04	0.15
1.12	281/55	0.28	0.17	3.38	309/63	0.02	0.09
1.13	042/37	0.04	0.19	3.45	101/34	0.14	0.03
1.15	044/79	0.26	0.02	3.46	303/51	0.09	0.17
1.41	290/82	0.06	0.04	3.53	283/67	0.03	0.02
1.43	014/68	0.02	0.02	3.58	142/78	0.01	0.01
1.46	117/49	0.07	0.04	3.61	281/67	0.04	0.17
1.47	202/64	0.09	0.13	3.65	271/67	0.11	0.13
1.51	021/88	0.22	0.16	3.70	197/66	0.03	0.04
1.56	005/23	0.04	0.06	3.73	055/43	0.09	0.07
1.64	283/82	0.38	0.42	3.77	294/62	0.35	0.44
1.66	163/30	0.08	0.07	3.85	300/48	0.40	0.26
1.67	006/46	0.03	0.02	3.88	076/65	0.07	0.06
1.69	230/70	0.14	0.07	3.94	199/66	0.03	0.04
1.72	163/70	0.02	0.01	3.96	035/20	0.04	0.03
1.76	019/60	0.03	0.02	3.98	200/54	0.06	0.03
1.80	341/78	0.02	0.03	4.03	052/64	0.04	0.06
1.90	020/89	0.06	0.04	4.05	309/48	0.24	0.18
1.92	152/28	0.04	0.02	4.06	038/35	0.03	0.04
1.96	010/26	0.02	0.04	4.14	308/68	0.15	0.13
2.01	217/62	0.04	0.03	4.28	305/65	0.18	0.29
2.04	331/45	0.01	0.03	4.34	033/50	0.06	0.07
2.07	128/60	0.07	0.15	4.37	249/15	0.19	0.22
2.10	044/42	0.07	0.06	4.40	220/63	0.01	0.01
2.12	297/70	0.03	0.03	4.50	238/69	0.02	0.01
2.15	304/61	0.19	0.07	4.54	318/88	0.05	0.07
2.17	206/32	0.05	0.07	4.55	032/50	0.09	0.09
2.31	064/64	0.14	0.13	4.58	015/63	0.02	0.04
2.35	106/80	0.42	0.11	4.65	250/42	0.18	0.13
2.40	342/18	0.06	0.22	4.76	035/46	0.14	0.13

SCANLINE 9A (cont.)

D (m)	Orientation	L_1 (m)	L_2 (m)	D (m)	Orientation	L_1 (m)	L_2 (m)
4.78	033/74	0.04	0.02	7.78	290/79	0.52	0.58
4.81	075/16	0.02	0.03	7.81	290/74	0.49	0.23
4.90	228/72	0.01	0.03	7.82	292/73	0.41	0.20
4.98	287/66	0.18	0.16	7.83	291/68	0.40	0.15
4.99	145/80	0.32	0.07	7.85	053/41	0.29	0.13
5.00	334/65	0.05	0.04	7.90	351/02	0.07	0.05
5.11	236/90	0.03	0.02	8.04	107/60	0.04	0.06
5.14	007/19	0.19	0.15	8.10	051/84	0.02	0.07
5.18	237/77	0.05	0.07	8.14	357/16	0.04	0.06
5.20	234/68	0.01	0.03	8.20	159/32	0.16	0.08
5.22	248/48	0.07	0.04	8.27	122/80	0.05	0.07
5.28	339/37	0.14	0.16	8.35	283/34	0.07	0.08
5.31	008/44	0.20	0.06	8.44	092/68	0.06	0.04
5.35	167/51	0.02	0.01	8.50	031/08	0.14	0.16
5.38	138/55	0.04	0.07	8.53	036/48	0.01	0.02
5.50	040/51	0.08	0.36	8.55	209/40	0.07	0.06
5.71	171/84	0.09	0.38	8.64	181/53	0.02	0.07
5.73	010/58	0.18	0.13	8.80	030/20	0.15	0.43
5.82	075/51	0.39	0.04	8.88	255/82	0.04	0.06
5.84	143/81	0.19	0.14	9.00	200/78	0.14	0.07
5.90	191/28	0.05	0.07	9.16	088/64	0.10	0.22
5.91	038/31	0.07	0.05	9.18	016/82	0.03	0.04
5.97	186/75	0.18	0.03	9.21	311/39	0.04	0.01
6.20	153/26	0.19	0.24	9.25	036/82	0.03	0.02
6.24	097/18	0.53	0.22	9.40	016/85	0.04	0.02
6.25	259/53	0.08	0.07	9.50	042/90	0.36	0.01
6.28	020/68	0.05	0.04	9.58	014/78	0.04	0.03
6.34	094/41	0.11	0.17	9.64	130/16	0.03	0.06
6.50	015/62	0.14	0.06	9.73	049/82	0.07	0.14
6.55	162/54	0.30	0.49	9.75	250/20	0.19	0.16
6.80	276/72	0.42	0.20	9.96	067/75	0.18	0.07
7.00	293/69	0.19	0.52	10.00	007/90	0.08	0.09
7.03	260/70	0.03	0.02	10.07	070/36	0.14	0.35
7.05	097/42	0.05	0.02	10.14	247/39	0.06	0.02
7.07	291/62	0.09	0.04	10.21	047/45	0.14	0.08
7.08	187/07	0.04	0.03	10.37	011/87	0.19	0.14
7.11	056/46	0.01	0.22	10.40	239/48	0.03	0.04
7.22	289/69	0.53	0.18	10.46	012/62	0.01	0.08
7.25	085/40	0.03	0.02	10.51	284/36	0.04	0.02
7.30	292/58	0.54	1.63	10.55	100/50	0.06	0.32
7.31	053/44	0.08	0.06	10.60	020/85	0.04	0.31
7.45	299/64	0.91	1.74				
7.47	172/73	0.05	0.07				
7.50	287/66	0.19	0.18				
7.54	038/72	0.03	0.02				
7.57	292/70	0.24	0.19				
7.63	299/63	0.14	0.12				
7.65	125/23	0.04	0.02				
7.67	297/71	0.05	0.04				
7.70	295/62	0.36	0.28				
7.73	187/81	0.02	0.05				

SCANLINE 10A

Scanline Orientation 100/00
Face Orientation 196/85

D (m)	Orientation	L_1 (m)	L_2 (m)	D (m)	Orientation	L_1 (m)	L_2 (m)
0.00	336/72	2.00	0.28	4.24	085/76	0.13	0.05
0.10	282/15	0.60	0.62	4.27	002/77	0.14	0.02
0.22	345/67	0.30	0.34	4.31	183/65	0.01	0.02
0.38	251/62	0.06	0.23	4.35	349/44	0.02	0.49
0.87	311/55	0.11	0.25	4.56	154/89	0.04	0.16
0.96	193/83	0.06	0.27	4.61	299/48	0.07	0.29
1.04	114/35	0.19	0.33	4.67	215/54	0.03	0.16
1.46	049/72	0.03	0.07	4.71	236/56	0.03	0.07
1.53	340/36	0.58	0.07	4.80	353/38	0.84	0.63
1.61	190/78	0.08	0.03	4.89	132/23	0.02	0.03
1.69	170/30	0.11	0.01	4.92	293/82	0.01	0.07
1.88	078/77	0.15	0.07	4.97	199/13	0.09	0.15
1.93	162/62	0.22	0.15	5.02	043/13	0.09	0.15
1.99	157/72	0.07	0.25	5.04	229/50	0.02	0.02
2.01	326/30	0.07	0.64	5.09	305/20	0.07	0.89
2.09	163/65	0.07	0.25	5.20	192/26	0.42	0.31
2.23	305/25	0.74	0.39	5.25	012/38	0.22	0.43
2.44	047/28	0.02	0.09	5.39	116/78	0.07	0.05
2.46	291/28	0.36	0.07	5.52	040/58	0.07	0.36
2.60	096/60	0.19	0.03	5.61	164/50	0.12	0.25
2.64	282/30	0.29	0.41	5.69	002/19	1.05	0.07
2.72	358/62	0.04	0.19	5.82	253/34	0.15	0.07
2.75	195/62	0.14	0.03	5.85	160/87	0.04	0.14
2.84	161/70	0.06	0.04	5.96	000/20	0.84	0.38
2.92	173/63	0.09	0.04	5.97	225/62	0.18	0.36
2.98	356/56	0.03	0.09	6.09	048/70	0.02	0.02
2.99	305/52	0.08	0.14	6.20	020/37	0.07	0.15
3.02	159/60	0.02	0.03	6.23	257/37	0.06	0.19
3.04	282/36	0.04	0.03	6.31	329/45	0.43	0.36
3.06	292/46	0.02	0.05	6.34	168/34	0.07	0.09
3.12	153/76	0.04	0.23	6.36	240/25	0.18	0.15
3.20	321/52	0.06	0.04	6.40	234/22	0.43	0.07
3.22	191/61	0.04	0.06	6.48	169/76	0.11	0.08
3.34	209/76	0.06	0.09	6.49	059/04	0.15	0.32
3.51	209/26	0.04	0.07	6.52	014/28	0.17	0.33
3.58	101/58	0.01	0.07	6.54	152/15	0.07	0.04
3.62	046/72	0.01	0.01	6.58	172/86	0.01	0.03
3.68	334/50	0.06	0.14	6.75	232/32	0.15	0.20
3.85	321/48	0.06	0.49	6.78	258/84	0.14	0.32
3.86	327/58	0.07	0.09	6.80	302/37	0.05	0.06
3.90	140/42	0.03	0.06	6.82	302/35	0.04	0.04
3.92	308/75	0.07	0.09	6.85	079/58	0.05	0.07
3.95	269/34	0.07	0.13	6.87	239/31	0.10	0.07
3.99	125/84	0.07	0.15	6.90	331/33	0.04	0.03
4.01	307/80	0.09	0.06				
4.03	134/30	0.07	0.10				
4.07	348/21	0.15	0.14				
4.12	259/74	0.08	0.08				
4.20	183/81	0.07	0.06				

SCANLINE 10B

Scanline Orientation 184/78
Face Orientation 196/85

D (m)	Orientation	L_1 (m)	L_2 (m)	D (m)	Orientation	L_1 (m)	L_2 (m)
0.00	175/48	0.09	0.25	2.98	157/84	0.02	0.04
0.11	247/75	0.07	0.14	3.00	150/83	0.05	0.02
0.15	284/23	0.14	0.06	3.04	314/42	0.03	0.01
0.19	223/54	0.46	0.20	3.05	324/75	0.01	0.07
0.20	205/15	0.03	0.04	3.09	215/90	0.07	0.02
0.22	176/90	0.03	0.07	3.14	179/57	0.04	0.02
0.25	227/52	0.02	0.25	3.16	080/05	2.00	2.00
0.27	038/73	0.01	0.01	3.18	049/84	0.12	0.03
0.30	215/31	0.04	0.07	3.20	359/16	0.07	0.18
0.34	211/28	0.04	0.23	3.22	193/84	0.17	0.18
0.37	323/28	0.01	0.04	3.29	206/43	0.24	0.17
0.40	213/32	0.05	0.07	3.32	023/44	0.18	0.33
0.45	003/09	0.12	0.08	3.42	312/14	0.19	0.32
0.51	214/20	0.72	0.19	3.50	009/30	0.25	0.18
0.57	138/75	0.03	0.07	3.52	226/27	0.32	0.17
0.61	196/90	0.01	0.05	3.60	194/54	0.32	0.16
0.69	242/20	0.01	0.25				
0.72	328/64	1.50	0.24				
0.91	331/70	0.72	0.19				
0.97	334/72	0.24	0.20				
1.14	160/13	0.15	0.07				
1.18	162/84	0.08	0.10				
1.19	063/80	0.07	0.01				
1.26	295/20	0.21	0.09				
1.34	175/75	0.04	0.03				
1.54	292/17	0.01	0.24				
1.58	251/77	0.05	0.18				
1.61	349/14	1.14	0.36				
1.63	323/80	0.14	0.11				
1.65	195/30	0.14	0.04				
1.70	189/41	0.13	0.07				
1.72	236/74	0.12	0.07				
1.76	339/58	0.09	0.07				
1.79	041/28	0.13	0.62				
1.84	256/10	0.15	0.22				
1.85	323/14	0.17	0.10				
1.88	270/36	0.06	0.05				
1.90	291/28	0.16	0.12				
1.91	035/28	0.01	0.03				
1.95	167/40	0.35	0.16				
2.11	313/20	0.94	0.72				
2.20	325/14	0.23	0.08				
2.26	327/67	2.00	0.32				
2.41	325/80	1.30	0.29				
2.66	059/05	0.22	2.00				
2.72	179/74	0.21	0.34				
2.78	177/81	0.02	0.15				
2.82	330/72	0.13	0.04				
2.94	178/16	0.25	0.19				

SCANLINE 10C

Scanline Orientation 189/00
Face Orientation 095/86

D (m)	Orientation	L_1 (m)	L_2 (m)
0.00	097/58	0.03	0.07
0.03	330/55	0.24	0.02
0.06	177/61	0.03	0.14
0.10	266/71	0.01	0.05
0.14	345/71	0.07	0.05
0.17	186/60	0.24	0.01
0.26	060/17	0.15	0.07
0.34	138/87	0.11	0.06
0.39	217/81	0.05	0.12
0.48	116/69	0.03	0.07
0.51	299/22	0.25	0.42
0.56	329/78	0.01	0.12
0.64	315/79	0.01	0.04
0.72	327/70	0.01	0.14
0.74	058/81	0.05	0.09
0.81	318/76	0.04	0.12
0.93	157/80	0.07	0.12
0.96	162/55	0.08	0.02
0.99	061/76	0.22	0.15
1.14	146/68	0.04	0.06
1.22	345/78	0.01	0.27
1.29	132/90	0.06	0.07
1.31	313/11	0.07	0.17
1.34	239/12	0.15	0.27
1.52	309/70	0.09	0.03
1.59	343/04	0.17	0.16
1.65	130/74	0.02	0.07
1.77	134/88	0.03	0.07
1.79	060/72	0.01	0.03
1.84	064/63	0.04	0.05
1.90	009/62	0.32	0.05
1.91	218/07	0.19	0.07
1.94	337/74	0.04	0.03
2.02	096/86	0.04	0.07
2.08	339/64	0.15	0.12
2.10	342/68	0.07	0.03
2.14	346/72	0.01	0.15
2.17	104/50	0.07	0.02
2.26	356/11	0.03	0.07
2.29	337/16	0.06	0.05
2.31	140/74	0.07	0.04
2.34	050/86	0.02	0.02
2.42	355/09	0.07	0.09
2.43	033/72	0.01	0.27
2.44	008/76	0.06	0.02
2.49	352/53	0.05	0.49
2.60	169/70	0.01	0.01
2.64	284/25	0.17	0.24
2.76	280/61	0.03	0.17
2.78	286/20	0.19	0.42
2.79	341/85	0.02	0.19
2.82	111/54	0.06	0.16
2.94	273/22	0.14	0.15
2.97	001/75	0.01	0.15
3.05	291/25	0.19	0.24
3.13	184/85	0.17	0.06
3.18	343/78	0.03	0.33
3.21	083/73	0.03	0.15
3.22	339/08	0.05	0.19
3.24	041/84	0.27	0.06
3.32	008/66	0.17	0.33
3.36	248/84	0.04	0.07
3.39	160/68	0.07	0.12
3.41	345/10	0.25	0.15
3.53	117/54	0.25	0.11
3.55	258/90	0.34	0.12
3.64	111/54	0.17	0.19
3.82	122/55	0.21	0.24
4.01	028/32	0.19	0.07
4.22	123/59	0.12	0.10
4.26	063/34	0.05	0.06
4.29	355/41	0.03	0.07
4.33	132/80	0.02	0.04
4.42	056/20	0.13	0.17
4.50	319/76	0.49	0.93
4.63	066/39	0.03	0.05
4.69	221/84	0.10	0.24
4.72	037/90	0.24	0.29
4.79	254/76	0.03	0.02
4.82	255/10	0.07	0.06
4.84	349/48	0.01	0.05
4.86	166/82	0.02	0.15
4.90	263/80	0.17	0.22

SHAFT

Horizontal Scanline

Depth 1.00 m

D (m)	Orientation	L_1 (m)	D (m)	Orientation	L_1 (m)
0.00	320/56	0.47	5.96	103/85	0.21
0.02	124/38	0.09	6.07	223/76	0.02
0.04	166/04	0.19	6.24	016/76	0.19
0.15	061/69	0.43	6.34	177/12	0.22
0.22	287/14	0.33	6.71	290/79	0.31
0.42	062/69	0.16	6.92	312/40	0.04
0.47	121/66	0.18	6.97	238/67	0.05
0.74	317/84	0.06	7.10	149/54	0.32
0.76	289/48	0.18	7.47	344/60	0.08
0.78	081/84	0.05	7.74	132/70	0.16
0.82	292/41	0.14	7.78	121/80	0.14
0.92	292/88	0.11	7.93	339/54	0.12
1.14	240/39	0.57	7.97	161/35	0.18
1.29	309/78	0.22	8.00	234/70	0.12
1.31	228/47	0.19	8.32	331/54	0.33
1.32	223/65	0.10	8.49	129/19	0.22
1.61	193/78	0.09	8.68	236/80	0.11
1.62	294/58	0.08	8.80	083/23	0.09
1.73	234/27	0.16	9.50	156/22	0.20
1.74	033/78	0.11	9.90	302/42	0.73
2.18	315/60	0.18	10.20	232/43	0.64
2.21	275/28	0.22	11.00	312/55	0.45
2.36	227/54	0.03	11.27	325/52	0.23
2.43	319/78	0.14	11.30	159/02	0.31
2.46	039/12	0.22			
2.50	176/70	0.17			
2.65	339/06	0.06			
2.70	004/82	0.16			
2.82	290/38	0.07			
2.85	323/44	0.04			
2.87	168/68	0.15			
3.00	333/51	0.09			
3.24	296/42	0.24			
3.35	327/52	0.07			
3.47	257/52	0.03			
3.55	357/75	0.09			
3.61	004/64	0.27			
3.63	308/46	0.11			
3.72	339/32	0.06			
3.79	310/38	0.09			
3.80	125/59	0.04			
4.30	070/42	0.39			
4.41	180/74	0.22			
4.53	283/38	0.41			
4.58	311/33	0.04			
4.83	055/55	0.44			
5.30	353/58	0.28			
5.78	335/61	0.16			

SHAFT

Horizontal Scanline

Depth 1.70 m

D (m)	Orientation	L_1 (m)	D (m)	Orientation	L_1 (m)
0.00	001/68	0.39	6.55	323/39	0.18
0.06	197/48	0.08	6.66	067/62	0.37
0.41	290/24	0.15	6.72	195/62	0.15
0.93	157/80	0.15	6.84	063/78	0.08
0.95	333/47	0.08	7.10	331/84	0.96
0.99	330/83	0.07	7.17	259/43	0.62
1.07	125/75	0.22	7.25	359/52	0.21
1.39	099/25	0.36	7.61	051/45	0.27
1.47	110/15	0.07	7.76	304/48	0.49
1.51	298/54	0.07	8.08	267/25	0.15
1.57	047/62	0.19	8.28	242/08	0.17
1.82	187/72	0.24	8.41	335/82	0.07
1.89	111/56	0.32	8.62	359/60	0.48
1.97	108/43	0.36			
2.12	097/45	0.06			
2.21	110/55	0.12			
2.34	186/36	0.14			
2.47	233/64	0.19			
2.53	255/68	0.07			
2.63	136/64	0.18			
2.73	189/49	0.18			
2.81	264/77	0.08			
2.93	005/16	0.19			
2.98	006/11	0.16			
3.06	209/89	0.05			
3.11	116/80	0.07			
3.23	224/36	0.14			
3.36	296/72	0.07			
3.38	349/40	0.15			
3.44	227/31	0.18			
3.56	330/38	0.03			
3.87	324/63	0.15			
4.30	289/14	0.86			
4.31	222/41	0.07			
4.57	128/81	0.87			
4.77	236/30	0.06			
4.84	091/82	0.08			
5.21	306/37	0.09			
5.33	336/89	0.07			
5.43	209/36				
5.58	318/32	0.09			
5.62	309/15	0.09			
5.74	329/52	0.25			
5.79	182/63	0.05			
5.91	291/62	0.57			
6.12	326/68	0.42			
6.31	162/24	0.08			
6.35	166/10	0.19			

SHAFT

Horizontal Scanline

Depth 2.50 m

D (m)	Orientation	L_1 (m)	D (m)	Orientation	L_1 (m)
0.00	235/47	0.19	4.19	325/79	0.05
0.07	004/80	0.07	4.23	303/79	0.02
0.21	195/33	0.07	4.54	213/12	0.53
0.25	171/68	0.02	4.56	166/68	0.05
0.38	209/32	0.08	4.72	297/76	0.04
0.41	251/32	0.08	4.74	199/41	0.18
0.49	211/34	0.25	4.81	276/44	0.22
0.67	326/28	0.04	4.98	212/47	0.43
0.87	205/42	0.04	5.00	000/42	2.00
0.88	241/14	0.06	5.11	348/69	0.07
0.93	177/87	0.05	5.19	327/43	0.16
1.10	242/26	0.36	5.21	026/47	0.09
1.14	190/30	0.06	5.27	348/43	0.09
1.26	034/80	0.12	5.29	318/21	0.24
1.28	215/32	0.06	5.34	255/62	0.03
1.48	349/84	0.07	5.39	352/78	0.16
1.53	266/85	0.07	5.47	100/53	0.08
1.54	155/72	0.05	5.61	042/79	0.03
1.57	169/84	0.05	5.62	125/65	0.02
1.59	070/82	0.03	5.65	138/58	0.07
1.60	163/77	0.11	5.69	174/35	0.07
1.64	011/12	0.07	5.74	263/26	0.32
1.66	193/13	0.15	5.83	355/80	0.06
1.82	202/90	0.02	5.91	353/50	0.36
2.00	177/84	0.23	6.33	157/80	0.11
2.04	154/66	0.25	6.36	215/20	0.78
2.48	231/32	0.26	6.47	338/24	0.42
2.69	020/90	0.07	6.55	352/73	0.07
2.82	023/82	0.06	6.61	199/78	0.16
2.87	208/60	0.04	6.64	234/71	0.08
2.89	306/79	0.14	6.88	178/46	0.08
2.98	043/52	0.08	6.89	315/50	0.17
3.09	304/66	0.08	6.92	000/48	0.29
3.18	219/51	0.09	7.14	234/20	0.42
3.19	071/36	0.25	7.30	030/78	
3.36	272/48	0.03	7.34	219/89	0.04
3.40	244/84	0.09	7.42	062/39	0.06
3.43	010/58	0.18	7.54	029/20	0.15
3.57	279/15	0.03	7.65	033/40	0.07
3.72	315/82	0.04	7.73	008/66	0.07
3.76	045/38	0.07	7.78	256/10	0.24
3.77	055/36	0.08	7.81	091/34	0.06
3.86	358/72	0.06	7.92	213/28	0.03
3.95	158/30	0.14	7.99	152/32	0.09
4.01	240/07	0.65	8.07	064/40	0.13
4.05	017/56	0.06	8.14	004/52	0.08
4.08	029/36	0.02	8.23	153/88	0.04
4.14	198/78	0.07	8.33	327/36	0.25

SHAFT

Horizontal Scanline

Depth 2.50 m (cont.)

D (m)	Orientation	L_1 (m)	D (m)	Orientation	L_1 (m)
8.48	244/39	0.08	3.39	108/70	0.16
8.55	316/46	0.09	3.44	204/68	0.16
8.67	356/49	0.32	3.50	044/86	0.13
8.72	310/58	0.42	3.68	226/67	0.14
8.77	225/13	0.04	3.91	168/79	0.06
8.83	132/70	0.09	3.96	005/90	0.05
8.89	299/84	0.36	4.07	004/83	0.02
8.93	188/71	0.15	4.34	224/21	2.00
8.95	233/14	0.15	4.62	085/83	0.15
			4.83	023/51	0.16
			5.12	304/14	0.21
			5.30	052/90	0.16
			5.38	241/55	0.29
			5.49	312/28	0.42
			5.64	311/23	0.44
			5.91	344/83	0.06
			6.24	332/36	0.29
			6.42	209/83	0.27
			6.45	124/28	0.19
			6.64	346/69	0.22
			6.78	283/48	0.39
			6.98	035/64	0.24
			7.14	041/24	0.29
			7.22	038/59	0.06
			7.29	170/22	0.14
			7.36	043/62	0.08
			7.42	038/53	0.19
			7.48	021/36	0.15
			7.78	211/33	0.02
			7.80	038/68	0.03
			7.88	220/28	0.16
			7.92	223/30	0.14
			7.99	222/38	0.07
			8.02	222/79	0.16
			8.06	224/22	0.15
			8.12	003/66	0.19
			8.18	179/60	0.02
			8.26	215/36	0.05
			8.29	353/58	0.06
			8.37	281/19	0.14
			8.44	018/62	0.39
			8.46	011/76	0.19
			8.48	267/84	0.12
			8.60	122/83	0.12
			8.62	016/82	0.14

SHAFT

Horizontal Scanline

Depth 3.80 m

D (m)	Orientation	L_1 (m)
0.11	025/80	0.16
0.24	080/08	0.39
0.34	326/62	0.19
0.37	271/87	0.14
0.39	102/79	0.22
0.45	291/72	0.04
0.46	009/87	0.34
0.49	074/54	0.04
0.51	205/40	0.06
0.59	202/59	0.14
0.67	299/82	0.15
0.89	055/22	0.14
1.02	216/78	0.22
1.24	083/50	0.13
1.34	199/82	0.03
1.41	306/76	0.04
1.50	148/20	0.14
1.59	321/72	0.42
1.74	051/60	0.06
1.75	199/80	0.14
1.80	122/60	0.15
1.84	322/22	0.39
2.18	090/12	0.16
2.22	300/68	0.23
2.54	013/80	0.14
2.71	210/80	0.14
2.74	030/71	0.12
2.96	034/84	0.12
3.06	028/84	0.16

SHAFT

Horizontal Scanline

Depth 5.10 m

D (m)	Orientation	L_1 (m)	D (m)	Orientation	L_1 (m)
0.00	231/72	0.09	7.10	338/20	0.49
0.27	015/42	0.24	7.34	301/25	0.17
0.41	083/42	0.22	7.48	326/70	0.39
0.44	304/58	0.04	7.51	222/26	0.18
0.53	055/57	0.19	7.55	063/44	0.22
0.59	082/50	0.17			
0.64	090/44	0.08			
0.78	056/70	0.23			
0.81	316/58	0.44			
0.83	028/68	0.09			
0.94	277/62	0.14			
1.09	191/40	0.32			
1.41	327/88	0.25			
1.58	326/44	0.19			
1.63	165/48	0.07			
1.72	320/69	0.49			
1.91	327/81	0.16			
2.15	322/78	0.07			
2.40	353/70	0.04			
2.44	068/73	0.18			
2.47	064/81	0.17			
2.72	347/62	0.08			
2.91	357/88	0.08			
3.11	066/51	0.03			
3.40	095/79	0.02			
3.44	333/74	0.18			
3.57	160/32	0.25			
3.91	294/82	0.57			
4.06	048/08	0.02			
4.09	107/69	0.06			
4.21	102/72	0.14			
4.30	330/72	0.06			
4.47	318/68	0.23			
4.52	226/40	0.07			
4.78	255/49	0.18			
4.95	125/66	0.07			
5.02	063/75	0.02			
5.14	010/74	0.17			
5.18	016/76	0.14			
5.44	338/83	0.09			
5.51	340/72	0.11			
5.61	316/30	0.07			
5.69	299/22	1.40			
5.78	191/18	0.07			
6.21	278/22	0.43			
6.48	118/80	0.03			
6.51	292/37	0.06			
6.58	301/53	0.42			
6.71	317/31	0.07			

SHAFT

Horizontal Scanline

Depth 6.35 m

D (m)	Orientation	L_1 (m)	D (m)	Orientation	L_1 (m)
0.00	010/61	0.25	4.69	201/33	0.14
0.09	118/58	0.09	4.74	200/73	0.06
0.14	214/90	0.17	5.12	307/50	0.39
0.24	069/80	0.15	5.24	227/31	0.15
0.31	321/66	0.52	5.35	292/32	0.24
0.39	007/67	0.14	5.41	239/21	0.07
0.44	078/70	0.39	5.42	281/23	0.16
0.67	314/29	0.14	5.44	261/23	0.07
0.80	139/78	0.08	5.46	263/17	0.09
0.85	218/20	0.09	5.50	333/70	0.06
0.96	069/72	0.03	5.59	254/23	0.19
1.02	193/40	0.01	5.62	157/35	0.19
1.11	015/47	0.04	5.70	288/76	0.19
1.14	029/72	0.39	5.83	334/56	0.18
1.15	286/43	0.19	5.84	092/31	0.09
1.28	292/10	0.07	5.88	115/56	0.04
1.54	085/67	0.14	5.90	323/46	0.37
1.61	113/38	0.74	6.31	001/77	0.07
1.64	122/38	0.19	6.64	033/80	0.14
1.85	063/67	0.14	6.65	332/24	0.14
2.14	240/55	0.13	6.74	253/73	0.13
2.27	350/07	0.19	6.80	171/31	0.49
2.30	343/82	0.04	6.92	035/11	0.15
2.49	224/59	1.80	7.03	196/80	0.13
2.51	335/16	0.04	7.26	308/44	0.14
2.81	310/82	0.19	7.55	235/79	0.20
2.87	044/71	0.47	7.56	335/72	0.06
2.89	048/51	0.19	7.59	258/75	0.11
2.94	204/52	0.36	7.81	327/50	0.16
3.18	218/20	0.37	7.87	206/47	0.13
3.47	138/32	0.17	7.99	177/50	0.06
3.57	033/67	0.17	8.00	232/63	0.33
3.59	160/42	0.29	8.09	162/58	0.13
3.62	018/77	0.14	8.22	190/28	0.04
3.64	353/60	0.13	8.25	332/63	0.44
3.70	351/32	0.04	8.38	190/21	0.07
3.83	006/50	0.19	8.54	321/61	0.06
3.92	273/74	0.19	8.59	133/40	0.19
3.95	235/48	0.17			
4.04	011/65	0.33			
4.11	243/44	0.16			
4.13	207/48	0.17			
4.23	040/84	0.16			
4.31	125/83	0.19			
4.34	319/72	0.16			
4.45	217/32	0.39			
4.56	312/66	0.49			
4.59	312/70	0.57			

SHAFT

Horizontal Scanline

Depth 7.40 m

D (m)	Orientation	L_1 (m)	D (m)	Orientation	L_1 (m)
0.00	207/74	0.06	5.70	123/40	0.13
0.41	273/78	0.14	5.79	148/85	0.13
0.64	184/67	0.13	5.87	307/35	0.19
0.73	116/50	0.12	5.97	174/69	0.06
0.89	608/34	0.42	6.02	052/55	0.07
0.92	006/22	0.39	6.14	009/60	0.13
1.10	133/38	0.14	6.31	025/49	0.17
1.25	023/90	0.04	6.44	105/08	0.14
1.34	163/56	0.07	6.58	005/68	0.45
1.48	179/84	0.06	6.67	316/42	0.19
1.59	044/46	0.12	6.83	322/38	0.41
1.60	331/71	0.15	7.02	285/73	0.17
1.64	136/61	0.04	7.16	354/34	0.31
1.92	070/79	0.16	7.26	164/68	0.19
1.94	190/57	0.12	7.30	010/32	0.19
2.00	240/53	0.17	7.54	205/56	0.07
2.01	015/34	0.07	7.64	234/32	0.20
2.11	038/71	0.14	7.84	200/40	0.13
2.18	046/72	0.31	7.87	192/50	0.14
2.21	292/70	0.23	7.91	204/27	0.06
2.25	074/57	0.13	7.99	091/88	0.16
2.29	289/33	0.21	8.01	106/85	0.13
2.30	191/76	0.18	8.07	082/57	0.13
2.44	331/72	0.12	8.16	287/59	0.31
2.50	326/65	0.13	8.31	264/33	0.07
2.58	085/83	0.22	8.33	091/38	0.19
2.60	350/58	0.11	8.34	337/80	0.15
2.80	146/76	0.24			
2.85	254/13	0.25			
2.99	041/31	0.06			
3.02	208/28	0.17			
3.34	208/40	0.17			
3.45	088/37	0.04			
3.47	225/24	0.49			
3.91	255/72	0.14			
3.98	147/82	0.09			
4.02	208/29	0.15			
4.15	079/77	0.06			
4.41	155/72	0.32			
4.44	294/74	0.16			
4.90	229/70	0.09			
4.93	028/48	0.14			
4.96	306/37	0.19			
5.09	194/81	0.17			
5.17	237/62	0.15			
5.33	343/69	0.18			
5.38	264/61	0.16			
5.48	120/90	0.15			

SHAFT

Horizontal Scanline

Depth 8.40 m

D (m)	Orientation	L_1 (m)	D (m)	Orientation	L_1 (m)
0.00	210/21	0.17	4.91	068/58	0.10
0.11	198/25	0.17	5.03	325/76	0.19
0.23	174/60	0.25	5.09	083/52	0.02
0.25	260/84	0.17	5.14	331/67	0.09
0.34	046/44	0.39	5.18	323/80	0.29
0.58	032/46	0.24	5.31	306/54	0.26
0.59	222/64	0.36	5.43	289/32	0.25
0.67	152/80	0.19	5.47	326/84	0.34
0.74	236/55	0.20	5.50	001/14	0.10
0.77	302/69	0.07	5.53	334/77	0.42
0.84	109/67	0.14	5.62	261/61	0.39
1.06	034/49	0.04	5.68	130/11	0.24
1.13	262/56	0.19	5.80	322/23	0.42
1.17	211/78	0.05	5.82	331/75	0.15
1.30	251/32	0.07	5.89	285/65	0.37
1.41	133/01	0.42	5.94	145/33	0.06
1.50	179/90	0.16	6.11	260/37	0.49
1.59	311/63	0.06	6.17	189/11	0.15
1.61	332/75	0.06	6.30	015/82	0.27
1.63	028/83	0.15	6.38	022/85	0.16
1.83	058/77	0.35	6.46	000/44	0.19
1.96	054/49	0.09	6.59	322/60	0.39
2.04	130/60	0.29	6.62	195/36	0.06
2.12	299/38	0.16	6.67	256/62	0.19
2.26	153/40	0.13	6.70	328/55	0.39
2.31	277/75	0.10	6.74	030/58	0.19
2.37	177/89	0.13	6.79	039/70	0.15
2.49	179/32	0.33	6.80	018/53	0.14
2.73	244/84	0.17	6.91	346/50	0.17
2.91	180/07	0.49	6.96	329/37	0.19
3.03	214/10	0.69	7.04	025/37	0.16
3.07	069/15	0.10	7.21	003/25	0.49
3.10	292/72	0.15	7.29	001/36	0.18
3.24	203/24	0.49	7.44	359/41	0.18
3.38	192/34	0.17	7.49	023/44	0.16
3.60	353/54	0.29	7.57	157/04	0.23
3.65	039/39	0.17	7.60	330/82	0.14
3.81	179/70	0.05	7.63	048/67	0.13
3.84	011/19	0.39	7.69	216/62	0.07
3.96	254/29	0.07	8.01	238/53	0.04
4.15	014/33	0.17	8.05	031/36	0.29
4.16	191/59	0.07	8.12	080/38	0.16
4.20	011/34	0.17	8.24	105/77	0.13
4.30	112/38	0.07	8.31	195/74	0.13
4.34	097/17	0.16	8.34	009/80	0.06
4.41	330/82	0.19	8.40	041/47	0.22
4.64	003/64	0.46			
4.79	256/57	0.34			

SHAFT

Horizontal Scanline

Depth 9.50 m

D (m)	Orientation	L_1 (m)	D (m)	Orientation	L_1 (m)
0.00	358/52	0.25	5.47	340/32	0.15
0.08	178/39	0.04	5.57	325/28	0.14
0.11	340/60	0.31	5.66	322/85	0.19
0.19	028/65	0.15	5.81	267/24	0.17
0.22	214/57	0.29	5.89	003/67	0.14
0.25	004/46	0.34	6.07	017/66	0.05
0.31	069/26	0.15	6.23	106/27	0.16
0.39	313/59	0.07	6.29	019/78	0.19
0.46	322/71	0.18	6.46	217/30	0.18
0.47	325/76	0.15	6.52	121/42	0.31
0.65	121/27	0.24	6.69	283/17	0.28
0.71	047/72	0.03	6.74	142/62	0.02
0.74	293/22	0.15	6.99	184/61	0.44
0.86	265/09	0.19	7.27	029/62	0.04
0.88	341/46	0.15	7.33	175/62	0.10
1.16	159/82	0.22	7.57	160/23	0.08
1.17	154/80	0.24	7.66	032/36	0.14
1.33	140/24	0.35	7.85	342/86	0.24
1.45	324/16	0.49	7.92	335/47	1.40
1.64	347/71	0.10	8.22	020/20	0.34
1.90	267/40	0.15	8.34	165/37	0.14
1.99	343/05	0.47	8.35	217/29	0.40
2.11	180/74	0.03			
2.23	262/88	0.05			
2.31	017/76	0.09			
2.36	249/19	0.20			
2.38	302/44	0.02			
2.62	170/25	0.11			
2.74	032/38	0.14			
3.08	068/54	0.28			
3.13	147/80	0.44			
3.20	209/20	1.87			
3.43	211/29	1.24			
3.64	153/68	0.19			
3.67	004/79	0.24			
4.03	192/82	0.15			
4.23	005/28	0.24			
4.25	024/66	0.18			
4.34	107/47	0.03			
4.36	282/20	0.04			
4.40	294/73	0.15			
4.51	335/48	0.16			
4.53	022/08	0.02			
4.64	295/59	0.18			
4.69	322/54	0.17			
4.71	295/51	0.10			
5.00	204/08	0.30			
5.33	117/60	0.05			
5.36	216/55	0.07			

SHAFT

Horizontal Scanline

Depth 10.20 m

D (m)	Orientation	L_1 (m)	D (m)	Orientation	L_1 (m)
0.00	350/62	0.06	5.09	085/08	0.31
0.12	178/18	0.11	5.14	052/22	0.02
0.17	232/69	0.11	5.30	054/19	0.22
0.32	341/80	0.29	5.36	226/82	0.07
0.33	334/83	0.34	5.44	023/33	0.27
0.49	040/50	0.13	5.53	334/80	0.14
0.54	314/34	0.25	5.64	171/14	0.39
0.71	289/45	0.24	5.68	174/27	0.20
0.76	087/30	0.20	5.79	230/19	0.25
0.81	187/37	0.40	5.82	339/32	0.07
1.12	031/81	2.00	5.84	068/15	0.02
1.18	313/72	0.15	5.87	356/78	0.02
1.23	260/18	0.19	5.89	002/80	0.07
1.29	288/59	0.17	6.04	025/40	0.10
1.30	244/53	0.10	6.10	344/80	0.07
1.33	344/78	0.05	6.15	130/75	0.20
1.37	079/65	0.05	6.31	034/74	0.04
1.38	270/25	0.33	6.40	182/11	0.17
1.40	334/80	0.07	6.42	144/32	0.01
1.44	095/34	0.03	6.54	150/80	0.24
1.56	227/80	0.13	6.64	196/58	0.17
1.57	293/21	0.20	6.67	350/36	0.10
1.62	130/90	0.12	6.82	337/86	0.31
1.64	072/08	1.04	6.88	085/81	0.49
2.01	167/63	0.25	6.93	077/83	0.43
2.07	170/68	0.29	6.98	182/75	0.39
2.23	195/08	0.21	7.11	024/66	0.31
2.53	124/38	0.25	7.30	158/07	0.14
2.56	012/08	0.13	7.32	155/10	0.17
2.63	127/30	0.16	7.43	148/28	0.17
2.65	110/43	0.10	7.52	173/66	0.23
2.74	132/38	0.15	7.57	238/79	0.25
2.77	354/25	0.02	7.81	061/74	0.06
2.94	218/26	0.15	7.85	016/44	0.20
3.11	331/82	0.41	7.89	124/23	0.19
3.23	222/33	0.20	7.94	001/72	0.16
3.24	210/28	0.25	7.96	244/54	0.01
3.72	258/52	0.17	8.00	161/66	0.10
3.77	228/33	0.41			
3.84	321/54	0.22			
4.01	340/23	0.24			
4.14	251/20	0.16			
4.36	336/29	0.21			
4.71	338/84	1.60			
4.81	220/29	0.11			
4.90	258/07	0.21			
4.96	254/27	0.15			
5.00	251/01	0.21			

SHAFT

Horizontal Scanline

Depth 11.2m

D (m)	Orientation	L_1 (m)	D (m)	Orientation	L_1 (m)
0.09	152/80	0.13	3.97	157/86	0.09
0.22	328/51	0.25	4.02	152/82	0.09
0.34	357/47	0.35	4.07	234/18	0.24
0.54	007/34	0.27	4.09	231/19	0.15
0.59	132/75	0.07	4.19	344/89	0.06
0.61	307/35	0.05	4.25	327/78	0.07
0.63	308/42	0.21	4.31	208/31	0.25
0.67	112/26	0.09	4.36	309/68	0.08
0.74	210/77	0.06	4.42	255/14	0.27
0.78	032/71	0.17	4.50	262/37	0.20
0.85	344/79	0.17	4.58	275/40	0.13
0.92	240/52	0.07	4.84	280/22	0.52
0.94	016/54	0.25	4.89	324/78	0.07
0.97	323/17	0.14	4.89	282/34	0.17
1.05	116/27	1.72	5.01	291/35	0.36
1.64	291/78	0.30	5.05	164/90	0.07
2.12	109/24	0.87	5.07	098/71	0.17
2.45	109/24	0.17	5.22	097/16	0.13
2.52	122/50	0.37	5.25	082/17	0.07
2.57	212/11	0.15	5.41	282/28	0.17
2.61	014/03	0.07	5.55	351/64	0.13
2.64	059/66	0.18	5.57	354/65	0.11
2.72	106/66	0.15	5.81	130/08	0.32
2.75	008/53	0.20	5.95	343/56	0.07
2.77	002/89	1.20	6.04	254/82	0.11
2.81	006/52	0.17	6.12	014/66	0.17
2.87	358/46	0.13	6.17	010/69	0.25
2.90	151/60	0.07	6.27	309/62	0.15
2.93	171/53	0.05	6.35	160/59	0.11
2.98	216/70	0.35	6.39	185/64	0.27
3.11	174/78	0.06	6.44	005/48	1.07
3.17	170/25	0.07	6.46	171/08	0.17
3.22	312/34	0.10	6.47	147/09	0.14
3.28	334/60	0.20	6.57	153/06	0.17
3.32	326/82	0.30	6.64	342/52	0.19
3.34	324/84	0.39	6.73	012/62	0.25
3.48	214/51	0.20	6.88	261/75	0.35
3.62	193/18	0.17	6.95	162/38	0.20
3.67	131/77	0.49	7.14	345/75	0.06
3.82	318/71	0.09	7.15	168/51	0.06
3.87	159/78	0.09	7.23	159/31	0.05
3.91	156/81	0.09	7.31	179/18	0.05

SHAFT

Horizontal Scanline

Depth 11.2m (cont.)

D (m)	Orientation	L_1 (m)
7.45	337/42	0.20
7.46	053/32	0.19
7.63	181/21	0.07
7.90	011/51	0.20
7.93	224/31	0.08
7.98	286/08	0.06

SHAFT

Horizontal Scanline

Depth 12.40 m

D (m)	Orientation	L_1 (m)	D (m)	Orientation	L_1 (m)
0.00	180/53	0.17	6.18	023/39	0.20
0.09	258/68	0.25	6.28	245/51	0.36
0.10	341/80	0.11	6.37	170/25	0.11
0.12	008/82	0.24	6.38	249/79	0.16
0.21	295/76	0.14	6.48	234/33	0.13
0.24	003/24	0.16	6.53	178/52	0.10
0.28	201/90	0.15	6.64	277/80	0.60
0.36	011/77	0.24	7.61	056/84	0.29
0.46	124/54	0.11	7.78	052/62	0.29
0.83	222/74	0.10	7.80	318/70	0.10
0.96	096/16	0.38	7.90	080/44	0.20
1.22	112/04	0.34	7.94	074/54	0.30
1.45	275/42	0.15	8.02	091/10	1.20
1.71	275/30	0.16			
2.01	090/14	0.49			
2.02	145/49	0.01			
2.10	190/70	0.29			
2.19	110/29	0.45			
2.29	311/42	0.17			
2.31	354/86	0.11			
2.52	075/65	0.22			
2.59	336/85	0.37			
2.74	301/17	0.39			
2.88	149/72	0.30			
2.94	158/72	0.15			
3.12	000/66	0.35			
3.21	120/78	0.11			
3.37	147/66	0.20			
3.53	312/24	0.29			
3.64	082/87	0.39			
3.84	126/68	0.39			
4.00	188/73	0.15			
4.12	334/61	0.20			
4.21	208/53	0.06			
4.63	326/75	0.07			
4.68	207/76	0.10			
4.72	140/36	0.22			
5.05	307/22	0.31			
5.23	208/68	0.08			
5.43	122/76	0.35			
5.61	224/65	0.25			
5.66	204/46	0.11			
5.73	247/47	0.08			
5.84	215/80	0.50			
5.86	295/28	0.23			
5.98	259/22	0.16			
6.02	266/50	0.29			
6.12	262/83	0.04			

SHAFT

Horizontal Scanline

Depth 13.6 m

D (m)	Orientation	L_1 (m)	D (m)	Orientation	L_1 (m)
0.00	053/82	0.35	5.68	355/15	0.23
0.34	355/70	0.16	5.98	338/16	1.30
0.51	037/23	0.29	6.16	162/66	0.33
0.85	039/77	0.06	6.24	141/89	0.33
1.00	336/07	1.30	6.32	017/86	0.13
1.02	164/90	0.07	6.46	108/85	0.23
1.24	021/56	0.11	6.66	269/86	0.25
1.34	138/72	0.06	6.74	206/66	0.23
1.53	062/85	0.11	6.76	110/81	0.25
1.61	000/82	0.10	6.97	305/74	0.25
1.62	116/28	0.25	6.99	217/72	0.14
1.67	205/57	0.06	7.03	219/85	0.06
1.73	298/10	0.11	7.10	282/73	0.15
1.77	210/74	0.20	7.14	354/22	0.17
1.79	236/06	0.33	7.54	071/26	0.10
1.83	314/56	0.29	7.64	277/82	0.44
1.88	060/74	0.06	7.86	332/35	0.17
2.00	106/k2	0.84	8.12	078/62	0.15
2.04	063/77	0.11	8.16	197/55	0.18
2.05	180/60	0.11	8.18	322/78	0.13
2.08	078/58	0.19	8.20	044/82	0.23
2.10	085/74	0.10			
2.12	073/35	0.10			
2.16	201/74	0.07			
2.31	275/80	0.25			
2.33	190/70	0.13			
2.37	109/64	0.16			
2.57	013/72	0.34			
2.59	293/87	0.15			
2.67	243/61	0.14			
2.81	153/66	0.15			
3.17	211/18	2.00			
3.54	167/52	0.25			
3.57	250/44	0.06			
3.62	159/88	0.16			
3.68	053/19	0.03			
3.72	073/49	0.18			
3.91	245/32	0.19			
3.99	097/72	0.13			
4.30	246/22	1.80			
4.74	041/75	0.16			
4.77	230/12	0.15			
4.79	249/05	0.09			
5.18	315/07	0.25			
5.33	278/18	0.24			
5.48	127/86	0.20			
5.52	146/24	0.08			
5.58	144/73	0.08			

SHAFT

Horizontal Scanline

Depth 14.60 m

D (m)	Orientation	L_1 (m)	D (m)	Orientation	L_1 (m)
0.15	273/81	0.06	5.81	260/27	0.39
0.16	202/70	0.23	5.90	024/78	0.38
0.21	072/58	0.13	5.97	147/38	0.16
0.26	063/60	0.44	6.42	293/26	0.64
0.32	281/42	0.25	6.57	122/49	0.17
0.42	138/53	0.16	6.59	288/27	0.44
0.62	139/29	0.13	6.62	026/79	0.22
0.78	353/80	0.22	6.69	260/86	0.24
1.11	094/44	0.12	6.74	111/15	0.22
1.23	278/88	0.22	6.87	318/74	0.16
1.41	108/59	0.44	6.95	195/37	0.25
1.99	253/21	0.22	7.02	274/80	0.24
2.04	092/81	0.06	7.33	328/77	0.24
2.11	076/56	0.12	7.44	090/79	0.33
2.28	035/47	0.16	7.71	218/42	0.15
2.41	003/58	0.16	7.74	169/80	0.44
2.45	272/24	0.19	7.80	072/53	0.17
2.52	046/73	0.06	7.86	302/68	0.13
2.53	029/57	0.08	7.90	032/46	0.19
2.56	263/87	0.39			
2.57	280/63	0.11			
2.74	048/82	0.13			
2.75	248/19	0.22			
2.87	310/82	0.25			
3.03	317/25	0.16			
3.24	350/69	0.15			
3.39	297/80	0.25			
3.54	298/85	0.16			
3.82	247/41	0.59			
3.86	351/20	0.18			
4.00	145/88	0.16			
4.02	316/67	0.07			
4.15	126/66	0.15			
4.32	295/34	0.18			
4.44	242/28	0.13			
4.47	121/45	0.10			
4.61	305/29	0.38			
4.66	171/26	0.15			
4.69	206/83	0.06			
4.73	277/72	0.15			
4.76	021/86	0.58			
4.94	259/22	0.19			
5.11	271/22	0.19			
5.15	300/30	0.25			
5.30	338/41	0.18			
5.34	324/34	0.72			
5.43	195/78	0.38			
5.46	315/34	0.12			

SHAFT

Horizontal Scanline

Depth 15.70 m

D (m)	Orientation	L_1 (m)	D (m)	Orientation	L_1 (m)
0.00	045/50	0.42	5.84	276/45	0.19
0.21	033/64	0.17	5.89	245/52	0.10
0.34	034/68	0.18	6.09	000/32	0.24
0.52	030/89	0.20	6.10	111/89	0.15
0.60	236/89	0.16	6.22	284/57	0.17
0.79	033/72	0.11	6.28	317/33	0.17
0.84	223/79	0.06	6.60	219/70	1.40
0.87	128/76	0.13	6.65	335/32	1.70
1.03	247/47	0.09	6.94	089/34	0.38
1.26	151/50	0.17	7.12	352/65	0.18
1.35	352/86	0.11	7.16	096/82	0.39
1.49	171/70	0.20	7.27	040/55	0.04
1.54	113/69	0.18	7.39	034/57	0.13
1.68	186/62	0.24	7.44	186/79	0.18
1.72	090/31	1.40	7.65	045/47	0.49
1.92	226/78	0.13			
2.08	201/76	0.15			
2.10	200/80	0.14			
2.37	196/73	0.13			
2.42	076/64	0.15			
2.77	217/56	0.13			
2.98	172/63	0.18			
3.10	351/33	0.16			
3.14	335/42	0.04			
3.24	071/77	0.31			
3.29	260/42	0.38			
3.31	304/32	0.16			
3.38	140/52	0.38			
3.44	043/47	0.29			
3.50	334/10	0.26			
3.74	333/26	0.58			
3.77	335/29	0.24			
3.81	161/56	0.48			
3.86	056/75	0.29			
4.02	301/44	0.10			
4.05	242/90	0.31			
4.09	217/81	0.49			
4.18	210/74	0.59			
4.47	117/64	0.16			
4.52	306/52	0.09			
4.61	328/35	0.25			
4.82	048/40	0.13			
5.02	093/74	0.34			
5.12	217/31	0.15			
5.42	084/68	0.13			
5.52	280/33	1.30			
5.64	045/56	0.19			
5.76	314/48	0.22			

SHAFT

Horizontal Scanline

Depth 16.90 m

D (m)	Orientation	L_1 (m)
0.00	356/47	0.30
0.13	352/52	0.19
0.18	039/68	0.10
0.23	284/86	0.41
0.44	037/75	0.20
0.66	095/50	0.09
0.78	132/49	0.52
0.83	300/60	0.24
0.99	128/52	0.07
1.08	302/52	0.16
1.22	068/71	0.41
1.28	014/79	0.07
1.34	071/79	0.06
1.43	136/49	0.06
1.45	129/40	0.20
1.59	352/86	0.19
1.66	137/48	0.12
1.75	089/42	0.05
1.90	183/82	0.15
2.10	348/60	0.69
2.34	258/57	0.38
2.48	212/43	0.16
2.60	250/80	0.15
3.10	207/79	0.16
3.24	009/50	0.16
3.37	273/85	0.15
3.38	244/52	0.17
3.42	246/48	0.04
3.52	196/63	0.34
3.62	124/80	0.15
4.21	296/52	2.00
5.01	081/48	0.24
5.07	294/48	0.13
5.23	177/88	0.15
5.26	349/86	0.15
5.29	315/85	0.24
5.31	008/73	0.22
5.37	180/49	0.18
5.41	351/41	2.00
5.80	336/35	0.44
5.95	000/53	0.07
6.17	299/24	0.08
6.26	268/64	0.11
6.35	238/80	0.05
6.40	233/47	0.02
6.65	235/82	0.40
6.77	035/17	0.35
7.10	203/78	0.24
7.24	095/49	0.15
7.27	343/30	0.23

Horizontal Scanline

Depth 17.90 m

D (m)	Orientation	L_1 (m)
0.25	336/78	0.15
0.40	309/82	0.24
0.42	140/83	0.13
0.68	287/20	0.27
0.82	094/81	0.10
1.42	160/08	0.13
1.60	222/78	0.10
1.66	314/78	0.49
1.70	148/08	0.22
1.72	147/10	0.23
1.86	172/32	0.15
1.90	326/87	0.12
2.02	187/09	0.85
2.50	187/72	0.07
2.63	213/84	0.06
3.00	150/38	0.18
3.04	143/46	0.13
3.10	173/42	0.18
3.24	003/50	0.12
3.25	267/86	0.19
3.36	083/70	0.04
3.45	160/77	0.09
3.62	114/69	0.08
3.64	277/62	0.19
3.75	217/45	0.16
3.96	142/84	0.15
4.05	186/64	0.12
4.10	230/32	0.30
4.40	217/56	0.24
4.68	279/48	0.06
4.70	324/76	0.13
4.72	190/52	0.13
4.85	175/80	0.13
4.88	009/76	0.12
5.20	156/63	0.04
5.30	158/67	0.19
5.32	233/49	0.10
5.50	342/56	0.28

SHAFT

Horizontal Scanline

Depth 17.90 m (cont.)

D (m)	Orientation	L_1 (m)
5.54	213/42	0.49
5.68	102/40	0.28
5.90	231/42	0.33
5.98	257/62	0.18
6.04	184/83	0.11
6.15	159/28	0.19
6.30	314/70	2.00
6.81	307/64	0.28
7.10	007/71	1.24
7.70	286/75	0.13
7.74	282/10	1.42
7.82	150/72	0.16
7.93	268/85	0.14
7.97	084/68	0.10
8.02	051/68	0.18
8.05	154/84	0.09

Horizontal Scanline

Depth 20.10 m

D (m)	Orientation	L_1 (m)
0.00	078/26	0.16
0.12	049/26	0.09
0.42	237/54	0.06
0.49	194/66	0.09
0.72	038/56	0.06
0.98	170/70	0.05
1.37	351/17	0.25
1.59	229/89	0.17
1.64	247/09	0.13
1.84	104/79	0.15
1.94	043/61	0.09
1.97	358/44	0.18
2.25	127/70	0.17
2.43	135/78	0.19
2.80	052/08	0.38
3.06	183/47	0.20
3.08	007/19	0.21
3.38	260/76	0.83
3.62	192/67	0.41
4.07	237/47	1.00
4.61	252/36	0.07
4.68	192/86	0.34
4.90	271/44	0.48
5.33	254/42	0.06
5.57	246/44	0.05
6.04	268/51	0.09
6.27	330/68	0.06
6.39	027/49	0.42
6.52	294/42	0.07
6.63	024/44	0.20
6.74	272/83	0.83
6.95	207/06	0.24
7.17	301/73	0.21
7.30	180/72	0.14
7.74	259/13	0.48
7.93	003/88	0.07
8.02	070/18	0.30
8.10	244/86	0.39

Horizontal Scanline

Depth 21.20 m

0.00	354/46	0.19
0.61	061/33	0.06
0.84	056/32	0.17
1.01	041/42	0.06
1.53	096/55	0.17
1.66	096/46	0.23
1.85	097/64	0.31
2.05	108/54	0.13
2.36	115/48	0.71
2.44	110/51	0.21
2.78	183/49	0.21
3.00	007/68	0.49
3.08	099/67	0.05
3.11	089/76	0.12
3.51	229/46	0.84
3.85	126/12	0.41
4.20	287/72	0.31
4.61	262/48	0.31
4.65	262/66	0.48
4.97	208/32	0.14
5.09	294/90	0.16
5.22	211/73	0.06
5.42	049/07	0.31
6.10	248/78	0.13
6.68	262/60	0.52
7.02	310/74	0.39
7.61	056/44	0.07
7.75	300/71	0.15
8.02	336/54	0.11
8.30	026/63	0.14

VERTICAL SCANLINE IN THE SHAFT

WEST SIDE

D (m)	Orientation	L_1 (m)	L_2 (m)	D (m)	Orientation	L_1 (m)	L_2 (m)
0.00	265/20	0.15	0.35	2.32	270/37	0.10	0.30
0.05	135/75	0.01	0.25	3.33	300/39	0.40	0.10
0.15	185/80	0.20	0.25	3.39	355/66	1.20	0.01
0.29	095/21	1.10	0.05	3.44	090/06	0.30	0.10
0.40	295/65	0.25	0.55	3.53	160/10	0.40	0.20
0.50	145/20	1.05	0.10	3.55	120/22	0.30	0.20
0.58	275/20	0.45	0.25	3.60	110/24	0.10	0.10
0.69	250/28	0.15	0.75	3.72	270/16	0.01	0.04
0.80	225/45	0.01	0.25	3.78	310/26	0.10	0.10
0.87	240/08	0.20	0.20	3.84	300/42	0.30	0.01
0.92	240/10	0.10	0.15	3.96	210/01	0.30	0.30
1.10	155/25	0.25	0.05	4.10	160/76	0.20	0.20
1.17	160/30	0.30	0.20	4.17	050/48	0.20	0.01
1.20	335/80	0.02	0.05	4.23	220/28	0.20	0.01
1.22	260/32	0.35	0.05	4.30	310/34	0.90	0.20
1.31	290/02	0.15	0.35	4.38	280/41	0.10	0.20
1.33	020/38	0.01	0.20	4.40	190/12	0.35	0.20
1.35	200/28	0.01	0.30	4.51	165/20	0.10	0.30
1.47	190/40	0.15	0.20	4.55	085/80	0.40	0.30
1.49	185/30	0.10	0.25	4.57	100/75	0.01	0.03
1.62	355/10	0.01	0.15	4.66	170/40	0.30	0.45
1.73	185/90	0.10	0.15	4.77	120/35	0.02	0.04
1.80	350/12	0.75	0.20	4.78	115/30	0.05	0.10
1.92	110/33	0.40	0.45	4.79	125/40	0.06	0.05
1.94	300/30	0.25	0.20	4.80	130/45	0.05	0.05
1.99	295/35	0.45	0.30	4.84	260/20	0.20	0.10
2.04	290/30	0.50	0.25	4.87	280/30	0.35	0.20
2.25	325/50	0.15	0.05	4.93	280/42	0.30	0.20
2.33	215/15	0.20	0.25	5.06	300/66	0.20	0.40
2.37	170/28	0.10	0.20	5.07	240/12	0.30	0.20
2.41	185/06	0.10	0.20	5.08	220/06	0.30	0.05
2.45	210/20	0.01	0.20	5.12	265/09	0.05	0.06
2.47	210/20	0.05	0.05	5.15	274/07	0.30	0.20
2.48	220/17	0.10	0.30	5.16	310/32	0.02	0.04
2.58	346/57	0.01	0.30	5.18	250/13	0.30	0.20
2.64	005/69	0.01	0.05	5.19	260/04	0.05	0.03
2.70	220/31	0.30	0.20	5.26	190/33	0.40	0.20
2.77	240/56	0.30	0.20	5.32	190/12	0.30	0.01
2.85	180/10	0.30	0.20	5.36	060/35	0.40	0.20
2.86	040/63	0.10	0.30	5.44	275/44	0.05	0.01
2.91	260/10	0.05	0.10	5.49	320/10	0.80	0.40
2.96	265/50	0.01	0.30	5.72	190/66	0.20	0.30
3.02	190/04	0.30	0.80	5.74	250/08	0.40	0.20
3.03	190/10	0.30	0.40	5.78	240/05	0.04	0.30
3.08	200/06	0.60	0.20	5.93	320/22	0.40	0.10
3.09	260/34	0.01	0.30	6.16	385/62	0.20	0.30
3.13	200/44	0.20	0.40	6.17	340/71	0.01	0.40
3.22	270/44	0.01	0.02	6.26	270/23	0.10	0.20
3.26	240/30	0.30	0.01	6.42	300/63	0.01	0.04

VERTICAL SCANLINE IN THE SHAFT

WEST SIDE (cont.)

D (m)	Orientation	L_1 (m)	L_2 (m)	D (m)	Orientation	L_1 (m)	L_2 (m)
6.64	330/39	0.10	0.20	11.48	190/44	0.20	0.20
6.68	200/48	0.40	0.20	11.61	012/82	0.10	0.30
6.77	340/60	0.30	0.10	11.75	285/59	0.01	0.30
6.80	340/48	0.10	0.30	11.82	340/59	0.30	0.01
6.84	275/35	0.20	0.10	11.95	260/64	0.30	0.10
6.88	310/24	0.20	0.10	12.15	350/80	0.01	0.20
6.92	340/53	0.30	0.20	12.18	335/38	0.30	0.10
6.97	355/44	0.20	0.40	12.21	200/04	0.30	0.20
6.98	275/56	0.05	0.05	12.36	285/07	0.30	0.10
7.00	025/39	0.05	0.10	12.41	320/67	0.10	0.05
7.31	348/76	0.10	0.30	12.52	310/63	0.30	0.01
7.41	165/06	0.20	0.20	12.56	325/61	0.20	0.01
7.56	170/09	0.30	0.20	12.62	280/36	0.20	0.01
7.71	173/44	0.10	0.01	12.67	275/33	0.10	0.20
7.77	190/13	0.20	0.10	12.78	270/09	0.40	0.50
7.98	260/20	0.20	0.01	12.85	190/82	0.10	0.30
8.04	035/55	0.01	0.20	13.00	265/50	0.30	0.20
8.32	310/15	0.01	0.20	13.12	040/42	0.20	0.50
8.35	320/25	0.01	0.05	13.19	110/46	0.20	0.20
8.82	190/13	0.20	0.30	13.20	260/20	0.15	0.01
9.00	170/87	0.50	0.30	13.27	280/62	0.10	0.10
9.25	035/84	0.20	0.40	13.36	250/08	0.10	0.10
9.37	350/08	0.20	0.40	13.39	250/08	0.10	0.10
9.45	020/78	0.10	0.20	13.40	250/08	0.10	0.10
9.71	340/08	0.20	0.40	13.44	250/08	0.10	0.10
9.74	345/16	0.20	0.04	13.67	260/17	0.10	0.01
9.80	010/42	0.10	0.10	13.84	270/32	0.30	0.20
9.95	200/72	0.10	0.10	13.94	005/07	0.30	0.20
9.98	290/30	0.10	0.15	14.03	298/54	0.80	0.01
10.00	296/36	0.10	0.05	14.10	200/85	0.30	0.20
10.01	105/48	0.01	0.30	14.30	250/65	0.10	0.20
10.05	105/62	0.01	0.20	14.34	260/11	0.40	0.20
10.07	293/36	0.15	0.05	14.45	280/16	0.10	0.90
10.20	340/90	0.40	0.30	14.49	280/24	1.20	0.30
10.31	350/04	0.10	0.20	14.50	295/20	0.60	0.30
10.35	210/19	0.10	0.30	14.57	320/46	2.00	0.40
10.45	200/16	0.10	0.30	14.70	340/72	0.20	0.40
10.46	200/16	0.10	0.01	14.84	185/41	0.10	0.20
10.48	200/16	0.20	0.01	14.89	190/18	0.10	0.30
10.52	200/16	0.30	0.01	14.92	340/36	0.30	0.50
10.58	215/05	0.20	0.01	14.98	340/32	0.30	0.50
10.70	310/80	0.30	0.10	14.99	340/39	0.10	0.40
10.74	350/90	0.10	0.01	15.51	280/46	2.00	1.50
10.79	265/80	0.30	0.45	15.70	310/45	0.50	0.70
10.95	080/88	0.20	0.10	15.78	355/09	0.50	0.60
11.15	215/49	0.01	0.30	15.79	250/09	0.50	0.10
11.20	350/22	0.30	0.01	15.87	270/68	0.10	0.30
11.32	320/58	0.01	0.05	16.15	265/16	0.10	0.05
11.35	280/21	0.05	0.20	16.20	250/69	0.10	0.60

VERTICAL SCANLINE IN THE SHAFT

WEST SIDE (cont.)

D (m)	Orientation	L_1 (m)	L_2 (m)
16.38	270/10	0.30	0.50
16.41	275/12	0.40	0.60
16.75	350/42	0.40	0.60
16.84	270/20	0.30	0.20
16.86	255/35	0.10	0.20
16.90	250/35	0.10	0.20
17.10	265/45	0.10	0.30
17.16	260/35	0.20	0.40
17.25	040/80	0.20	0.40
17.50	340/80	0.30	0.50
17.68	340/05	0.50	0.70
17.75	110/90	0.10	0.30
17.79	278/20	0.20	0.30
17.95	280/80	0.30	0.50
17.97	210/10	0.20	0.20
18.09	275/08	0.03	0.50
18.41	000/10	0.30	0.50
18.43	000/10	0.30	0.50
18.48	000/10	0.30	0.50
18.51	000/10	0.30	0.50
18.62	250/46	0.30	0.06
18.90	310/50	0.40	0.30
19.05	250/59	0.10	0.01
19.25	280/02	0.30	0.01
19.60	330/05	0.50	0.01
19.80	180/12	0.70	0.10
20.10	270/64	0.30	0.20
20.15	100/60	0.10	0.30
20.35	210/10	0.40	0.30
20.40	350/40	0.30	0.20
20.48	245/30	0.40	0.60
20.93	200/15	2.00	1.50
21.15	240/85	0.10	0.20
21.35	080/60	0.20	0.30
21.56	120/25	1.50	1.50
21.70	150/10	1.00	1.40
21.85	090/35	0.10	0.60
21.90	090/15	0.10	0.30
21.92	100/60	0.40	0.30
21.98	050/29	0.30	0.20
22.00	025/75	0.10	0.01

VERTICAL SCANLINE IN THE SHAFT

EAST SIDE

D (m)	Orientation	L_1 (m)	L_2 (m)
0.00	108/62	0.15	0.25
0.22	257/10	0.20	0.25
0.26	108/75	0.10	0.30
0.35	154/59	0.05	0.15
0.45	275/43	1.40	1.05
0.55	110/50	0.05	0.06
0.57	100/60	0.01	0.01
0.59	105/65	0.05	0.10
0.65	110/35	0.15	0.35
0.80	025/60	0.30	0.20
0.95	140/75	0.26	0.50
1.04	205/25	0.10	0.75
1.07	105/25	0.10	0.15
1.10	205/42	0.05	0.20
1.19	085/52	0.01	0.10
1.21	095/60	0.01	0.15
1.24	175/63	0.05	0.10
1.26	265/26	0.05	0.20
1.34	196/08	0.15	0.20
1.45	125/58	0.35	0.01
1.55	030/77	0.10	0.10
1.62	185/08	0.30	0.05
1.64	350/07	0.15	0.01
1.70	135/65	0.35	0.01
1.75	115/47	0.20	0.15
1.80	295/45	0.30	0.20
2.02	140/38	0.05	0.05
2.07	065/70	0.05	0.15
2.08	065/70	0.01	0.10
2.16	000/43	0.01	0.01
2.18	030/15	0.40	0.60
2.28	300/71	0.20	0.20
2.34	330/26	0.10	0.40
2.42	350/21	0.40	0.30
2.46	170/58	0.10	0.05
2.52	120/36	0.40	0.20
2.56	090/08	0.01	0.01
2.57	010/50	0.01	0.30
2.63	080/50	0.20	0.60
2.67	080/16	0.30	0.20
2.83	160/24	0.30	0.01
2.88	180/10	0.01	0.20
3.07	200/46	0.30	0.04
3.08	030/50	0.20	0.10
3.17	190/38	0.20	0.10
3.22	200/10	0.10	0.30
3.30	280/70	0.30	0.20
3.40	185/54	0.10	0.01
3.47	275/20	0.05	0.02

VERTICAL SCANLINE IN THE SHAFT

EAST SIDE (cont.)

D (m)	Orientation	L_1 (m)	L_2 (m)
3.54	320/24	0.30	0.10
3.67	350/37	0.10	0.20
3.74	000/73	0.20	0.30
3.77	260/04	0.60	0.20
3.86	330/39	0.01	0.02
3.89	190/56	0.10	0.20
3.94	100/38	0.40	0.20
4.02	060/44	0.30	0.10
4.15	270/57	0.70	0.10
4.23	350/54	0.01	0.02
4.27	160/52	0.20	0.01
4.69	070/12	0.30	0.30
4.76	090/32	0.01	0.02
4.85	080/26	0.30	0.20
4.92	180/18	0.10	0.20
4.97	015/50	0.50	0.05
5.05	005/44	0.50	0.30
5.12	210/67	0.01	0.20
5.17	310/40	0.01	0.30
5.28	355/60	0.05	0.05
5.32	020/55	0.01	0.01
5.40	170/56	0.60	0.01
5.47	005/19	0.20	0.01
5.48	170/15	0.30	0.50
5.64	274/63	0.40	0.20
5.65	095/08	2.00	2.00
5.70	245/10	0.10	0.10
5.76	350/30	0.10	0.10
5.83	350/30	0.30	0.30
5.89	150/68	0.10	0.10
5.96	150/66	0.20	0.30
5.98	180/30	0.20	0.30
5.99	180/30	0.20	0.05
6.04	180/69	0.01	0.01
6.05	005/38	0.01	0.20
6.10	340/04	0.30	0.20
6.13	000/10	0.10	0.20
6.16	350/12	0.30	0.20
6.18	350/10	0.30	0.20
6.19	335/10	0.30	0.10
6.22	170/60	0.01	0.01
6.25	300/16	0.30	0.20
6.36	120/62	0.30	0.30
6.47	320/64	0.10	0.10
6.50	210/29	0.20	0.01
6.64	040/64	0.60	0.20
6.73	020/14	0.20	1.20
6.83	005/27	0.10	0.20
6.88	060/14	0.01	0.01
6.92	080/17	0.10	0.01
6.93	030/62	0.20	0.01
6.98	300/68	0.20	0.20
7.05	180/46	0.05	0.01
7.24	064/11	0.50	0.30
7.32	016/14	0.30	0.01
7.48	177/36	0.50	0.01
7.64	079/08	0.05	0.06
7.66	131/04	0.30	0.60
7.80	004/11	1.20	0.40
7.94	194/88	0.30	0.60
7.99	206/06	0.30	0.10
8.04	200/28	2.00	0.03
8.26	091/05	1.30	0.20
8.36	351/13	1.50	0.30
8.42	006/20	2.40	2.60
8.45	316/23	0.10	0.25
8.51	141/09	1.40	2.00
8.75	236/23	1.60	0.30
8.83	024/13	0.10	0.10
8.87	020/07	0.15	0.10
8.92	017/06	0.20	0.20
9.02	069/53	0.01	0.03
9.04	266/10	0.07	0.10
9.35	046/62	0.15	0.13
9.43	092/08	2.00	2.20
9.75	076/17	0.75	1.00
9.92	332/76	0.15	0.22
10.25	176/12	0.17	0.85
10.55	115/06	0.30	0.30
10.70	060/28	0.10	0.30
10.75	200/38	0.10	0.20
10.78	065/52	0.10	0.20
11.05	175/34	0.30	0.01
11.22	030/08	2.00	1.00
11.29	030/08	0.05	0.02
11.56	042/20	0.20	0.05
11.66	005/76	0.02	0.20
11.75	050/25	0.60	0.20
11.90	115/68	0.15	0.20
12.00	220/86	0.01	0.50
12.25	110/10	0.30	0.20
12.27	040/06	1.50	0.10
12.35	320/32	0.01	0.20
12.39	280/13	2.00	3.00
12.41	300/12	0.50	2.00
12.55	035/74	0.10	0.30
12.76	075/42	0.20	0.20
12.82	065/44	0.20	0.80
12.87	045/56	0.10	0.20
12.93	035/62	0.10	0.40

VERTICAL SCANLINE IN THE SHAFT

EAST SIDE (cont.)

D (m)	Orientation	L_1 (m)	L_2 (m)
13.00	035/44	0.01	0.03
13.11	280/41	0.05	0.70
13.13	300/45	0.01	0.03
13.23	281/33	0.40	0.05
13.26	300/39	0.30	0.40
13.33	275/39	0.01	0.20
13.70	285/40	0.01	0.30
13.79	165/54	0.20	0.60
14.10	174/52	1.20	0.50
14.30	090/62	0.30	0.10
14.45	200/80	0.01	0.30
14.55	100/40	0.30	0.20
14.60	150/44	0.10	0.10
14.74	320/58	0.10	0.20
15.04	340/28	0.10	0.20
15.06	005/18	0.20	0.40
15.24	030/15	0.30	0.50
15.45	150/38	0.50	0.10
15.62	340/52	0.10	0.10
15.86	340/57	0.20	0.01
16.14	310/56	0.30	0.20
16.28	100/23	0.40	0.30
16.42	140/23	0.30	0.01
16.52	260/21	0.10	0.05
16.54	010/16	0.01	0.30
16.58	160/83	0.10	0.20
16.65	300/90	0.20	0.01
16.84	250/04	1.00	2.00
16.93	010/08	1.50	2.00
17.17	200/07	2.00	1.50
17.30	100/20	0.01	0.04
17.80	100/12	3.00	2.50
17.81	100/12	3.00	2.50
17.83	100/12	3.00	2.50
17.85	100/12	3.00	2.50
17.98	100/06	2.00	0.50
18.27	280/63	0.50	0.01
18.38	335/10	0.10	0.30
18.50	350/10	0.10	0.30
18.64	190/10	1.00	1.50
18.78	180/10	0.50	0.30
18.88	020/71	0.05	0.20
19.40	010/76	0.40	0.20
19.60	180/09	2.00	2.00
19.90	180/03	0.70	0.40
19.93	271/20	0.30	0.01
20.00	280/35	0.10	0.30
20.14	253/40	0.30	0.20
20.64	015/20	0.40	0.20
20.66	025/15	0.50	0.30
20.69	006/10	0.40	0.30
20.76	010/15	0.05	0.05
20.77	035/60	0.01	0.03
20.80	045/45	0.01	0.02
21.15	080/20	0.01	0.02
21.32	200/20	0.30	0.10
21.43	265/30	0.10	0.20
21.55	340/30	0.40	0.60
21.77	210/80	0.03	0.05
21.80	320/25	0.10	0.20

CHINNOR TUNNEL

Chainage 9.9m

Vertical Scanline

D (m)	Orientation	L_1 (m)	L_1 (m)
0.16	005/10	0.10	0.20
0.57	350/62	0.02	0.04
0.75	275/75	1.30	1.20
0.88	345/24	0.30	1.50
1.00	290/70	1.30	1.50
1.15	340/53	1.20	0.04
1.20	335/25	0.50	0.50
1.77	000/42	1.60	2.40
2.07	345/50	0.22	0.15
2.25	340/80	0.24	0.16
2.51	330/10	2.30	3.00
2.55	320/15	1.00	2.60
2.80	330/35	0.40	0.30
2.92	335/20	0.40	0.60
3.07	325/10	0.05	0.05
3.10	325/10	1.00	0.05
3.20	185/85	1.10	0.40
3.30	010/80	0.10	0.10
3.35	275/75	0.05	0.01
3.40	000/10	0.05	0.20
3.58	155/60	0.01	0.10
3.60	300/60	0.50	0.25
4.02	290/65	0.20	0.15
4.40	165/45	0.21	0.05

Horizontal Scanline

0.50	340/30	0.20	0.15
0.70	345/30	0.25	0.25
0.80	335/85	0.04	0.55
0.95	025/80	0.10	0.05
1.20	095/85	0.05	0.02
1.27	235/75	0.25	0.10
1.90	205/50	0.20	0.10
2.30	330/10	2.30	3.00
2.40	320/15	1.00	2.60
2.74	120/90	0.50	1.20
2.95	025/40	0.03	0.01
2.96	025/40	0.01	0.01
4.20	165/65	0.36	0.24
4.50	255/70	0.40	0.05
4.70	250/70	0.16	0.01

Chainage 11.5m

Vertical Scanline

D (m)	Orientation	L_1 (m)	L_2 (m)
0.04	315/11	0.45	0.07
0.24	325/35	0.15	0.55
0.34	340/20	0.25	0.30
0.38	331/82	0.05	0.12
0.43	125/15	0.05	0.25
0.45	354/30	0.05	0.25
0.48	171/79	0.05	0.30
0.50	053/82	0.05	0.05
0.73	352/33	0.15	0.20
0.84	170/19	0.05	2.00
0.85	039/69	0.01	0.05
1.06	012/22	0.10	0.01
1.15	334/44	0.01	0.08
1.44	340/36	2.00	1.20
1.46	341/26	0.80	0.30
1.55	328/32	0.10	0.10
1.72	354/24	0.15	0.05
1.75	149/57	0.10	0.05
2.06	348/21	0.10	0.10
2.13	349/35	0.05	0.01
2.16	259/85	0.05	0.01
2.17	354/52	0.05	0.01
2.30	348/42	0.10	0.10
2.37	166/68	0.01	0.01
2.50	352/12	0.01	0.30
2.83	016/30	0.01	0.35
2.87	295/36	0.01	0.50
2.89	294/30	0.01	0.50
3.14	028/58	0.15	0.35
3.25	306/73	0.05	0.10
3.67	031/56	0.02	0.05
3.81	010/18	0.10	0.15
4.00	337/34	0.15	0.20
4.10	087/90	0.01	0.01
4.14	327/48	0.01	0.05
4.22	227/80	0.05	0.01
4.25	196/84	0.02	0.05
4.71	051/67	0.01	0.01

Horizontal Scanline

0.60	176/62	0.01	0.25
0.75	213/74	0.10	0.05
0.79	202/80	0.10	0.10
0.95	318/87	0.20	0.10
1.04	232/82	0.15	0.01
1.07	307/63	0.15	0.01
1.22	135/88	0.15	1.20
1.54	340/18	0.80	1.40

CHINNOR TUNNEL

Chainage 11.5m (cont)

Horizontal Scanline

D (m)	Orientation	L_1 (m)	L_2 (m)
1.92	031/15	0.35	0.20
2.18	307/14	0.25	0.45
2.44	307/41	0.01	0.10
2.45	005/22	0.05	0.10
2.60	294/62	0.35	0.85
2.82	005/44	0.10	0.01
2.89	110/70	0.10	0.15
3.12	107/42	0.10	0.20
3.91	275/02	0.50	0.20
4.30	110/39	0.30	0.10
4.65	276/17	0.01	1.50

Chainage 12.1m

Vertical scanline

0.09	322/62	0.01	1.30
0.10	136/66	0.05	0.05
0.11	046/48	0.10	0.01
0.12	338/09	0.30	0.30
0.13	340/10	0.30	0.35
0.14	352/28	0.20	1.20
0.32	122/75	0.15	0.05
0.41	349/22	1.40	1.20
0.56	327/69	0.01	0.10
0.67	165/84	0.01	0.15
0.75	340/08	0.30	2.00
0.78	346/08	1.50	2.50
0.80	332/07	1.50	2.50
0.87	329/09	0.80	1.00
1.10	334/15	1.50	1.50
1.19	341/25	0.05	0.05
1.26	162/88	0.01	0.20
1.48	345/16	0.40	3.50
1.60	350/10	0.05	0.05
1.77	348/77	0.05	0.10
1.90	351/80	0.30	0.50
2.20	073/41	0.05	0.60
2.40	060/49	0.05	0.01
2.60	132/90	0.01	0.01
2.65	286/74	0.05	0.10
2.66	195/82	0.01	0.01
2.90	173/90	0.30	1.20
3,00	004/69	0.30	1.20
3.18	324/84	0.01	0.05
3.24	215/69	0.05	0.10
3.30	305/55	0.10	0.60
3.35	310/48	0.20	0.60
3.45	115/86	0.05	0.05
3.46	004/10	0.10	0.01
3.75	298/59	0.01	0.05
3.80	245/10	0.30	0.02
3.85	333/74	0.30	0.01
3.95	349/31	0.01	0.50
4.05	172/19	0.05	0.05
4.15	175/10	0.01	0.10
4.30	292/80	0.05	0.01
4.40	107/85	0.01	0.02
4.45	115/18	0.10	0.10

Horizontal Scanline

0.25	305/28	0.25	0.01
0.69	287/30	1.60	1.90
1.71	343/08	1.30	2.50
1.75	319/78	0.01	0.15
1.90	042/40	0.01	0.30
2.00	346/43	0.01	0.02
2.04	098/82	0.15	0.15
2.08	212/44	0.14	0.15
2.35	354/40	0.05	0.01
2.40	125/88	0.01	0.30
2.45	037/30	0.01	0.04
2.48	210/51	0.06	0.10
2.50	196/52	0.25	0.01
2.57	024/72	0.10	0.05
2.70	323/71	1.50	0.30
2.88	085/51	0.25	0.01
3.00	157/52	0.01	0.01
3.27	314/31	0.05	0.01
3.65	037/82	0.01	0.01
3.78	014/52	0.05	0.01
3.83	014/32	0.05	0.03
3.97	312/90	0.10	0.10
4.00	007/56	0.10	0.10
4.21	316/58	0.10	0.01
4.30	241/09	1.00	1.10
4.40	092/56	0.35	0.01
4.50	000/78	0.45	0.01
4.67	326/90	1.90	1.30
4.80	336/63	1.50	0.01
4.83	125/88	0.30	0.45

CHINNOR TUNNEL

Chainage 14.0m

Vertical Scanline

D (m)	Orientation	L_1 (m)	L_2 (m)
0.25	296/25	0.01	0.20
0.27	308/32	0.60	0.01
0.50	315/22	2.00	3.00
0.54	322/18	0.01	3.00
0.58	061/73	0.05	0.05
0.67	327/14	2.00	2.20
0.74	322/15	1.50	1.50
0.78	315/12	1.50	3.00
0.85	160/74	0.05	0.05
1.06	311/47	0.13	0.05
1.18	306/17	1.50	2.50
1.20	322/01	0.01	1.20
1.25	289/48	0.01	0.01
1.28	203/62	0.05	0.05
1.38	035/23	0.01	0.01
1.47	308/27	0.10	0.05
1.56	357/17	0.30	1.40
1.80	352/18	0.40	0.80
1.87	352/18	0.03	0.04
1.97	247/12	0.10	0.30
2.14	345/44	0.05	0.20
2.19	009/30	0.06	0.01
2.20	202/40	0.20	0.10
2.28	339/30	0.20	2.50
2.69	342/00	1.00	1.50
2.76	340/15	0.10	0.10
2.78	340/14	0.10	0.10
2.98	353/44	0.30	0.60
3.01	353/44	0.40	0.20
3.02	353/44	0.40	0.20
3.09	322/86	0.10	0.30
3.41	334/06	0.40	0.20
3.45	348/12	0.15	0.40
3.58	096/60	0.01	0.05
3.80	323/52	0.25	1.50
3.86	354/33	0.50	0.35
3.99	282/60	0.11	0.15
4.04	329/42	0.04	0.05
4.10	306/58	0.02	0.05
4.16	317/60	0.02	0.07

Horizontal Scanline

D (m)	Orientation	L_1 (m)	L_2 (m)
0.00	290/21	0.80	0.01
0.30	288/45	0.01	0.30
0.58	305/40	0.01	0.05
0.59	194/46	0.01	0.10
0.77	134/85	0.30	0.10
0.88	345/59	0.10	0.30
1.20	306/27	0.30	0.60
1.40	332/50	0.10	0.30
1.91	339/41	3.00	1.00
3.71	131/48	0.01	0.01
4.10	333/48	0.20	2.20
4.30	258/52	0.50	0.20
4.61	158/60	0.03	0.05
4.70	339/35	0.01	0.05
4.82	165/54	0.50	0.01

CHINNOR TUNNEL

Chainage 18.1m

Vertical Scanline

D (m)	Orientation	L_1 (m)	L_2 (m)
0.04	113/11	0.05	0.16
0.26	345/31	0.45	1.50
0.35	330/24	0.01	1.00
0.36	341/21	1.20	2.00
0.74	328/77	0.01	0.60
0.84	206/90	0.01	0.02
0.87	354/27	0.05	0.01
1.02	004/18	1.20	2.50
1.04	335/31	0.05	1.20
1.07	349/23	0.50	0.50
1.08	336/24	0.60	0.05
1.67	352/18	0.20	0.10
1.72	034/74	0.10	0.10
1.83	017/37	0.05	0.10
2.02	350/62	0.01	0.20
2.07	340/27	0.10	0.30
2.28	347/25	0.01	0.05
2.68	302/59	0.30	0.50
2.70	037/18	0.05	0.01
2.71	312/22	0.01	0.04
2.73	140/20	0.01	0.05
2.79	319/19	0.50	2.00
2.82	133/22	0.30	0.10
2.86	313/73	0.01	2.00
2.91	147/26	0.01	0.05
3.11	305/76	0.01	0.02
3.17	036/78	0.01	0.82
3.22	308/30	0.30	0.20
3.41	043/35	0.01	0.05
3.58	304/19	2.50	0.30
3.59	309/20	0.30	0.20
3.60	200/21	0.05	0.06
3.82	331/63	0.01	0.05
3.83	026/19	0.01	0.04
3.92	311/65	0.03	0.04
4.01	218/52	0.01	0.02
4.17	212/86	0.01	0.20
4.25	327/46	0.18	0.30
4.31	346/42	0.03	0.07
4.38	224/42	0.01	0.03

Horizontal Scanline

D (m)	Orientation	L_1 (m)	L_2 (m)
0.20	343/15	0.03	0.05
0.23	044/79	0.02	0.01
1.19	063/80	0.05	0.06
1.22	309/09	0.04	0.15
1.41	324/74	0.10	0.60
1.53	247/62	0.05	0.04
1.57	333/76	0.05	0.01
1.72	313/34	1.00	0.30
1.82	106/54	0.02	0.10
1.83	276/76	0.05	0.02
1.90	005/47	0.10	0.05
2.03	132/68	0.01	0.03
2.14	323/29	0.14	0.30
2.69	108/68	0.01	0.03
2.74	005/72	0.04	0.03
2.78	116/70	0.05	0.05
2.90	299/60	0.01	0.01
3.31	019/22	0.01	0.03
3.33	174/11	0.01	0.01
3.41	297/24	0.01	0.06
3.60	304/14	0.35	0.20
3.61	124/71	0.20	0.01
3.72	118/21	0.06	0.10
3.84	196/48	0.05	0.10
4.00	236/28	0.10	0.10
4.10	303/24	0.20	0.01
4.32	112/37	0.10	0.20
4.60	166/02	0.01	0.01
4.87	342/14	0.03	0.15

CHINNOR TUNNEL

Chainage 20.4m

Vertical Scanline

D (m)	Orientation	L_1 (m)	L_2 (m)
0.09	024/12	0.05	0.05
0.14	022/72	0.10	0.20
0.15	134/32	0.10	1.50
0.22	327/24	0.10	0.05
0.24	024/24	0.10	0.70
0.27	141/12	0.25	0.20
0.37	227/04	0.30	1.40
0.38	321/16	0.30	1.50
0.39	306/12	0.40	1.50
0.41	353/13	0.30	1.50
0.44	357/10	0.30	1.40
0.45	354/17	0.40	1.30
0.64	346/30	0.30	0.20
0.76	305/59	0.10	0.30
1.15	174/65	0.10	0.01
1.16	027/16	0.20	0.01
1.34	341/20	0.05	0.05
1.45	005/36	0.05	0.01
1.65	016/38	0.01	0.30
1.76	344/30	0.20	0.30
1.80	010/34	0.01	0.05
2.00	335/50	0.15	1.00
2.25	323/85	0.05	0.01
2.32	166/46	0.20	0.40
2.43	004/03	0.10	0.30
2.60	347/32	0.05	0.05
3.13	356/10	0.50	2.00
3.14	014/09	0.30	0.80
3.20	343/17	0.01	0.20
3.62	133/45	0.20	0.10
3.73	046/38	0.10	0.05
3.92	023/43	0.01	0.05
4.01	309/31	0.05	0.30
4.11	317/56	0.02	0.05
4.17	299/69	0.20	0.20
4.30	014/57	0.05	0.10
4.34	013/57	0.50	0.30
4.41	254/86	0.04	0.05

Horizontal Scanline

D (m)	Orientation	L_1 (m)	L_2 (m)
0.05	240/52	0.20	0.01
0.44	330/48	1.00	0.50
0.95	329/20	1.50	0.50
1.15	309/13	1.50	0.30
1.40	322/11	1.30	0.40
1.52	334/02	1.20	0.40
1.62	193/15	1.40	0.60
2.00	121/32	0.05	0.01
2.22	102/32	0.01	0.05
2.40	323/37	0.01	0.60
2.80	110/26	0.20	0.60
3.24	020/14	0.05	0.30
3.71	119/76	0.80	0.20
4.12	321/22	0.01	0.01
4.85	346/39	0.15	0.01
4.91	016/39	0.01	0.05

CHINNOR TUNNEL

Chainage 35.9m

Vertical Scanline

D (m)	Orientation	L_1 (m)	L_2 (m)
0.23	362/09	0.80	0.90
0.29	348/05	0.90	0.50
0.49	148/52	0.01	0.05
0.61	344/64	0.30	0.10
0.66	207/08	0.40	0.20
0.76	295/66	0.05	0.03
0.83	121/29	0.01	0.02
0.91	319/66	0.01	0.03
1.10	070/04	0.01	0.05
1.21	139/76	0.01	0.02
1.45	307/42	0.30	0.10
1.50	359/60	0.40	0.20
1.53	123/82	0.05	0.02
1.75	308/26	0.05	0.10
1.88	147/34	0.02	0.20
1.90	318/44	0.03	0.05
1.91	318/44	0.02	0.04
1.92	318/44	0.03	0.05
1.94	342/26	0.30	0.40
2.00	332/76	0.30	0.40
2.19	196/27	0.05	0.30
2.40	306/18	0.30	0.10
2.59	163/40	0.04	0.02
2.74	353/08	0.40	0.05
2.86	346/51	0.20	0.01
2.97	329/77	0.01	0.10
3.01	327/60	0.01	0.01
3.10	143/69	0.02	0.03
3.16	333/61	0.15	0.30
3.35	338/57	0.01	0.10
3.36	233/49	0.01	0.20
3.47	205/66	0.01	0.20
3.56	353/72	0.05	0.10
3.64	057/77	0.10	0.20
3.68	216/14	0.10	0.40
3.74	207/24	0.20	0.30
3.76	030/75	0.01	0.10
3.80	007/12	0.01	0.01
3.81	315/74	0.01	0.03
3.82	050/72	0.02	0.04
3.85	334/82	0.01	0.04
4.00	345/10	0.50	1.50
4.02	344/14	0.10	0.40
4.04	005/14	0.30	0.02
4.07	333/26	0.40	0.80

Horizontal Scanline

D (m)	Orientation	L_1 (m)	L_2 (m)
0.11	310/40	0.20	0.05
0.20	295/44	0.02	0.03
0.82	186/76	0.30	0.20
0.91	334/20	0.03	0.04
0.92	336/25	0.01	0.04
0.95	189/54	0.03	0.30
1.19	301/37	0.02	0.04
1.55	313/56	0.03	0.06
1.59	041/65	0.20	0.30
1.90	329/90	0.20	0.10
2.26	324/58	0.20	0.30
2.62	325/56	0.01	0.05
2.81	208/55	0.10	0.05
2.84	286/40	0.03	0.01
2.94	322/15	2.00	0.80
3.34	133/78	0.01	0.01
3.35	016/18	0.02	0.01
3.37	302/58	0.04	0.05
3.62	356/60	0.30	0.10
3.70	156/78	0.30	0.20
3.81	074/68	0.20	0.10
3.82	326/68	0.01	0.01
3.90	316/64	0.30	0.10
4.08	175/74	0.20	0.10
4.32	176/74	0.20	0.10
4.82	186/54	0.05	0.01
4.98	177/54	0.25	0.01

CHINNOR TUNNEL

Chainage 55.4m

Vertical Scanline

D (m)	Orientation	L_1 (m)	L_2 (m)
0.02	175/59	0.03	0.04
0.15	219/60	0.05	0.01
0.29	232/49	0.70	0.20
0.64	237/08	0.20	0.50
0.94	016/48	0.01	0.05
0.98	157/60	0.20	0.01
1.06	321/52	0.30	0.80
1.20	203/68	0.40	0.30
1.32	307/37	0.30	0.20
1.35	176/36	0.05	0.20
1.47	322/33	0.01	0.20
1.56	022/52	0.01	0.30
1.59	020/44	0.01	0.20
1.77	014/30	0.01	0.05
1.84	040/57	0.01	0.05
1.86	301/62	0.01	0.02
1.87	031/54	0.20	0.01
1.89	039/58	0.01	0.01
1.92	038/65	0.01	0.30
2.04	031/58	0.30	0.20
2.14	030/53	0.20	0.10
2.51	017/49	0.20	0.20
2.56	329/17	0.01	0.20
2.64	202/55	0.20	0.10
2.68	002/68	0.03	0.02
2.70	014/49	0.80	0.01
2.92	243/72	0.30	0.01
3.04	354/22	1.70	0.01
3.23	081/32	0.01	0.03
3.27	031/10	2.00	0.20
3.41	104/38	0.01	0.02
3.47	346/22	0.02	0.03
3.51	031/51	0.01	0.02
3.54	337/32	0.03	0.05
3.55	331/28	0.10	0.10
3.60	266/28	0.20	0.30
3.61	330/66	0.20	0.01
3.62	201/65	0.10	0.10
3.64	243/26	0.10	0.01
3.65	015/47	0.30	0.20
3.68	152/43	0.10	0.01
3.72	228/62	0.01	0.20
3.79	347/11	0.20	0.30
3.86	044/64	0.30	0.10
3.98	040/68	0.10	0.30
4.09	336/12	0.01	0.20
4.12	319/16	0.20	0.30
4.27	226/80	0.01	0.01
4.30	093/90	0.04	0.01
4.42	025/52	0.04	0.06
4.50	222/80	0.30	0.30
4.70	219/46	0.20	0.10

Horizontal Scanline

D (m)	Orientation	L_1 (m)	L_2 (m)
0.07	085/74	0.30	0.40
0.20	150/64	0.20	0.20
0.29	210/48	0.05	0.10
0.36	214/36	0.10	0.20
0.47	210/59	0.30	0.01
0.57	014/07	0.20	0.20
0.90	156/90	0.20	0.05
0.96	026/30	0.20	0.10
1.07	031/20	0.30	0.20
1.20	179/72	0.30	0.20
1.29	119/58	0.10	0.01
1.44	219/64	0.20	0.20
1.66	007/70	0.30	0.01
1.74	186/83	0.20	0.10
1.83	302/74	0.30	0.50
2.02	234/74	0.30	0.30
2.17	226/70	0.10	0.40
2.34	016/60	0.10	0.40
2.61	289/74	0.70	0.30
2.83	350/02	0.01	0.02
2.93	111/81	0.02	0.02
3.13	238/62	0.05	0.10
3.21	119/36	0.40	0.40
3.30	343/58	0.02	0.01
3.32	029/79	0.20	0.30
3.36	108/85	0.40	0.20
3.53	205/34	0.01	0.03
3.67	005/26	0.04	0.20
3.68	020/40	0.20	0.20
3.83	135/79	0.01	0.20
4.32	089/56	0.10	0.20
4.71	206/53	0.01	0.02

CHINNOR TUNNEL

Chainage 57.5m

Vertical Scanline

D (m)	Orientation	L_1 (m)	L_2 (m)
0.14	350/19	0.10	0.20
0.15	007/32	0.20	0.10
0.16	127/20	0.40	0.30
0.18	353/11	0.30	0.50
0.19	317/11	0.10	0.70
0.27	006/04	0.70	0.90
0.30	354/04	0.50	0.60
0.62	268/12	0.40	0.20
1.07	294/16	0.01	0.40
1.34	006/32	0.01	0.03
1.36	210/46	0.30	0.10
1.37	157/50	0.02	0.04
1.41	348/60	0.30	0.20
1.47	352/72	0.40	0.20
1.55	192/88	0.30	0.20
1.65	236/84	0.10	0.30
1.72	151/47	0.30	0.20
1.74	120/84	0.50	0.01
1.97	356/32	0.10	0.20
2.32	322/24	0.30	0.10
2.59	343/43	0.20	0.10
2.70	356/24	0.30	0.20
2.78	306/05	0.01	0.20
2.93	044/29	0.60	0.20
3.02	164/24	0.60	0.10
3.13	104/90	0.30	0.20
3.16	001/13	0.70	0.01
3.21	320/21	0.70	0.70
3.39	045/28	0.10	0.20
3.47	119/62	0.10	0.05
3.54	057/64	0.40	0.20
3.65	117/79	0.20	0.01
3.72	352/78	0.80	0.20
3.88	249/10	0.90	0.30
3.92	024/59	0.10	0.10
3.98	352/08	1.50	0.30
3.99	180/32	0.10	0.10
4.02	048/69	0.01	0.30
4.04	277/36	0.20	0.01
4.10	294/12	0.80	0.30
4.20	053/49	0.10	0.30
4.24	332/30	0.10	0.50
4.27	002/36	0.10	0.30
4.29	159/63	0.10	0.10
4.32	274/75	0.01	0.02
4.37	348/34	0.10	0.20
4.45	335/72	0.20	0.30
4.52	304/77	0.10	0.30

Horizontal Scanline

D (m)	Orientation	L_1 (m)	L_2 (m)
0.04	342/18	0.02	0.03
0.24	025/20	0.30	0.20
0.31	010/11	0.10	0.10
0.42	005/05	0.01	0.02
0.43	005/07	0.10	0.06
0.72	126/31	0.30	0.20
0.84	154/18	0.90	0.40
0.87	118/90	0.10	0.20
0.93	051/28	0.10	0.20
1.30	132/27	0.10	0.20
1.49	253/58	0.10	0.01
1.61	167/56	0.10	0.10
1.81	242/38	0.01	0.30
1.82	207/48	0.01	0.30
2.09	233/54	0.01	0.04
2.24	218/47	0.30	0.20
2.47	212/63	0.01	0.02
2.51	163/74	0.10	0.20
2.62	220/80	0.10	0.01
2.68	010/44	0.30	0.01
2.74	220/70	0.30	0.20
2.77	015/11	0.10	0.10
2.86	031/72	0.30	0.10
2.86	003/52	0.10	0.10
3.02	332/68	0.30	0.01
3.06	298/14	0.01	0.04
3.12	161/08	0.40	0.20
3.15	251/64	0.01	0.05
3.18	324/52	0.01	0.05
3.34	295/52	0.01	0.02
3.35	218/72	0.01	0.02
3.38	328/08	0.20	0.40
3.58	211/31	0.10	0.20
3.63	117/32	0.20	0.40
3.69	110/40	0.40	0.50
3.71	004/62	0.10	0.10
3.74	304/60	0.10	0.50
3.87	186/82	0.30	0.10
4.00	164/66	0.20	0.10
4.14	205/54	0.20	0.20
4.15	048/20	0.10	0.01
4.29	202/74	0.20	0.10
4.34	155/56	0.10	0.01
4.40	341/22	0.10	0.20
4.46	226/30	0.30	0.10
4.55	345/50	0.20	0.30
4.56	302/60	0.30	0.50
4.90	168/72	0.20	0.40

CHINNOR TUNNEL

Chainage 60.6m

Vertical Scanline

D (m)	Orientation	L_1 (m)	L_2 (m)
0.06	349/16	0.02	0.04
0.07	203/52	0.20	0.10
0.27	207/32	0.90	1.10
0.38	161/83	0.01	0.02
0.56	327/79	0.20	0.50
0.63	183/04	0.10	0.40
0.66	184/18	0.30	0.20
0.89	017/25	0.01	0.02
0.99	212/82	0.20	0.40
1.03	007/84	0.20	0.40
1.06	266/50	0.01	0.20
1.15	116/86	0.04	0.05
1.31	025/62	0.03	0.02
1.32	183/85	0.03	0.04
1.37	183/86	0.20	0.40
1.40	206/90	0.20	0.10
1.52	189/74	0.20	0.10
1.58	269/20	0.05	0.30
1.60	274/15	0.20	0.30
1.62	195/85	0.20	0.40
1.84	186/57	0.20	0.10
1.88	349/76	0.20	0.20
2.02	357/66	0.40	0.30
2.17	277/24	0.20	0.30
2.56	005/08	0.10	0.20
2.58	224/82	0.01	0.02
2.71	156/90	0.20	0.40
2.78	232/80	0.30	0.20
2.82	082/72	0.01	0.02
2.83	085/75	0.02	0.03
2.90	066/52	0.03	0.05
2.91	045/50	0.05	0.01
3.18	341/04	0.10	0.20
3.21	314/16	0.10	0.10
3.23	316/18	0.30	0.30
3.27	054/61	0.01	0.02
3.37	140/70	0.02	0.30
3.42	217/88	0.01	0.30
3.43	261/42	0.20	0.30
3.46	316/27	0.01	0.80
3.50	237/47	0.10	0.50
3.58	159/09	0.10	0.20
3.60	299/22	0.05	0.01
3.69	292/19	1.50	2.50
3.85	189/84	1.20	1.40
4.09	230/64	0.01	0.03
4.10	006/74	0.10	0.20
4.11	126/19	0.20	0.20
4.29	319/58	0.30	0.40
4.33	354/19	0.50	0.30
4.42	334/72	0.01	0.02
4.47	028/76	0.20	0.15

Horizontal Scanline

D (m)	Orientation	L_1 (m)	L_2 (m)
0.20	148/64	0.20	0.30
0.44	119/52	0.02	0.02
0.60	339/86	0.02	0.03
0.64	217/58	0.01	0.01
0.84	040/54	0.20	0.10
0.91	212/90	0.01	1.50
0.97	281/80	0.01	0.02
0.99	226/30	0.30	0.40
1.07	010/80	0.30	0.40
1.31	228/18	0.40	0.20
1.44	200/72	0.01	0.01
1.51	304/62	0.04	0.05
1.52	308/71	0.02	0.04
1.67	352/88	0.02	0.04
1.85	204/39	0.20	0.30
1.91	036/09	0.05	0.10
2.24	218/12	0.30	0.30
2.64	280/09	0.05	0.01
2.71	015/50	1.50	0.01
2.96	202/15	0.10	0.05
2.97	210/10	0.05	0.05
2.98	082/82	0.10	0.01
3.10	220/50	0.01	0.02
3.36	213/58	0.03	0.10
3.48	022/85	0.10	0.20
3.55	295/69	0.10	0.10
3.58	304/79	0.01	0.20
3.64	207/26	0.10	0.30
3.85	317/48	0.10	0.40
3.86	306/51	0.20	0.35
4.00	216/56	0.30	0.20
4.08	219/47	0.02	0.04
4.28	116/22	0.04	0.05
4.29	116/22	0.04	0.05
4.58	341/59	0.02	0.02
4.86	353/40	0.05	0.05

CHINNOR TUNNEL

Chainage 65.2m

Vertical Scanline

D (m)	Orientation	L_1 (m)	L_2 (m)
0.10	124/78	0.01	0.02
0.19	184/14	0.30	0.20
0.24	004/04	0.30	0.20
0.30	323/52	0.20	0.30
0.39	329/66	0.02	0.03
0.42	297/46	0.02	0.03
0.57	290/17	0.25	0.30
0.59	284/12	0.20	0.30
0.60	284/12	0.40	0.20
0.79	286/13	0.50	0.10
1.15	296/20	0.30	0.40
1.16	298/23	0.20	0.50
1.17	297/21	0.20	0.40
1.18	298/33	0.20	0.01
1.39	123/60	0.01	0.01
1.53	100/73	0.01	0.01
1.54	332/17	0.20	0.30
1.57	138/07	0.10	0.10
1.64	356/24	0.02	0.02
1.65	224/13	0.01	0.01
1.78	343/32	0.30	0.30
1.87	347/22	0.30	0.30
1.94	237/84	0.20	0.40
2.09	325/24	0.02	0.50
2.21	041/54	0.20	0.10
2.44	069/61	0.01	0.02
2.50	160/63	0.10	0.20
2.53	321/26	0.10	0.20
2.60	123/84	0.10	0.20
2.66	325/58	0.10	0.25
2.74	336/67	0.30	0.05
2.75	315/76	0.20	0.20
2.88	322/65	0.05	0.20
2.96	019/04	0.10	0.20
3.01	164/10	0.25	0.15
3.17	316/32	0.70	0.90
3.22	298/27	0.50	0.10
3.23	298/27	0.90	1.40
3.54	320/70	0.20	0.20
3.63	300/28	0.01	1.50
3.66	309/22	0.01	0.02
3.71	300/42	0.05	0.10
3.76	318/32	0.02	0.80
4.02	299/54	0.04	0.05
4.07	284/17	0.05	0.05
4.24	178/20	0.02	0.02
4.31	357/18	0.40	0.20
4.32	333/33	0.10	0.50
4.46	176/70	0.01	0.02
4.50	000/31	0.50	0.30
4.60	260/76	0.04	0.10

Horizontal Scanline

D (m)	Orientation	L_1 (m)	L_2 (m)
0.17	190/53	0.04	0.02
0.18	321/41	0.02	0.03
0.50	350/27	0.02	0.02
0.62	263/31	0.05	0.01
0.92	294/18	0.40	0.20
1.21	307/08	0.40	0.20
1.22	355/10	0.20	0.10
1.41	254/12	0.20	0.10
1.75	116/16	0.20	0.20
1.77	216/55	0.30	0.30
1.90	028/28	0.05	0.06
2.20	166/20	0.80	0.50
2.36	168/60	0.40	0.50
2.46	075/45	0.01	0.06
2.56	019/70	0.01	0.02
2.68	340/22	0.01	0.02
2.93	019/22	0.03	0.03
3.11	300/32	0.40	0.10
3.20	280/50	0.10	0.20
3.36	249/40	0.30	0.30
3.92	111/50	0.02	0.03
4.41	180/10	0.10	0.20
4.43	190/05	0.20	0.30
4.57	293/22	0.20	0.10
4.59	197/10	0.10	0.20
4.82	221/61	0.02	0.05
4.86	139/44	0.02	0.01

CHINNOR TUNNEL

Chainage 70.2m

Vertical Scanline

D (m)	Orientation	L_1 (m)	L_2 (m)
0.09	050/74	0.01	0.02
0.11	130/55	0.03	0.02
0.14	233/28	0.25	0.35
0.19	112/10	0.20	0.30
0.21	242/15	0.20	0.10
0.22	248/10	0.35	0.20
0.23	118/03	0.20	0.25
0.26	327/13	0.05	0.10
0.28	336/10	0.25	0.40
0.31	314/07	0.20	0.50
0.36	126/02	0.20	0.50
0.40	310/50	0.10	0.20
0.73	358/08	0.30	0.60
0.82	328/54	0.20	0.20
0.84	328/62	0.01	0.10
0.87	128/62	0.05	0.03
0.88	304/22	0.90	0.80
1.00	202/89	0.10	0.40
1.02	346/06	0.04	0.05
1.12	201/84	0.10	0.10
1.26	250/24	0.20	0.60
1.29	262/08	0.30	0.70
1.30	260/10	0.20	0.10
1.31	309/08	0.60	0.50
1.69	312/25	0.10	0.15
1.76	133/90	0.01	0.02
1.80	050/42	0.20	0.30
1.91	007/41	1.00	0.20
2.05	011/54	0.20	0.10
2.08	206/62	0.30	0.20
2.16	087/24	0.10	0.20
2.20	015/84	0.20	0.10
2.30	260/05	0.10	0.30
2.31	162/12	0.10	0.30
2.34	002/26	0.40	0.20
2.35	342/12	0.20	0.20
2.38	345/12	0.10	0.50
2.39	012/29	0.05	0.05
2.42	113/66	0.10	0.20
2.59	012/53	0.01	0.01
2.60	223/10	0.40	0.10
2.61	320/16	0.10	0.30
2.62	293/10	0.30	0.20
2.79	267/13	0.10	0.30
2.81	261/10	1.00	1.50
2.84	348/06	0.20	0.50
2.86	344/00	0.50	0.10
2.96	011/09	1.50	1.00
2.99	358/08	0.80	0.40
3.05	352/04	0.10	0.70
3.06	153/08	0.20	0.40
3.33	339/06	0.40	0.20
3.49	293/47	0.20	0.01
3.51	311/44	0.01	0.20
3.58	212/02	0.20	0.30
3.73	297/12	0.10	0.05
3.83	020/18	1.30	1.00
3.99	328/14	0.50	0.20
4.00	328/14	0.30	0.40
4.07	320/20	0.60	0.10
4.12	350/10	0.10	0.20
4.13	350/10	0.20	0.30
4.14	000/16	0.20	0.40
4.24	352/12	0.90	0.50
4.30	256/80	0.10	0.20
4.32	360/90	0.10	0.10
4.45	045/56	0.20	0.30
4.60	026/73	0.10	0.20
4.75	160/55	0.05	0.20
4.80	200/81	0.05	0.05

CHINNOR TUNNEL

Chainage 70.2m (cont.)

Horizontal Scanline

D (m)	Orientation	L_1 (m)	L_2 (m)
0.34	303/18	0.20	0.20
0.44	040/86	0.02	0.02
0.75	333/09	0.20	0.10
0.84	358/86	0.01	0.02
0.90	212/88	0.10	0.10
1.06	331/16	0.20	0.30
1.10	166/90	0.01	0.02
1.14	248/10	0.01	0.05
1.38	124/89	0.10	0.20
1.51	294/89	0.10	0.20
1.73	202/80	0.20	0.30
1.83	097/78	0.01	0.02
2.21	108/77	0.20	0.01
2.24	114/75	0.20	0.20
2.36	068/32	0.02	0.10
2.40	025/50	0.05	0.10
2.54	295/04	0.10	0.20
2.56	110/84	0.10	0.10
2.68	220/50	0.30	0.20
3.05	002/47	0.20	0.20
3.16	208/90	0.10	0.10
3.24	222/26	0.20	0.10
3.26	189/90	0.05	0.10
3.51	053/22	0.40	0.20
3.53	097/15	0.30	0.20
3.62	039/10	0.40	0.20
3.98	113/89	0.01	0.01
4.00	207/88	0.01	0.01
4.06	051/49	0.10	0.10
4.16	182/90	0.10	0.01
4.21	064/75	0.30	0.10
4.27	204/66	0.20	0.20
4.30	060/36	0.10	0.10
4.35	043/45	0.10	0.10
4.42	129/42	0.10	0.10
4.46	346/40	0.05	0.01
4.52	169/50	0.10	0.30
4.55	237/67	0.50	0.01
4.58	195/90	0.10	0.30
4.71	301/44	0.20	0.30
4.73	161/58	0.01	0.02
4.95	012/12	0.10	0.05

Chainage 72.7m

Vertical Scanline

D (m)	Orientation	L_1 (m)	L_2 (m)
0.11	257/68	0.10	0.10
0.19	144/32	0.10	0.30
0.26	246/86	0.20	0.10
0.32	342/28	0.20	0.20
0.38	357/14	0.10	0.15
0.40	223/32	0.05	0.40
0.42	227/85	0.05	0.10
0.46	344/66	0.01	0.30
0.49	024/60	0.20	0.40
0.50	314/30	0.60	0.40
0.55	113/47	0.20	0.10
0.68	292/08	1.50	3.00
0.88	302/18	0.30	2.20
0.94	308/15	0.30	0.70
0.98	312/30	0.50	0.05
1.00	199/78	0.05	0.30
1.04	311/23	0.20	0.20
1.08	317/32	0.10	0.40
1.18	089/87	0.20	0.05
1.46	266/51	0.05	0.10
1.77	276/24	0.30	0.40
1.97	024/68	0.05	0.10
2.06	030/67	0.20	0.30
2.21	228/80	0.20	0.30
2.31	282/69	0.20	0.30
2.34	094/08	0.20	0.30
2.47	198/72	0.10	0.10
2.51	332/70	0.10	0.30
2.52	193/10	0.10	0.20
2.56	347/84	0.20	0.05
2.66	149/78	0.20	0.40
2.79	331/78	0.10	0.20
2.80	345/11	0.20	0.30
2.93	292/14	0.01	0.02
3.04	213/81	0.05	0.02
3.10	349/80	0.04	0.10
3.17	327/73	0.10	0.30
3.31	198/44	0.20	0.05
3.38	313/21	0.10	0.20
3.41	304/17	0.20	1.30
3.50	180/79	0.10	0.10
3.61	348/44	2.10	1.50
3.69	185/60	0.20	0.50
3.70	164/60	0.20	0.30
3.77	004/46	0.30	1.50
3.78	006/44	0.50	2.30
3.80	001/46	0.20	0.60
3.83	174/37	0.02	0.30

CHINNOR TUNNEL

Chainage 72.7m (cont.)

Vertical Scanline

D (m)	Orientation	L_1 (m)	L_2 (m)
3.96	119/76	0.40	0.30
4.08	030/12	0.40	0.70
4.18	166/78	0.30	0.90
4.20	056/39	0.05	0.20
4.35	010/30	0.20	0.30
4.45	198/74	0.20	2.50

Horizontal Scanline

0.23	312/72	0.20	0.30
0.34	129/72	0.20	0.30
0.38	003/52	0.10	0.30
0.47	037/80	0.20	0.10
0.54	217/11	1.50	0.60
0.61	281/30	0.20	0.40
0.66	340/84	0.04	0.02
1.37	104/19	1.60	0.40
1.54	345/30	0.20	0.30
1.63	118/88	0.20	0.10
1.72	241/11	0.30	0.20
1.79	120/88	2.60	2.50
1.92	152/81	0.20	0.30
1.93	027/48	2.50	0.30
2.06	351/24	0.10	0.15
2.19	025/52	0.20	0.20
2.23	202/82	0.35	0.10
2.65	329/56	0.10	0.05
2.67	023/18	0.20	1.30
2.70	132/90	0.10	0.01
2.78	226/30	0.10	0.10
2.90	007/24	0.50	0.40
2.99	188/80	0.05	0.10
3.10	185/46	0.30	0.20
3.16	007/40	0.05	0.20
3.19	131/78	0.30	0.30
3.61	201/80	1.50	3.00
3.77	234/17	0.10	0.30
3.81	114/82	0.20	0.10
3.87	200/24	0.20	0.20
4.22	213/14	0.30	0.60
4.23	200/84	0.50	0.10
4.28	049/52	0.30	0.20
4.48	339/33	0.20	0.05
4.62	000/16	0.30	0.05
4.63	186/62	0.05	0.10
4.71	359/36	0.20	0.40
4.80	231/85	0.20	0.40
4.87	019/60	0.05	0.05

Chainage 84.95m

Vertical Scanline

D (m)	Orientation	L_1 (m)	L_2 (m)
0.07	159/85	0.05	0.10
0.12	340/63	0.20	0.30
0.24	316/36	0.01	0.05
0.25	114/28	0.05	0.02
0.29	015/48	0.02	0.04
0.32	205/57	0.05	0.10
0.34	351/39	0.10	0.10
0.49	024/14	0.20	0.10
0.53	008/24	0.30	0.15
0.59	024/39	0.20	0.10
0.68	314/40	0.20	0.04
0.83	323/76	0.20	0.10
0.88	327/47	0.40	0.05
0.96	282/04	0.30	0.20
0.97	354/80	0.20	0.10
0.99	231/90	0.05	0.01
1.14	303/20	0.30	0.20
1.17	206/66	0.01	0.05
1.20	118/83	0.20	0.10
1.24	024/24	0.05	0.10
1.32	312/29	0.10	0.30
1.34	295/26	0.10	0.01
1.36	206/88	0.20	0.10
1.42	318/24	0.20	0.20
1.43	341/22	0.10	0.40
1.64	326/44	0.30	0.20
1.66	173/86	0.10	0.15
1.72	318/16	0.20	0.40
1.73	318/16	0.20	0.40
1.78	263/05	0.25	0.10
1.81	280/46	0.01	0.03
1.83	000/70	0.20	0.10
1.87	321/32	0.10	0.15
1.90	324/73	0.30	0.20
1.94	162/74	0.20	0.10
2.04	060/46	0.10	0.15
2.08	242/35	0.10	0.10
2.11	352/21	0.20	0.10
2.16	015/10	0.20	0.10
2.18	327/75	0.01	0.01
2.22	200/10	0.05	0.05
2.27	238/52	0.10	0.01
2.36	230/41	0.20	0.01
2.42	225/75	0.10	0.01
2.47	124/66	0.30	0.20
2.48	040/90	0.20	0.05
2.61	236/78	0.30	0.20
2.65	018/30	0.70	0.20
2.95	018/06	1.50	0.20

CHINNOR TUNNEL

Chainage 84.95m (cont.)

Vertical Scanline

D (m)	Orientation	L_1 (m)	L_2 (m)
3.03	358/04	0.10	1.70
3.08	199/90	0.30	0.20
3.16	009/72	0.20	0.30
3.17	152/85	0.30	0.60
3.32	077/22	0.30	0.10
3.56	219/61	0.10	0.40
3.62	024/32	0.30	0.20
3.66	240/23	0.80	0.20
3.69	044/29	0.30	0.01
3.76	208/50	0.60	0.20
3.86	350/88	0.40	0.20
3.91	341/07	0.60	0.10
3.93	331/10	0.20	0.50
3.94	337/10	0.10	0.05
3.96	344/08	0.20	0.25
4.22	284/15	0.30	0.20
4.25	043/04	0.10	0.01
4.42	033/04	0.30	0.05

Horizontal Scanline

0.15	000/90	0.30	0.60
0.38	244/20	0.30	0.80
0.68	115/84	0.30	0.05
0.93	216/86	0.30	0.70
0.97	281/10	0.30	1.00
1.07	040/76	0.30	0.25
1.17	140/82	0.30	0.15
1.34	202/41	0.30	0.35
1.55	215/05	0.45	0.30
1.57	061/53	0.20	0.05
1.62	030/42	0.20	0.10
1.92	010/11	0.30	0.30
1.94	015/10	0.20	0.10
1.95	043/68	0.01	0.01
2.34	005/88	0.01	0.03
2.37	027/49	0.10	0.16
2.47	026/49	0.30	0.20
2.62	222/79	0.30	0.55
2.68	009/66	0.05	0.10
2.76	008/32	0.20	0.60
2.91	202/77	0.30	0.35
2.98	122/85	0.01	0.03
3.03	352/09	0.40	0.20
3.06	101/77	0.25	0.20
3.23	259/08	0.10	0.40
3.31	180/53	0.20	0.25
3.38	286/58	0.30	0.20

D (m)	Orientation	L_1 (m)	L_2 (m)
3.46	214/46	0.40	0.10
3.51	005/30	0.05	0.10
3.67	293/74	0.15	0.10
4.01	124/86	0.30	0.20
4.21	185/63	0.40	0.20
4.34	187/88	0.20	0.40
4.62	180/79	0.10	0.20
4.81	292/78	0.10	0.10

KIELDER EXPERIMENTAL TUNNEL

Sandstone Heading

Vertical Scanline

D (m)	Orientation	L_1 (m)	L_2 (m)
0.18	045/11	Bedding	
0.31	056/11	"	
0.32	070/05	"	
0.39	158/08	"	
0.45	284/76	0.30	0.70
0.52	018/11	0.05	0.05
0.68	149/05	0.10	0.15
0.79	100/90	0.30	0.10
0.92	127/03	Bedding	
0.97	301/75	0.10	0.40
1.08	107/09	0.30	0.10
1.15	063/82	0.05	0.30
1.28	293/81	0.30	0.50
1.51	065/04	Bedding	
1.53	099/88	0.40	0.10
1.62	108/03	Bedding	
1.76	027/69	0.10	0.15
1.79	289/85	0.10	0.05
1.92	063/04	Bedding	
2.12	067/04	"	
2.18	044/08	"	
2.23	032/04	"	
2.54	052/87	"	

Vertical Scanline

D (m)	Orientation	L_1 (m)	L_2 (m)
0.00	115/02	Bedding	
0.14	228/84	0.10	0.10
0.18	150/07	Bedding	
0.38	246/90	0.20	0.30
0.52	107/05	Bedding	
0.74	250/85	0.10	0.30
0.79	129/08	Bedding	
0.81	149/05	"	
0.89	071/04	"	
0.94	072/04	"	
0.96	119/06	"	
0.98	195/10	"	
1.02	045/83	0.10	0.05
1.05	242/44	0.20	0.01
1.10	337/40	0.10	0.30
1.18	091/10	0.10	0.01
1.35	130/60	0.05	0.10
1.39	055/05	Bedding	
1.46	067/07	"	
1.65	269/87	0.15	0.30
1.73	079/08	Bedding	

Vertical scanline

D (m)	Orientation	L_1 (m)	L_2 (m)
1.86	076/08	Bedding	
1.88	076/11	"	
1.94	144/06	"	
1.95	144/06	"	
1.97	144/06	"	
1.99	160/08	"	
2.07	293/07	"	
2.19	173/03	"	
2.44	118/78	0.01	0.40
2.57	126/73	0.01	0.20
2.70	234/78	0.40	0.20

Horizontal Scanline

D (m)	Orientation	L_1 (m)	L_2 (m)
0.00	146/87	2.00	0.20
0.08	068/07	0.30	0.40
0.11	069/87	0.80	0.03
0.22	069/05	0.20	0.40
0.29	149/86	0.40	0.01
0.30	242/70	0.40	0.20
0.31	331/77	0.05	0.30
0.34	075/73	0.10	0.05
0.40	143/83	0.01	0.30
0.42	075/73	0.10	0.05
0.73	243/79	0.50	0.04
0.95	254/82	0.30	0.01
1.32	261/88	0.30	0.40
1.36	253/82	0.70	0.60
1.48	351/14	0.10	0.30
1.63	185/84	0.20	0.40
1.83	216/78	0.20	0.50
1.94	165/04	0.30	0.60
2.13	186/80	0.10	0.40
2.27	117/84	0.40	0.01
2.46	063/06	0.50	1.20
2.58	261/80	0.40	0.01
2.81	324/83	0.50	0.01
3.02	048/83	0.01	0.40
3.38	140/83	0.01	0.04
3.47	146/89	1.00	1.00
3.53	077/84	0.20	0.10
3.78	023/84	0.20	0.10
3.89	029/82	0.30	0.40
3.97	000/87	0.10	0.01
4.01	331/86	1.20	0.40
4.19	148/83	0.10	0.30
4.98	078/85	0.05	0.10

KIELDER EXPERIMENTAL TUNNEL

Sandstone Heading

Horizontal Scanline (cont.)

D (m)	Orientation	L_1 (m)	L_2 (m)
5.13	163/82	0.30	0.15
5.22	252/85	1.50	1.50
5.67	179/83	0.40	0.10
6.00	163/83	0.40	0.30

Horizontal Scanline

D (m)	Orientation	L_1 (m)	L_2 (m)
0.00	074/06	Bedding	
0.64	272/90	0.10	0.25
0.74	359/83	0.01	0.40
0.89	194/73	0.60	0.01
0.98	121/04	Bedding	
1.28	126/21	0.30	0.20
1.37	339/69	0.01	0.40
1.98	129/06	0.05	0.02
2.16	137/80	2.50	2.10
2.33	158/04	0.30	0.20
2.35	158/10	0.20	0.05
2.43	261/90	0.40	0.01
2.58	238/88	0.01	0.03
2.59	137/62	0.01	0.02
2.68	156/60	0.05	0.01
2.75	240/80	0.40	1.50
2.75	069/87	0.10	0.40
2.81	048/89	0.30	0.30
3.50	120/08	0.05	0.05
3.64	206/82	0.10	0.10
3.73	133/82	0.10	0.10
3.80	230/89	0.05	0.02

Horizontal Scanline

D (m)	Orientation	L_1 (m)	L_2 (m)
0.00	244/82	0.01	0.50
0.14	062/16	Bedding	
0.17	337/70	0.05	0.40
0.42	299/79	0.20	0.40
0.51	308/82	0.01	0.30
0.53	098/88	0.30	0.40
0.85	100/60	0.30	0.30
1.10	326/80	0.15	0.15
1.25	267/83	0.20	0.20
1.38	329/85	0.30	0.30
1.86	186/85	0.10	0.14
1.93	192/83	0.01	0.30
2.07	268/88	1.20	0.30
2.08	138/81	0.10	0.05
2.28	263/87	0.05	0.05

D (m)	Orientation	L_1 (m)	L_2 (m)
2.55	199/89	0.30	1.00
2.68	335/83	0.20	1.50
2.78	268/88	0.01	0.30
2.87	000/83	0.30	0.40
3.12	028/83	0.10	0.30
3.28	147/05	Bedding	
3.48	137/11	"	
3.49	044/03	"	

Orientation of discontinuities in the Limestone Heading and the Quarry face.

1.	153/84
2.	255/77
3.	162/80
4.	250/82
5.	156/85
6.	249/87
7.	166/83
8.	249/77
9.	160/88
10.	253/87
11.	064/88
12.	138/85
13.	234/88
14.	212/77
15.	242/88
16.	138/89

KIELDER EXPERIMENTAL TUNNEL

Mudstone Heading

Chainage 29.7m

Vertical Scanline

D (m)	Orientation	L_1 (m)	L_2 (m)
0.04	355/04	0.20	0.60
0.07	062/86	0.10	0.05
0.10	347/02	Bedding	
0.13	002/10	0.20	0.40
0.18	282/04	Bedding	
0.19	282/04	"	
0.20	282/04	"	
0.21	282/04	"	
0.23	282/04	"	
0.24	220/89	0.05	0.02
0.25	220/89	Bedding	
0.26	220/89	"	
0.29	015/81	0.10	0.10
0.34	212/06	Bedding	
0.35	212/06	"	
0.43	330/86	0.15	0.30
0.44	232/06	Bedding	
0.46	232/06	"	
0.48	232/06	"	
0.49	033/83	0.05	0.10
0.52	223/13	Bedding	
0.57	223/13	"	
0.59	055/36	0.40	0.20
0.67	225/83	0.10	0.30
0.72	244/80	0.40	0.20
0.81	230/75	0.30	0.01
0.86	243/80	0.30	0.01
0.96	236/35	0.40	0.30
1.18	070/84	0.50	0.01
1.32	230/80	0.30	0.10
1.33	065/04	Bedding	
1.34	065/04	"	
1.35	065/04	"	
1.37	065/04	"	
1.38	233/79	0.10	0.15
1.40	087/78	0.10	0.01
1.42	339/39	0.02	0.04
1.47	273/60	0.05	0.05
1.48	273/60	0.01	0.01
1.49	015/09	Bedding	
1.55	015/09	"	
1.58	015/09	"	
1.62	230/80	0.70	0.20
1.63	034/02	Bedding	
1.65	157/89	0.10	0.15
1.78	031/37	0.40	0.30
1.86	227/74	0.30	0.40
1.89	280/84	0.20	0.01
1.91	137/90	0.01	0.01
1.92	303/09	0.30	0.15
2.04	317/60	0.20	0.10
2.14	066/15	0.10	0.13
2.17	242/73	0.40	0.30
2.22	233/72	0.10	0.10
2.24	346/80	0.10	0.01
2.32	077/77	0.01	0.05
2.37	210/81	0.20	0.15
2.50	050/88	0.10	0.30
2.52	234/76	0.15	0.01
2.62	004/46	0.40	0.01
2.63	257/72	0.05	0.01
2.68	017/45	0.20	0.01
2.70	237/75	0.01	0.01
2.76	169/51	0.20	0.01

KIELDER EXPERIMENTAL TUNNEL

Mudstone Heading

Chainage 29.7m

Horizontal Scanline

D (m)	Orientation	L_1 (m)	L_2 (m)
0.00	239/81	0.30	0.20
0.12	244/81	0.40	0.30
0.15	348/62	0.05	0.10
0.22	240/74	0.30	0.05
0.23	238/71	0.05	0.01
0.24	239/75	0.05	0.01
0.28	239/75	"	
0.29	239/75	"	
0.30	239/75	"	
0.31	239/75	"	
0.34	242/77	0.30	0.20
0.37	163/55	0.30	0.15
0.39	045/90	0.30	0.40
0.43	232/88	0.20	0.30
0.44	239/89	0.30	0.20
0.45	233/85	0.10	0.20
0.47	233/85	0.10	0.05
0.52	153/79	0.10	0.20
0.54	144/90	0.01	0.30
0.59	323/39	0.20	0.30
0.63	231/70	0.10	0.01
0.70	225/80	0.90	0.40
0.74	234/59	0.30	0.40
0.91	059/82	0.10	0.20
0.99	070/23	0.10	0.20
1.17	226/75	0.50	0.30
1.19	234/76	0.30	0.10
1.24	346/09	0.10	0.50
1.30	233/76	0.80	0.01
1.36	242/79	0.01	0.03
1.39	040/06	0.01	0.01
1.44	222/81	1.50	0.20
1.48	313/76	1.50	0.01
1.52	344/08	0.10	0.20
1.56	239/73	0.15	0.30
1.59	245/70	0.01	0.02
1.63	240/73	0.20	0.01
1.65	359/10	0.20	0.10
1.67	253/72	0.05	0.01
1.72	262/60	1.30	0.40
1.74	262/60	1.30	0.40
1.75	233/90	0.05	0.03
1.80	137/88	0.10	0.05
1.87	244/81	0.30	0.10
1.92	161/80	0.10	0.05
1.94	252/75	0.05	0.05
1.97	357/06	0.01	0.05
2.00	212/84	0.01	0.10
2.12	351/74	0.10	0.10
2.23	320/77	0.05	0.05
2.28	145/80	0.20	0.10
2.30	198/82	0.50	1.00
2.80	212/72	0.60	0.80
2.85	007/66	0.05	0.10
2.99	218/82	0.40	0.60
3.11	334/06	0.15	0.01
3.14	299/58	0.01	0.02

KIELDER EXPERIMENTAL TUNNEL

Mudstone Heading

Chainage 57.0m

Vertical Scanline

D (m)	Orientation	L_1 (m)	L_2 (m)
0.00	099/22	0.10	0.05
0.03	277/65	0.30	0.20
0.04	044/12	0.20	0.40
0.06	228/41	0.20	0.14
0.07	213/38	0.05	0.02
0.09	213/38	0.10	0.05
0.11	213/38	0.01	0.05
0.13	208/36	0.30	0.20
0.16	262/75	0.20	0.30
0.17	223/89	0.20	0.15
0.18	256/43	0.10	0.70
0.20	200/88	0.10	0.05
0.23	260/16	0.80	0.40
0.27	258/49	0.40	0.30
0.30	243/02	0.50	0.05
0.32	160/89	0.30	0.10
0.36	016/07	0.30	0.20
0.38	016/07	0.10	0.10
0.41	333/06	0.30	0.15
0.44	344/04	0.10	0.05
0.45	348/04	0.02	0.05
0.46	289/07	0.05	0.20
0.48	340/80	0.10	0.05
0.50	350/06	0.30	0.20
0.51	350/06	0.10	0.05
0.54	342/04	0.05	0.01
0.57	319/77	0.05	0.01
0.62	255/61	0.05	0.10
0.64	256/58	0.90	0.30
0.68	015/10	0.50	0.10
0.70	318/08	0.05	0.03
0.73	005/10	0.30	0.20
0.75	295/03	0.10	0.15
0.77	247/05	0.30	0.60
0.79	247/05	0.10	0.30
0.82	238/64	0.30	0.05
0.84	247/05	0.20	0.15
0.86	247/05	0.40	0.15
0.87	247/05	0.10	0.10
0.89	054/41	0.20	0.10
0.91	070/63	0.20	0.30
0.97	232/83	0.01	0.05
0.98	042/06	0.10	0.40
0.99	042/06	0.10	0.05
1.00	042/06	0.30	0.10
1.02	257/88	0.05	0.10
1.05	172/90	0.01	0.05
1.07	254/90	0.01	0.05
1.12	012/59	0.20	0.10
1.14	270/30	0.02	0.03
1.15	033/04	0.20	0.10
1.16	033/04	0.10	0.15
1.18	033/04	0.05	0.01
1.19	033/04	0.05	0.03
1.24	036/18	0.20	0.40
1.29	220/84	0.40	0.70
1.31	224/89	0.40	0.15
1.36	257/78	0.01	0.02
1.49	212/90	0.30	0.20
1.54	149/82	0.20	0.30
1.64	207/90	0.30	0.40
1.75	146/80	0.30	0.10

KIELDER EXPERIMENTAL TUNNEL

Mudstone Heading

Chainage 57.0m

Horizontal Scanline

D (m)	Orientation	L_1 (m)	L_2 (m)
0.03	342/06	0.02	0.01
0.08	329/05	0.20	0.40
0.14	239/60	0.10	0.30
0.19	248/83	0.10	0.20
0.24	193/90	0.05	0.05
0.29	200/07	0.20	0.15
0.38	211/11	0.03	0.10
0.40	254/83	0.02	0.30
0.51	305/62	0.05	0.20
0.56	242/81	0.05	0.15
0.59	240/82	0.01	0.05
0.60	244/81	0.20	0.30
0.67	228/02	0.05	0.01
0.68	248/84	0.01	0.02
0.72	242/83	0.20	0.25
0.81	015/73	0.20	0.50
0.84	248/81	0.02	0.10
0.90	247/83	0.10	0.15
0.91	253/58	0.20	0.30
0.92	253/58	0.10	0.15
0.94	258/67	0.20	0.10
0.95	241/64	0.40	0.20
0.99	152/90	0.10	0.50
1.00	241/68	0.30	0.01
1.12	166/86	0.20	0.15
1.15	257/61	0.20	0.01
1.16	139/87	0.30	0.40
1.22	257/80	1.50	0.30
1.26	307/07	0.30	0.20
1.27	280/09	0.30	0.10
1.35	240/80	0.10	0.30
1.38	301/07	0.20	0.10
1.45	153/84	0.30	0.30
1.49	060/55	0.30	0.20
1.50	324/02	0.20	0.01
1.54	333/02	0.30	0.10
1.56	243/81	0.10	0.01
1.59	245/82	0.05	0.20
1.66	075/72	0.05	0.10
1.69	045/05	0.20	0.30
1.74	224/72	0.20	0.30
1.86	058/80	0.10	0.20
1.88	245/75	0.20	0.15
1.96	225/85	0.05	0.20
2.05	029/08	0.10	0.30
2.13	226/81	0.04	0.30
2.17	296/47	0.05	0.10
2.18	144/78	0.01	0.01
2.19	131/00	0.01	0.10
2.27	217/80	0.10	0.01
2.34	345/09	0.01	0.30
2.42	209/72	0.10	0.30
2.47	145/87	0.40	0.70
2.56	049/50	0.60	0.50
2.69	158/86	0.40	0.70
2.75	259/78	0.40	0.60
2.87	245/03	0.05	0.10
2.90	019/06	0.20	0.40
2.95	031/08	0.40	0.20

KIELDER EXPERIMENTAL TUNNEL

Mudstone Heading

Chainage 68.9m

Vertical Scanline

D (m)	Orientation
0.00	056/87
0.01	148/86
0.04	030/16
0.07	030/16
0.08	030/16
0.10	030/16
0.11	030/16
0.14	167/88
0.18	007/04
0.21	013/06
0.24	019/08
0.28	019/08
0.29	019/08
0.32	032/32
0.35	357/07
0.37	000/02
0.41	356/02
0.45	002/04
0.47	298/03
0.48	298/03
0.52	240/80
0.53	354/06
0.58	013/11
0.59	022/19
0.60	238/80
0.66	020/22
0.68	013/22
0.70	223/89
0.76	041/38
0.77	028/37
0.84	025/28
0.85	259/90
0.86	210/84
0.91	215/85
0.92	335/05
0.93	335/05
0.94	335/05
0.95	335/05
0.97	242/82
0.99	256/80
1.02	009/07
1.04	256/72
1.06	166/14
1.09	157/04
1.12	342/02
1.14	026/08
1.18	340/02
1.20	340/02
1.22	208/83
1.28	020/62
1.37	297/06
1.38	304/02
1.40	300/02
1.47	327/02
1.52	318/01
1.59	208/62
1.60	300/06
1.72	058/52
1.77	248/83
1.79	301/04
1.83	301/04
1.84	220/83
1.90	222/79
1.94	333/08
1.99	211/85
2.04	236/68
2.08	333/10
2.14	263/72
2.19	263/38
2.22	214/60
2.30	301/60
2.31	050/35

Horizontal Scanline

D (m)	Orientation
0.00	200/25
0.01	213/62
0.04	338/11
0.05	136/84
0.07	149/78
0.11	209/09
0.14	333/01
0.24	294/21
0.39	176/86
0.57	048/47
0.59	347/55
0.64	358/57
0.69	239/70
0.75	240/75
0.78	062/51
0.81	350/01
0.85	228/73
0.89	356/02
0.93	347/04
0.94	255/80

Horizontal Scanline

D (m)	Orientation
0.95	255/80
0.99	009/02
1.00	066/40
1.04	342/03
1.06	347/06
1.10	198/85
1.18	017/07
1.22	026/05
1.26	216/85
1.28	257/87
1.30	247/87
1.32	008/04
1.35	258/87
1.38	025/03
1.40	234/86
1.42	237/88
1.47	035/09
1.50	140/79
1.53	252/89
1.56	154/86
1.57	246/84
1.58	215/81
1.60	029/15
1.61	131/81
1.70	119/82
1.71	252/85
1.73	248/86
1.78	066/80
1.85	031/02
1.95	346/02
2.00	129/74
2.06	008/20
2.09	156/89
2.17	247/62
2.19	006/06
2.20	160/84
2.30	072/63

KIELDER EXPERMENTAL TUNNEL

Mudstone Heading

Chainage 87.6m

Vertical Scanline

D (m)	Orientation
0.00	303/06
0.01	118/17
0.08	330/62
0.09	354/04
0.12	083/02
0.16	027/05
0.17	187/83
0.23	308/06
0.30	341/01
0.32	162/85
0.36	186/73
0.39	058/28
0.45	251/82
0.49	158/89
0.50	245/79
0.53	042/03
0.55	036/03
0.56	036/03
0.57	260/90
0.60	196/88
0.69	244/81
0.75	238/89
0.92	001/02
1.14	240/77
1.33	339/07
1.47	244/85
1.55	010/02
1.58	348/03
1.60	017/02
1.66	148/03
1.80	245/81
1.81	010/22
1.86	348/12
1.89	296/85
1.93	278/73
2.02	081/46
2.04	286/78
2.05	316/85
2.06	069/42
2.12	036/31

Horizontal Scanline

D (m)	Orientation
0.00	003/10
0.04	141/86
0.12	237/81
0.14	147/71
0.24	211/84
0.26	121/80
0.35	240/90
0.42	234/81
0.51	077/19
0.75	341/01
0.82	349/02
1.02	021/04
1.13	124/26
1.21	315/84
1.25	099/04
1.32	089/06
1.40	062/33
1.42	070/31
1.48	243/18
1.54	035/59
1.61	200/90
1.69	038/47
1.73	155/78
1.75	036/12
1.76	320/78
1.78	171/83
1.80	358/07
1.85	358/03
1.88	182/88
1.93	072/10
2.00	052/28
2.11	038/10

Vertical Scanline

D (m)	Orientation
0.03	306/88
0.06	032/01
0.07	107/04
0.09	036/01
0.12	036/01
0.13	104/06
0.17	242/06
0.24	242/83
0.25	096/12
0.36	160/90
0.37	332/02
0.39	003/03
0.45	084/10
0.49	106/08
0.53	006/66
0.56	068/03
0.64	259/18
0.66	078/31
0.74	008/05
0.89	169/88
1.00	160/03

Horizontal Scanline

D (m)	Orientation
0.00	020/04
0.11	120/82
0.14	240/74
0.30	143/82
0.32	064/86
0.39	074/87
0.48	061/86
0.53	315/02
0.58	011/04
0.62	229/84
0.72	155/04
0.79	155/04
0.81	079/83
0.82	312/03
0.91	264/81
0.94	0.4/73
0.95	179/02
1.00	151/77

CHANNEL TUNNEL, MACHINE ERECTION CHAMBER

Vertical Scanline 1

D (m)	Orientation	L_1 (m)	L_2 (m)
0.31	258/40	0.80	2.00
0.34	135/39	0.05	0.10
0.46	281/47	0.50	0.01
0.52	253/68	0.30	0.01
0.67	318/48	0.40	0.20
0.69	277/78	0.50	0.20
1.07	344/16	2.00	2.00
1.20	055/28	2.00	2.00
2.44	238/24	2.00	0.30
2.50	273/50	2.00	2.00
2.52	238/24	2.00	0.20
2.75	292/70	0.50	0.10

Vertical Scanline 2

0.16	116/60	0.20	0.10
0.17	232/43	0.10	0.20
0.18	075/36	0.30	0.50
0.25	261/52	0.20	0.50
0.28	050/74	0.20	0.30
0.56	342/49	0.20	0.10
0.68	312/20	0.30	2.00
0.76	328/20	0.30	0.60
0.79	311/18	0.10	0.40
0.99	073/12	0.20	0.40
1.12	282/79	0.10	0.01
1.65	060/80	0.30	0.20
2.18	086/00	2.00	2.00
2.35	072/82	0.10	0.30
2.62	218/84	0.30	0.60
2.67	208/77	0.20	0.01
2.71	214/62	0.40	0.20
2.75	128/24	0.01	0.20
2.81	151/69	0.10	0.30
2.95	258/88	0.30	0.50

Vertical Scanline 3

0.15	255/88	0.50	0.50
0.37	228/17	0.30	1.00
0.42	259/41	0.30	0.10
1.55	045/52	0.10	0.30
1.58	061/04	0.10	0.20
1.90	259/85	0.60	2.00
2.08	138/41	0.20	0.20
2.14	259/41	0.40	0.30
2.43	268/47	0.80	0.30
2.61	120/65	0.20	0.10
2.77	300/58	0.01	0.10

Vertical Scanline 3 (cont.)

2.83	308/64	0.05	0.10
2.90	269/50	0.01	0.15
2.93	340/51	0.20	0.20

Vertical Scanline 4

0.06	267/02	0.10	0.50
0.10	274/05	0.30	0.10
0.14	081/60	0.30	0.20
0.21	224/36	0.05	0.10
0.25	090/50	0.05	0.10
0.41	322/50	0.02	0.05
0.43	222/58	0.05	0.01
0.53	293/23	0.10	0.40
0.83	204/35	0.01	0.05
0.96	055/68	0.05	0.01
1.25	325/49	0.10	0.01
2.13	278/15	0.20	0.01
2.16	278/15	0.25	0.01
2.61	300/14	0.40	0.30
2.64	354/65	0.10	0.05
2.70	092/84	0.10	0.20

Vertical Scanline 5

0.09	087/44	0.30	0.20
0.24	270/16	1.50	0.80
0.27	265/05	0.30	0.30
0.37	315/15	0.10	0.05
0.44	122/10	0.30	0.05
0.54	121/07	0.30	0.10
0.58	036/27	0.05	0.10
0.68	122/20	0.20	0.10
0.92	089/39	0.30	0.05
1.75	244/02	0.05	0.10
1.97	310/60	0.01	0.01
2.22	332/16	0.30	0.80
2.98	272/40	0.01	0.40
3.00	105/71	0.10	0.02

Vertical Scanline 6

0.09	080/68	0.40	0.30
0.38	092/55	0.30	0.40
0.65	272/24	0.40	0.50
0.82	276/30	0.60	0.80
1.16	242/18	0.05	0.20
1.59	246/11	0.01	0.03

CHANNEL TUNNEL, MACHINE ERECTION CHAMBER

Vertical Scanline 6 (cont.)

D (m)	Orientation	L_1 (m)	L_2 (m)
1.80	274/82	1.20	0.20
2.11	328/03	0.50	0.50
2.30	269/78	2.00	1.50
2.39	320/09	0.40	0.10
2.53	329/07	0.60	1.00
2.83	305/74	0.30	0.20

Horizontal Scanline 1

0.14	288/58	0.01	0.15
1.80	088/19	2.00	2.00
2.20	287/60	2.00	0.50
2.35	114/28	0.30	0.01
2.95	098/17	1.00	0.20
3.30	042/10	0.20	0.01
3.68	069/42	0.30	0.05
4.03	286/38	0.20	0.01
4.42	298/16	0.05	0.10
4.92	322/64	0.05	0.01
5.80	254/80	0.30	1.00
7.42	214/10	0.30	0.80
8.74	164/12	0.10	0.30
9.12	143/25	0.30	0.50
9.40	260/35	0.10	0.50

Horizontal Scanline 2

0.05	036/24	2.00	2.00
0.15	274/40	0.01	2.00
0.22	166/74	0.01	0.30
4.94	074/69	0.40	0.30
5.52	234/87	0.05	0.10
6.33	155/42	0.10	0.01
7.11	224/90	0.10	0.01
8.73	065/22	2.00	2.00
10.20	284/82	1.00	1.00

Horizontal Scanline 3

D (m)	Orientation	L_1 (m)	L_2 (m)
0.27	305/80	0.30	0.01
0.57	068/78	0.10	0.10
0.85	307/81	0.05	0.01
1.30	092/87	0.20	0.10
2.12	062/85	0.70	0.05
2.25	061/82	0.05	0.01
2.82	257/23	0.10	0.01
3.24	334/35	0.01	0.01
3.73	311/72	0.10	0.30
5.28	038/83	0.10	0.05
5.32	295/86	0.30	0.20
6.57	260/16	0.01	0.01
9.34	288/89	0.05	0.10
10.00	269/85	0.20	1.50

APPENDIX C

DESCRIPTION OF THE COMPUTING TECHNIQUES USED TO PLOT DISCONTINUITY ORIENTATION DATA

Discontinuity orientation data presented in Chapters 2, 3 and 5 were processed using a computer program written by Attewell and Woodman (1971) on file at the University of Durham. The program rapidly processes large volumes of orientation data and displays the resulting discontinuity fabric, smoothed and contoured, on an equal area or equal angle upper or lower hemisphere projection or as a whole sphere projection, as required.

Discontinuity orientation is measured in the field in terms of the direction of maximum dip, expressed as a geographical azimuth ranging from 0^{o} - 360^{o} counting in clockwise rotation, and the amount of maximum dip recorded as an angle ranging from 0^{o} - 90^{o}. The discontinuity orientation, uniquely defined by these two angles can then be represented by a line (or pole) extending upwards normal to the discontinuity surface. The orientation of this pole is therefore defined by the two angles described above which represent the direction and amount of inclination of the pole from the vertical (Figure C.1). The point P in Figure C.1 can be regarded as forming the centre of a hemisphere of radius r, and i the point where the pole intersects the surface of the hemisphere. If a straight line is drawn from i to a point (the "south pole") a distance r directly below P, the intersection point I of this line with the horizontal plane of the upper hemisphere is known as the upper hemisphere projection of the orientation of the pole. This upper hemisphere projection therefore displays uniquely in two dimensions the orientation

of the discontinuity plane under consideration.

In the computer program, the properties of the pole to each of the discontinuity surfaces, expressed in terms of polar co-ordinates, are regarded as approximating to a Dirac delta function. The total sample of discontinuity orientations, regarded as a sum of Dirac delta functions, must be smoothed to give a better representation of the true population characteristics. This is achieved by allocating to each data point i on the hemisphere a small circular area centred on i having a projected area equal to $k\pi r^2$ where k is the fraction of the total area of the hemisphere of projection (k would often, by convention, be taken as 0.01, or 1%). This circular area is then scanned for other data points in order that a weighting factor can be applied to the initiating point proportional to the number of points found within the circular area. When each data point has been scanned and weighted in this way a choice of normalisation procedures is initiated in order that the weightings can be expressed as a more meaningful percentage value. Following this an output matrix holding character information is generated and printed out in the form presented in Chapters 2, 3 and 5.

For all survey locations except the Chinnor tunnel, the '12 o'clock' position on the projections presented in this thesis represents the geographical north direction ($000^{o} = 360^{o}$). In the case of orientation data obtained in the Chinnor tunnel, the '12 o'clock' position represents the tunnel drive direction, just 10^{o} east of geographical north. On all projections, therefore, the '6 o'clock' position represents the due south (180^{o}) direction or the reverse drive direction, counting the angles in a clockwise rotation. Reference to Figure C.1 shows that data points near

the centre of the projection represent sub-horizontal planes, whilst those near the perimeter represent sub-vertical planes, with the position of the point round the perimeter indicating the dip direction (that is azimuth) of the plane.

The discontinuity orientation density distribution data presented on the upper hemisphere projections in Chapters 2, 3 and 5 are in the form of clusters of matrices. These matrices consist of numbers representing percentage values between 0 and 9, with letters representing the higher percentages, O = 10, A = 11, B = 12, C = 13 etc. These are area normalised values representing the smoothed percentage of data points having an orientation within the one percent area of projection centred on the point in question.

Interpretation of the data presented on the projections is a largely qualitative procedure involving the recognition of preferred orientation patterns within the discontinuity orientation fabric. This work is coupled with systematic comparison between projections, obtained from surveys taken at different locations, in order to identify trends or patterns in discontinuity orientation. The computer program is particularly suited to this procedure because grouping and re-grouping of sample data-sets can be achieved relatively quickly once the orientation data have been recorded on punch cards.

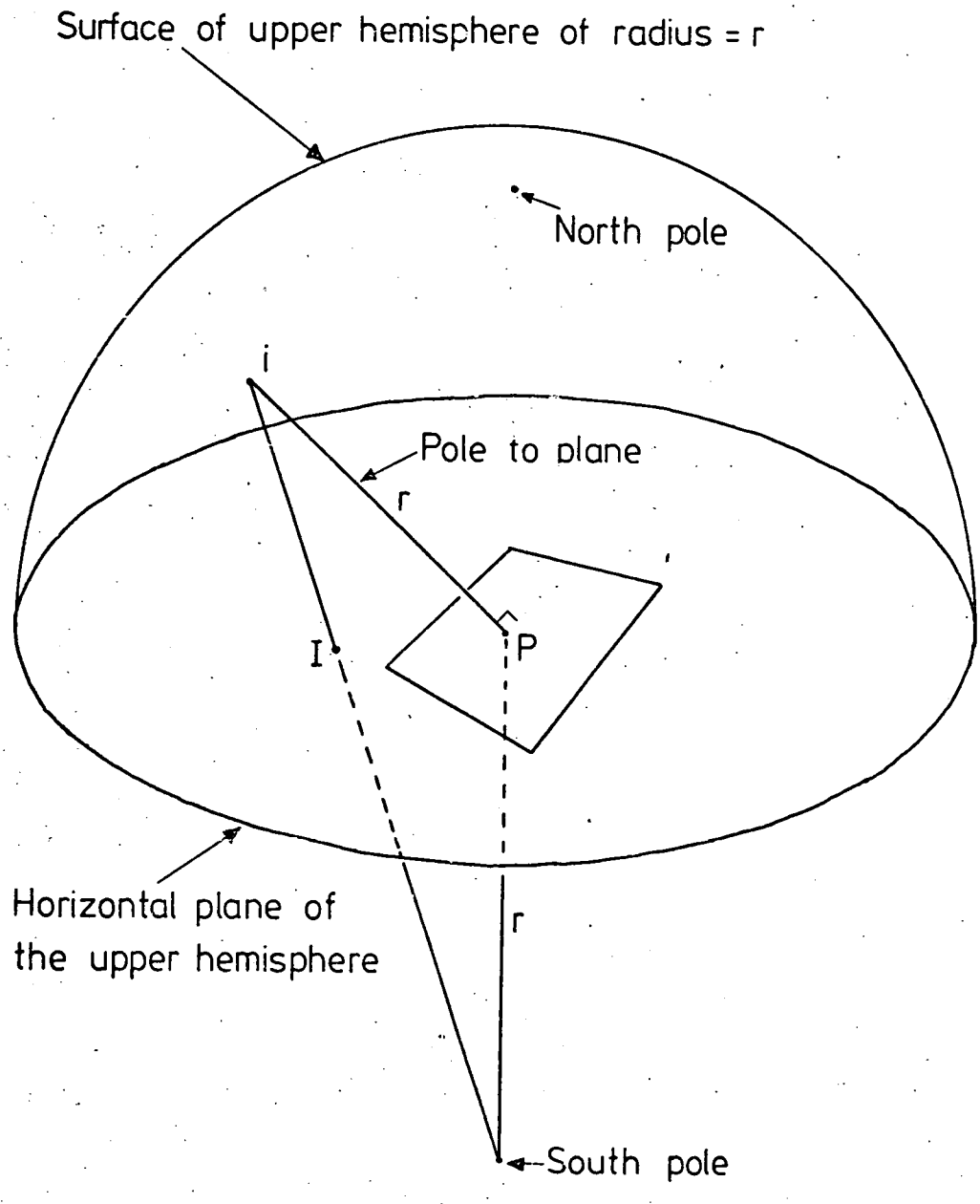

Fig. C.1 UPPER HEMISPHERE PROJECTION OF A POLE TO A PLANE.

APPENDIX D

TESTS CARRIED OUT BY SOIL MECHANICS LTD. AT CHINNOR

D.1 Point load strength index

Cores recovered during the site investigation programme at Chinnor were tested by Soil Mechanics Ltd., using a portable hydraulic point load tester, to obtain an indication of rock strength variability. Franklin (1972) gives a full description of the theoretical and practical aspects of the test, and in particular demonstrates the good correlation between the point load index and uniaxial compressive strength.

For each test, a section of core of length at least 1.4D (where D is the core diameter) is compressed diametrically between two rounded conical points having a tip radius of 5mm and a cone angle of 60^{0}. The load P required to produce failure is used to calculate the strength index P/D^{2}. When D ≠ 50mm the index is corrected to an equivalent value (Is_{50}) for the same material having a tested diameter of 50mm. The conversion of the strength index to Is_{50}, done using standard charts, allows a comparison to be made between strength values obtained from different diameter cores.

D.2 Pressuremeter tests

The Menard pressuremeter is a device designed for use in boreholes to measure the *in situ* shear strength and deformation modulus of soils and rocks. The pressuremeter apparatus consists essentially of two parts:

1. A probe which is lowered down the borehole to the required test level.

2. A pressure-volumeter located on the ground surface connected by plastic tubes to the probe.

The probe consists of three flexible cylindrical metal cells containing rubber membranes which can be pressurised, thus expanding the metal cells inside the borehole. During a test the central measuring cell is inflated by water under pressure from the ground surface, thus exerting a radial pressure on the walls of the borehole. The two guard cells, one at each end of the probe, are inflated with gas to the same pressure as the measuring cell, thereby minimising end effects near the central measuring cell.

The pressure-volumeter is a volume measuring device connected to a supply of gas under pressure. During the test, measured increments of pressure are applied through the probe to the walls of the borehole. The volume changes associated with expansion of the measuring cell during deformation of the ground are monitored in the calibrated volumeter.

After applying suitable corrections to the results a graph is plotted of pressure against volume change. The resulting pressure-volume relation is commonly similar in form to the graph shown in Figure D.1. The graph is composed essentially of three stages:

1. Initial stage of low apparent modulus during which the horizontal ground stress condition is being restored.

2. Elastic stage; the slope of this linear part of the curve is proportional to E_p, the deformation modulus of the ground near the test cell.

3. The final stage is marked by rapidly increasing deformation as the pressure increases to the limit pressure. This limit pressure is a measure of the ultimate bearing capacity of the material.

D.3 Seismic velocity measurements*

Seismic velocity was measured in boreholes using a velocity sonde consisting of two transducers, the upper one being a transmitter and the lower one a receiver, set at separations of 305mm, 915mm or 1830mm within the probe. Short sinusoidal acoustic pulses, containing frequencies between 22.5 kHz and 33.5 kHz, are periodically transmitted and propogate through the rock near the borehole. The resultant signals from the receiver transducer are recorded on an oscilloscope-type photographic chart recorder whose writing scan speed is varied according to the transducer spacing. The record produced is of the variable intensity type in which positive half cycles of the signals appear as dark images whose intensities are proportional to the signal amplitude.

Analysis of the log gives values for the velocity of propogation of both compressional (P) waves and shear (S) waves. The P and S wave

---

*Details obtained from the Soil Mechanics Ltd. Report to the Transport and Road Research Laboratory, 1975 (Part 2).

velocities can be taken as a broad indication of rock quality near the test probe.

D.4 Water injection tests*

Water injection tests carried out by Soil Mechanics Ltd. were of the 'pumping in' type, during which the lower 3m of each borehole was sealed off using a pneumatic packer. Water was then pumped under pressure into the isolated section of borehole, ensuring that the maximum water pressure did not exceed the effective overburden pressure. At each test pressure the water was allowed to flow until the rate of flow reached a constant value (Q) which was then recorded. At least three measurements were taken at each pressure.

The magnitude of Q is a function of (a) the water pressure difference between the isolated section of the borehole and the ground (b) the size of the isolated borehole section, and (c) the permeability of the ground:

$$k = \frac{Q}{2\pi LH}\left(\ln \frac{2L}{D}\right) \qquad \text{when } L \geq 5D$$

$$k = \frac{Q}{2\pi LH}\left(\sinh^{-1} \frac{L}{D}\right) \qquad \text{when } 5D > L \geq 0.5D.$$

---

*Details obtained from the Soil Mechanics Ltd. Report to the Transport and Road Research Laboratory, 1974 (Part 1).

where

k = permeability of the ground

Q = constant rate of flow into the hole

L = length of the portion of the hole tested

H = differential head of water

D = diameter of hole tested

$\ln$ = natural logarithm

$\sinh^{-1}$ = arc hyperbolic sine

These formulae, valid when the thickness of the stratum tested is at least 5L, are consequently applicable at Chinnor.

For convenience the formulae can be written:

$$k = C_p \left(\frac{Q}{H}\right)$$

where C_p is a shape factor defined by the geometric part of the above formulae. Where the test length is below the water table, H is the distance in metres from the water table to the level of the pressure gauge plus the applied pressure in metres of water head. Where the test length is above the water table, H is the distance in metres from the centre of the length tested to the pressure gauge plus the applied pressure in metres of water head. Reduction of effective head applied at the test level occurs as a result of resistance to flow through the supply hoses and rods. Corrections for this effect are made using standard charts and calibrations.

For each test a corrected pressure-flow curve is drawn up so that changes of flow pattern during the test, if any, can be seen. Permeability is then calculated for the appropriate values of excess head.

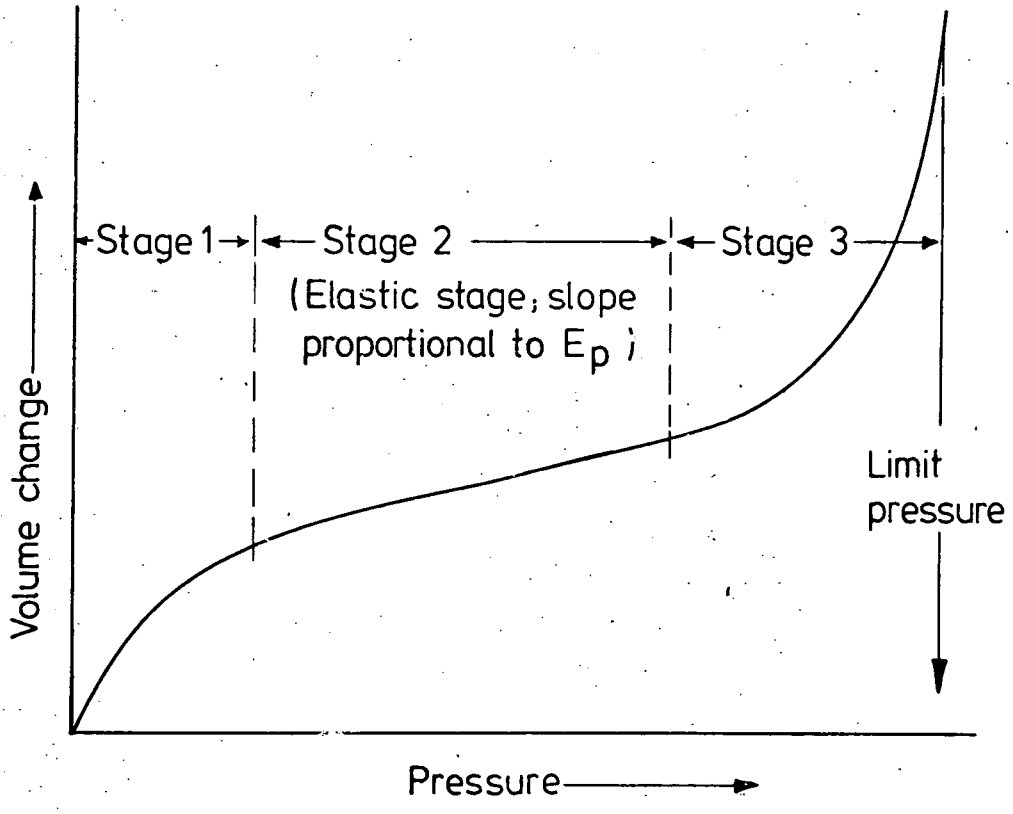

Fig. D.1 TYPICAL PRESSURE-VOLUME CURVE FOR A PRESSUREMETER TEST.

APPENDIX E

X-RAY ANALYSIS OF CHALK SAMPLES FROM CHINNOR

E.1 Introduction

Detailed X-ray analyses of samples taken at selected depths in borehole 105 were carried out by Mr R. G. Hardy of the Department of Geological Sciences at the University of Durham. The analyses were of two types:

1. X-ray diffraction (X.R.D.). Using this technique a thin film of the powdered sample is irradiated with X-rays thus producing diffracted beams inclined at varying angles to the plane of the sample. The diffraction angles, measured using a geiger-counter, are a measure of the crystal structures (and therefore the mineral content) of the sample. Analysis of the diffraction charts, which plot the relation between diffraction angle and radiation intensity, allowed semi-quantitative analyses of mineral content to be made. This was possible because the concentration of a given mineral is proportional to the area under the radiation peak generated by that mineral. The analysis at Durham was carried out on a PW 1130 Philips 3 kW generator-diffractometer using cobalt K_α radiation.

2. X-ray fluorescence (X.R.F.). Using this technique the chemical composition of a sample is accurately determined from the emission spectrum produced when the sample is irradiated with X-rays.

The analysis was carried out on a Philips PW 1212 Automatic Spectrometer.

E.2 X.R.D., results and discussion

The results of the X.R.D. analysis suggest that the samples from borehole 105 contain three main minerals:

1. Calcite

2. Quartz

3. Lussatite. This mineral is a 'semi-amorphous' form of silica consisting of extended sheets of SiO_4 tetrahedra that show considerable stacking disorder and consequently produce X-ray diffraction maxima attributable to tridymite (Calvert, 1974). The structure of lussatite suggests that it could behave in a similar way to a montmorillonitic clay mineral, with an expanding lattice that could respond to pressure release or the presence of water.

Samples from borehole 105 range in composition between two end member types depending on the amount of lussatite present. The end members are:

1. Samples consisting of approximately 65% calcite, 20% quartz together with a small percentage ($\lesssim$10%) of a semi-amorphous mixed layer clay mineral and only a small amount of lussatite. Samples of this type were found at depths 9.7m, 11m, 12m, 15m and 27m in borehole 105.

2. Samples containing calcite, quartz and lussatite in approximately equal proportions of 30% together with a small percentage (<5%) of mixed layer clay mineral. Samples of this type were found at depths 13m, 19m, 20m and 21m in borehole 105.

In general one can say that all samples are calcite-rich together with varying amounts of quartz and lussatite and a negligible amount of clay mineral. It is likely that the engineering properties of the chalk at Chinnor will be dominated by the behaviour of the lussatite (when present), such that large amounts of this mineral may lend a 'clayey' character to the chalk.

E.3 X.R.F., results and discussion

The following elements (as the oxides) were determined using X.R.F. techniques: SiO_2 (silica), Al_2O_3 (aluminium oxide), Fe_2O_3 (iron oxide), MgO (magnesium oxide), CaO (calcium oxide), Na_2O (sodium oxide), K_2O (potassium oxide), TiO_2 (titanium oxide), S (sulphur) and P_2O_5 (phosphorous oxide). The per cent by weight of these oxides (and elements) in the samples from borehole 105 are listed in Table E.1.

In order to calculate the calcium carbonate ($CaCO_3$) content it was assumed that all the CaO was combined in the chalk with carbon dioxide (CO_2) as $CaCO_3$:

$$CaO + CO_2 \rightarrow CaCO_3$$

Molecular weight: 56.08 + 44.01 → 100.09

Table E.1 X.R.F. chemical analysis, borehole 105 Chinnor

Sample depth (m)	Chemical composition, per cent by weight													
	SiO_2	Al_2O_3	Fe_2O_3	MgO	CaO	Na_2O	K_2O	TiO_2	S	P_2O_5	Total, (Non volatile oxides)	Estimated CO_2	Total	Estimated $CaCO_3$
2.2	31.80	4.60	1.35	1.10	31.75	0.00	1.10	0.25	0.00	0.08	72.03	24.92	96.95	56.67
3	21.00	3.45	0.90	0.94	40.50	0.00	0.75	0.16	0.00	0.21	67.93	31.79	99.72	72.29
4	17.80	2.40	0.90	0.86	44.50	0.00	0.55	0.10	0.00	0.16	67.11	34.93	102.04	79.43
6	24.60	4.00	1.10	1.00	38.00	0.00	0.85	0.17	0.00	0.13	69.85	29.83	99.68	67.83
7	28.40	3.70	1.25	1.20	35.25	0.06	0.95	0.20	0.00	0.05	71.06	26.43	97.49	61.68
7(duplicate)	23.40	4.40	1.10	1.34	37.50	0.26	0.88	0.16	0.02	0.05	69.11	29.44	98.55	66.94
8	32.20	4.90	1.35	1.16	32.00	0.00	1.10	0.23	0.00	0.02	72.96	25.12	98.08	57.12
9	26.40	4.10	1.10	1.04	36.00	0.00	0.90	0.18	0.00	0.08	69.80	28.26	98.06	64.26
9.7	39.80	4.60	1.28	1.10	28.00	0.00	0.90	0.21	0.00	0.00	75.89	21.98	97.87	49.98
11	44.40	2.60	1.18	0.70	29.00	0.00	0.65	0.15	0.00	0.00	78.68	22.77	101.45	51.77
12	40.40	3.30	1.12	0.84	29.50	0.00	0.83	0.18	0.00	0.00	76.17	23.16	99.33	52.66
13	51.90	4.00	1.28	0.86	24.75	0.00	0.85	0.22	0.00	0.00	83.86	19.43	103.29	44.18
14	32.00	2.90	1.10	0.82	33.50	0.00	0.60	0.15	0.00	0.63	71.07	26.30	97.37	59.80
15	42.00	3.50	1.12	0.87	29.25	0.03	0.83	0.19	0.00	0.01	77.80	22.96	100.76	52.21
16	26.40	4.50	1.32	1.10	35.75	0.02	0.98	0.17	0.00	0.08	70.32	28.06	98.38	63.81
19	50.40	5.60	2.10	1.25	23.25	0.03	1.23	0.27	0.00	0.00	84.13	18.75	102.38	41.50
20	61.00	4.50	1.10	0.83	19.30	0.09	0.88	0.26	0.02	0.00	89.09	15.15	104.24	34.45
21	56.60	2.40	1.20	0.54	25.00	0.07	0.50	0.13	0.00	0.00	86.44	19.63	106.07	44.63
22	18.00	2.40	1.00	0.84	44.75	0.00	0.52	0.10	0.00	0.10	67.71	35.13	102.84	79.88
23	26.40	3.60	1.10	1.02	33.30	0.02	0.75	0.14	0.00	0.10	66.43	26.14	92.57	59.44
24	20.70	2.70	0.90	0.80	43.25	0.01	0.70	0.14	0.03	0.10	69.33	33.95	103.28	77.20
25	36.00	4.60	1.35	1.04	32.50	0.06	0.90	0.20	0.00	0.01	76.66	25.51	102.17	58.01
26	33.60	4.60	1.40	1.05	30.00	0.05	1.15	0.20	0.33	0.01	72.39	23.55	95.94	53.55
27	44.70	5.30	1.80	1.30	25.00	0.04	1.37	0.30	0.62	0.01	80.44	19.63	100.07	44.63
28	34.80	6.70	1.72	1.23	27.50	0.04	1.35	0.26	0.60	0.01	74.21	21.59	95.80	49.09

Therefore, if x is the per cent by weight CaO

the per cent by weight $CO_2 = \frac{44.01}{56.08} x = 0.785x$

The CO_2 contents estimated in this way are listed in Table E.1 together with the $CaCO_3$ contents obtained by summing the CaO and CO_2 contents.

An indication of the validity of the assumption that all the CaO is combined as $CaCO_3$ can be obtained by summing the per cent by weight CO_2 and the total per cent by weight of non volatile oxides. This should give a total percentage of 100. Examination of Table E.1 shows that in general this summed total is within 5% of 100%, thus confirming the validity of the assumption concerning the combination of CaO.

Examination of Table E.1 shows that the samples from depths 13m, 19m, 20m and 21m in borehole 105 have a significantly higher SiO_2 content than the other samples. If this SiO_2 were present as the silicate portion of clay minerals in the samples one would expect a corresponding increase in the Al_2O_3 contents since this oxide is also combined in the clay mineral lattice. The lack of any corresponding increase in Al_2O_3 contents is clearly demonstrated in Table E.1 and tends to suggest that the SiO_2 is in the form of free silica. Reference to the X.R.D. results in Section E.2 shows that samples from depths 13m, 19m, 20m and 21m in borehole 105 are rich in the mineral lussatite. This serves to explain the increased amounts of free silica in these samples.

APPENDIX F

LIST OF MICROFOSSILS IDENTIFIED FROM SAMPLES TAKEN IN THE SHAFT AT CHINNOR

Zone 9, *Marssonella Ozawai*

≤ 114m A.O.D. to approximately 123m A.O.D.

These samples contain rich and typical assemblages of Zone 9 benthonics including:

Arenobulimina anglica

truncata

Bulbophragmium westfalicum

'Cibicides' aff. *voltziana*

Dorothia gradata

Gaudryina quadrans

sp. 25.

Gavelinella ammonoides

baltica

cenomanica

Gyroidina nitida

Hagenowella courta

Hagenowina advena

'Lituola' globigerinoides

Marssonella ozawai

oxycona

Plectinaaruthenica

'Pernerina' sp.

Pseudotextulariella cretosa

Ramulina spp.

Spiroplectammina rectangularis

Tristrix excavata

Tritaxia pyramidata

Vaginulina kochi

Planktonics are very rare or absent and include only *Hedbergellae*.

Lower Part of Zone 10 (*Quinqueloculina Antiqua* Zone)

Approximately 123m A.O.D. to 130m A.O.D.

These samples contain assemblages closely similar to those from below but lacking *Marssonella ozawai*. Since this species often is rare near the top of its range additional splits of material were processed using hydrochloric acid. The agglutinated species are resistant to this treatment and, although the full range of agglutinated species were recovered in each case this did not include *Marsonnella ozawai*. No specimens of *Plectina* sp. 21 were recovered.

Lower Part of Zone 11 (II), (Upper *Plectina* Sp. 21 Zone)

Approximately 130m A.O.D. to the top of the shaft

Arenobulimina anglica (advanced forms)

Bulbophragmium westfalicum

Cibicides sp. 21

'Discorbis' sp. 21

Dorothia gradata

Flourensina orenata

Gavelinella baltica

cenomanica

Hagenowina advena

Plectina sp. 21

Tritaxia pyramidata

and a very rich assemblage (61% of the whole) of planktonics dominated by *Hedbergellae* but including *Rotalipora cushmani*.

APPENDIX G

UPPER HEMISPHERE PROJECTIONS OF DISCONTINUITY ORIENTATION AT SELECTED LEVELS IN THE SHAFT

The upper hemisphere projections presented in Figures G.1 to G.20 represent discontinuity orientation data obtained from horizontal scanline surveys taken at selected levels in the shaft at Chinnor. The computer plotting of these data is described in Appendix C. It is worth reiterating here that the '12 o'clock' position on the projections represents the geographical north azimuth direction (000^{o} = 360^{o}) whilst the '6 o'clock' position represents geographical south = 180^{o}, counting the degrees in a clockwise rotation.

The data presented in Figures G.1 to G.20 are discussed in Chapter 3 in the context of additional data collected in the shaft and tunnel at Chinnor.

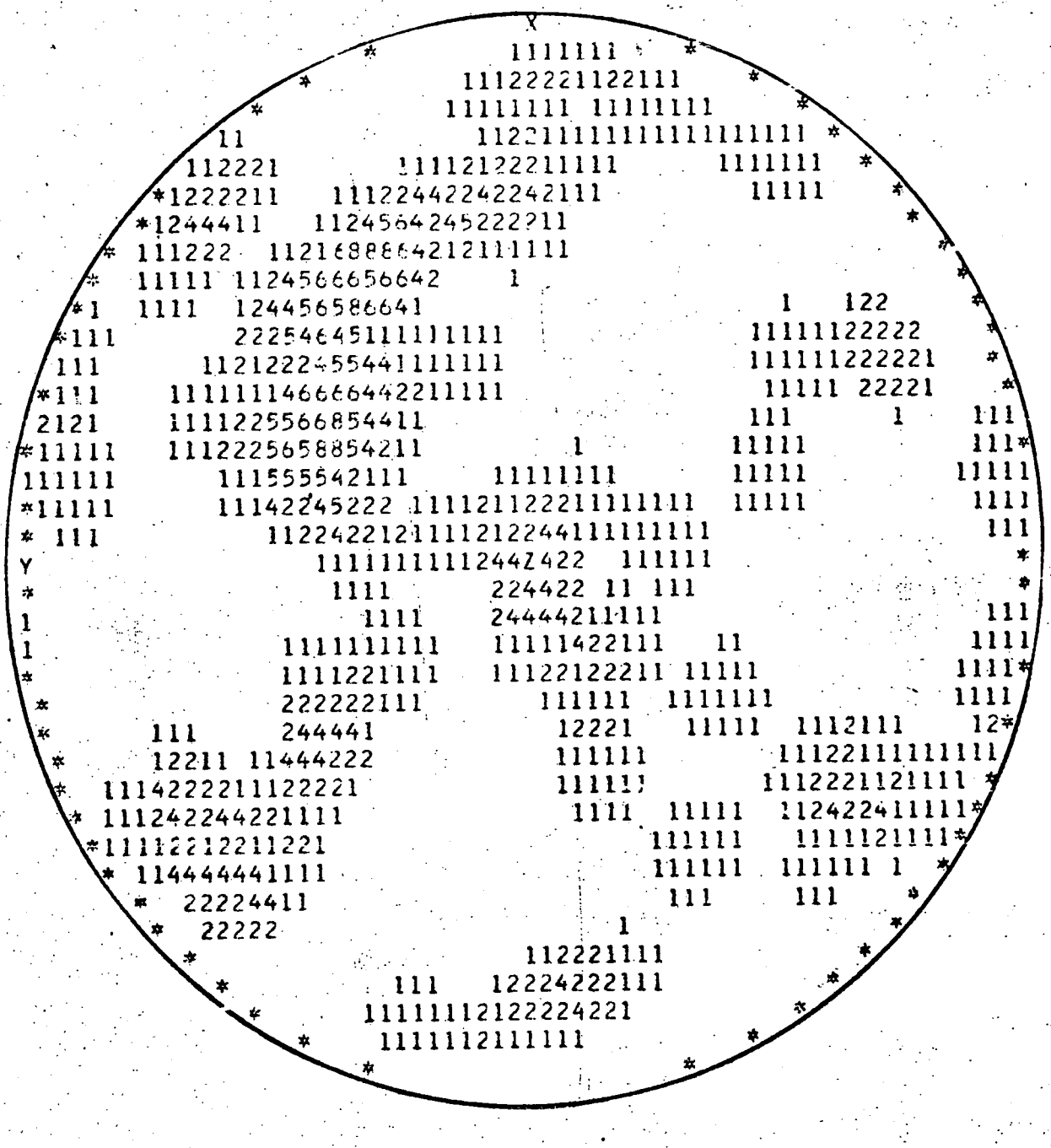

73 readings

Fig. G.1 UPPER HEMISPHERE PROJECTION OF DISCONTINUITY ORIENTATION HORIZONTAL SCANLINE IN THE SHAFT, DEPTH 1·0 m.

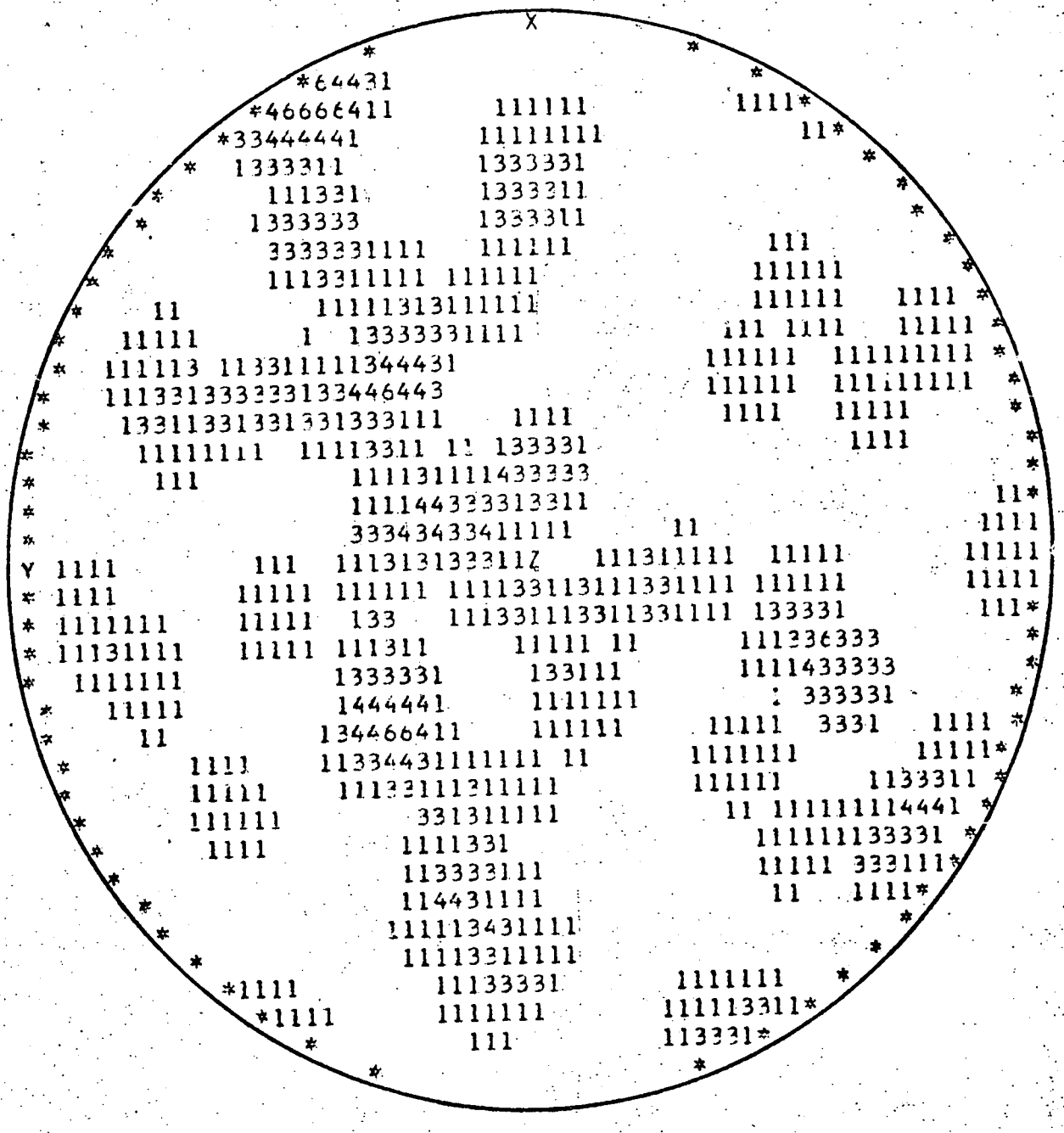

61 readings

Fig. G.2 UPPER HEMISPHERE PROJECTION OF DISCONTINUITY ORIENTATION, HORIZONTAL SCANLINE IN THE SHAFT DEPTH 1·7m.

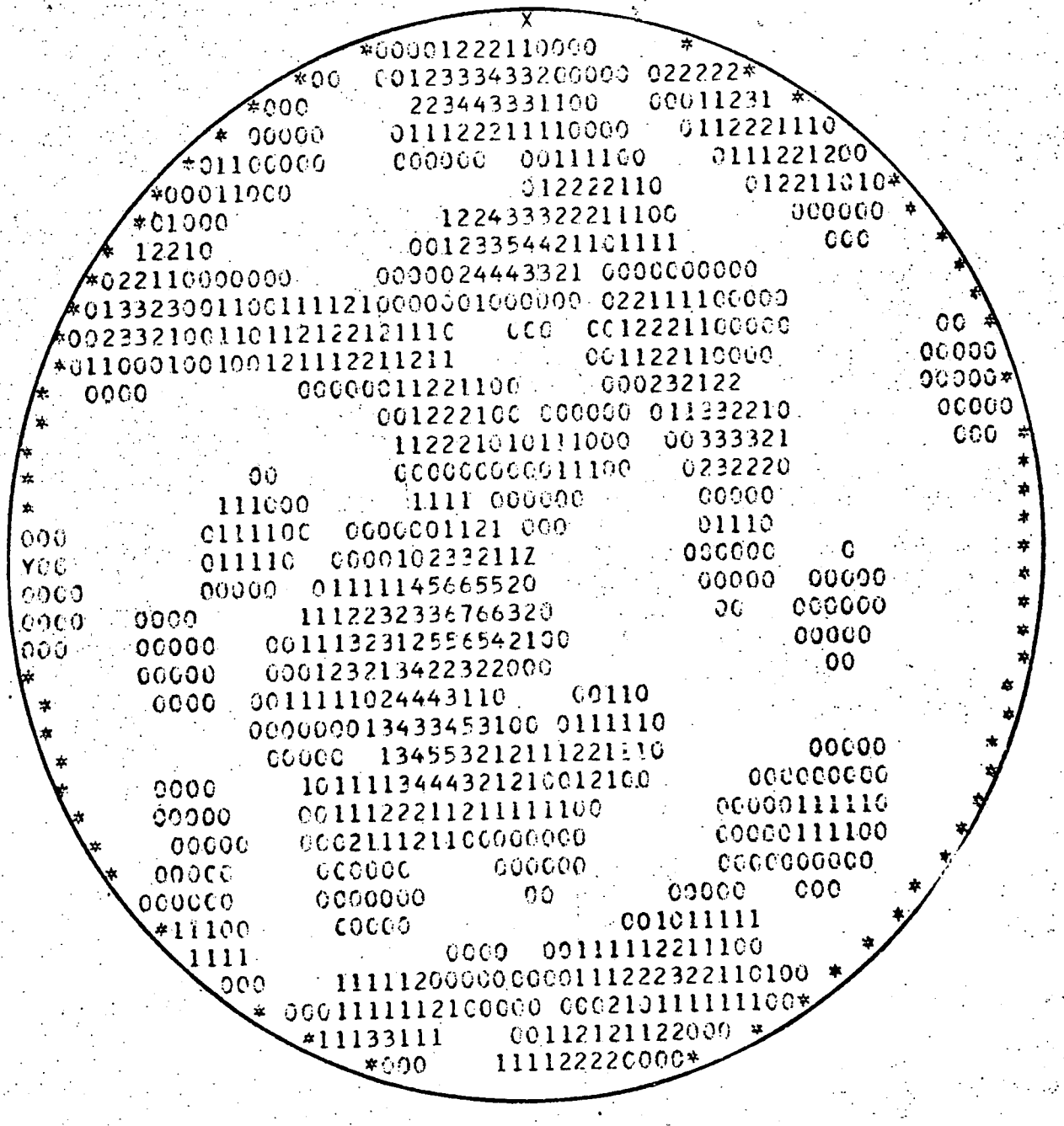

105 readings

Fig. G.3 UPPER HEMISPHERE PROJECTION OF DISCONTINUITY ORIENTATION, HORIZONTAL SCANLINE IN THE SHAFT DEPTH 2·5m.

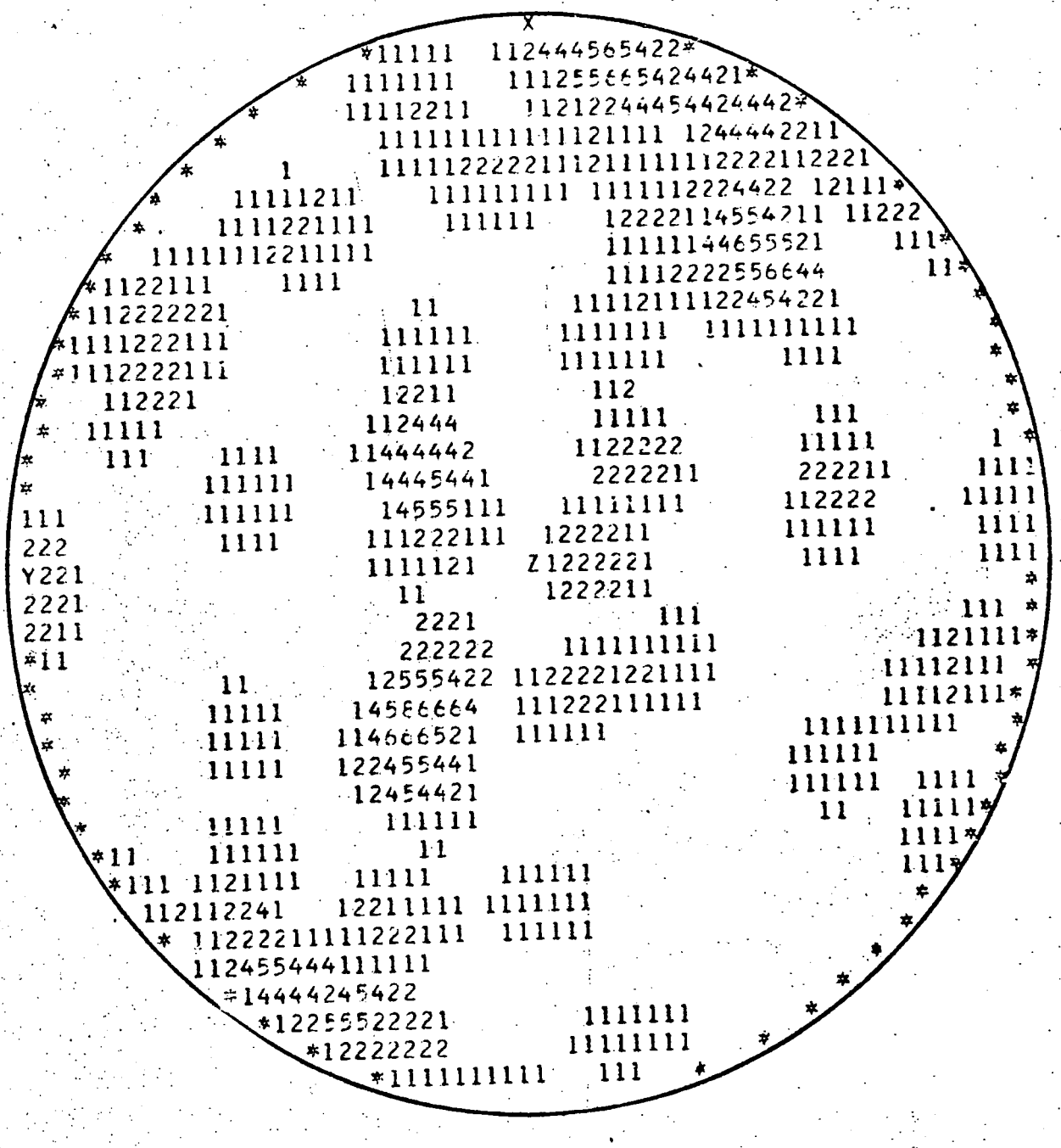

74 readings

Fig.G.4 UPPER HEMISPHERE PROJECTION OF DISCONTINUITY ORIENTATION, HORIZONTAL SCANLINE IN THE SHAFT DEPTH 3·8m.

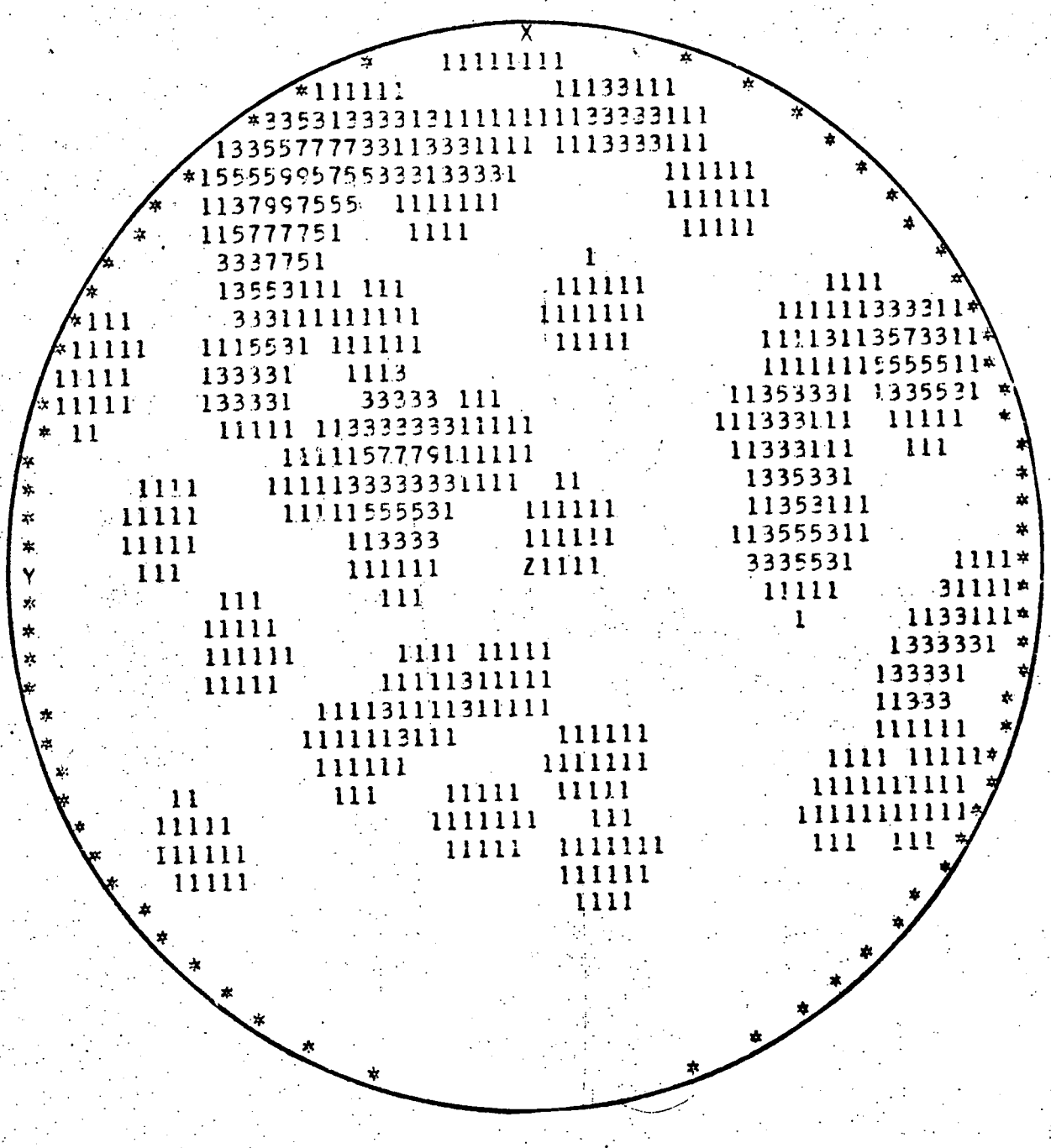

54 readings

Fig. G.5 UPPER HEMISPHERE PROJECTION OF DISCONTINUITY ORIENTATION, HORIZONTAL SCANLINE IN THE SHAFT DEPTH 5·1 m.

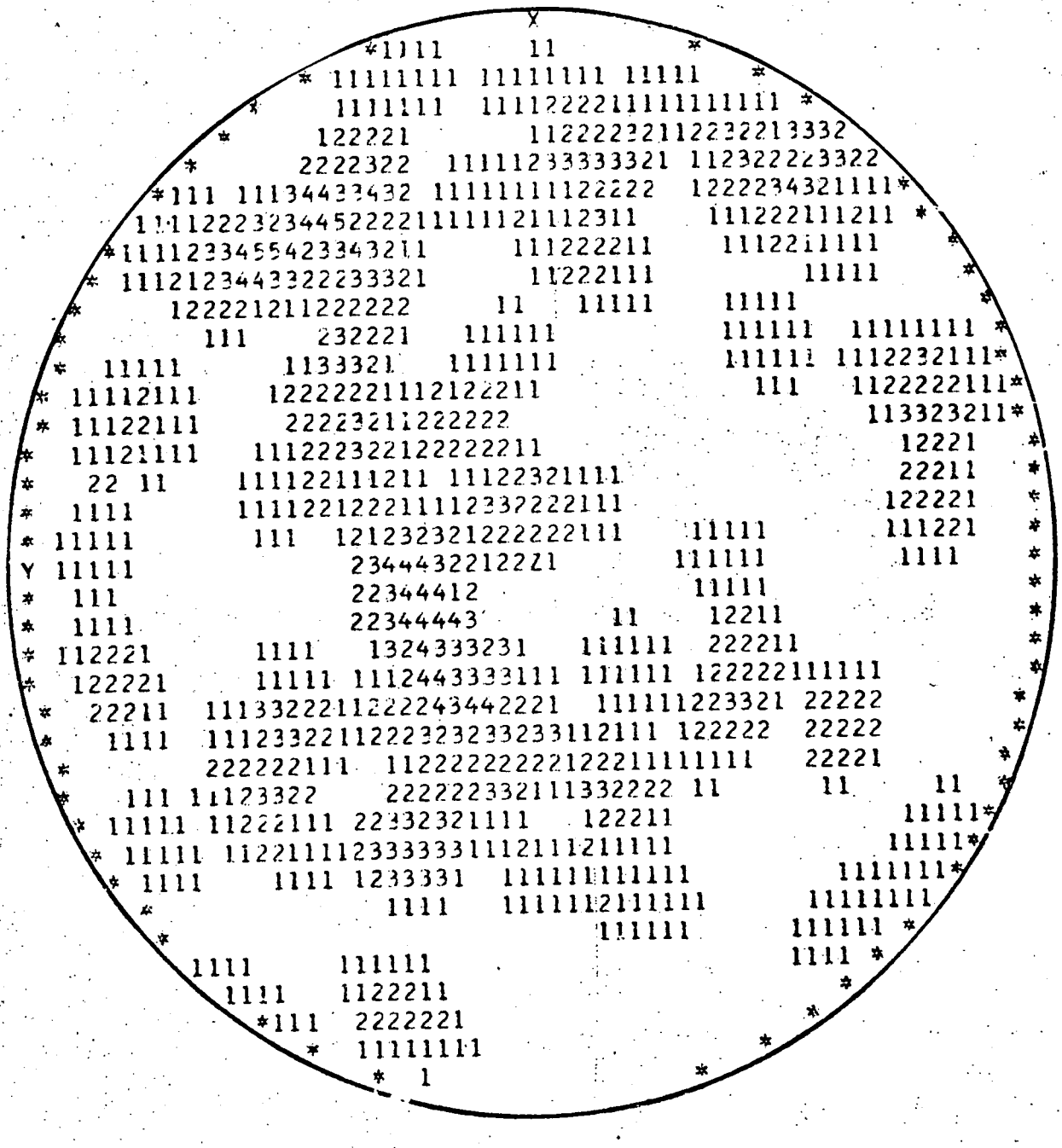

87 readings

Fig. G.6 UPPER HEMISPHERE PROJECTION OF DISCONTINUITY ORIENTATION, HORIZONTAL SCANLINE IN THE SHAFT DEPTH 6·4 m.

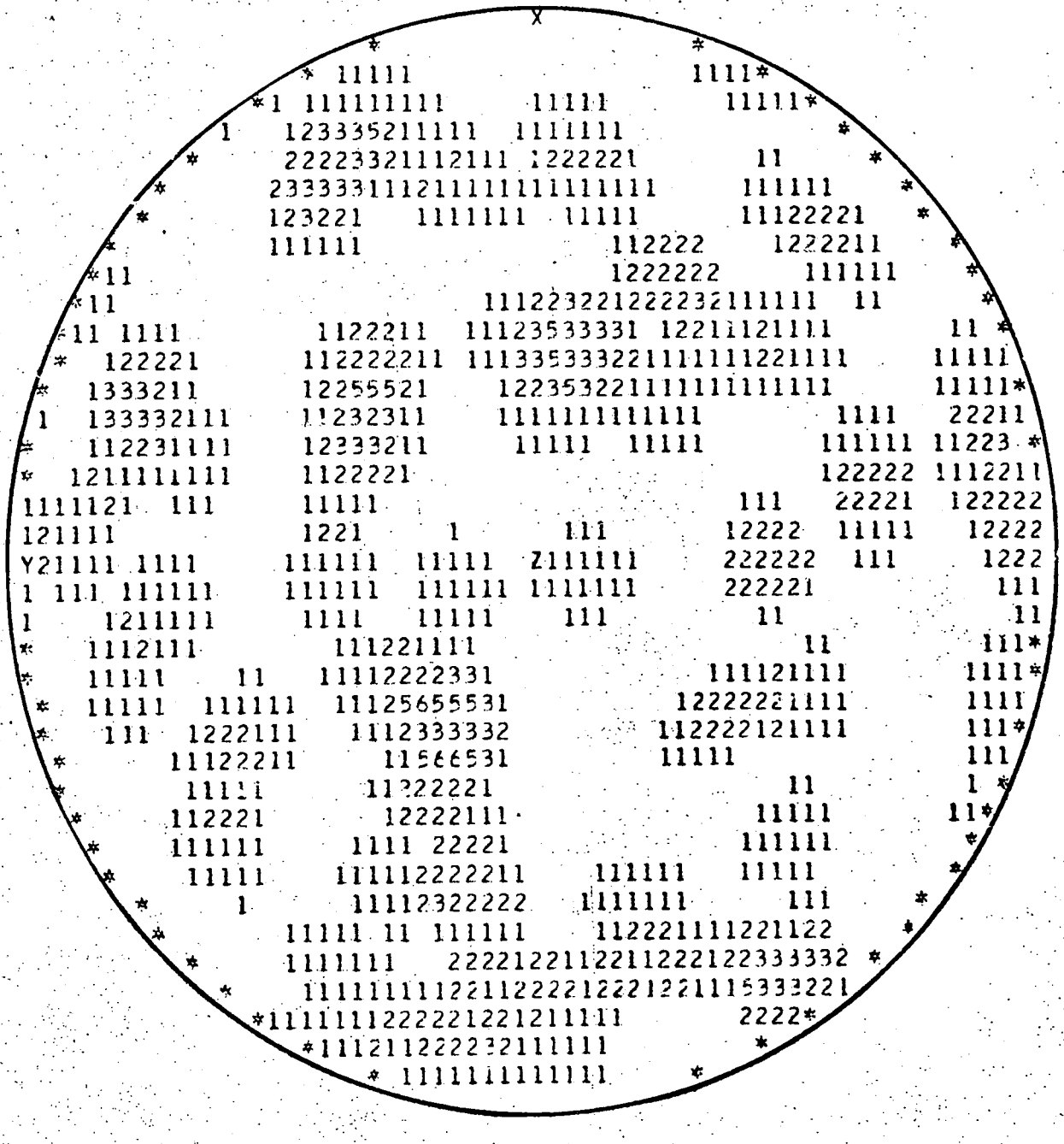

75 readings

Fig. G.7 UPPER HEMISPHERE PROJECTION OF DISCONTINUITY ORIENTATION, HORIZONTAL SCANLINE IN THE SHAFT DEPTH 7·4 m.

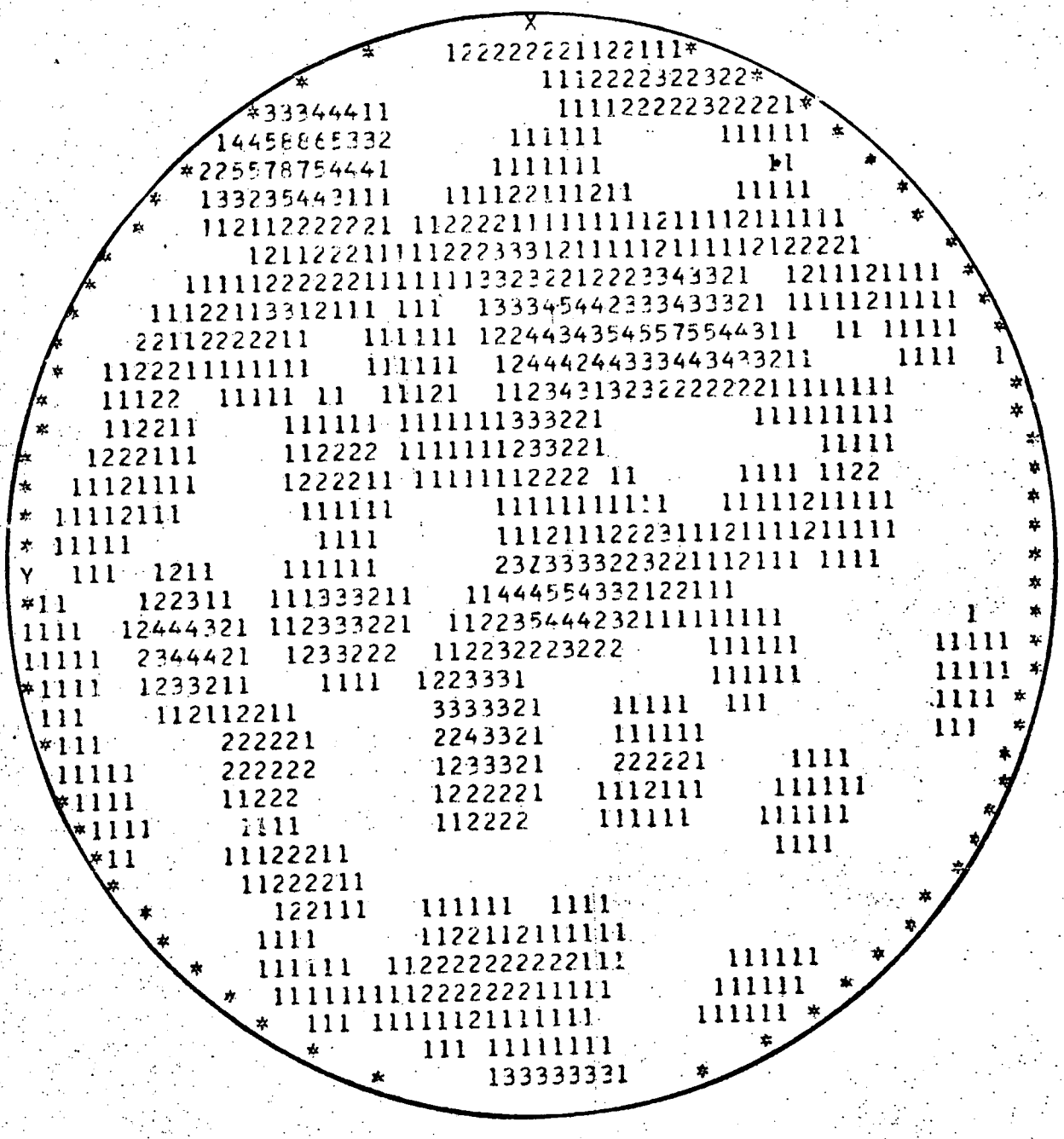

95 readings

Fig.G.8 UPPER HEMISPHERE PROJECTION OF DISCONTINUITY ORIENTATION, HORIZONTAL SCANLINE IN THE SHAFT DEPTH 8·4 m.

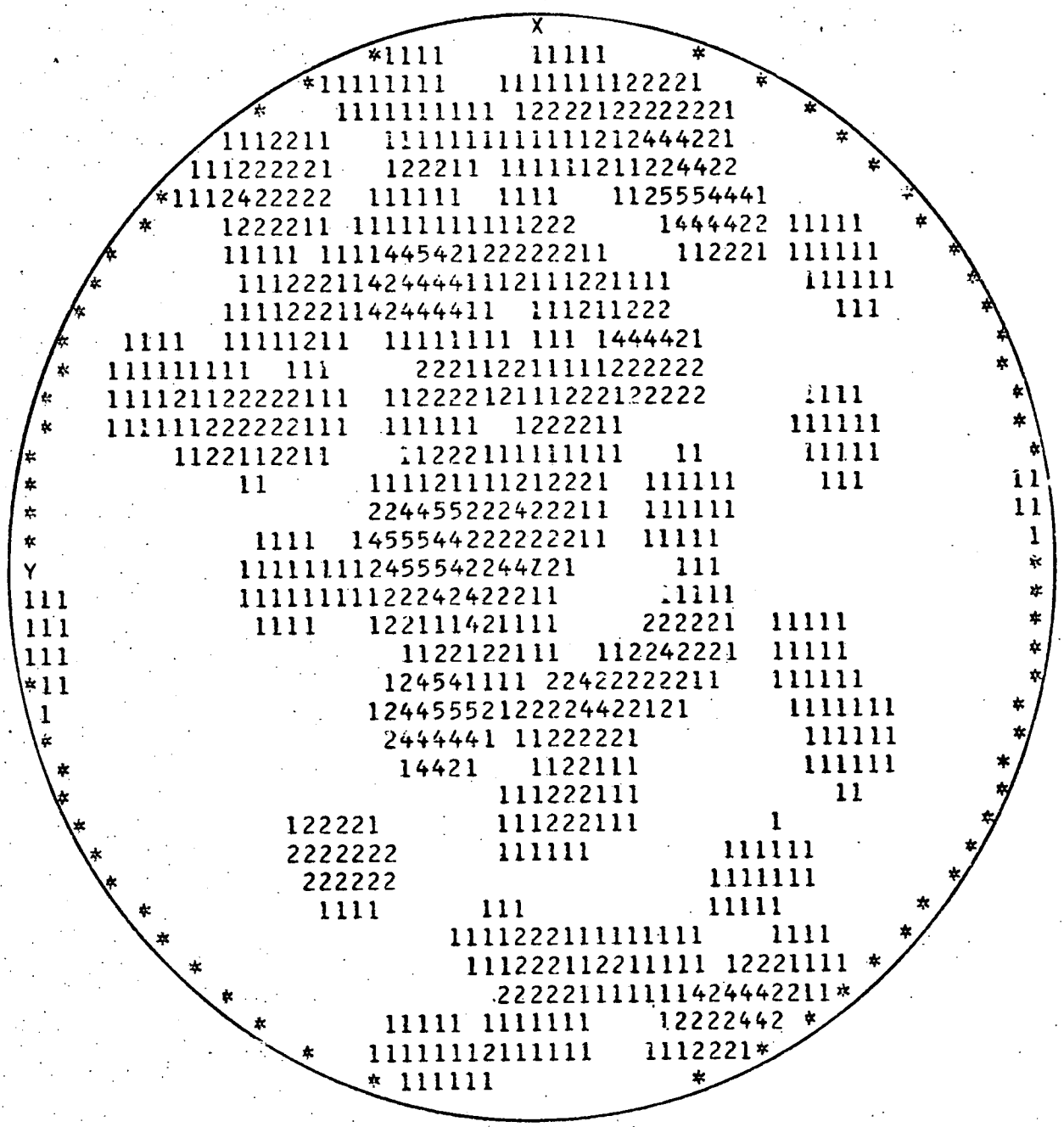

71 readings

Fig.G.9 UPPER HEMISPHERE PROJECTION OF DISCONTINUITY ORIENTATION, HORIZONTAL SCANLINE IN THE SHAFT DEPTH 9·5 m.

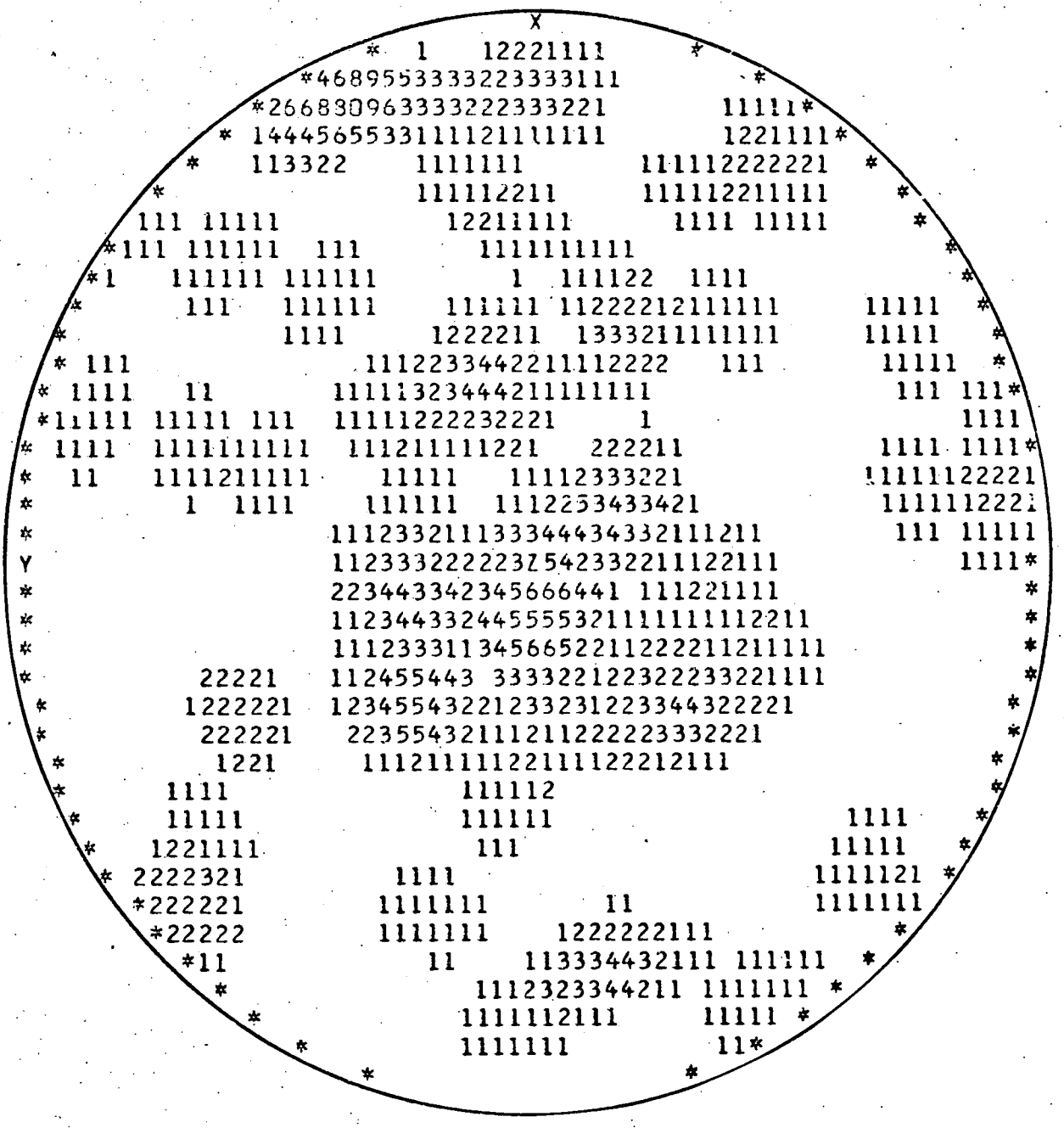

86 readings

Fig.G.10 UPPER HEMISPHERE PROJECTION OF DISCONTINUITY ORIENTATION, HORIZONTAL SCANLINE IN THE SHAFT DEPTH 10·2 m.

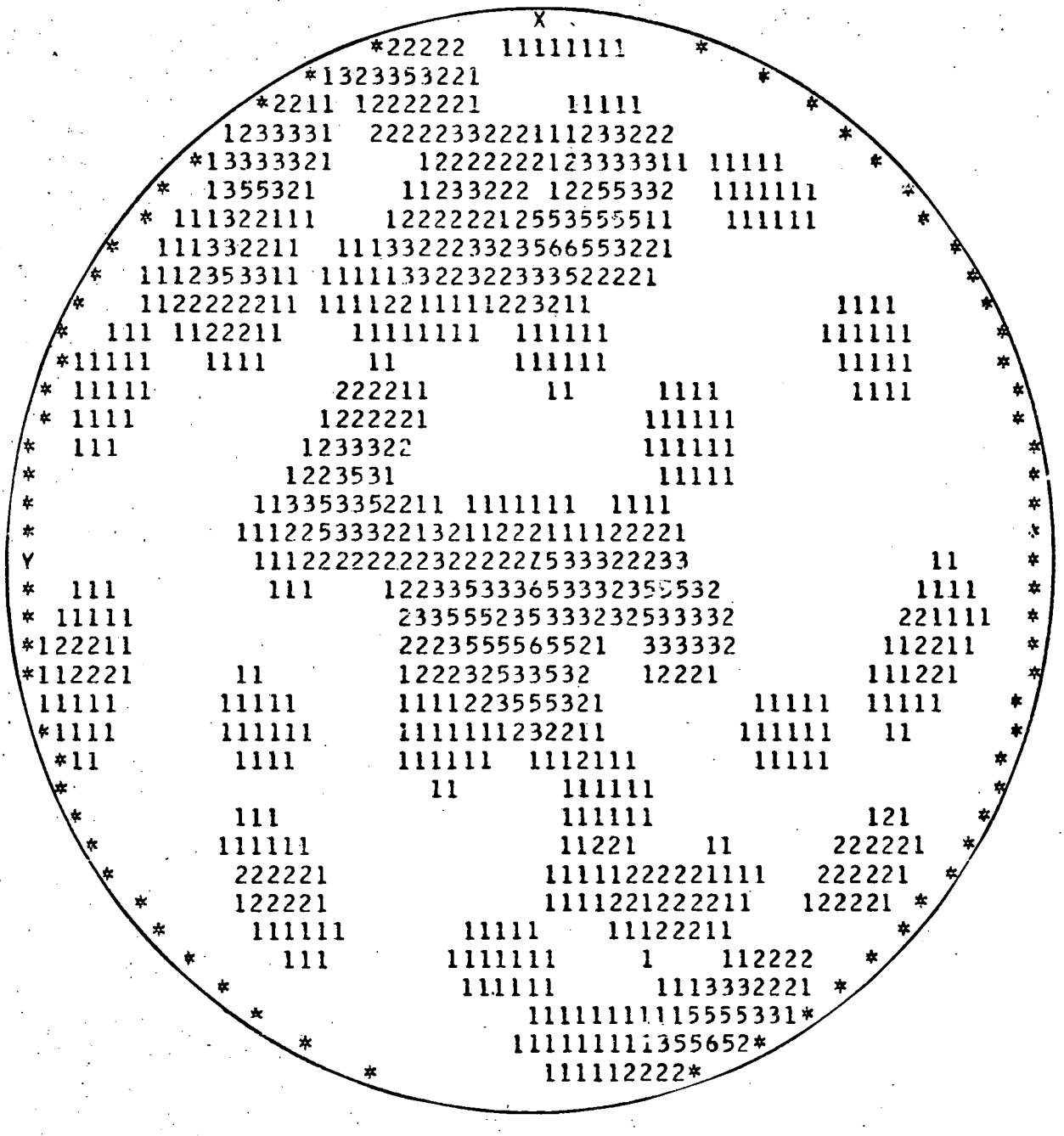

78 readings

Fig. G.11 UPPER HEMISPHERE PROJECTION OF DISCONTINUITY ORIENTATION, HORIZONTAL SCANLINE IN THE SHAFT, DEPTH 11·2 m .

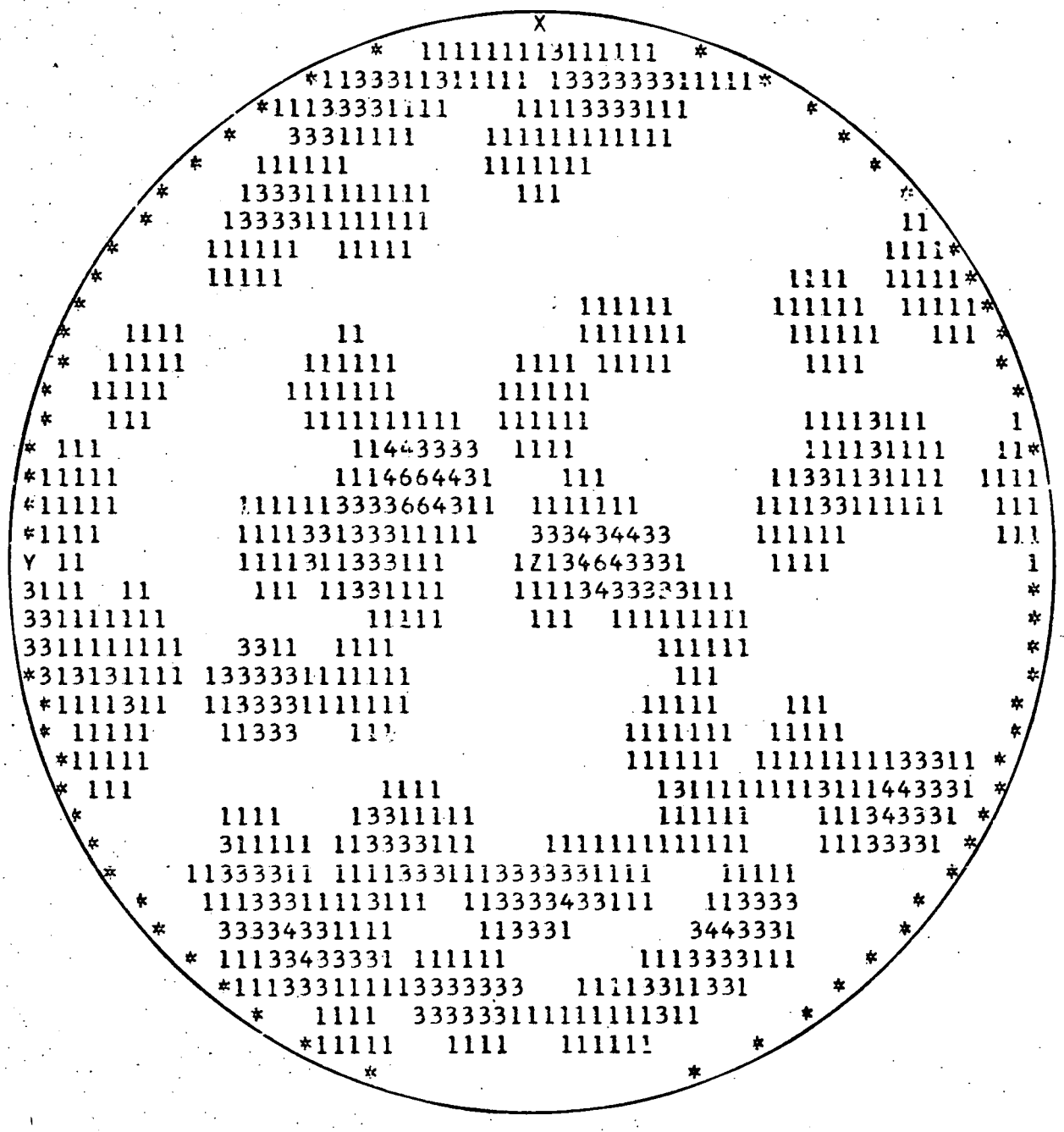

61 readings

Fig. G.12 UPPER HEMISPHERE PROJECTION OF DISCONTINUITY ORIENTATION, HORIZONTAL SCANLINE IN THE SHAFT, DEPTH 12·4m.

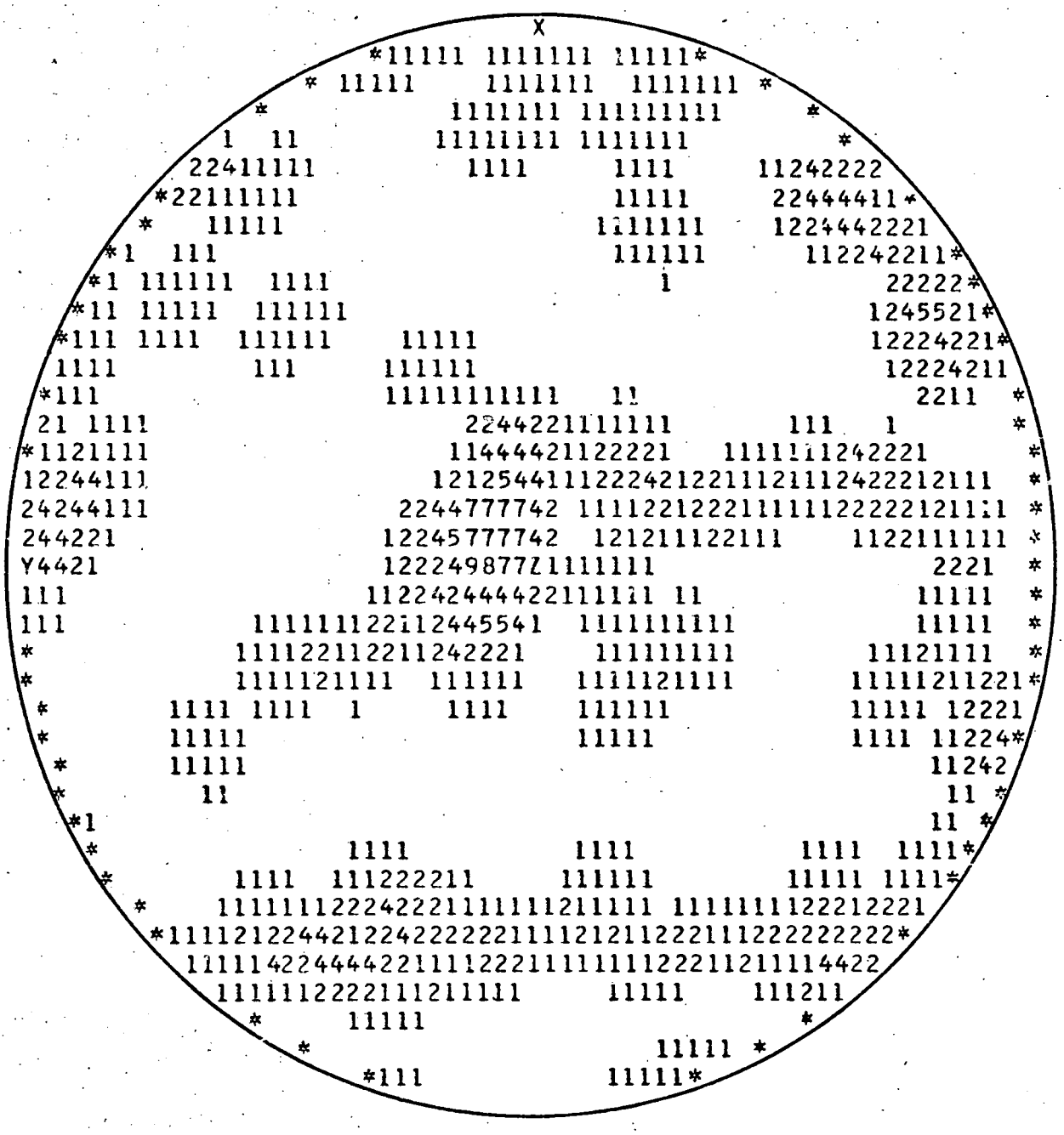

70 readings

Fig. G.13 UPPER HEMISPHERE PROJECTION OF DISCONTINUITY ORIENTATION, HORIZONTAL SCANLINE IN THE SHAFT, DEPTH 13·6m.

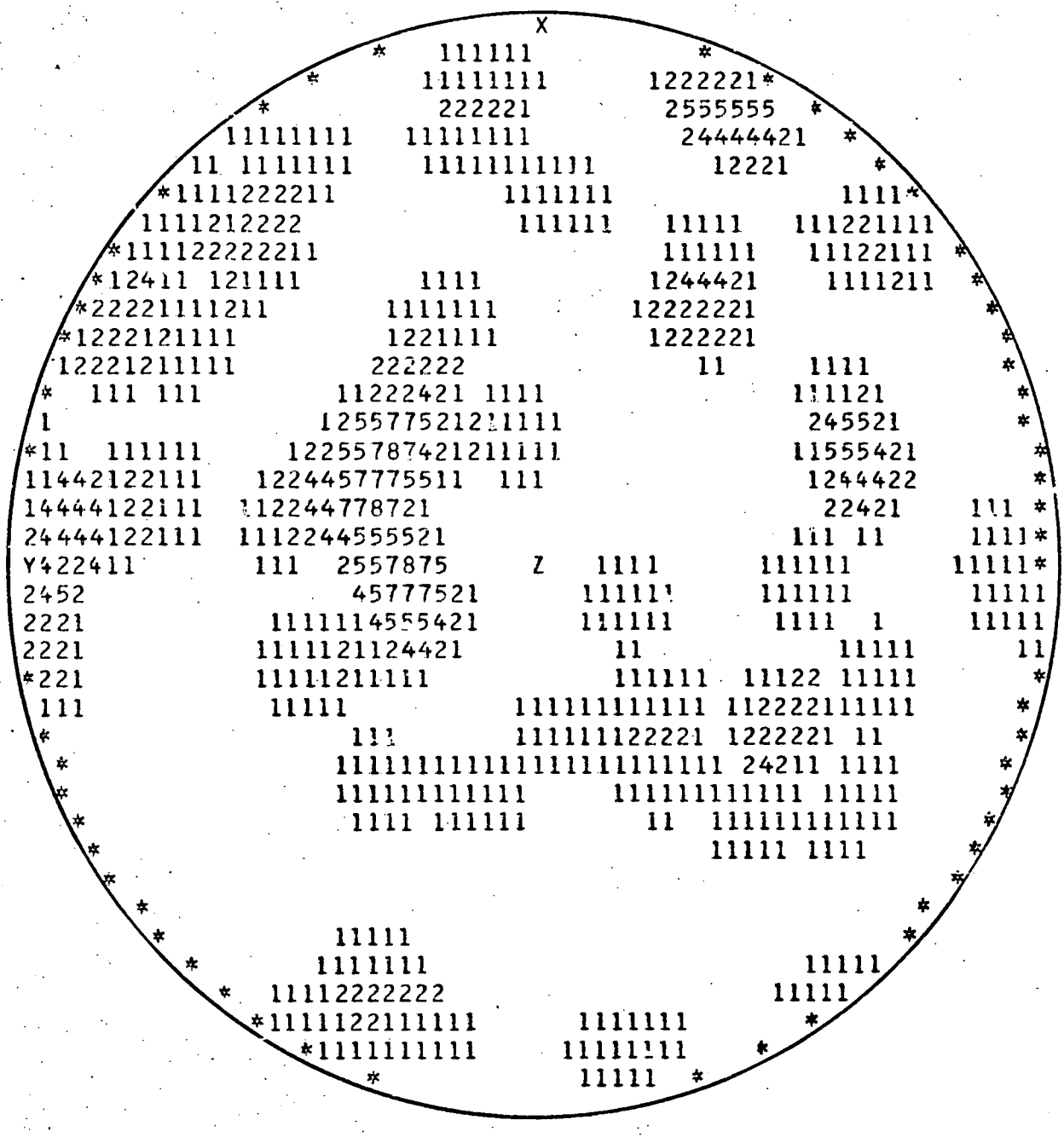

67 readings

Fig. G.14 UPPER HEMISPHERE PROJECTION OF DISCONTINUITY ORIENTATION, HORIZONTAL SCANLINE IN THE SHAFT, DEPTH 14·6m.

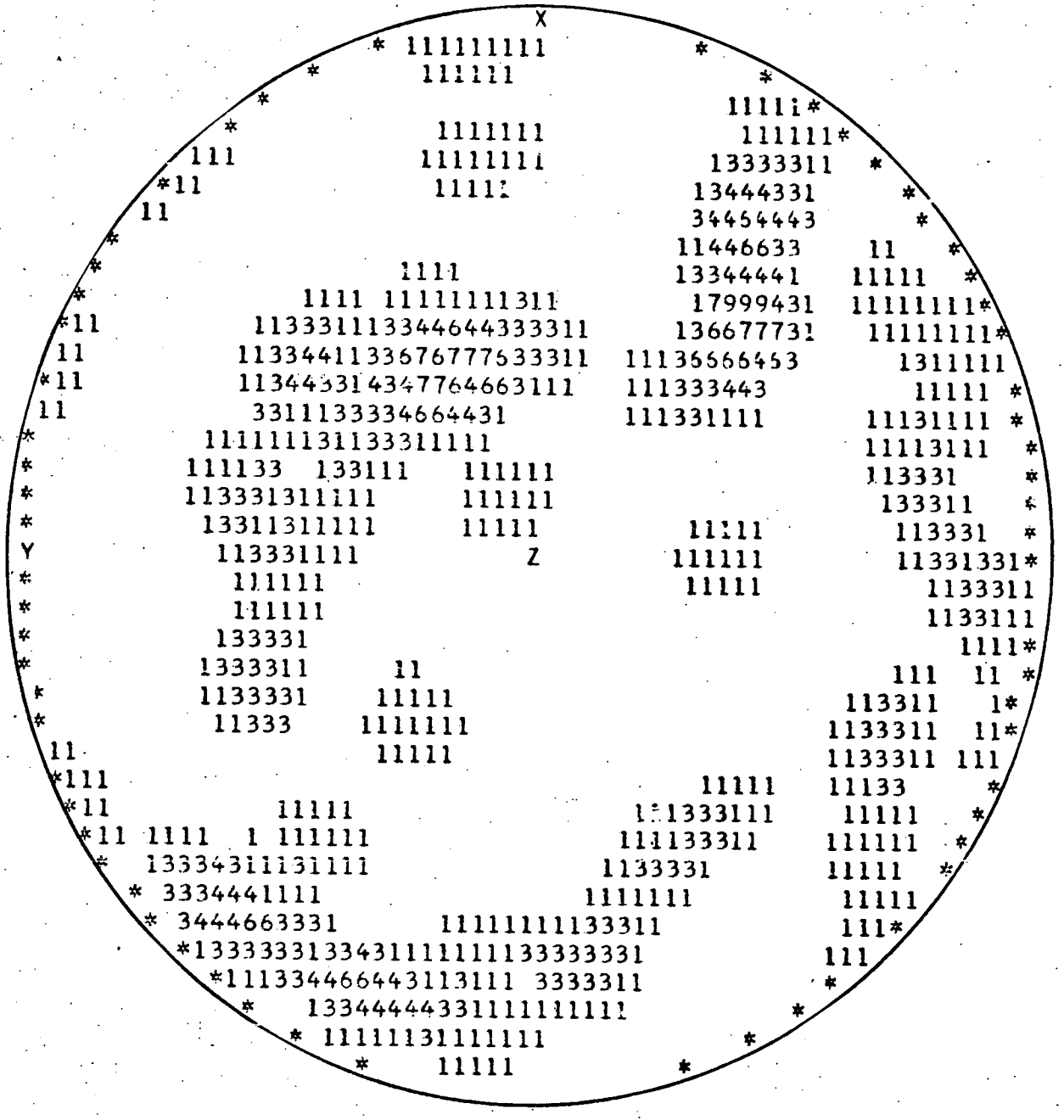

63 readings

Fig. G.15 UPPER HEMISPHERE PROJECTION OF DISCONTINUITY ORIENTATION, HORIZONTAL SCANLINE IN THE SHAFT, DEPTH 15·7m.

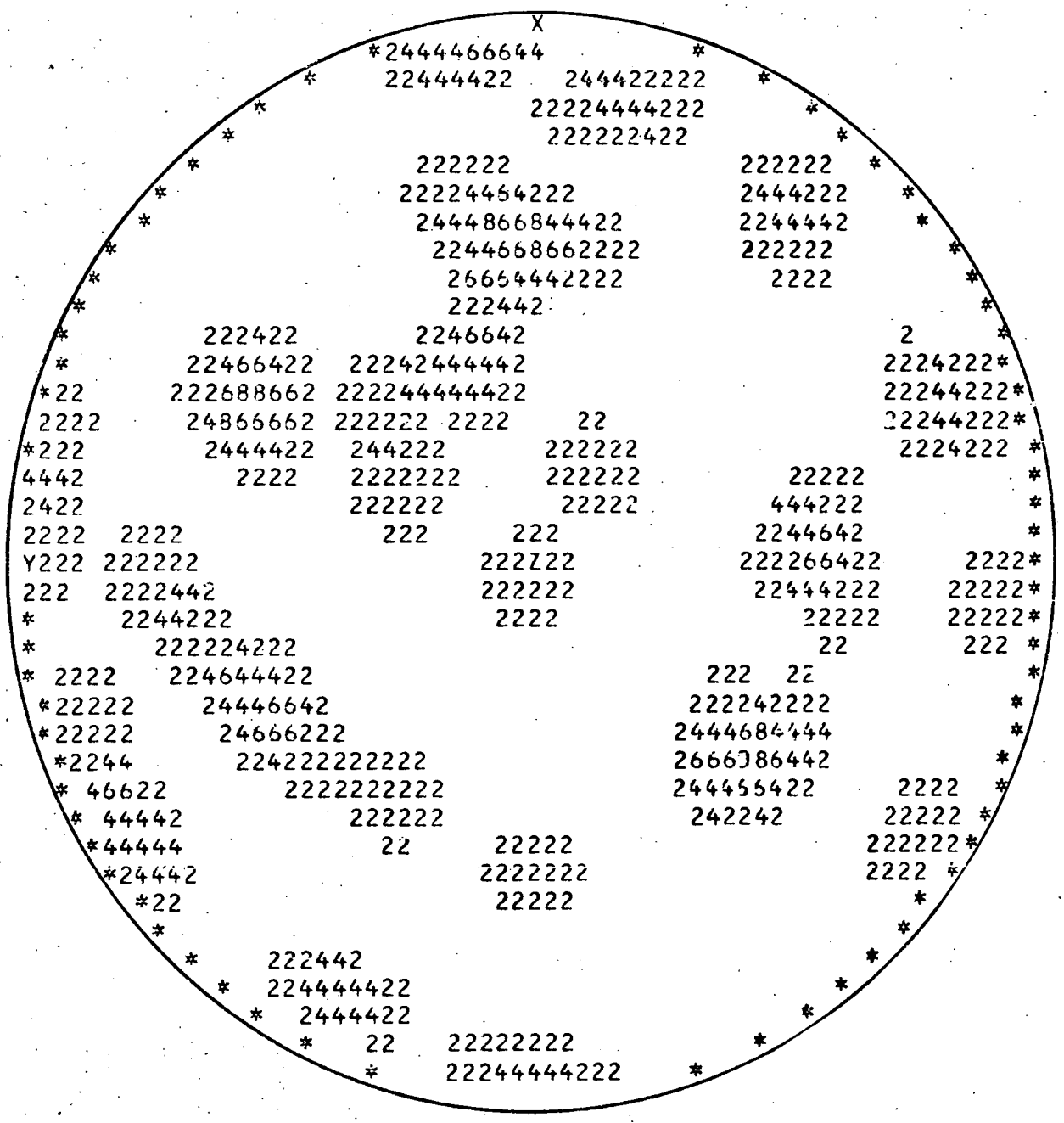

Fig.G.16 UPPER HEMISPHERE PROJECTION OF DISCONTINUITY ORIENTATION, HORIZONTAL SCANLINE IN THE SHAFT, DEPTH 16·9 m.

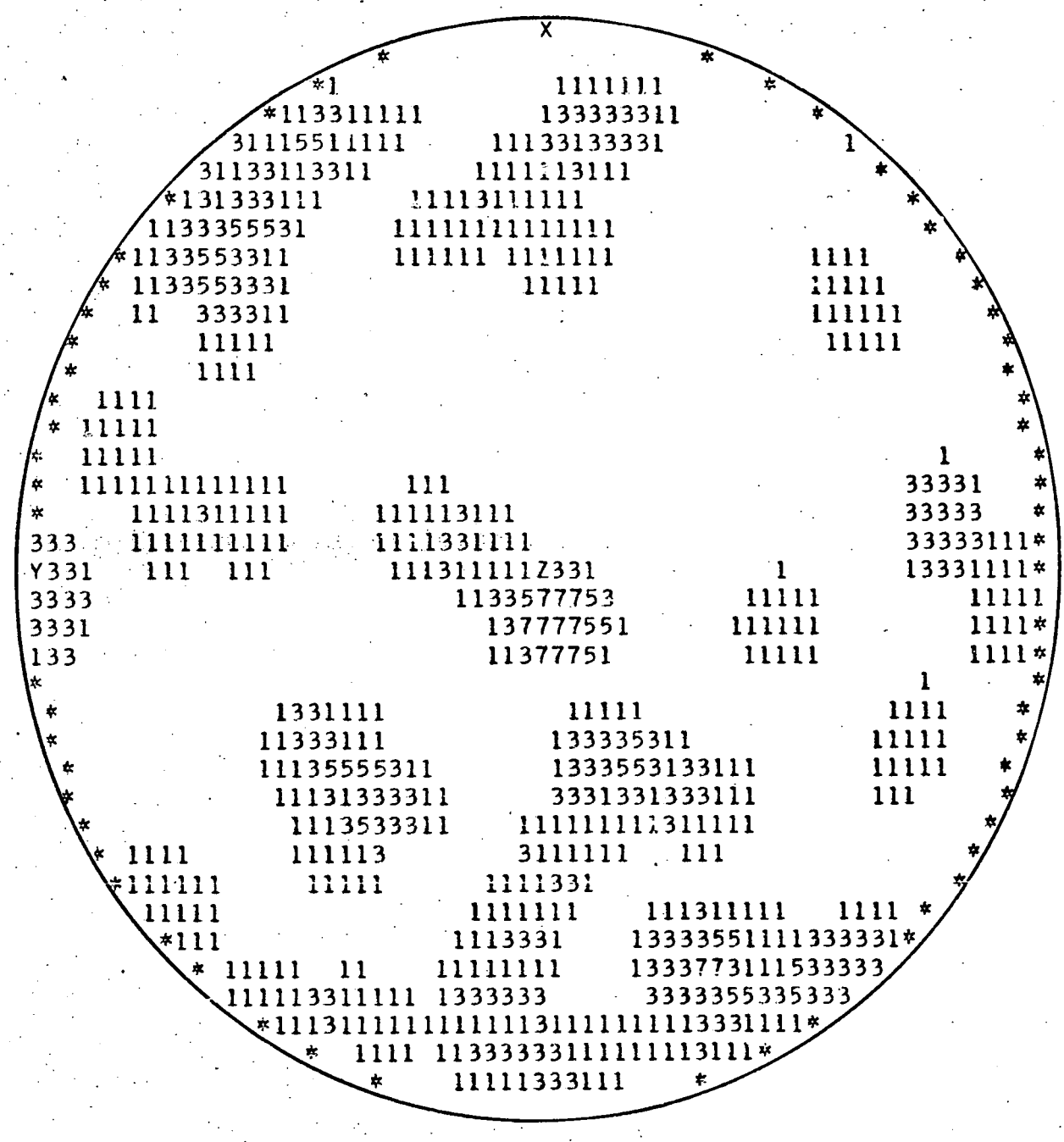

54 readings

Fig. G.17 UPPER HEMISPHERE PROJECTION OF DISCONTINUITY ORIENTATION, HORIZONTAL SCANLINE IN THE SHAFT, DEPTH 17·9m.

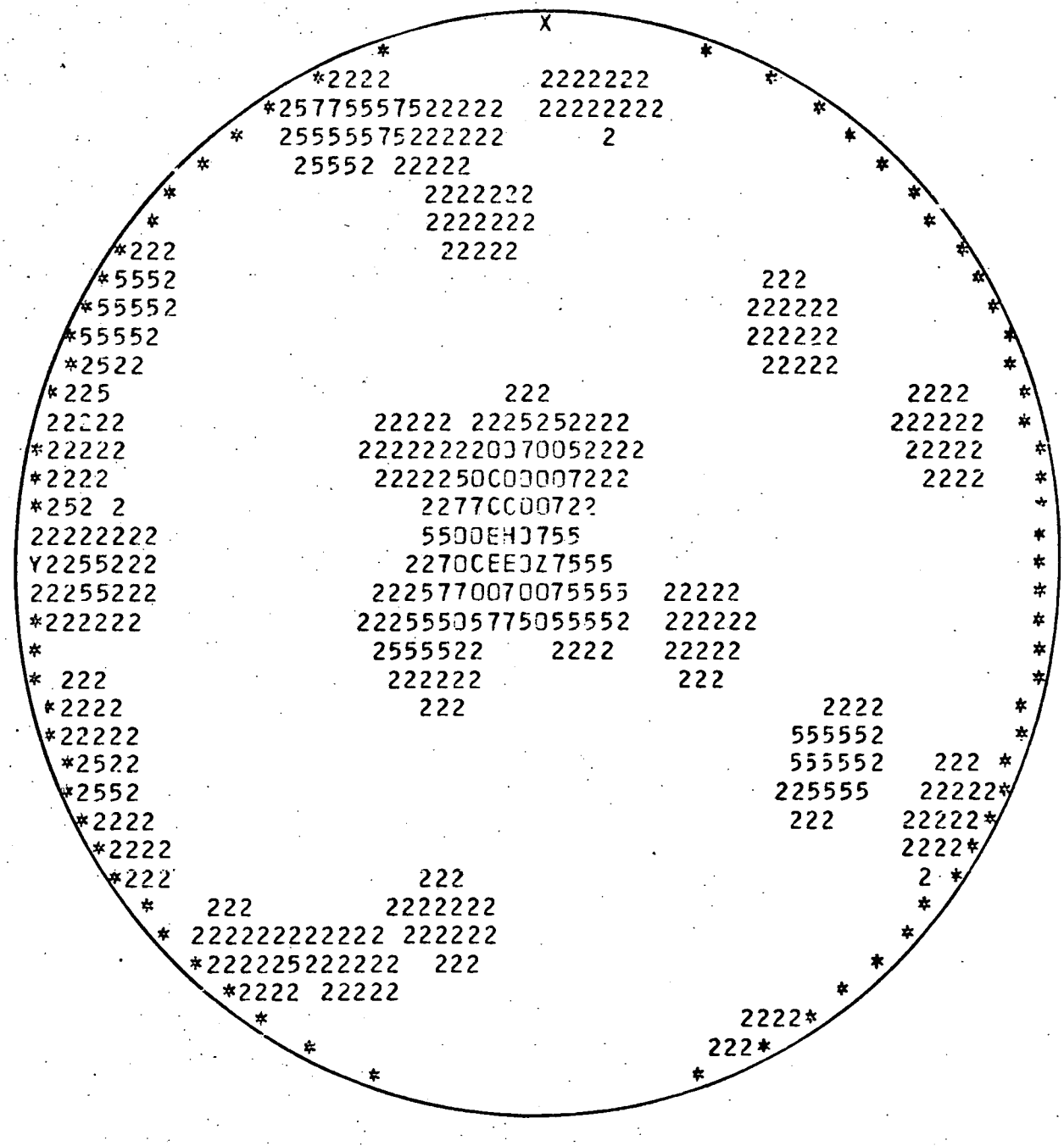

38 readings

Fig.G.18 UPPER HEMISPHERE PROJECTION OF DISCONTINUITY ORIENTATION, HORIZONTAL SCANLINE IN THE SHAFT, DEPTH 19·0m.

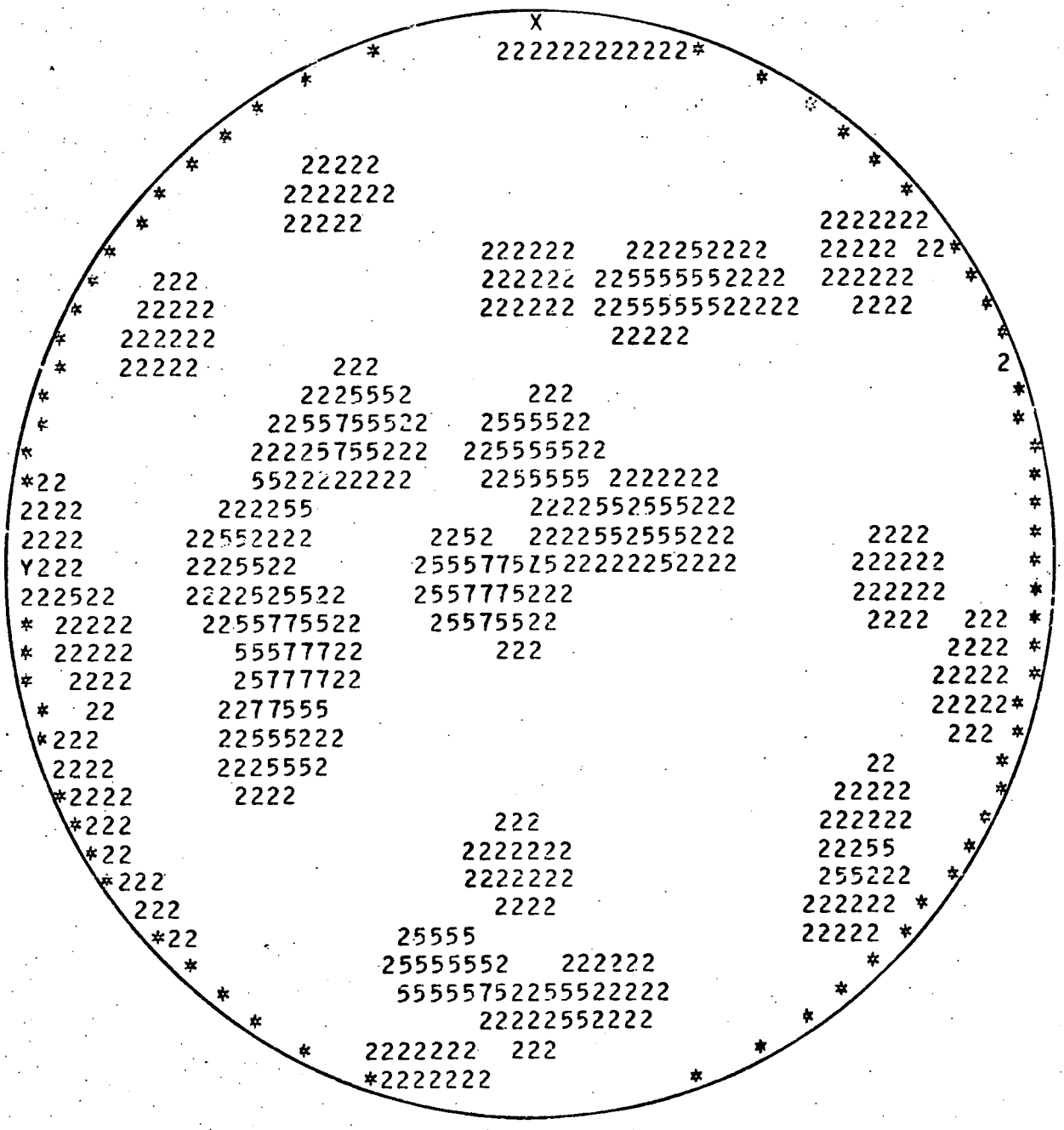

40 readings

Fig. G.19 UPPER HEMISPHERE PROJECTION OF DISCONTINUITY ORIENTATION, HORIZONTAL SCANLINE IN THE SHAFT, DEPTH 20·1m.

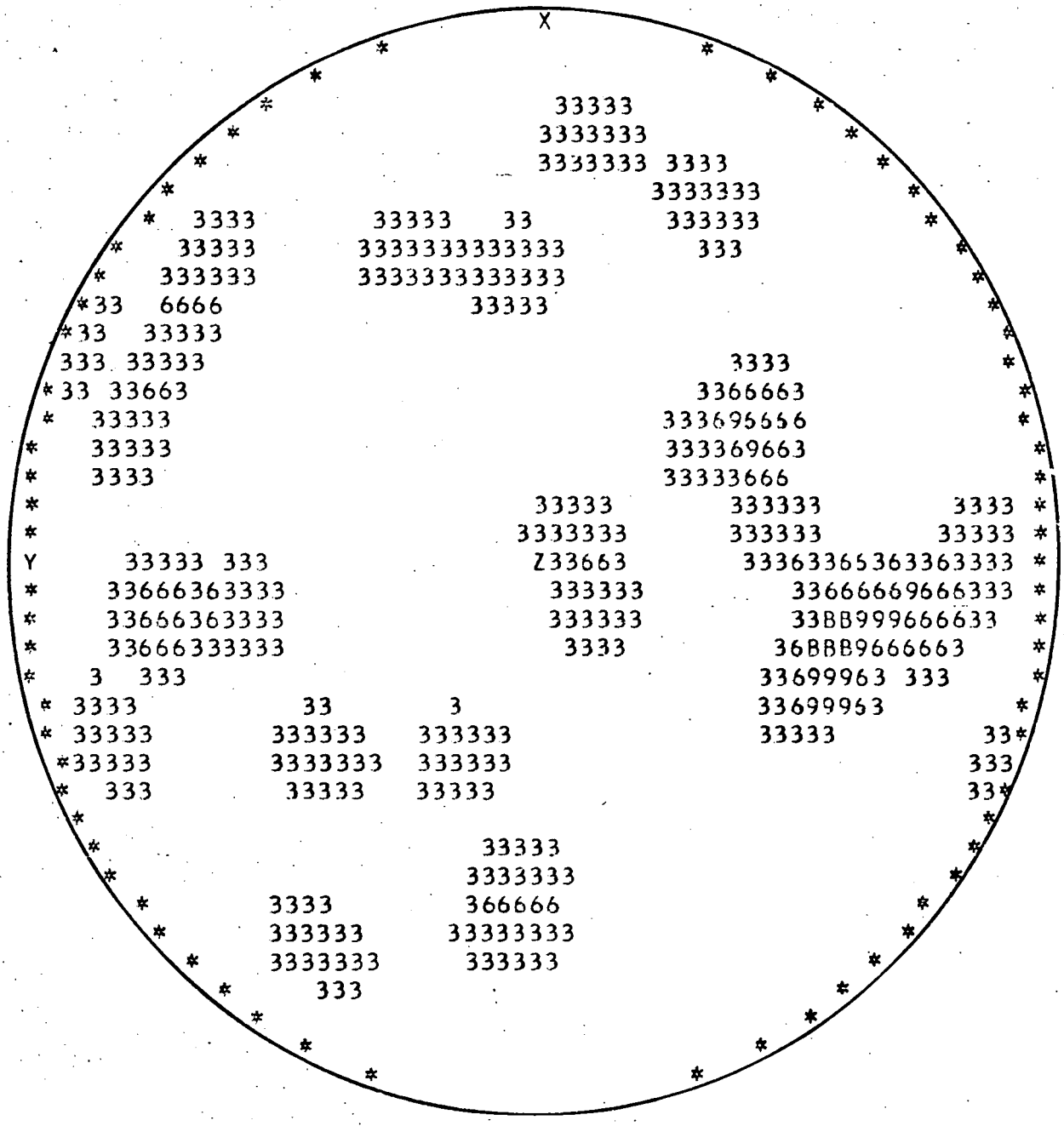

Fig. G.20 UPPER HEMISPHERE PROJECTION OF DISCONTINUITY ORIENTATION, HORIZONTAL SCANLINE IN THE SHAFT, DEPTH 21·2m.

APPENDIX H

DISCONTINUITY SPACING AND ORIENTATION DATA FROM SELECTED FACES IN THE FIRST 85m OF TUNNEL

Figures H.1 to H.17 are discontinuity spacing histograms constructed from data obtained from scanline surveys at seventeen separate tunnel faces at Chinnor. Each histogram contains a fitted negative exponential probability density distribution together with additional statistical data relating to the scanline surveys.

Figures H.18 to H.31 contain discontinuity orientation data obtained from scanline surveys at selected faces in the Chinnor tunnel. The computer plotting of these data is described in Appendix C. It is worth reiterating here that the '12 o'clock' position on the projections represents the tunnel drive direction (geographical azimuth 010^{o}) whilst the '6 o'clock' position, counting the angles in clockwise rotation, represents the reverse drive direction (geographical azimuth 190^{o}).

The data presented in Figures H.1 to H.31 are discussed in Chapter 5 in the context of additional data collected in the tunnel at Chinnor.

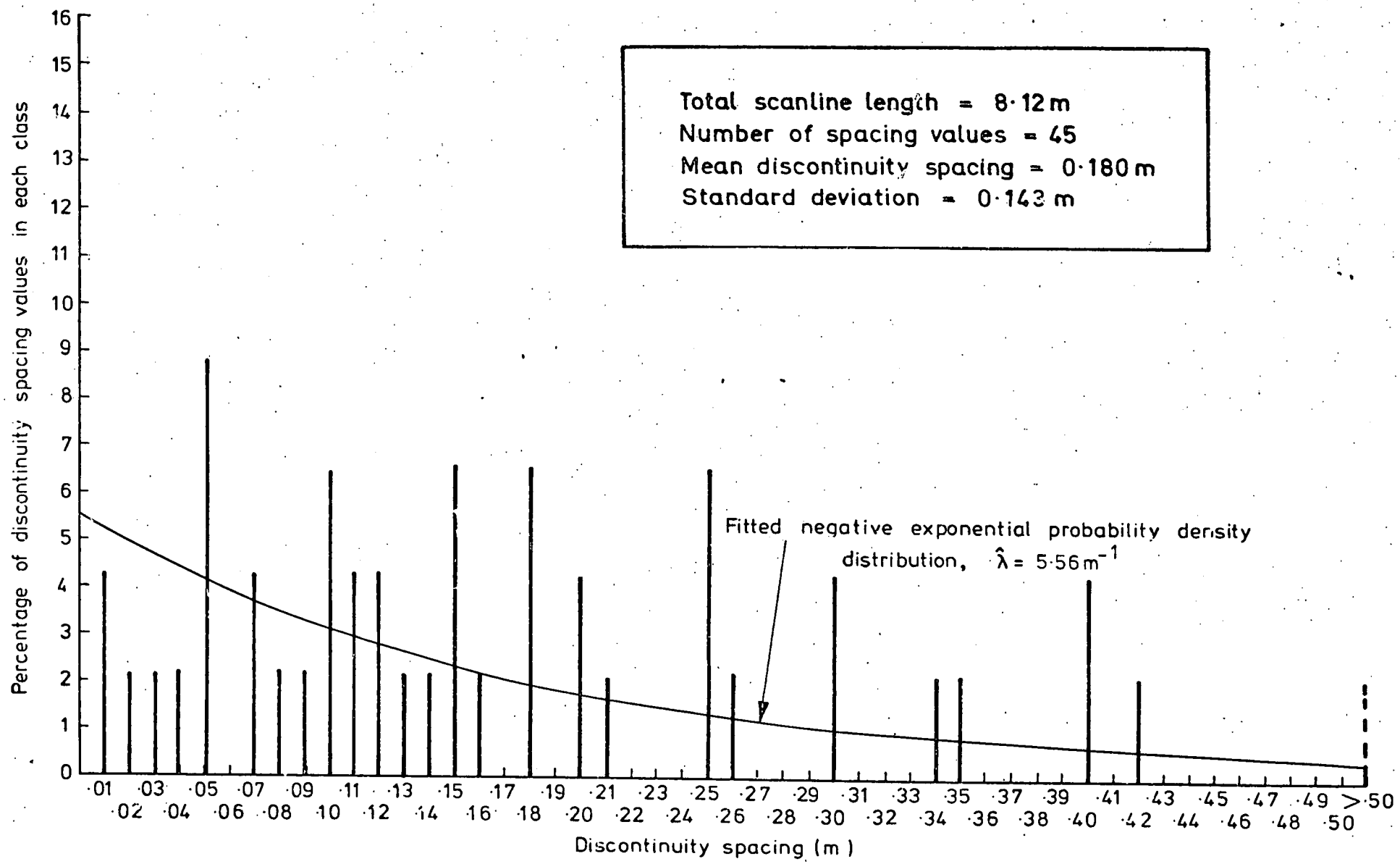

Fig. H.1 DISCONTINUITY SPACING HISTOGRAM, SCANLINES AT THE TUNNEL FACE, CHAINAGE 9·9m

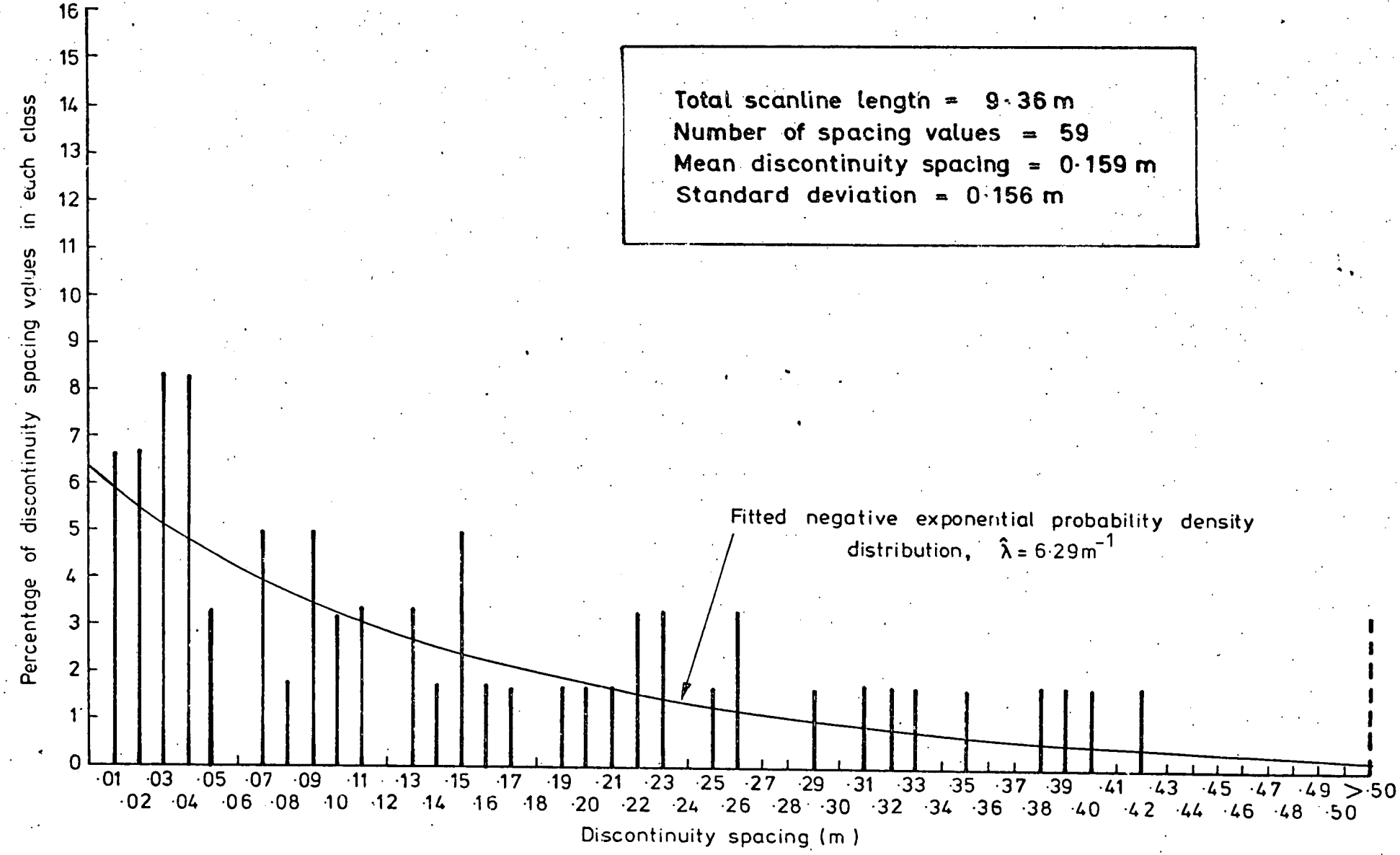

Fig.H.2 DISCONTINUITY SPACING HISTOGRAM, SCANLINES AT THE TUNNEL FACE, CHAINAGE 11·5m

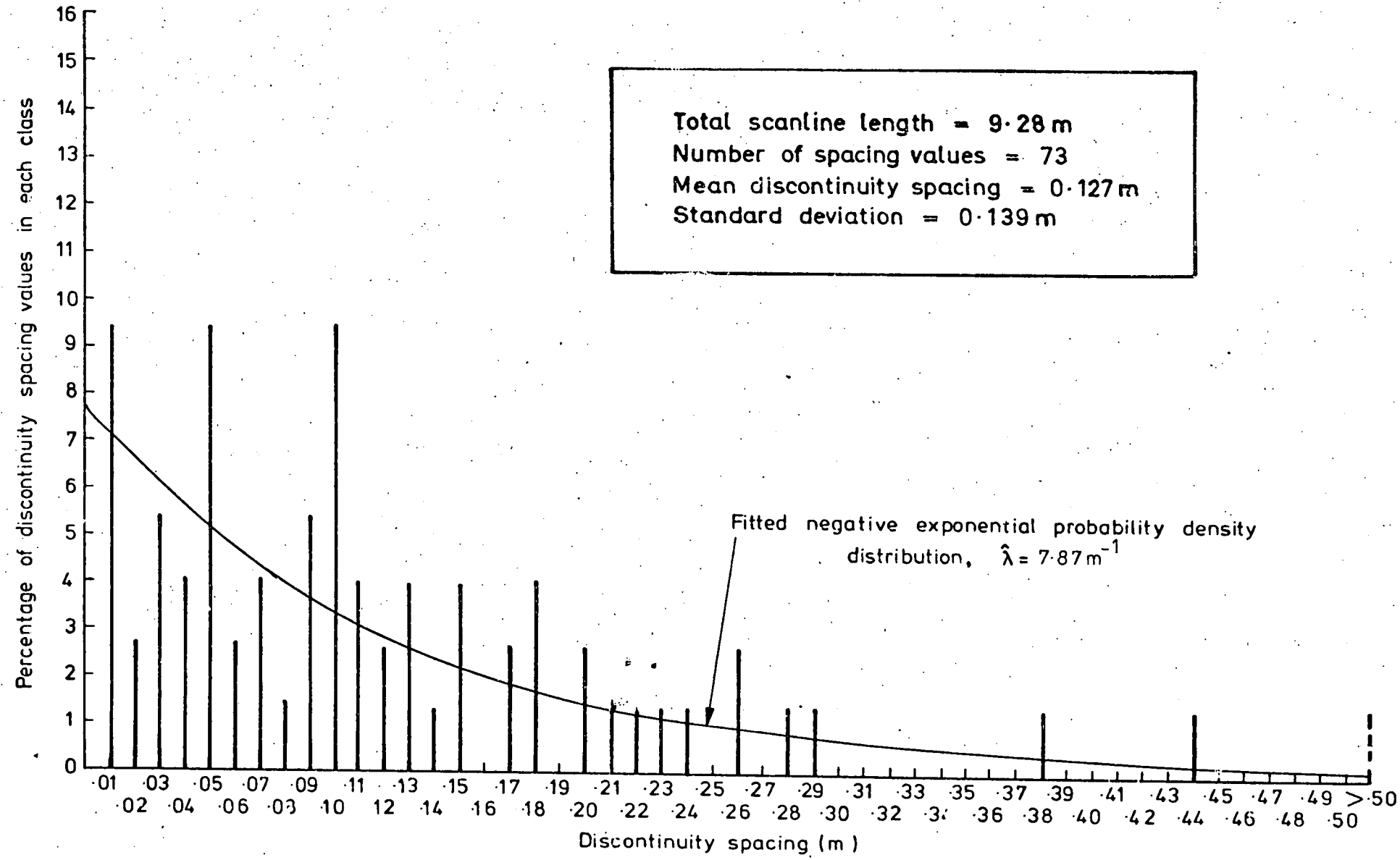

Fig. H. 3 DISCONTINUITY SPACING HISTOGRAM, SCANLINES AT THE TUNNEL FACE, CHAINAGE 12·1m

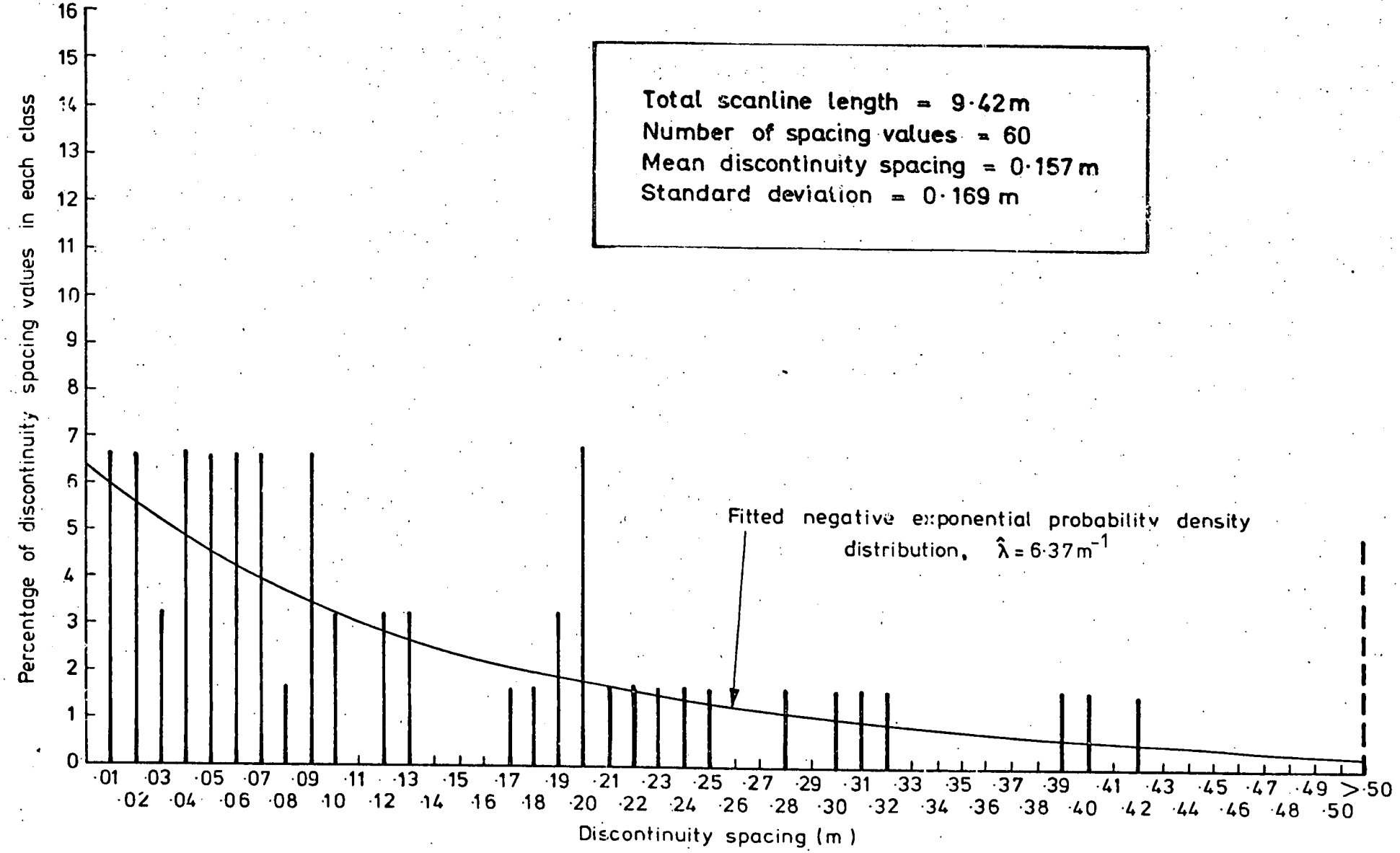

Fig.H.4 DISCONTINUITY SPACING HISTOGRAM, SCANLINES AT THE TUNNEL FACE, CHAINAGE 14·0m

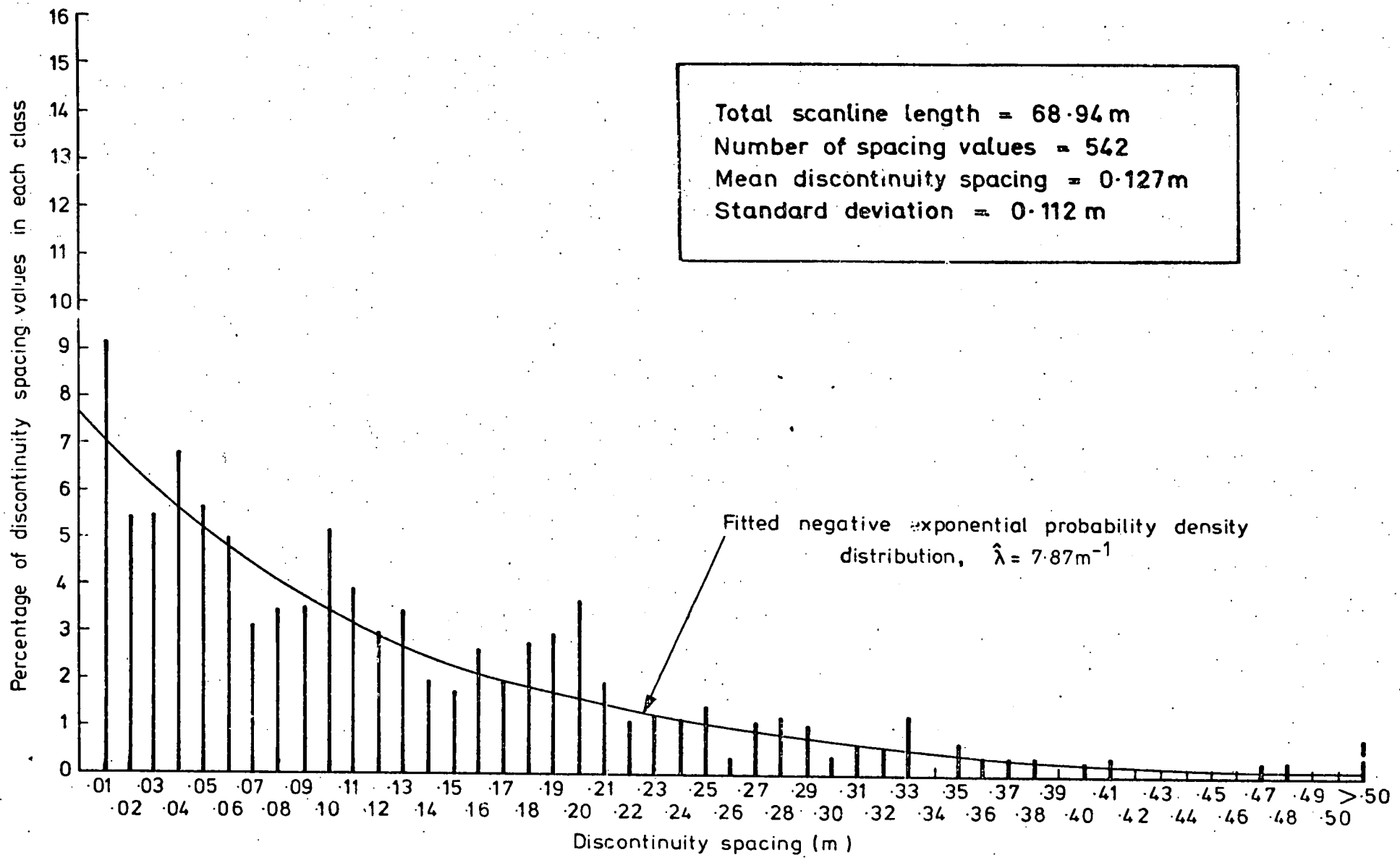

Fig. H.5 DISCONTINUITY SPACING HISTOGRAM, SCANLINES AT THE TUNNEL FACE, CHAINAGE 18·1m

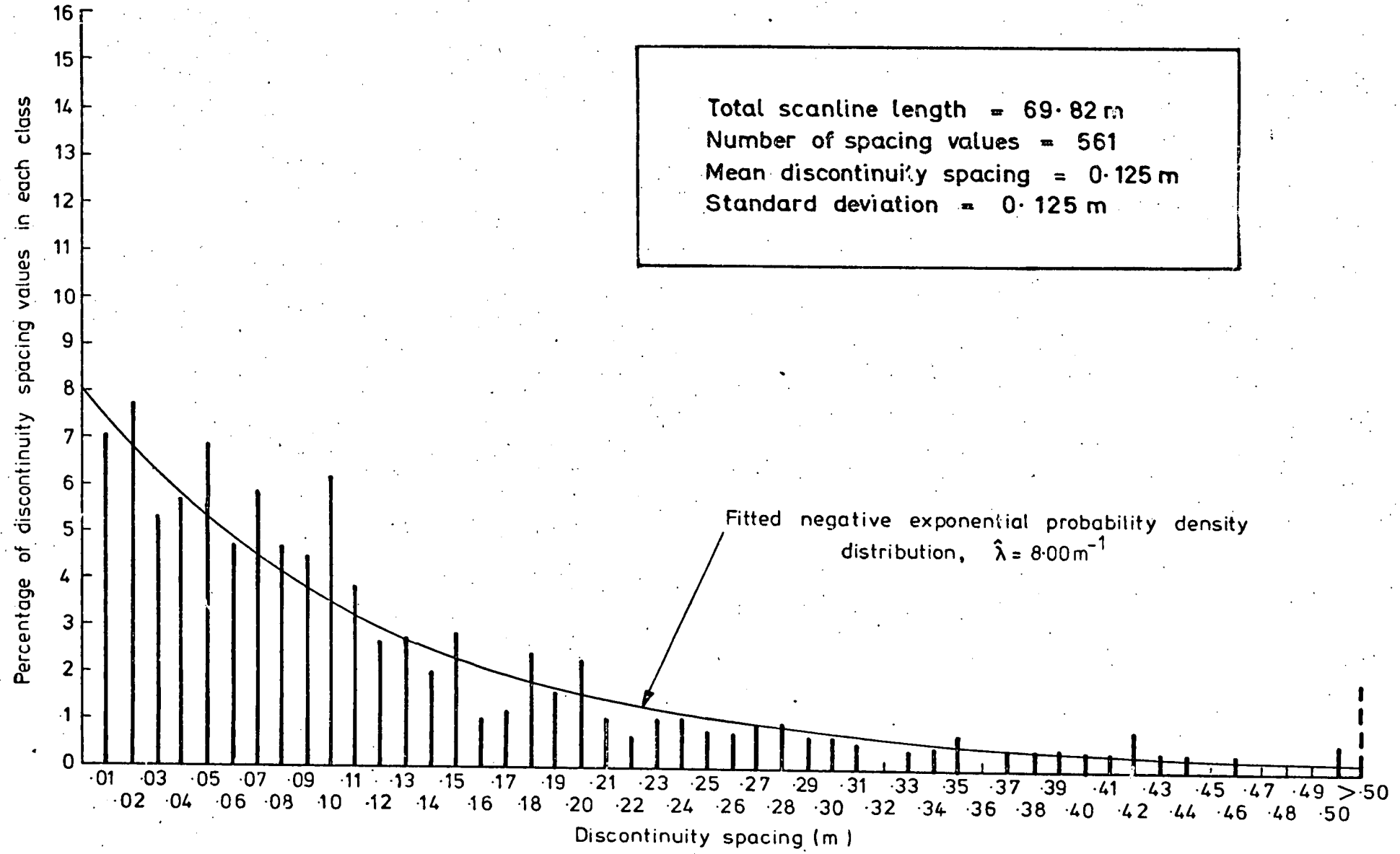

Fig. H.6 DISCONTINUITY SPACING HISTOGRAM, SCANLINES AT THE TUNNEL FACE, CHAINAGE 20·4 m

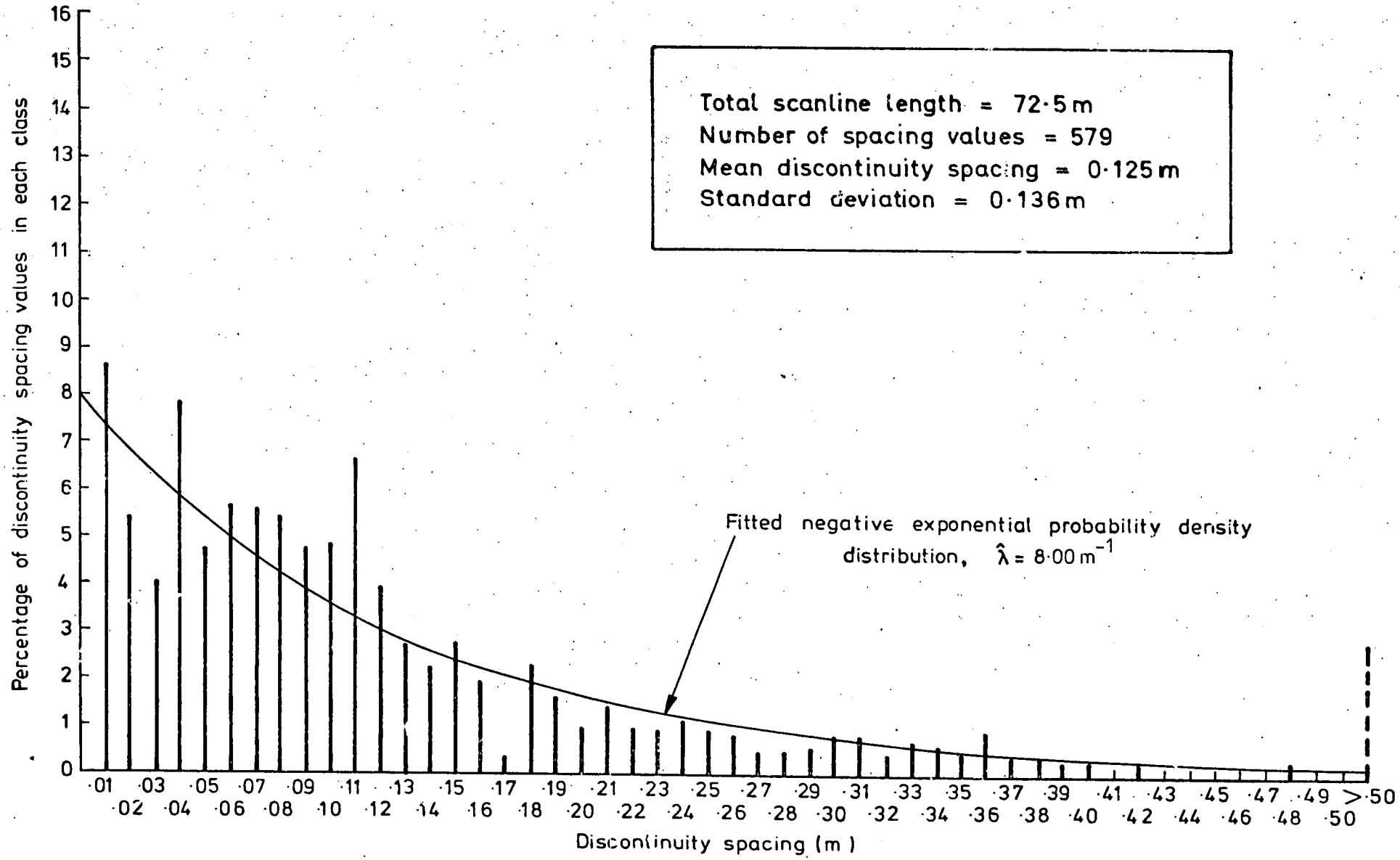

Fig.H.7 DISCONTINUITY SPACING HISTOGRAM, SCANLINES AT THE TUNNEL FACE, CHAINAGE 35·9m

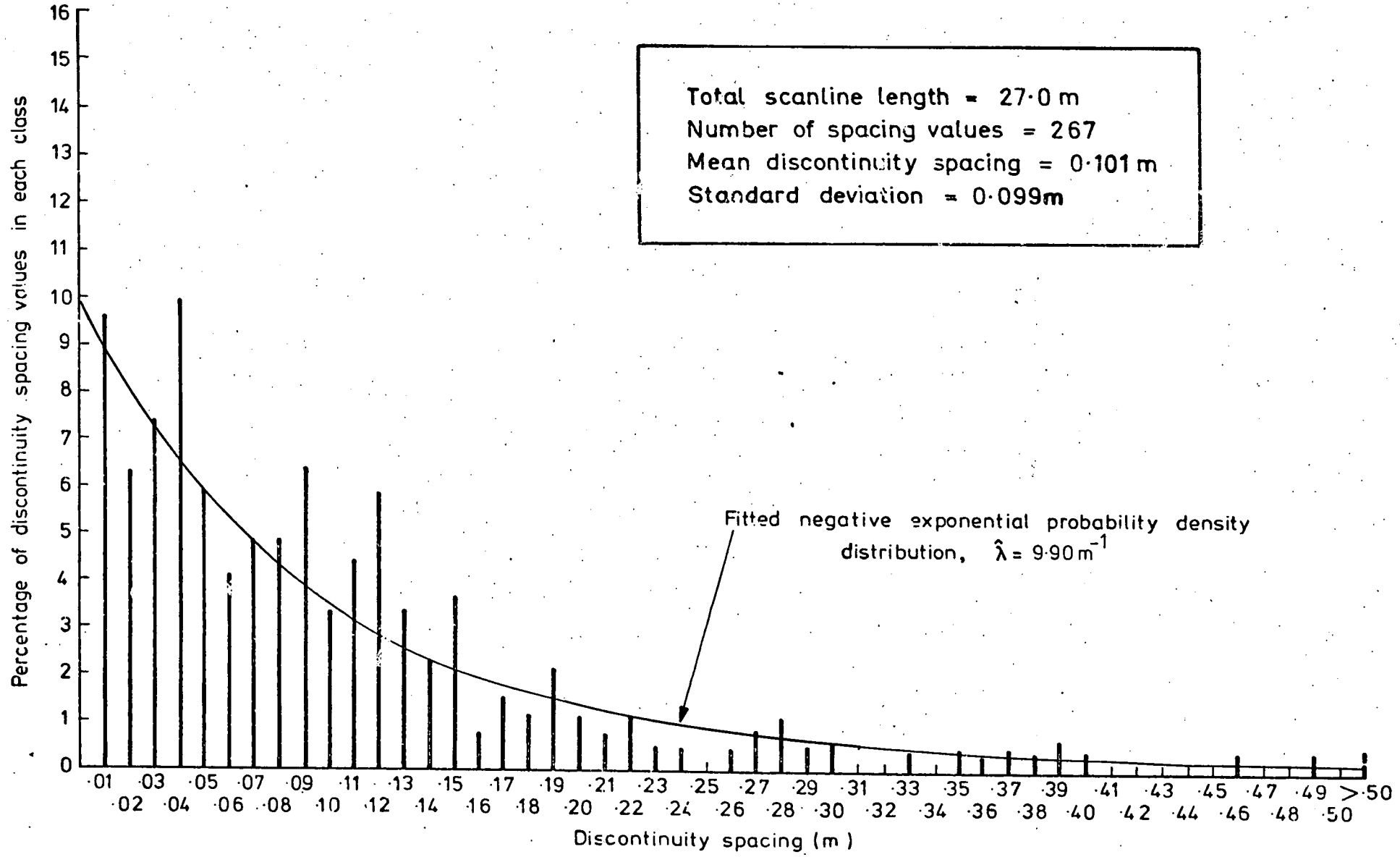

Fig.H.8 DISCONTINUITY SPACING HISTOGRAM, SCANLINES AT THE TUNNEL FACE, CHAINAGE 55·4m

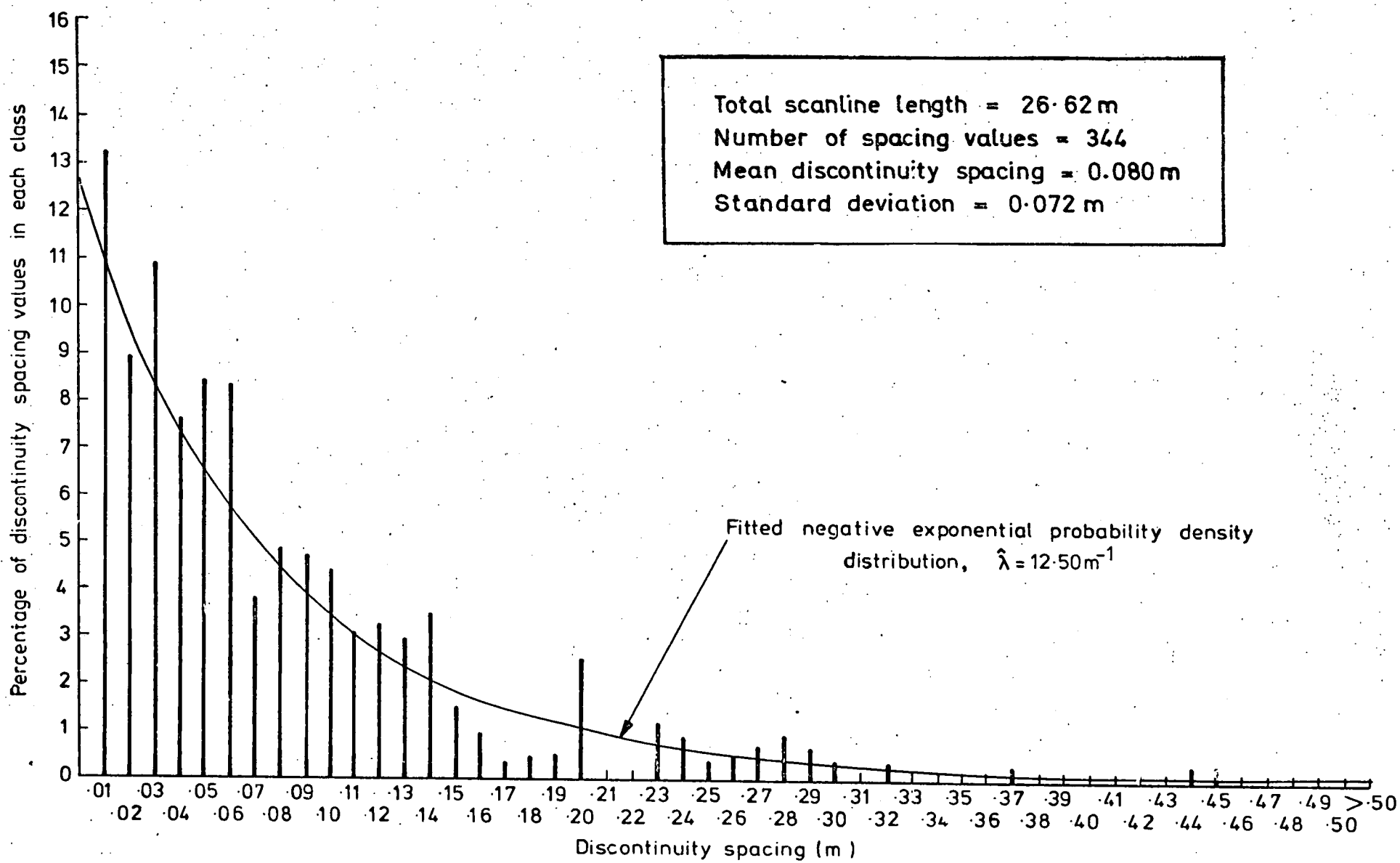

Fig. H.9 DISCONTINUITY SPACING HISTOGRAM, SCANLINES AT THE TUNNEL FACE, CHAINAGE 57·5 m

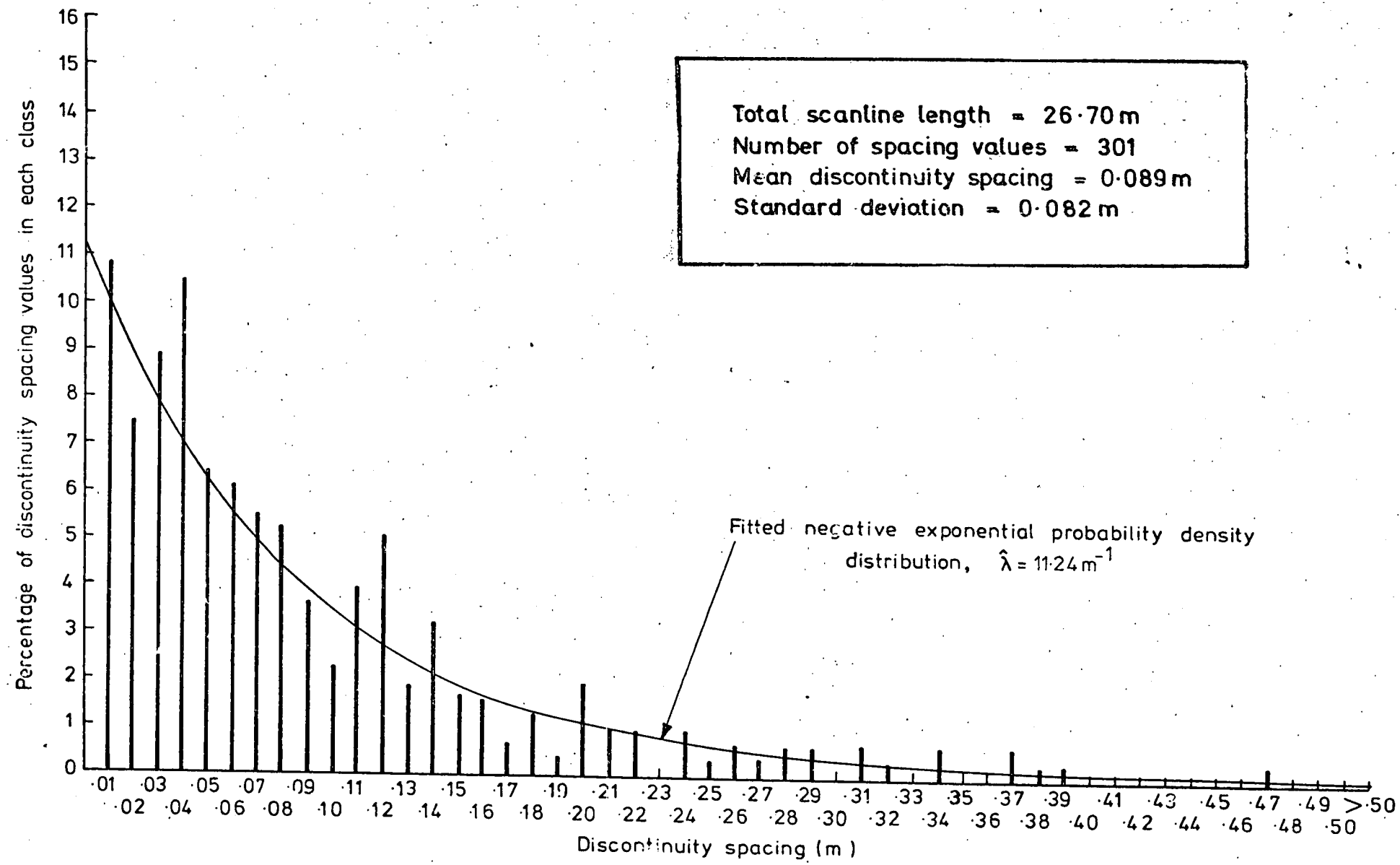

Fig. H.10 DISCONTINUITY SPACING HISTOGRAM, SCANLINES AT THE TUNNEL FACE, CHAINAGE 60·6m

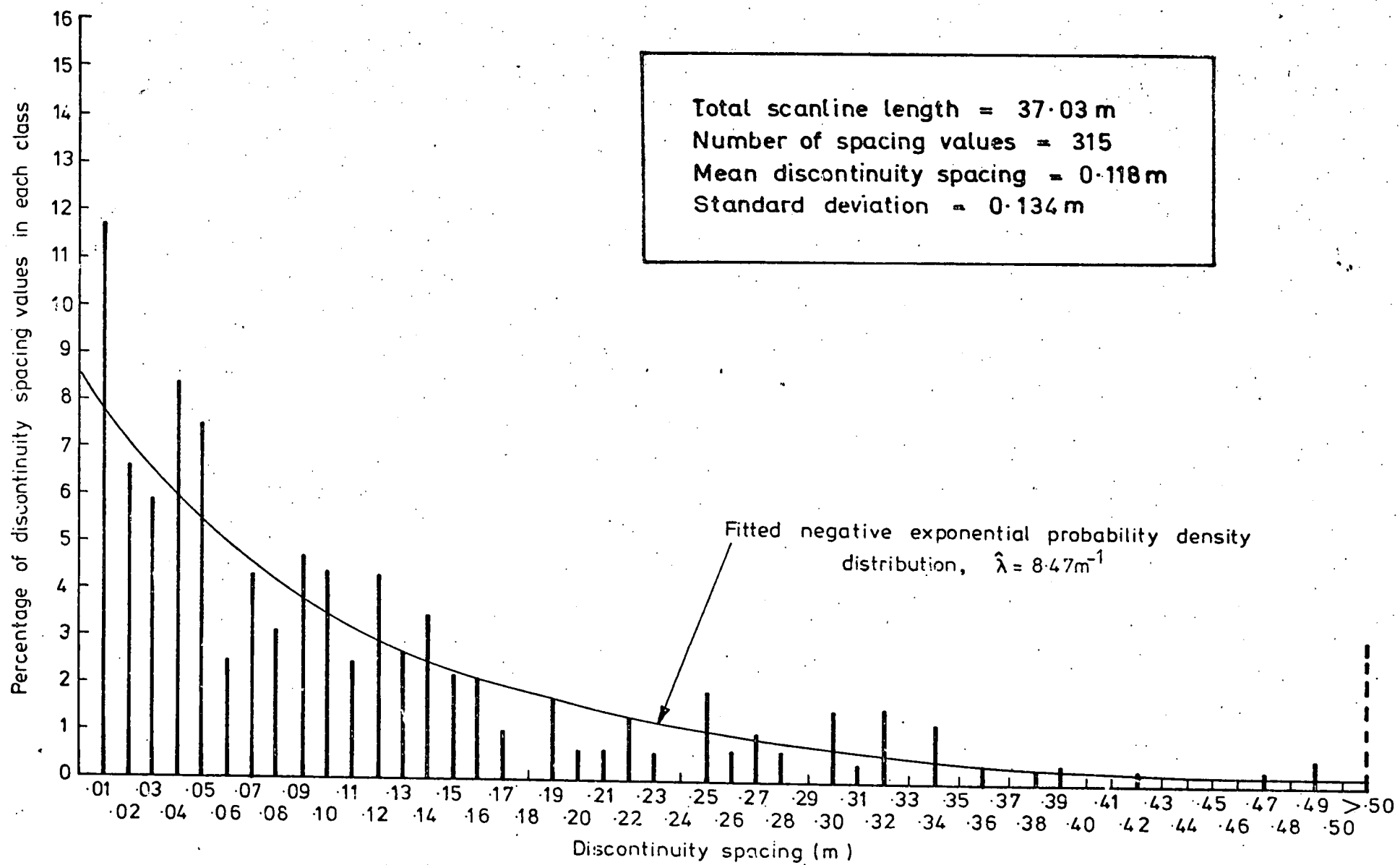

Fig. H.11 DISCONTINUITY SPACING HISTOGRAM, SCANLINES AT THE TUNNEL FACE, CHAINAGE 65·2m

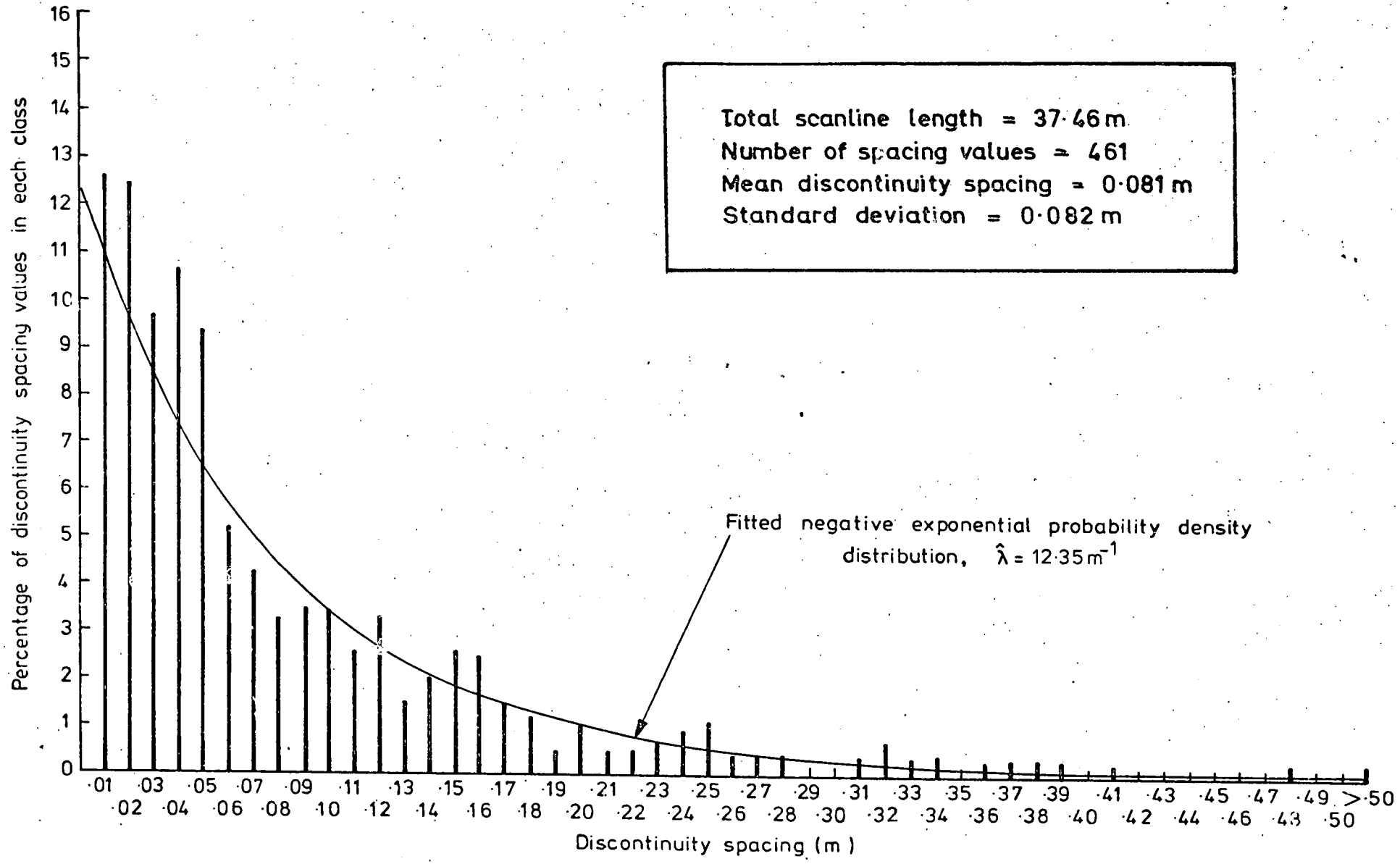

Fig.H.12 DISCONTINUITY SPACING HISTOGRAM, SCANLINES AT THE TUNNEL FACE, CHAINAGE 70·2m

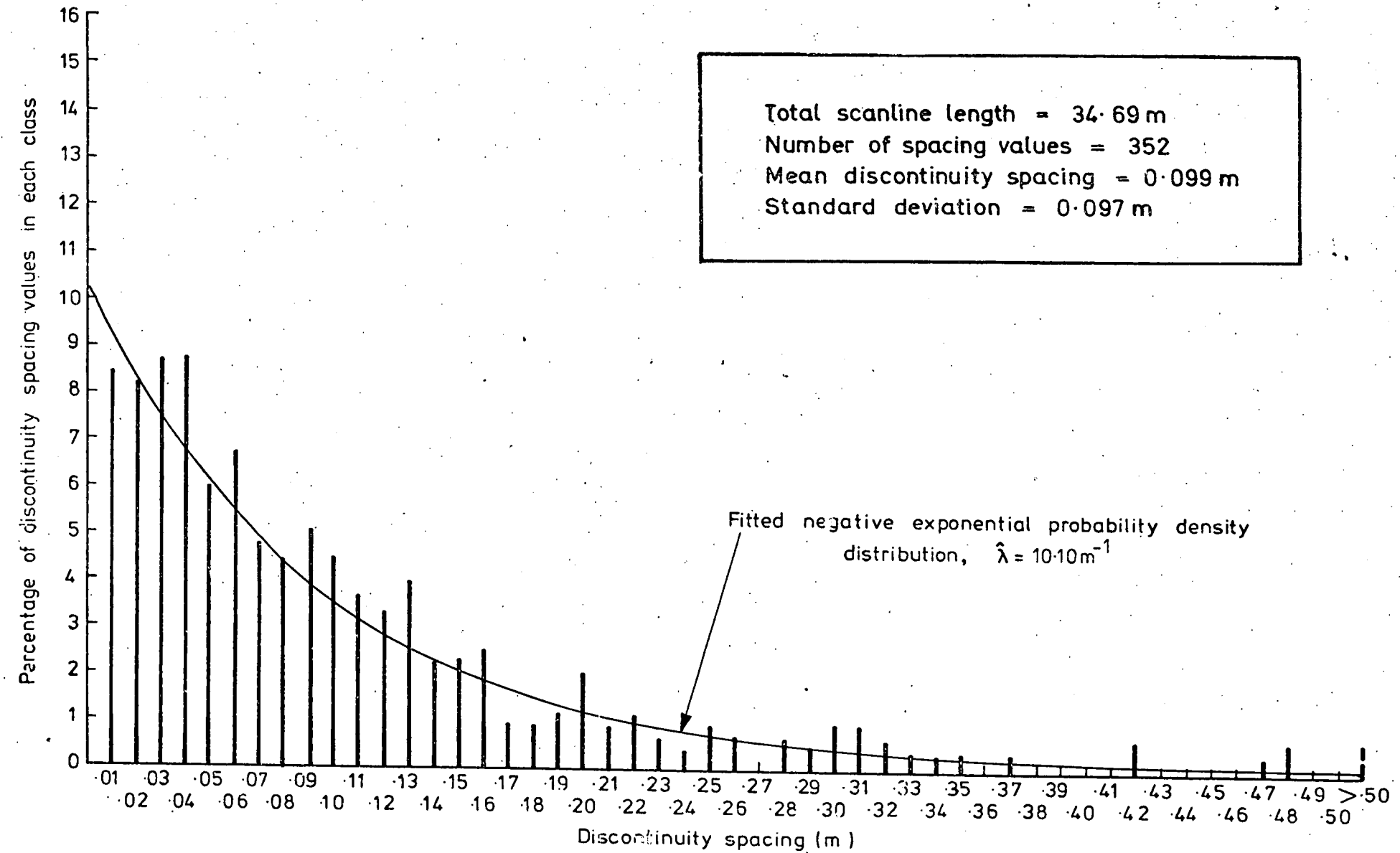

Fig. H.13 DISCONTINUITY SPACING HISTOGRAM, SCANLINES AT THE TUNNEL FACE, CHAINAGE 72·7m

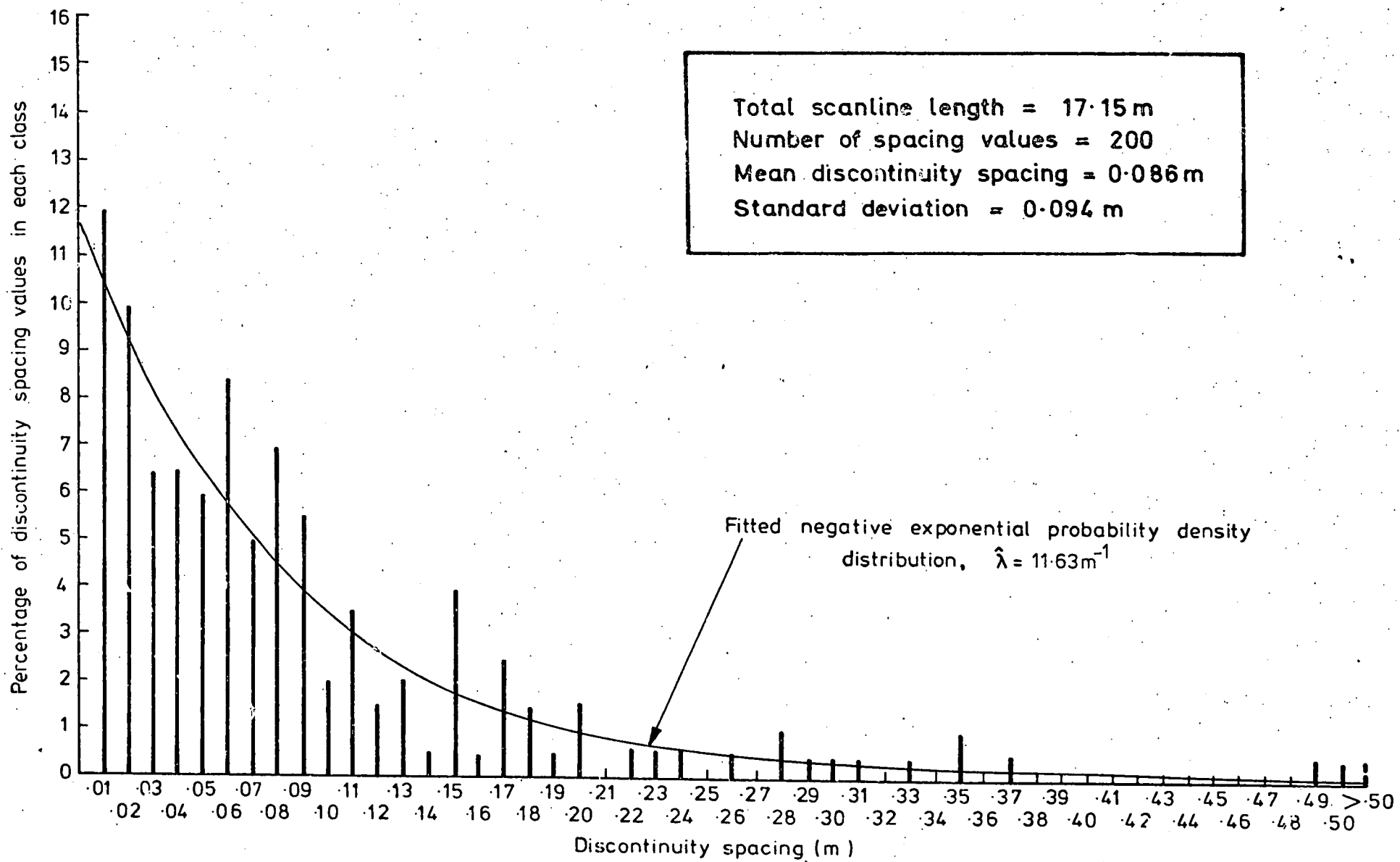

Fig. H.14 DISCONTINUITY SPACING HISTOGRAM, SCANLINES AT THE TUNNEL FACE, CHAINAGE 73·9m

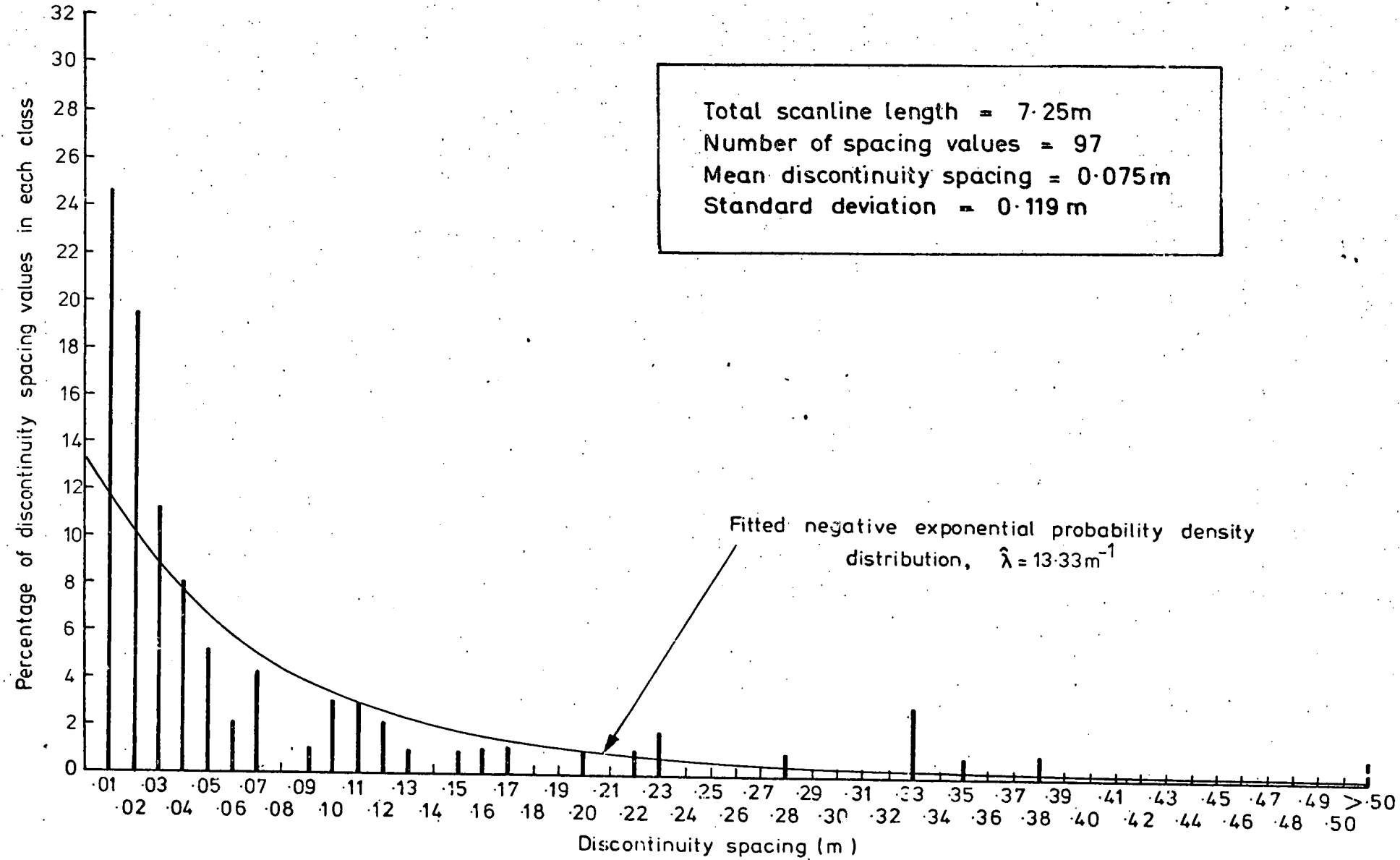

Fig.H.15 DISCONTINUITY SPACING HISTOGRAM, SCANLINES AT THE TUNNEL FACE, CHAINAGE 76·1m

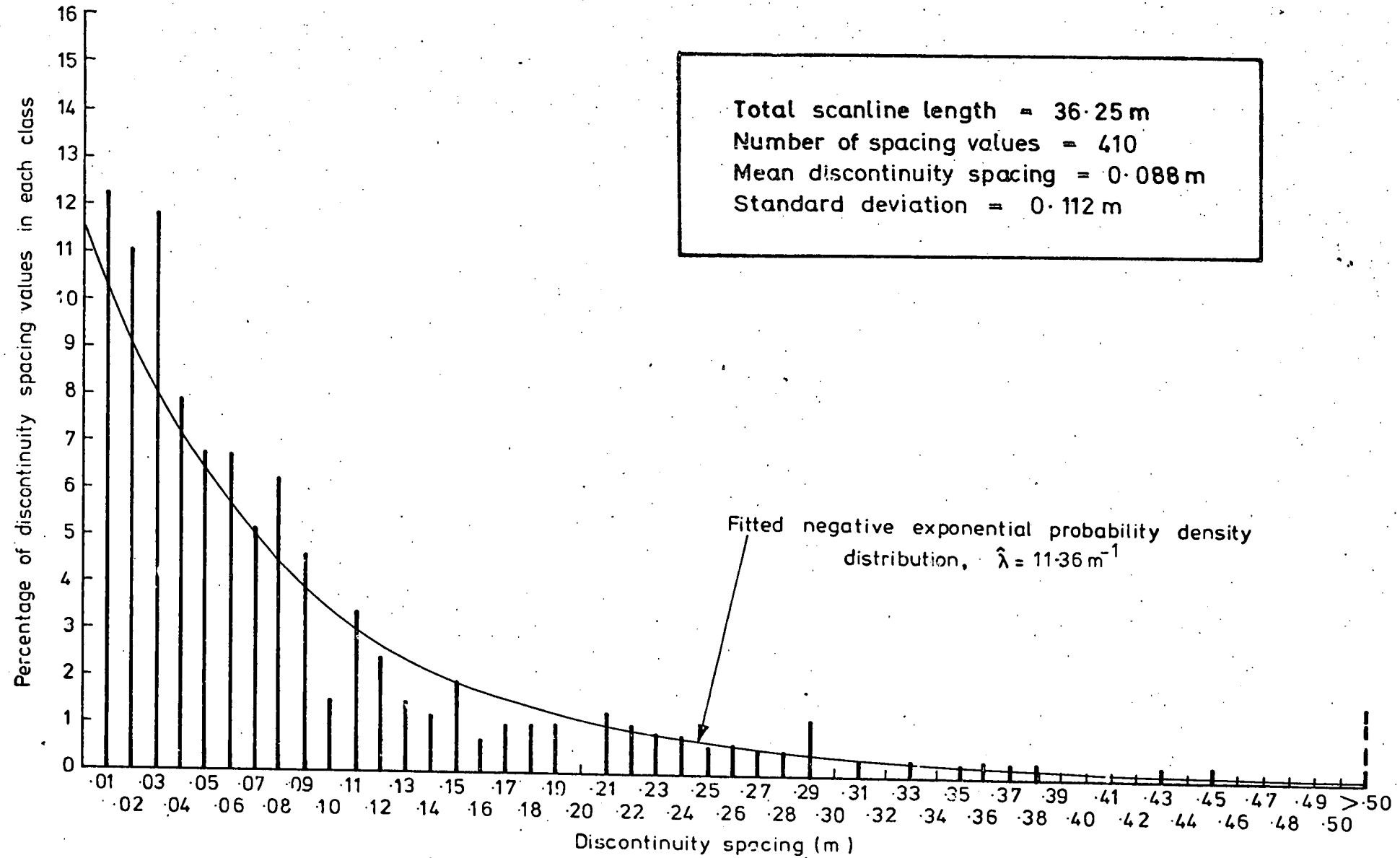

Fig. H.16 DISCONTINUITY SPACING HISTOGRAM, SCANLINES AT THE TUNNEL FACE, CHAINAGE 79·3 m

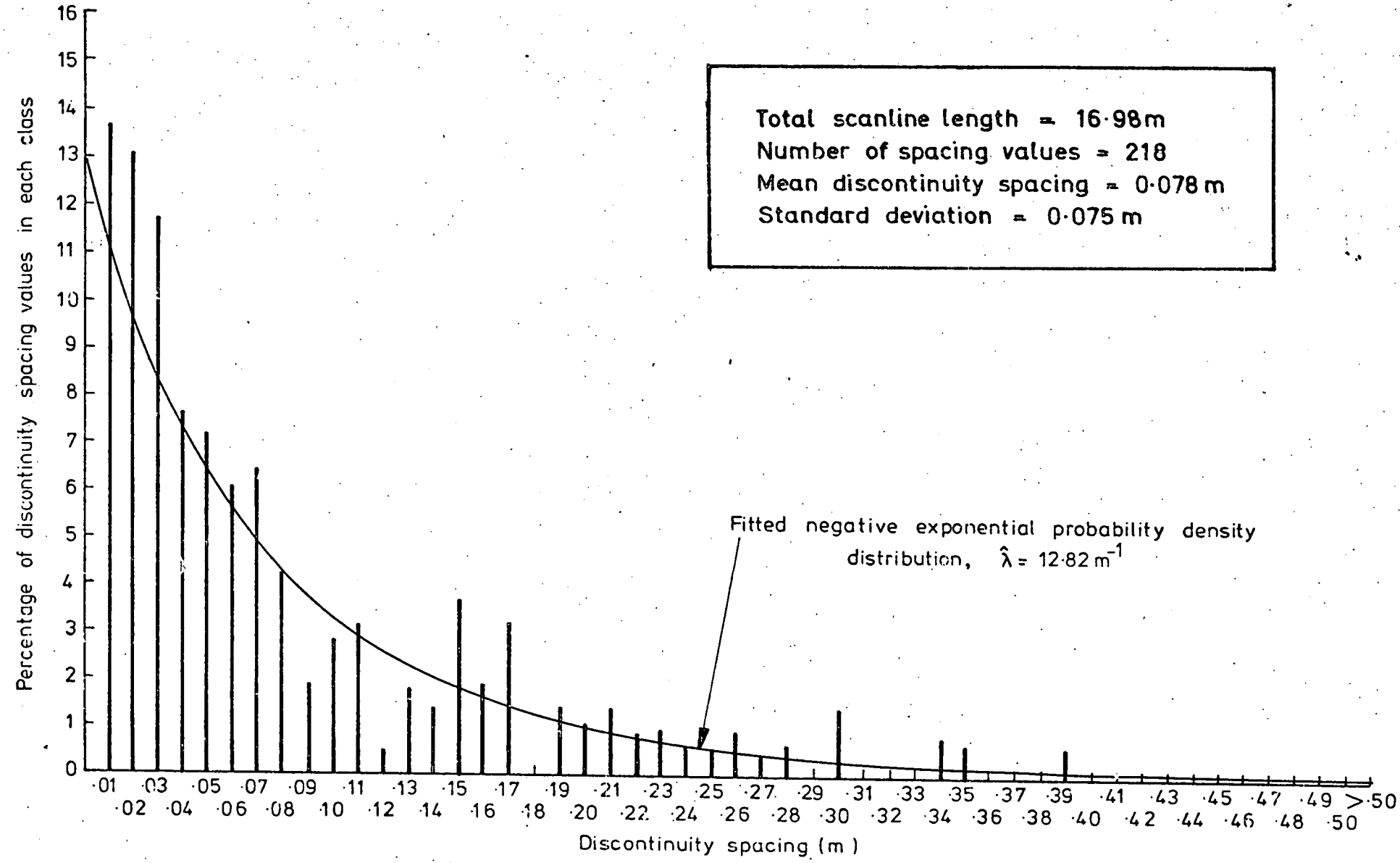

Fig. H.17 DISCONTINUITY SPACING HISTOGRAM, SCANLINES AT THE TUNNEL FACE, CHAINAGE 85·0m

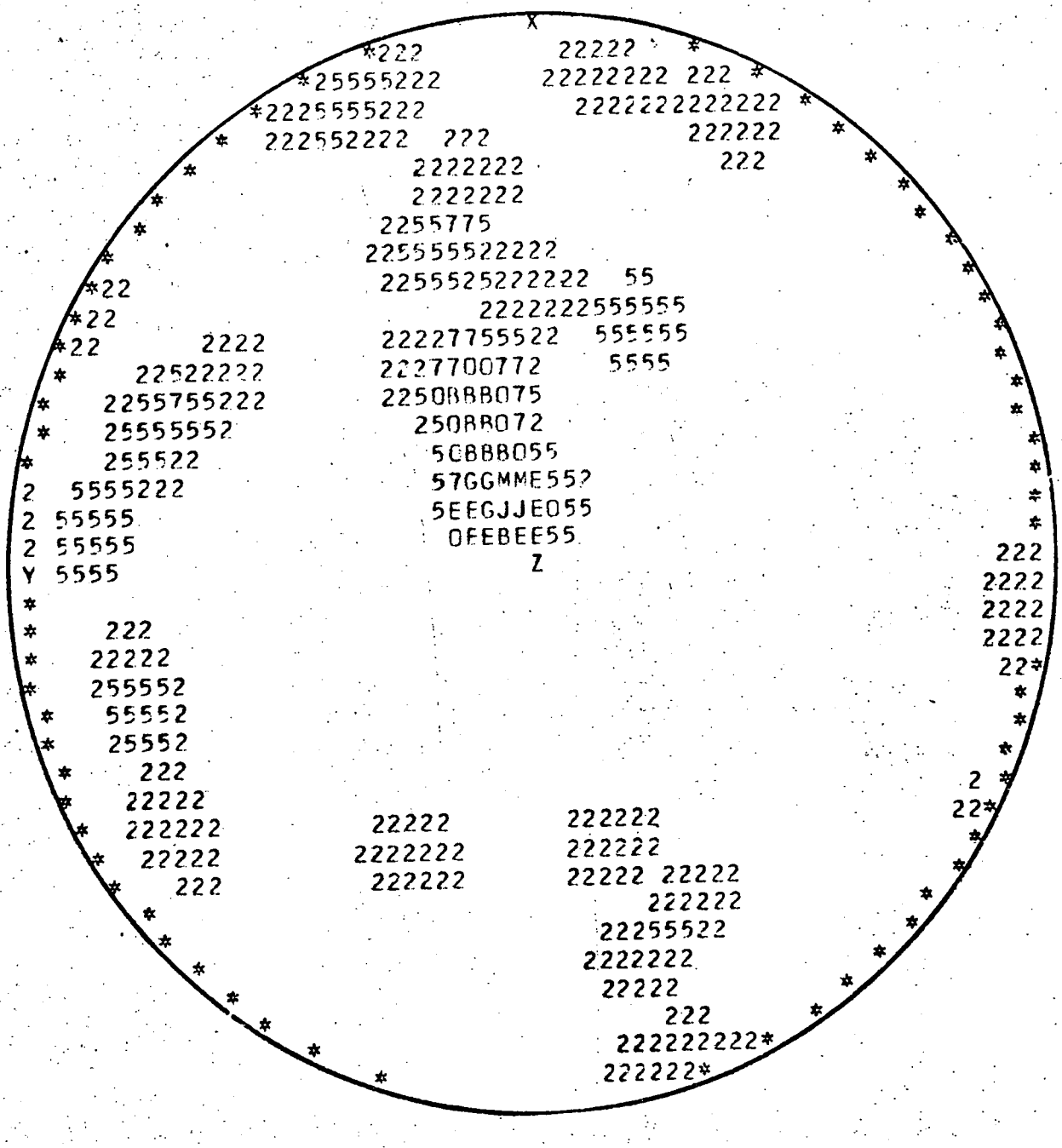

Fig. H.18 UPPER HEMISPHERE PROJECTION OF DISCONTINUITY ORIENTATION, TUNNEL CHAINAGE 9·9m.

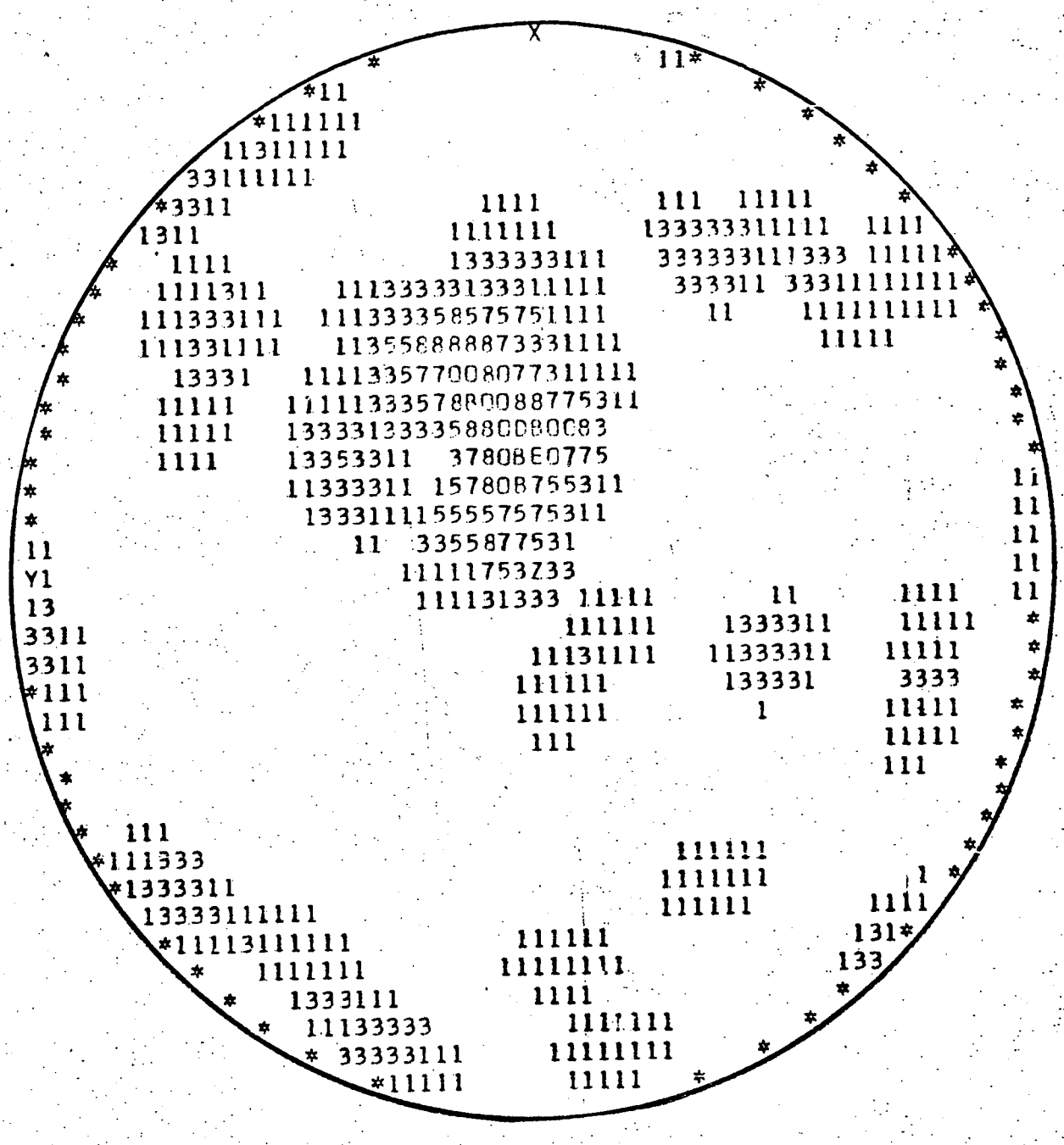

57 readings

Fig. H.19 UPPER HEMISPHERE PROJECTION OF DISCONTINUITY ORIENTATION, TUNNEL CHAINAGE 11·5m.

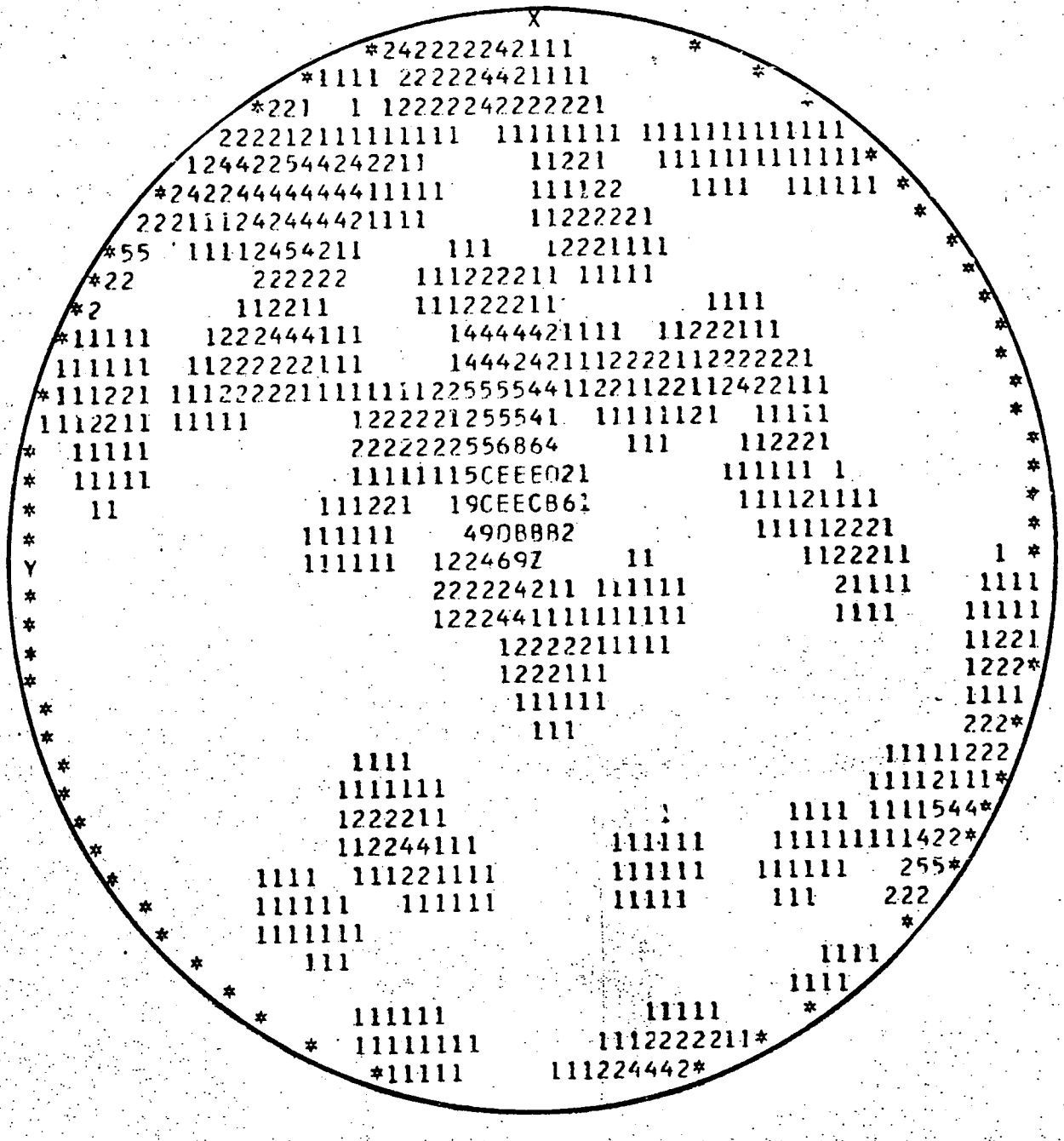

Fig. H.20 UPPER HEMISPHERE PROJECTION OF DISCONTINUITY ORIENTATION, TUNNEL CHAINAGE 12·1m.

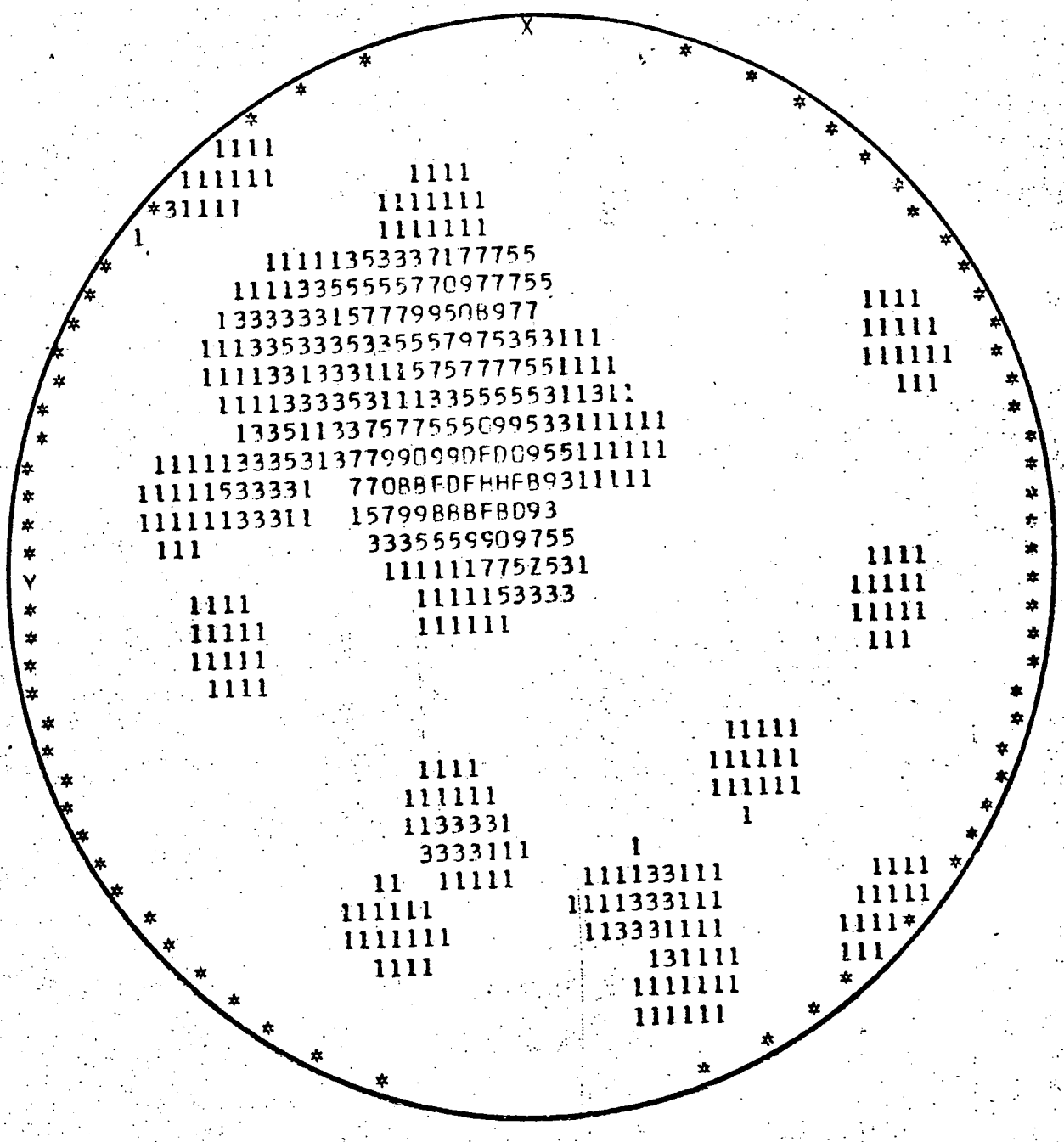

Fig. H.21 UPPER HEMISPHERE PROJECTION OF DISCONTINUITY ORIENTATION, TUNNEL CHAINAGE 14·0m.

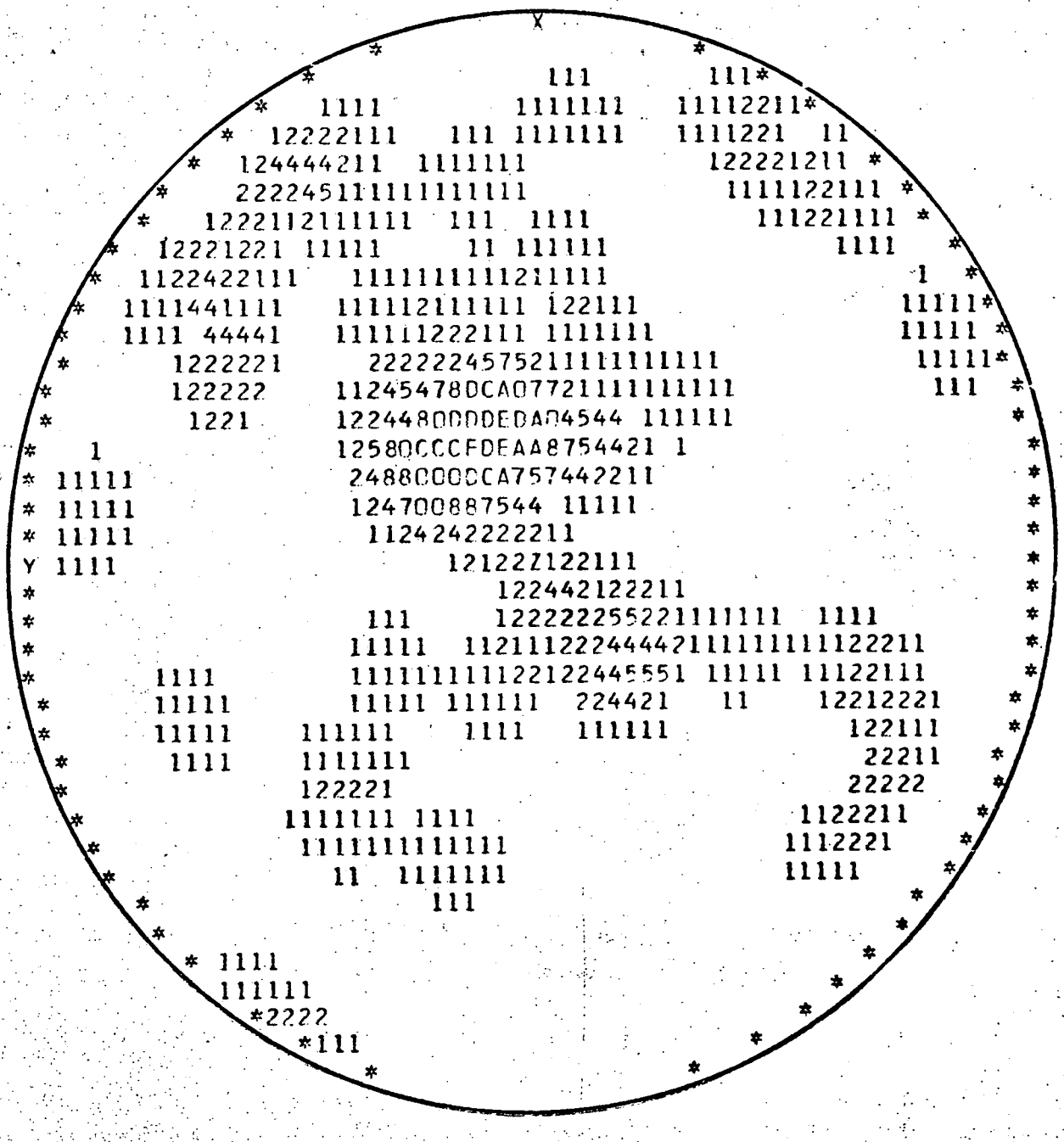

69 readings

Fig. H.22 UPPER HEMISPHERE PROJECTION OF DISCONTINUITY ORIENTATION, TUNNEL CHAINAGE 18·1m.

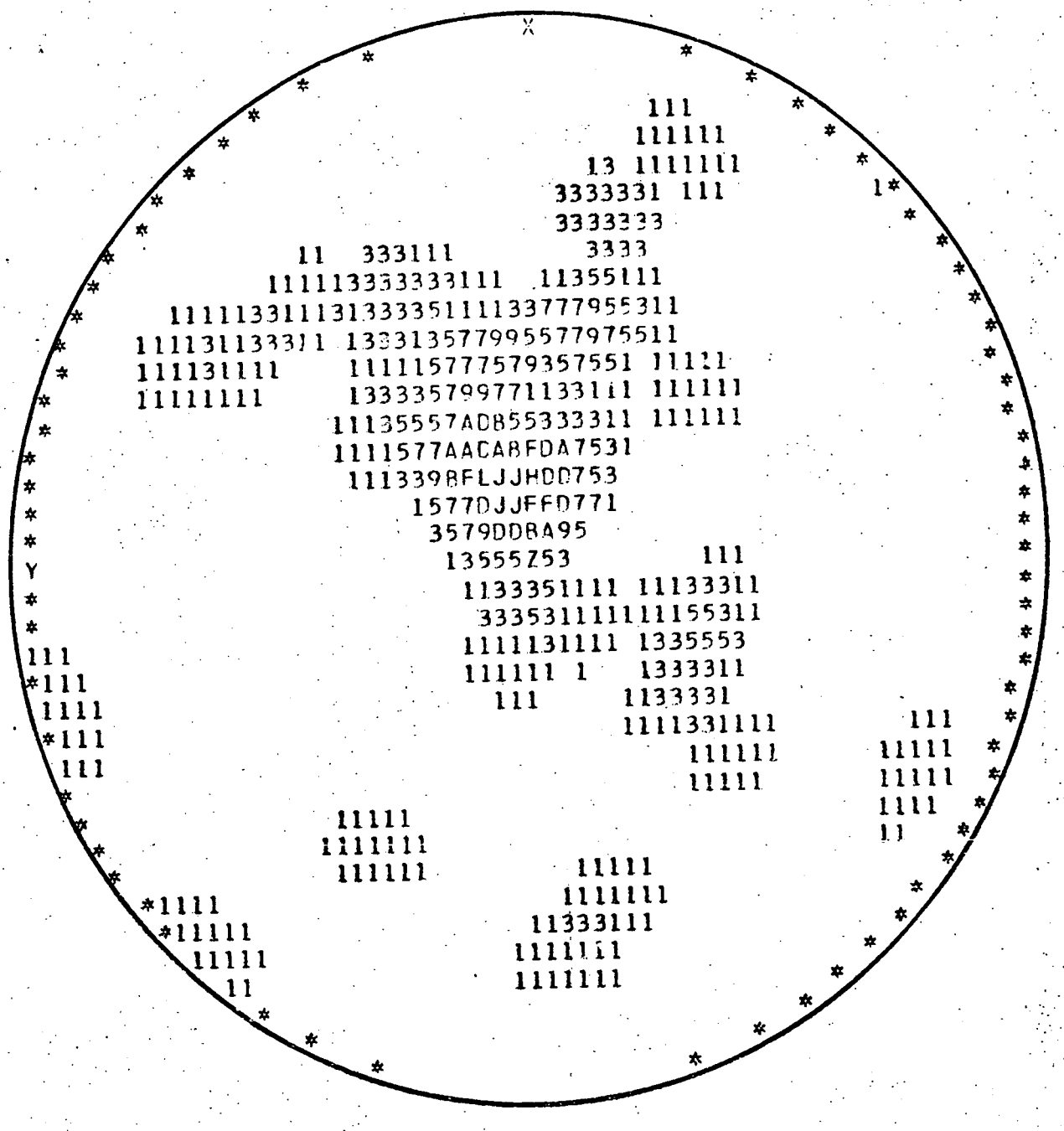

54 readings

Fig.H.23 UPPER HEMISPHERE PROJECTION OF DISCONTINUITY ORIENTATION, TUNNEL CHAINAGE 20·4 m.

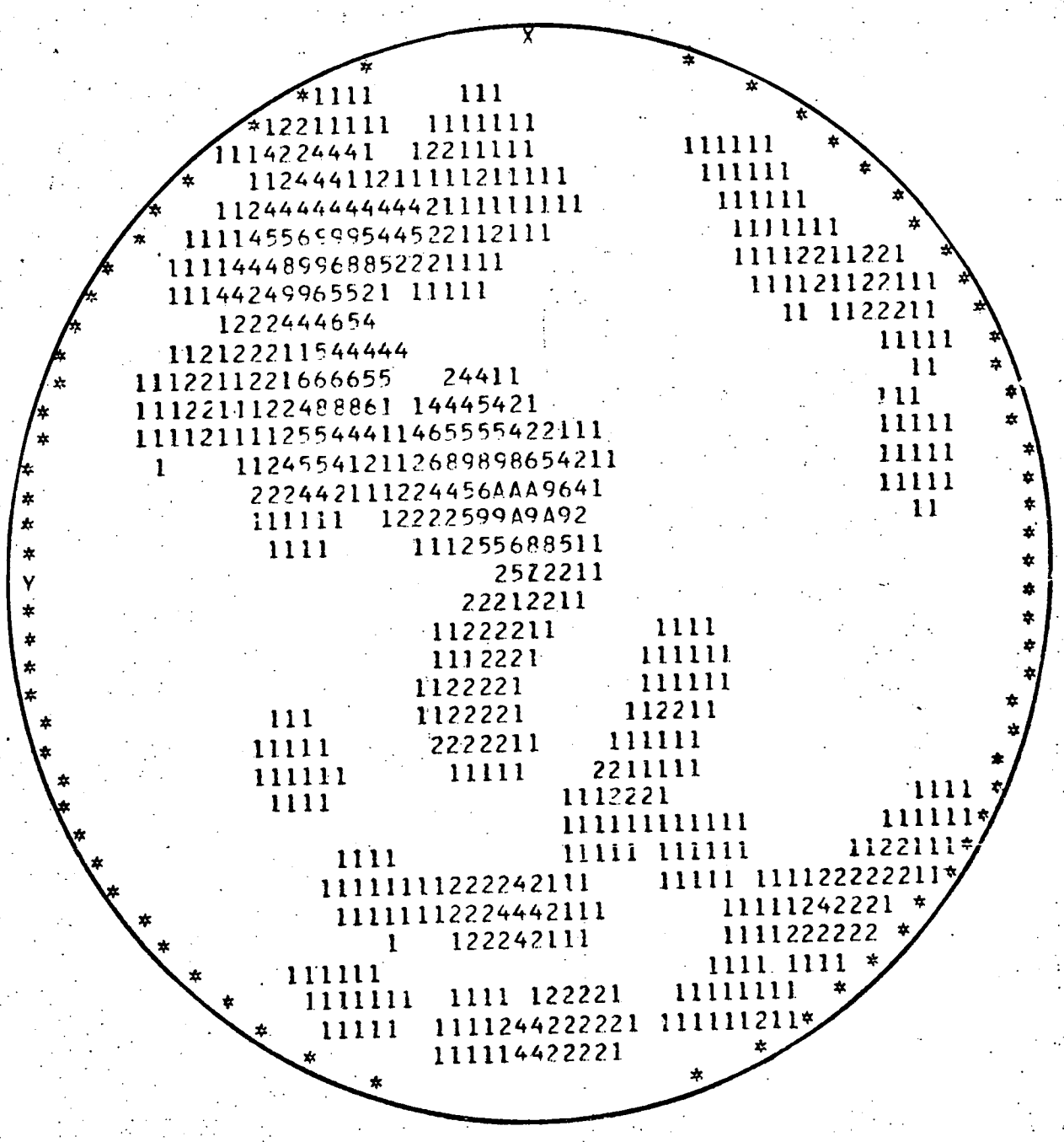

72 readings

Fig.H.24 UPPER HEMISPHERE PROJECTION OF DISCONTINUITY ORIENTATION, TUNNEL CHAINAGE 35·9m.

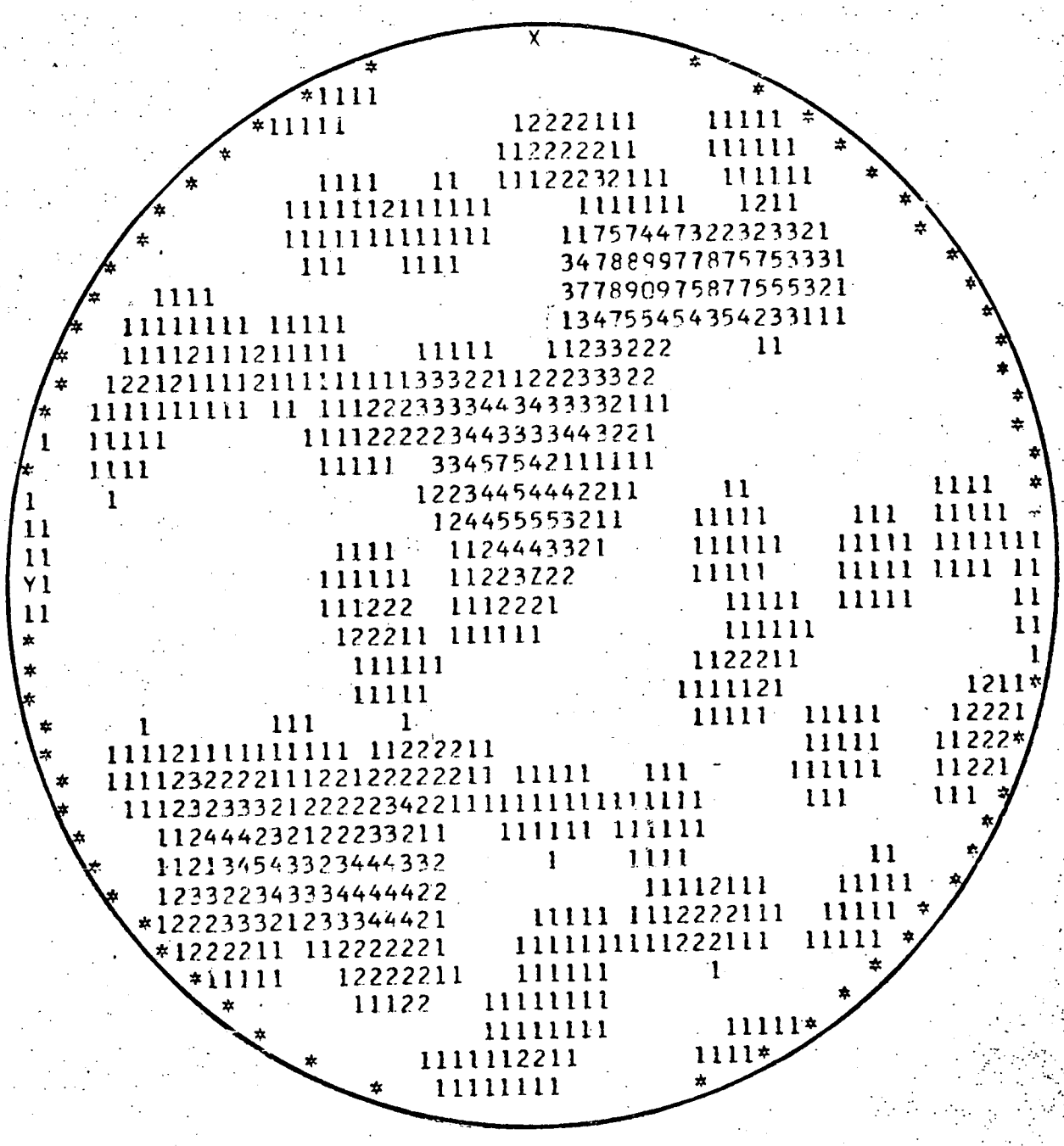

84 readings

Fig. H.25 UPPER HEMISPHERE PROJECTION OF DISCONTINUITY ORIENTATION, TUNNEL CHAINAGE 55·4m.

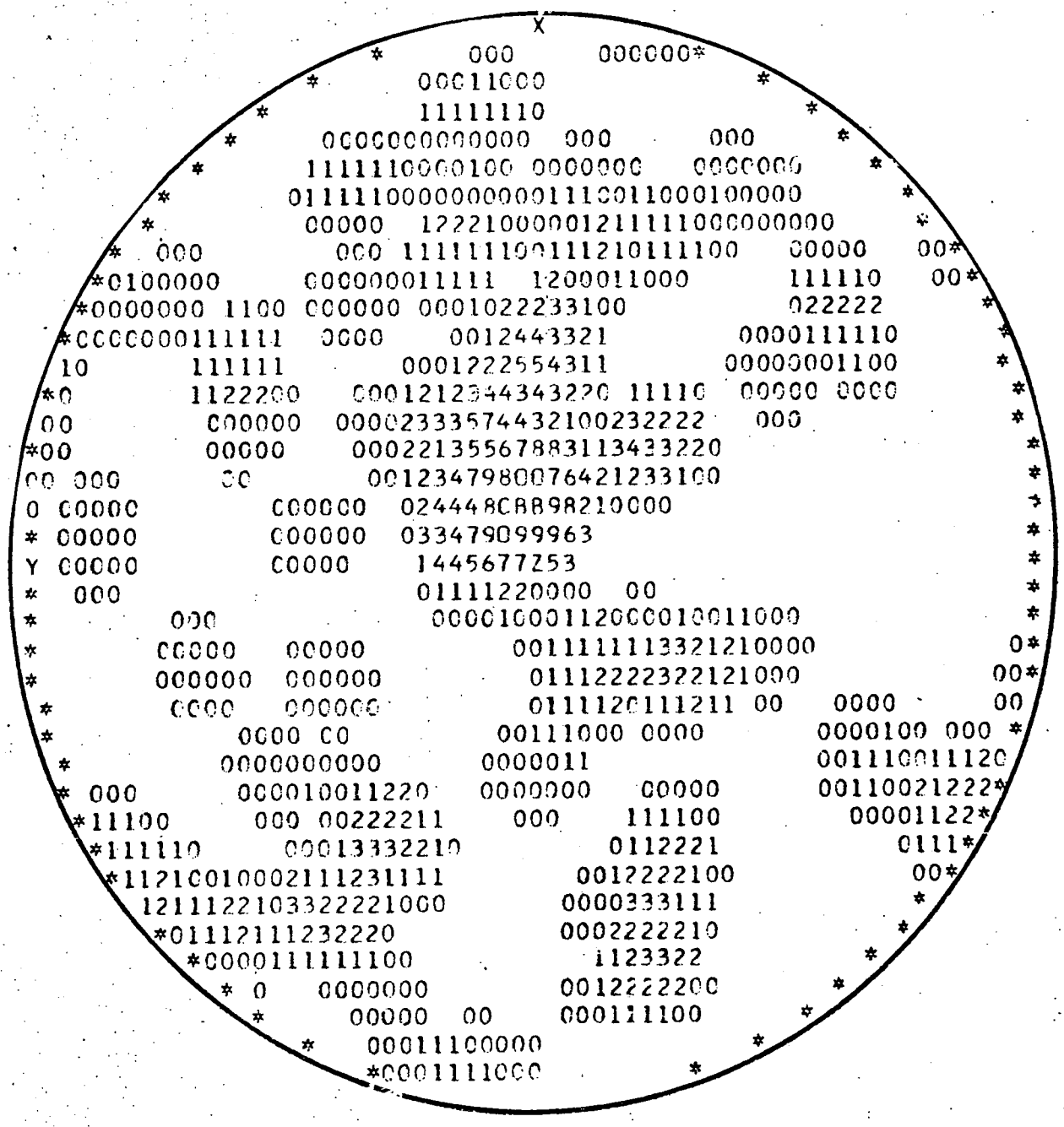

101 readings

Fig.H.26 UPPER HEMISPHERE PROJECTION OF DISCONTINUITY ORIENTATION, TUNNEL CHAINAGE 57·5m.

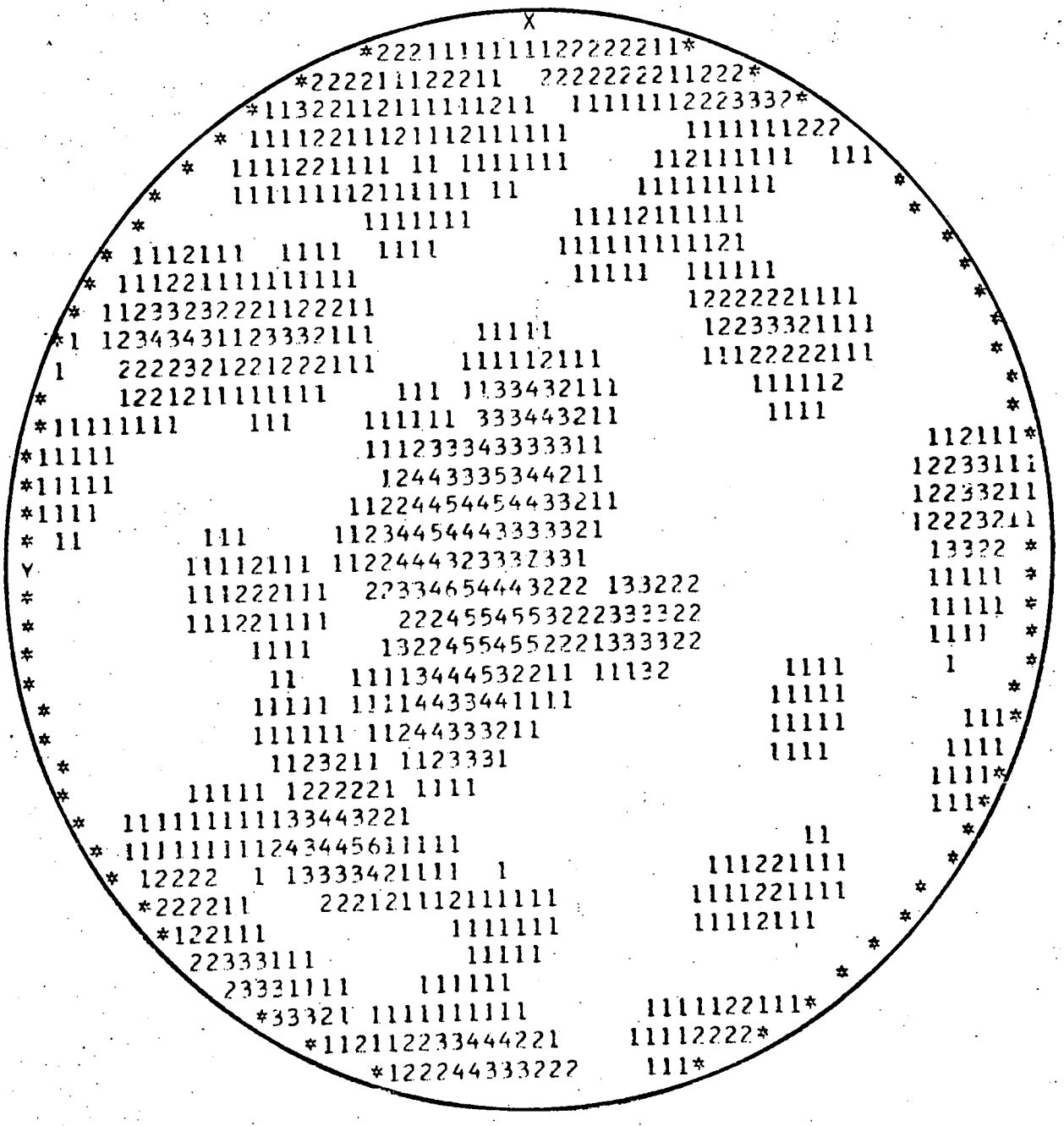

89 readings

Fig.H.27 UPPER HEMISPHERE PROJECTION OF DISCONTINUITY ORIENTATION, TUNNEL CHAINAGE 60·6m.

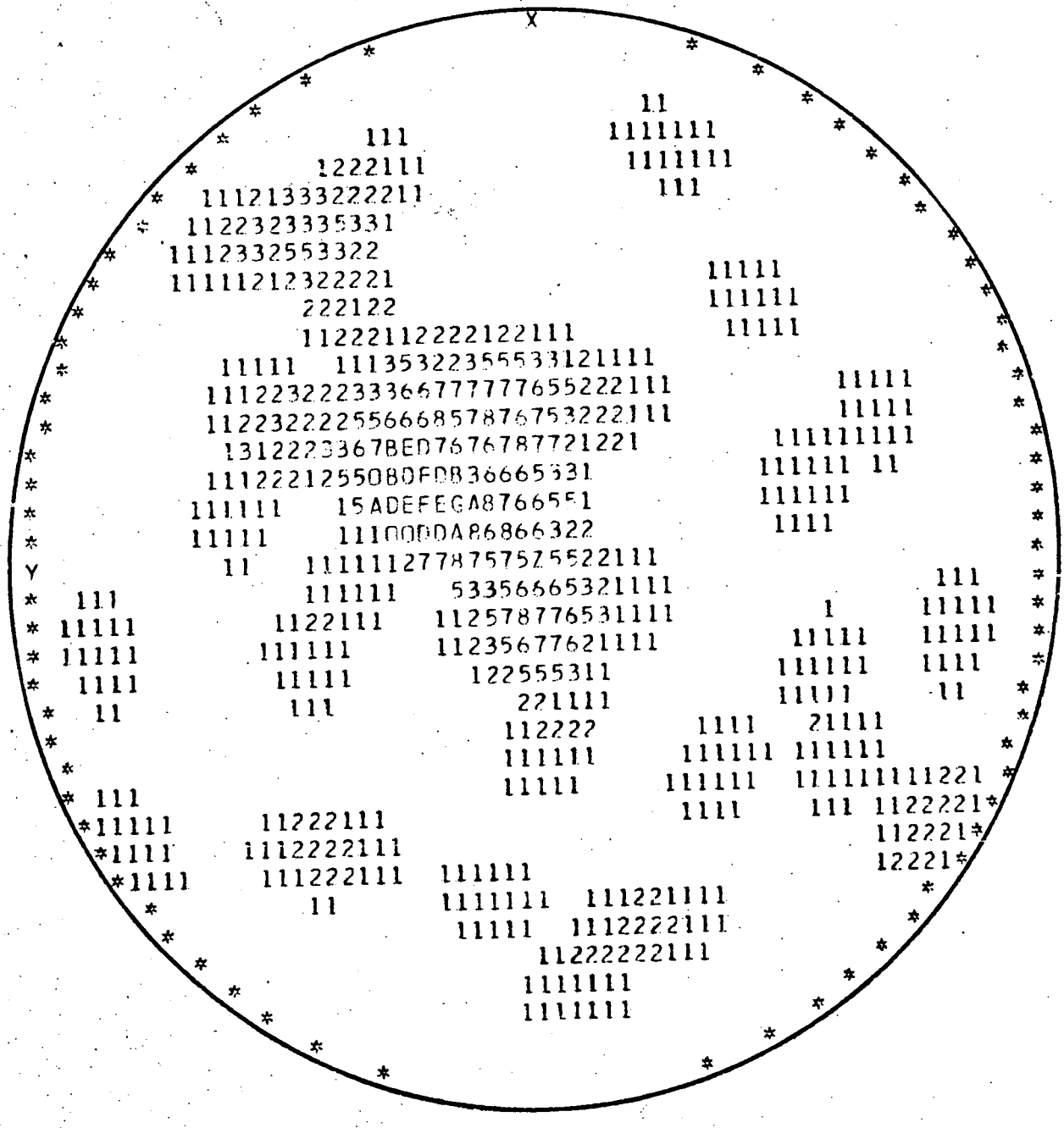

78 readings

Fig.H.28 UPPER HEMISPHERE PROJECTION OF DISCONTINUITY ORIENTATION, TUNNEL CHAINAGE 65·2m.

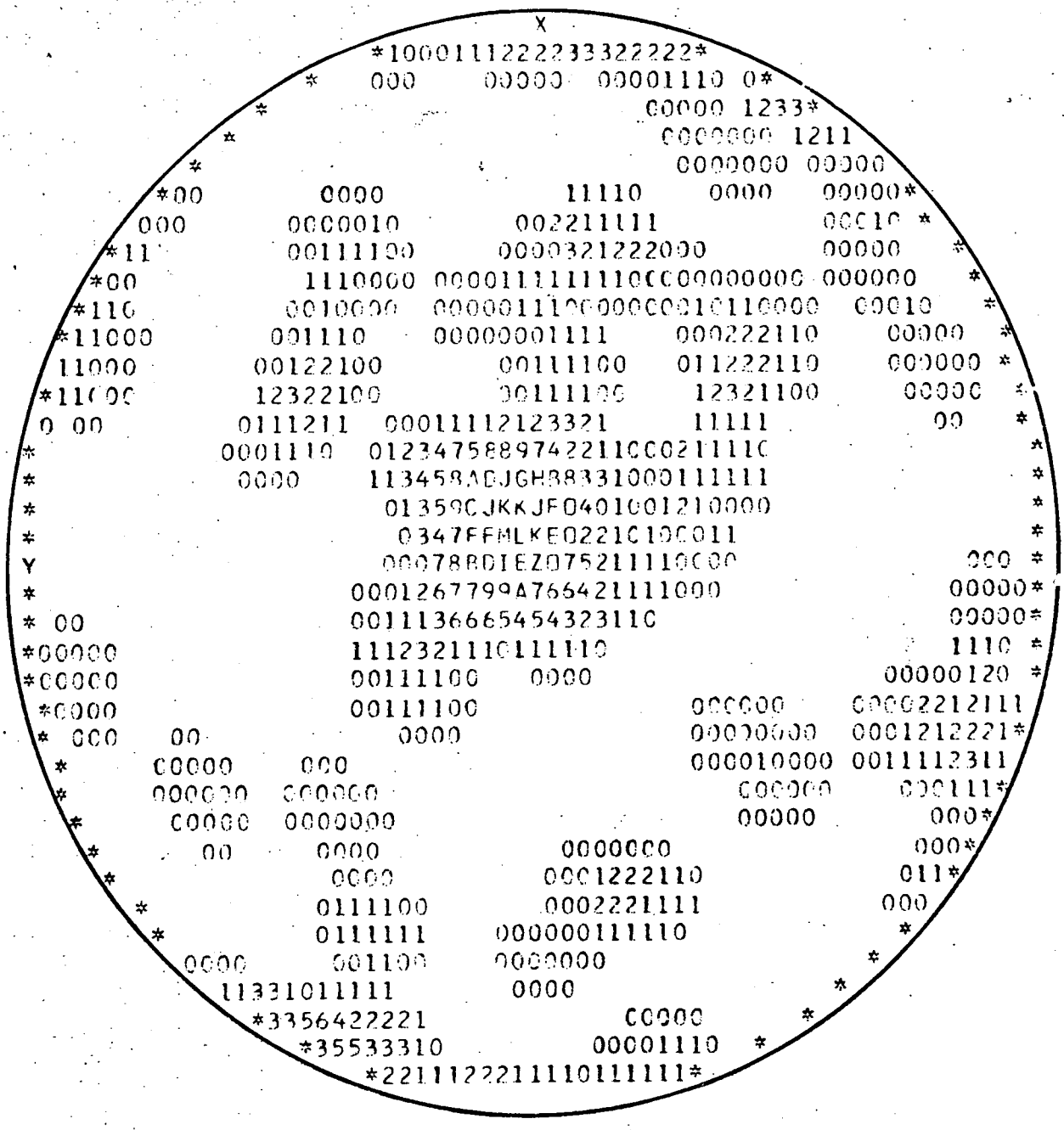

113 readings

Fig.H.29 UPPER HEMISPHERE PROJECTION OF DISCONTINUITY ORIENTATION, TUNNEL CHAINAGE 70·2m.

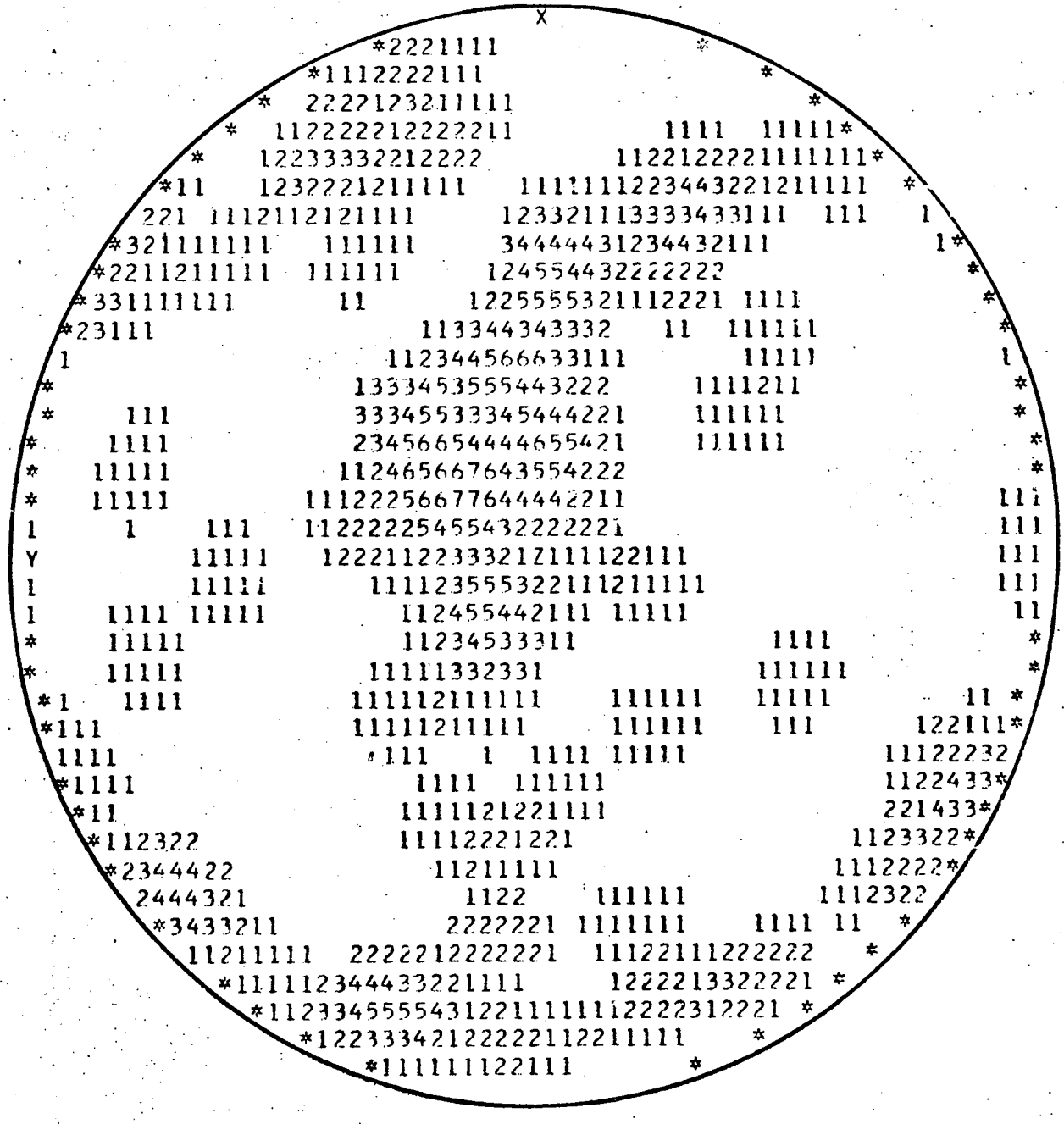

94 readings

Fig.H.30 UPPER HEMISPHERE PROJECTION OF DISCONTINUITY ORIENTATION, TUNNEL CHAINAIGE 72·7m.

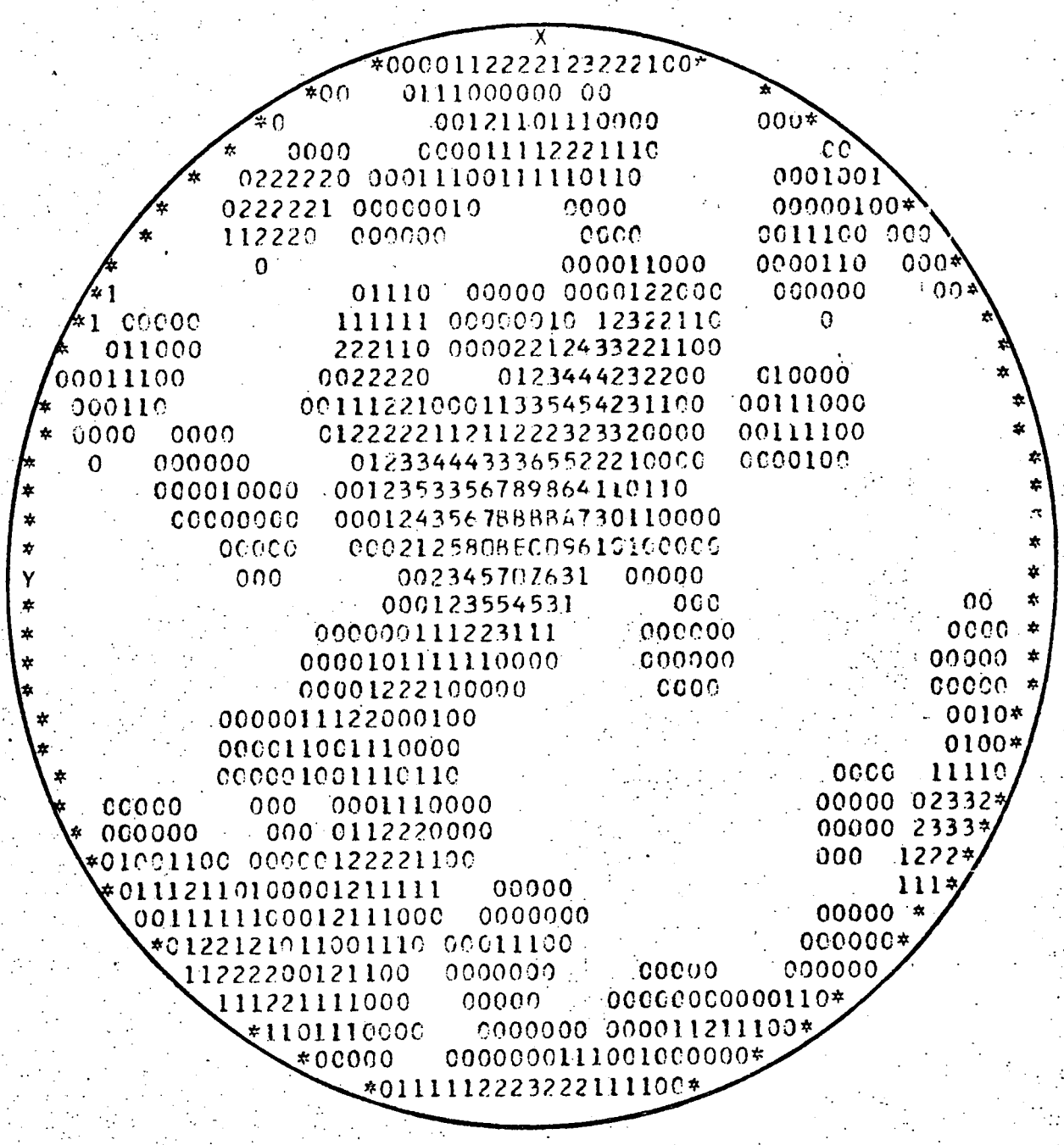

104 readings

Fig.H.31 UPPER HEMISPHERE PROJECTION OF DISCONTINUITY ORIENTATION, TUNNEL CHAINAGE 85·0m.

APPENDIX I

RAW DATA FROM DEMEC GAUGE READINGS

In this Appendix, raw data obtained from measurements of Demec spans set up in the trench across the tunnel line are presented. This work is described fully in Chapter 7.

The data, presented in matrix form, can be interpreted using Tables I.1 and I.2. The six matrices A to F are presented in Tables I.3 to I.8. In Table I.1 the column numbers in matrices A to F are related to time: for example column numbers 26, 23, 19, 23, 23 and 11 in matrices A, B, C, D, E and F respectively, represent readings taken on 29 April 1974. In Table I.2 the row numbers are related to position: for example in matrix F, row number 10 represents readings on a Demec span 2.6m east of the tunnel centre line. In matrices A and B the type of discontinuity movement monitored by each Demec span is indicated: rows designated "N" record normal movement, rows designated "P" record parallel movement.

The positive and negative numbers listed in Tables I.3 to I.8 are the deviations in Demec gauge readings from the initial reading. The processing of these results is explained fully in Section 7.3.3. Matrices A and D represent the 'short' Demec gauge, matrices B, E and F the 'long' Demec gauge and matrix C the 'medium' Demec gauge. The conversion of the deviation readings to strain values is done by applying the appropriate gauge factor. The strain value corresponding to a deviation of one unit on the Demec gauge, for each of the gauges used, is listed below:

'short' gauge, deviation = 1, strain = 1.99×10^{-5}

'medium' gauge, deviation = 1, strain = 0.98×10^{-5}

'long' gauge, deviation = 1, strain = 0.50×10^{-5}

Therefore in matrix F, $D_{48,12}$, the deviation of the 12th reading on span 48, is 2. This represents a tensile strain of 1×10^{-4} at 10.00 am on 30 April 1974 at a position 12.6m to the west of the tunnel centre line.

The presentation of the Demec gauge readings in matrix form simplified the recording, retrieval and processing of data and consequently facilitated the analysis of the results presented in Chapter 7.

Table I.1

Correlation between column numbers and time in matrices A to F

Time	1974 Date	Column number in matrices						
		A	B	C	D	E	F	
	10 Jan	1						
	14 Jan	2						
	18 Jan	3						
	21 Jan	4	1		1	1		
	23 Jan	5	2		2	2		
	28 Jan	6	3		3	3		
	31 Jan	7	4		4	4		
	4 Feb	8	5	1	5	5		
	7 Feb	9	6	2	6	6		
	11 Feb	10	7	3	7	7		
	14 Feb	11	8	4	8	8		
	18 Feb	12	9	5	9	9		
	21 Feb	13	10	6	10	10		
	25 Feb	14	11	7	11	11		
	28 Feb	15	12	8	12	12		
	4 Mar	16	13	9	13	13		
	7 Mar	17	14	10	14	14		
	12 Mar	18	15	11	15	15		
	13 Mar						1	
	18 Mar	19	16	12	16	16		
	20 Mar						2	
	25 Mar	20	17	13	17	17		
	29 Mar	21	18	14	18	18	3	
	1 Apr						4	
	4 Apr	22	19	15	19	19		
	5 Apr						5	
	10 Apr	23	20	16	20	20	6	
	16 Apr	24	21	17	21	21	7	
	22 Apr	25	22	18	22	22	8	
	24 Apr						9	
	26 Apr						10	
	29 Apr	26	23	19	23	23	11	
10.00	30 Apr						12	
15.30	30 Apr						13	
09.15	1 May						14	
12.00	1 May						15	Reaction ring jacking tests
14.15	1 May						16	
15.35	1 May						17	
16.05	1 May						18	
10.15	2 May						19	
	7 May	27	24	20	24	24	20	
	13 May	28	25	21	25	25	21	
	24 May	29	26	22	26	26	22	
	31 May	30	27	23	27	27	23	
	6 June	31	28	24	28	28	24	
	14 June	32	29	25	29	29	25	
	28 June	33	30	26	30	30	26	
	21 July	34	31	27	31	31	27	

Table I.2

Correlation between row number and position in matrices A to F

	Matrix A		Matrix B		Matrix C	Matrices D and E	Matrix F
Row number in matrices	Dip (direction and value) of discontinuity monitored	Distance from centre line (m)	Dip (direction and value) of discontinuity monitored	Distance from centre line (m)	Distance from centre line (m)	Distance from centre line (m)	Distance from centre line (m)
1							East 6.2
2	West 15°	East 6.3	West 35°	East 7.4	East 6.0		5.8
3						West 13.0	5.4
4					East 3.5		5.0
5	West 70°	East 6.1	West 10°	East 4.0			4.6
6					East 0.6		4.2
7							3.8
8	West 45°	East 3.4	West 45°	East 1.1	West 0.3		3.4
9							3.0
10	West 20°	East 2.9	West 10°	East 0.3	West 3.9		2.6
11							2.2
12	West 50°	East 2.2			West 6.3		1.8
13							1.4
14	West 15°	East 1.7	West 60°	West 0.3			1.0
15							0.6
16							0.2
17	West 40°	East 1.5	West 40°	West 1.9			West 0.2
18							0.6
19							1.0
20	West 30°	West 1.2	West 30°	West 2.5			1.4
21							1.8
22							2.2
23	East 25°	West 5.6	West 40°	West 3.2			2.6
24							3.0
25							3.4
26	West 20°	West 5.9	West 40°	West 4.5			3.8
27							4.2
28							4.6
29			West 65°	West 5.0			5.0
30							5.4
31							5.8
32			West 80°	West 5.6			6.2
33							6.6
34							7.0
35			West 35°	West 7.6			7.4
36							7.8
37							8.2
38							8.6
39							9.0
40							9.4
41							9.8
42							10.2
43							10.6
44							11.0
45							11.4
46							11.8
47							12.2
48							12.6

Table I.3

Matrix A, short gauge deviation readings

		1	2	3	4	5	6	7	8	9	10	11	12	13	14	15	16	17	18	19	20	21	22	23	24	25	26	27	28	29	30	31	32	33	34
P	1	-5	-5	-5	-4	-4	1	-5	-10	-5	-7	-6	-7	-14	-9	-7	-9	-10	-14	-12	-14	-13	-6	-12	-12	-240	-220	-327	-323	-290	-268	-233	-250	-239	-238
P	2	-9	-12	-8	-14	-13	-14	-14	-23	-19	-20	-21	-27	-32	-30	-32	-38	-44	-38	-42	-45	-50	-50	-50	-37	-36	-59	-74	-80	-68	-53	-58	-69	-64	-59
N	3	3	4	11	10	14	7	8	6	10	7	10	8	8	7	2	3	2	1	1	8	7	6	13	35	79	71	70	72	71	108	118	115	116	117
N	4	7	5	-4	-3	-6	-7	-17	-15	-15	-15	-17	-23	-26	-22	-21	-24	-28	-27	-29	-29	-32	-37	-41	-34	-37	-51	-47	-56	-48	-36	-42	-40	-39	-38
P	5	5	16	26	26	26	25	26	22	25	23	23	25	25	25	19	14	24	16	17	24	16	15	-5	-13	-18	-8	-12	-3	-39	-41	-45	-45	-44	-43
N	6	-1	-1	-4	-3	-9	-4	-11	-11	-7	-10	-8	-13	-12	-7	-3	-10	-6	-7	-8	-8	-10	-12	-27	-65	-77	-38	-31	-24	-79	-140	-148	-144	-145	-147
N	7	-6	6	-4	-3	-7	-6	14	7	9	10	8	4	5	9	10	3	1	-1	-1	-3	-3	3	14	51	44	-22	-63	-71	-56	-16	-23	-29	-23	-22
P	8	5	6	13	19	22	18	29	18	29	29	24	26	25	28	27	26	28	24	26	33	23	32	21	-23	-16	-49	-48	-42	-55	-66	-131	-120	-117	-116
N	9	4	6	2	2	2	1	11	3	8	8	8	8	7	11	12	9	7	5	7	7	6	9	17	36	34	-27	-61	-67	-57	-22	-73	-100	-93	-92
N	10	1	2	-2	7	6	9	12	12	18	19	18	10	13	12	0	2	8	3	8	7	6	-34	-41	-59	-60	-59	-52	-37	-55	-41	-93	-72	-62	-62
P	11	-3	4	2	-3	2	-3	-4	-8	-6	-7	-9	-19	-13	-13	-7	-14	-22	-22	-21	-21	-26	-3	-6	11	5	-15	-22	-25	-23	-9	-12	-23	-22	-21
N	12	1	1	3	1	4	1	1	-8	-3	-1	-3	-6	-6	-1	-3	-5	-10	-5	-6	-4	-4	-24	-2	32	34	58	-74	-78	-71	-69	-121	-146	-135	-134
N	13	3	2	12	10	10	11	8	11	16	14	15	12	11	14	12	12	11	11	12	11	12	12	11	-2	-9	-1	13	14	14	-6	-6	16	6	7
P	14	3	-5	-6	-9	-8	-7	-6	-7	-9	-6	-9	-8	-10	-4	-8	-10	-11	-11	-10	-10	-10	-8	-14	-28	-31	-23	-18	-17	-19	-38	-44	-35	-39	-38
N	15	-9	-9	-4	-4	-5	-6	-5	-6	-3	-5	-5	-6	-8	-5	-6	-6	-7	-7	-6	-6	-8	-6	-14	-29	-38	-27	-12	-10	-15	-28	-34	-12	-29	-26
N	16	3	-41	-35	-43	-36	-35	-50	-48	-53	-56	-55	-57	-57	-57	-53	-53	-58	-63	-53	-56	-58	-57	-60	-59	-65	-67	-73	-73	-85	-92	-88	-89	-92	-90
P	17	-8	-1	-1	-1	-1	3	0	0	0	0	0	-6	-8	-4	-5	-5	0	-4	-3	-8	-8	-8	-19	-11	-10	-21	-24	-24	-26	-28	-24	-21	-23	-22
N	18	5	2	3	3	3	3	3	3	3	3	3	2	-1	1	1	1	1	-1	0	1	1	3	5	7	1	-5	-26	-24	-22	-20	-28	-31	-30	-30
N	19	-6	0	2	5	4	1	6	1	4	2	4	4	2	5	6	4	-5	-9	-5	0	-6	-3	-10	-20	-27	-37	-27	-26	-43	-48	-67	-64	-65	-66
P	20	19	5	9	11	12	9	9	9	10	9	10	7	7	7	11	3	2	-2	6	8	5	8	5	12	12	-4	-5	-13	-10	-4	-30	-39	-30	-30
N	21	0	-2	4	4	2	3	1	4	7	5	5	-1	1	1	-4	0	-3	-2	-6	-2	-7	-7	0	44	58	-6	-23	-21	-15	-68	-77	-57	-72	-72
N	22	8	13	13	16	13	16	22	24	25	24	29	31	32	33	37	32	33	29	37	44	67	86	226	490	606	255	124	71	593	648	426	234	244	247
P	23	-3	-13	-28	-28	-26	-26	-36	-34	-35	-35	-29	-31	-28	-23	-17	-23	-23	-33	-25	-21	-5	7	175	441	569	308	89	13	233	551	502	288	198	204
N	24	-2	-5	8	7	14	3	8	9	13	12	15	22	16	21	35	22	12	12	22	29	49	75	-167	-178	-69	250	110	52	314	421	421	254	231	230
N	25	-2	-8	-18	-15	-9	-17	-18	-14	-3	-5	-12	-12	-19	-19	-14	-14	-20	-11	-11	-10	-10	-19	-27	-50	-69	-57	-24	14	-8	-29	-44	-13	-39	-40
P	26	-10	-19	-23	-22	-13	-14	-26	-20	-20	-20	-21	-24	-27	-12	-10	-22	-26	-25	-22	-18	-23	-22	-22	-23	-34	-77	-96	-145	-136	-144	-217	-206	-209	-214
N	27	-4	1	-7	1	2	7	-5	13	15	14	4	11	10	21	15	20	16	14	13	17	11	11	-5	-34	-50	-7	-31	-34	-41	-70	-108	-75	-99	-98

Note: Demec spans measuring normal movement: rows 'N'.
Demec spans measuring parallel movement: rows 'P'.

Table I.4

Matrix B, long gauge deviation readings

		1	2	3	4	5	6	7	8	9	10	11	12	13	14	15	16	17	18	19	20	21	22	23	24	25	26	27	28	29	30	31
N	1	1	2	5	4	5	6	7	5	6	5	8	6	3	12	17	27	18	13	16	-6	-93	-134	-122	-42	30	29	-203	-292	-103	-93	-83
P	2	5	5	12	11	7	8	9	16	14	14	14	20	19	23	22	29	32	31	33	6	7	-147	-102	48	152	102	-54	42	107	110	110
N	3	4	-5	-2	-8	-3	-1	-3	5	2	-2	-1	0	-6	3	-14	-5	-1	-6	0	-11	14	-129	-93	-72	-38	-97	-235	-391	-158	-155	-155
N	4	0	0	1	6	6	12	12	10	7	5	10	12	5	10	4	11	11	12	21	15	-37	-4	-25	-23	-14	-68	-90	-76	-58	-75	-64
P	5	-3	-7	-7	3	13	13	13	14	14	11	8	8	13	4	-1	9	14	19	41	52	12	22	47	97	128	145	133	123	185	184	187
N	6	-1	3	5	-2	7	12	14	12	10	7	8	8	13	9	11	7	11	18	40	25	-34	0	20	28	40	3	2	5	45	48	42
N	7	-14	-19	-33	-58	-63	-70	-75	-104	-118	-126	-125	-124	-130	-137	-154	-165	-172	-175	-168	-144	-111	-93	-144	-392	-481	-529	-495	-483	-483	-483	-483
P	8	-31	-32	-38	-58	-64	-63	-66	-72	-75	-75	-88	-94	-95	-90	-107	-106	-121	-112	-106	-100	-148	-191	-262	-243	-218	-209	-287	-388	-182	-181	-180
N	9	-3	-7	-32	-52	-62	-60	-61	-103	-108	-109	-104	-107	-102	-114	-123	-131	-139	-139	-140	-129	-147	-170	-232	-421	-496	-586	-634	-678	-611	-610	-609
N	10	5	5	9	2	2	2	2	-8	-10	-13	-13	-9	-9	-8	-13	-11	-14	-18	-13	-8	-13	-20	-57	-185	-223	-270	-283	-322	-323	-323	-314
P	11	15	8	20	22	25	35	39	52	62	65	63	62	72	69	71	89	70	79	85	83	70	63	78	366	490	634	629	608	682	681	681
N	12	-1	3	2	22	23	30	36	43	43	40	40	41	42	50	55	60	54	57	56	52	21	4	22	57	88	95	71	83	86	87	89
N	13	-22	-14	-22	-22	-27	-20	-22	-19	-26	-31	-27	-23	-32	-34	-38	-45	-45	-51	-50	-50	-29	-28	-27	-134	-165	-192	-210	-195	-232	-231	-230
P	14	-8	-2	-10	-9	-13	-15	-14	-16	-17	-19	-22	-16	-24	-23	-24	-34	-34	-33	-35	-40	-32	-41	-40	-82	-92	-105	-122	-121	-127	-126	-125
N	15	-13	-17	-15	-8	-11	-14	-16	-7	-11	-15	-13	-8	-15	-17	-21	-22	-21	-23	-15	-16	-23	-30	-2[illegible]	-83	-98	-115	-167	-143	-146	-144	-147
N	16	4	4	9	9	13	9	10	17	17	14	6	10	9	9	4	4	9	5	13	-17	-55	-78	-98	-83	-79	-58	-94	-130	-72	-71	-65
P	17	2	3	4	10	6	9	6	10	3	-1	4	-4	-5	2	-10	8	7	2	13	-24	-96	-40	-62	-98	-19	-21	-52	-117	-117	-106	-106
N	18	-5	-5	5	-2	0	1	1	-1	-1	-6	-5	-5	-5	-7	-10	-7	-4	-8	-1	-39	-98	-145	-183	-160	-116	-124	-160	-207	-190	-179	-210
P	19	3	0	-7	-2	-2	3	5	5	4	0	4	8	5	-5	1	3	-1	-5	-4	1	20	25	-9	-81	-107	-121	-120	-127	-99	-128	-97
N	20	-2	-3	-1	6	2	6	7	0	-3	1	1	7	-3	1	0	0	5	8	24	21	-46	-133	-185	-120	-72	-48	-27	-33	-66	-63	-71
P	21	-1	4	0	2	7	12	15	3	3	9	3	14	11	11	8	7	10	6	7	7	19	19	-33	-59	-58	-68	-70	-109	-76	-75	-77
N	22	1	8	9	15	16	19	22	11	13	18	13	19	22	24	25	29	27	28	42	57	-23	-85	-155	-59	-62	-51	-31	-33	80	77	73
N	23	6	-5	0	2	4	6	7	-2	-3	-6	-1	-1	3	4	0	5	3	2	5	-6	-48	-83	-94	68	112	146	125	111	167	167	165
P	24	-26	-20	-28	-22	-23	-24	-26	-35	-42	-44	-43	-39	-42	-48	-49	-51	-57	-55	-51	-60	-81	-88	-114	-206	-229	-248	-278	-290	-290	-290	-284
N	25	-9	-8	-14	-11	-13	-10	-9	-11	-11	-11	-11	-6	-6	-13	-16	-21	-19	-14	-12	-2	14	18	8	4	2	22	22	25	21	22	23
N	26	-8	-5	-8	-7	-7	-6	-6	-3	-3	-4	-3	-7	-3	-4	-8	-1	1	-2	-4	-57	9	8	-24	18	30	-41	-77	-23	45	43	45
P	27	-6	-5	-11	-5	-5	-8	-7	-6	-6	-9	-8	-2	-6	-4	-6	-5	-1	-6	-2	-6	9	3	32	58	64	41	43	99	107	110	118
N	28	-3	0	1	9	11	11	[illegible]	12	12	6	6	13	9	5	7	8	10	11	12	-54	-46	-233	-201	36	69	11	-154	-176	35	50	101
N	29	-9	-9	-22	-12	-22	-14	-11	-17	-14	-18	-21	-7	-11	-17	-22	-27	-28	-26	-10	-26	-137	-158	-257	-172	-166	-154	-154	-177	-181	-179	-172
P	30	-23	-29	-46	-42	-34	-57	-55	-58	-59	-73	-71	-68	-73	-74	-88	-101	-90	-94	-68	-83	-122	-130	-148	-204	-202	-216	-234	-268	-243	-241	-246
N	31	-19	-8	-8	-12	-13	-13	-13	-13	-16	-16	-14	-21	-21	-17	-20	-17	-22	-24	-32	-46	29	17	-43	-19	-9	-13	-19	-20	-2	-5	-4
N	32	15	13	5	4	3	4	4	7	-5	3	6	5	1	-2	-5	-3	3	-4	8	5	-20	-6	-6	4	0	3	-5	0	-22	-10	-11
P	33	-4	8	2	5	9	10	11	4	2	-1	-1	-6	4	-5	-6	-3	-2	-8	-9	-88	-148	-159	-69	-80	-65	-158	-230	-196	-66	-95	-124
N	34	-4	1	-11	-7	-4	-7	-6	-7	-10	-11	-12	-13	-10	-17	-19	-16	-12	-16	-13	-48	-74	-83	-95	-66	-44	-82	-95	-118	-34	-68	-85
N	35	4	3	-4	6	2	3	4	3	1	2	0	0	-7	-5	-7	-7	-6	-7	-1	-10	-12	-43	-153	-195	-189	-145	-115	-174	-157	-173	-214
P	36	-1	0	0	-6	1	-2	0	-1	-1	-7	-9	-19	-22	-11	-17	-8	-12	-15	-15	-77	-254	-336	-427	-427	-382	-412	-476	-574	-620	-615	-655
N	37	0	0	0	2	-1	-2	-1	-5	-7	-7	-8	-16	-18	-11	-18	-19	-24	-33	-36	-110	-222	-223	-430	-430	-348	-437	-444	-503	-232	-255	-270

Note: Demec spans measuring normal movement: rows 'N'.
Demec spans measuring parallel movement: rows 'P'.

Table I.5

Matrix C, medium gauge deviation readings

	1	2	3	4	5	6	7	8	9	10	11	12	13	14	15	16	17	18	19	20	21	22	23	24	25	26	27
1	-3	-3	-3	0	3	-1	-5	-3	-6	0	-4	-11	-3	-4	-4	-11	-23	-32	-14	-20	-13	-29	-38	-32	-28	-23	-23
2	5	6	5	5	5	5	6	4	2	4	6	3	12	7	10	-5	-26	-34	-1	-5	7	-30	-63	-45	-7	-13	-14
3	1	-2	-2	-1	2	5	8	17	17	26	31	35	32	36	33	123	93	146	173	172	177	128	176	187	197	192	193
4	0	1	0	4	4	3	-6	0	-1	0	-1	-1	-2	0	0	0	0	8	-4	6	1	-3	1	1	6	7	6
5	5	6	5	5	5	8	15	16	16	15	15	17	19	16	20	15	14	13	18	14	15	10	6	-2	10	5	6
6	2	7	5	10	10	7	15	9	12	14	20	21	21	19	15	10	-12	-20	2	19	24	14	-7	-23	26	23	22
7	-7	-1	-3	-3	-3	-5	-5	-4	1	-1	-1	-3	2	-2	-6	-5	-10	-16	-4	-11	-8	-12	-21	-21	-20	-15	-22
8	-1	-3	-2	-3	-2	0	-1	0	1	0	0	3	2	2	3	3	-2	-4	-1	-3	0	-3	-14	-17	-10	-8	-4
9	-8	1	1	0	1	-2	0	1	9	2	8	11	6	8	-5	1	-14	-6	-12	-18	-17	-19	-28	-36	-27	-30	-29
10	3	0	0	0	2	-1	0	-4	0	-5	-1	3	5	6	6	-26	-83	-93	-73	-49	-36	-80	-121	-122	-56	-61	-62
11	3	-3	-2	-2	-3	0	2	-7	2	10	3	1	2	-3	0	-37	-64	-75	-39	-53	-27	-88	-102	-89	-72	-75	-79
12	3	5	4	1	3	1	8	0	3	0	-2	-6	-8	-7	-7	-26	-34	-44	-11	-12	3	-30	-44	-33	-2	-22	-21

Table I.6

Matrix D, short gauge deviation readings

	1	2	3	4	5	6	7	8	9	10	11	12	13	14	15	16	17	18	19	20	21	22	23	24	25	26	27	28	29	30	31
1	0	-9	-9	-4	-8	-9	-9	-9	-10	-12	-7	-5	-10	-4	-2	1	-5	-1	-1	0	-5	2	-8	-3	0	-1	-5	-3	-7	-3	-6
2	-6	-4	-2	0	0	4	3	3	2	4	7	12	9	13	13	7	10	8	10	5	6	10	3	17	20	24	16	13	9	12	12
3	-2	-2	-3	-3	-3	-3	-3	-4	-3	-3	-1	-2	-3	-2	-3	-4	-1	-3	-5	-3	2	11	9	19	17	25	21	30	27	29	30
4	2	0	7	4	4	4	0	0	2	3	4	7	8	12	4	4	5	0	3	1	-3	-1	0	7	11	8	5	5	10	7	8
5	0	-1	2	4	4	6	5	2	0	1	3	6	6	5	-6	6	6	7	9	10	12	14	12	8	10	8	13	12	15	14	15
6	0	1	1	0	2	4	3	3	3	1	1	7	4	7	6	9	8	10	11	15	22	26	22	18	19	17	20	21	25	22	23

Table I.7

Matrix E, long gauge deviation readings

	1	2	3	4	5	6	7	8	9	10	11	12	13	14	15	16	17	18	19	20	21	22	23	24	25	26	27	28	29	30	31
1	4	4	-5	-4	-7	-4	-5	-5	-7	-7	-7	-2	-1	-7	1	-1	-1	-1	5	0	0	8	21	55	65	71	61	46	0	6	7
2	-2	-2	-5	-6	-6	-3	-4	-5	-5	-7	-7	-5	-4	-3	-4	-5	-6	-7	-5	-12	-4	8	22	61	79	86	72	56	6	10	6
3	3	-1	-7	-4	-8	-7	-7	-7	-7	-6	-11	-8	-12	-16	-12	-13	-13	-15	-10	-6	-8	8	18	47	58	65	47	31	-2	3	6
4	-1	0	-1	-1	-4	-1	-1	-1	-1	-1	-1	-1	-6	-4	-5	-5	-3	-3	-6	-6	-4	-9	-1	-41	-47	-45	-43	-40	-40	-40	-40
5	-2	-2	1	6	4	8	8	9	9	6	15	16	13	15	8	11	15	17	20	13	6	5	23	-9	-13	-15	-16	-11	-8	-8	-3
6	0	-1	-6	0	2	8	6	10	10	9	18	20	16	20	13	17	22	25	24	25	26	26	38	4	-2	-1	-1	5	8	8	14

Table I.8

Matrix F, long gauge deviation readings

	1	2	3	4	5	6	7	8	9	10	11	12	13	14	15	16	17	18	19	20	21	22	23	24	25	26	27
1	1	4	6	2	3	6	4	5	3	-7	-20	-25	-23	-18	-24	-24	-22	-16	-21	-31	-20	-25	-35	-39	-40	-49	-48
2	0	3	2	1	0	4	4	7	26	26	17	17	16	21	22	21	21	21	21	17	29	24	22	23	2	2	3
3	-1	0	1	-1	4	6	-3	-21	-26	-30	-35	-31	-32	-33	-29	-29	-28	-30	-33	-30	-19	-35	-49	-65	-64	-61	-63
4	-1	-1	-2	-2	-8	-4	-8	-17	-16	-16	-27	-20	-22	-21	-17	-22	-18	-20	-22	-25	-10	-19	-27	-34	-34	-34	-37
5	0	1	1	1	-15	-24	-44	-53	-61	-65	-59	-62	-61	-64	-59	-59	-55	-57	-63	-61	-53	-79	-89	-104	-98	-97	-96
6	0	0	-2	1	5	14	16	20	24	17	13	6	5	5	9	5	8	1	5	-5	-2	-17	-10	-10	-16	-12	-16
7	-1	-3	0	0	-19	-30	-44	-29	-43	-16	-40	-56	-57	-62	-58	-66	-50	-60	-61	-90	-103	-159	-150	-146	-156	-150	-159
8	1	0	0	4	2	16	18	20	18	31	21	20	16	18	25	19	25	25	21	10	13	4	-8	2	6	8	10
9	-2	0	-2	-2	-9	-3	0	-2	0	-2	-14	-24	-26	-26	-20	-26	-19	-22	-25	-44	-46	-50	-53	-47	-52	-52	-46
10	-1	0	2	2	6	12	22	18	19	24	14	12	14	20	25	20	25	24	21	23	30	42	44	44	48	47	49
11	-1	0	-1	-1	-15	-9	1	-4	4	-10	-22	-37	-40	-39	-33	-40	-30	-35	-41	-58	-81	-86	-50	-49	-61	-58	-57
12	-1	-1	0	0	9	8	9	-9	-16	5	44	56	64	70	76	69	86	79	189	141	174	177	105	62	62	64	63
13	-1	0	1	1	-10	-17	-20	-21	-25	-42	-82	-78	-202	-245	-242	-252	-248	-258	-312	-733	-935	-1119	-1105	-1096	-1086	-1090	-1080
14	-2	-1	-3	0	17	21	33	39	38	31	32	22	18	21	28	26	32	26	27	37	48	46	44	47	47	47	54
15	1	-1	2	2	-7	-7	-15	-18	-24	-19	-9	-11	-15	-10	-6	-9	-5	-7	-14	-17	-13	-24	-44	-48	-42	-44	-50
16	1	-2	2	-6	-18	-30	-38	-41	-51	-51	-56	-56	-61	-57	-53	-54	-52	-56	-62	-82	-80	-86	-94	-103	-109	-103	-100
17	-1	5	0	1	11	16	39	47	47	-10	44	24	20	17	28	18	37	18	6	-13	-25	-44	-32	-38	-55	-49	-48
18	0	1	1	-1	-16	-15	-34	-44	-66	-36	-25	-28	-27	-26	-21	-25	-22	-22	-26	-29	-28	-36	-68	-79	-56	-68	-67
19	0	-8	-5	-5	-17	-17	-28	-39	-46	-44	-5	-17	-19	-18	-10	-16	-9	-13	-28	-56	-68	-90	-111	-115	-115	-114	-113
20	0	2	4	4	-12	-6	2	13	11	5	19	-1	-6	-9	6	8	16	7	20	-13	-15	-44	-44	-40	-30	-36	-41
21	-1	3	3	4	2	-1	-8	-21	-24	-31	-38	-40	-37	-34	-32	-36	-26	-25	-17	-16	-2	-25	-49	-45	-45	-46	-55
22	0	1	5	4	0	0	-12	-30	-36	-48	-72	-78	-80	-84	-77	-84	-69	-79	-81	-78	-64	-84	-101	-102	-116	-114	-120
23	1	1	0	0	8	12	25	15	8	-6	-23	-40	-42	-47	-39	-47	-31	-43	-53	-58	-48	-58	-61	-62	-61	-60	-65
24	-1	0	-1	-2	-9	0	19	6	27	11	-41	-69	-74	-80	-72	-81	-67	-81	-86	-113	-121	-126	-105	-120	-115	-114	-116
25	-1	4	1	3	0	-3	-20	-48	-60	-67	-106	-102	-105	-102	-94	-99	-86	-96	-105	-92	-25	-42	-92	-100	-103	-99	-97
26	-5	7	6	5	14	21	21	22	21	9	-14	-53	-61	-68	-65	-72	-56	-75	-77	-123	-244	-245	-155	-161	-166	-165	-164
27	4	0	0	0	-14	-19	-56	-76	-87	-73	34	26	29	27	31	23	36	32	32	19	22	14	-41	-27	-19	-21	-26
28	1	0	5	4	7	4	15	20	18	36	13	-2	0	-1	0	-2	14	-3	-6	-30	-30	-50	-26	-31	-36	-31	-35
29	3	0	-1	1	-14	-14	-25	-33	-33	-53	-38	-46	-45	-41	-42	-42	-40	-42	-30	-40	-35	-49	-71	-69	-74	-73	-82
30	-1	-1	2	-1	-4	-5	-29	-39	-39	-40	-45	-44	-40	-36	-38	-40	-31	-35	-33	-30	-11	-14	-42	-40	-40	-40	-34
31	-1	7	7	8	9	15	39	44	45	73	44	37	40	41	40	36	38	39	46	31	26	37	74	66	70	67	77
32	-1	-1	-1	0	8	6	30	25	29	19	24	21	22	27	24	27	26	28	38	27	31	21	20	26	20	24	26
33	-1	-3	-2	-3	-14	-14	-27	-36	-42	-49	-56	-50	-47	-41	-40	-36	-41	-36	-40	-20	-7	-5	-18	-21	-25	-24	-23
34	-1	-10	-10	-10	-17	-17	-18	-27	-27	-39	-48	-51	-47	-45	-43	-43	-44	-43	-46	-51	-44	-39	-58	-51	-59	-57	-56
35	-3	-1	-8	-7	-8	-8	-21	-30	-28	-36	-47	-47	-42	-35	-36	-39	-40	-36	-35	-49	-41	-28	-35	-40	-45	-44	-45
36	-1	0	-1	-1	14	22	63	84	90	92	100	94	91	101	102	101	97	99	102	118	97	102	168	167	179	173	178
37	0	1	1	1	0	0	-24	-37	-41	-45	-56	-50	-48	-46	-43	-42	-41	-44	-44	-50	-39	-30	-79	-73	-85	-80	-84
38	-2	-2	-2	-2	-5	-2	3	4	6	6	1	3	3	6	7	9	9	9	11	16	28	26	29	35	25	25	26
39	-1	-1	-1	-1	-16	-15	-26	-32	-25	-21	-29	-25	-25	-24	-21	-22	-21	-21	-18	-27	-7	-1	-43	-36	-36	-37	-37
40	1	-1	0	0	20	22	51	48	39	29	30	23	25	35	37	32	22	19	22	61	54	50	119	109	104	106	101
41	-3	-2	-1	-1	-14	-15	-42	-59	-57	-52	-58	-56	-58	-54	-52	-45	-37	-40	-42	-62	-51	-56	-82	-82	-87	-86	-85
42	-2	-2	-2	-1	-3	-2	20	10	11	19	10	14	13	22	20	16	29	21	25	18	19	19	12	12	14	13	9
43	-2	-3	-3	-3	11	7	8	9	12	9	2	-1	3	4	6	6	4	6	6	12	-1	-3	13	17	16	17	18
44	-3	-2	-4	-1	18	1	-2	2	11	2	-20	-25	-26	-14	-17	-15	-19	-17	-18	-1	-10	-17	19	7	16	16	17
45	-1	0	-1	2	-12	-17	-17	-23	-27	-22	-2	2	3	4	9	-6	1	12	9	-28	-12	8	-31	-12	-20	-20	-18
46	0	-1	-1	-1	0	6	39	67	72	66	69	66	64	68	68	70	65	66	67	80	59	52	132	124	132	131	132
47	-2	-2	-2	-2	3	7	5	-11	-7	-15	-16	-16	-16	-16	-7	-11	-10	-10	-5	5	27	30	6	12	0	4	5
48	0	-1	-1	-1	-6	-4	-11	-14	-14	-20	-3	2	6	12	13	12	10	13	14	45	61	50	31	23	20	25	26

APPENDIX J

DETAILS OF THE FINITE ELEMENT ANALYSIS TECHNIQUE

The techniques adopted when modelling the behaviour of a tunnel/ground situation using finite element methods can be divided into four stages:

1. Construction of a finite element mesh consisting of an assemblage of simplex triangular elements. The mesh models to scale in two dimensions a section through the ground and tunnel, normal to the tunnel axis.

2. The statement of boundary conditions and material properties.

3. The formulation of the mesh, material properties and boundary conditions into the finite element computer program, followed by computer processing to give the required output in terms of stress and deformation.

4. Extraction, presentation and interpretation of the appropriate results from the computer output.

J.1 Construction of the finite element mesh

The mesh used in the analysis is shown in Figure 8.1. The mesh, constructed within a rectangular framework models to scale the right-hand half of the tunnel system. Each triangle, or element, is allocated an element number. Each triangle corner, or node, is allocated a node number and located in two dimensional space in terms of xy coordinates.

The mesh is constructed to satisfy two main criteria:

1. Smaller elements are used in areas likely to produce steeper stress gradients.

2. The difference between node numbers for any element is kept at a minimum. This is done to economise on computer storage space by reducing the size of the banded matrix.

J.2 Statement of boundary conditions and material properties

Boundary conditions may be considered in terms of the four margins to the mesh.

1. The left-hand margin of the mesh represents a line of symmetry, the nodes of this margin are therefore constrained to move in the vertical direction only.

2. The nodes on the lower margin of the mesh, being sufficiently far from the tunnel are constrained to move in the horizontal direction only.

3. The nodes on the upper margin of the mesh (at ground level) are not loaded and are free to move in both vertical and horizontal directions, except as specified in 1 above.

4. The nodes on the right-hand margin of the mesh are loaded and are free to move in both vertical and horizontal directions, except as specified in 2 above.

The boundary conditions described above are summarised diagrammatically in Figure J.1.

The material properties for the mesh are obtained from tests on samples of the ground to be modelled in the finite element analysis. The following properties are used:

1. bulk density

2. Young's modulus, input as a multi-linear stress-strain curve defined in terms of strain increments

3. Poisson's ratio, ν, and the horizontal earth pressure at rest, K_o. An approximate value of K_o may be obtained from a knowledge of the Poisson's ratio ν, from the relation $K_o = \frac{\nu}{(1-\nu)}$ (Coates, 1970).

Where a tunnel is lined, material properties for both the ground and the lining must be defined.

J.3 Computer analysis

Much of the description in this Section is based directly on Zienkiewicz and Cheung (1967) and Roberts (1970). The mesh is formulated numerically in terms of element numbers, each of which is defined by three node numbers and node co-ordinates. These data, together with boundary conditions and material properties are analysed by the computer program. The characteristic behaviour of each element is formulated in terms of its size, shape, position and material properties. Once compatibility between elements and boundary conditions is achieved the behaviour of the continuum is satisfactorily modelled.

J.3.1 The simplex triangular element

The triangular element is adopted for two-dimensional analysis because its formulation is simple and it is readily adaptable to modelling complicated structures. Figure J.2 shows a typical triangular element with nodes i, j, m. The displacements δ of each node have two components, vertical v and horizontal u.

For node i

$$\left\{ \delta_i \right\} = \left\{ \begin{matrix} u_i \\ v_i \end{matrix} \right\}$$

There are therefore three paired components of nodal displacements required to describe the displacement $\{\delta\}^e$ of the element. These may be listed as a vector

$$\{\delta\}^e = \left\{ \begin{matrix} \delta_i \\ \delta_j \\ \delta_m \end{matrix} \right\}$$

The displacement of any point within the element must be uniquely defined by these components. Considering the displacement $(u,v) = \{f\}$ of this point within the element in terms of two polynomials

$$u = \alpha_1 + \alpha_2 x + \alpha_3 y$$
$$v = \beta_1 + \beta_2 x + \beta_3 y$$

The six constants can be evaluated by solving the six simultaneous equations produced by considering the nodal coordinates and nodal displacements for the whole element.

$$u_i = \alpha_1 + \alpha_2 x_i + \alpha_3 y_i$$
$$v_i = \beta_1 + \beta_2 x_i + \beta_3 y_i$$
$$u_j = \alpha_1 + \alpha_2 x_j + \alpha_3 y_j$$
$$v_j = \beta_1 + \beta_2 x_j + \beta_3 y_j$$
$$u_m = \alpha_1 + \alpha_2 x_m + \alpha_3 y_m$$
$$v_m = \beta_1 + \beta_2 x_m + \beta_3 y_m$$

Adopting matrix techniques we therefore have

$$\begin{Bmatrix} u_i \\ v_i \\ u_j \\ v_j \\ u_m \\ v_m \end{Bmatrix} = \begin{bmatrix} 1 & 0 & x_i & 0 & y_i & 0 \\ 0 & 1 & 0 & x_i & 0 & y_i \\ 1 & 0 & x_j & 0 & y_j & 0 \\ 0 & 1 & 0 & x_j & 0 & y_j \\ 1 & 0 & x_m & 0 & y_m & 0 \\ 0 & 1 & 0 & x_m & 0 & y_m \end{bmatrix} \begin{Bmatrix} \alpha_1 \\ \beta_1 \\ \alpha_2 \\ \beta_2 \\ \alpha_3 \\ \beta_3 \end{Bmatrix} \quad \ldots\ (J.1)$$

$$\text{ie} \quad \{\delta\}^e = [A] \cdot \{a\} \quad \ldots\ (J.2)$$

from Equation J.1

$$u = \frac{1}{2\Delta} \left\{ (a_i + b_i x + c_i y)u_i + (a_j + b_j c + c_j y)u_j + (a_m + b_m x + c_m y)u_m \right\} \quad \ldots\ (J.3)$$

and

$$v = \frac{1}{2\Delta} \left\{ (a_i + b_i x + c_i y)v_i + (a_j + b_j x + c_j y)v_j + (a_m + b_m x + c_m y)v_m \right\} \quad \ldots\ (J.4)$$

in which Δ = area of triangle ijm

and $a_i = x_j y_m - x_m y_j$

$b_i = y_j - y_m$

$c_i = x_m - x_j$

$a_j = x_m y_i - x_i y_m$

$b_j = y_m - y_i$

$c_j = x_i - x_m$

$a_m = x_i y_j - x_j y_i$

$b_m = y_i - y_j$

$c_m = x_j - x_i$

Therefore the displacements $(u,v) = \{f\}$ at any point within the element may be defined by

$$\{f\} = [N] \{\delta\}^e \qquad \ldots. (J.5)$$

in which the components of $[N]$ are functions of position within the element.

The total plane strain at any point within the element can be defined by three components (Timoshenko and Goodier, 1951)

$$\{\varepsilon\} = \begin{Bmatrix} \varepsilon_x \\ \varepsilon_y \\ \gamma_{xy} \end{Bmatrix} = \begin{Bmatrix} \frac{\partial u}{\partial x} \\ \frac{\partial v}{\partial y} \\ \frac{\partial u}{\partial y} + \frac{\partial v}{\partial x} \end{Bmatrix}$$

Using Equations J.3 and J.4 we obtain

$$\{\varepsilon\} = \frac{1}{2\Delta} \begin{bmatrix} b_i & 0 & b_j & 0 & b_m & 0 \\ 0 & c_i & 0 & c_j & 0 & c_m \\ c_i & b_i & c_j & b_j & c_m & b_m \end{bmatrix} \{\delta\}^e$$

ie $\{\varepsilon\} = [B] \{\delta\}^e \qquad \ldots. (J.6)$

Assuming an elastic behaviour and ignoring initial strains, the relation between stresses and strains will be of the linear form

$$\{\sigma\} = [D] \{\varepsilon\} \qquad \ldots. (J.7)$$

where $[D]$ is a matrix containing the appropriate material properties.

The total plane stress within the element may be defined by three components

$$\{\sigma\} = \begin{Bmatrix} \sigma_x \\ \sigma_y \\ \tau_{xy} \end{Bmatrix}$$

The D matrix may be determined by considering the isotropic stress-strain relation

$$\varepsilon_x = \frac{1}{E}\sigma_x - \frac{\nu}{E}\sigma_y$$

$$\varepsilon_y = -\frac{\nu}{E}\sigma_x + \frac{1}{E}\sigma_y$$

$$\gamma_{xy} = \frac{2(1+\nu)}{E}\tau_{xy}$$

giving $[D] = \frac{E}{1-\nu^2}\begin{bmatrix} 1 & \nu & 0 \\ \nu & 1 & 0 \\ 0 & 0 & \frac{(1-\nu)}{2} \end{bmatrix}$

where E is Young's modulus and ν is Poisson's ratio of the material.

The starting point for analysis of the triangular element was based on nodal displacements δ_i. It is now necessary to consider the nodal forces for the element, $\{F\}^e$.

Let $\{F\}^e = \begin{Bmatrix} F_i \\ F_j \\ F_m \end{Bmatrix}$

define the nodal forces which are statically equivalent to the boundary

stresses and distributed loads on the element. Each of the forces $\{F_i\}$ contains the same number of components as the corresponding nodal displacements $\{\delta_i\}$.

The distributed loads $\{p\}$ are defined as the forces acting on a unit volume of material with directions corresponding to those of the displacements $\{f\}$ at that point.

Referring to Figure J.2 the nodal forces for node i, $\{F_i\}$ are $\begin{Bmatrix} U_i \\ V_i \end{Bmatrix}$. For the distributed load $\{p\}$ we have the body force components $\begin{Bmatrix} X \\ Y \end{Bmatrix}$.

By imposing an arbitrary nodal displacement and equating external and internal work done by the forces during this displacement it is possible to make the nodal forces statically equivalent to the actual boundary stresses and distributed loads.

Let $\{\delta^*\}^e$ be the arbitrary nodal displacement, and $\{f^*\}$ and $\{\varepsilon^*\}$ the corresponding displacements and strains within the element.

From Equations J.5 and J.6

$$\{f^*\} = [N]\{\delta^*\}^e$$

and $$\{\varepsilon^*\} = [B]\{\delta^*\}^e$$

By equating the work done by the nodal forces to the sum of the products of the individual force components and corresponding displacements we get

$$(\{\delta^*\}^e)^T . \{F\}^e = \text{work done by nodal forces}$$

The internal work per unit volume done by the stresses and distributed forces is

$$\{\varepsilon^*\}^T\{\sigma\}-\{f^*\}^T\{p\}$$

ie $$(\{\delta^*\}^e)^T([B]^T\{\sigma\} - [N]^T\{p\})$$

Equating external work with the total internal work, obtained by integrating over the volume of the element, we get

$$(\{\delta^*\}^e)^T \{F\}^e = (\{\delta^*\}^e)^T (\int [B]^T\{\sigma\}d(vol) - \int [N]^T\{p\}\, d(vol))$$

where the integration is with respect to volume.

Substituting Equations J.6 and J.7

$$\{F\}^e = (\int [B]^T[D][B]d(vol))\ \{\delta\}^e - \int [N]^T\{p\}d(vol)$$

in which the nodal forces due to distributed loads $\{F\}_p^e$ are

$$\{F\}_p^e = -\int [N]^T\{p\}d(vol)$$

For two-dimensional elements, which in effect have a constant thickness, the matrices under the integral are constant with respect to volume.

$$\{F\}^e - \{F\}_p^e = [k]^e\{\delta\}^e$$

where

$$[k]^e = [B]^T\,[D][B]\Delta \qquad \ldots\ (J.8)$$

$[k]^e$ is known as the element stiffness matrix, and forms part of the composite stiffness matrix [K]for the whole continuum considered. By applying a force matrix [F] of all nodal forces, resolved into their x and y directions, to the stiffness matrix the displacements of the nodes can be determined as solutions to a large set of simultaneous equations

$$[\delta] = [F].[K^{-1}] \qquad \ldots\ (J.9)$$

The strains, and therefore the stresses, in individual elements may be calculated from the displacements of the nodes using Equations J.2, J.6 and J.7.

The stiffness matrix [K] has the dimensions 2N x 2N where N is the number of nodes in the structure. Maxwell's Reciprocal Theorem states that if a deflection is caused in a structure at a point m by a force acting at point n, then the same force acting at m will cause the same deflection at n, from which it follows that $[k]^e_{nm} = [k]^e_{mn}$. The compsite stiffness matrix is therefore symmetrical about the diagonal. In addition, nodes that are not connected directly through an element will have a stiffness coefficient of zero. Therefore only a small part of the composite stiffness matrix need be examined during computation, enabling great savings in computer storage space.

J.3.2 The computer program

The previous Section summarised some of the basic mathematical procedures used in finite element analysis. This Section deals with the operations of the computer program. This program was written in the Engineering Geology Laboratories of the University of Durham originally as an Engineering Geology M.Sc. Advanced Course dissertation by Roberts (1970) but subsequently modified by Attewell and Woodman (Attewell, 1975) in order to achieve economy of storage. This economy of storage was achieved by introducing a new banded matrix facility which not only

facilitated banded matrix decomposition but also created a true multi-linear stress-strain facility through both tensile and compressive stress regimes.

The computer program consists of a number of subroutines, each of which performs a specific job. The functions of the important subroutines are listed below.

Subroutine INPUT

This subroutine has the sole function of reading all the input data to the program and writing most of it out again. All arrays and variables are placed in a common store block such that a variable used in several subroutines is stored in the same location for each subroutine, thus achieving storage economy.

Subroutine ELEMST (I)

Subroutines with the notation (I) each work on individual elements and are therefore called inside a loop which is operated for each element in turn.

Subroutine ELEMST formulates the stiffness matrix for each element, in terms of the nodal co-ordinates and material properties, a procedure involving the formation of $[k]^e$ in Equation J.8 using matrix algebra. Various subroutines for matrix operations are used which are called from the Scientific Subroutine Package (SSP) which is supplied by IBM as a standard program available to all users.

Subroutine TRIG (I)

This subroutine calculates the area of each element using the nodal co-ordinates.

Subroutine POST(I)

This subroutine places the terms of each element stiffness matrix into the relevant places in the overall banded stiffness matrix [K]. It was mentioned earlier that [K] is symmetrical about the diagonal, therefore only half of the matrix is stored and used. As the stiffness matrix [K] is built up, non zero terms will only appear where nodes are connected directly to one another. Therefore the bandwidth, ie the range within which non zero terms can occur, is fixed by the largest difference between node numbers for any element. This criterion was noted earlier when constructing the mesh in order to achieve the greatest economy in computer storage space.

Subroutine LORAX

In the case of a lined tunnel this subroutine calculates the equivalent nodal forces for the tunnel lining loading situation.

Subroutine LOAD

This subroutine calculates, when appropriate, the equivalent nodal forces for the lining weight loading.

Subroutine ULOAD

This subroutine applies any appropriate nodal loadings specified in the input data, such as vertical loading due to overburden or an air pressure in a tunnel.

Subroutine BOUND

This subroutine fixes the boundary conditions discussed earlier. The input data specify the constraints on the boundary nodes in terms of freedom to move

in the x and y directions. Nodal constraint in the program is achieved by modifying the appropriate terms of the stiffness matrix [K] such that interaction between the constrained node and its neighbours is minimised whilst the constrained node itself is fixed.

Subroutine CHOLS

This subroutine is the solution routine for the simultaneous Equations J.9. It is based on the Choleski 'square root' method of solution, decomposing the stiffness matrix and then using a back substitution to find the nodal displacements.

Subroutine STRAIN (I)

This subroutine uses Equations J.2, J.6 and J.7 to find the strains in each element using the nodal displacements found by CHOLS.

Subroutine MATER (I)

This subroutine is used to alter material properties between load increments. Two load increments are used, operating on a multi-linear stress-strain curve describing the material properties. Following the first load increment, material properties are re-specified for each element according to the amount of strain in the element.

Subroutine PRINC

This subroutine calculates the principal stresses (and their directions) and the radial and tangential stresses to the tunnel from the general stress values σ_x, σ_y and τ_{xy} using matrix algebra subroutines called from the SSP.

The operation of the subroutines, described above, in the finite element program is summarised in Figure J.3.

J.4 Extraction, presentation and interpretation of the computer output

The computer output presents information on the incremental and total stresses and strains at the centroid of each element. These data include the following:

1. Direction and magnitude of the principal stresses and principal strains.
2. Vertical and horizontal stresses and strains, together with shear stresses and strains.
3. Radial and tangential stresses and strains together with shear stresses and strains related to any specified centre.

In addition, nodal movements, expressed as x and y components are presented for each load increment. To obtain the total nodal movements it is necessary to sum the nodal movements for each load increment, in this case two.

Presentation and interpretation of the finite element analysis output are discussed in Chapter 8.

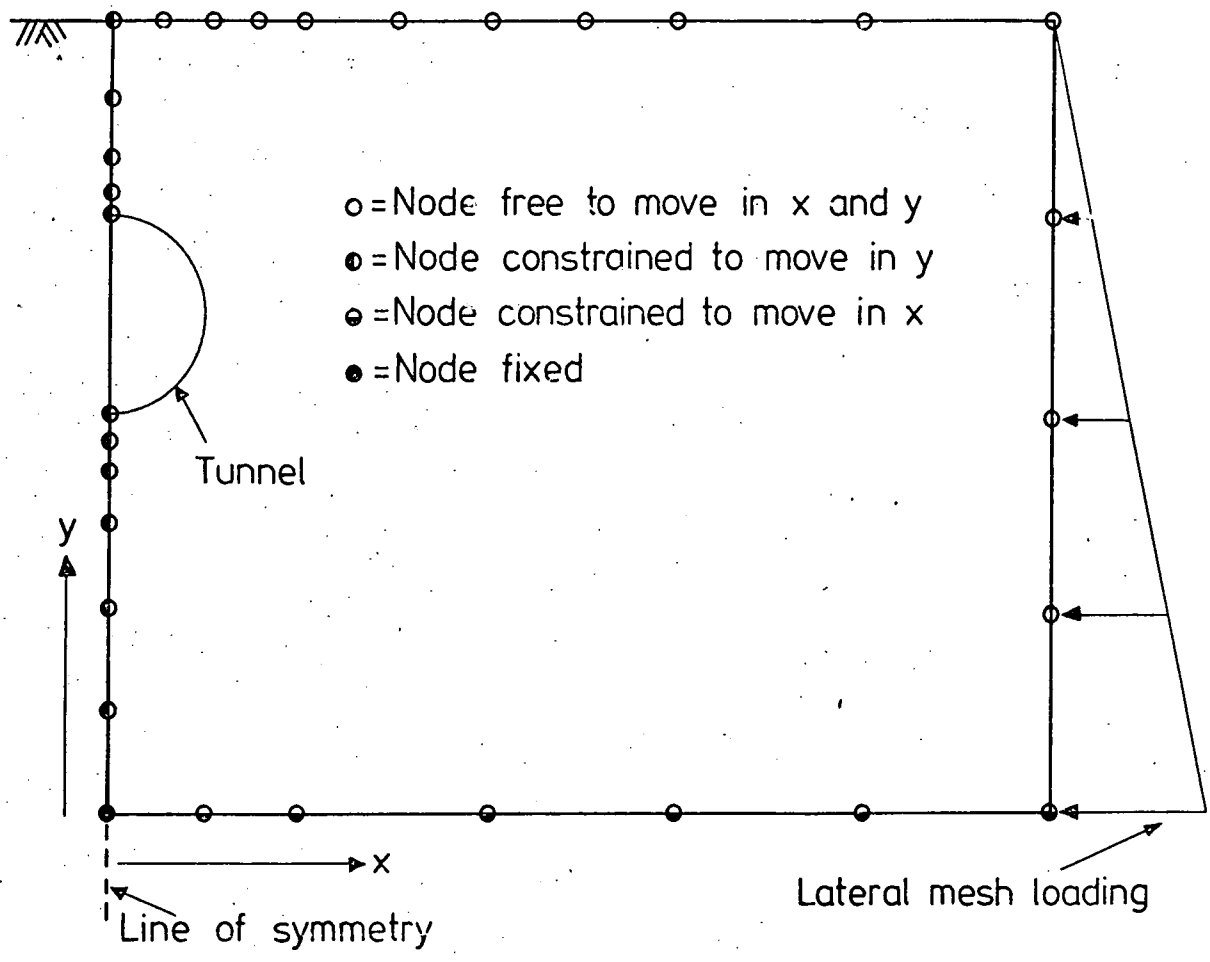

Fig. J.1 DIAGRAMMATIC SUMMARY OF BOUNDARY CONDITIONS APPLIED TO FINITE ELEMENT MESH.

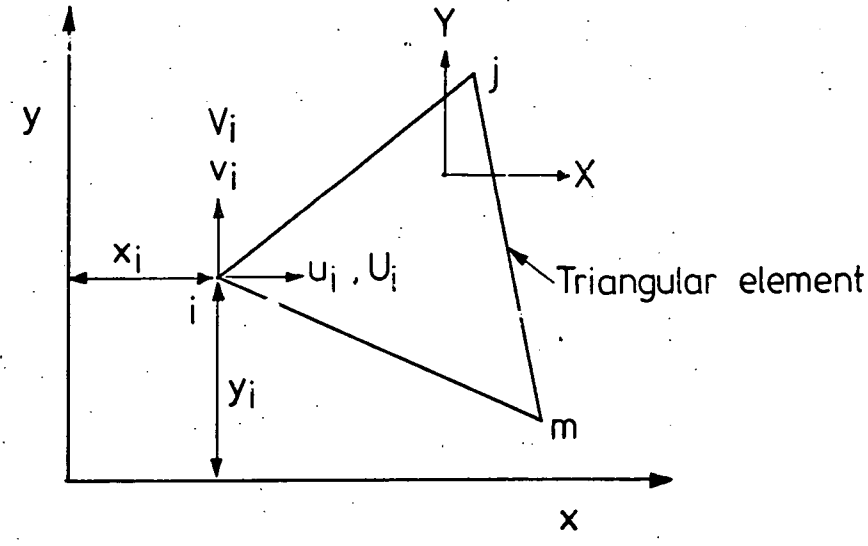

Fig. J.2 THE SIMPLEX TRIANGULAR ELEMENT.

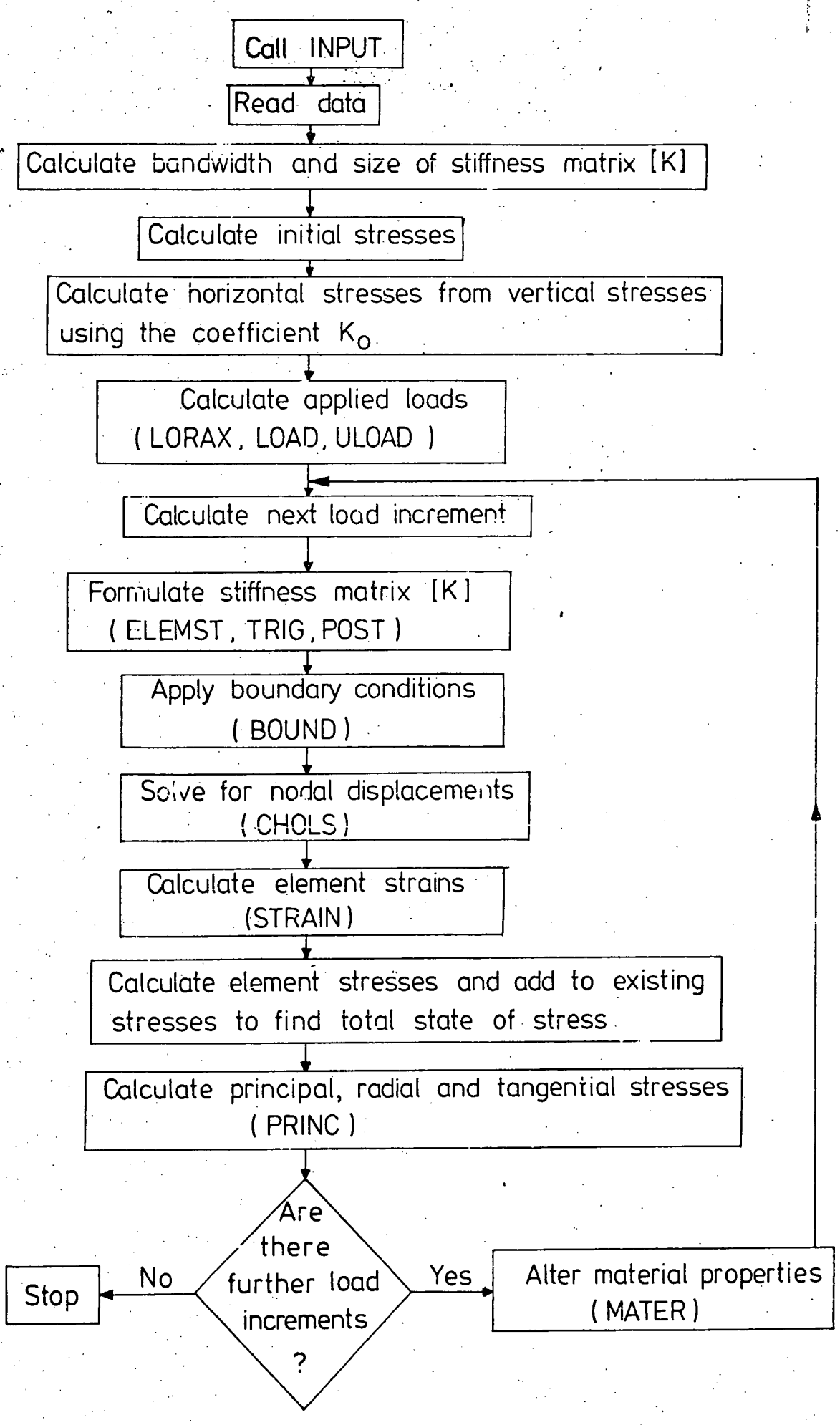

Fig. J.3 SIMPLIFIED FLOW DIAGRAM OF THE MAIN FINITE ELEMENT ANALYSIS COMPUTER PROGRAM.

APPENDIX K

SHEAR BOX TEST RESULTS

In this Appendix a series of graphs is presented showing the relation between τ_{max} and σ'_n for shear box tests carried out on discontinuity surfaces taken from borehole cores sampled in the Lower Chalk at Chinnor. These tests are described in detail in Chapter 9.

Figures K.1 to K.12 show the variation of τ_{max} (the maximum shear stress mobilised) with σ'_n (the effective normal stress acting across the discontinuity) for the series of tests carried out on dry samples. Figures K.13 to K.24 show the variation of τ_{max} with σ'_n for tests carried out on wet (saturated) samples. In each of the Figures K.1 to K.24 the first cycle shear tests are represented by circular data points and a solid line, the parameters of which are c'_p and ϕ'_p. The second cycle shear tests are represented by crossed data points and a dashed line, the parameters of which are c'_{ult} and ϕ'_{ult}. Additional data relating to each test (described fully in Chapter 9) are also tabulated in Figures K.1 to K.24.

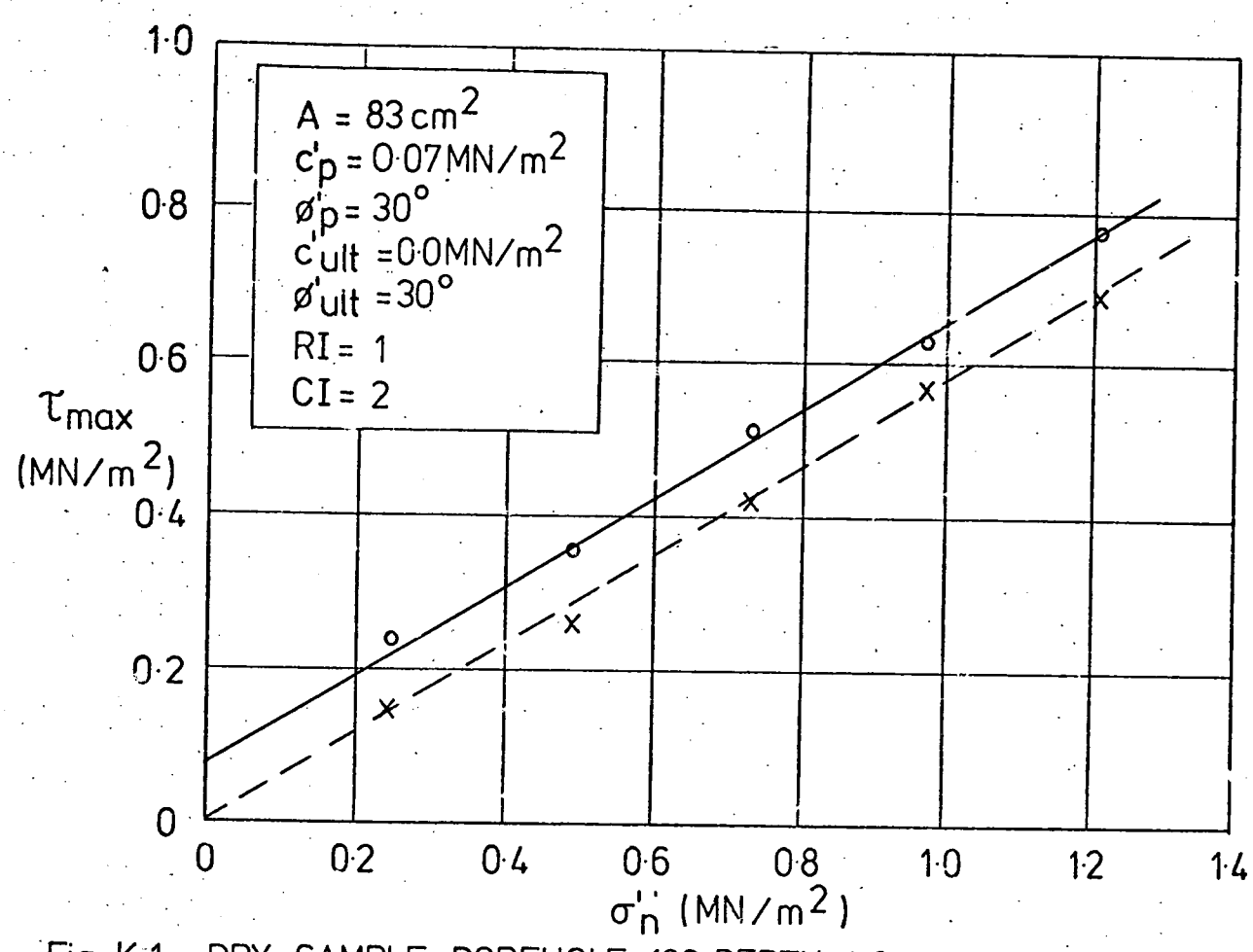

Fig. K.1 DRY SAMPLE, BOREHOLE 100, DEPTH 4·0m.

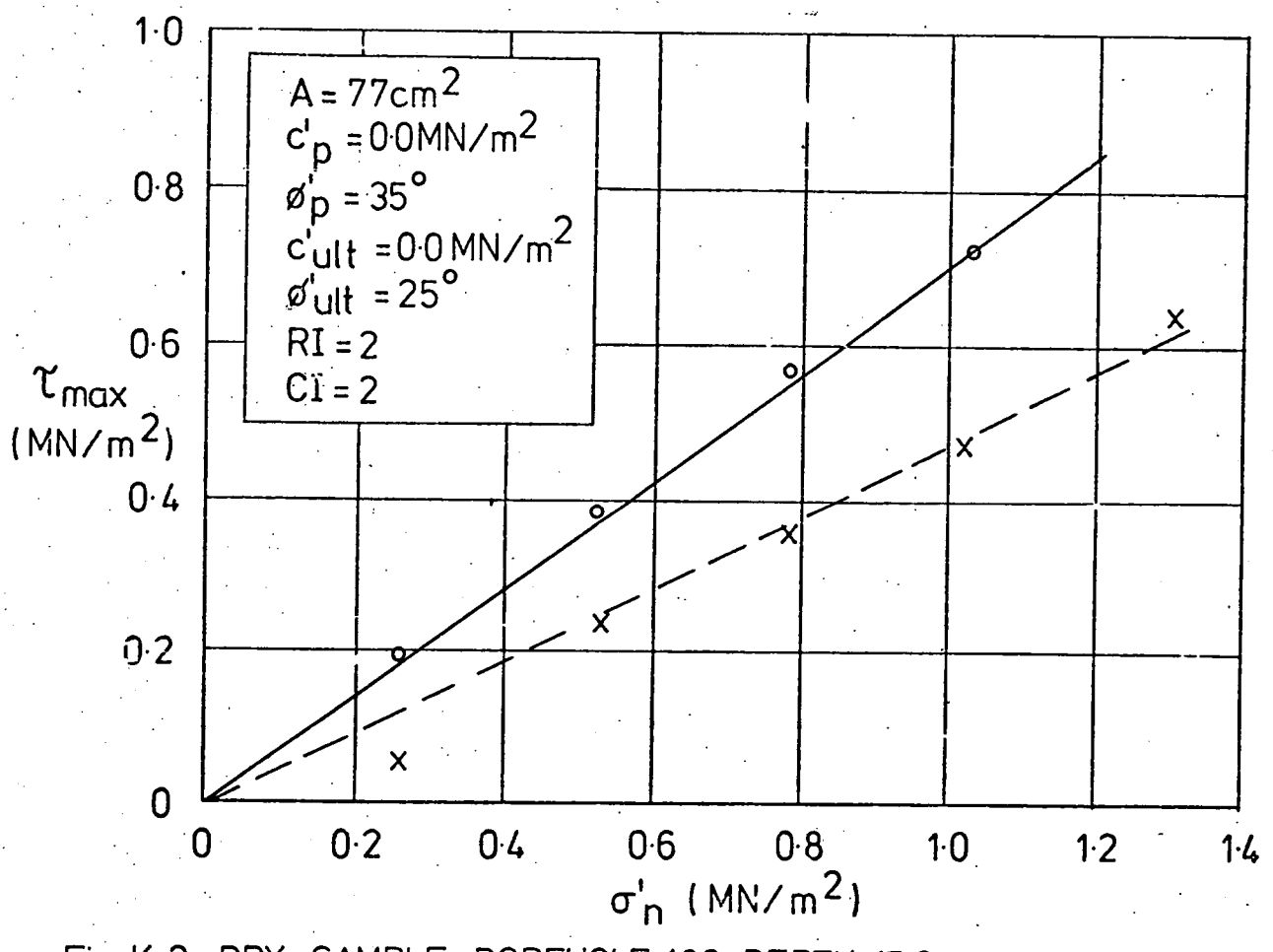

Fig. K.2 DRY SAMPLE, BOREHOLE 100, DEPTH 15·0m.

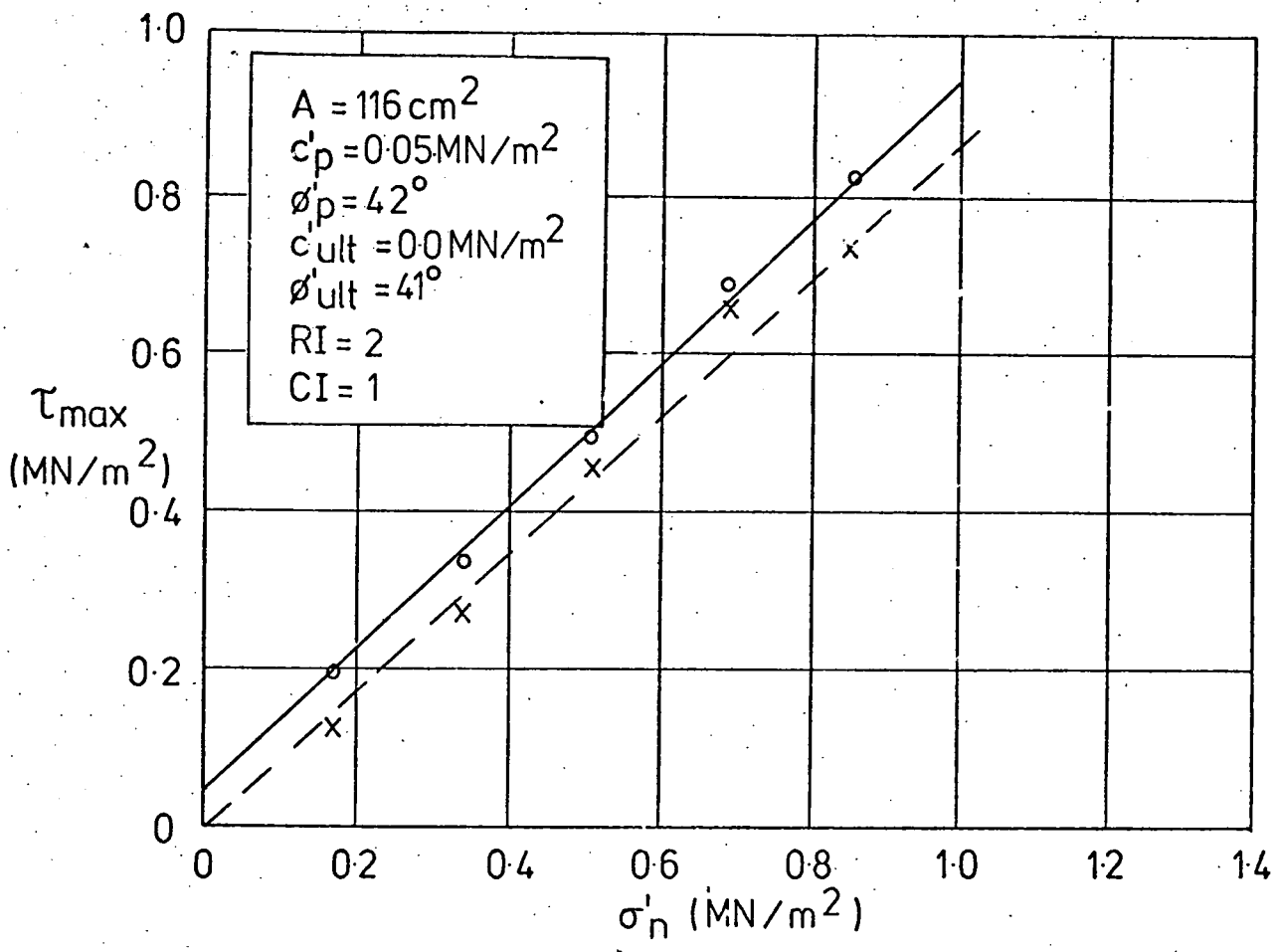

Fig. K.3 DRY SAMPLE, BOREHOLE 100, DEPTH 17·6m.

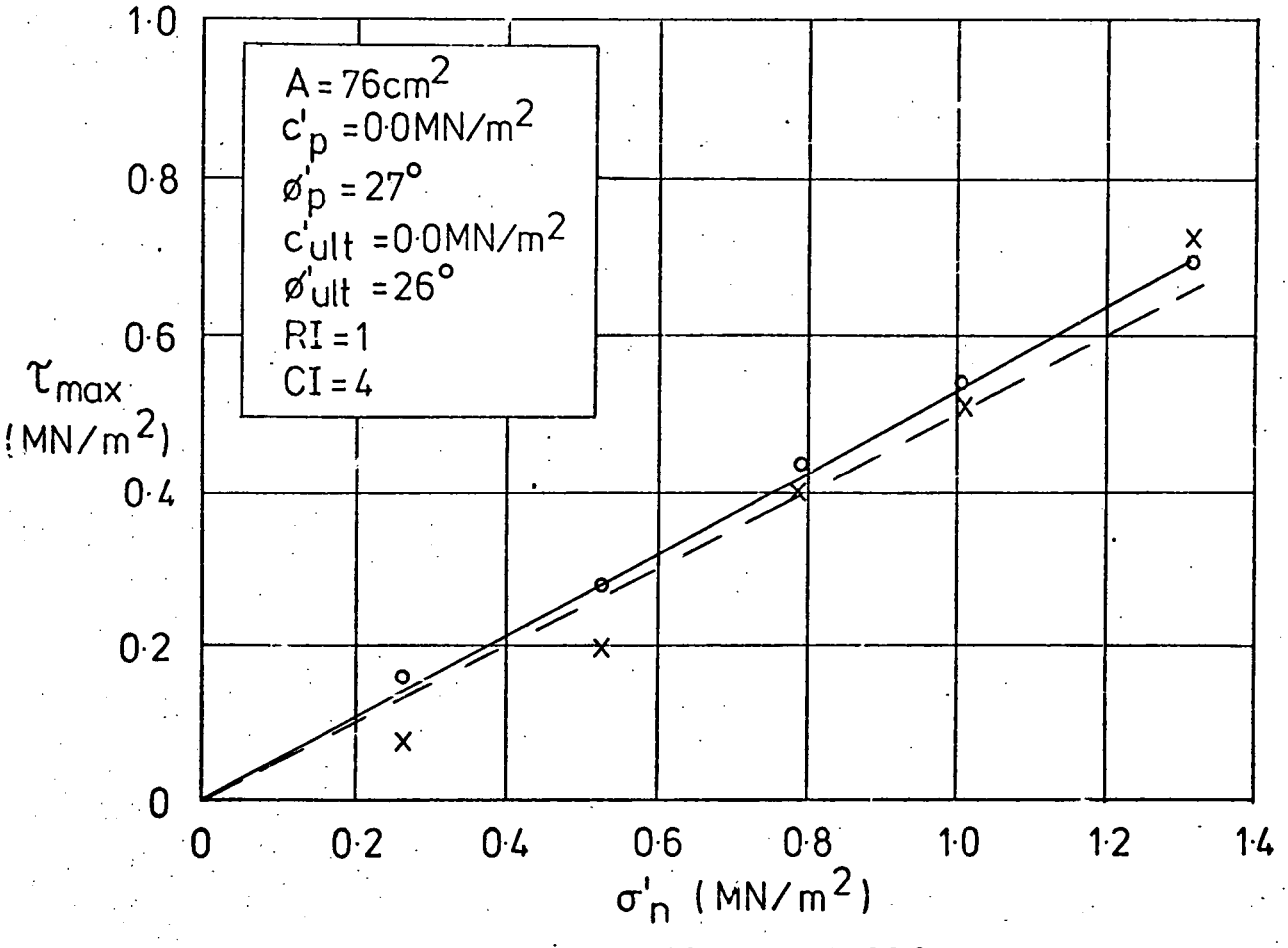

Fig. K.4 DRY SAMPLE, BOREHOLE 100, DEPTH 29·8m

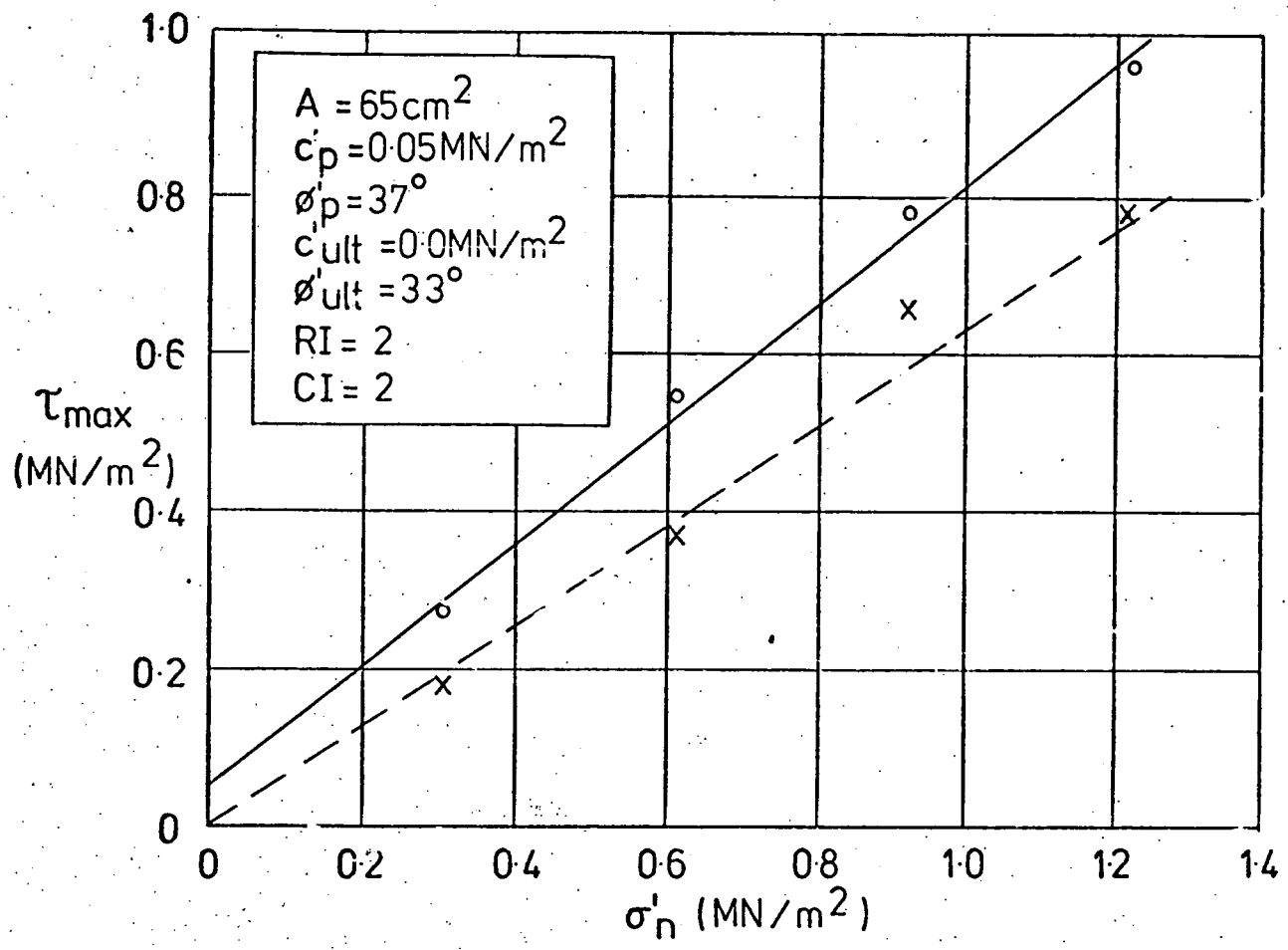

Fig. K.5 DRY SAMPLE, BOREHOLE 101, DEPTH 4·0m.

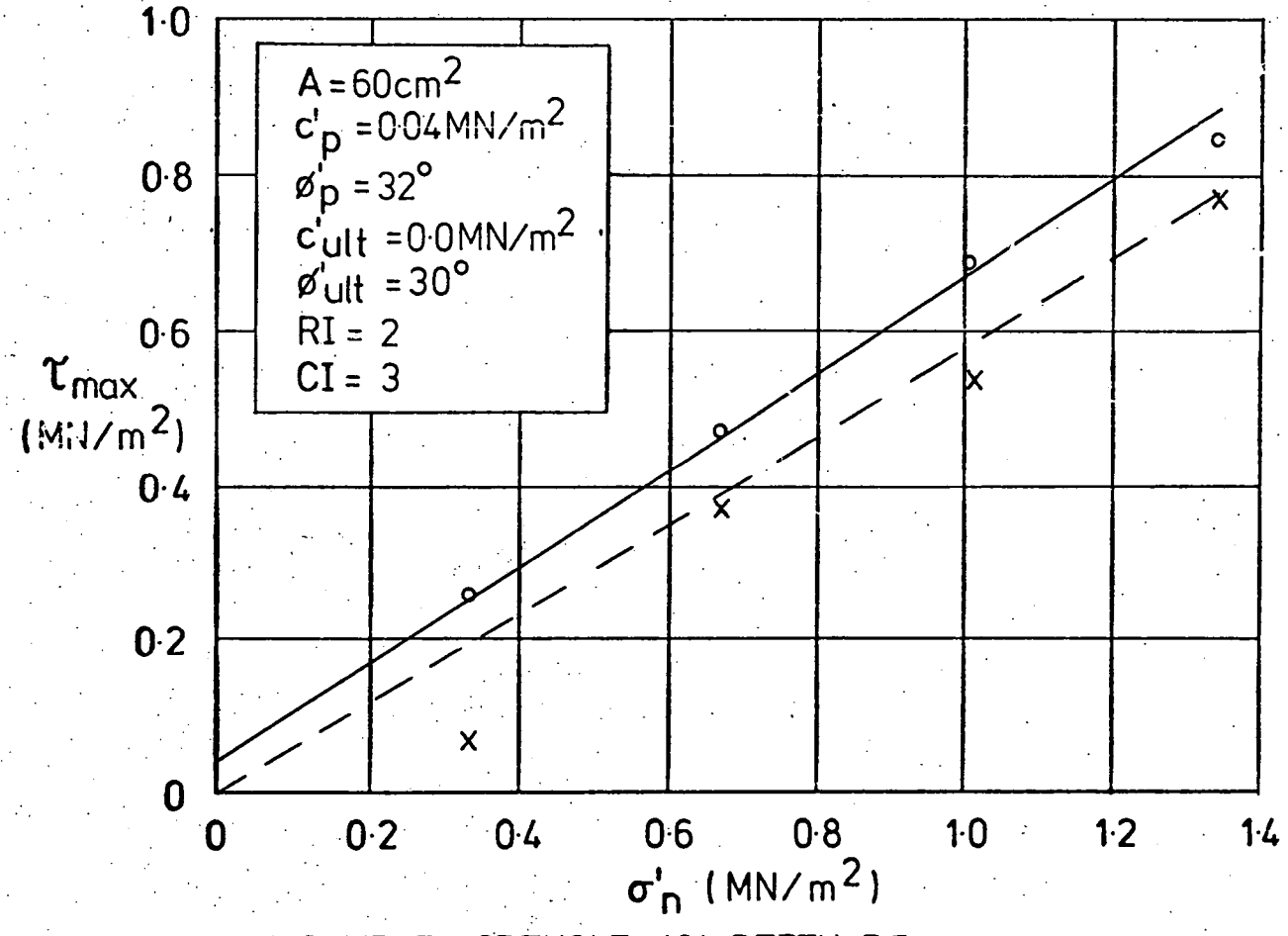

Fig. K.6 DRY SAMPLE, BOREHOLE 101, DEPTH 5·5m.

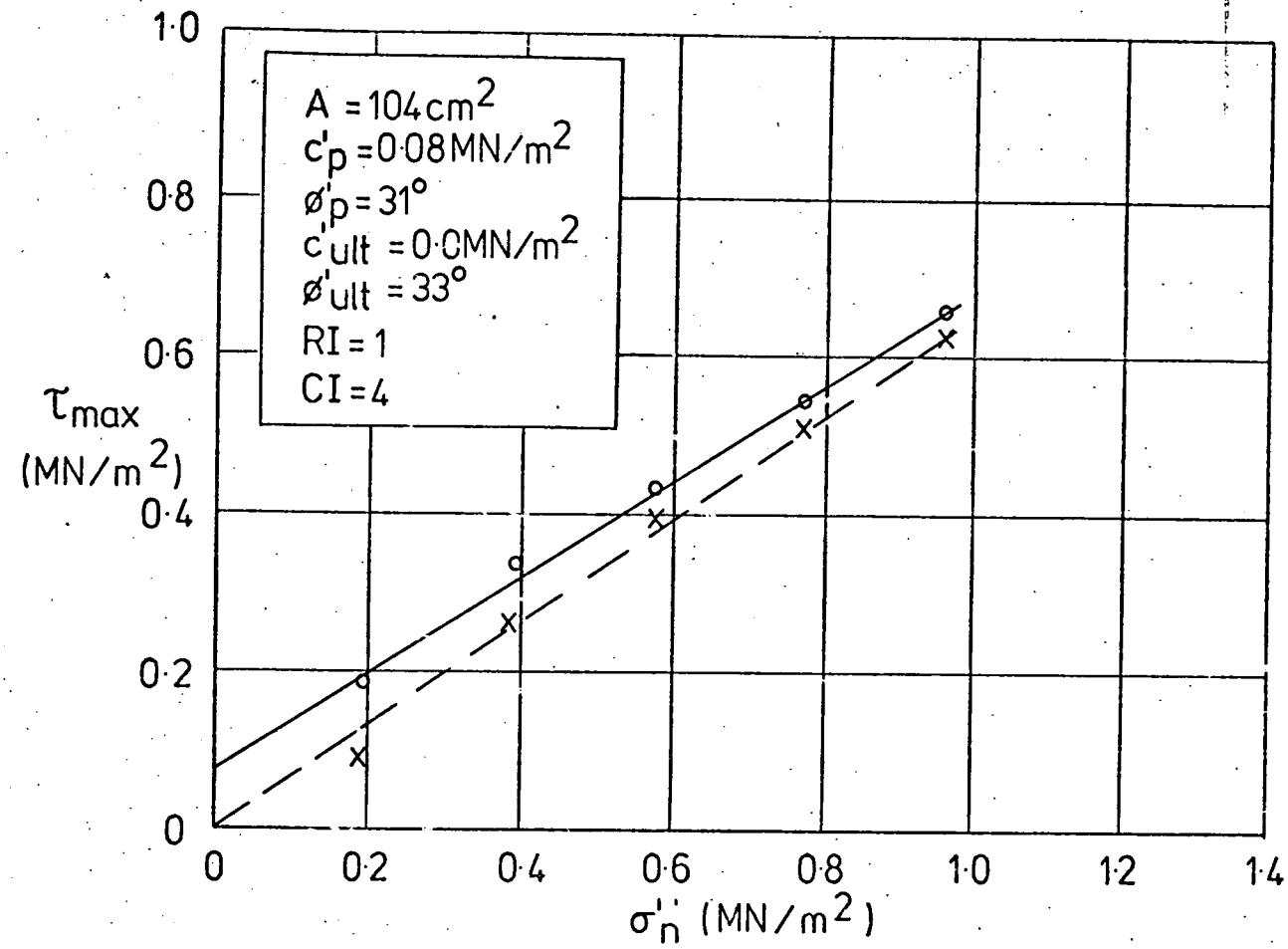

Fig.K.7 DRY SAMPLE, BOREHOLE 101, DEPTH 12·8m.

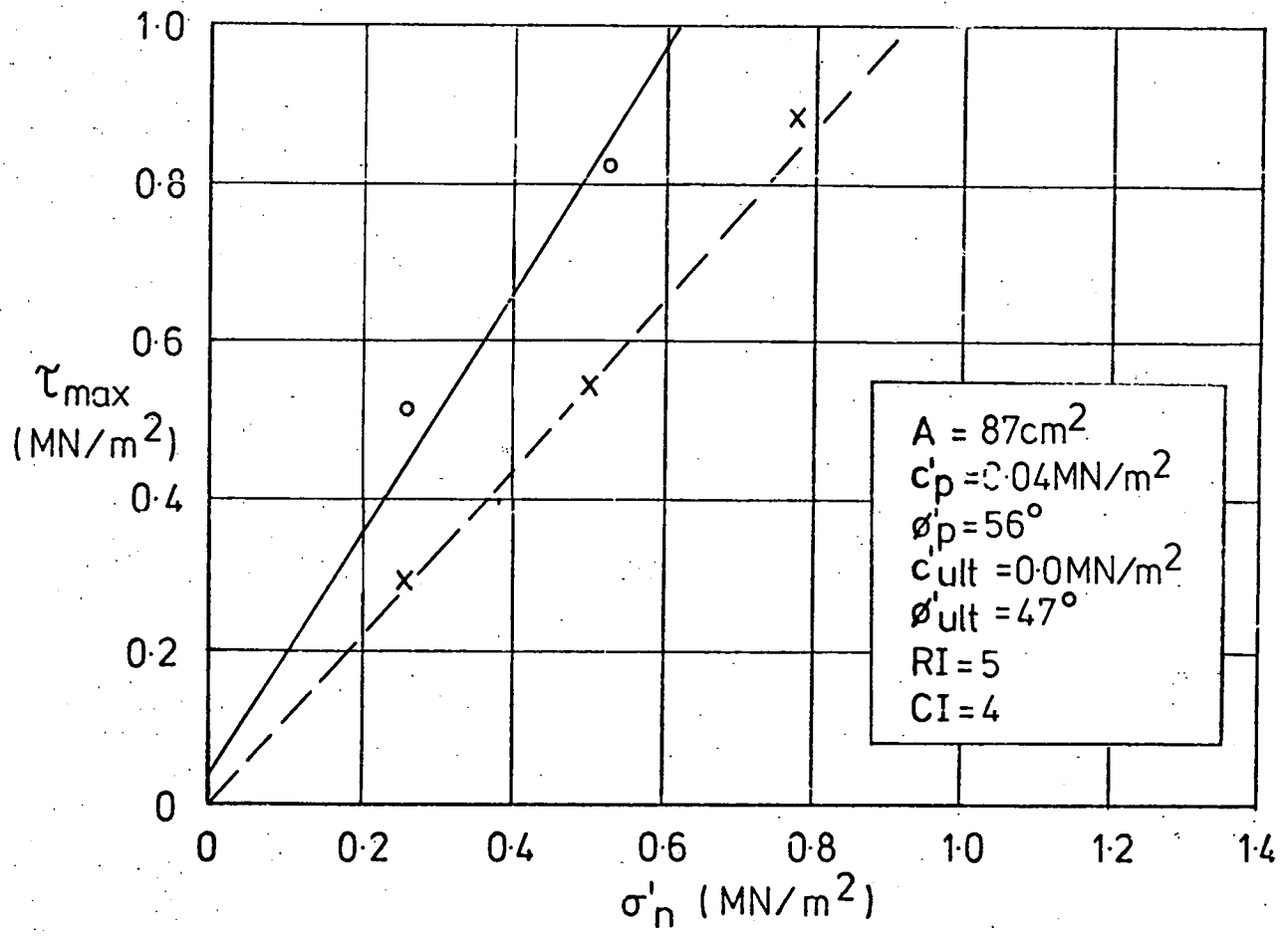

Fig.K.8 DRY SAMPLE, BOREHOLE 101, DEPTH 18·2m.

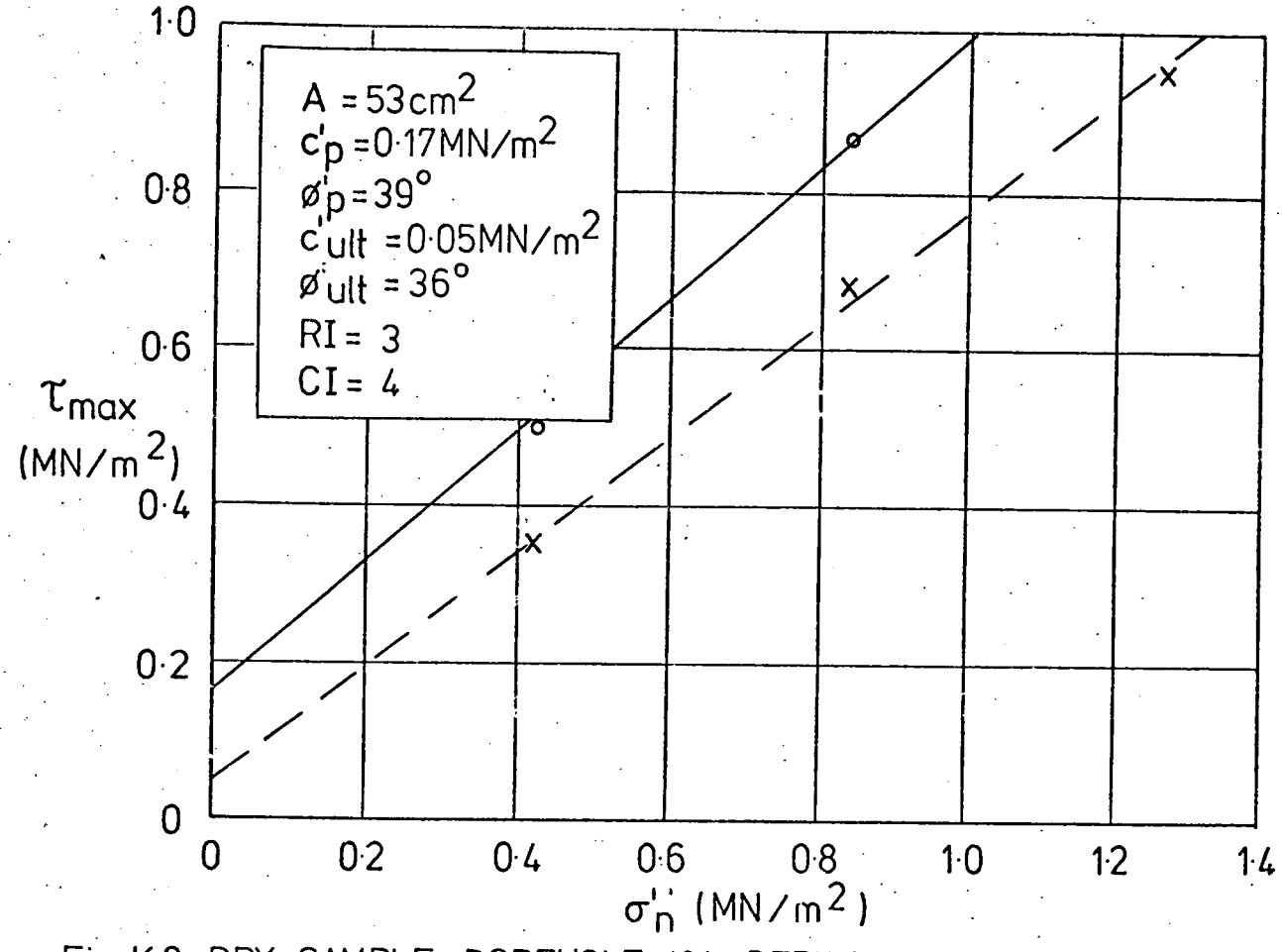

Fig.K.9 DRY SAMPLE, BOREHOLE 101, DEPTH 19·2m.

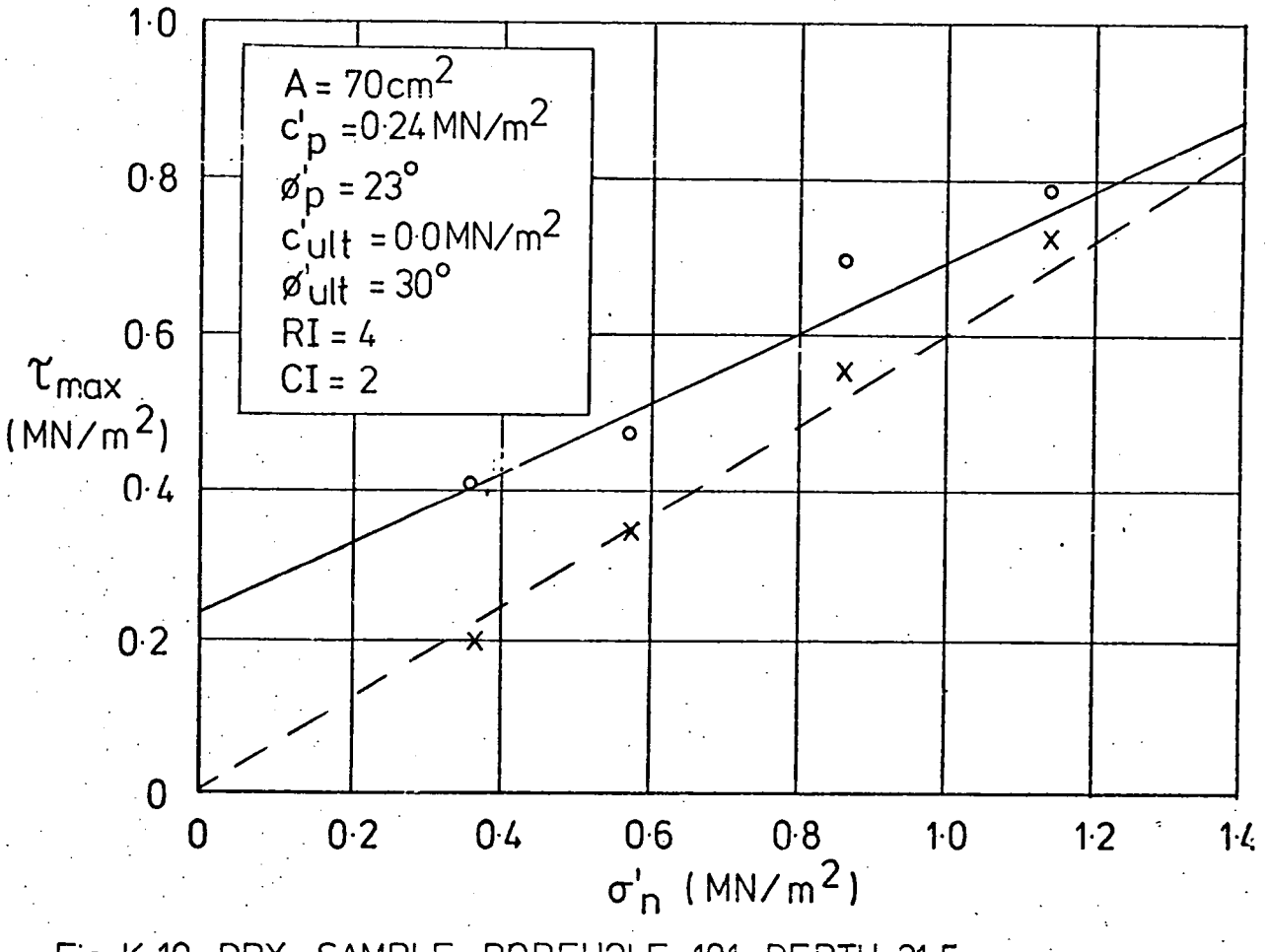

Fig.K.10 DRY SAMPLE, BOREHOLE 101, DEPTH 21·5m.

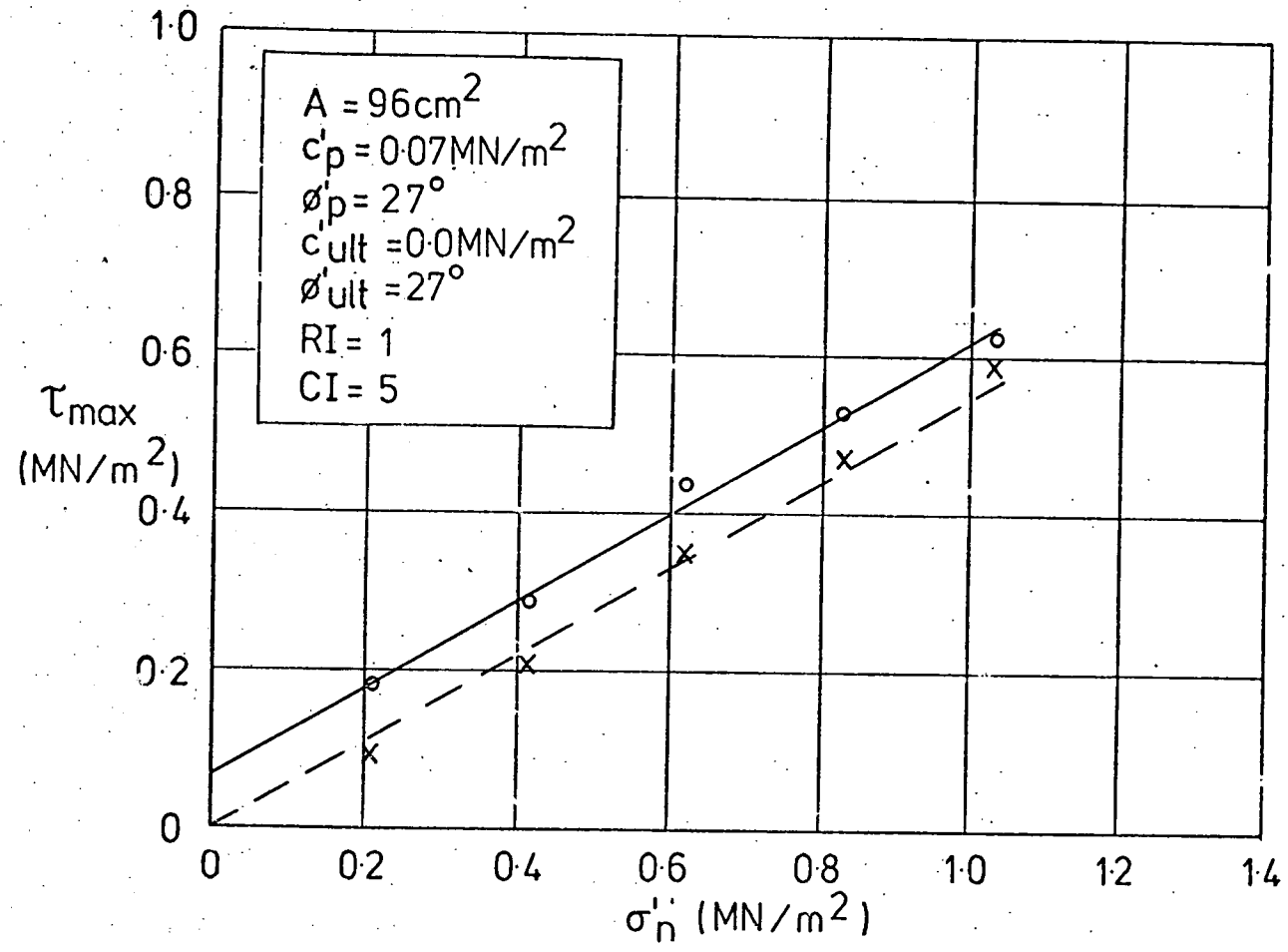

Fig. K.11 DRY SAMPLE, BOREHOLE 101, DEPTH 22·6m.

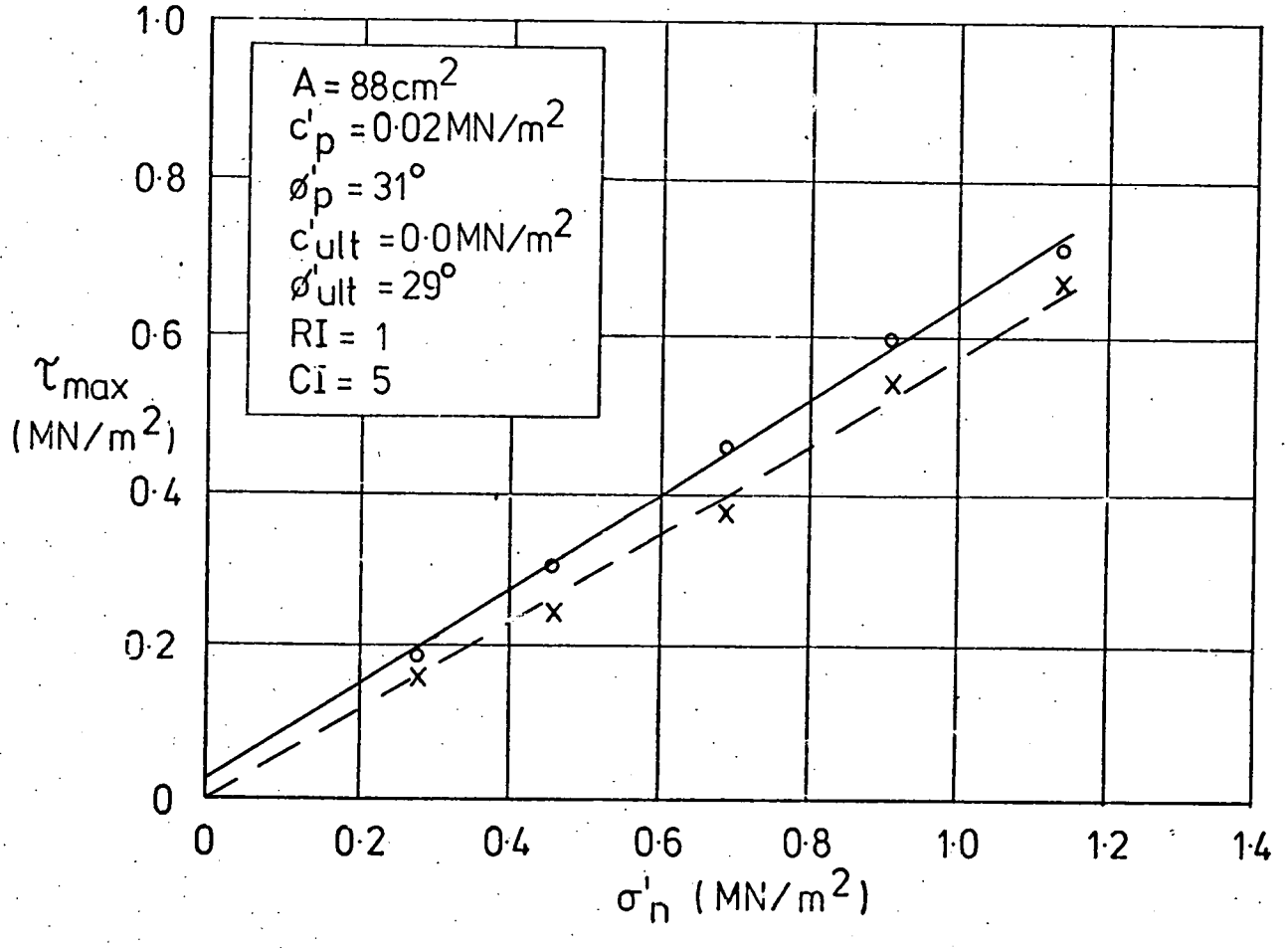

Fig. K.12 DRY SAMPLE, BOREHOLE 101, DEPTH 22·8m.

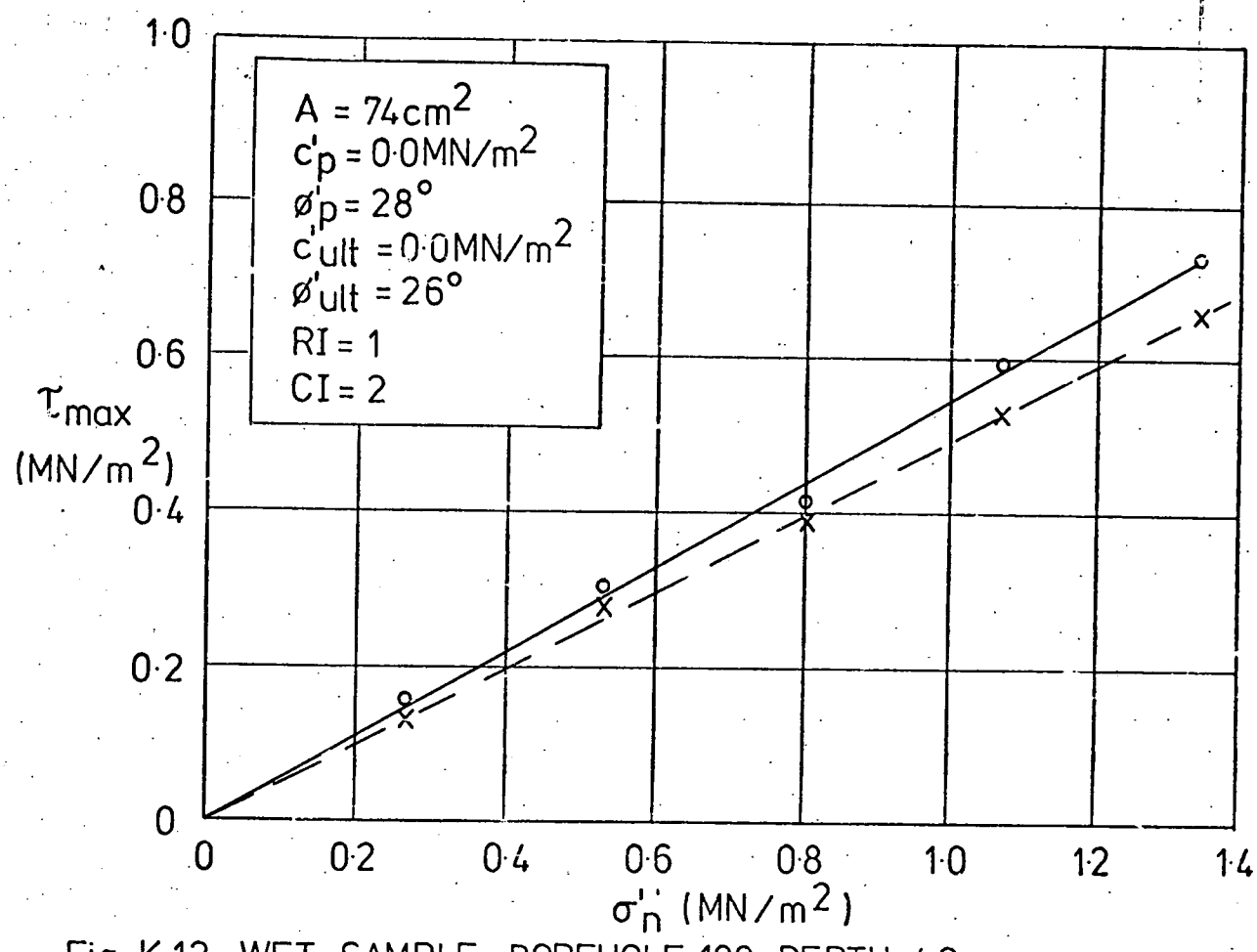

Fig. K.13 WET SAMPLE, BOREHOLE 100, DEPTH 4·2m.

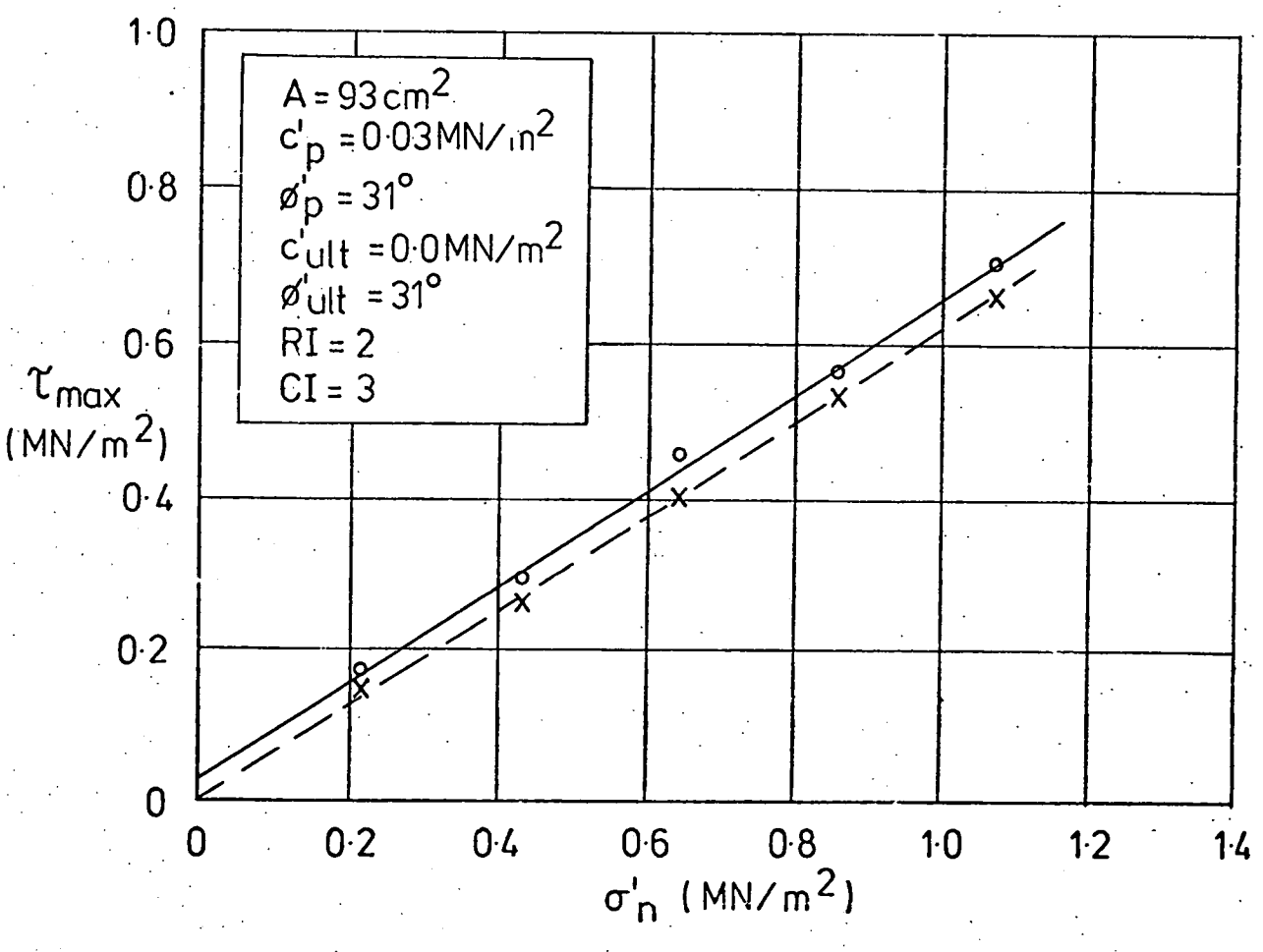

Fig. K.14 WET SAMPLE, BOREHOLE 100, DEPTH 7·7m.

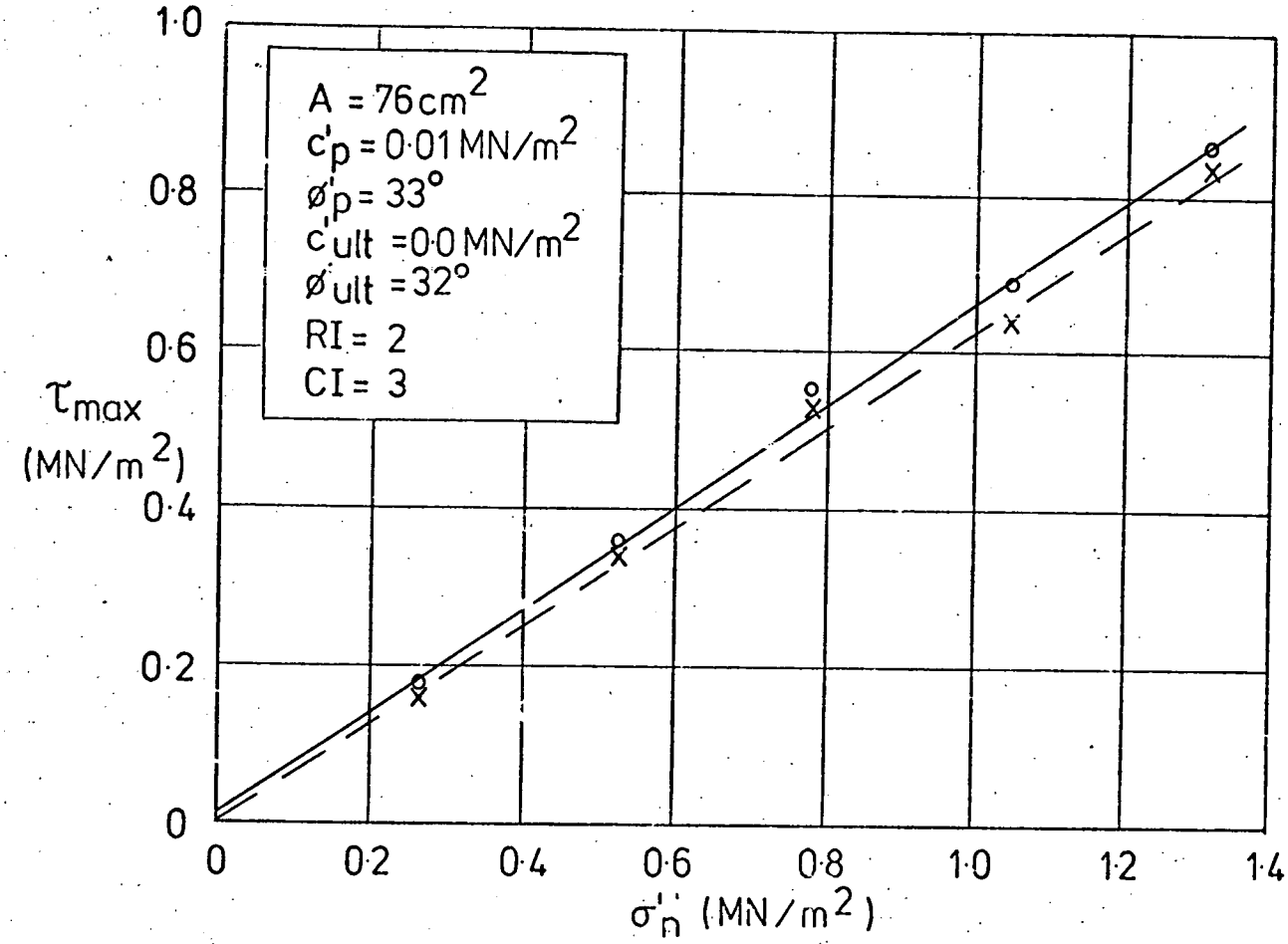

Fig. K.15 WET SAMPLE, BOREHOLE 101, DEPTH 3·7m.

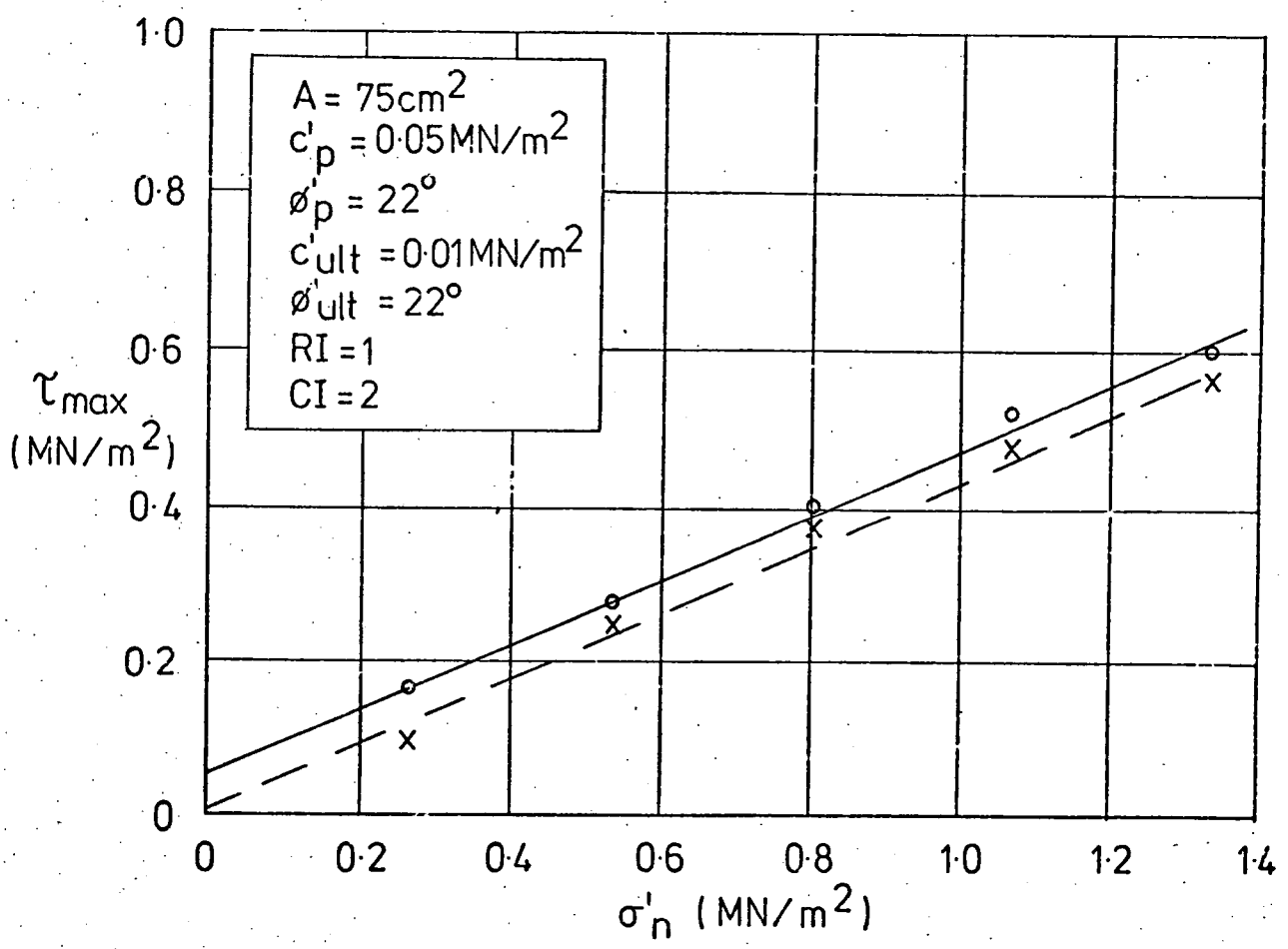

Fig. K.16 WET SAMPLE, BOREHOLE 101, DEPTH 7·6m

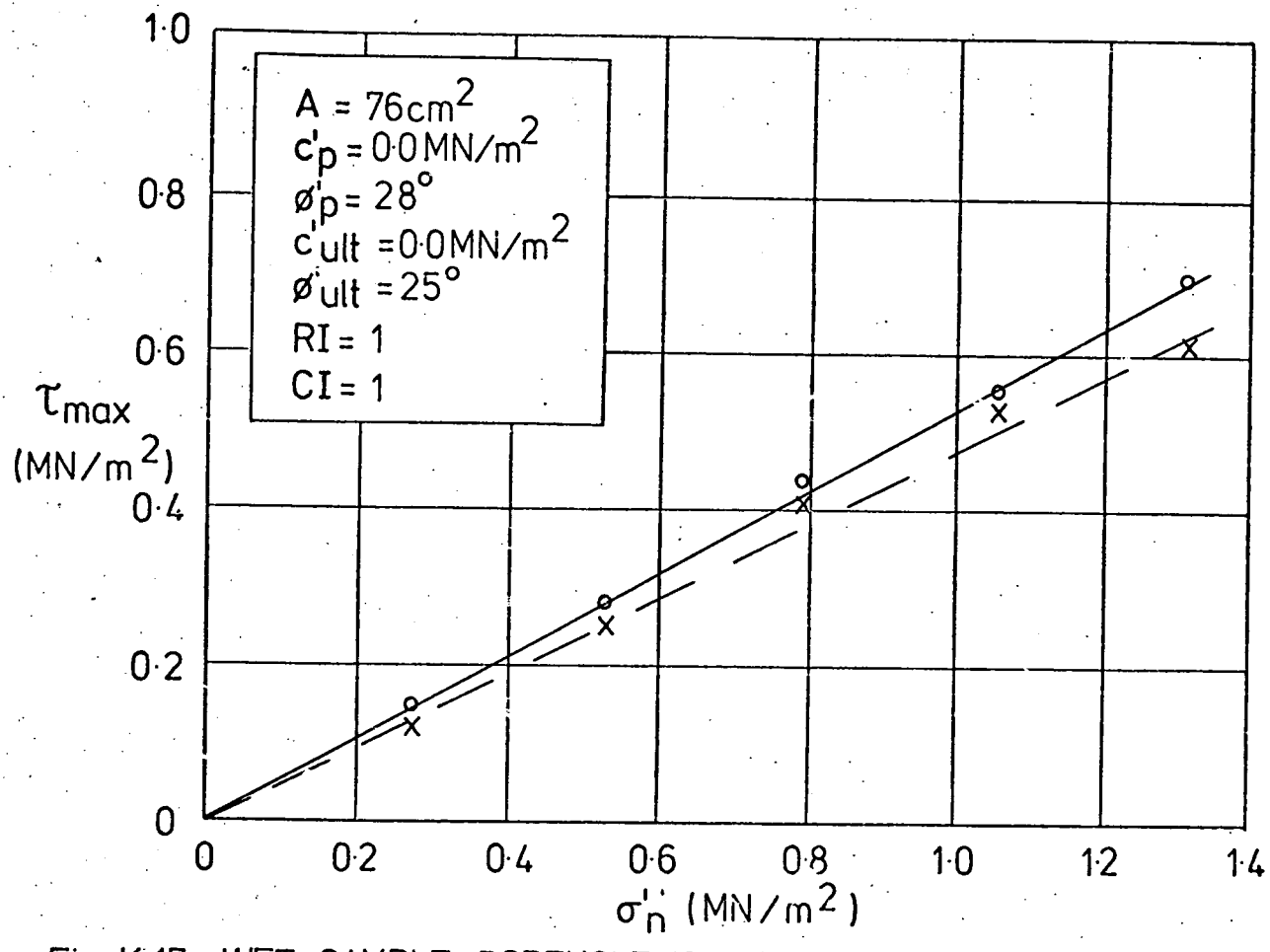

Fig. K.17 WET SAMPLE, BOREHOLE 101, DEPTH 15m.

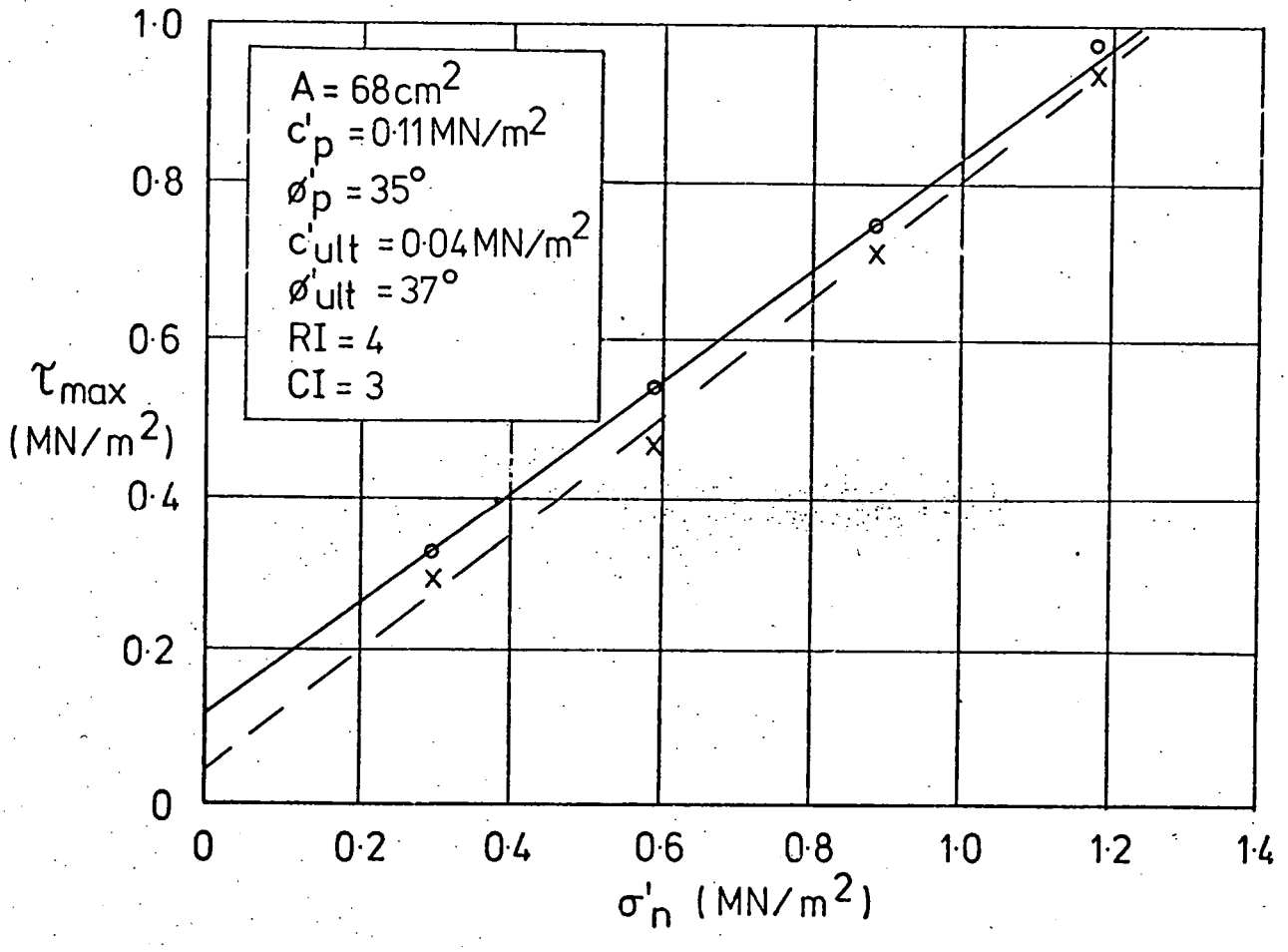

Fig. K.18 WET SAMPLE, BOREHOLE 102, DEPTH 6·0m.

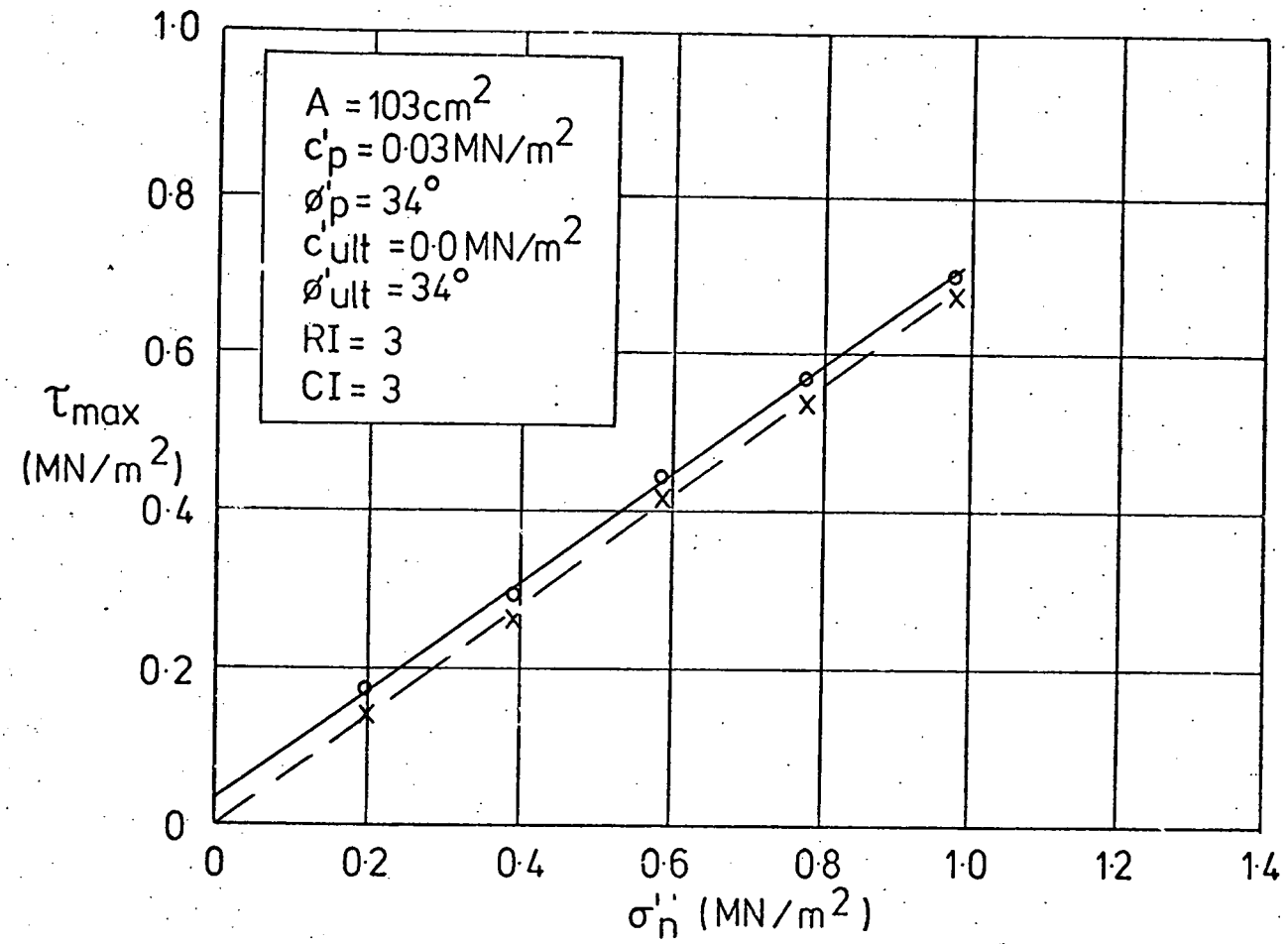

Fig. K.19 WET SAMPLE, BOREHOLE 102, DEPTH 18·8m.

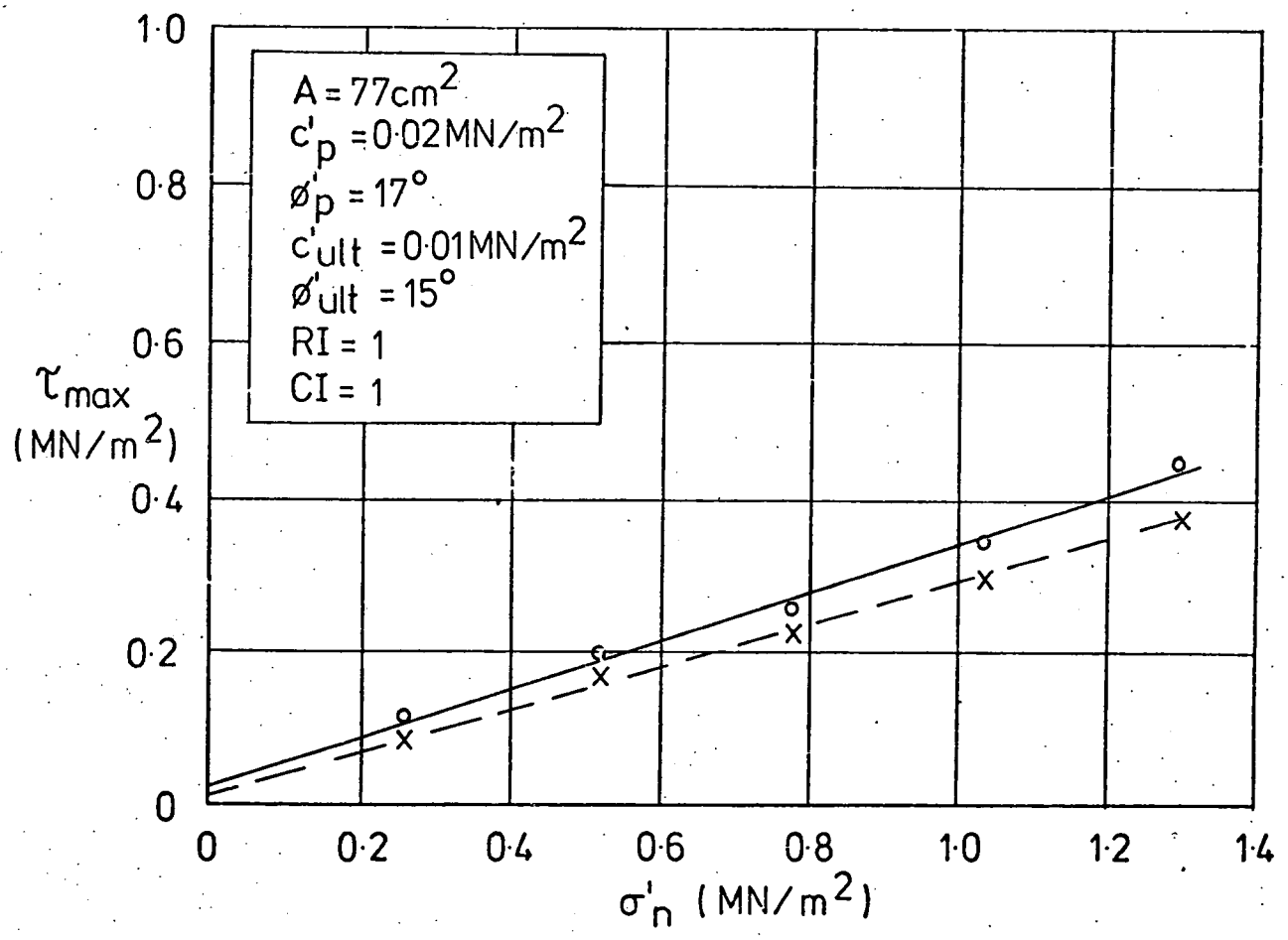

Fig. K. 20 WET SAMPLE, BOREHOLE 104, DEPTH 17·9m.

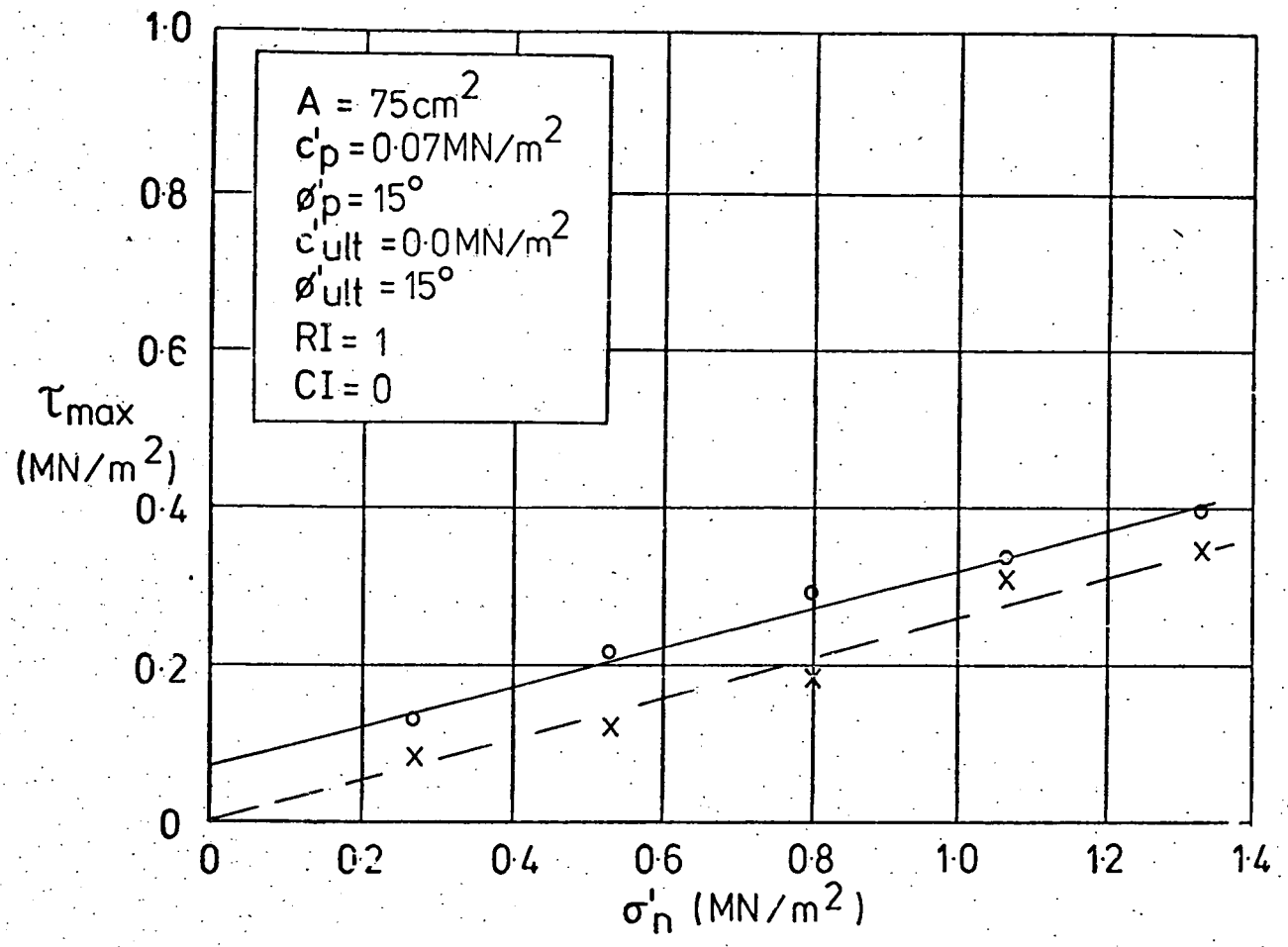

Fig. K. 21 WET SAMPLE, BORHOLE 104, DEPTH 18·2m.

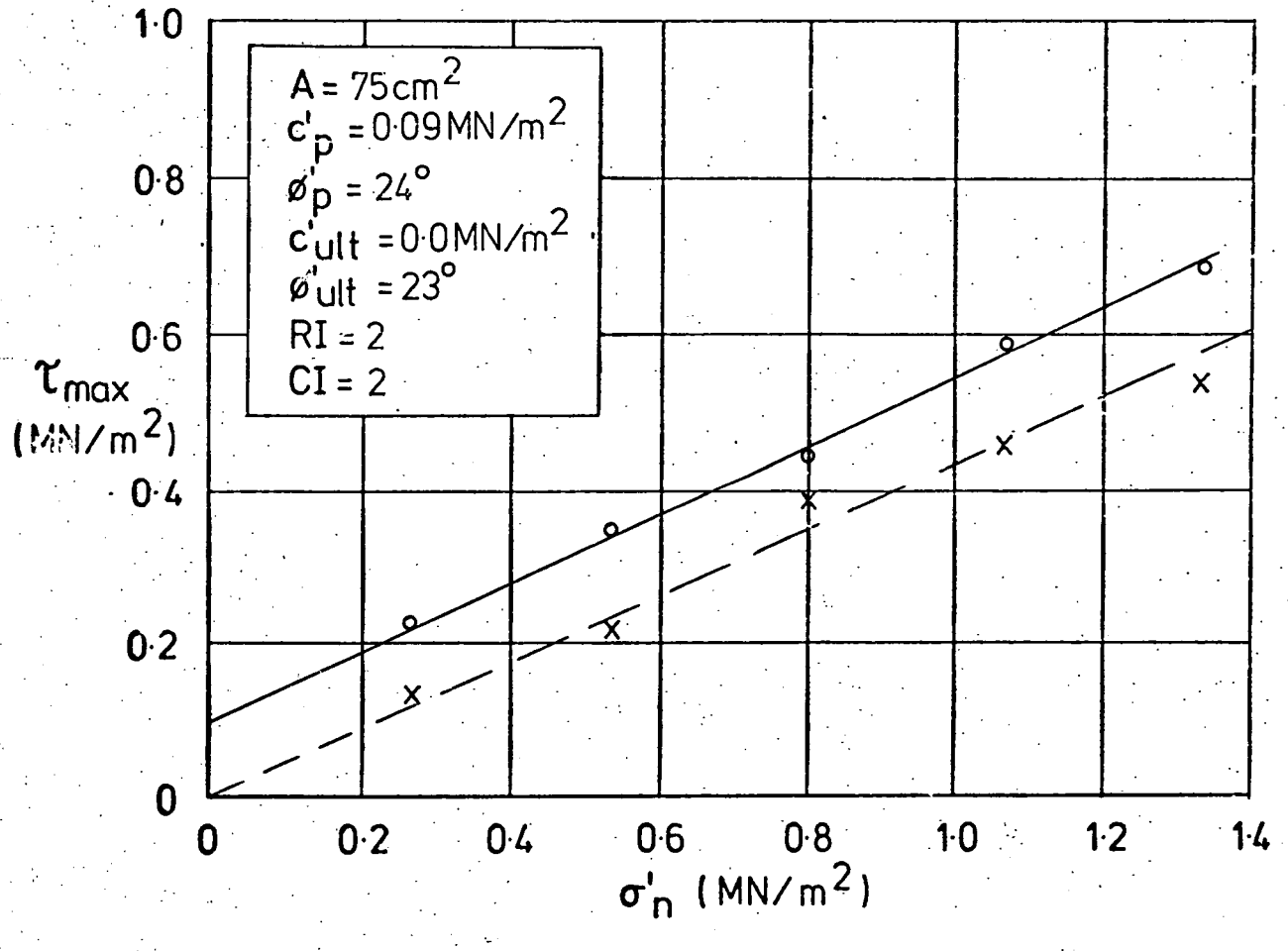

Fig. K. 22 WET SAMPLE, BOREHOLE 105, DEPTH 3·0m.

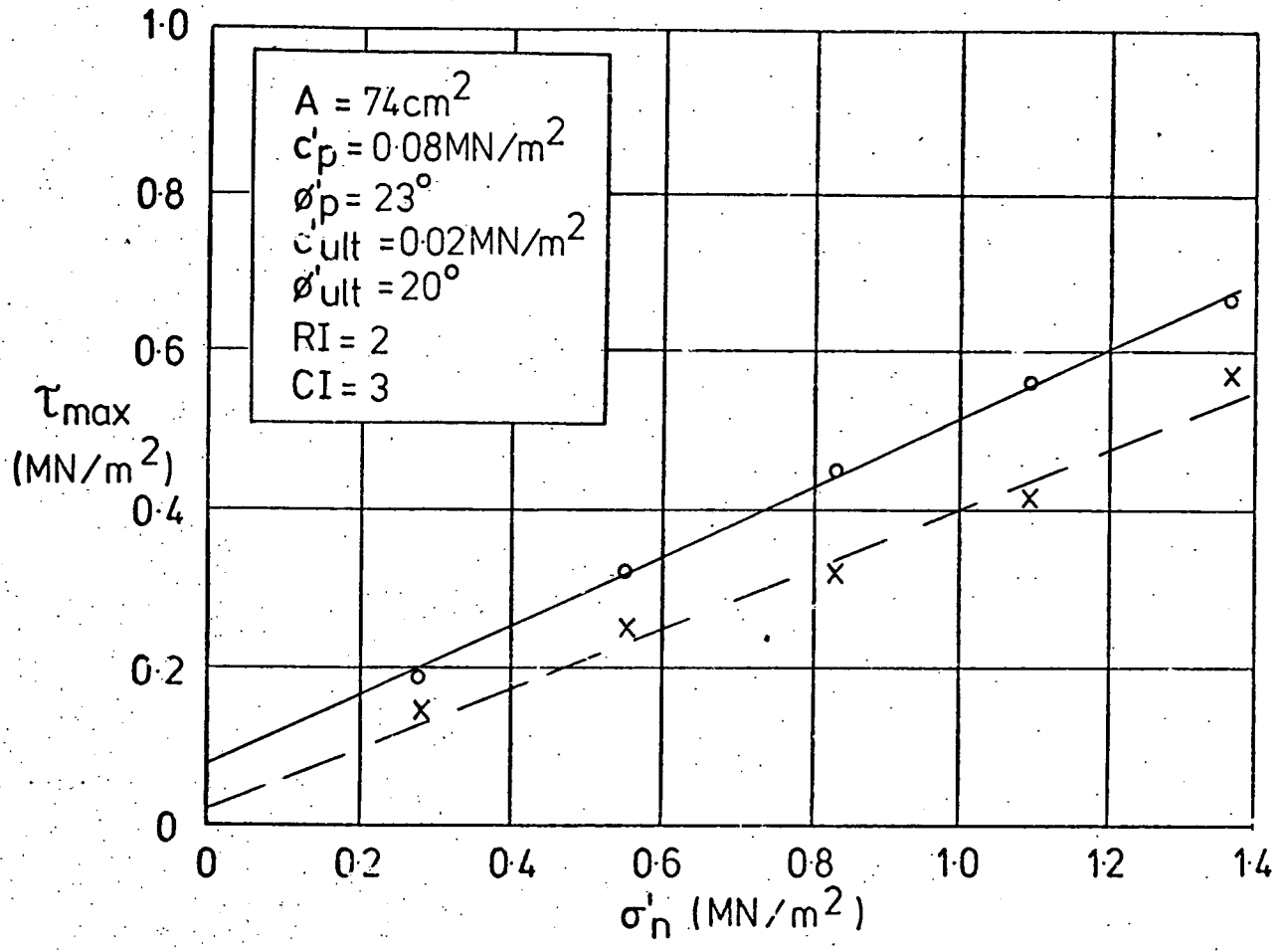

Fig. K.23 WET SAMPLE, BOREHOLE 105, DEPTH 20·3m.

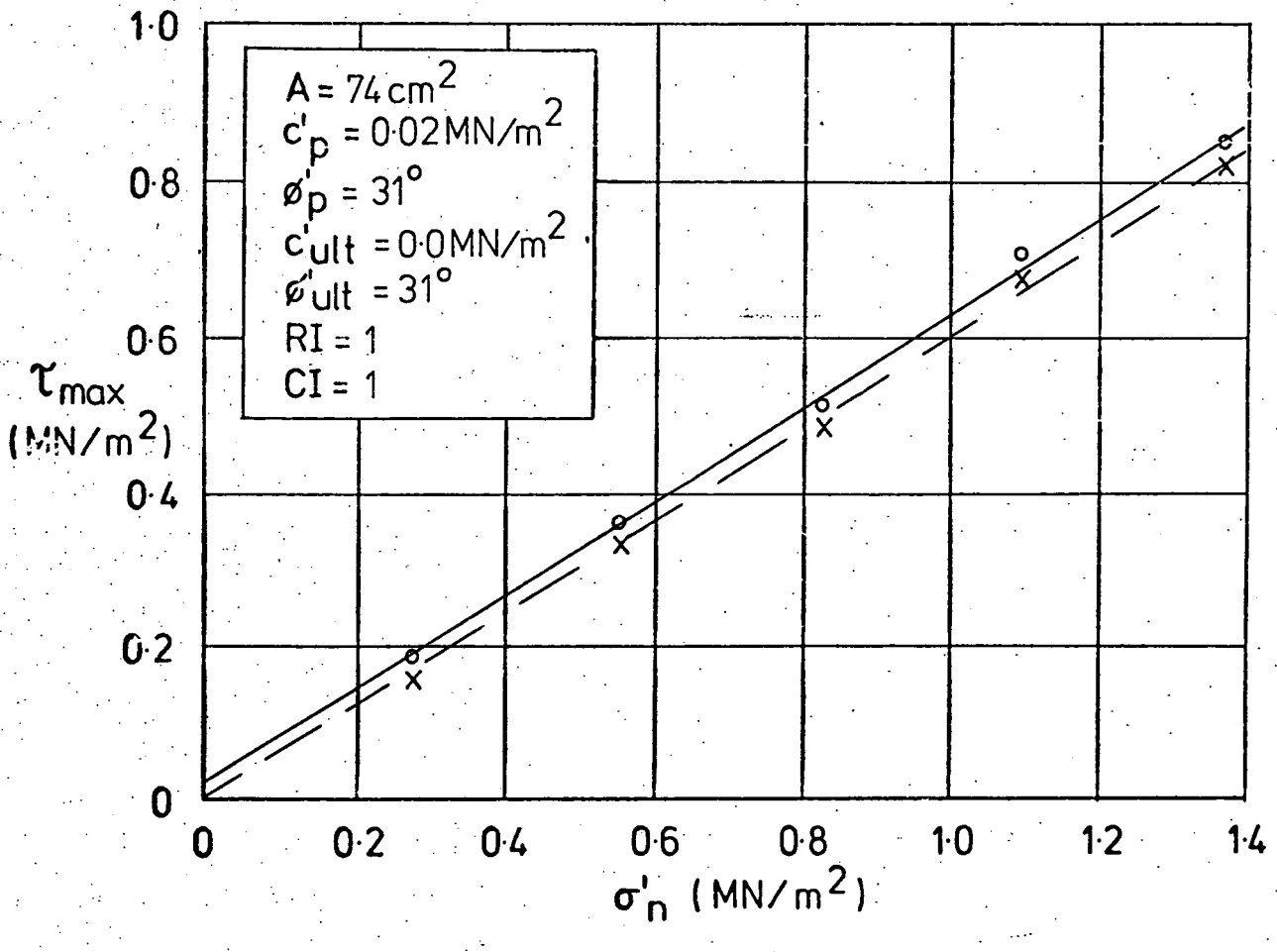

Fig. K.24 WET SAMPLE (FROM ROAD CUTTING)

APPENDIX L

DISCONTINUITY SPACINGS IN ROCK; STATISTICAL ASPECTS

L.1 The Poisson and negative exponential distributions

Using the scanline technique, discontinuity spacings are measured by setting up a measuring tape across the rock face and noting the tape positions where discontinuities are present. If it is assumed that each small section of scanline has an equal chance of containing a discontinuity, the discontinuity positions are random and the spacing distribution can be studied in two ways:

a) the discrete case - a small unit length of rock (say, 10mm) is considered intact if no discontinuity is present, and fractured if a discontinuity is present; the total scanline length must then be an integral multiple of the unit length;

b) the continuous case - the unit lengths become infinitely small and the total scanline length can be any real number.

In the discrete case, the binomial and geometric distributions provide the probabilities associated with frequency of discontinuity occurrence and spacing values respectively. In the continuous case, the equivalent distributions are the Poisson and negative exponential functions. The discrete case can be explained via a coin tossing analogy and the continuous case as a limit to the discrete case when the number of units becomes infinite. The coin tossing analogy is useful because it provides an intuitive understanding of why the most likely spacing value is zero when the discontinuities are randomly positioned.

L.1.1 Discrete case

Consider, in analogy, an unbiased coin tossing sequence of heads and tails where a head represents a unit length of intact chalk and a tail represents a unit length containing a discontinuity. For example

Coin sequence: T H H T H H T H T T T H H T H T T H T

Scanline: 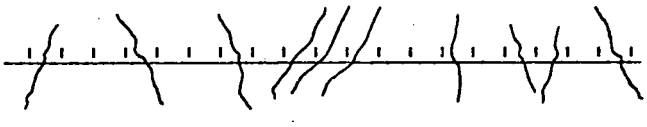

There is an analogy between the number of tails that will occur in n tosses and the number of discontinuities that will occur along a scanline of length n units. In addition, the spacings between successive tails and the spacings between successive discontinuities are analogous. In practice, the probability of a small unit length of scanline being intersected by a discontinuity need not be one half as for the unbiased coin. Thus, the analogy becomes direct for a biased coin* with a different probability value for tails producing a random sequence such as

H H H T H H H H T H T H H H H H T T H H T

The probability of k tails occurring in n tosses, or k discontinuities in a length n units, is given by the binomial distribution as:

$$P\left(\begin{matrix}k \text{ tails in} \\ n \text{ tosses}\end{matrix}\right) = (n!/(n-k)!k!)\, q^k p^{n-k} \qquad \text{.....(L.1)}$$

where $P(x)$ = probability of x occurring

p = probability of a head

$q = 1-p$ = probability of a tail

---

* Although biased, the result is still random - similar to selecting a ball from a bag containing different numbers of black and red balls.

The probabilities associated with encountering a certain number of discontinuities in a given length of scanline can be calculated from Equation L.1 given q the probability of a discontinuity intersecting a unit length of scanline. The mean and standard deviation of the binomial distribution are np and $\sqrt{npq}$ respectively.

However, we are also interested in the distribution of spacings between successive tails and, by analogy, the distribution of spacings between discontinuities. In this case, the probability of each sequence is considered. Assuming that a tail has just occurred, the sequences in Table L.1 can follow:

Table L.1 Spacing sequences between successive tails

Sequence	No. of heads (spacing between tails)	Probability	Probability for unbiased coin ($p=^1/2$)
T-T	0	q	$^1/2$
T-HT	1	pq	$^1/4$
T-HHT	2	ppq	$^1/8$
T-HHHT	3	pppq	$^1/16$
T-HHHHT	4	ppppq	$^1/32$

This probability density distribution is called the geometric distribution because the probability is reduced by the constant factor p for each unit increase of spacing.

Thus $$P\left(\begin{matrix}\text{k heads between}\\ \text{successive tails}\end{matrix}\right) = p^k q = p^k(1-p) \qquad \ldots\ldots (L.2)$$

This distribution is plotted in Figure L.1 for a specific value of p. For $p = \frac{1}{2}$ the coin is unbiased, for other p values the coin is biased but the coin tossing sequence is still random. Note that for all p values, the most frequently occurring spacing value is zero. The mean of the geometric distribution is equal to $p/(1-p)$.

L.1.2 Continuous case

In the coin tossing analogy, the coin can only be thrown an integral number of times and hence the scanline length can only be an integral multiple of the unit length. The equivalent distribution that characterises the number of events occurring in a continuous interval x is the Poisson distribution. The probability of k events occurring in the interval x is given by

$$P(\text{k events in interval x}) = e^{-\lambda x}(\lambda x)^k/k! \qquad \ldots\ldots \text{(L.3)}$$

where λ is the mean number of events occurring in a unit interval. In the Poisson distribution, the values of the mean and variance are both λ.

Since we are interested in the discontinuity spacing probability density distribution, consider the distance l from one discontinuity to the next:

$$P(l \leq x) = 1 - P(l > x)$$

$$= 1 - P(\text{no discontinuities in distance x})$$

and from Equation L.3, with k = 0

$$P(l \leq x) = 1 - e^{-\lambda x} \qquad \ldots.(L.4)$$

This is a negative exponential cumulative probability distribution. The probability density distribution (f(x)) is the derivative of Equation L.4 with respect to x:

$$f(x) = \lambda e^{-\lambda x} \qquad \ldots.(L.5)$$

This spacing distribution (Equation L.5) is plotted in Figure L.1 for a specific value of λ. The mean and standard deviation are both equal to $1/\lambda$. In both the geometric and negative exponential distributions, the most likely spacing value is zero. Lindley (1965) suggests that this is the reason for the phrase "it never rains but it pours" since rare events such as accidents follow a Poisson distribution. In the discontinuity context, an apparent clustering of discontinuities will occur as a natural consequence of the random positions.

L.2 Precision of the mean discontinuity frequency estimate ($\hat{\lambda}$)

The parameter λ in the negative exponential distribution (cf. Equation 11.2) is estimated by counting the number of discontinuities intersecting a scanline and then dividing by the scanline length. The estimated number of discontinuities per metre ($\hat{\lambda}$) is given by

$$\hat{\lambda} = n/L \qquad \ldots.(L.6)$$

where n is the number of discontinuities encountered

and L is the scanline length.

We wish to know the probability of estimating λ within a certain error band as a function of the scanline length.

For example, if the true $\lambda = 10m^{-1}$ and a scanline length of one metre is taken, then 10 discontinuities must occur for $\hat{\lambda}$ to be within 5% of the value $10m^{-1}$; if 9 or 11 discontinuities occurred, $\hat{\lambda}$ would be 10% in error.

Equation L.3 gives the probability of k events occurring in an interval x

Thus, for the example above

$$P(\text{10 discontinuities in one metre}) = e^{-10}\, 10^{10}/10! = 0.125$$

In this case, for a true λ of $10m^{-1}$ and taking a scanline length of 1m, the probability of estimating λ within 5% is only 0.125. Note that the use of 5% is artificial here because the same probability applies to estimating λ to within any percentage less than 10% - ie when ten discontinuities are measured, $\hat{\lambda}$ will be exactly equal to λ.

In general for $\hat{\lambda}$ to lie within a certain error band, $\pm \varepsilon$,

$$\lambda(1 - \varepsilon) \leq \hat{\lambda} \leq \lambda(1 + \varepsilon) \qquad \ldots.(L.7)$$

and, from Equation L.6

$$\lambda L(1 - \varepsilon) \leq n \leq \lambda L(1 + \varepsilon) \qquad \ldots.(L.8)$$

From Equation L.3, the probability of this occurring is

$$\sum_{k=n_1}^{k=n_2} e^{-\lambda L}(\lambda L)^k/k! \qquad \text{.....(L.9)}$$

for integral values of n_1 to n_2, satisfying inequality L.8. If, for example, the scanline length is 20 times the mean discontinuity spacing ($\lambda L = 20$) and a 10% error band is allowed ($\varepsilon = 0.1$), n can take the values $n_1 = 18, 19, 20, 21$, $n_2 = 22$. The probability of this occurring is 0.423 - calculated from Equation L.9. A graph summarising the probabilities predicted by Equation L.9 is presented as Figure 11.5.

Because of the artificiality of the error band, it is preferable to use the upper and lower limits of λL from the observed number of discontinuities at, say, the 98% or 90% confidence limit (Garwood, 1936) as in Table L.2 below. A larger Table is available in Pearson and Hartley (1954).

Table L.2 Variation of λL at 98% and 90% confidence levels given the observed number of discontinuities (from Garwood, 1936)

		Possible variation of λL	
		98% confidence	90% confidence
Observed number of discontinuities	0	0 - 4.61	0 - 3
	1	0.01 - 6.64	0.05 - 4.74
	5	1.28 - 13.11	1.97 - 10.51
	10	4.13 - 20.14	5.43 - 16.96
	15	7.48 - 26.74	9.25 - 23.10
	20	11.08 - 33.10	13.25 - 29.06
	25	14.85 - 39.31	17.38 - 34.92
	30	18.74 - 45.40	21.59 - 40.69
	40	26.77 - 57.35	30.20 - 52.07
	50	35.03 - 69.07	38.96 - 63.29

If 50 discontinuities are observed in a scanline length of 5m, λL varies from 38.96 to 63.29 at the 90% confidence level (Table L.2); ie λ varies between $7.79m^{-1}$ and $12.66m^{-1}$. From Equation 11.5, the theoretical RQD* value then varies from 82% to 64%. This illustrates the high sampling error in using short scanlines or short borehole lengths for RQD determinations.

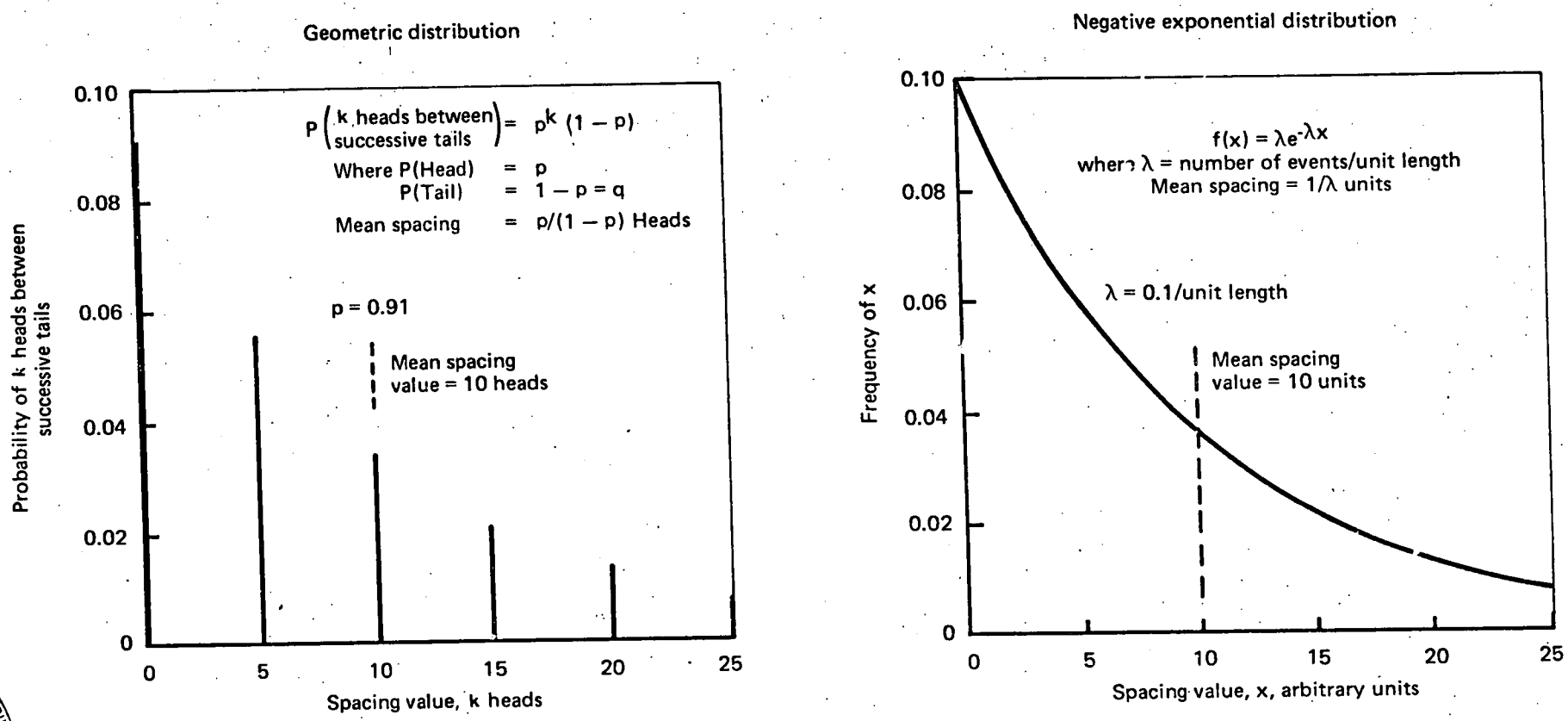

Fig.L.1 GEOMETRIC AND NEGATIVE EXPONENTIAL DISTRIBUTIONS